The rift-drift transition on magma-rich margins: Insights into the evolution of seaward dipping reflectors

James Richard Norcliffe

Submitted in accordance with the requirements for the degree of

Doctor of Philosophy

The University of Leeds

Institute of Applied Geoscience

School of Earth and Environment

June, 2019

The candidate confirms that the work submitted is his/her own, except where work which has formed part of jointly authored publications has been included. The contribution of the candidate and the other authors to this work has been explicitly indicated below. The candidate confirms that appropriate credit has been given within the thesis where reference has been made to the work of others.

The work presented in Chapter 5 of this thesis is based on a publication in *Earth and Planetary Science Letters*, which became available online on the 11th October 2018:

Norcliffe, J.R., Paton, D.A., Mortimer, E.J., McCaig, A.M., Nicholls, H., Rodriguez, K., Hodgson, N. and Van Der Spuy, D. 2018. Laterally Confined Volcanic Successions (LCVS); recording rift-jumps during the formation of magma-rich margins. Earth and Planetary Science Letters. 504,pp.53–63.

As primary author, I was responsible for seismic interpretation, seismic velocity analysis, analysis of results, and for writing the manuscript. The additional authors contributed through discussing the validity and implications of the results, they also provided editorial suggestions.

Acknowledgements

Firstly, I would like to thank my supervisors, Douglas Paton, Estelle Mortimer, and Andrew McCaig, whose advice and guidance have been invaluable.

In addition to my supervisors, I would like to extend special thanks to Mohamed Gouiza, discussions with whom have shaped my thinking on rifted margins. I am also grateful to Diego Costantino for both the interest he took in my work and the encouragement he gave me. Both the IT knowledge and willingness to help of Ben Craven has also been invaluable throughout my PhD.

I would like to thank Spectrum for providing data. Special thanks extend to Neil Hodgson and Karyna Rodriguez for assisting with data-release and for their interest and feedback.

For their encouragement and support, I would like to thank my colleagues, past and present, within the Basin Structure Group: Tobias Dalton; Simon Oldfield; Benjamin Allen; Holly Rowlands; Ahmad Schmela; Saleh Alqahtani; Tim Cullen; Bonita Barret; Ulises Rodriguez; Sergio Gamez Galicia; Charlotte Botter; Roxana Stanca; Michael Shotton; Alan Coventry; and Lulu Wu. I would also like to thank several other fellow PhD students, notably George Taylor, Amicia Lee and Kathy Doyle. Thanks also to Paul Markwick for several tectonics and data-management related discussions.

Taking a hiatus from my PhD to work in an exploration team at Equinor reminded me the importance of seeing the big picture. For this I would like thank Tore Hansen, Andrew Robinson and all of the members of regional exploration team I was part of.

For her continual support I would like to express deep thanks to my partner Autumn. For encouraging me to follow my interests I am grateful to my mother, who unfortunately passed away during my time as a PhD student. For their continued support, I am thankful to my father, my brothers, my sister-in-law and the rest of my family.

Abstract

Magma-rich margins are characterised by thick sequences of seaward dipping reflectors (SDRs), which consist of basalts interbedded with variable amounts of clastic and volcaniclastic material. The processes responsible for the emplacement and tilting of SDRs remain uncertain, as does the composition of the crust that they overlie. In this thesis, novel insights into SDR emplacement are gained through analysing new seismic reflection data from the Orange Basin, offshore South Africa and Namibia.

It is demonstrated that a series of abandoned sites of SDR emplacement are embedded within the Orange Basin SDRs. Analysis of their 3D structure indicates that these features record rift-jumps resulting from the interaction between separate magmatic segments.

Abandoned sites of SDR emplacement record the syn-emplacement geometry of SDRs, providing new constraints on models of SDR formation. The stratal geometries observed were compared to predictions from numerical and conceptual models. This analysis indicates that the dips within SDRs result from magmatic-loading. It also suggests that SDRs are emplaced subaerially as the uppermost part of an entirely magmatic crust.

Magnetic lineations were then correlated from within oceanic crust to within SDR-bearing magmatic crust, providing new insights into the lateral variability of spreading dynamics. The along-strike continuity of these lineations suggest that, during South Atlantic opening, magmatic spreading occurred along a continuous axial zone, part of which was submarine and part of which was subaerial. This organised spreading centre was not segmented by transfer zones active earlier in the rifting process. This provides an example of magmatic process overprinting structural segmentation present earlier in the rifting process.

Finally, the processes accommodating asymmetric SDR emplacement were analysed. In contrast to previous studies, here it is demonstrated that three processes control asymmetry: asymmetric magmatic spreading; rift-jumps; and asymmetric continental stretching. The dominance of each of these processes varies both spatially and temporally.

Table of Contents

List of Figures

List of Tables

Abbreviations

CVWs	Conjugate volcanic wedges
Km	Kilometre
LCVS	Laterally Confined Volcanic Succession
LMA	Large Marginal Anomaly
LoCC	Limit of continental crust
LoOC	Limit of oceanic crust
Ma	Millions of years from present
Myr	Millions of years
s	Seconds
SDRs	Seaward dipping reflectors

xxx

Chapter 1 Introduction

1.1 Rationale

Observations from active (e.g. Ebinger and Casey, 2001; Wolfenden et al., 2005; Wright et al., 2006) and ancient (e.g. Hinz, 1981; White and McKenzie, 1989; Skogseid, 2001) rifts indicate that rifting is often accompanied by magmatism. However, the ways in which magmatism influences the rifting process remain ambiguous, standing in contrast to our increasingly refined understanding of rifting in the absence of magmatic activity (e.g. Whitmarsh et al., 2001; Manatschal, 2004; Reston, 2005; Jagoutz et al., 2007; Péron-Pinvidic and Manatschal, 2008; Mohn et al., 2012; Lymer et al., 2019).

From rift-initiation to the onset of seafloor spreading, rifted margins contain a detailed record of the rifting process. They are commonly classified via the amount of magmatic material they contain relative to predictions of rifting above a *normal* asthenosphere, which is considered as undepleted and having a potential temperature of 1300±30°C (e.g. McKenzie and Bickle, 1988; White and McKenzie, 1989). The majority of present-day rifted margins are classified as either ‘magma-rich’ (‘magma-dominated’) or ‘magma-poor’ (‘magma-starved’; Sawyer et al., 2007; Reston, 2009; Doré and Lundin, 2015), although there are also margins containing ‘moderate’ amounts of magmatic material (Larsen et al., 2018).

Magma-rich margins, the focus of this thesis, provide the opportunity to study the interaction between tectonic and magmatic processes during rifting. Globally, these margins are characterised by two features (Figure 1.1): high-velocity lower crust (White et al., 1987; Eldhom, 1991; Eldhom and Grue, 1994; Gladczenko et al., 1997; White et al., 2008); and seaward dipping reflectors (Hinz, 1981; Mutter et al., 1982; Planke and Eldhom, 1994; Planke et al., 2000). The composition and structure of the crust situated vertically between these two features (labelled with question marks in Figure 1.1) is uncertain and subject to much ongoing debate (Pindell et al., 2014; Quirk et al., 2014; McDermott et al., 2015; Clerc et al., 2015; Geoffroy et al., 2015; Nemčok and Rybár., 2017; Paton et al., 2017; Collier et al., 2017; Reuber, 2017; McDermott et al., 2018; Senkans et al., 2018).

High-velocity lower crust (HVLC) was first identified in seismic refraction data (White et al., 1987) and is commonly interpreted as either underplated igneous material (Autin et al., 2016) or highly intruded continental crust (White et al., 2008). Seaward dipping reflectors (SDRs) occur in the uppermost crust and were originally identified in seismic reflection data (Hinz, 1981). Drilling from offshore Norway (Mutter et al., 1982; Planke and Eldhom, 1994), SE Greenland (Hopper et al., 2003), the U.K. (Roberts et al., 1984), and Namibia (Wickens and McLachlan, 1990; Jackson et al., 2000) has shown that SDRs consist of tholeiitic flood basalts interbedded with variable amounts of volcaniclastic and clastic material. SDRs often occur in sequences that are over 100 km wide (margin-perpendicular extent) and up to 2500 km long (margin-parallel extent; e.g. McDermott et al., 2018). Globally, the vertical thickness of SDRs is typically between 2 and 6 km (Morgan and Watts, 2018), although in places thicknesses can exceed 10 km (Stica et al., 2014; Reuber et al., 2016; Reuber, 2017). The dip of the reflectors is generally between 5-15°, with extremes of 30° occasionally being reached (Morgan and Watts, 2018).

Understanding the mechanisms responsible for the emplacement and tilting of SDRs is essential for understanding how lithospheric extension is accommodated in a magma-rich setting. However, the process of SDR emplacement is highly debated, with discussion focusing on the relative roles of faulting (Geoffroy, 2005; Quirk et al., 2014; Clerc et al., 2015; Geoffroy et al., 2015; Nemčok and Rybár., 2017; Senkans et al., 2018; Guan et al., 2019) and magmatic loading (Mutter et al., 1982; Corti et al., 2015; Paton et al., 2017; Buck, 2017; Morgan and Watts, 2018; Tian and Buck, 2019) in producing their characteristic geometry. This debate also has implications for understanding the structure and composition of the sub-SDR crust (Figure 1.1), with different models of SDR emplacement suggesting that it is either stretched continental crust (Clerc et al., 2015; Geoffroy et al., 2015; Nemčok and Rybár., 2017; Senkans et al., 2018) or entirely new magmatic crust (Mutter et al., 1982; Paton et al., 2017).

Given the occurrence of magma-rich margins worldwide (Hinz, 1981; Mutter et al., 1982; Austin and Uchupi, 1982; Oh et al., 1995; Gladczenko et al., 1997; Larsen and Saunders, 1998; Skogseid, 2001; Calvès et al., 2011; Senkans et al., 2018), and the presence of SDRs on each of them, these ambiguities are of

fundamental importance to understanding the rifting process. As such, it is the primary aim of this thesis use data from the South Atlantic to provide new constraints on the processes accommodating the emplacement and tilting of SDRs.

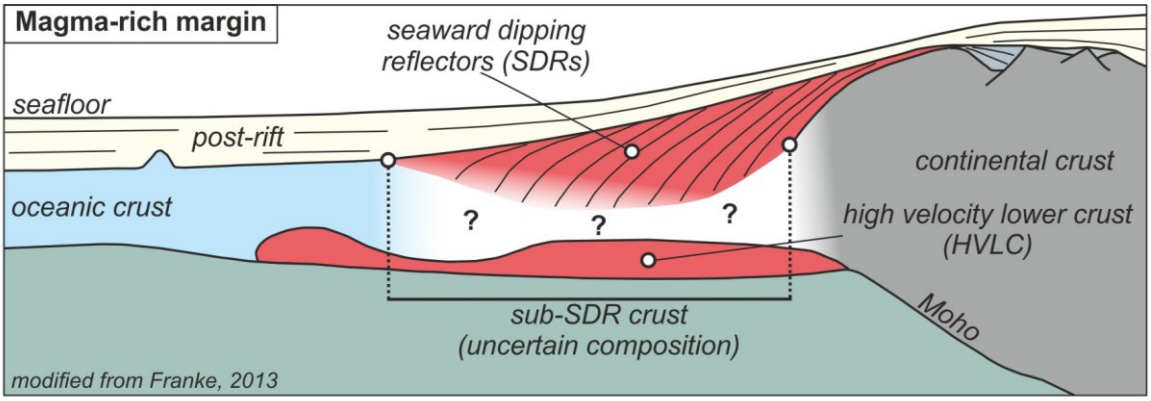

Figure 1.1. The archetypal architecture of a magma-rich margin, namely: seaward dipping reflectors (SDRs); and high velocity lower crust (HVLC). The nature of the crust between the SDRs and the HVLC is disputed and here is annotated with question marks. Modified from Franke, 2013.

1.2 Research questions

In order to provide new insights into SDR emplacement and magma-rich margin evolution, four specific research questions were addressed, each of which is presented below. To answer these questions seismic reflection data from the South Atlantic conjugate magma-rich margins were analysed. The primary study area for this thesis is the Orange Basin, which is located offshore South Africa and Namibia. An overview of this basin and the dataset used to study it area provided in section 1.3.

Research question 1: Do jumps of the rift-axis occur during SDR emplacement?

Models of magma-rich margin evolution indicate that conjugate wedges of SDRs were emplaced either side of a central axial zone (Mutter et al., 1982; Quirk et al., 2014; Paton et al., 2017; Buck, 2017; McDermott et al., 2018; Morgan and Watts, 2018). This axial zone can be referred to as the rift-axis (Figure 1.2). Recent analytical models of SDR emplacement have incorporated jumps of the rift-axis, or 'rift-jumps' (Buck, 2017), to explain two defining features of magma-rich margins (Figure 1.2): firstly, that SDRs often occur in a series of seaward stepping wedges (e.g. Franke et al., 2007; Koopmann et al., 2013; McDermott et al., 2018); and secondly, that conjugate SDR sequences

are often asymmetrical, meaning that one margin will contain a wider sequence of SDRs than the other (Becker et al., 2016).

The occurrence of such rift-jumps has not yet been investigated through detailed seismic interpretation, meaning that the applicability of these numerical models is uncertain. Here two seismic surveys were used to investigate a newly identified volcano-stratigraphic package embedded within the Orange Basin SDRs (Chapter 5). This package is interpreted as an abandoned site of SDR emplacement resulting from a rift-jump. Through analysing its 3D structure, the processes driving this rift-jump were assessed. The results of this detailed study were then used to explain features that are observed across the Orange Basin (Chapter 6).

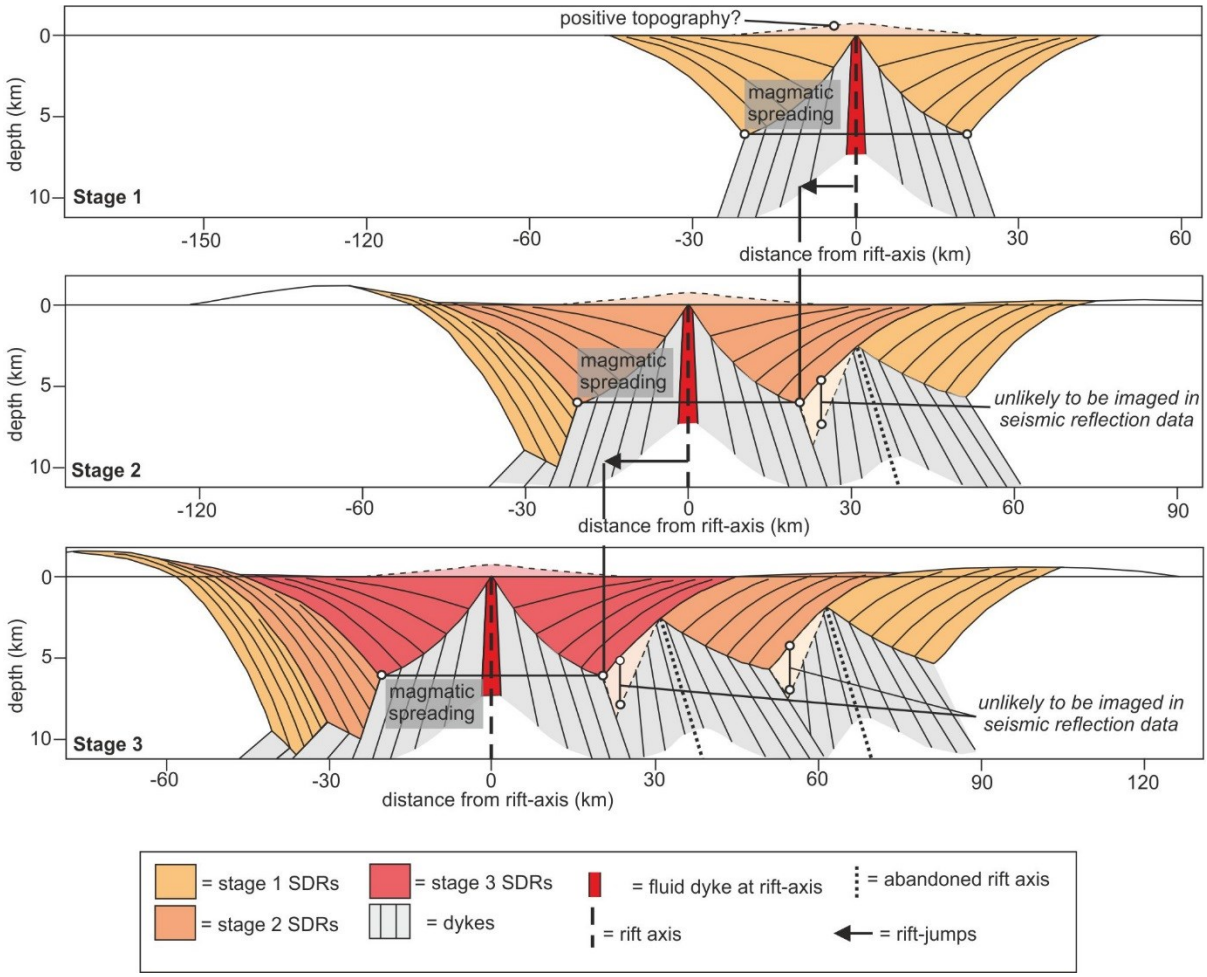

Figure 1.2. Three stage model showing the occurrence of two rift-jumps during SDR emplacement (modified from Buck, 2017). Here, the geometry SDRs results from magmatic loading either side of the rift-axis (Buck, 2017). However rift-jumps could also occur during fault-controlled SDR emplacement (e.g. Quirk et al., 2015).

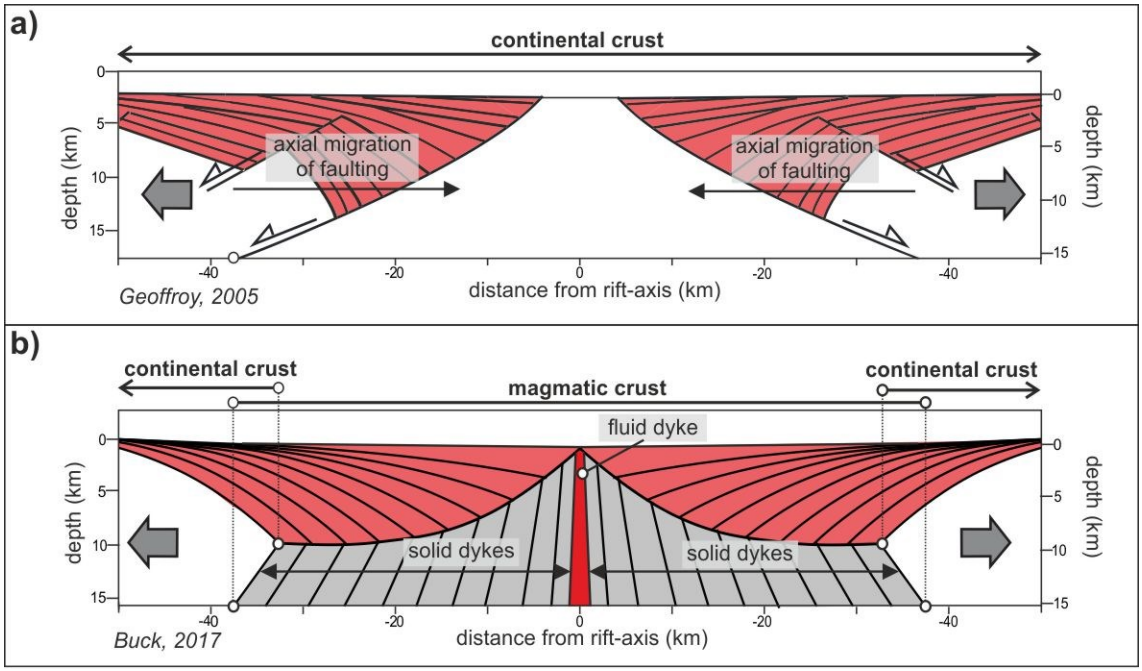

Figure 1.3. Two different models of SDR emplacement. a) fault-controlled SDR emplacement, here the SDRs entirely overlie continental crust (modified from Geoffroy, 2005). b) magmatic-loading model of SDR emplacement, here the SDRs are emplaced as the uppermost part of thickened oceanic crust (modified from Buck, 2017).

Research question 2: What are the roles of faulting and loading in generating the dips displayed by SDRs?

Models of SDR emplacement can be separated into two categories: those where SDRs are considered as fault-controlled features (Figure 1.3a); and those where SDRs are considered as loading-controlled features (Figure 1.3b). These two sets of models assume fundamentally different extension mechanisms and crustal compositions. In the former set of models, it is assumed that SDRs were emplaced during continental stretching and that extension was accommodated primarily by faulting (Geoffroy, 2005; Quirk et al., 2014; Geoffroy et al., 2015; Clerc et al., 2015; Nemčok and Rybár., 2017; Senkans et al., 2018; Guan et al., 2019). In the latter set of models, SDRs are interpreted to have formed as part of an entirely magmatic crust (Mutter et al., 1982; Eldhom and Grue, 1994; Gladczenko et al., 1998; Hopper et al., 2003; McDermott et al., 2015; Paton et al., 2017; Collier et al., 2017) within which extension was accommodated by axial igneous accretion (Mutter et al., 1982; Buck, 2017; Paton et al., 2017; Morgan and Watts, 2018; McDermott et al., 2018; Tian and Buck, 2019). Hence being able to distinguish between these

models is vital for understanding the structure and evolution of magma-rich margins (Tugend et al., 2018).

Here, new insights into this debate were gained through studying a number of abandoned sites of SDR emplacement. These features provide constraints on the syn-emplacement geometry of SDRs; something that is lacking in fully developed SDR sequences. In order to answer the question posed above, observations and interpretations from these features were compared to the predictions of fault-controlled and loading-controlled models of SDR emplacement (Chapter 6).

Research question 3: What were the spatial and temporal relationships between subaerial and submarine magmatic spreading during South Atlantic opening?

In the magma-rich portion of the South Atlantic there is a growing consensus that the outermost SDRs were emplaced as the uppermost part of an entirely magmatic crust (Figure 1.4a; Gladczenko et al., 1998; Bauer et al., 2000; McDermott et al., 2015; Paton et al., 2016; Collier et al., 2017; McDermott et al., 2018). This *magmatic crust* differs from oceanic crust in two ways: firstly, it has thicknesses exceeding those typical of oceanic crust (White et al., 1992); secondly its uppermost layer consists not of pillow-lavas but of subaerially erupted flood basalts (SDRs; Paton et al., 2017; Collier et al., 2017; McDermott et al., 2018). Following the emplacement of this SDR-bearing magmatic crust the spreading axis subsided below sea-level (Figure 1.4b), leading to the emplacement of oceanic crust (Mutter et al., 1982; Planke et al., 2000; McDermott et al., 2015; Paton et al., 2017; Collier et al., 2017; McDermott et al., 2018). This spreading-axis subsidence is well documented in two-dimensions (Mutter et al., 1982; Planke et al., 2000; Hopper et al., 2003; Paton et al., 2017) but its three-dimensionality is less well understood.

The South Atlantic opened from south to north (Jackson et al., 2000; Moulin et al., 2010; Heine et al., 2013; Collier et al., 2017), meaning that both spreading styles were active coevally but along different parts of the evolving basin. In Chapter 7, new constrains are provided on the spatial and temporal relationship between subaerial and submarine spreading. This was accomplished by coupling the interpretation of seismic reflection data with that of a total magnetic anomaly grid. Linear magnetic anomalies, representative of magmatic spreading, were correlated from within oceanic crust to within magmatic crust.

This provides new insights into the lateral variability of spreading dynamics during ocean opening.

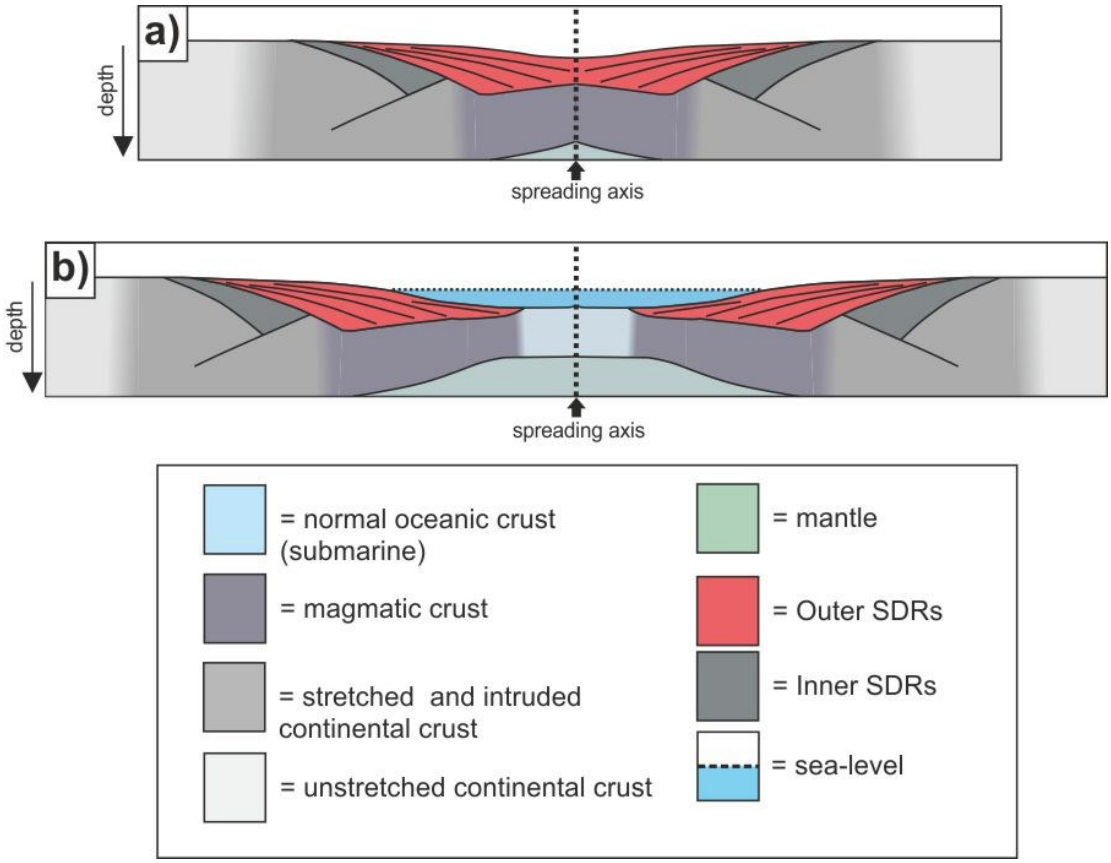

Figure 1.4. Subsidence of a magmatic spreading system during magma-rich margin formation. a) subaerial SDR emplacement as the uppermost part of an entirely magmatic crust. b) submarine oceanic crust generation along the same spreading axis that was present in a).

Research question 4: What are the mechanisms and causes of asymmetric SDR emplacement?

Conjugate SDR sequences worldwide are asymmetric (Hopper et al., 2003; Blaich et al., 2009; Misra et al., 2015; Becker et al., 2016; Horni et al., 2017; Buck, 2017), meaning that one margin contains a wider and/or thicker SDR sequence than the other. This is problematic as the majority of models explaining SDR emplacement consider a symmetrical system (Mutter et al., 1982; Quirk et al., 2014; Geoffroy et al., 2015; Paton et al., 2017; Buck, 2017; Morgan and Watts, 2018; McDermott et al., 2018). Furthermore, the models that do address asymmetry have failed to reach a consensus, with three mechanisms being proposed (Figure 1.5): asymmetrical magmatic spreading (Figure 1.5a; Hopper et al., 2003); rift-jumps resulting in the transfer of material

from one side of the basin to the other (Figure 1.5b; Buck, 2017); and, different emplacement mechanisms operating on either side of the basin (Figure 1.5c; Becker et al., 2016).

Each of these models makes predictions concerning the geometry, thickness and width of the conjugate SDR belts. Here, three conjugate pairs of seismic lines from the South Africa-Argentina and Namibia-Uruguay conjugate margins were selected to test these models (Chapter 8). The model predictions were compared, qualitatively and quantitatively, with observations and interpretations from seismic data, thus constraining the mechanisms and causes of asymmetric SDR emplacement.

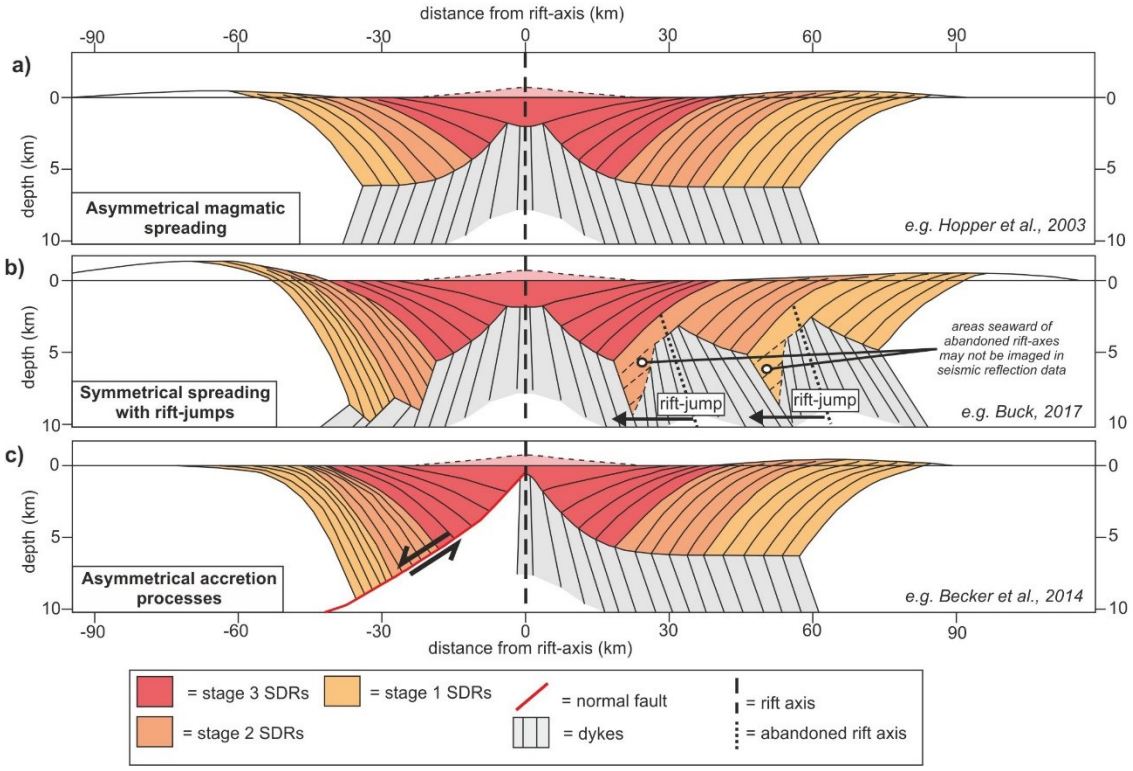

Figure 1.5. Three models of asymmetric SDR emplacement: a) asymmetric magmatic spreading (modified from Hopper et al., 2003). b) rift-jumps resulting in the transfer of material from one side of the rift to the other (modified from Buck, 2017). c) different emplacement mechanisms operating either sides of the rift-axis (modified from Becker et al., 2014). In c) SDRs are fault-controlled (Fig 1.4a) on the left-hand-side of the rift-axis and loading controlled (Fig. 1.4b) on the right-hand-side of the rift-axis.

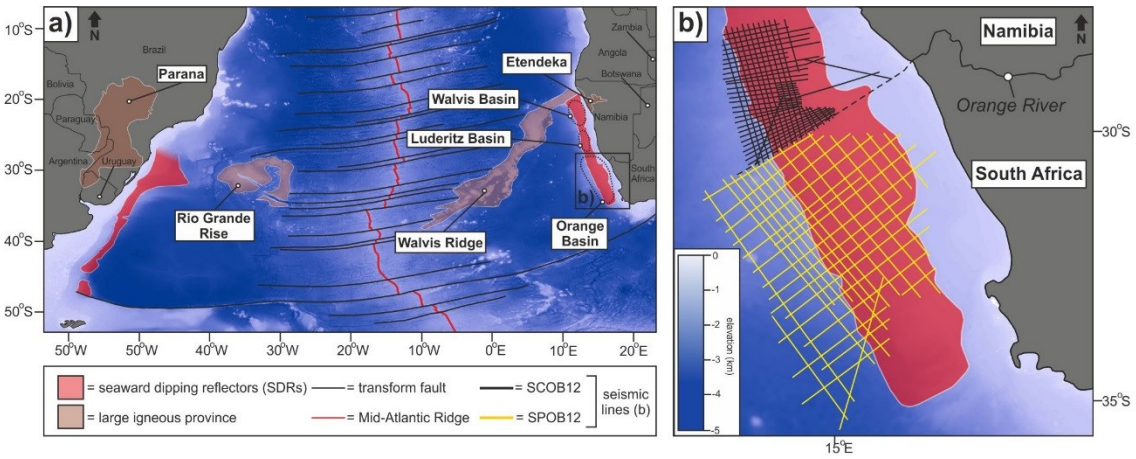

Figure 1.6. a) regional map of the South Atlantic with several geological features labelled: seaward dipping reflectors; large igneous provinces; the Mid-Atlantic Ridge; and prominent transform faults (see key for colours). On both the South American and African margins, the presence of seaward dipping reflectors demarks the location of a magma-rich margin. On the African margin, the sedimentary basins south of the Walvis Ridge are annotated. b) map of the study area showing the location of seismic lines from two surveys, one of which is located offshore Namibia and the other offshore South Africa. The location of b) is shown as an inset on a).

1.3 Study area and data

The primary study area is the Orange Basin, which is located offshore South Africa and Namibia. It is the southernmost sedimentary basin along the 1800 km long magma-rich portion of the African Atlantic margin (Figure 1.6a). This margin, alongside its conjugate offshore South America (Figure 1.1a), has been instrumental in developing our understanding of the architecture and evolution of magma-rich margins (Hinz, 1981; Austin and Uchupi, 1982; Gladczenko et al., 1997; Gladczenko et al., 1998; Bauer et al., 2000; Franke et al., 2007; Koopmann et al., 2013; Stica et al., 2014; McDermott et al., 2015; Clerc et al., 2015; Geoffroy et al., 2015; Paton et al., 2017; McDermott et al., 2018).

This thesis is based primarily on the interpretation of two seismic reflection surveys from the Orange Basin (Figure 1.6b). One of these surveys, SCOB12, is located over the Namibian side of the basin (Figure 1.6b), and the other, SPOB12, is located over the South African side of the basin (Figure 1.6b). The South African dataset has a total length of 10,460 km, whilst the Namibian dataset has a length of 8,156 km. Both datasets were acquired by Spectrum Geo in 2012 and utilised long-recording times (10 s) and long-streamers (10.05 km) to image rifted-margin structure. Both surveys were also pre-stack time

migrated (PSTM) and pre-stack depth migrated (PSDM). Together, they provide the opportunity to study the along-strike variability of a magma-rich margin at an unprecedented resolution. The datasets are fully described in Chapter 4.

In addition to these two newly acquired datasets, two additional vintage surveys were used to facilitate along-strike correlations and produce 3D structure maps (Chapter 5, Chapter 6). As these surveys are only used in specific parts of this thesis, they will be introduced accordingly.

In areas with limited seismic coverage, a regional total magnetic anomaly grid was used to correlate features between 2D seismic lines. It was also used to map magnetic chrons identified in earlier studies (Koopmann et al., 2014b; Collier et al., 2017).

Chapter 8 addresses margin asymmetry in the South Atlantic and utilises three 2D seismic reflection lines over the South American margin. Again, the dataset containing these lines will be described in the relevant part of this thesis.

1.4 Thesis outline

In this thesis, Chapters 1-4 provide geological and methodological background, Chapters 5-8 focus on results and analysis, and Chapter 9 summarises the conclusions from earlier chapters. Each of the results-based chapters (5-8) are relatively self-contained and include: a brief summary of the relevant literature; a description of the specific methodology; and, a contextualised discussion of the results. A brief summary of each chapter is given below.

Chapter 2 provides an overview of the architecture and evolution of magma-rich margins. The first part of the chapter focuses on the causes of magmatism during lithospheric extension. The second part then addresses our current understanding of SDR emplacement.

Chapter 3 summarises the tectono-magmatic evolution of the South Atlantic magma-rich margins. It also describes the architecture of the Orange Basin and juxtaposes previous interpretations of stratal geometry and crustal type.

Chapter 4 describes the data and methods used throughout this thesis. It introduces methods of seismic stratigraphy and demonstrates how they have been applied to the dataset.

Chapter 5 is modified from a publication in *Earth and Planetary Science Letters* (Norcliffe et al., 2018) and addresses the first research question presented above: *Do jumps of the rift-axis occur during SDR emplacement?* Within this chapter, data from a small part of the South African Orange Basin are used to characterise a newly identified volcano-stratigraphic package. Through the interpretation of stratal geometry and seismic velocities, it is demonstrated that this package results from a rift-jump during SDR emplacement. Through mapping its 3D structure, the processes driving intra-SDR emplacement rift-jumps are determined.

Chapter 6 addresses the second research question posed above (section 1.2): *What are the roles of faulting and loading in generating the dips displayed by SDRs?* To answer this question, the findings from the previous chapter are used to identify five separate abandoned sites of SDR emplacement within the Orange Basin. Each of these features records the syn-emplacement geometry of SDRs, which is not recorded in fully developed SDR sequences. These stratal geometries are compared with the predictions made by conceptual and numerical models of SDR emplacement. It is demonstrated that during SDR emplacement large amounts of axial subsidence is generated without faulting. This supports magmatic-loading models of SDR emplacement and suggests that SDRs constitute the uppermost part of an entirely magmatic crust.

Chapter 7 focuses on the third research question posed in section 1.2: What were the spatial and temporal relationships between subaerial and submarine magmatic spreading during South Atlantic opening? This chapter uses findings from Chapter 6 to map the distribution of different crustal types across the Orange Basin. This crustal framework is then used to constrain the interpretation of linear magnetic anomalies. It is shown that magnetic lineations within the oceanic crust can be correlated within the SDRs. These results are then used to investiage the along-strike variability of spreading-dynamics during South Atlantic opening.

Chapter 8 addresses the fourth question posed in section 1.2: *What are the mechanisms and causes of asymmetrical SDR emplacement?* Here, data from the conjugate magma-rich margins of the South Atlantic are uses to test, qualitatively and quantitatively, different models of asymmetric SDR

emplacement. In particular this chapter focuses on the role of rift-jumps in producing the asymmetry observed in the present day.

Chapter 9 provides a summary of how the central four research questions (section 1.2) have been addressed. Future directions in rift-related research are considered also considered

Chapter 2 The architecture and evolution of magma-rich rifted margins

2.1 Introduction

This chapter evaluates our current understanding of magmatism during rifting. It covers both the processes responsible for magmatism and the consequences magmatism may have on an evolving rift basin. A significant portion of this chapter is also given to describing the architecture of SDRs (section 2.3.1) and discussing different models for their evolution (section 2.3.2). The regional setting for the study will be outlined in Chapter 3.

2.2 The occurrence of magmatism during rifting

Here, the fundamentals of melt-production during rifting are revisited. The models presented in this section act as a benchmark for the more recent observations and models described in subsequent sections (sections 2.2.3) and Chapters (chapter 8).

2.2.1 Reference model for melt-generation during rifting

Classic models of melt-generation during lithospheric stretching (Figure 2.1a) make several assumptions: firstly, that the lithosphere thins via pure shear; secondly, that the temperature at the base of the plate remains constant; thirdly, that the asthenosphere is isothermal; and fourthly, that in order to maintain isostatic equilibrium the asthenosphere rises passively during lithospheric thinning (McKenzie, 1978; McKenzie, 1984; McKenzie and Bickle, 1988; White and McKenzie, 1989).

Under these conditions, the lithospheric stretching factor, β, can be used to calculate the amount of lithospheric thinning (Chappell and Kusznir, 2008). As β increases the asthenosphere decompresses, a consequence of which can eventually be adiabatic partial melting (Figure 2.1b). Following melt generation, it is assumed that all of the melt is extracted from matrix and moves vertically upwards, where it is emplaced intrusively (within the lithosphere) or extrusively (at the surface; McKenzie and Bickle, 1988; White and McKenzie, 1989). If we assume a *normal* asthenosphere, then initial melt generation occurs where β is

between 2.2-3.8 (Figure 2.1b). A *normal* asthenosphere is considered as undepleted and as having a potential temperature of 1300±30 °C (White and McKenzie, 1989; Chappell and Kusznir, 2008). In this situation, the amount of melt generated will then increase with increasing β (Figure 2.1b). Given that rifted margins worldwide record β factors in excess of 2.2-3.8, it follows that they should all contain magmatic additions.

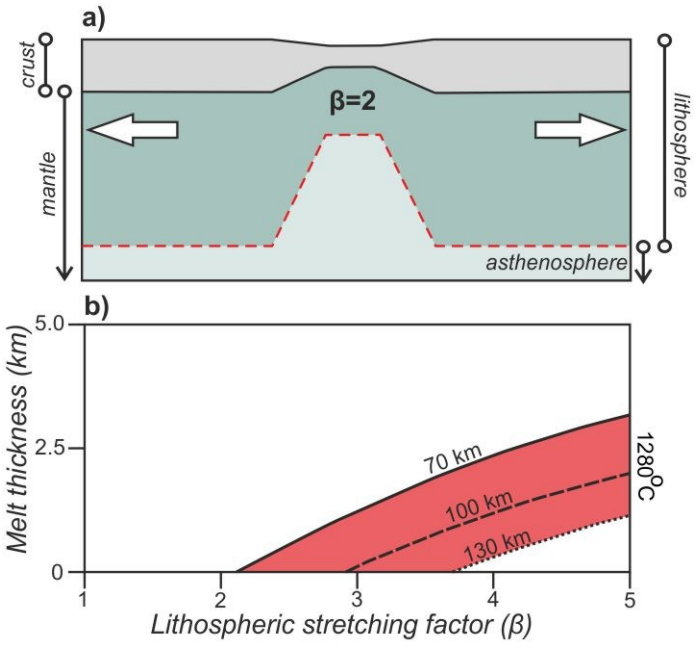

Figure 2.1. Models of lithospheric stretching and melt production. a) Schematic diagram demonstrating the pure shear stretching of the continental lithosphere, (modified from McKenzie, 1978; and Allen and Allen, 2013). b) Melt thickness during lithospheric extension, as a function of β (McKenzie and Bickle, 1988). Curves are shown for three initial lithospheric thicknesses (70 km, 100 km, and 130 km). The potential temperature of the asthenosphere is 1280 °C, which is considered *normal*. Graph is modified from Chappell and Kusznir (2008).

2.2.2 Global observations of rift-related magmatism

The model presented above (section 2.2.1) predicts that magmatic material should be common in highly stretched rift basins, and ubiquitous in places where rifting culminated in continental breakup (McKenzie and Bickle, 1988; White and McKenzie, 1989). This model can be tested against observations from rift-systems worldwide.

The process of rifting can be studied in three settings: active rift basins (e.g. Ebinger and Casey, 2001; Corti, 2009; Keir et al., 2013); present-day rifted margins and failed-rifts (e.g. Reston, 2009; Péron-Pinvidic et al., 2013; Franke,

2013); and fossil rift systems (e.g. Manatschal, 2004; Mohn et al., 2012; Abdelmalak et al., 2015). Rifted margins define the transition from unstretched continental crust (β = 0) to oceanic crust (β ≈ ∞). Hence they provide an ideal setting to test the model presented above (section 2.2.1), where the amount of melt is a result of β (Figure 2.1b). Data from rifted-margins indicate that the amount of magmatic material can vary greatly both between (e.g. Sawyer et al., 2007; Franke, 2013) and along (Shillington et al., 2009; Koopmann et al., 2013; Gouiza and Paton, 2019) margins. This indicates that factors other than β are influencing magma production during rifting (White and McKenzie, 1989; Nielsen and Hopper, 2002; Armitage et al., 2010; Koopmann et al., 2014a; Taposeea et al., 2016).

The interpretation of present-day rifted margins and fossil rift-systems worldwide, has led to them being classified as either ‘magma-rich’ (also known as ‘magma-dominated’) or ‘magma-poor’ (also known as ‘magma-starved’; Sawyer et al., 2007; Péron-Pinvidic and Manatschal, 2008; Reston, 2009). This classification can also be extended to active rifts (Ebinger and Casey, 2001; Wright et al., 2006). These terms, magma-rich and magma-poor, refer to the amount of magmatic material observed relative to that predicted by lithospheric extension above a *normal* asthenosphere (White and McKenzie, 1989). Hence it appears that rifting is often accompanied by either more or less magmatism than predicted by base-case scenario presented above (section 2.2.1).

There are several well-constrained examples of magma-rich and magma-poor margins, namely the NE Atlantic magma-rich margin (e.g. Mutter et al., 1982; Planke and Eldhom, 1994; Eldhom and Grue, 1994; Skogseid, 2000; White et al., 2008) and the Iberian magma-poor margin (Boillot et al., 1980; Whitmarsh et al., 2001; Reston, 2005; Pérez-Gussinyé et al., 2008). In these cases both margin-architecture and the distribution of magmatic material are well-constrained by seismic reflection, seismic refraction, borehole and potential fields data. Elsewhere, rifted-margins are classified by their architecture as compared to these well-defined examples from the North Atlantic. These archetypal margin geometries are described in detail below (sections 2.2.2.1 and 2.2.2.2).

Prior to describing the characteristics of these end-members, it is worth noting that the data available over rifted margins do not adequately resolve moderate

amounts of magmatic material (Reston, 2009). Hence some margins currently classified as magma-poor may actually contain more magmatic material than is appreciated. For example, the architecture of the South China Sea margins are indicative of a magma-poor environment, however recent drilling indicates that rifting was accompanied by a *normal* (White and McKenzie, 1989) amount of magmatic material (Larsen et al., 2018)

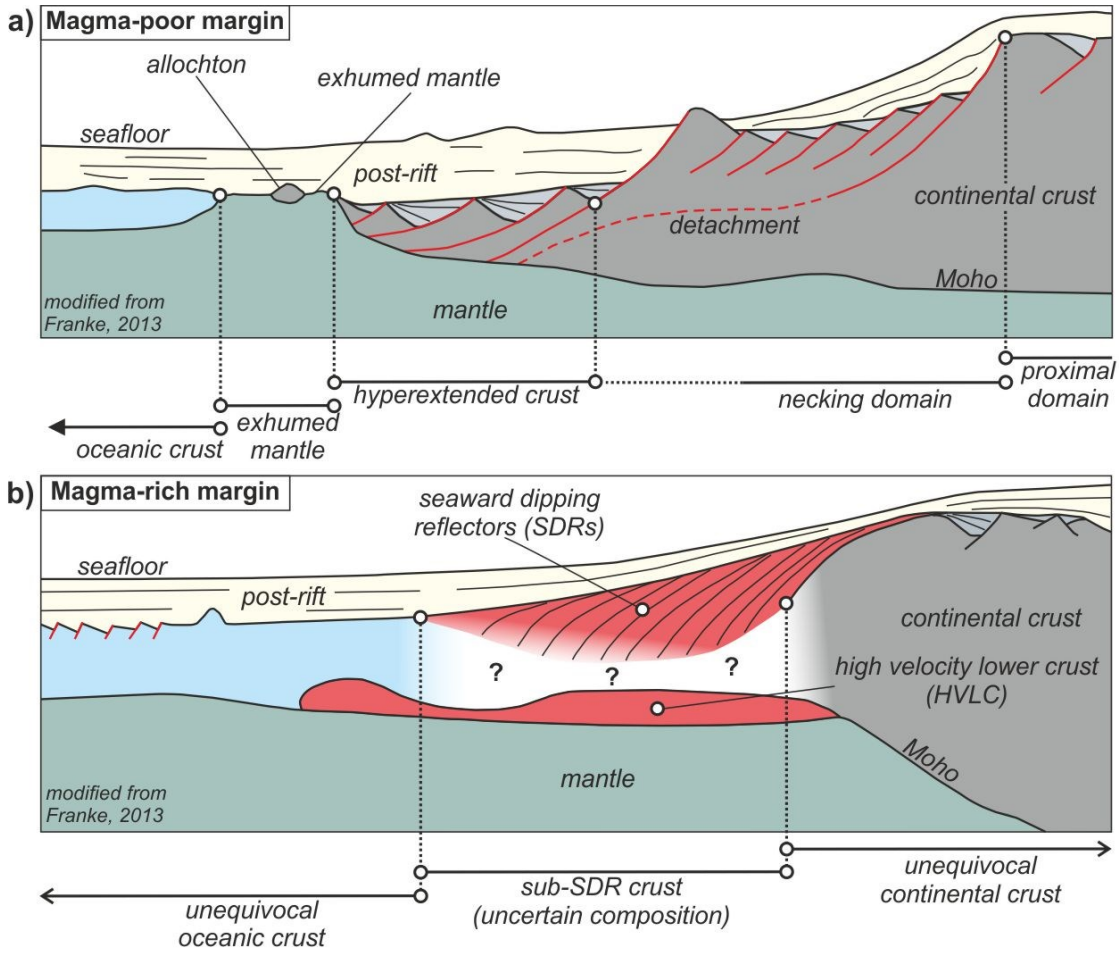

Figure 2.2. Archetypal architecture of rifted margins, modified from Franke (2013). a) magma-poor margin characterised by seaward dipping detachment faults, hyperextended continental crust, exhumed mantle, and oceanic crust. b) magma-rich margin characterised by the occurrence of seaward dipping reflectors (SDRs) and high-velocity lower crust (HVLC). The composition of the sub-SDR crust is uncertain and is annotated with question marks.

2.2.2.1 Magma-poor margins

Magma-poor margins (Figure 2.2a) consist of a series of seaward stepping domains, each of which contains distinct structural features (Péron-Pinvidic et al., 2013; Franke, 2013; Tugend et al., 2015; Doré and Lundin, 2015). As the process of rifting progressives, strain localises towards the rift-axis resulting a

narrowing of the zone affected by deformation (Whitmarsh et al., 2001; Péron-Pinvidic et al., 2013; Naliboff et al., 2017). A consequence of this strain localisation is that each of the seaward-stepping domains observed in the present-day records a distinct phase of the rifting process (Péron-Pinvidic et al., 2013).

The landward-most part of a magma-poor margin contains isolated half-grabens that overlie relatively unthinned crust (Péron-Pinvidic et al., 2013; Franke, 2013; Tugend et al., 2015). The faults controlling these half-grabens often overlie basement heterogeneities (e.g. Osmundsen et al., 2002), leading to the interpretation that structural inheritance controlled early basin evolution (Manatschal et al., 2015). This innermost part of a rifted margin is often named the *proximal domain* (Péron-Pinvidic et al., 2013).

Moving seawards, large seaward dipping detachment faults (Figure 2.2a) offset the top-basement surface (e.g. Osmundsen and Ebbing, 2008; Osmundsen and Péron-Pinvidic, 2018). These faults overlie a zone of major crustal thinning (Whitmarsh et al., 2001; Osmundsen and Ebbing, 2008; Péron-Pinvidic and Manatschal, 2008; Mohn et al., 2012), leading to this area often being named the *necking domain/zone* (Péron-Pinvidic and Manatschal, 2008; Péron-Pinvidic et al., 2013).

Seawards of the *necking domain*, the seaward-dipping detachment faults cross-cut the entire crust (Figure 2.2a). This signifies that the entire crust was brittle, or *hyperextended*, during their formation (Reston, 2005; Péron-Pinvidic et al., 2013; Tugend et al., 2015). Clear examples of hyperextended crust have been documented in both geophysical data (e.g. Reston, 2005; Reston, 2009; Lymer et al., 2019) and in outcrop (Manatschal, 2004).

A zone of exhumed and serpentinised mantle may be present seawards of this hyperextended crust (e.g. Boillot et al., 1980; Boillot et al., 1987; Manatschal, 2004). The occurrence of serpentinite signifies that the mantle was exposed at the seafloor during extension (Boillot et al., 1987). In seismic reflection and refraction data, the occurrence of exhumed mantle is evident from the merging of the top-basement and Moho at the edge of the hyperextended crust (e.g. Gillard et al., 2015). Recent studies have demonstrated that the exhumed mantle itself may contain several generations of detachment faults (Gillard et al., 2015; Gillard et al., 2016). Magmatic additions may be also be present

within this zone, where they result from pulses of magmatism that did not culminate in magmatic spreading (Jagoutz et al., 2007; Gillard et al., 2016; Gillard et al., 2017).

Oceanic crust is present seawards of the exhumed mantle (Figure 2.2a), although in these settings the earliest oceanic crust may be 'magma-starved' (Jagoutz et al., 2007). In these situations, the presence of oceanic crust is defined by the occurrence of mid-ocean ridge basalt (MORB) magmatism (Jagoutz et al., 2007).

2.2.2.2 Magma-rich margins

Magma-rich margins (Figure 2.2b) worldwide are characterised by two features (Menzies and Klemperer, 2002; Franke, 2013): high velocity lower crust (HVLC), and seaward dipping reflectors (SDRs). HVLS is defined by P-wave velocities of ≥7.2 km/s (White et al., 2008) and is identifiable in seismic refraction data. Integrated studies of seismic refraction and gravimetric data indicate that these high-velocities correspond to high-densities (e.g. Hirsch et al., 2009; Maystrenko et al., 2013). Accordingly these features are sometimes referred to as high-density lower crustal bodies (Autin et al., 2016). In seismic reflection data, reflections have been recorded from the boundaries of the HVLC (Gernigon et al., 2004; Abdelmalak et al., 2017) and from within the crustal body itself (White et al., 2008; Quirk et al., 2014; Geoffroy et al., 2015; Clerc et al., 2015). Despite its widespread occurrence, the nature of HVLC remains disputed (Hopper et al., 2003; Gernigon et al., 2004; White et al., 2008; Abdelmalak et al., 2017). Its velocities are typical of mafic igneous material generated via the melting of a hotter-than-normal asthenosphere (White et al., 2008). However, studies diverge on whether HVLC consists of entirely new magmatic material, (an underplate; Eldhom and Grue, 1994; Hopper et al., 2003) or highly intruded continental crust (White et al., 2008).

Seaward dipping reflectors (SDRs) are the second diagnostic feature of magma-rich margins (Figure 2.2b). Drilling from the offshore Norway (Mutter et al., 1982; Planke and Eldhom, 1994), the U.K. (Roberts et al., 1984), SE Greenland (Larsen and Saunders, 1998), and Namibia (Wickens and McLachlan, 1990; Jackson et al., 2000) demonstrate that SDRs consist of basic volcanics interbedded with variable amounts of clastic material. SDRs partially

overlie the HVLC and are located between unequivocal continental crust and unequivocal oceanic crust (Figure 2.2b). They are generally considered as the extrusive counterpart to the intrusive lower crustal bodies (e.g. Eldhom and Grue, 1994; Gladczenko et al., 1998; White et al., 2008). The processes responsible for the seaward tilting of SDRs remain contentious (Mutter et al., 1982; Pindell et al., 2014; Quirk et al., 2014; Clerc et al., 2015; Geoffroy et al., 2015; Paton et al., 2017; Buck, 2017; McDermott et al., 2018; Morgan and Watts, 2018). Given that this debate is the main focus of this thesis, a detailed description of our current understanding of SDR emplacement is provided in section 2.3.

The nature of the crust located vertically between the SDRs and the HVLC is interpreted either as intruded continental crust (White et al., 2008; Clerc et al., 2015; Geoffroy et al., 2015) or as entirely new *magmatic crust* (Mutter et al., 1982; Hopper et al., 2003; Paton et al., 2017). Again, debates concerning this issue are described in detail in subsequent sections (sections 2.3.2).

Immediately seawards of the SDRs is *normal* oceanic crust (Figure 2.2b), which is identifiable by its seismic character (McDermott et al., 2015; Paton et al., 2017) and velocity structure (White et al., 2008; Hirsch et al., 2009; Taposeea et al., 2016). It also often contains alternating magnetic anomalies, indicating the occurrence of organised seafloor spreading (Koopmann et al., 2014b; Collier et al., 2017). The oceanic crust located adjacent to the SDRs is typically thicker (Franke, 2013; Taposeea et al., 2016) than the global average of 7.1±0.8 km (White et al., 1992). However, with increasing distance seaward, the crustal thickness decreases towards the global average (Franke, 2013). Accompanying this seaward decrease in thickness, there is often a change in the morphology (Elliott and Parson, 2008; McDermott et al., 2015; Geissler et al., 2017). Adjacent to the SDRs, the top of the oceanic crust is relatively smooth and flat-lying (Figure 2.2b). However, with distance seawards this surface becomes increasingly disrupted by seaward dipping normal faults (Figure 2.2b), giving a classic ‘abyssal hills’ geometry (Elliott and Parson, 2008; McDermott et al., 2015).

Landwards of the SDRs is unequivocal continental crust, which shows marked variability between different rifted margins. Along the Norwegian margin, the SDRs sit outboard of a wide zone of stretched continental crust that is often

over 200 km wide (e.g. Skogseid, 2000; Osmundsen and Ebbing, 2008; Gernigon et al., 2015). This region formed in response to multiple periods of magma-poor rifting, and is possibly floored by hyperextended continental crust (Osmundsen and Ebbing, 2008; Gernigon et al., 2015). This contrasts examples from offshore Namibia and Brazil (Stica et al., 2014; Clerc et al., 2015; Geoffroy et al., 2015; Reuber, 2017; McDermott et al., 2018), where the crust inboard of the SDRs is only moderately thinned (as is the case in Figure 2.2b).

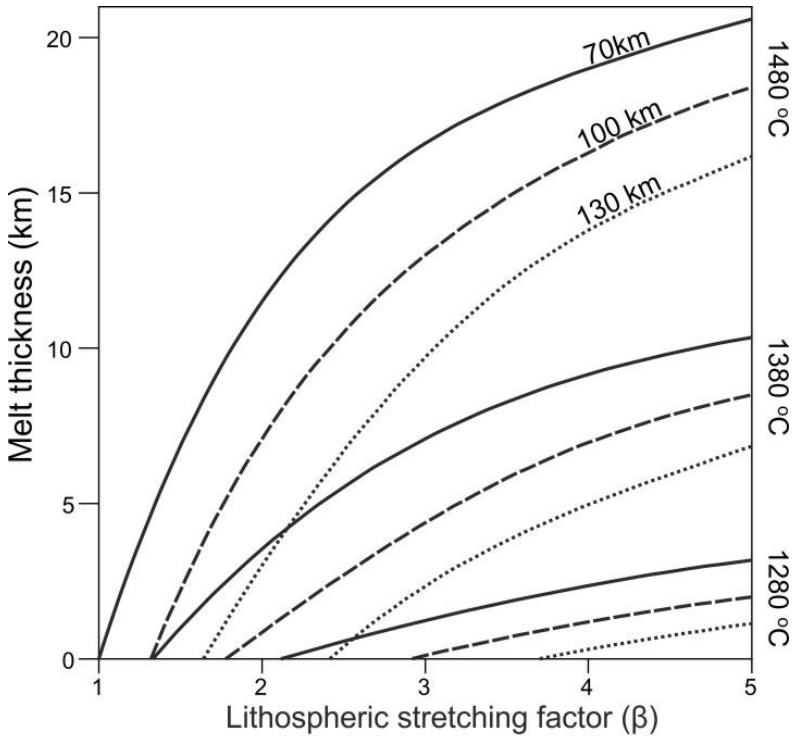

Figure 2.3. The generation of melt during lithospheric stretching (White and McKenzie, 1989), redrawn from Chappell and Kusznir, 2011. Three asthenospheric potential temperatures are shown, 1280 °C (ambient), 1380 °C, and 1480 °C. For each of these potential temperatures, the initial thickness of the lithosphere is also modified (curves show starting thicknesses of 70 km, 100, km, and 130 km). It is demonstrated that, for the same value of β, increases in temperature result in a greater melt thickness.

2.2.3 Causes of variable amounts of magmatism during rifting

The variable amounts of magmatic material contained on margins worldwide suggest that melt volumes are not solely controlled by the amount of lithospheric extension (section 2.1.1). Deficits in magmatism during rifting can be attributed to depth-dependent stretching (Minshull et al., 2008), slow extension-rates (Pérez-Gussinyé et al., 2006), a depleted or sub-depleted

asthenosphere (Pérez-Gussinyé et al., 2008; Gouiza and Paton, 2019), and/or cool asthenospheric temperatures (Reston and Morgan, 2004). Meanwhile, normal amounts of magmatism may result from fast extension above an already thin lithosphere (Larsen et al., 2018). Magma-rich margins are commonly attributed to a hotter-than-normal asthenosphere (White and McKenzie, 1989; Nielsen and Hopper, 2002; Armitage and Collier, 2017) alongside several other factors (Nielsen et al., 2002; Armitage et al., 2010; Koopmann, et al., 2014a; Taposeea et al., 2016). Given that magma-rich margins are the focus of this thesis, each of the factors influencing excessive melt volumes are described below.

2.2.3.1 Causes of excessive amounts of magmatic activity during rifting

During lithospheric extension, excessive amounts of magmatism can be attributed to the presence of an underlying thermal anomaly (White and McKenzie, 1989). Such anomalies occur where mantle plumes impinge on the base of the lithosphere (White and McKenzie, 1989). Theoretical models suggest that, for any one value of β, a greater melt thickness will be produced by an increase of asthenospheric potential temperature above ambient (Figure 2.3).

Magma-rich margins often correlate, spatially and temporally (White and McKenzie, 1989), with the occurrence of mantle plumes and onshore large igneous provinces (LIPs): the magma-rich margins of the North Atlantic are associated with the Iceland Plume and the North Atlantic Igneous Province (NAIP) LIP (White et al., 1987; Skogseid, 2000; Nielsen et al., 2002; Smallwood and White, 2012); the magma-rich margins of the South Atlantic are associated with the Tristan plume and the Parána-Etendeka LIP (Gladczenko et al., 1997; Taposeea et al., 2016; Collier et al., 2017); the GOP rift in the NE Indian Ocean is associated with the Reunion plume and the Deccan LIP (Collier et al., 2009; Armitage et al., 2010; Corfield et al., 2010; Misra et al., 2015); and, the less well studied magma-rich margins of the Central Atlantic are associated with the Central Atlantic Magmatic Province (CAMP) LIP. Additionally, the active magmatic rifts of northern Ethiopia are also associated with a hotter-than-normal asthenosphere (Armitage and Collier, 2017). These spatio-temporal relationships support a causal link between magma-rich rifting and mantle plumes (White and McKenzie, 1989).

However, at a finer scale, complexities arise with a simple relationship between rifting and asthenospheric temperature (Nielsen et al., 2002; Armitage et al., 2010; Franke, 2013; Koopmann et al., 2014a). One such complication is related to mantle dynamics during rifting. The model of White and McKenzie (1989) assumes a *passive* asthenosphere. That is, an asthenosphere that passively rises and melts in response to lithospheric thinning. It has been suggested that the active upwelling of asthenospheric material, at rate faster than plate separation, may generate excessive amounts of melt without excess temperatures (Mutter et al., 1988). In these models, active upwelling takes the form of small-scale convection that is triggered by either the rifting process (Mutter et al., 1988; van Wijk et al., 2001) or changes in the thickness of the pre-rift lithosphere (King and Anderson, 1998). Dynamic models of melt generation demonstrate that small-scale convection does indeed increase the amount of asthenospheric melting (Nielsen and Hopper, 2002). However, they also demonstrate that this convection alone does not produce the amounts of melt typical of a magma-rich margin and instead emphasise the need for anomalously high temperatures in the asthenosphere (Nielsen and Hopper, 2002).

A second complication of the model of White and McKenzie (1989) is related to the amount of magmatic material generated through time. Interpretations of seismic refraction and reflection data indicate that magma-rich margins record a transient pulse of magmatic activity (Mutter et al., 1982; Eldhom and Grue, 1994; Hopper et al., 2003; Paton et al., 2017; McDermott et al., 2018). This interpretation is based primarily on two observations: that SDRs and HVLC record excess amounts of asthenospheric melting, yet they transition seawards into oceanic crust with ‘normal’ thickness. This relationship indicates that the magma-budget decreased through time (Mutter et al., 1982; Eldhom and Grue, 1994; Hopper et al., 2003). The transient pulse of excess magmatism has been reproduced through modelling an exhaustible ‘hot layer’ in the uppermost asthenosphere (Keen and Boutilier, 2000; Nielsen and Hopper, 2002; Armitage et al., 2010; Taposeea et al., 2016; Armitage and Collier, 2017), a scenario consistent with rifts that overlie a laterally extensive plume head (Hopper et al., 2003).

Several studies have also elucidated the relationship between pre-existing structures in the lithosphere and thermal anomalies (Nielsen and Hopper, 2002; Armitage et al., 2010; Taposeea et al., 2016). In the North Atlantic, the Iceland plume impinged the base a lithosphere that had already been thinned by rifting (Skogseid, 2000; Nielsen et al., 2002; Armitage et al., 2010). Prior to continental breakup the plume was centred beneath the unthinned Greenland craton (Figure 2.4; Nielsen et al., 2002). It is suggested that the plume head was then channelled towards areas of thinner lithosphere (Nielsen et al., 2002). This flow of plume material is only possible prior to melting, after which its viscosity increases due to dehydration and cooling, preventing further lateral flow (Nielsen et al., 2002). The distribution of rift-related magmatic material in the South Atlantic provides further insights into the relationship between asthenospheric thermal anomalies and 3D lithospheric structure (Taposeea et al., 2016). However, this will be discussed in more detail in the Chapter 3, which focuses on the magma-rich margins of the South Atlantic.

In conclusion, observations and models suggest that asthenospheric temperatures are the primary control on excessive melt-volumes during rifting (White and McKenzie, 1989). However, it is also clear that the pre-existing structure of the lithosphere controls when and where melting occurs (White and McKenzie, 1989; Nielsen and Hopper, 2002; Taposeea et al., 2016; Armitage and Collier, 2017).

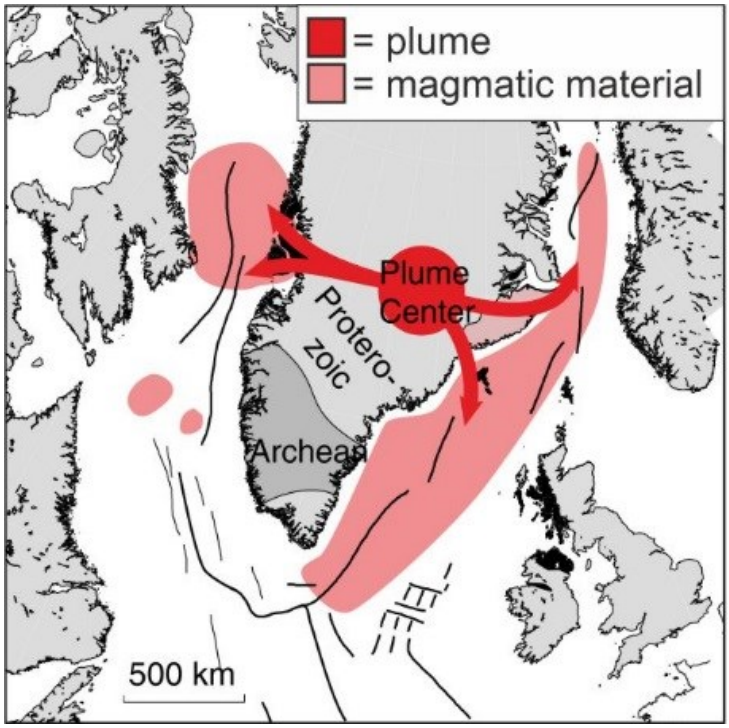

Figure 2.4. Conceptual model (modified from Nielsen et al., 2002) showing the channeling of plume material by changes in lithospheric thickness. Here, the plume impinged the lithosphere beneath the Greenland craton. Plume material was then channelled towards the zones of thinned lithosphere (the rifts of the North Atlantic and the Davis Strait).

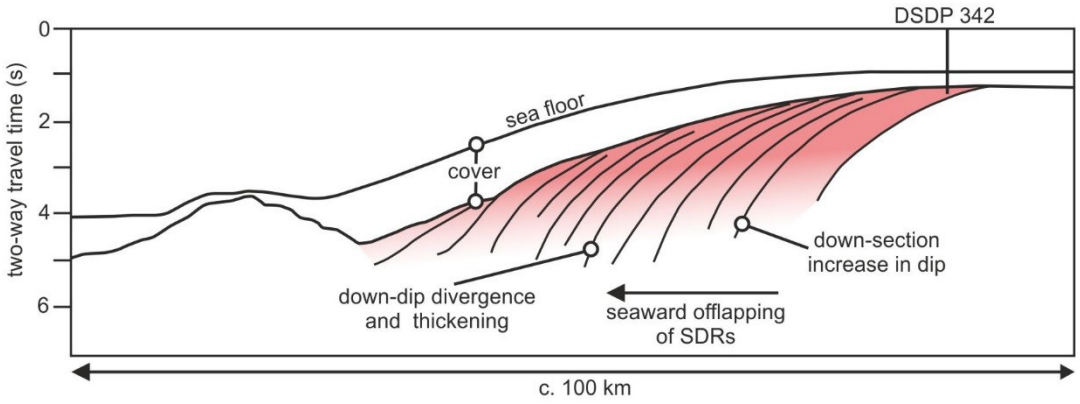

Figure 2.5. Schematic diagram showing the archetypal geometry of SDRs (Mutter et al., 1982) based on data from the Vøring margin, offshore Norway. Redrawn from Mutter et al. (1982) and Jackson et al. (2000).

2.3 The architecture and evolution of seaward dipping reflectors

Now that the processes controlling magma-rich margin formation have been addressed, our current understanding of SDR architecture (section 2.3.1) and emplacement (section 2.3.2) will be discussed. It is demonstrated that in order to understand the evolution of magma-rich margins, it is crucial to understand the processes controlling the emplacement and tilting of SDRs.

2.3.1 The architecture and lithology of SDRs

In seismic reflection data SDRs have been identified on margins worldwide (Hinz, 1981; Austin and Uchupi, 1982; Mutter et al., 1982; Gladczenko et al., 1997; Hopper et al., 2003; Collier et al., 2009; Calvès et al., 2011; Norton et al., 2015; Senkans et al., 2018; Gouiza and Paton, 2019). They have also been observed in outcrop in SE Greenland (Karson and Brooks, 1999), W Greenland (Geoffroy et al., 2001), and NE Norway (Abdelmalak et al., 2015).

A dominantly volcanic SDR-lithology was confirmed by Ocean Drilling Program (ODP) campaigns on the Norwegian Vøring margin (Mutter et al., 1982; Planke and Eldhom, 1994), the SE Greenland margin (Larsen and Saunders, 1998), and the Rockall margin (Roberts et al., 1984). In each of these locations the SDRs consist of tholeiitic flood basalts interbedded with variable amounts of sediment and volcaniclastic material (Mutter et al., 1982; Roberts et al., 1984; Planke and Eldhom, 1994; Larsen and Saunders, 1998). Dykes and sills were also encountered in several wells (Planke and Eldhom, 1994; Larsen and

Saunders, 1998). In addition to these ODP boreholes, SDRs have been encountered by several industry wells on the Namibian margin (Wickens and McLachlan, 1990; Jackson et al., 2000) where again they have a dominantly volcanic lithology.

The Kudu gas field wells, offshore Namibia, encountered flood basalts intercalated with fluvial sediments and aeolian sandstones, indicating that SDRs were emplaced in a subaerial environment (Wickens and McLachlan, 1990). A similar conclusion is supported by data from the North Atlantic, where the erosion and alteration of recovered flow tops indicate subaerial exposure (Planke and Eldhom, 1994; Larsen and Saunders, 1998). In seismic reflection data, SDRs are defined by a diagnostic reflector configuration (Figure 2.5), whereby all of the reflectors: dip seawards; have an arcuate geometry; increase in dip angle with depth, diverge downdip; show no evidence of bottomsets; and, offlap seawards (Mutter et al., 1982). In this context, the term 'offlap' refers to the seaward migration of the updip SDR-terminations (Figure 2.5).

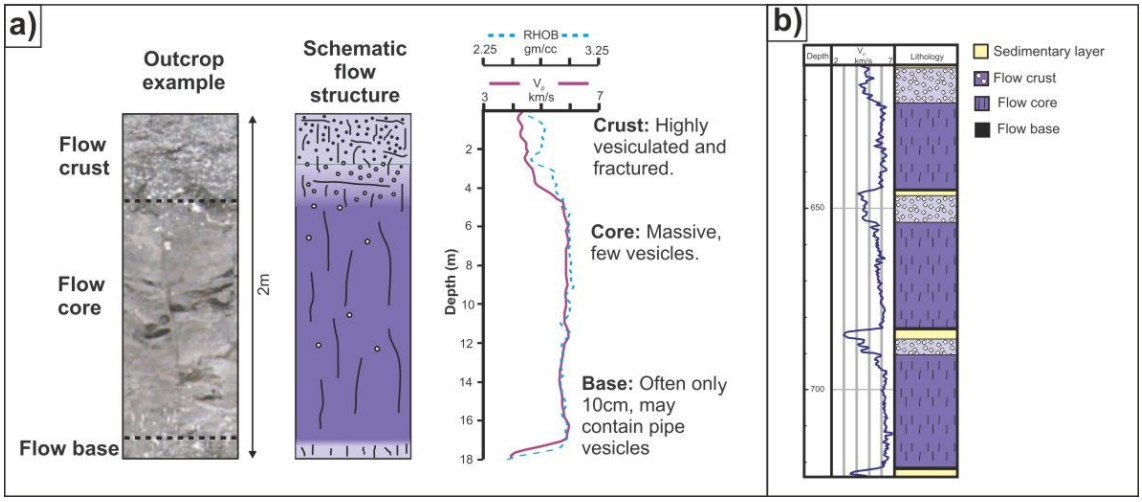

Figure 2.6. The structure and geophysical characteristics of lava flows (modified from Nelson et al., 2009). a) outcrop example of a basaltic lava flow, alongside the petrophysical properties of a lava flow from the Lopra-1 borehole (note scale difference between outcrop and wireline log data). Vp = p-wave velocity (km/s), RHOB = density log. b) P-wave velocity data through lava flows encountered in the Glyvursnes-1 borehole. Note velocity lows resulting from both the presence of interbedded sediments and lava flow tops.

Individual SDR-reflectors are highly variable in terms of amplitude and continuity (Planke and Eldhom, 1994). This variability is a result of the range of geological scenarios that can produce reflectivity. Borehole constrained synthetic seismograms demonstrate that SDR-reflections often result from tuning effects from numerous basalt flow-sediment interfaces (Planke and Eldhom, 1994). However, continuous reflections can also be generated from particularly thick and extensive lava flows (Planke and Eldhom, 1994). Field and laboratory studies demonstrate that the uppermost part of a lava flow, the 'flow crust' has a relatively low p-wave velocity due to its highly vesicular and weathered nature (Figure 2.6; Nelson et al., 2009). Velocity then increases with depth towards the higher-density flow centre (Nelson et al., 2009). These intra-lava flow density/velocity variations are sufficient to generate reflections, meaning that intercalated sediments are not a requisite for reflectivity. Two dimensional seismic forward modelling also demonstrates that SDR reflectivity can also result from interbedded lava flows and volcaniclastics (Morgan and Watts, 2018).

The dimensions of SDR sequences vary both along (Koopmann et al., 2013; McDermott et al., 2018) and between (e.g. Mutter et al., 1982; Stica et al., 2014) margins. They are characterised by widths (*margin-perpendicular distance*) between 30-500 km (Norton et al., 2015; McDermott et al., 2018), with the greater widths often being associated with hotspot tracks (McDermott et al., 2018). Regionally, they can be continuous along-strike for over 2000 km although they may be locally disrupted by transfer zones (Koopmann et al., 2013; McDermott et al., 2018). Vertical thicknesses of 3-6 km are common (Morgan and Watts, 2018) but extremes of >15 km have been reported, which again are associated with hot-spot tracks (McDermott et al., 2018). On average, SDRs dip between 5-15° (Morgan and Watts, 2018). However given that dip angle increase with depth, greater than average dips are common (as will be evident in subsequent chapters).

2.3.1.1 Different types of SDRs

The geometrical description presented above (Mutter et al., 1982) should hold for the large majority of reflectors within a succession/sequence of SDRs. Within this framework, many studies have demonstrated that SDR sequences can sub-divided into a series of packages (Planke et al., 1999; Bauer et al.,

2000; Planke et al., 2000; Franke et al., 2007; Elliott and Parson, 2008; Rey et al., 2008; Calvès et al., 2011; Koopmann et al., 2013; McDermott et al., 2015; Geissler et al., 2017; Horni et al., 2017; McDermott et al., 2018) via changes in: seismic character (Planke et al., 2000; Elliott and Parson, 2008; Calvès et al., 2011; McDermott et al., 2018); reflector dimensions (Planke et al., 2000; Calvès et al., 2011; McDermott et al., 2018); downdip termination character (Paton et al., 2017; McDermott et al., 2018); and, the type of crust that they overlie (Elliott and Parson, 2008; McDermott et al., 2015; Paton et al., 2017).

The most common way of categorising SDRs is to separate them into Inner SDRs and Outer SDRs (Planke et al., 1999; Bauer et al., 2000; Planke et al., 2000; Calvès et al., 2011; McDermott et al., 2015; Paton et al., 2017; Horni et al., 2017; Geissler et al., 2017). In these scenarios, the Inner SDRs are always located landwards of the Outer SDRs (Figure 2.7).

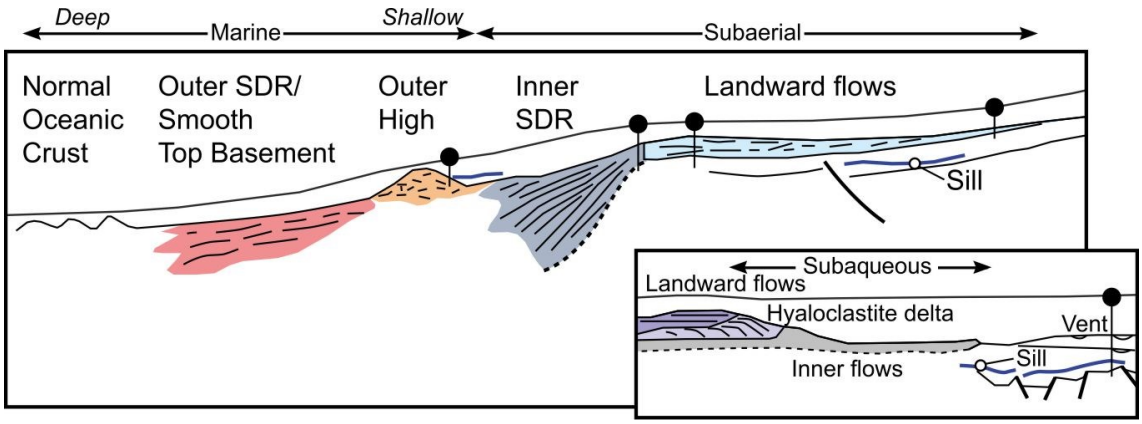

Figure 2.7. Seismic volcano-stratigraphic classification of a magma-rich margins, modified from Planke et al. (2000). Each of the separate seismic facies units is annotated, as are the interpreted emplacement environments.)

Interpretations of Inner SDRs and Outer SDRs are based on the seismic volcano-stratigraphic classification established by Planke et al. (2000). This classification system is explained in Chapter 4 and relies on defining different *seismic facies units* via consistent changes in parameters such as reflector configuration, reflector continuity, reflector amplitude and interval velocity (Planke et al., 2000). In addition to Inner and Outer SDRs this generic seismic volcano-stratigraphic classification (Figure 2.7) contains several seismic facies units (i.e. landward flows, lava deltas, and flat-lying flows) that are not the focus of this thesis (Planke et al., 2000).

Interestingly, the definitions of Inner SDRs and Outer SDRs are near identical (Table 2.1). Both seismic facies units are ‘wedge shaped’ and contain ‘divergent arcuate reflectors’ with ‘non-systematic truncations’ (Planke et al., 2000). The distinguishing characteristics of Outer SDRs are that they have lower amplitudes (Table 2.1) and are typically thinner than the Inner SDRs (Figure 2.7), they also sometimes contain planar reflectors that are interpreted as sills (Planke et al., 2000).

In this original classification, the two sets of SDRs were separated by a hyaloclastic mound known as the Outer High (Planke et al., 2000). The Outer High is interpreted to have been emplaced in shallow water, as the basin subsided to below sea-level (Planke et al., 2000). This lead to a model where the Inner SDRs, which pre-date the Outer High, were emplaced subaerially (Table 2.1). Whilst the Outer SDRs, which post-date the Outer High, were emplaced in a submarine environment (Table 2.1; Planke et al., 2000).

Dominant characteristics of main volcanic extrusive seismic facies units on rifted margins

Seismic facies unit	Reflector characteristics			Volcanic facies	Emplacement environment
	Shape	Boundaries	Internal		
Outer SDR	Wedge	Top: high-amplitude, smooth. Pseudoescarpments. Base: seldom defined.	Divergent-arcuate or -planar. Disrupted, nonsystematic truncations.	Flood basalts mixed pillow basalts, sediments, and sills.	Deep marine (>1-200 m)
Outer High	Mound	Top: high-amplitude event. Often planated. No base.	Chaotic.	Hyaloclastic flows and volcaniclastics.	Shallow marine (<1-200 m)
Inner SDR	Wedge	Top: high-amplitude, smooth. Pseudoescarpments. Base: seldom defined.	Divergent-arcuate. Disrupted, nonsystematic truncations.	Flood basalts.	Subaerial
Landward Flows	Sheet	Top: high-amplitude, smooth. Base: low-amplitude, disrupted.	Parallel to subparallel. High-amplitude, very disrupted.	Flood basalts.	Subaerial
Lava Delta	Bank	Top: high-amplitude, or reflector termination. Base: reflector termination.	Prograding clinoform. Disrupted.	Massive and fragmented basalts. Volcaniclastics.	Coastal
Inner Flows	Sheet	Top: high-amplitude, disrupted. Base: negative, but often obscured.	Chaotic or disrupted, subparallel.	Massive and fragmented basalts. Volcaniclastics.	Subaqueous

Table 2.1. Characteristics of the main extrusive seismic facies units on magma-rich margins, modified from Planke et al. (1999).

This model was based on the Norwegian margin, where the Outer High is a regional feature. However, such basement highs are not ubiquitous across magma-rich margins worldwide and in their absence the Outer SDRs directly overlie the Inner SDRs (e.g. Franke et al., 2007; Koopmann et al., 2013; McDermott et al., 2015; Geoffroy et al., 2015; Paton et al., 2017; Horni et al., 2017; Geissler et al., 2017). This has implications for understanding the emplacement environment of SDRs: If an Outer High records the subsidence of

the basin below sea-level then its absence may indicate that Inner SDRs and Outer SDRs do not record different emplacement environments. In the absence of an Outer High, several recent studies have instead classified Inner SDRs and Outer SDRs via their structural position on the margin and the nature of their downdip terminations (McDermott et al., 2015; Paton et al., 2017; McDermott et al., 2018). These classifications are discussed in the underlying section (2.3.2.3).

Figure 2.8. Three stage model for the emplacement and tilting of seaward dipping reflectors (Mutter et al., 1982). The 'Initial Phase' and 'Middle Phase' diagrams (top and middle) show a subaerial spreading axis where

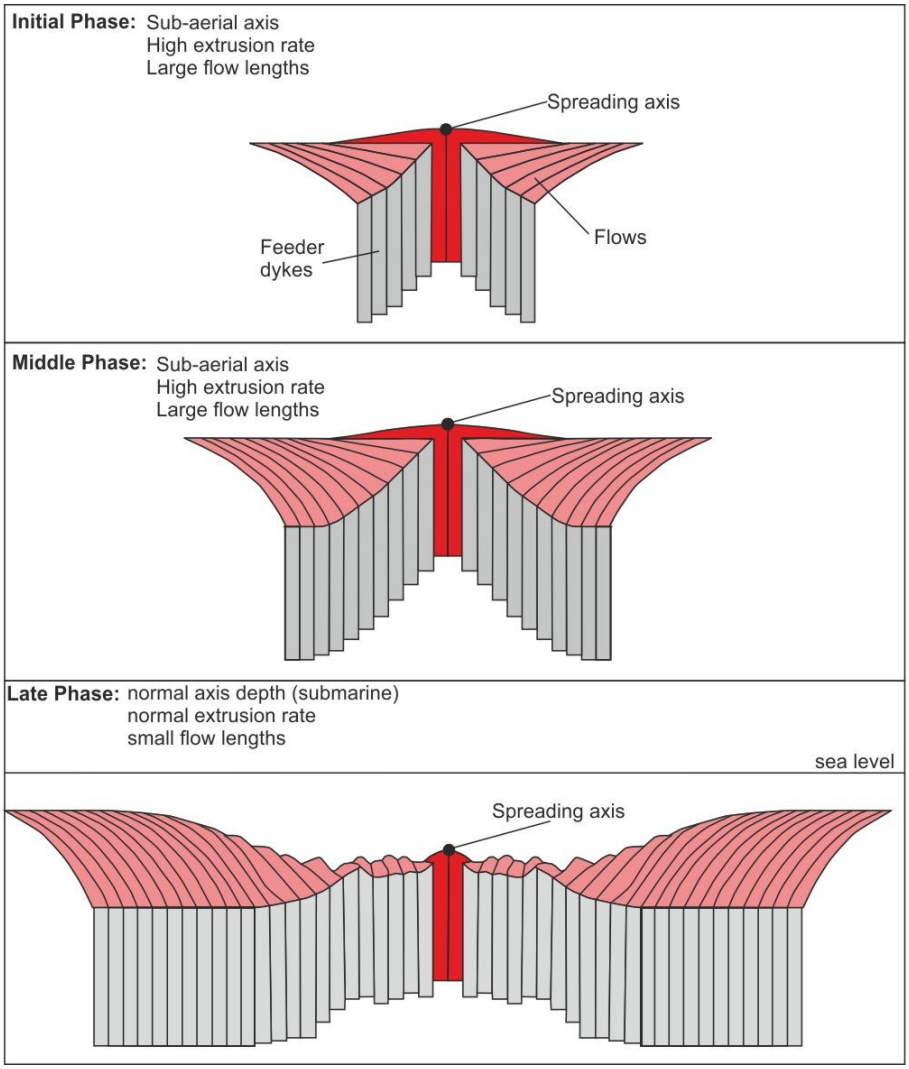

lava flows flow away from the axis and load the surrounding crust. This loading results in the subsidence of older lava flows and dykes. In the 'Late Phase' diagram (bottom) the spreading axis has subsided to the normal depth of a mid-ocean ridge.

2.3.2 The emplacement and tilting of SDRs

Despite ongoing research, the tectonic and magmatic processes responsible for the emplacement and tilting of SDRs remain contentious (Mutter et al., 1982; Quirk et al., 2014; Clerc et al., 2015; Geoffroy et al., 2015; Paton et al., 2017; Buck, 2017; Morgan and Watts, 2018; McDermott et al., 2018) . Many of these models can be categorised as to whether subsidence and rotation is driven by magmatic-loading (section 2.3.2.1; Mutter et al., 1982; Buck, 2017; Paton et al., 2017; Morgan and Watts, 2018) or by normal faulting (section 2.3.2.2; Quirk et al., 2014; Geoffroy et al., 2015; Clerc et al., 2015). These different models assume different composition of the sub-SDR crust, leading to contrasting interpretation of continent-ocean boundaries worldwide (Mutter et al., 1982; Larsen and Saunders, 1998; Stica et al., 2014; Clerc et al., 2015; Geoffroy et al., 2015; Norton et al., 2015; Paton et al., 2017; Nemčok and Rybár., 2017; McDermott et al., 2018; Senkans et al., 2018). Composite models (section 2.3.2.3) have also have been proposed, where both faulting and magmatic-loading control SDR emplacement occur but during different phases of basin evolution (Paton et al., 2017; McDermott et al., 2018). Below, an overview of each of these models is provided.

2.3.2.1 Magmatic-loading models of SDR emplacement

Models within this category interpret the geometry of SDRs to result from the magmatic loading of the thin and weak lithosphere (Mutter et al., 1982; Paton et al., 2017; Buck, 2017; Morgan and Watts, 2018; McDermott et al., 2018). By analogy with the regional architecture of lava-flows in Iceland, Mutter et al. (1982) presented the first detailed model of loading-driven SDR emplacement. SDRs were considered to be emplaced above a subaerial magmatic spreading system (Figure 2.8). Due to the subaerial environment and the high-extrusion rates, lavas erupted at the spreading centre flow km's away from the axial zone (early phase in Figure 2.8). Continuous axial dyke intrusion (middle phase in Figure 2.8) results in the splitting of older dykes and lava flows (Mutter et al., 1982). The emplacement of new lava flows results in the subsidence of the older lava flows and dykes (Mutter et al., 1982). Hence during emplacement, this models predict two sub-surface wedges of axially dipping lava flows located either side of the spreading axis (Figure 2.8). Through time, magma-supply is interpreted to decrease due to the waning of the underlying thermal anomaly

(Mutter et al., 1982), resulting in shorter flow lengths and the subsidence of the spreading centre below sea level (Figure 2.8). This leads to the generation of *normal* oceanic crust at the spreading centre (Mutter et al., 1982), resulting in the preservation of SDRs at the rifted margins (Figure 2.8). This model was proposed via comparison with the present-day geometry of Iceland, where lava flows dip regionally towards the spreading axes (Bodvarsson and Walker, 1964; Pálmason, 1973; Palmason and Saemundsson, 1974).

Recent analytical models have examined several variations from the model presented above (Corti et al., 2015; Buck, 2017; Morgan and Watts, 2018). The model of Mutter et al. (1982) assumes Airy isostasy, where loads are accommodated locally within a lithosphere with no flexural strength. Recent models have instead considered a system operating under flexural isostasy, whereby loads are accommodated by the regional bending of the elastic lithosphere (Corti et al., 2015; Buck, 2017; Morgan and Watts, 2018). Through comparison with Afar, Corti et al. (2015) demonstrated that regional flexure within a basin can result from axial magma-intrusion. The magnitude and wavelength of axial subsidence results both from the strength of the plate and the nature of the load (Corti et al., 2015). This initial flexural subsidence can be increased via the infilling of accommodation space with extrusive material (Corti et al., 2015).

Buck (2017) applied a variation of this model to explain the kinematic evolution of SDRs (Figure 2.9a). An infinitely thin fluid dyke was modelled as being permanently present at a spreading axis (Figure 2.9a). As older dykes move away from the spreading axis they instantaneously cool, resulting in a density increase. This density increase drives flexural subsidence (Figure 2.9a), the magnitude of which increases with distance from the spreading axis (Buck, 2017). The geometry of SDRs can then be produced through sequentially infilling the accommodation space generated by dyke solidification (Buck, 2017).

Morgan and Watts (2018) modelled a slightly different scenario to that described above (Buck, 2017). Instead of modelling a permanent fluid dyke at the rift-axis, they instead considered dyke emplacement to be episodic (Figure 2.9b). The geometry of SDRs was generated by iterations of the following process: a fluid dyke is emplaced at the rift-axis and the top of the dyke

reaching the surface; the instantaneous solidification of this dyke causes flexural subsidence that is infilled and amplified by volcanics; a new fluid dyke splits this volcanic mini-basin; once again this dyke solidifies and subsides, leading to volcanic infilling of the mini-basin; this mini-basin is split via an axial dyke, etc (Morgan and Watts, 2018).

These analytical models assume that the dimensions of the axially emplaced intrusive material remain constant through time (Buck, 2017; Morgan and Watts, 2018). However, geophysical data from margins worldwide indicate that the crust beneath the SDRs thins with distance seawards (e.g. Quirk et al., 2014; Geoffroy et al., 2015; Clerc et al., 2016; Paton et al., 2017; Reuber, 2017; Nemčok and Rybár., 2017; McDermott et al., 2018). Such thinning would result in continual subsidence of the spreading centre (Paton et al., 2017), potentially resulting in the formation of a thick mini-basin at the axial zone (Figure 2.9c).

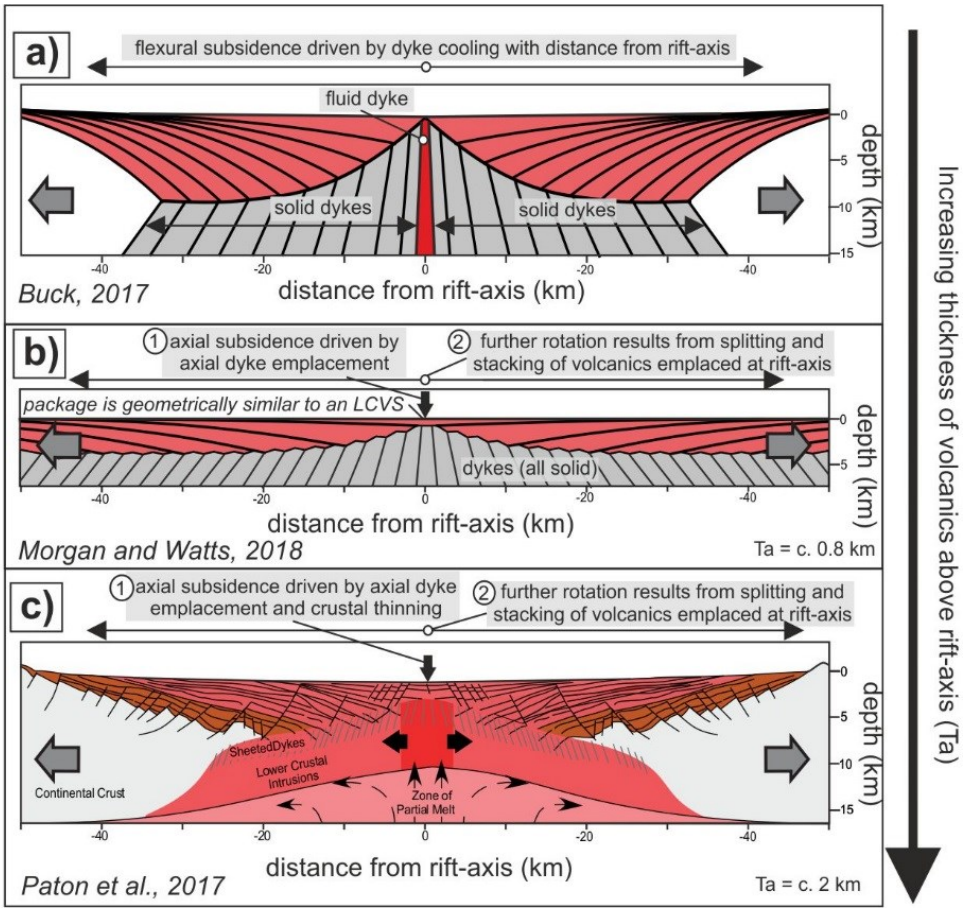

Figure 2.9. Three models of loading-driven SDR emplacement. a) loading results from the cooling of dykes as they move away from a spreading axis characterised by a permanent 'fluid dyke' (Buck, 2017). b) loading results from episodic axial dyke emplacement (Morgan and Watts, 2018). c) in addition to axial magmatic loading, decreasing crustal thickness also drives axial subsidence (Paton et al., 2017).

Models of magmatic loading have gained support from the interpretation of modern long-recording time long-offset seismic reflection data. In the South Atlantic the downdip termination of many of the SDRs is diffuse and sub-horizontal (McDermott et al., 2015; Paton et al., 2017; McDermott et al., 2018). This has been interpreted as evidence of an SDR-sheeted dyke contact as opposed to an SDR-faulted basement contact (McDermott et al., 2015; Paton et al., 2017; McDermott et al., 2018).

Magmatic-loading models of SDR emplacement assume, implicitly (Buck, 2017; Morgan and Watts, 2018) or explicitly (Mutter et al., 1982; Paton et al., 2017; McDermott et al., 2018), that SDRs are emplaced as the uppermost part of thickened oceanic crust. In these cases, the sub-SDR crust is often referred to as *magmatic crust* (Paton et al., 2017; McDermott et al., 2018; Morgan and Watts, 2018). Within these models, the continent-ocean boundary can be defined as the downdip termination of the landward most SDR (Skogseid, 1994; Gladczenko et al., 1998; Bauer et al., 2000; Hopper et al., 2003).

These models also assume that, during SDR emplacement, extension was accommodated primarily by magma-intrusion along a narrow axial zone (Mutter et al., 1982; Corti et al., 2015; Buck, 2017; Paton et al., 2017; Morgan and Watts, 2018). Specifically, extension in the brittle upper crust would have been accommodated by dyke intrusion (Mutter et al., 1982; Paton et al., 2017; Buck, 2017; Morgan and Watts, 2018) whilst in the lower crust it would be accommodated by gabbroic accretion (Paton et al., 2017; McDermott et al., 2018). These models have the advantage of being analogous with present-day high-magma supply extensional settings. In both northern Ethiopia (Ebinger and Casey, 2001; Wright et al., 2006) and Iceland (Mutter et al., 1982; Wright et al., 2012), extension is accommodated primarily through magma-intrusion, with faulting being a second-order process (see section 1.3.3).

2.3.2.2 Fault-controlled models of SDR emplacement

In these models (Figure 2.10), the SDR-dips result from the emplacement of lava-flows into half-grabens controlled by continent-dipping normal faults (Geoffroy, 2005; Stica et al., 2014; Quirk et al., 2014; Clerc et al., 2015; Geoffroy et al., 2015; Nemčok and Rybár., 2017; Senkans et al., 2018; Guan et al., 2019). These normal faults are interpreted to detach against a ductile lower

crust (Quirk et al., 2014; Clerc et al., 2015; Geoffroy et al., 2015), that is typically considered as intruded continental crust (Clerc et al., 2015; Geoffroy et al., 2015). However there are also suggestions that this lower crust is dominantly magmatic and contains only slithers of continental material (Figure 2.11; Quirk et al., 2014).

Fault-controlled model of SDR emplacement (modified from Guan et al. 2019, and Geoffroy et al., 2015). The SDRs are controlled by continent-dipping normal faults that young axial-ward, thus implying that the axial horst block narrows with time. The faults detach against a ductile and highly intruded lower crust (Figure 2.10).

The generation of SDRs in this manner requires the presence of an axial horst block during their emplacement (Quirk et al., 2014; Geoffroy et al., 2015; Clerc et al., 2016). This horst block would have separated the conjugate sequences of SDRs located either side of it (Figure 2.10, Figure 2.11). To produce the seaward-younging faults invoked in these models, this axial horst block would have narrowed through time with new faults successively nucleating within it (Quirk et al., 2014; Geoffroy et al., 2015; Clerc et al., 2016).

Several studies have also proposed that sub-SDR landward dipping faults exhume the lower crust in their footwalls (Clerc et al., 2015; Geoffroy et al., 2015). A consequence of this scenario is that, in the present day, the crust located immediately seawards of SDRs would consist of exhumed lower continental crust not oceanic crust (Senkans et al., 2018).

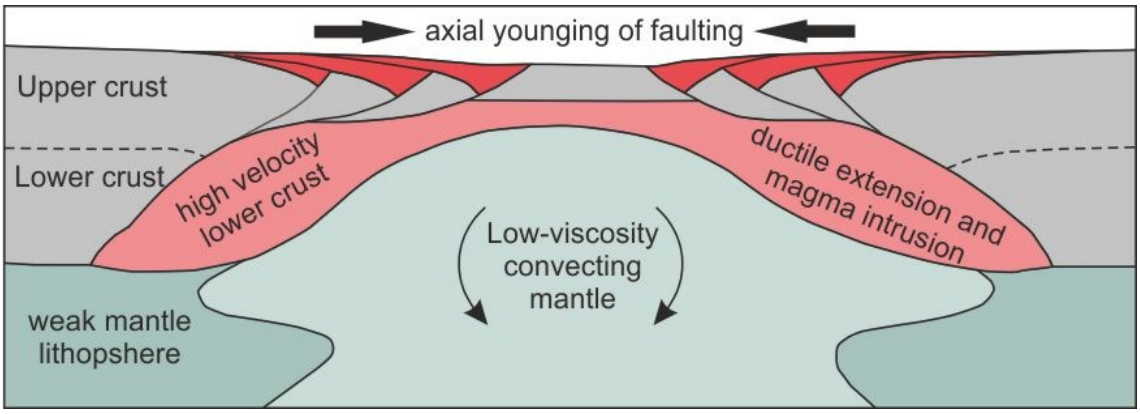

Figure 2.10. Fault-controlled model of SDR emplacement (modified from Guan et al. 2019 and Geoffroy et al., 2015). The SDRs are controlled by continent-dipping normal faults that young axial-ward, thus implying that the axial horst block narrows with time. The faults detach against a ductile and highly intruded lower crust.

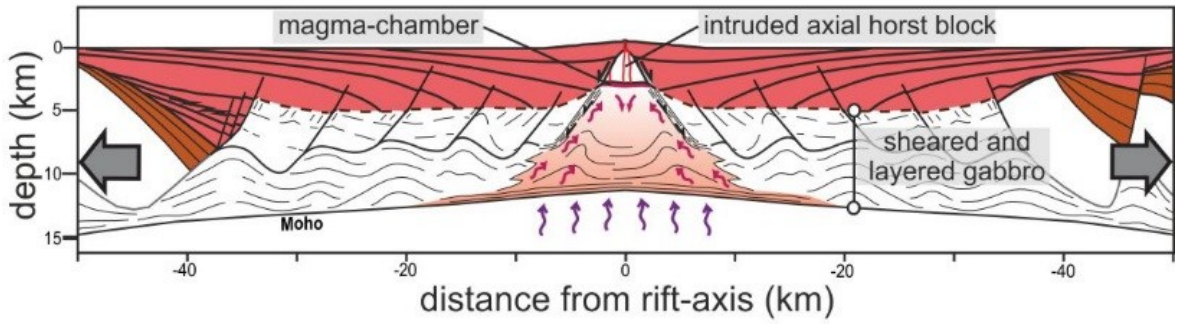

Figure 2.11. Fault-controlled model of SDR emplacement (modified Quirk et al., 2014). Here the SDRs are emplaced from a magma-chamber beneath the axial horst block. The sub-SDR crust consists mainly of new magmatic material but also contain slices of continental crust that have been shed off the axial horst block, according this axial horst narrows through time as new faults nucleate within it.

Many fault-controlled models of SDR emplacement are based on the interpretation of long recording time long offset seismic reflection data (Stica et al., 2014; Quirk et al., 2014; Geoffroy et al., 2015; Clerc et al., 2015; Nemčok and Rybár., 2017; Senkans et al., 2018). Undulations in the basal SDR surface are interpreted as landward-dipping normal faults. Lower crustal reflectivity can also be interpreted as shear zones with kinematics matching that of the overlying landward-dipping normal faults (Clerc et al., 2015; Geoffroy et al., 2015). Fault-controlled SDR emplacement is also supported by outcrop data in west Greenland. Here, outcrops of seaward dipping volcanics are cross-cut by landward dipping normal faults (Geoffroy, 2001). These volcanics however have dips of up to 60°, which is far steeper than is observed in offshore SDR sequences (Morgan and Watts, 2018).

Fault-controlled models of SDR emplacement suggest that, during magma-rich rifting, extension is accommodated primarily through the generation of large-throw normal faults. This is strikingly different to a scenario where strain is accommodated via magma-intrusion in a narrow axial zone (section 2.3.2.1). The majority of these models also assume that SDRs were emplaced during the stretching of the continental lithosphere, as opposed to during the accretion of new oceanic lithosphere (section 2.3.2.1). Hence many of these models place the location of the earliest oceanic crust seaward of the SDRs (Stica et al., 2014; Quirk et al., 2014; Clerc et al., 2015; Geoffroy et al., 2015; Nemčok and Rybár., 2017; Senkans et al., 2018).

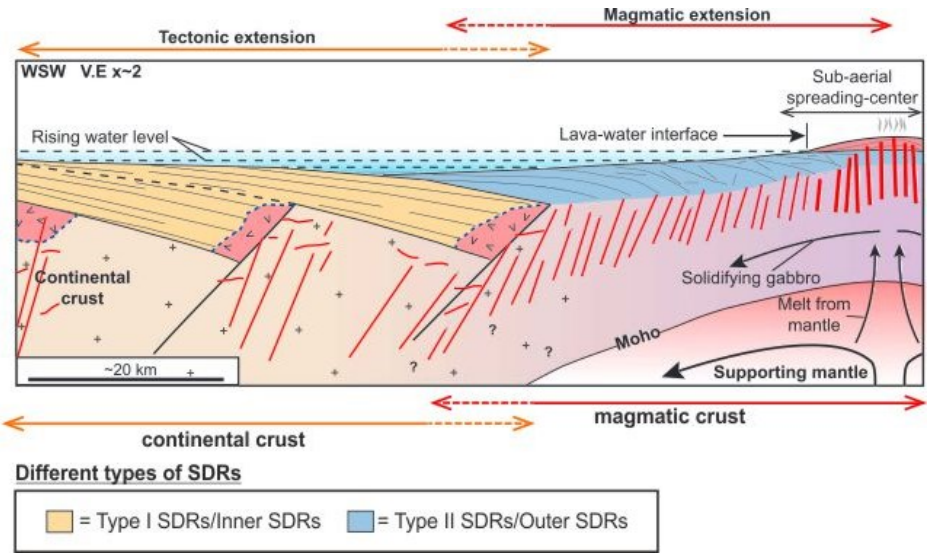

Figure 2.12. Composite model of SDR emplacement, modified from McDermott et al. (2018). The earliest SDRs (Type I SDRs/Inner SDRs) are fault controlled whereas the latest SDRs (Type II SDRs/Outer SDRs) are loading controlled.

2.3.2.3 Composite models of SDR emplacement

Recent models have suggested that both fault and loading models may apply, but during different phases of basin evolution (McDermott et al., 2015; Paton et al., 2017; McDermott et al., 2018). It is suggested that the innermost SDRs are fault-controlled (Figure 2.12) and formed during the extension of the continental lithosphere. The outermost SDRs meanwhile are interpreted as magmatic-loading controlled features (Figure 2.12) that formed during oceanic accretion (McDermott et al., 2015; Paton et al., 2017; McDermott et al., 2018). Temporally, the boundary between these two sets of SDRs records the transition from extension being accommodated by tectonic to magmatic processes (Figure 2.12; McDermott et al., 2015; Paton et al., 2017; McDermott et al., 2018). Spatially, this boundary represents the transition from stretched continental crust to new magmatic crust (McDermott et al., 2015; Paton et al., 2017; McDermott et al., 2018). Whilst this model has gained support from several studies, the terminology used to define these two sets of SDRs is contentious. McDermott et al. (2018) define the fault-controlled and loading-controlled SDRs as *Type I SDRs* and *Type II SDRs* respectively. Other authors instead define the fault-controlled SDRs as *Inner SDRs* and the loading-controlled SDRs as *Outer SDRs* (McDermott et al., 2015; Paton et al., 2017).

These models are based primarily on the interpretation of seismic reflection data. With reference to the South Atlantic magma-rich margins, it is noted that the innermost SDRs often terminate downdip against landward dipping interfaces interpreted as normal faults (McDermott et al., 2018). The outermost SDRs meanwhile terminate downdip against a diffuse sub-horizontal surface interpreted as an SDR-sheeted dyke contact (Paton et al., 2017; McDermott et al., 2018). These outermost SDRs are coincident with linear magnetic anomalies, indicating that they were emplaced from an organised magmatic spreading centre (Collier et al., 2017).

Composite models of SDR emplacement also draw support from petrological data from the SE Greenland margin. Here, the geochemistry of the innermost SDRs suggests that the melt rose through continental crust, whilst that of the outermost SDRs is more typical of melt generated as a seafloor spreading centre (Larsen and Saunders, 1998).

2.3.3 Extension mechanisms in active magmatic systems

Both Iceland (Mutter et al., 1982; McDermott et al., 2018) and the northernmost parts of East African Rift System (EARS; Wolfenden et al., 2005; Bastow and Keir, 2011; Corti et al., 2015; Paton et al., 2017) have been proposed as modern analogues for SDR emplacement. Both regions have similarities to magma-rich margins: extension is occurring above asthenospheric thermal anomalies (White and McKenzie, 1989; Corti, 2009; Smallwood and White, 2012; Keir et al., 2013; Armitage and Collier, 2017); more magmatism is observed than predicted by models of extension above a *normal* asthenosphere (White and McKenzie, 1989; Armitage and Collier, 2017); lava flows dip towards the rift-axis (Bodvarsson and Walker, 1964; Mutter et al., 1982; Corti et al., 2015); flexural deformation is observed at the flanks of the magmatic systems (Karson and Brooks, 1999; Wolfenden et al., 2005). The tectonic setting of both active systems may also be analogous to different stages of SDR emplacement: The northernmost segments of the EARS, comprising the Main Ethiopian Rift and the Afar depression, capture the transition from continental rifting to incipient seafloor spreading (Hayward and Ebinger, 1996; Ebinger and Casey, 2001; Corti, 2009; Corti et al., 2015; Paton et al., 2017); Iceland, meanwhile is an example of oceanic accretion above a mantle plume (e.g. White et al., 1995; Smallwood and White, 2012).

Both settings provide insights into the roles of tectonic and magmatic processes in accommodating deformation where magma-supply is high (Ebinger and Casey, 2001; Wright et al., 2012; Corti et al., 2015). Upper-crustal deformation in both regions is accommodated in narrow zones characterised by both active faulting and magmatism (e.g. Wright et al., 2012). Geodetic and seismological data demonstrate that the majority of extension is accommodated through dyke injection (Wright et al., 2006; Wright et al., 2012), with individual dykes propagating along strike for 10's km. The faulting observed in these settings is a result of dyke propagation at depth (Wright et al., 2012; Sigmundsson et al., 2014). These dyke-induced faults have low displacements in comparison to those that form purely in response to lithospheric extension (Paton et al., 2017). Extrusive material in both regions is fed from both volcanoes and fissure-eruption (Mutter et al., 1982; Ebinger and Casey, 2001; Corti, 2009; Keir et al., 2013).

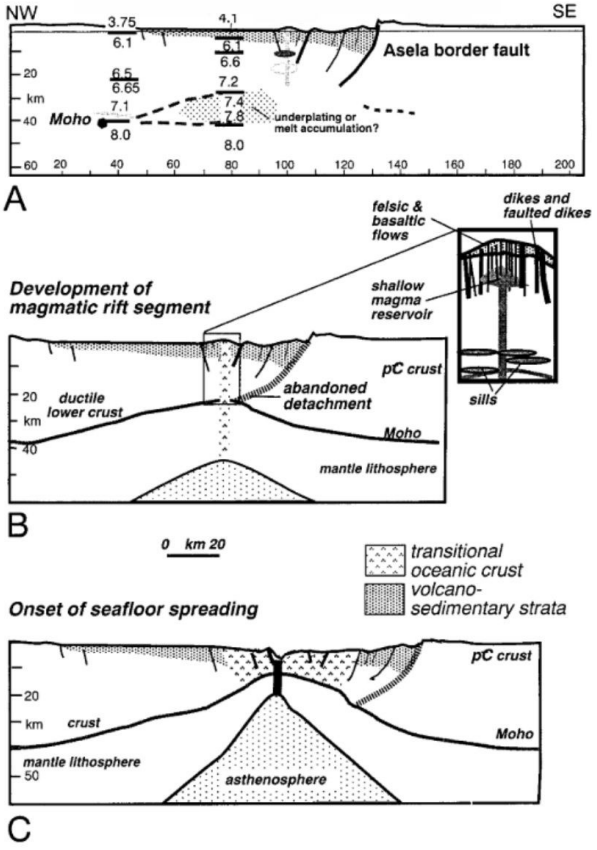

Figure 2.13. Model of continental breakup from Ebinger and Casey (2001). a) cross-section through the Main Ethiopian rift with seismic velocities shown. b) conceptual model where border faults have been abandoned in favour of an axial magmatic system. c) continued axial magmatic accretion results in the formation of transitional oceanic crust.

In both the Main Ethiopian Rift and Afar depression, the dating of volcanic rocks indicates that magma-maintained rifting commenced in the Quaternary (Hayward and Ebinger, 1996; Ebinger and Casey, 2001; Wolfenden et al., 2005). Prior to this, extension was accommodated through the formation of large-displacement normal faults (Ebinger and Casey, 2001; Wolfenden et al., 2005; Corti, 2009; Keir et al., 2013). The scarps of these basin-bounding normal faults still exist in the present-day, although they are now largely inactive (Ebinger and Casey, 2001). This has lead to a rifting model whereby extension is initially accommodated through tectonic processes (Figure 2.13a) but that magmatic processes come to dominate (Figure 2.13b and c) once the lithosphere has been thinned sufficiently for the asthenosphere to melt (Hayward and Ebinger, 1996; Ebinger and Casey, 2001). This interpretation is supported by numerical models indicating that dyke emplacement can occur under lower effective stresses than faulting (Buck, 2004; Bialas et al., 2010; Rivalta et al., 2015). This concept is also supported by observations and models of extension mechanisms at mid-ocean ridges (e.g. Morgan and Chen, 1993).

Chapter 3 Regional setting: magma-rich margins in the South Atlantic

3.1 Introduction

This thesis aims to provide new constraints on the processes involved in magma-rich margin formation. Primarily it does this through analysing data from the Orange Basin, located offshore South Africa and Namibia (Chapters 5-7). However, in order to assess margin asymmetry data from the conjugate portions of the Argentinian and Uruguayan margins are also interpreted (Chapter 8). Here, the regional setting of these conjugate margins is provided, with emphasis being placed on the processes controlling magma-rich margin occurrence and variability (section 3.2). An overview of the architecture and evolution of the Orange Basin is also given (section 3.3), providing a framework for the results presented in subsequent chapters.

3.2 Regional setting

3.2.1 Distribution of rifted margin end-members in the South Atlantic

The conjugate margins of the South Atlantic consist of magma-rich (Gladczenko et al., 1997; Blaich et al., 2009; Koopmann et al., 2014b; McDermott et al., 2015; Collier et al., 2017; McDermott et al., 2018), magma-poor (Unternehr et al., 2010; Péron-Pinvidic et al., 2015), and transform conjugate pairs (Figure 3.1).

Transform margins are located in the northernmost and southernmost South Atlantic (Heine et al., 2013). To the north (Figure 3.1), they are located offshore equatorial Africa and South America (Mercier de Lépinay et al., 2016). To the south (Figure 3.1), they are bounded by the Agulhas-Falkland Fracture Zone and are located offshore Argentina and South Africa (Koopmann et al., 2013; Mercier de Lépinay et al., 2016).

The rifted margins that occur between these sets of transform-pairs, formed under near-orthogonal extension (Heine et al., 2013). The architecture and end-member classification of these margins vary either side of two conjugate

aseismic ridges (Figure 3.1): the Walvis Ridge on the African plate, and the Rio Grande Rise on the South American plate (O'Connor and Duncan, 1990). Both of these features are associated with the Tristan plume, which in the present-day is located beneath the island of Tristan Da Cunha (O'Connor and Duncan, 1990). Northwards of these two aseismic ridges are the salt-bearing rifted margins (Figure 3.1) of Brazil, Angola, Democratic Republic of the Congo, Congo, and Gabon (Jackson et al., 2000; Karner and Gambôa, 2007; Davison, 2007; Lentini et al., 2010; Quirk and Hertle, 2013). Several studies have suggested that the distal parts of these margins are floored by hyperextended crust and possibly even exhumed mantle, leading to them being classified as *magma-poor* (Unternehr et al., 1988; Péron-Pinvidic et al., 2015). However, it also sometimes suggested that they are situated between the extremes of either magma-rich or magma-poor (Quirk and Hertle, 2013; Norton et al., 2015).

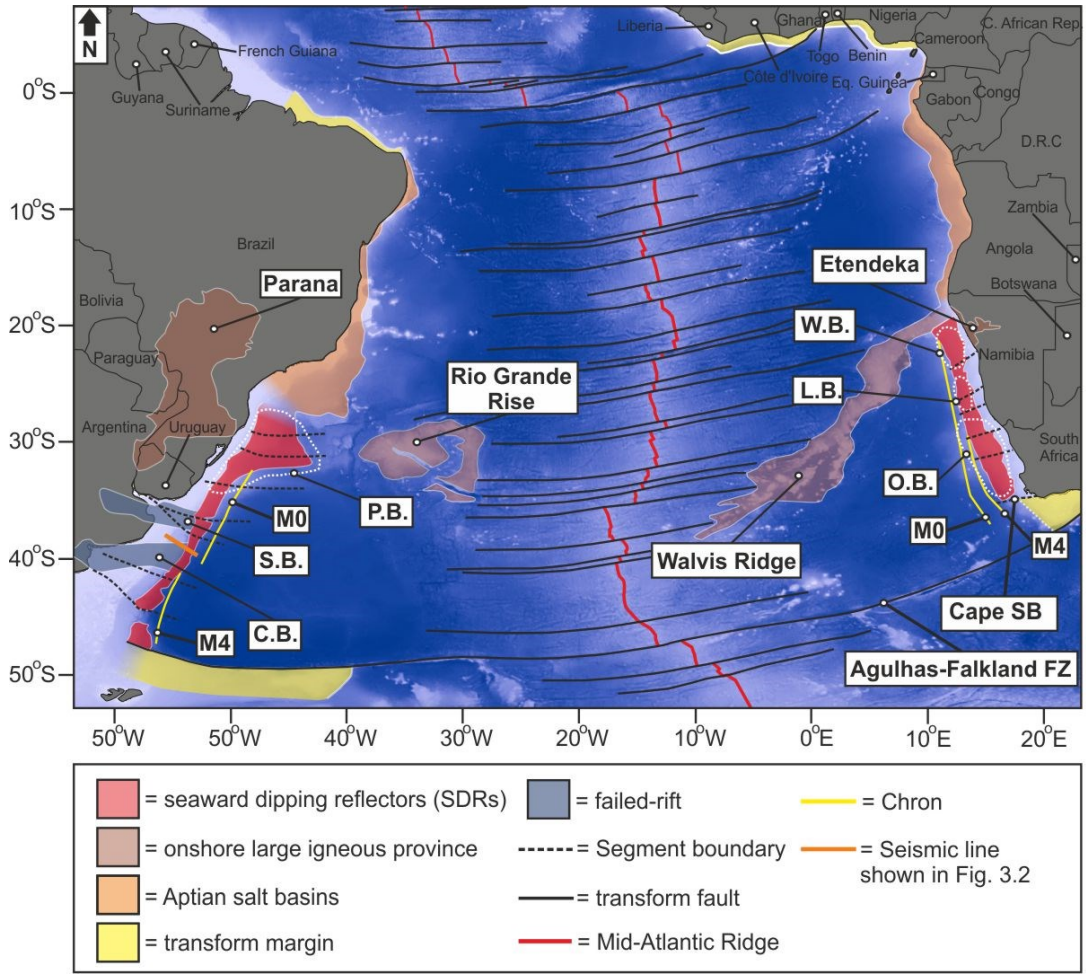

Figure 3.1. Regional map of the South Atlantic, with key geological features and sedimentary basins annotated. C.B. = Colorado Basin, S.B. = Salado Basin, P.B. = Pelotas Basin, W.B. = Walvis Basin, L.B. = Luderitz Basin, O.B. = Orange Basin, Cape SB = Cape Segment Boundary.

To the south of the Walvis Ridge and Rio Grande Rise (Figure 3.1), the conjugate rifted margins of the South Atlantic are magma-rich (Gladczenko et al., 1997; Gladczenko et al., 1998; Blaich et al., 2009; McDermott et al., 2015; Paton et al., 2017; McDermott et al., 2018). Both conjugates are defined by the occurrence of SDRs (Hinz, 1981; Austin and Uchupi, 1982; Gladczenko et al., 1997; Clemson et al., 1997; Corner et al., 2002; Franke et al., 2010; Koopmann et al., 2014b; McDermott et al., 2015; Paton et al., 2017; McDermott et al., 2018) and high-velocity lower crust (HVLC; Bauer et al., 2000; Stewart et al., 2000; Hirsch et al., 2009; Maystrenko et al., 2013; Becker et al., 2014; Autin et al., 2016). Given that this thesis focuses solely on the magma-rich parts of the South Atlantic, their architecture and evolution are described in detail below.

3.2.2 Magma-rich margins of the South Atlantic

The magma-rich segments of the South Atlantic (Figure 3.1) are located offshore Brazil (Pelotas Basin), Uruguay, Argentina, Namibia (Walvis, Luderitz and Orange Basins), and South Africa (Orange Basin.). The extent of these margins is demonstrated by the regional distribution of SDRs (Figure 3.1), which have been mapped using seismic reflection and magnetic anomaly data (Gladczenko et al., 1998; Franke et al., 2007; Koopmann et al., 2013; Stica et al., 2014; McDermott et al., 2015; Collier et al., 2017; McDermott et al., 2018).

On the South American margin, SDRs are present between the Rio Grande Rise in the north and the Agulhas-Falkland Fracture Zone in the south (Franke et al., 2007; Franke et al., 2010; Stica et al., 2014; McDermott et al., 2018). Along this margin the SDRs show pronounced variations in width (where *width* is measured as margin-perpendicular distance): In the Pelotas basin they reach widths in excess of 500 km (Stica et al., 2014; McDermott et al., 2018) whereas south of this widths are in the range of 60-180 km (Figure 3.1; Franke et al., 2007; Franke et al., 2010; McDermott et al., 2018). On the African margin the SDRs extend between the Walvis Ridge in the north and the Cape Segment Boundary in the south (Gladczenko et al., 1998; Koopmann et al., 2013). The mapped width of the SDRs on this margin varies between 115-225 km (Koopmann et al., 2013). On the African margin the SDRs have been encountered by several industry boreholes: one in the Walvis Basin (Jackson et al., 2000) and several offshore southern Namibia (Wickens and McLachlan, 1990). All of these wells reveal the SDRs to have a dominantly volcanic

lithology (more detail is given in section 3.2 and in Chapter 2). The A-C1 borehole offshore South Africa (see Fig. 3.4 in section 3.1 for location) also penetrated c. 690 m of basic volcanics prior to reaching crystalline basement (Gerrard and Smith, 1982). Given its location it is likely that this borehole too encountered the landward pinchout of the SDRs.

Analysis of refraction profiles indicate that the African SDRs overlie high velocity/density lower crustal bodies (Bauer et al., 2000; Hirsch et al., 2009) which have been interpreted as the intrusive counterpart to the SDRs. Using constraints from seismic refraction profiles, gravity data has been inverted to demonstrate that these high-velocity bodies are continuous along the SW African margin, with their trend matching that of the SDRs (Maystrenko et al., 2013). Similar methods have been used to demonstrate that high density/velocity bodies underlie the South American SDRs, where they too trend-margin parallel (Autin et al., 2016).

Along both margins, the SDRs are cross-cut by basement heterogeneities known as segment boundaries (Figure 3.1; Clemson et al., 1997; Koopmann et al., 2013) and/or transfer zones (Franke et al., 2007; Collier et al., 2017; McDermott et al., 2018). These features often correlate with along-strike variations in the width of the SDRs and rift-related features (Clemson et al., 1997; Koopmann et al., 2013; Stica et al., 2014; McDermott et al., 2018). This has led to the interpretation that they segmented the rift from its initiation to its breakup (Clemson et al., 1997; Franke et al., 2010; Stica et al., 2014; Koopmann et al., 2014b). Regional variations in the thickness of ‘syn-rift’ packages further support this conclusion (Clemson et al., 1997).

On the African margin, the trend of rift-related features is similar to that of the Pan-African fold-belts mapped onshore (Clemson et al., 1997). Similarly, half-grabens on the proximal part of the margin overlie intra-basement reflectors interpreted as Pan-African thrust-faults (Clemson et al., 1999; Mohammed et al., 2016; Paton et al., 2016). These relationships suggest that structural inheritance controlled both rift-initiation and subsequent strain localisation. It is also notable that the segment boundaries/transfer zones identified offshore correlate with features mapped onshore (Clemson et al., 1997). In these cases, segment boundaries correlate with onshore features that segmented or cross-cut the margin-parallel fold-belts. Hence the location of segment boundaries

demonstrates an additional way that structural inheritance shaped the rifted margin (Clemson et al., 1997). Although less well documented, the structure and segmentation of the South American margin is also often attributed to structural inheritance (Pángaro and Ramos, 2012; Reuber, 2017).

Offshore Argentina and Uruguay there are a series of failed rifts located inboard of the SDRs (Soto et al., 2011; Heine et al., 2013; Autin et al., 2016). These failed rifts are named the Salado and Colorado basins and are highly oblique to the margin-parallel trend of the SDRs (Fig. 3.1). Potential fields modelling and seismic interpretation suggest that the crust is as thin as 15 km beneath part of the Colorado basin (Autin et al., 2016). The presence of these failed rifts on the South American margin results in marked asymmetry when compared to the African conjugate, which contains no comparable features (Autin et al., 2016).

3.2.3 Contrasting interpretations of the South Atlantic magma-rich margins

The nature of the sub-SDR crust in the South Atlantic is a topic of ongoing debate (Stica et al., 2014; Clerc et al., 2015; Geoffroy et al., 2015; Paton et al., 2017; Reuber, 2017; McDermott et al., 2018). Here this is demonstrated by showing different interpretations of a seismic line from offshore Argentina (Figure 3.2a). Two of the interpretations shown (Figure 3.2b and c) are taken directly from previous studies (Paton et al., 2017; McDermott et al., 2018), whilst the others (Figure 3.2a and d) are extrapolated from studies elsewhere along the South American (Clerc et al., 2015) or the African margin (Bauer et al., 2000; Reuber, 2017).

Several authors interpret all of the SDRs to have formed as the uppermost part of thickened oceanic crust (Bauer et al., 2000; Reuber, 2017). This sub-SDR crust is often termed *magmatic crust* (McDermott et al., 2015; Paton et al., 2017; McDermott et al., 2018), however in this section the term oceanic crust is used for simplicity. This interpretation is based on velocities from seismic refraction data (Bauer et al., 2000) and conceptual models from other margins (e.g. Mutter et al., 1982). These interpretations place the boundary/transition between continental and oceanic crust at the first downdip termination of the oldest SDR (Figure 3.2a).

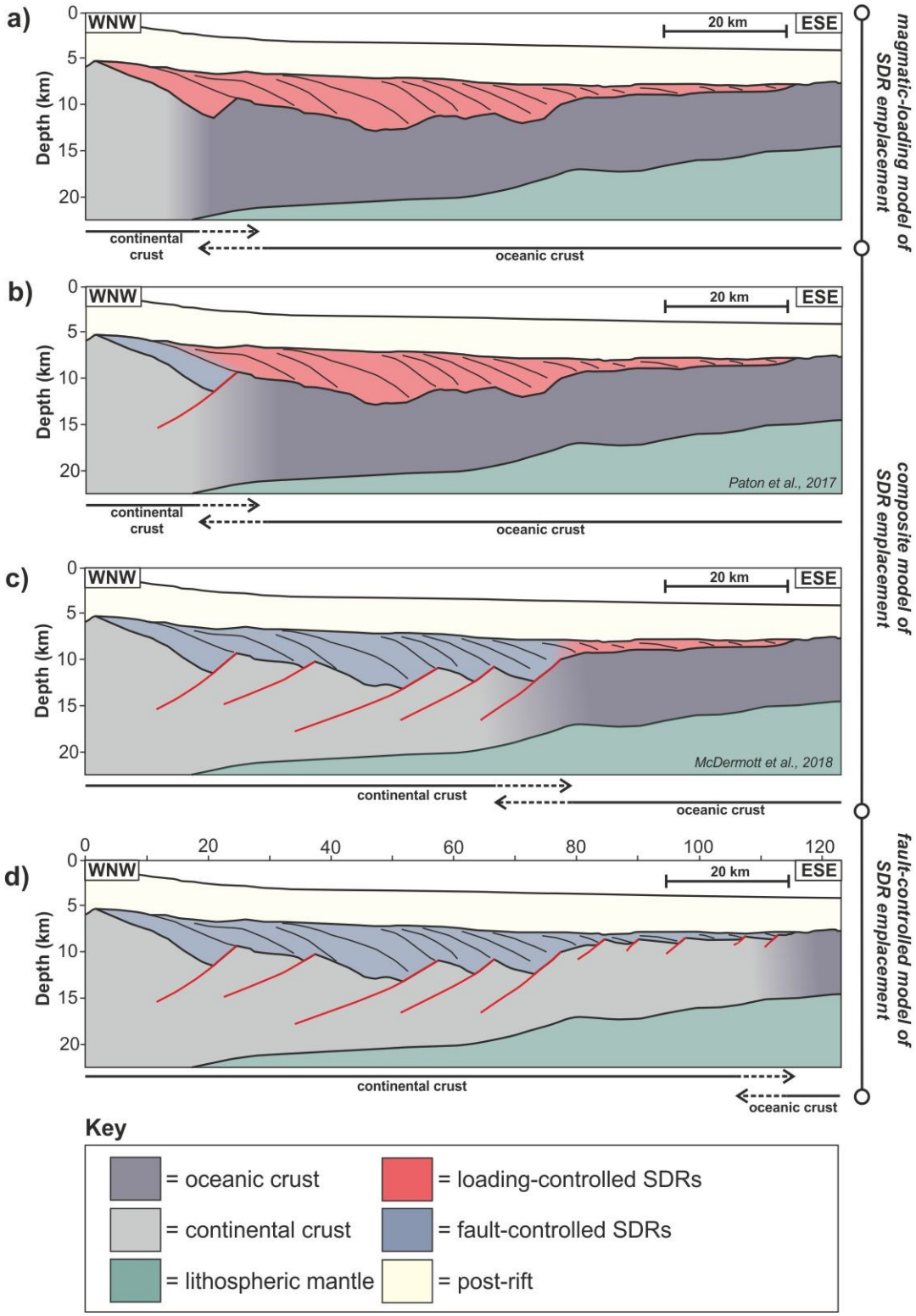

Figure 3.2. Three interpretations of the South American magma-rich margin (line location is shown in Figure 3.1). a) all SDRs are interpreted as loading controlled (based on the interpretations of Bauer et al., 2000 and Reuber, 2017). b) composite interpretation of the SDRs, modified from Paton et al. (2017). c) composite interpretation of the SDRs, modified from McDermott et al. (2018). d) all of the SDRs are interpreted as fault-controlled (based on the interpretation presented in Clerc et al., 2015).

Alternatively, several authors favour a *composite model* of SDR emplacement (section 2.2.2.3), wherein the innermost SDRs were emplaced during continental thinning and the outermost SDRs were emplaced during magmatic accretion (McDermott et al., 2015; Paton et al., 2017; Collier et al., 2017; McDermott et al., 2018). In these models the innermost SDRs are interpreted as fault-controlled, whilst the outermost SDRs are interpreted as loading-controlled (McDermott et al., 2015; Paton et al., 2017; McDermott et al., 2018). The transition from continental to oceanic crust hence occurs at the transition between these two SDR-types (McDermott et al., 2015; Paton et al., 2017; Collier et al., 2017; McDermott et al., 2018). However, different interpretations of the same seismic reflection line place this boundary in markedly different locations (Figure 3.2b and c; Paton et al., 2017; McDermott et al., 2018).

Finally, several authors interpret all of the SDRs to have been emplaced during the thinning of the continental lithosphere (Clerc et al., 2015; Geoffroy et al., 2015). Accordingly the SDRs are interpreted as fault-controlled features that overlie thinned and intruded continental crust (Clerc et al., 2015; Geoffroy et al., 2015). These models place the boundary between the continental crust and oceanic crust at the seaward extent of the SDRs (Figure 3.2d). This places the boundary between continental and oceanic crust up to ≤95 km seawards of the models presented above (Figure 3.2).

Hence, whilst the occurrence and architecture of magma-rich margins in the South Atlantic is well documented, our understanding of crustal structure and composition remains contentious. This leads to large uncertainties in calculating the amount of magmatic material emplaced during and immediately after breakup (Tugend et al., 2018). It also leads to uncertainties in our understanding of magma-rich margin evolution.

3.2.4 Opening of the South Atlantic

The South Atlantic opened from south to north, with a time difference of up to 15 Ma between the earliest (Valanginian) and latest (Barremian) breakup (Heine et al., 2013). This section focuses on the opening of the magma-rich portion of the South Atlantic, which opened across a shorter amount of time (Heine et al., 2013).

The magma-rich margins of the South Atlantic are a result of *Atlantic rifting*, that is, the phase of rifting that resulted in the opening of the South Atlantic (Austin and Uchupi, 1982; Gladczenko et al., 1997; Clemson et al., 1997; Autin et al., 2016; Paton et al., 2016). The margin-parallel trend of the SDRs and other rift-related features indicate that Atlantic Rifting responded to ENE-WSW extension (Blaich et al., 2011; Heine et al., 2013; Franke, 2013). This regional interpretation is supported by recent plate reconstructions indicating a very low angle of obliquity between the modelled extension direction and local rift trend (Brune et al., 2018).

It has been speculated that Atlantic rifting was preceded by earlier phases of extension (Maslanyj et al., 1992; Light et al., 1993; Clemson et al., 1997; Gladczenko et al., 1998; Autin et al., 2016; Paton et al., 2016). The most convincing evidence for this is the presence of the two failed-rifts offshore Uruguay and Argentina (Soto et al., 2011; Autin et al., 2016). The trend of these basins (Figure 3.2) indicate a phase of NNE-SSW oriented extension that preceded the NNE-SSW oriented Atlantic rifting (Autin et al., 2016).

On the African margin, a phase of either Triassic-Mid Jurassic (Clemson et al., 1997) or Permo-Triassic (Gladczenko et al., 1998) rifting has been speculated via the presence of unconformites within rift-related seismic stratigraphy. The trend of this potential earlier rift matches that of the Atlantic rift (Clemson et al., 1997; Gladczenko et al., 1998) and hence indicates a similar extension direction. However, due to a lack of borehole data, the timing and existence of these events remains speculative.

In the southernmost South Atlantic, Atlantic rifting began in the Late Jurassic as has been constrained via offshore drilling (Gerrard and Smith, 1982). In the northern part of the South Atlantic magma-rich margin, rifting is instead thought to have began in the Early Cretaceous (Jackson et al., 2000; Franke, 2013), demonstrating regional diachroneity.

The identification of seafloor spreading anomalies allow for the regional dating of the earliest *normal* oceanic crust (Koopmann, et al., 2014b; Collier et al., 2017). Here, *normal* oceanic crust is defined as crust with a velocity structure and thickness typical of oceanic crust emplaced in a submarine environment. The earliest magnetic chrons within this *normal* oceanic crust young with distance northwards (Figure 3.1), supporting a model of northward oceanic

propagation (Koopmann, et al., 2014b; Collier et al., 2017). A recent study indicates that the oldest chron identified in southernmost South Atlantic is M10r, corresponding to an age of 134.2 Ma. Meanwhile, the oldest chron in the northernmost part of the magma-rich South Atlantic is M3, corresponding to an age of 129.3 Ma (Collier et al., 2017).

Depending on the interpretation of the sub-SDR crust (Figure 3.2), it is debatable whether the age of the earliest *normal* oceanic crust is representative of the age of continental breakup (Collier et al., 2017). Given these uncertainties, these chrons can be considered as providing an estimate of the *latest* possible breakup age in any one location.

3.2.5 An example of plume influenced rifting?

In Chapter 2 (section 2.2.3.1), the role of mantle plumes in generating magma-rich margins was discussed with emphasis on the North Atlantic (e.g. Nielsen et al., 2002; Hopper et al., 2003). The rift-history of the South Atlantic also provides insights into the relationship between rifting and asthenospheric thermal anomalies. This is explained in the underlying text, which also provides context for the discussion on margin asymmetry in Chapter 8.

The occurrence of magma-rich margins in the South Atlantic is commonly attributed to the presence of the Tristan plume (White and McKenzie, 1989; Gladczenko et al., 1997; Bauer et al., 2000; McDermott et al., 2015; Taposeea et al., 2016; Paton et al., 2017; Collier et al., 2017; McDermott et al., 2018). The post-breakup influence of the Tristan Plume on the African and South American plates is evident through the presence of the Walvis Ridge and the Rio Grande Rise (O'Connor and Duncan, 1990). These conjugate aseismic ridges are asymmetric either side of the Mid-Atlantic Ridge, with the Walvis Ridge being longer than the Rio Grande Rise (Figure 3.1). This asymmetry is attributed to the plume migrating from beneath the Mid-Atlantic Ridge to beneath the African plate at c. 70 Ma (O'Connor and Duncan, 1990). Up to the present-day, the plume has remained beneath the African plate, where it is currently centred beneath the volcanic island of Tristan da Cunha (O'Connor and Duncan, 1990).

Recent studies of seafloor spreading anomalies suggest that the diachronous breakup of the South Atlantic was coeval with the emplacement of the onshore Paraná-Etendeka flood basalts, which are also a product of the Tristan Plume

(Collier et al., 2017). This supports a long-held notion that the magmatic material contained by the offshore rifted margins should be considered part of the Paraná-Etendeka large igneous province (Gladczenko et al., 1998).

Despite the temporal and spatial link between the South Atlantic magma-rich margins and the Tristan plume, there are several problems with applying a classic plume model in this region (Blaich et al., 2009; Franke, 2013; Koopmann, et al., 2014b). Based on observations of present-day seafloor swells, plume heads can be considered as having a diameter of c. 2000 km (White and McKenzie, 1989). Within this diameter the potential temperature of the asthenosphere is greatest in the centre, where the narrow (c. 200 km, Fromm et al., 2015) plume stem is located. With increasing distance away from this central point, the potential temperature of the plume head decreases until ambient temperatures are reached after 1000 km (White and McKenzie, 1989).

Prior to flood basalt emplacement (Figure 3.3a), the Tristan plume was centred beneath the conjugate Pelotas and Walvis Basins (Fig. 3.1 shows the location of these basins prior their separation onto conjugate plates, O'Connor and Duncan, 1990; Heine et al., 2013; Fromm et al., 2015; Taposeea et al., 2016; McDermott et al., 2018). This position suggests that there should be a progressive decrease in the amount of magmatic material along the rifted margins to the north and south of these basins. Contrary to this prediction, the margins located directly north of the Walvis Ridge and the Rio Grande Rise are generally classified as magma-poor (Unternehr et al., 2010; Péron-Pinvidic et al., 2015) or 'intermediate' (Reston, 2009; Quirk and Hertle, 2013). Southwards of these conjugate aseismic ridges, magma-rich margins extend for > 2000 km on the African and South American plates (Figure 3.3a). Hence on both margins rift-related magmatic material extends significantly farther than would be expected if the Tristan plume had a diameter of 2000 km (Figure 3.3a).

This distribution has resulted in previous authors questioning the role of a plume in controlling excessive melt-volumes in the South Atlantic (Koopmann et al., 2013; Franke, 2013). Instead it has been suggested that the along-strike segmentation of the rift was the primary control on magmatic activity (Koopmann et al., 2013; Franke, 2013; Koopmann et al., 2014b).

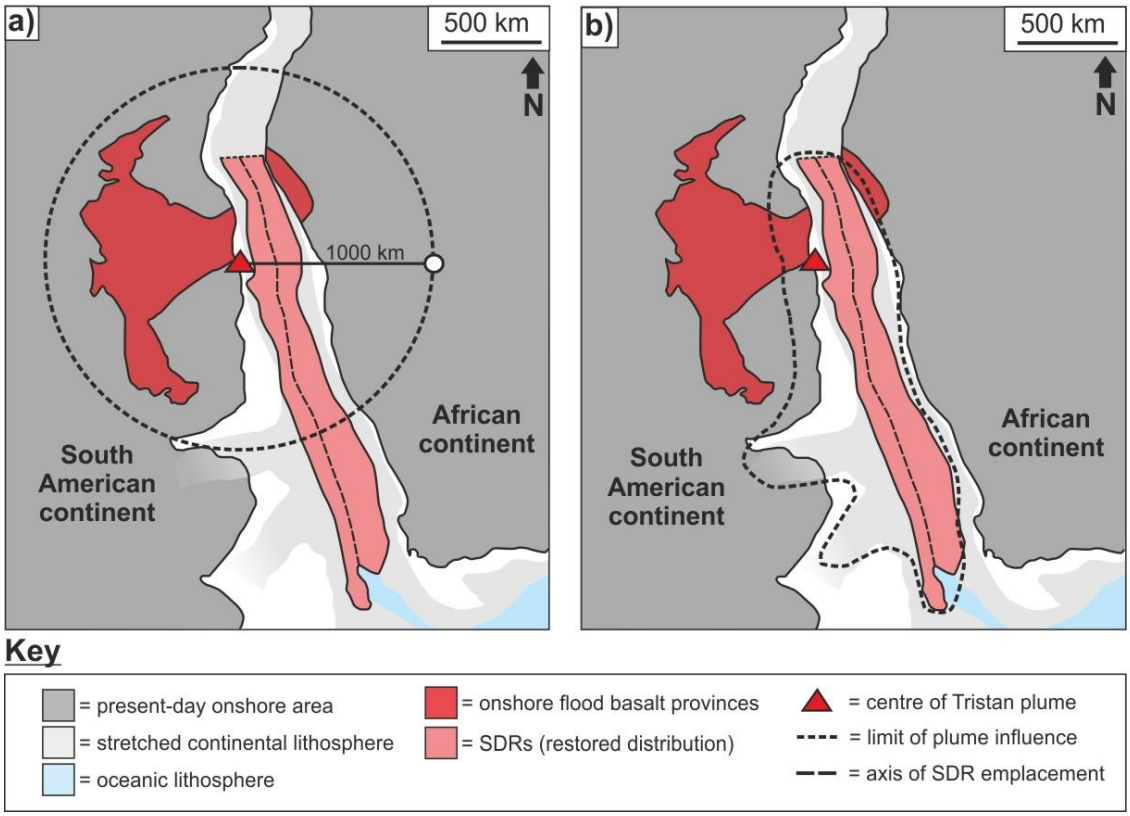

Figure 3.3. Reconstruction of the South Atlantic at 133 Ma. The reconstructed position of the SDRs, present-day onshore areas, oceanic crust, onshore flood basalt provinces, and the centre of the Tristan plume are from Heine et al. (2013). The distribution of thinned continental lithosphere is inferred from the distribution of rift basins in Heine et al. (2013). a) shows a plume with a radius of 2000 km, after White and McKenzie (1989). b) shows a plume that has been channelled southwards by the distribution of thinned continental lithosphere (after Taposeea et al. 2016, and McDermott et al. (2018).

However, studies of the regional distribution of SDRs (McDermott et al., 2018) and oceanic crust (Taposeea et al., 2016; Collier et al., 2017) are supportive of a plume-model, just one that has a different geometry to suggested in White and McKenzie (1989). When studying mantle plumes in the present day, it is simplest to study their influence on oceanic lithosphere (e.g. White and McKenzie, 1989; White et al., 1995; Smallwood and White, 2012). Indeed, it is residual depth anomalies within oceanic crust that indicate plumes have diameters of ≤2000 km (White and McKenzie, 1989). In these settings the plume is impinging against the base of a relatively uniform lithosphere, which contrasts a scenario of impingement against the base of the continental lithosphere (as was mentioned in section 2.2.3.1; Nielsen et al., 2002). In the South Atlantic, both rift-propagation and craton-distribution may have affected lithospheric thickness at the time of plume impingement. Rifting propagated

northwards in the South Atlantic (Jackson et al., 2000) and at the time of plume impingement the area to the south had already undergone thinning (Franke, 2013; Taposeea et al., 2016; Collier et al., 2017). Meanwhile, the lithosphere to the north was relatively thick due to two factors: the presence of the Congo Craton; and, limited lithospheric thinning (Taposeea et al., 2016). Hence it has been proposed that the plume head was channelled southwards (Figure 3.3b), resulting in a sheet of hot asthenosphere beneath the area currently occupied by the conjugate magma-rich margins (Taposeea et al., 2016). Continued extension above this hot-layer would have resulted in igneous bodies observed in the present day (Taposeea et al., 2016).

The main conclusions to be drawn from the distribution of magma-rich margins in the South Atlantic are similar to those presented in Chapter 2 (section 2.2.3.1): that thermal anomalies are required to explain the distribution of magma-rich margins (Nielsen and Hopper, 2002; Armitage and Collier, 2017), but that the distribution observed cannot be explained by a classic plume model.

3.3 The architecture and evolution of the Orange Basin

Now that the regional framework has been provided, our current understanding of the architecture and evolution of the Orange Basin will be discussed. In the present-day this basin is fed by the Orange River, which also marks the westernmost boundary between South African and Namibia (Séranne and Anka, 2005). The basin extends along the SW African margin for approximately 750 km, and is located offshore South Africa and Namibia (Figure 3.4a). As a result of its geographic location, previous studies have tended to focus on either the Namibian (Light et al., 1993; Clemson et al., 1997; Gladczenko et al., 1998; Bauer et al., 2000; Corner et al., 2002; McDermott et al., 2015; Mohammed et al., 2016) or the South African (Muntingh and Brown, 1993; Jungslager, 1999; Blaich et al., 2009; Paton et al., 2016) side of the basin. As a result of this, and despite several cross-border studies (Austin and Uchupi, 1982; Gerrard and Smith, 1982; Blaich et al., 2013; Koopmann et al., 2013), a detailed understanding of regional along-strike variability is lacking.

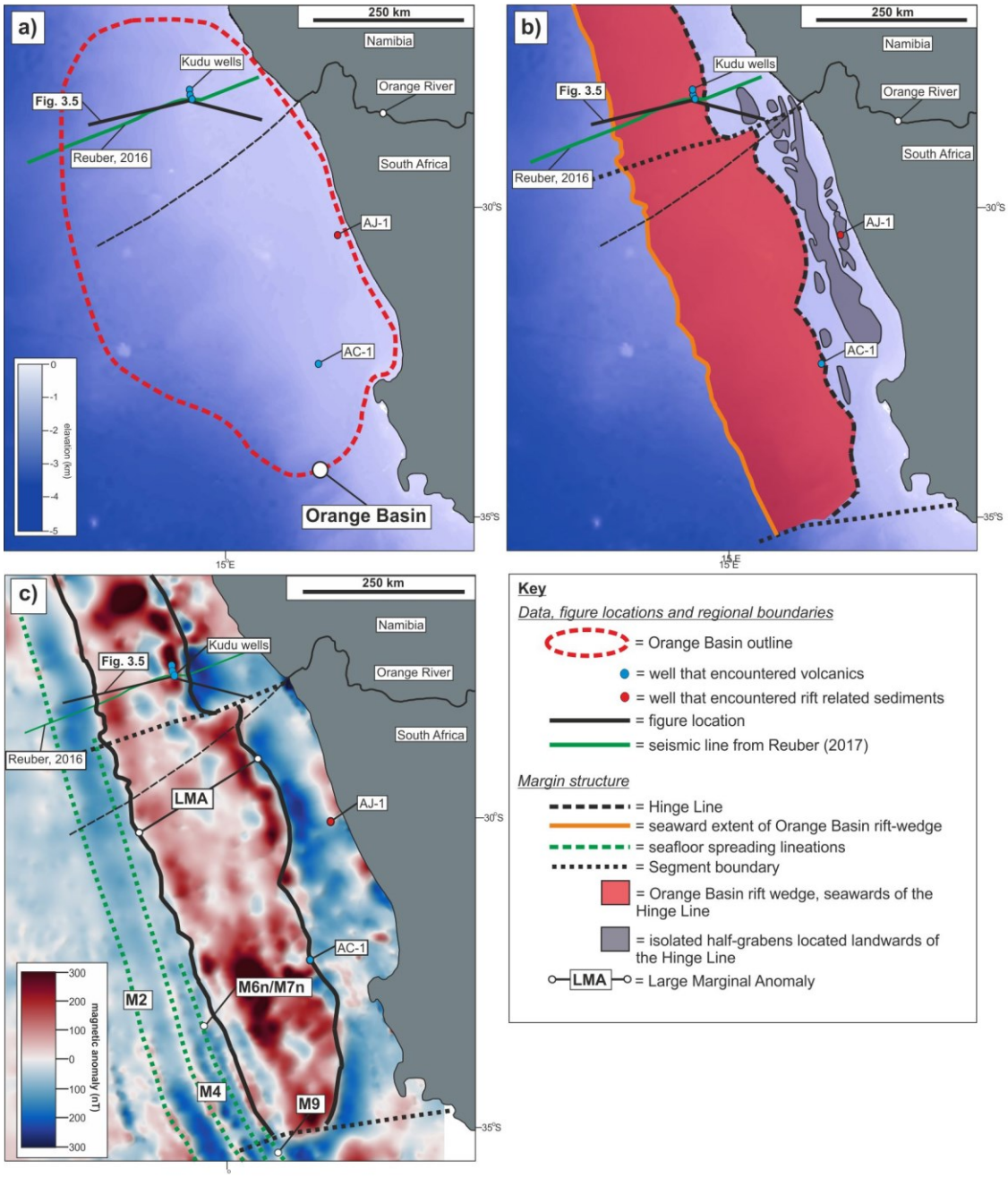

Figure 3.4. a) map showing the approximate outline of the Orange Basin (red-dashed line) and figure locations. b) map showing key regional features and figure locations. c) total magnetic intensity map showing the Large Magnetic Anomaly (LMA) and magnetic chrons (Collier et al., 2017). Symbols, line styles and colours and explained in the key.

3.3.1 Basin architecture

The architecture of the Orange Basin is illustrated on a regional cross section (Figure 3.5a). This cross-section is located through the Namibian Orange Basin and is modified from a seismic reflection profile presented in Mohammed et al. (2016, see line location in Fig. 3.4). The Moho location was correlated onto the line-of-section from a nearby long-recording time long-offset seismic section (Reuber, 2017). The close proximity of the cross-section (Mohammed et al., 2016) and the seismic line (Reuber, 2017) validate this along-strike correlation (Figure 3.4a).

The packages deposited during regional thermal subsidence are separated from those deposited/emplaced during rifting and oceanic accretion via a regional unconformity known as either: *seismic horizon R* (Gerrard and Smith, 1982); *AII* (Austin and Uchupi, 1982); *6At1* (Muntingh and Brown, 1993), *Top Basalt* (Gladczenko et al., 1998); the *Early Cretaceous rift unconformity* (Gladczenko et al., 1998); or, the *Breakup Unconformity* (Granado et al., 2009; Franke, 2013). The use of these latter terms, *Breakup Unconformity* and *Early Cretaceous rift unconformity* can lead to debate as to what process/processes the unconformity records. Here the term *seismic horizon R* (Gerrard and Smith, 1982) is used as it is both objective and regionally applicable.

Throughout this section, the term *basement* is used to describe the crust underlying the packages that were deposited and/or emplaced during rifting and subsequent seafloor spreading (Figure 3.5a). A regionally extensive margin-parallel basement high partitions the rift (Figure 3.5a) and is known either as the Hinge Zone (Austin and Uchupi, 1982), the Medial Hinge Zone (Jungslager, 1999) or the Kudu Basement Ridge (Mohammed et al., 2016). In this chapter the former of these terms is used due to its regional applicability (Figure 3.5a). Landwards of the Hinge Zone are a series of isolated half-grabens (Figure 3.5a) that are bounded by seaward dipping normal faults (Gerrard and Smith, 1982; Light et al., 1993; Jungslager, 1999; Mohammed et al., 2016). Long-offset long-recording seismic reflection data demonstrate that there is significant seaward crustal thinning beneath these isolated half-grabens (Figure 3.5; McDermott et al., 2015; Reuber, 2017). Offshore South Africa, drilling of one such half-grabens (AJ-1; Figure 3.5a) has revealed that the basin fill consists of continental ‘red-beds’ and lacustrine shales (Jungslager, 1999).

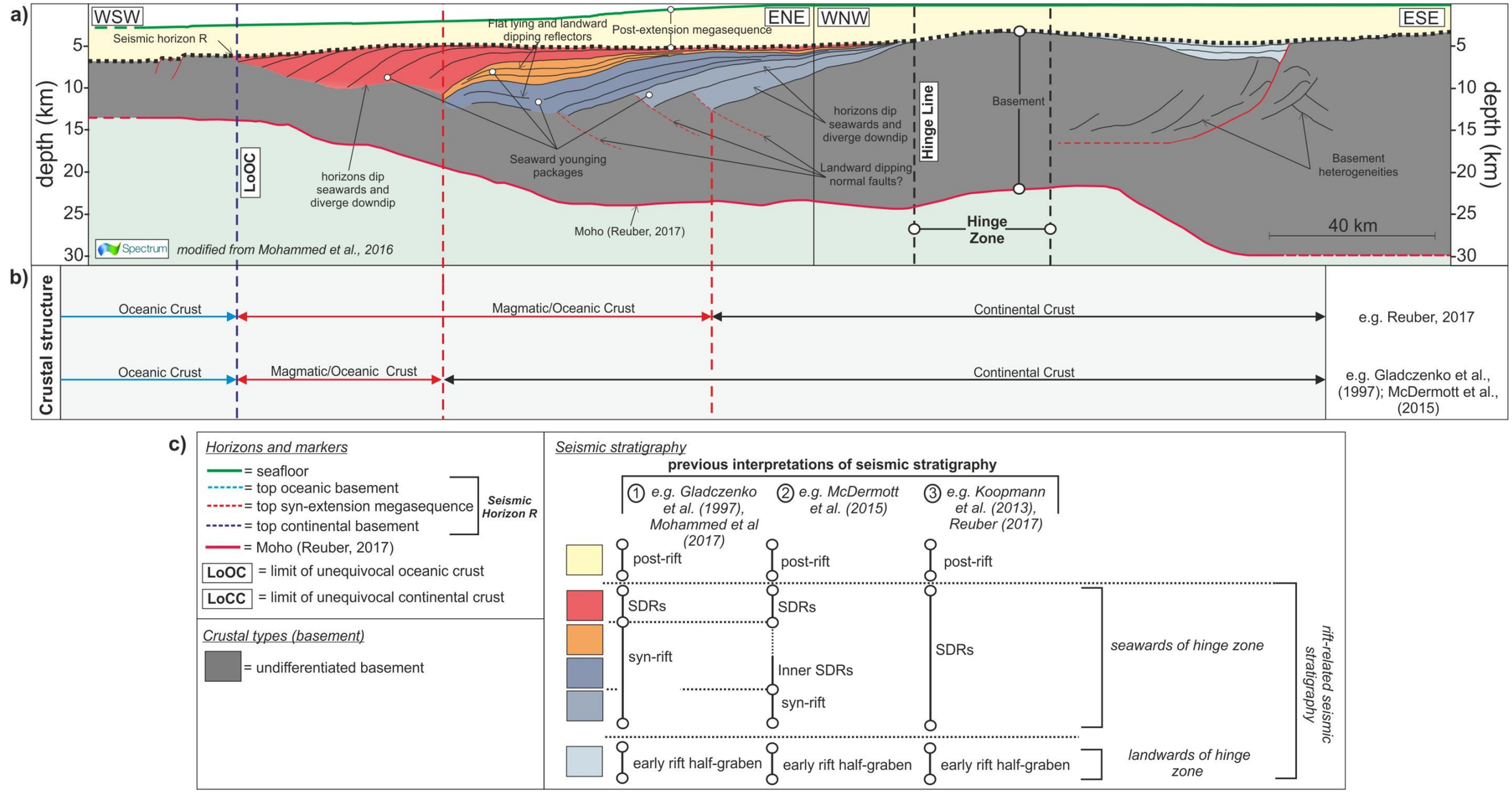

Figure 3.5. Regional cross-section through the Namibian Orange Basin demonstrating the key features of basin architecture, modified from Mohammed et al. (2016) and Reuber (2017). a) regional section (location shown in Fig. 3.4a) displaying crustal structure (Reuber, 2017; Mohammed et al., 2016) and key stratal relationships (Mohammed et al., 2016). b) different interpretations of the crustal structure shown in a). c) key for the horizons, and crustal types and seismic stratigraphy shown in a). Different interpretations of the rift-related stratigraphy are also annotated.

Seawards of the Hinge Zone (Figure 3.5a) is a wedge of seaward-younging packages (Austin and Uchupi, 1982; Clemson et al., 1997; Gladczenko et al., 1998; Bauer et al., 2000; McDermott et al., 2015; Mohammed et al., 2016; Paton et al., 2016; Reuber, 2017) that overlie a zone of major seaward crustal thinning (Bauer et al., 2000; Hirsch et al., 2009; Maystrenko et al., 2013; McDermott et al., 2015; Reuber, 2017). The landward pinchout of this wedge is often referred to as the Hinge Line (Figure 3.5a) and has been mapped across the basin in several previous studies (Figure 3.4b; Gerrard and Smith, 1982; Clemson et al., 1997; Koopmann et al., 2013). The packages comprising this wedge often contain horizons that dip seawards and diverge downdip (Gerrard and Smith, 1982; Austin and Uchupi, 1982; Clemson et al., 1997; Gladczenko et al., 1998; Corner et al., 2002; Koopmann et al., 2013; Mohammed et al., 2016), although relatively flat-lying and landward dipping reflectors have also been identified (Gladczenko et al., 1998; Bauer et al., 2000; Mohammed et al., 2016). Seawards this wedge pinches against crust that is consistently interpreted as oceanic crust (see below; Figure 3.5a and b). The seaward-most extent of this wedge has also been mapped across the region (Gladczenko et al., 1998; Koopmann et al., 2013) and trends approximately margin-parallel (Figure 3.4b). A margin-parallel positive magnetic anomaly, the Large Marginal Anomaly (LMA; Moulin et al., 2010), correlates closely with this wedge and demonstrates that, in places, it has a margin-perpendicular width of over 200 km (Figure 3.4b and c; Koopmann et al., 2013; Collier et al., 2017).

In the Namibian Orange Basin, the rift-related wedge situated seaward of the Hinge Line has been encountered by the Kudu gas field wells (Figure 3.4b). These wells penetrated the uppermost part of the succession, showing it to consist of terrestrial flood basalts, and volcaniclastic and clastic sediments (Wickens and McLachlan, 1990). In the South African side of the basin (Figure 3.4b) the A-C1 borehole, situated slightly seawards of the Hinge Line, encountered c. 690 m of basaltic lava flows interbedded with sediments and pyroclastic layers (Gerrard and Smith, 1982). The wedge was also drilled further north along the Namibian margin, where again a dominantly volcanic succession was encountered (Jackson et al., 2000; McDermott et al., 2015).

Seawards of this wedge, seismic horizon R is flat-lying and defines the top of a new crustal type characterised by thicknesses of ≤7.5 km (Figure 3.5a). In

seismic reflection data this crust has been described as largely featureless (Gladczenko et al., 1997). Seismic horizon R is occasionally offset by normal faults, the occurrence of which becomes more common with distance seawards (McDermott et al., 2015). The analysis of seismic refraction (Bauer et al., 2000; Hirsch et al., 2009) and potential fields (Hirsch et al., 2009; Maystrenko et al., 2013; Collier et al., 2017) data indicate that this is *oceanic crust* (Figure 3.5a and b). That landward most limit of this unequivocal oceanic crust is often referred as the LoOC (*limit of oceanic crust*).

3.3.2 Previous interpretations of margin structure

Previous interpretations of the Orange Basin rift-structure have been juxtaposed onto the regional cross-section (Figure 3.5b and c). These interpretations were correlated onto the cross-section from published maps (Gladczenko et al., 1998; Koopmann et al., 2013), interpreted seismic sections (Gladczenko et al., 1998; McDermott et al., 2015; Reuber, 2017), and regional cross-sections (Gladczenko et al., 1998; Jungslager, 1999).

Interpretations of the zone of isolated half-grabens lying inboard of the Hinge Zone have remained relatively consistent across different studies (Figure 3.5b and c). They are interpreted as forming early during the rifting process (Gerrard and Smith, 1982; Jungslager, 1999; Mohammed et al., 2016; Paton et al., 2016) and here are annotated as *early rift half-grabens* (Figure 3.5c). The normal faults controlling these half-grabens overlie basement heterogeneities (Figure 3.5a) interpreted as pre-rift compressional features (Light et al., 1993; Mohammed et al., 2016; Paton et al., 2016; Reuber, 2017). This suggests that during the early stages of rifting, extension was accommodated by the reactivation of pre-existing structures (Mohammed et al., 2016; Paton et al., 2016; Reuber, 2017).

The interpretation of the rift-related wedge located seawards of the Hinge Zone is more contentious (Figure 3.5c). This wedge of reflectors is consistently separated into a series of seaward-stepping and seaward-younging packages (Light et al., 1993; Clemson et al., 1997; Gladczenko et al., 1998; Bauer et al., 2000; McDermott et al., 2015; Mohammed et al., 2016; Paton et al., 2016). Whilst the structural position of these different packages remains relatively

consistent across different studies (Figure 3.5a), they have been interpreted in a number of different ways (Figure 3.5c).

The bulk lithology of the wedge, as can be constrained by geological and geophysical data, can be used to constrain these different interpretations. As is mentioned above, drilling has consistently encountered successions that consist mainly of basic volcanics (Wickens and McLachlan, 1990; Jungslager, 1999). A dominantly volcanic lithology is also supported by the interpretation of regional magnetic grids. The spatial correlation between the LMA and this wedge (Figure 3.4c) suggests that their composition is, at least in part, responsible for this positive magnetic anomaly. Several authors have used geometries picked from seismic reflection data to forward-model the LMA (Bauer et al., 2000; Corner et al., 2002; Koopmann, et al., 2014b; Collier et al., 2017). Two of these studies have used profiles from further north along the Namibian magma-rich margin (Bauer et al., 2000; Corner et al., 2002), however given the regional continuity of these features (Gladczenko et al., 1998; Corner et al., 2002; Moulin et al., 2010; Koopmann et al., 2013; Koopmann et al., 2014b; Collier et al., 2017) the findings are still applicable to the Orange Basin.

The LMA consists of a long-wavelength high-amplitude positive magnetic anomaly, and a series of shorter-wavelength anomalies that are superimposed on this (Collier et al., 2017). Collier et al. (2017) use several profiles from the SW African magma-rich margin to demonstrate that the amplitude and wavelength of the LMA can be reproduced via a uniformly magnetised wedge of basalt, the geometry of this wedge was constrained by seismic reflection data. It was also demonstrated that the influence of basement dykes on the LMA would be relatively minor in comparison that from the overlying volcanics (Collier et al., 2017), suggesting that the anomaly is not the result of a deeper ‘crustal’ magnetic source. In Collier et al. (2017) it proved difficult to match the shorter wavelength anomalies, and other studies produced a closer match by modelling changes of magnetic polarity within the volcanics (Bauer et al., 2000; Koopmann, et al., 2014b). Failures to exactly match these short wavelength anomalies may also be explained by the presence of intercalated sediments (Corner et al., 2002) or basement dykes (Collier et al., 2017). However, the importance of these studies lies not in obtaining a precise match, but in showing that the long wavelength component of the LMA requires these packages to

consist predominantly of basic volcanics. This does not rule out the possibility that certain parts of the succession, spatially and/or temporally, may be more clastic-dominated, but it does provide a regional context within which interpretations should be grounded. Several early studies of the Namibian Margin (Maslanyj et al., 1992; Light et al., 1993) interpreted the packages comprising this wedge to consist almost entirely of clastic material (i.e. the packages coloured light blue, dark blue, and orange in Fig. 3.5a), with only the uppermost layers (the package coloured red in Fig. 3.5a) being volcanic. Interpretations such as this are problematic in light of the evidence presented above.

Interpretations that do account for the volcanic nature the succession located seaward of Hinge Zone fall into three categories (Figure 3.5c). Firstly (see *previous interpretations of seismic stratigraphy* 1 in Figure 3.5c), the innermost packages are interpreted as *syn-rift*, and the outer as *SDRs* (Gladczenko et al., 1998; Mohammed et al., 2016; Paton et al., 2016). These interpretations suggest that the innermost packages, the *syn-rift*, terminate downip against landward dipping normal faults (annotated on Figure 3.5a). The SDRs meanwhile are interpreted as loading related features. In the second interpretation category (*see previous interpretations of seismic stratigraphy* 2, in Figure 3.5c, the wedge is divided into *syn-rift*, *Inner SDRs* and *Outer SDRs* (Bauer et al., 2000; Blaich et al., 2011; McDermott et al., 2015). In these models, the *Inner SDRs* are interpreted as fault-controlled and the *Outer SDRs* as loading controlled (McDermott et al., 2015). It has also been suggested that the *Inner SDRs* are more clastic-rich than the *Outer SDRs* (McDermott et al., 2015). In the third interpretation category (see *previous interpretations of seismic stratigraphy* 3 in Figure 3.5), the entire succession is interpreted as *SDRs* (Granado et al., 2009; Koopmann et al., 2013; Franke, 2013; Becker et al., 2014; Koopmann et al., 2014; Reuber, 2017).

These contrasting interpretations of stratal geometry correlate with differing interpretations of crustal structure (Figure 3.5b). Models assuming that the entire succession consists of SDRs interpret the underlying crust as new oceanic crust (Reuber, 2017), often named *magmatic crust* (Figure 3.5b, Reuber, 2017; Paton et al., 2017). Meanwhile, interpretations including *syn-rift* packages assume that they overlie stretched continental crust (Figure 3.5b),

resulting in a narrower zone of oceanic/magmatic crust (Gladczenko et al., 1998; McDermott et al., 2015).

3.3.3 Timing constraints

In the Orange Basin the onset Atlantic rifting is highly uncertain (Heine et al., 2013). This is because the boreholes that penetrate the rift-related succession either do not reach its base (Wickens and McLachlan, 1990; Jungslager, 1999) or were unable to date the volcanic rocks encountered (Gerrard and Smith, 1982). In the absence of these constraints, the onset of rifting is generally considered as occurring between 160-140 Ma, during the Late Jurassic (Jackson et al., 2000; Franke, 2013).

As was described above, the earliest *normal* oceanic crust can be dated by the interpretation of linear magnetic anomalies (Koopmann et al., 2014b; Collier et al., 2017). This oceanic crust is located immediately seawards of the SDRs, which may also overlie oceanic/magmatic crust (Gladczenko et al., 1998; McDermott et al., 2015; Collier et al., 2017). Regardless of the nature of the sub-SDR crust, the date of the earliest *normal* oceanic crust also records the end-of SDR emplacement. In the southernmost part of the Orange Basin, forward modelling of a 2D ship-track line suggests that the oldest chron present is M10r, giving an age of 134.2 Ma (Collier et al., 2017). In the northern part of the Orange Basin the oldest chron is M4, giving an age of 130.6 Ma (Collier et al., 2017).

Hence the Orange Basin syn-rift succession and SDRs can be considered as forming between 160-140 Ma (Jackson et al., 2000) and 134.2-130.6 Ma (Collier et al., 2017). The time at which SDR emplacement began within this broad time-range is uncertain.

Chapter 4 Data and methods

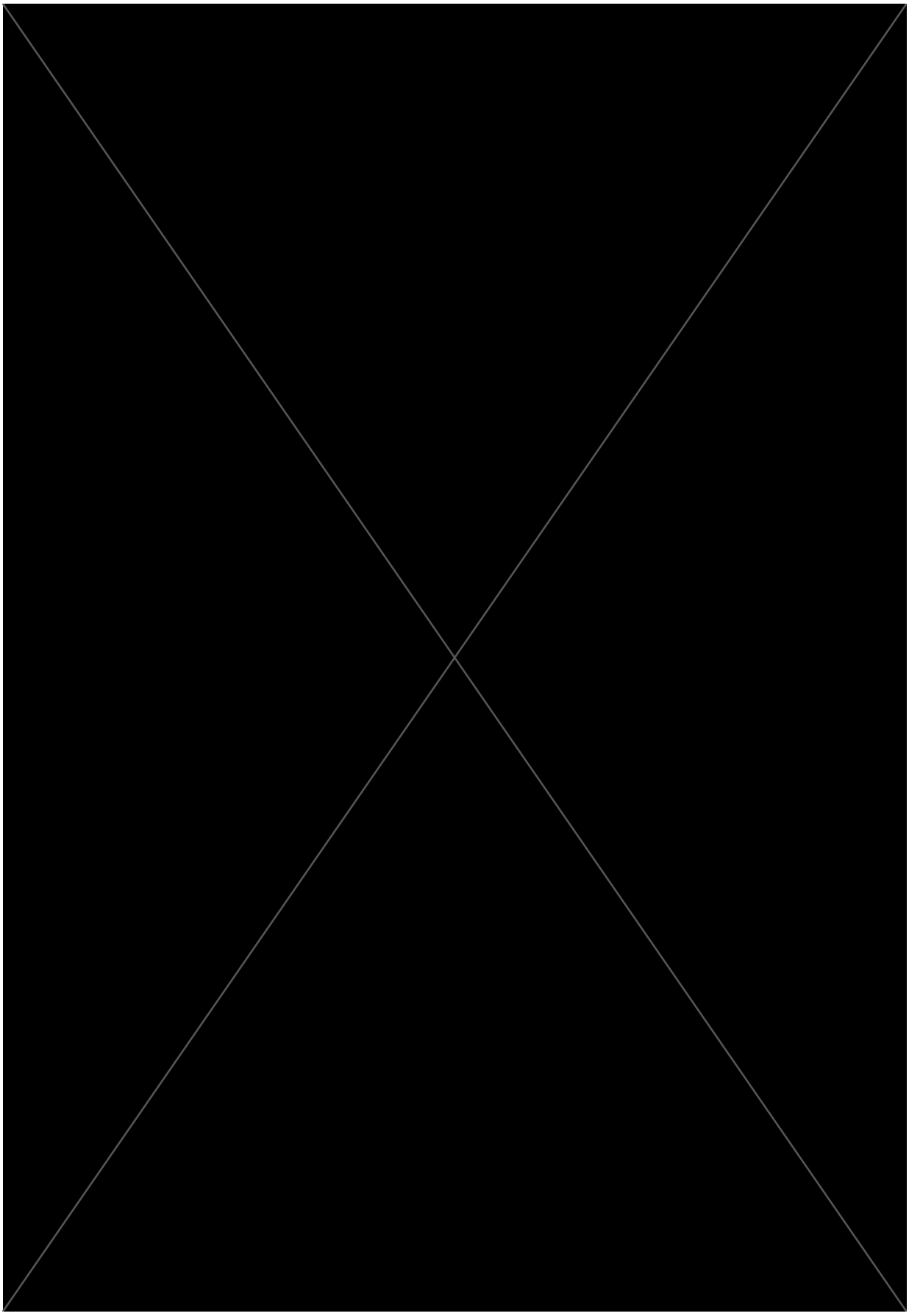

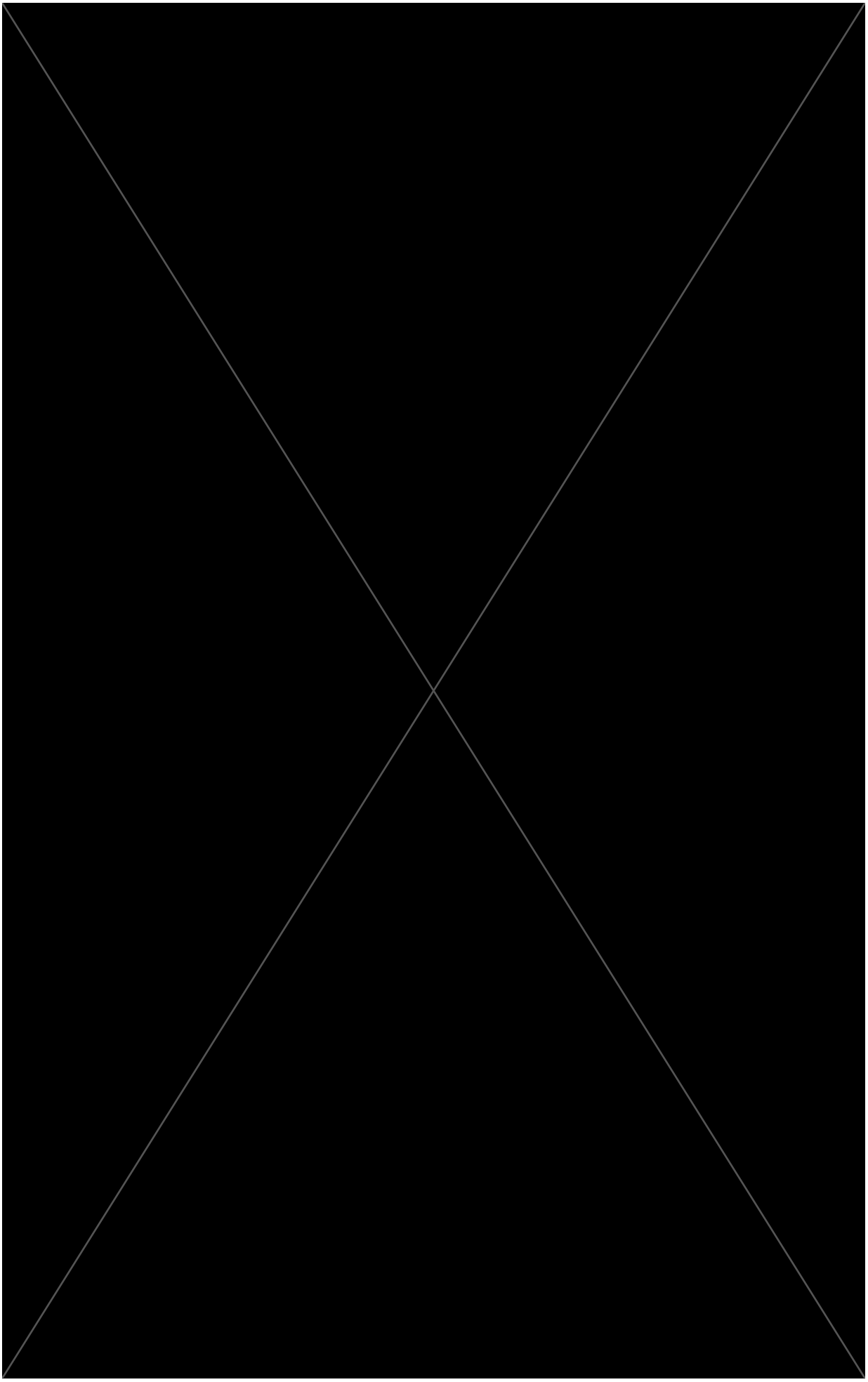

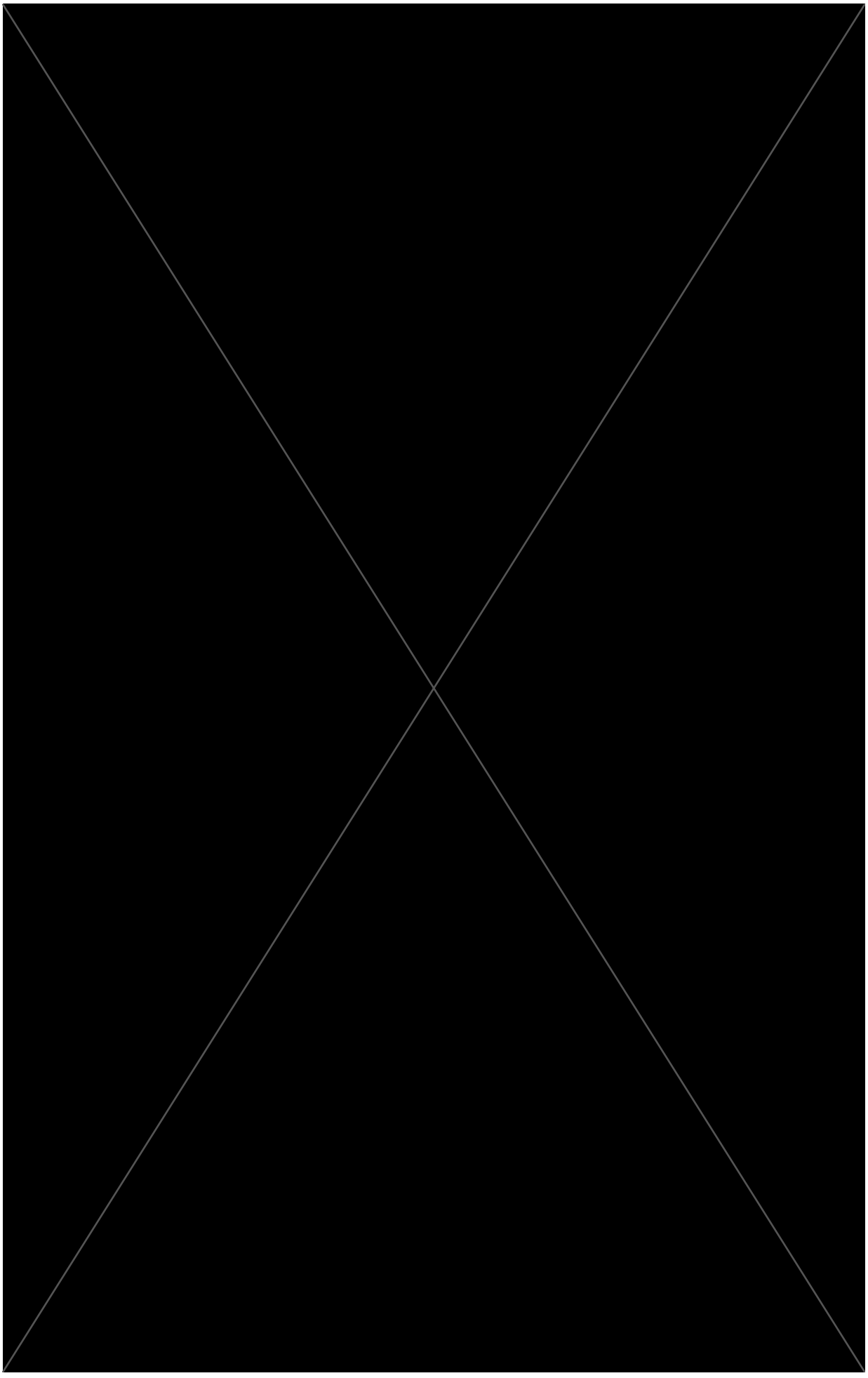

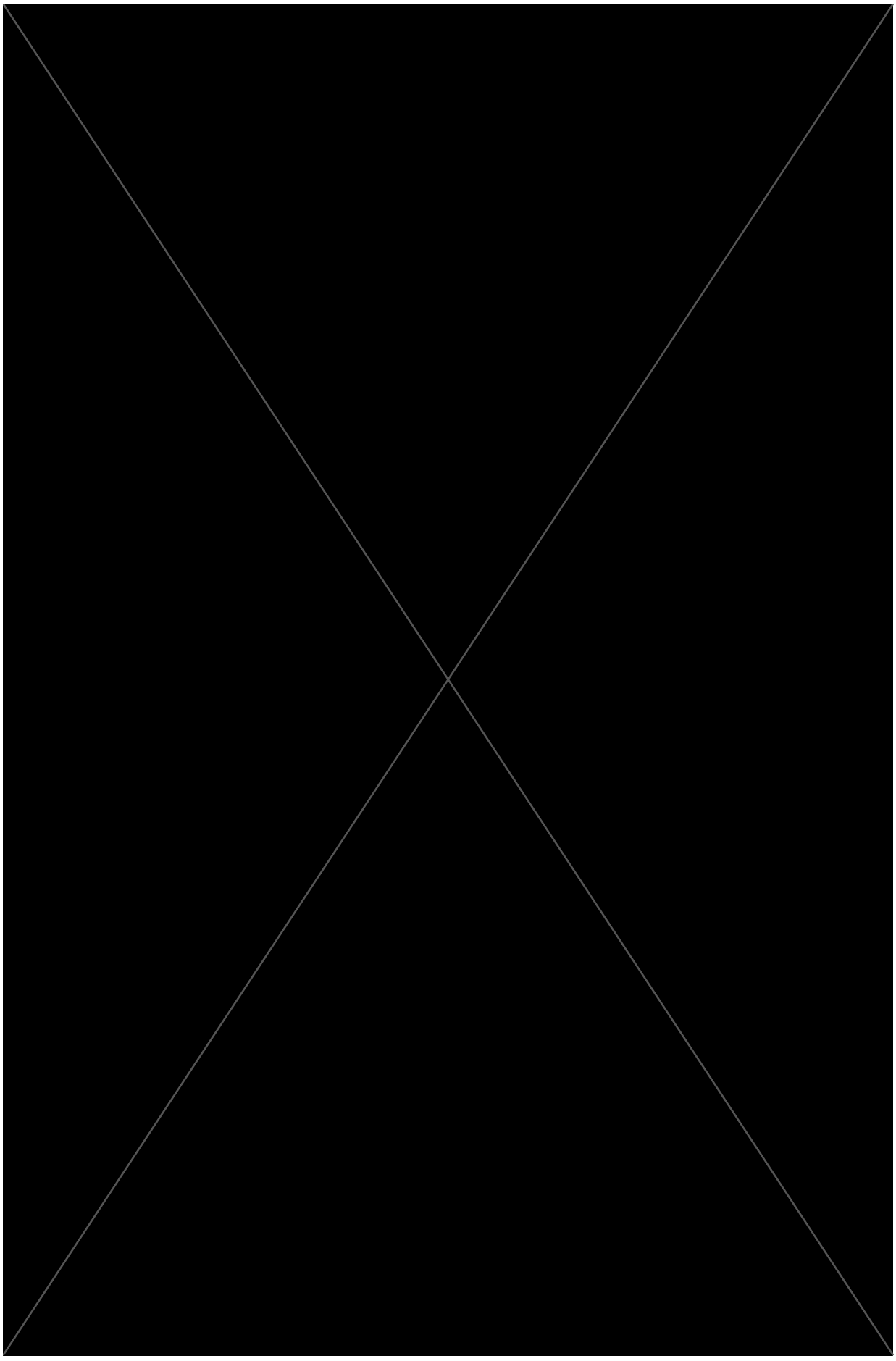

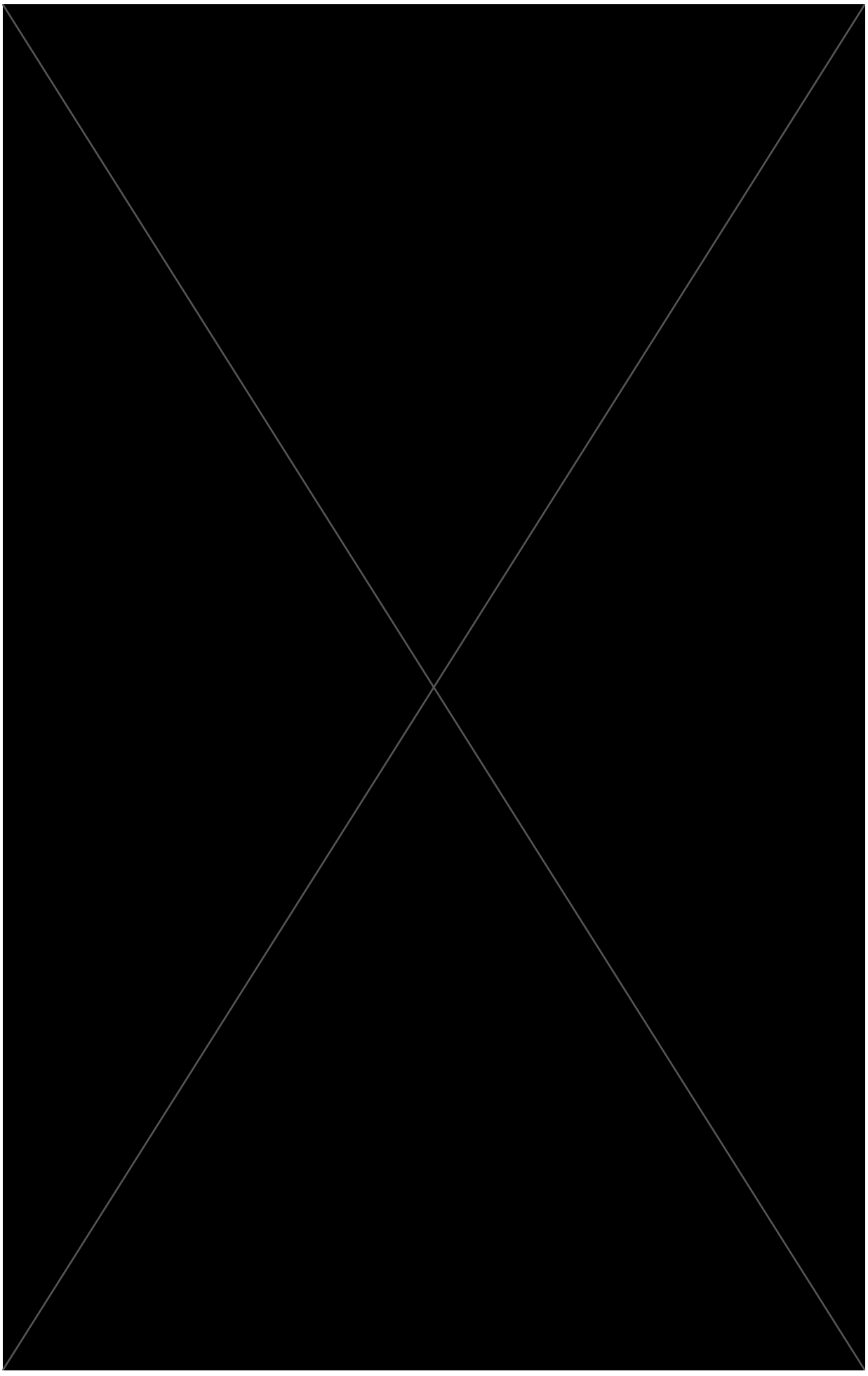

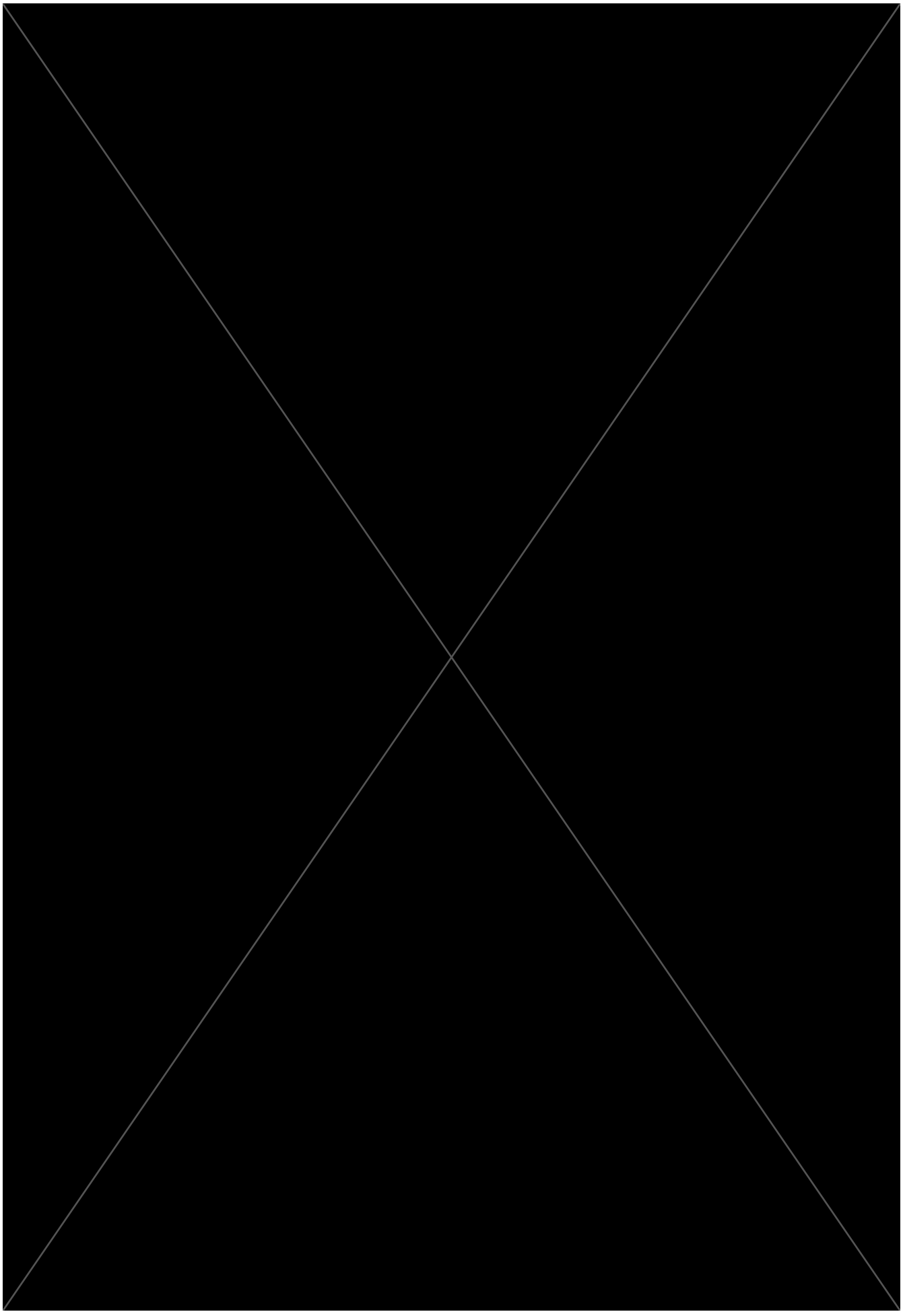

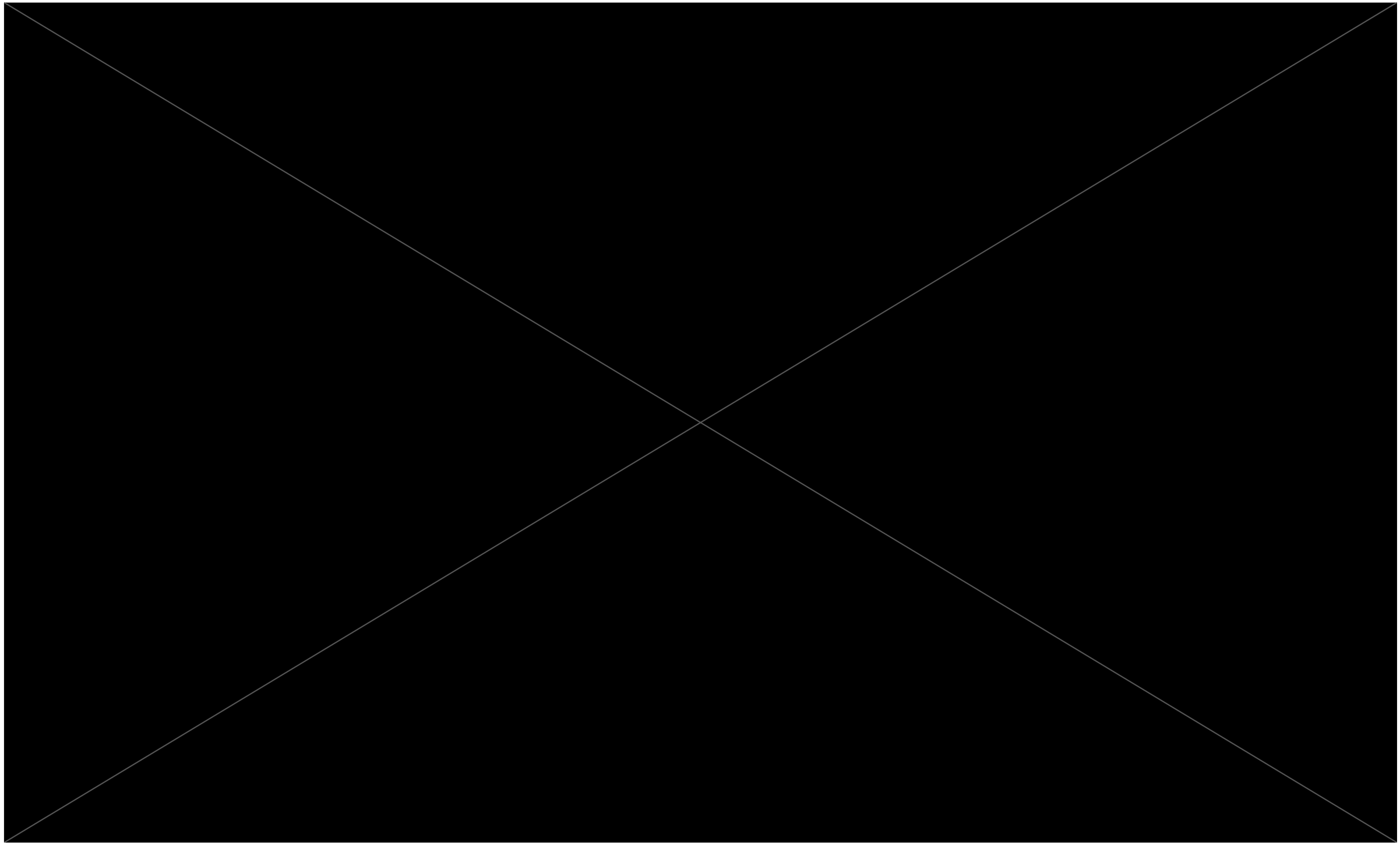

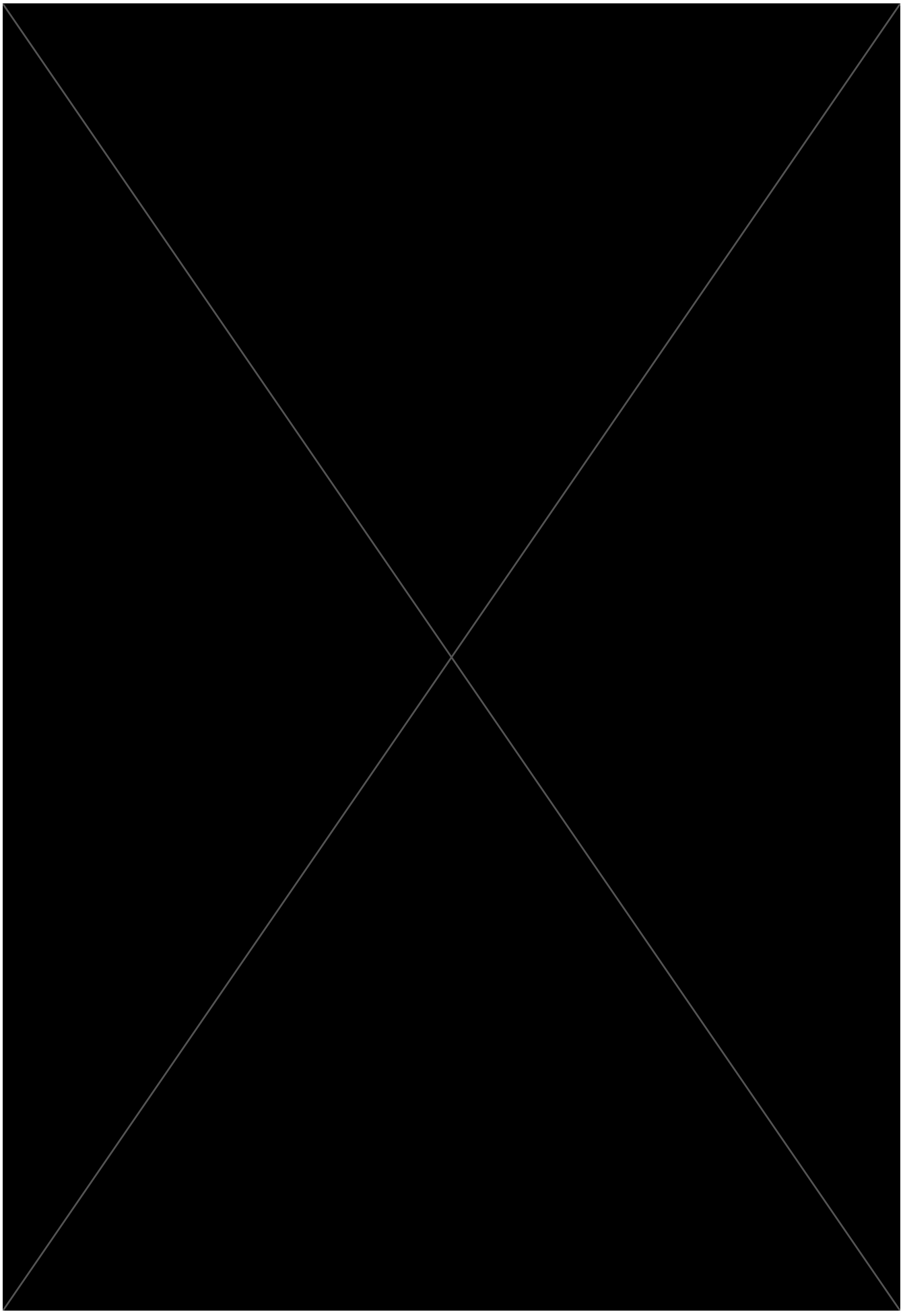

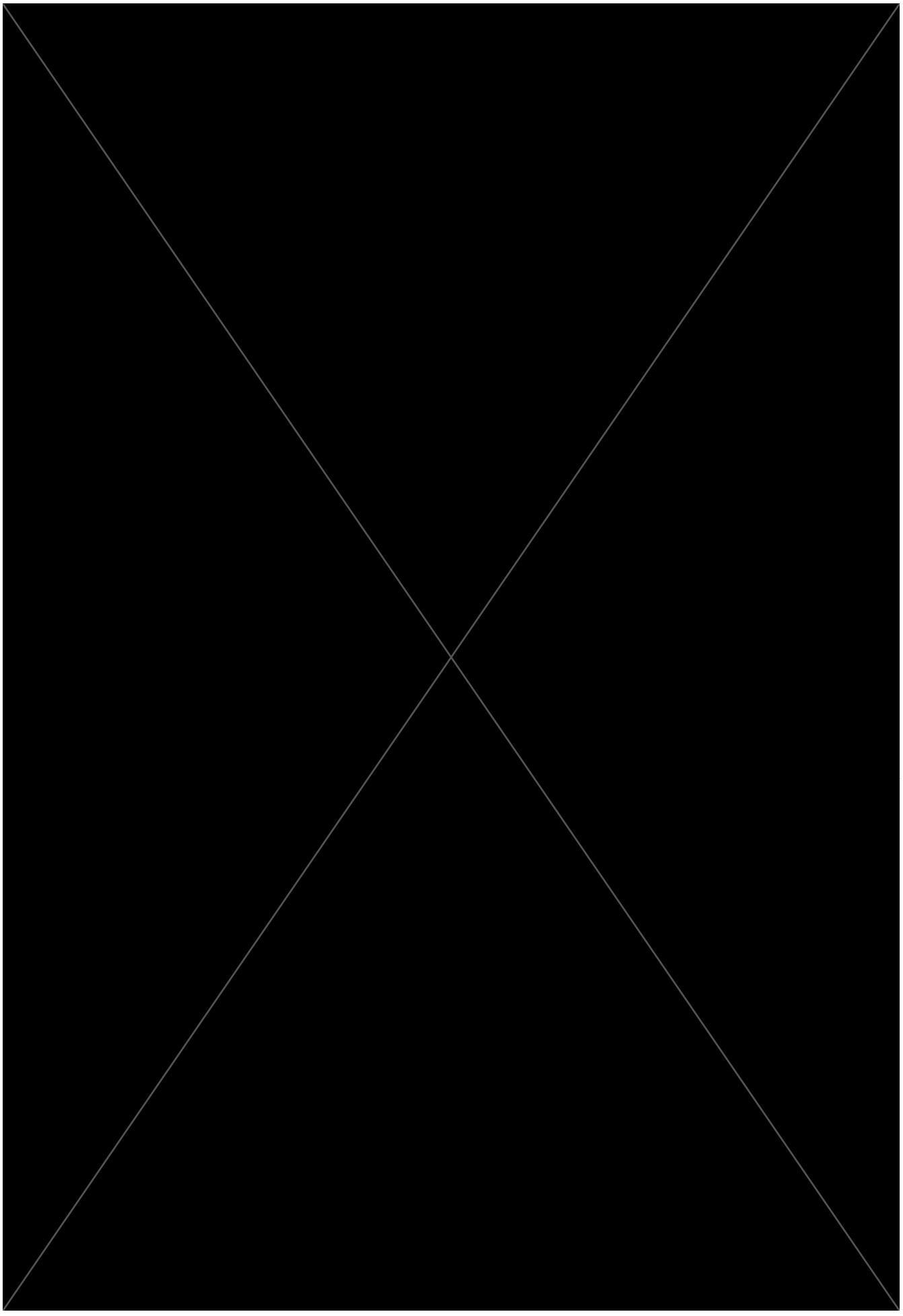

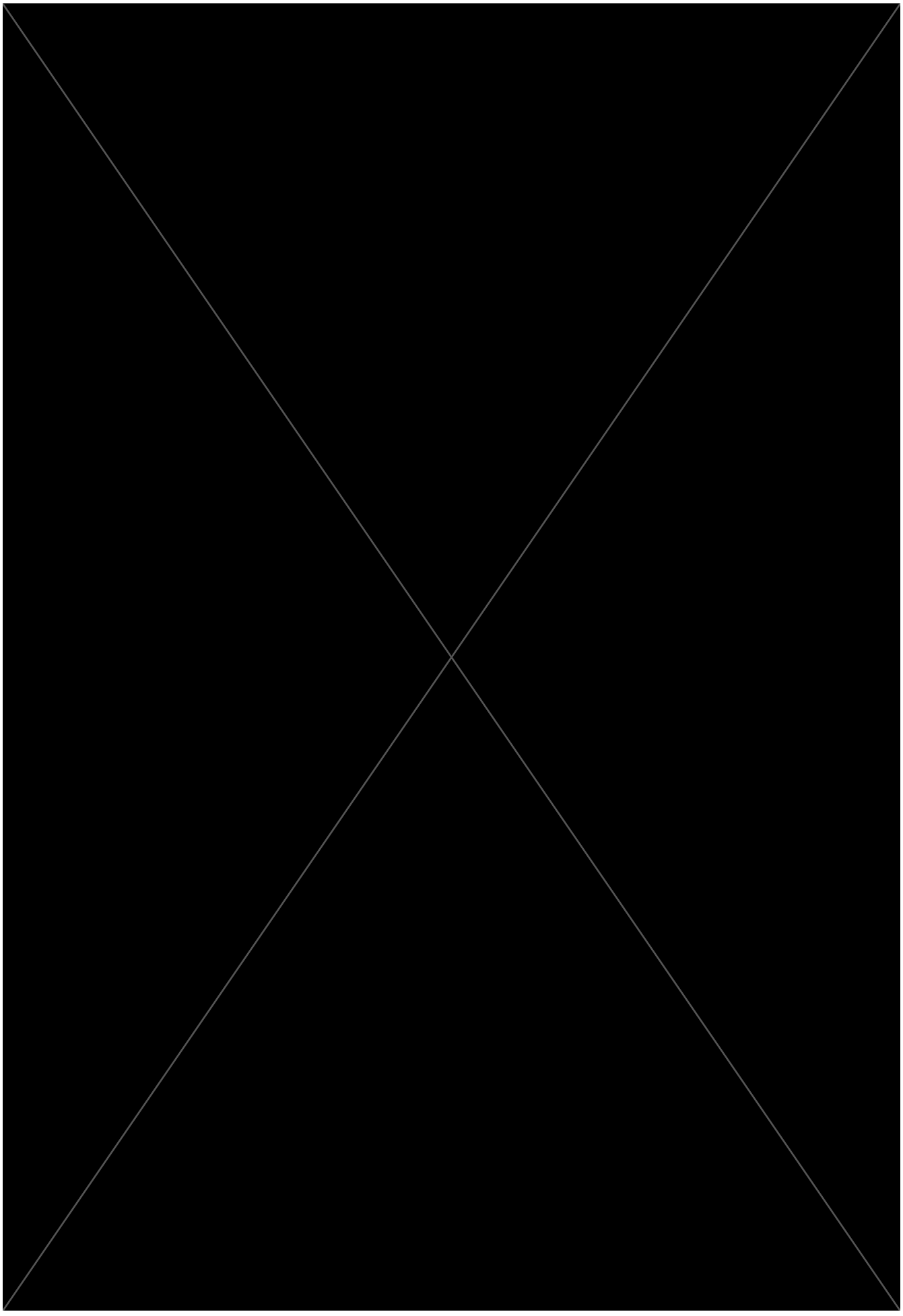

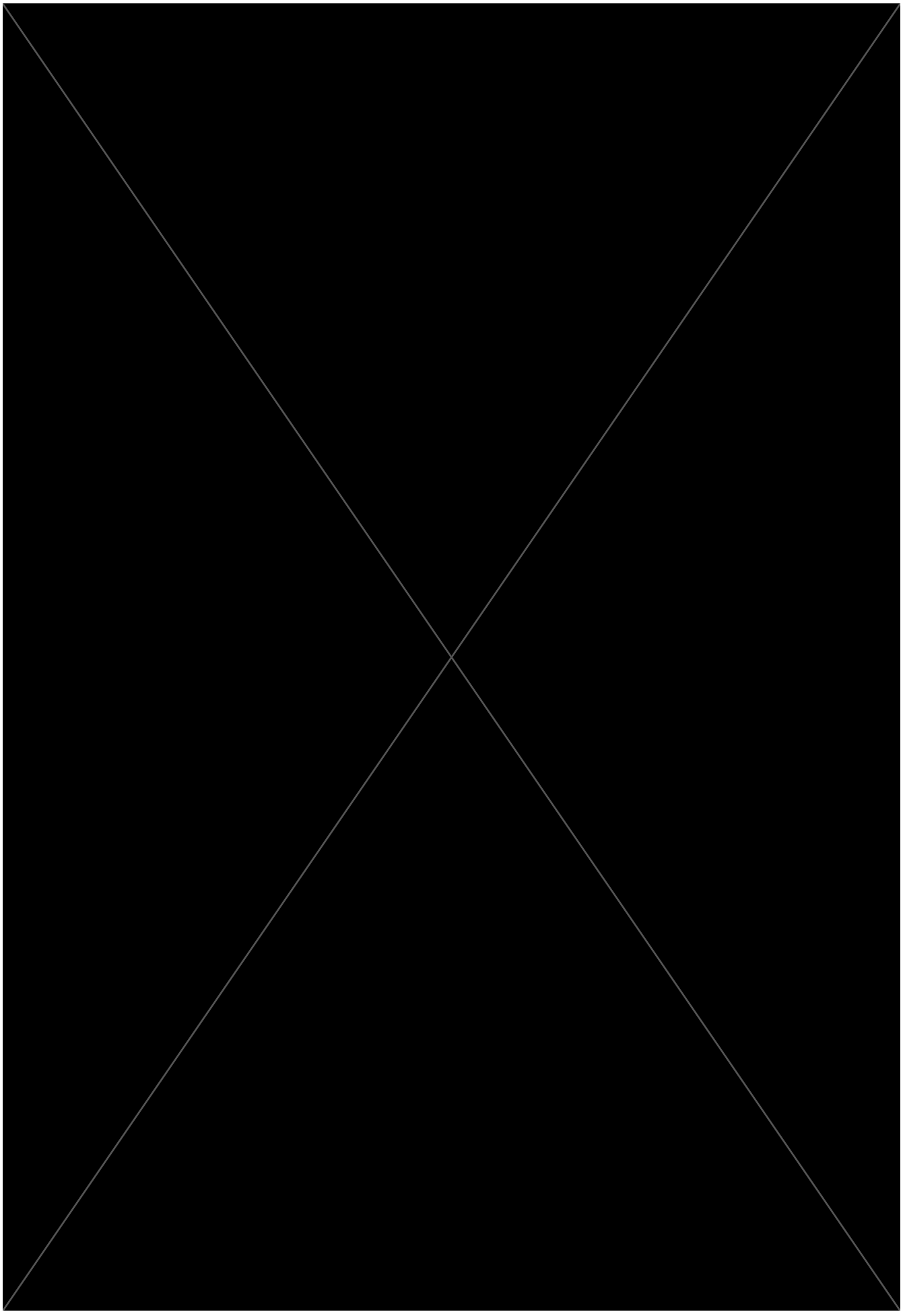

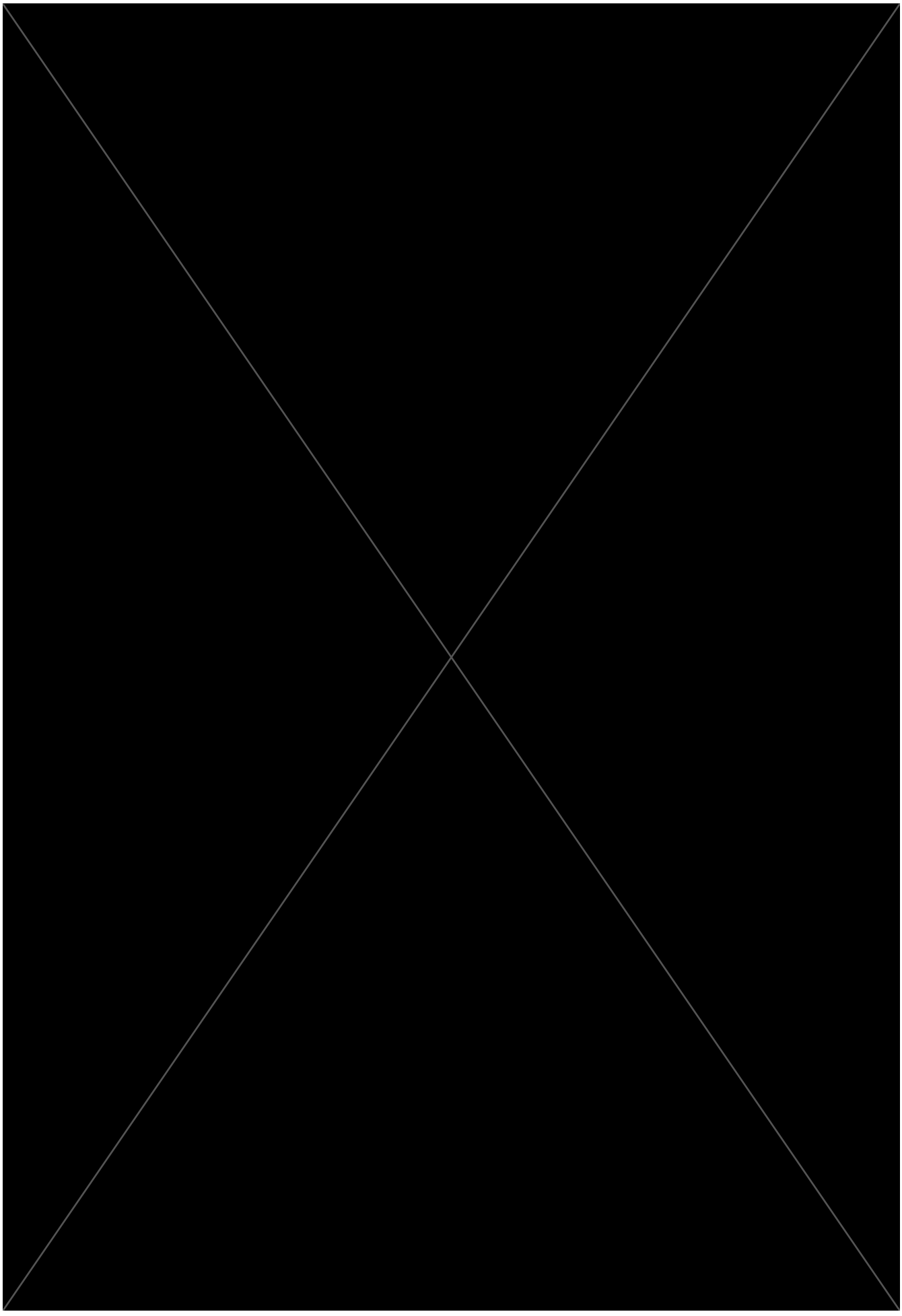

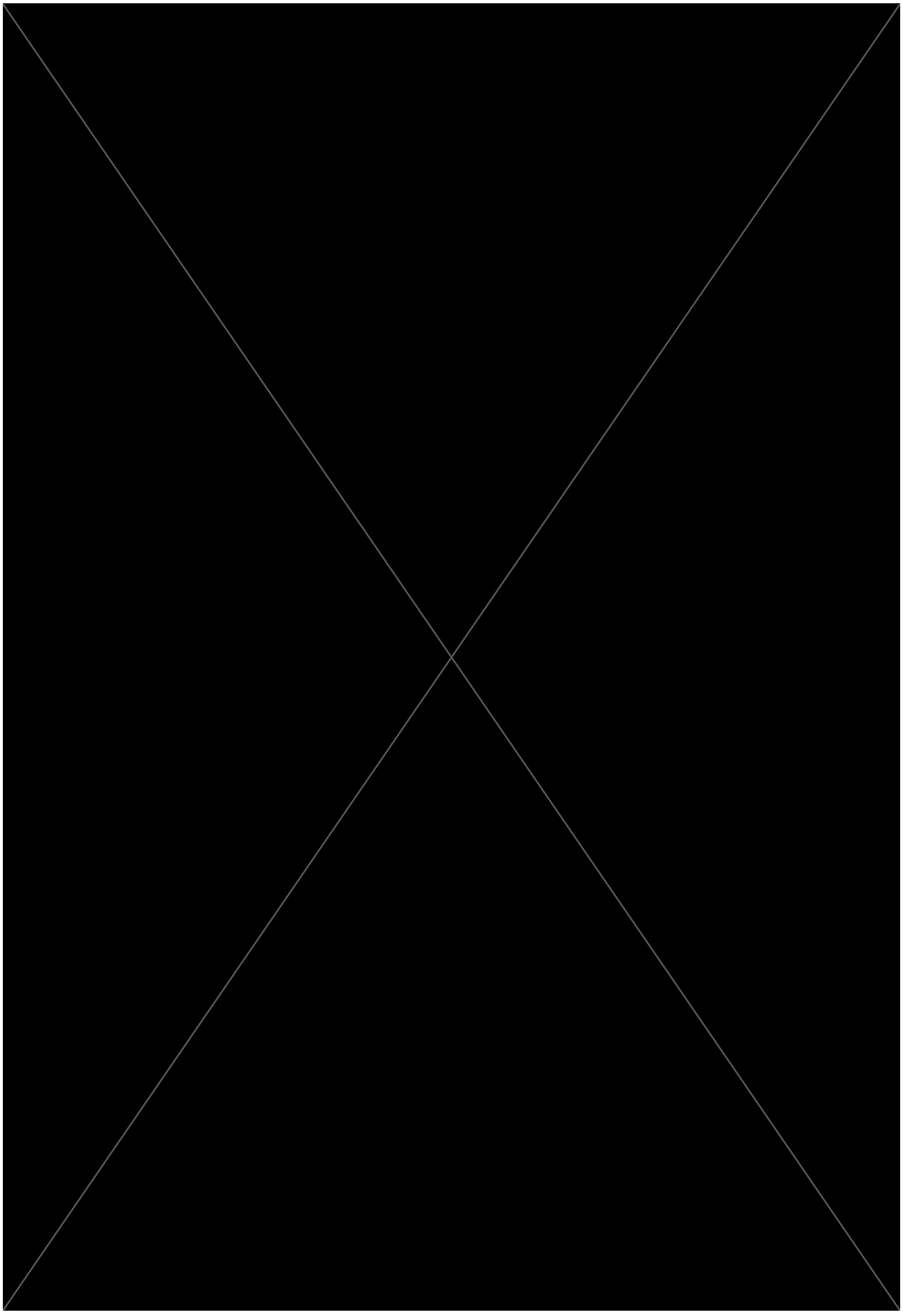

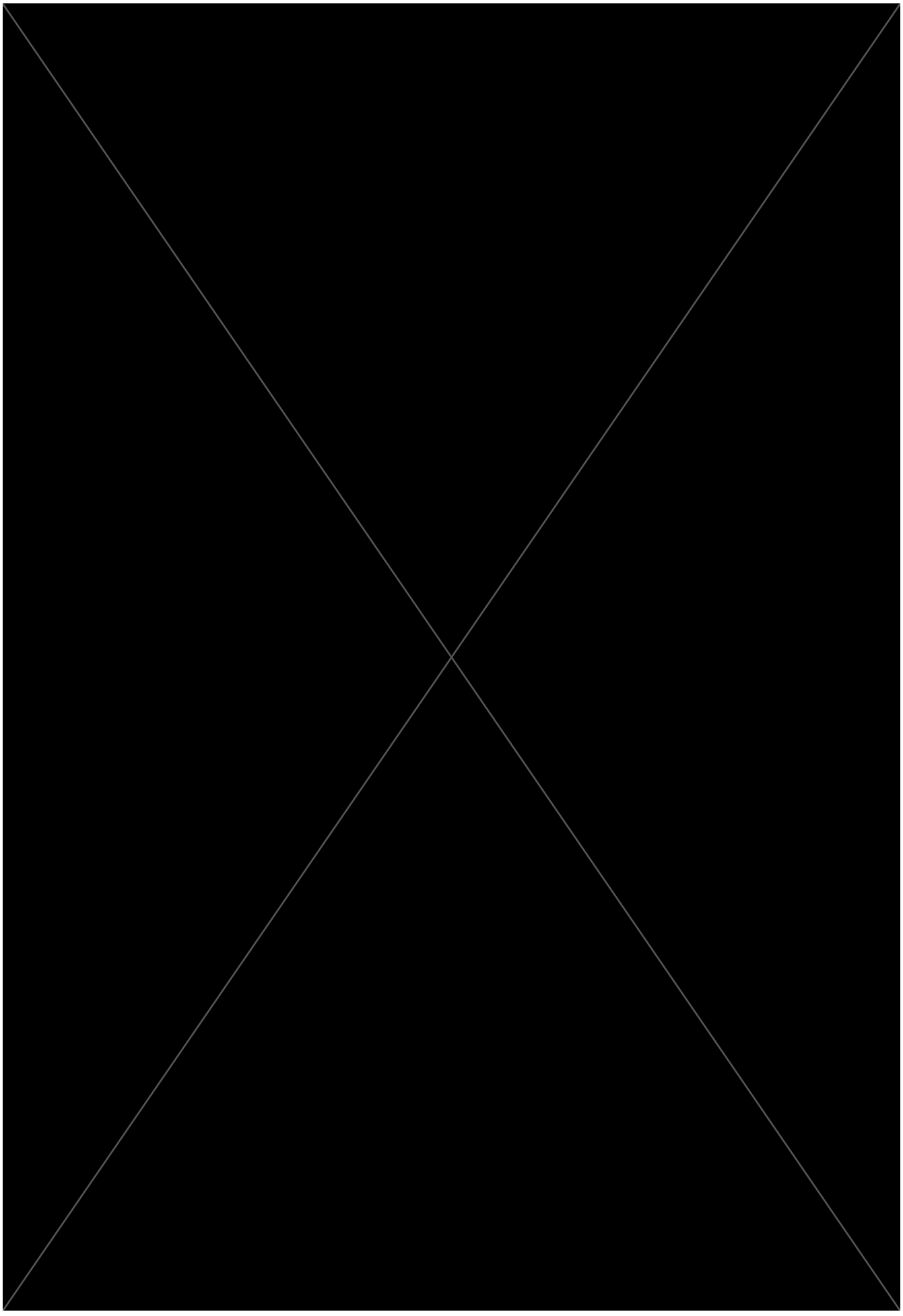

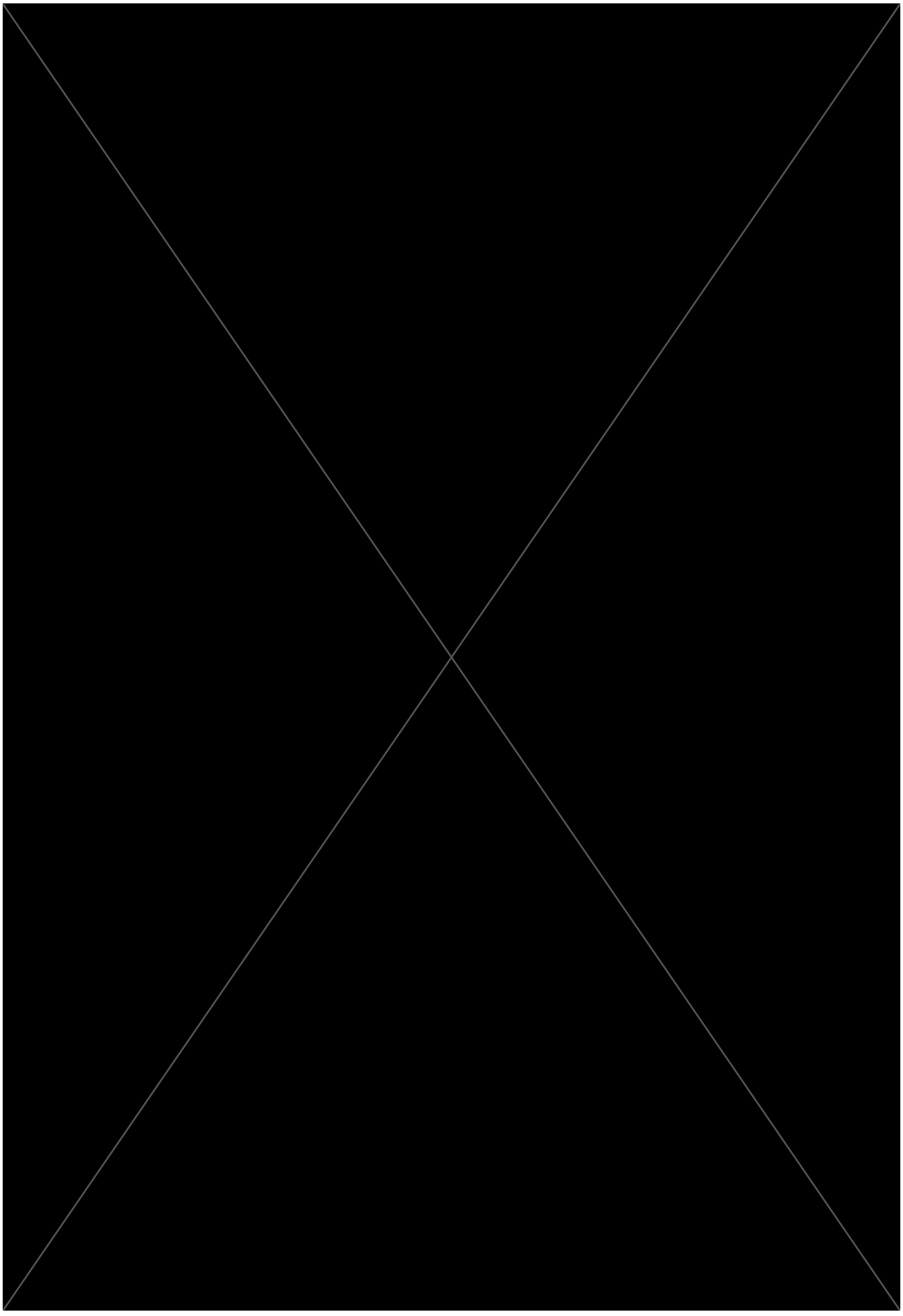

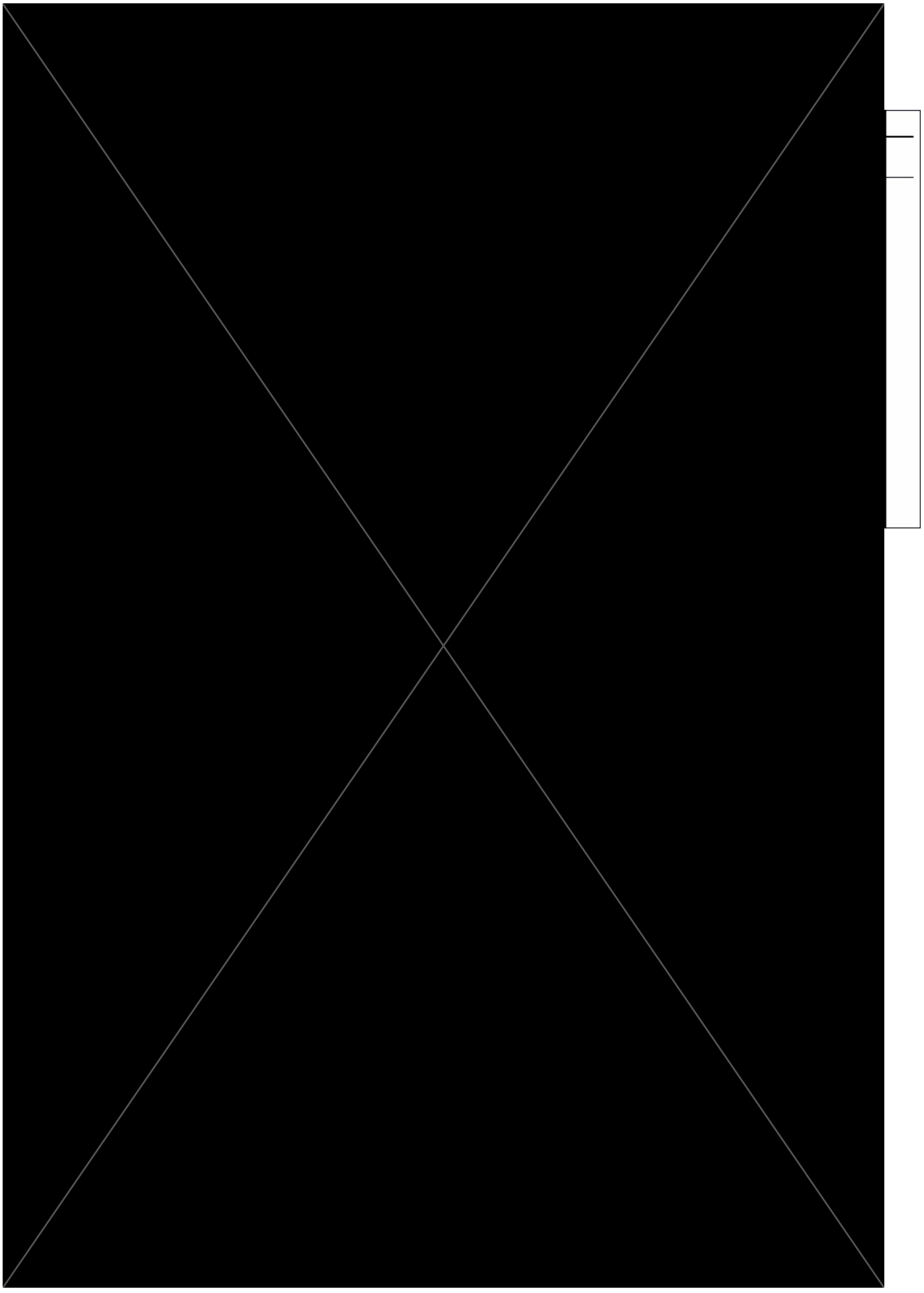

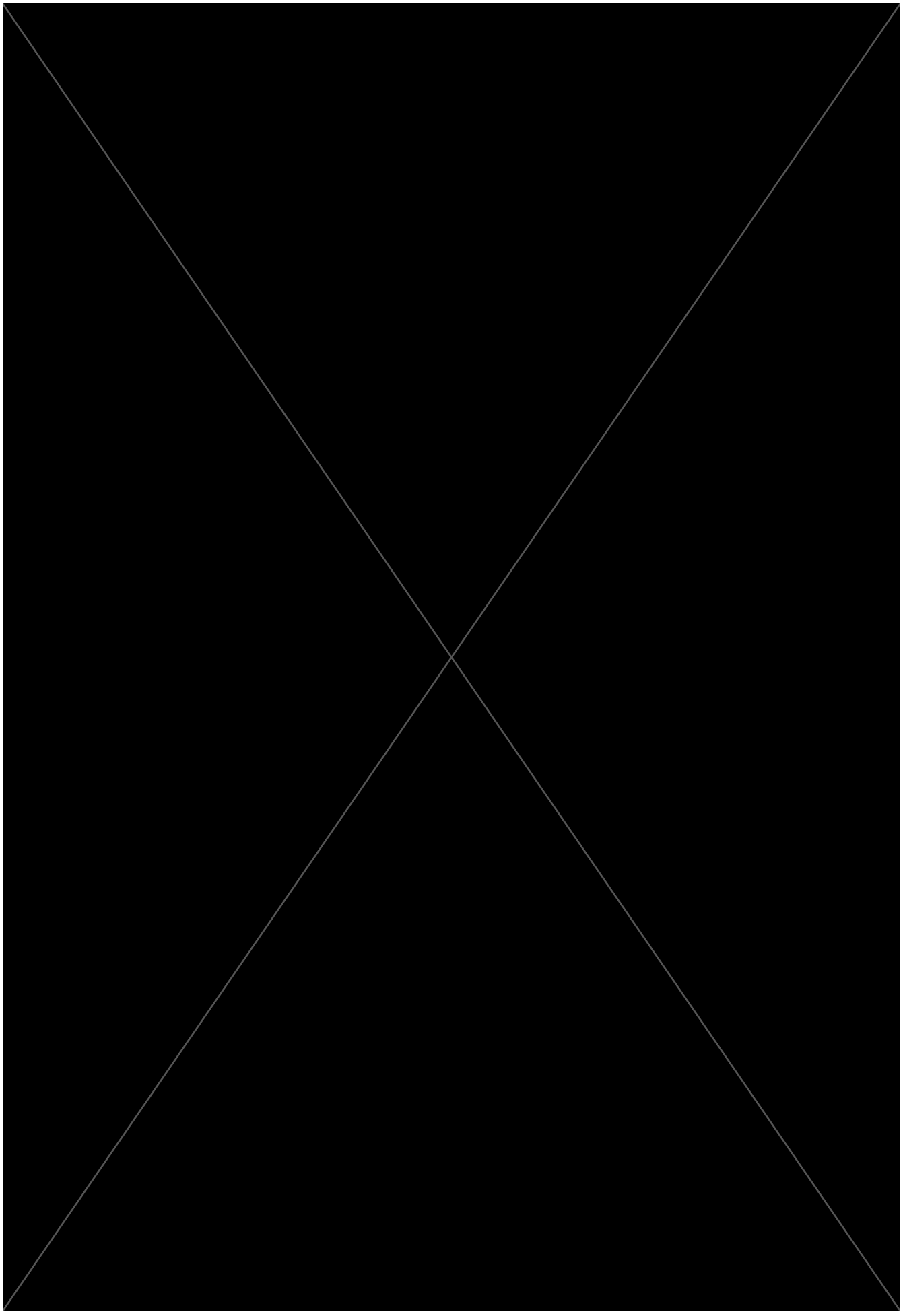

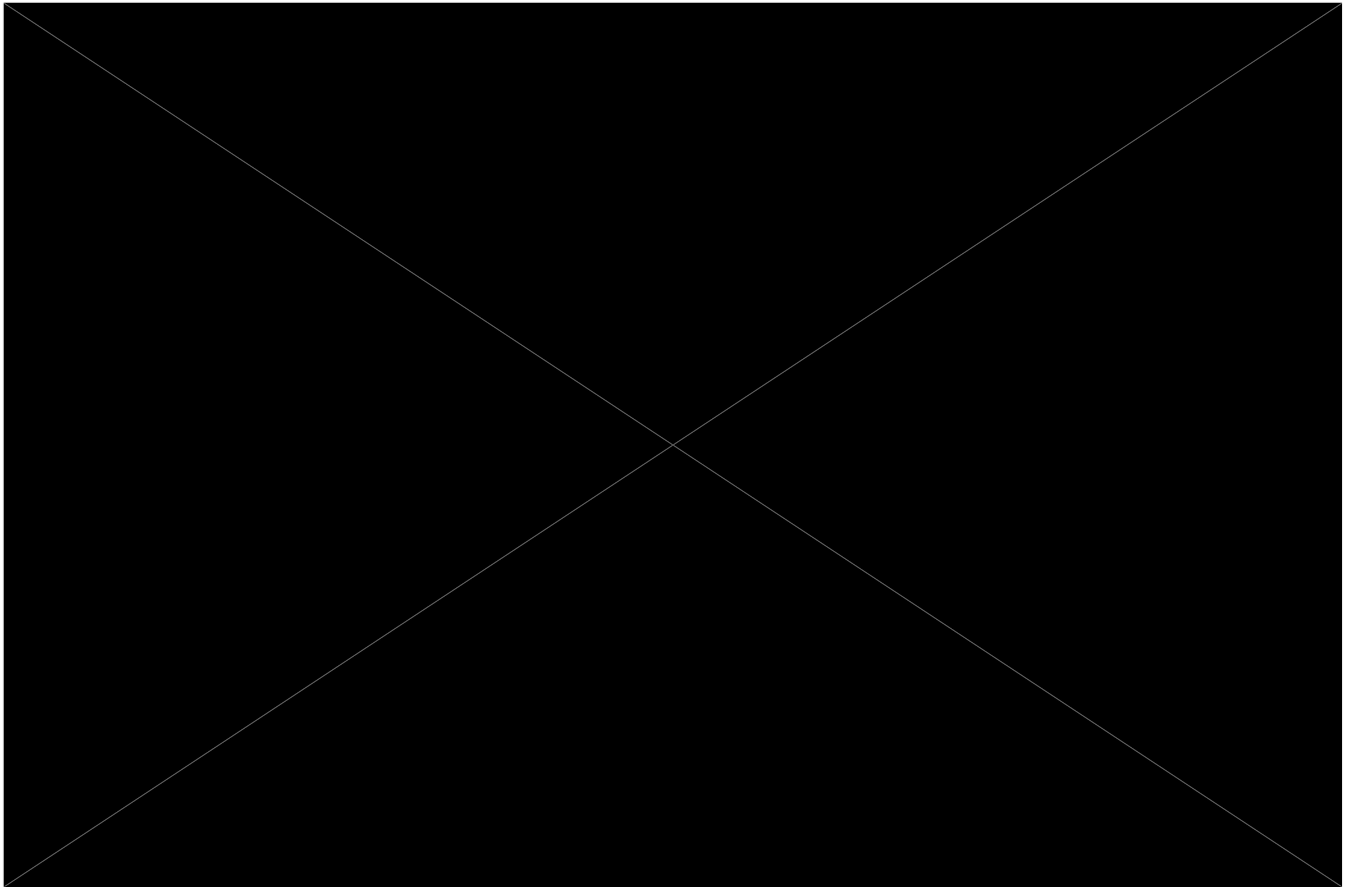

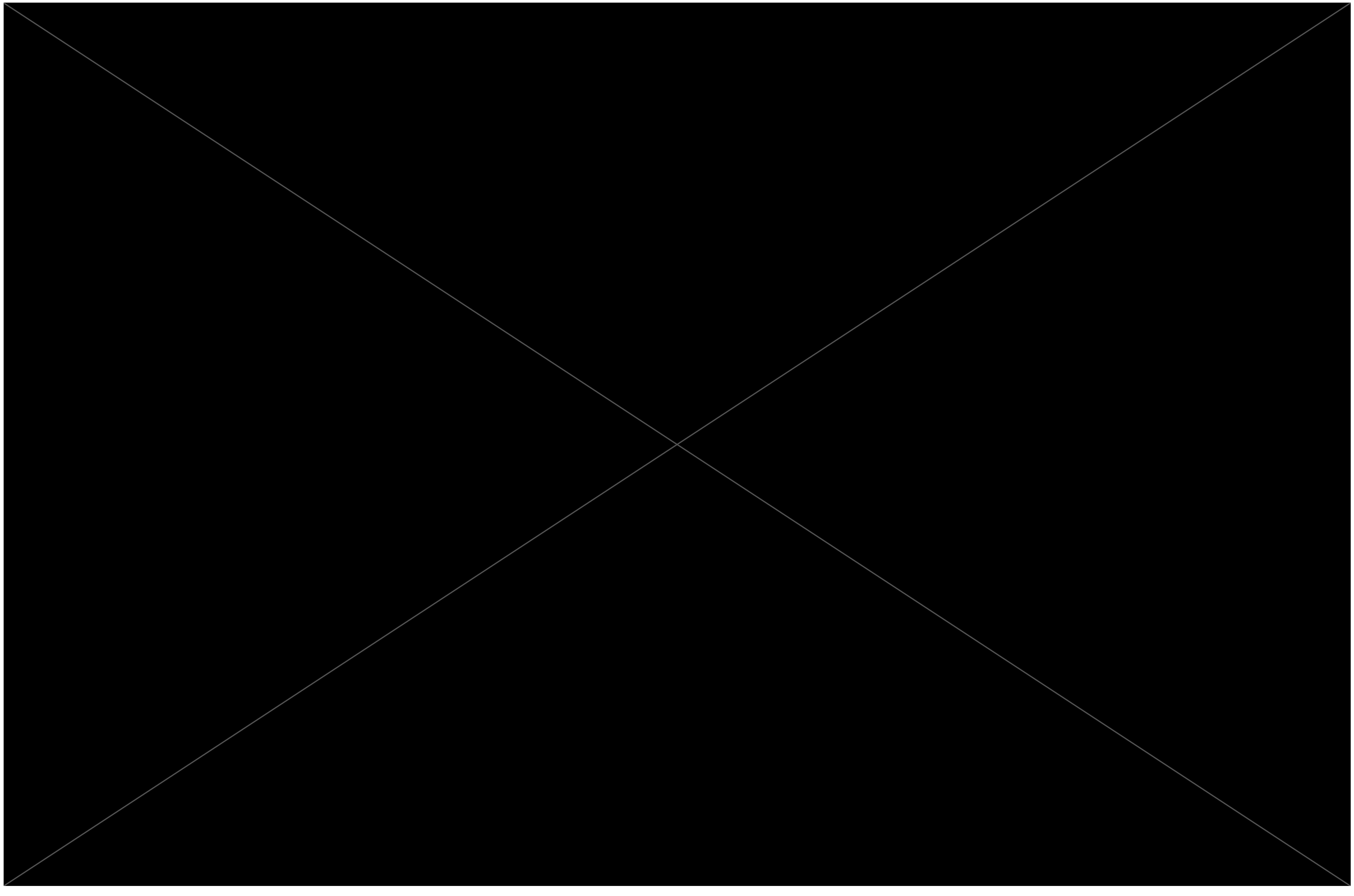

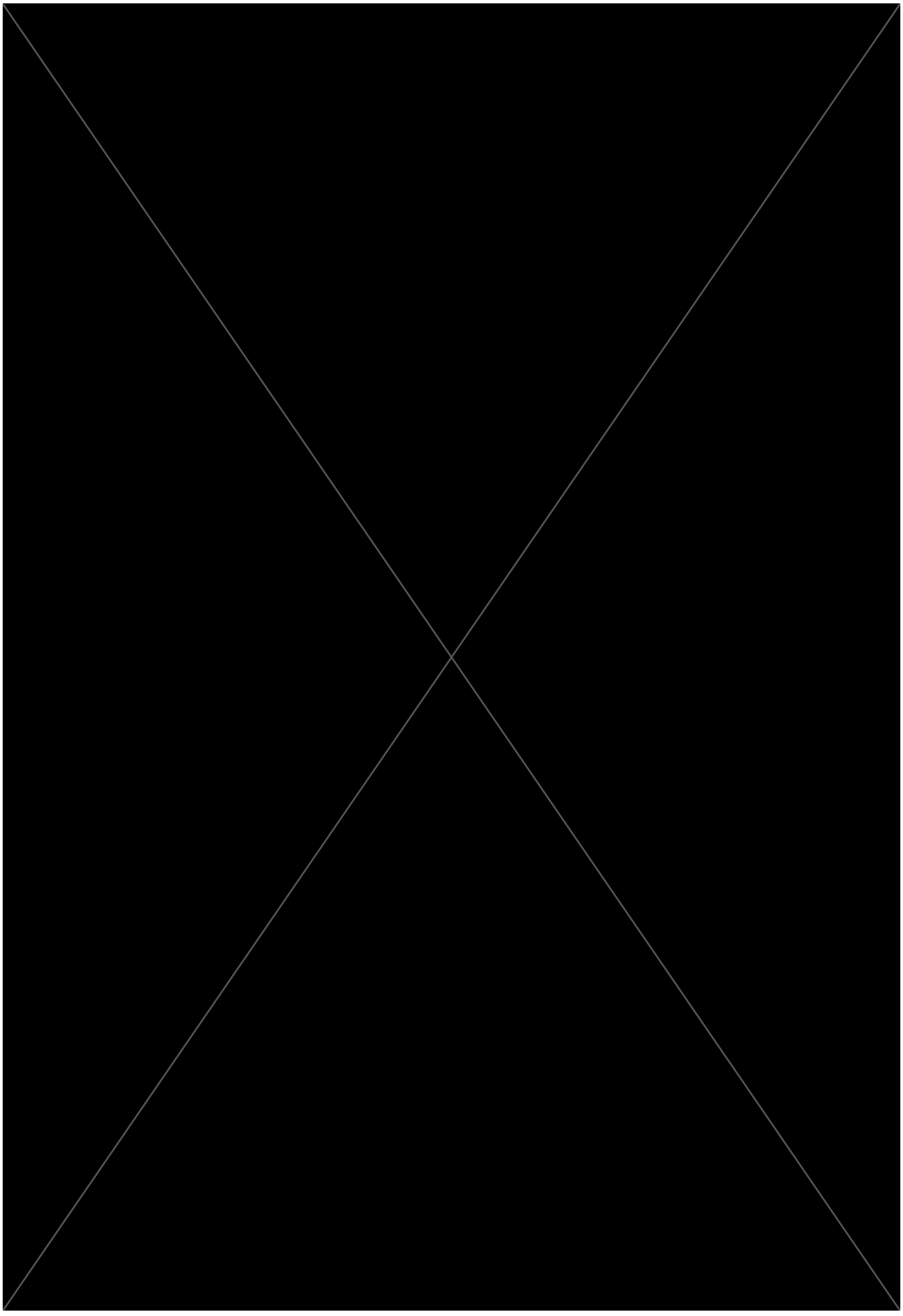

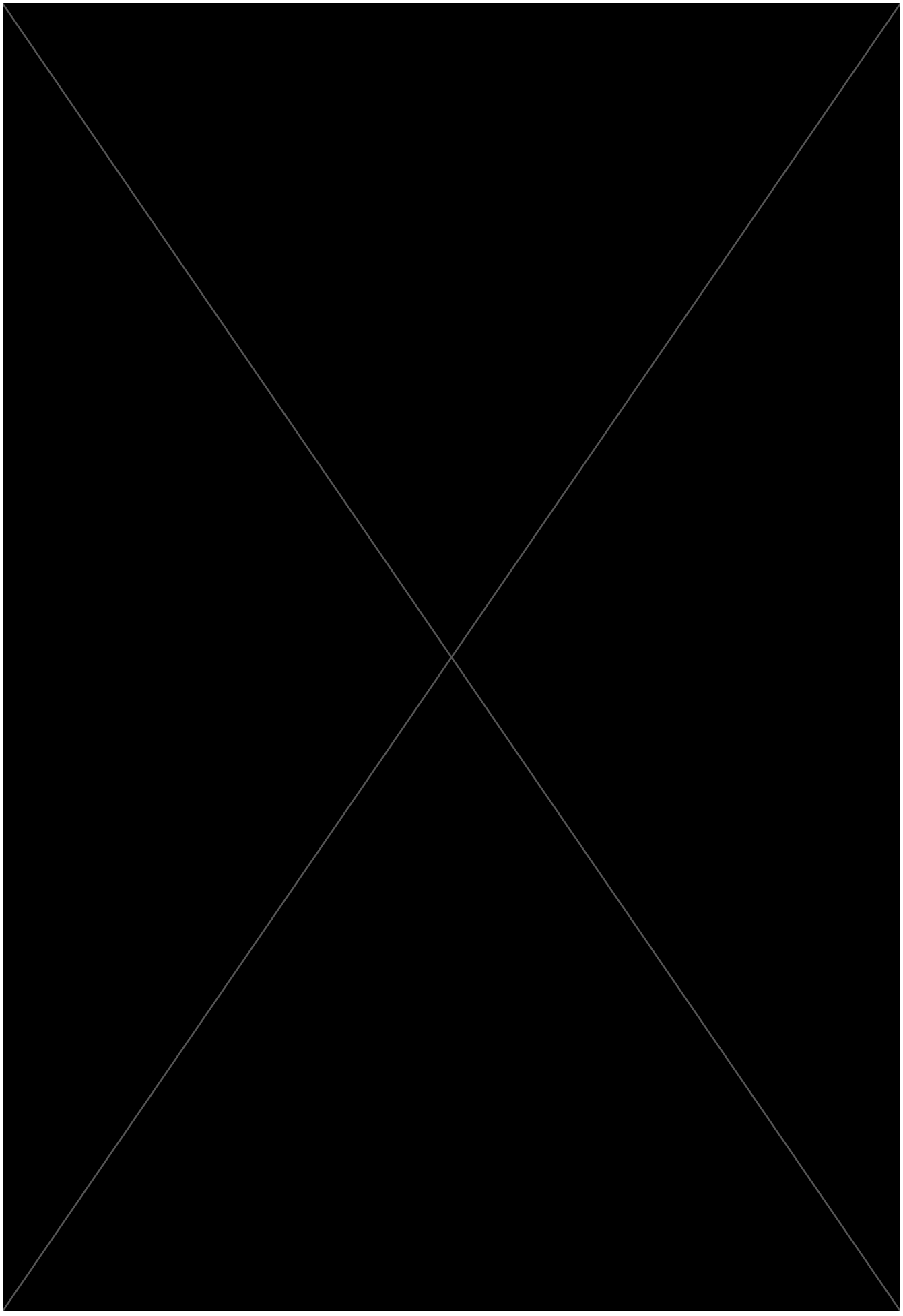

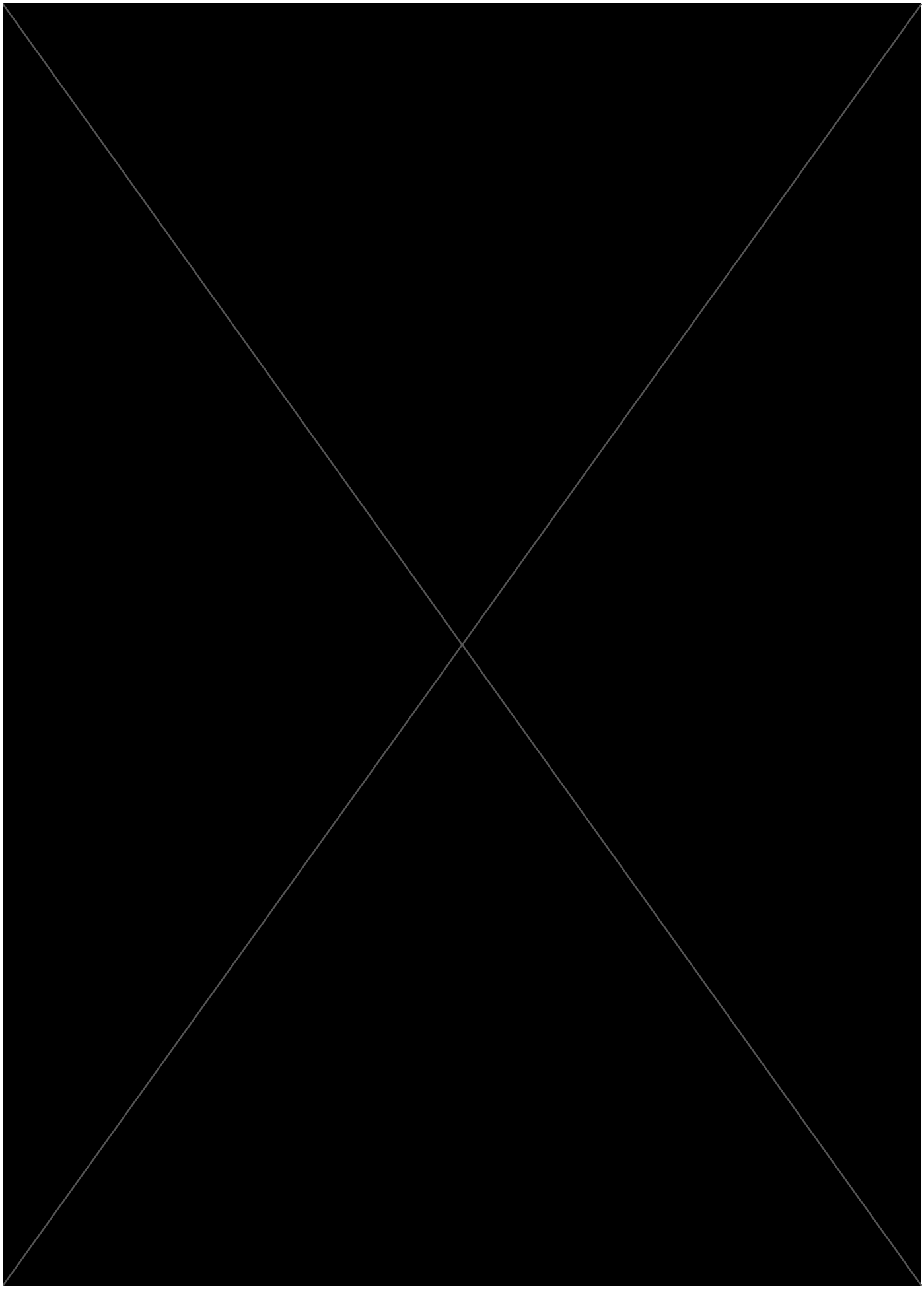

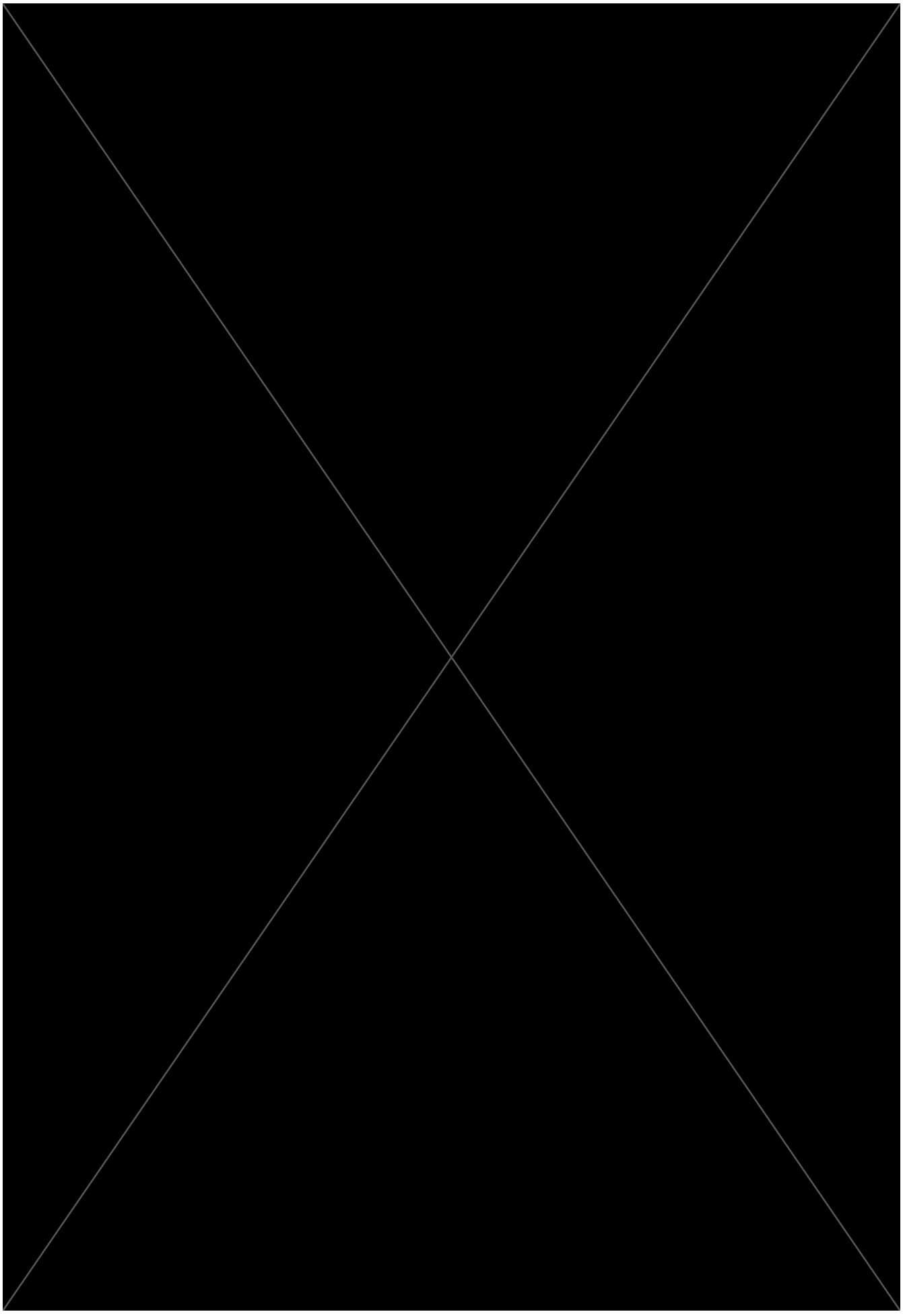

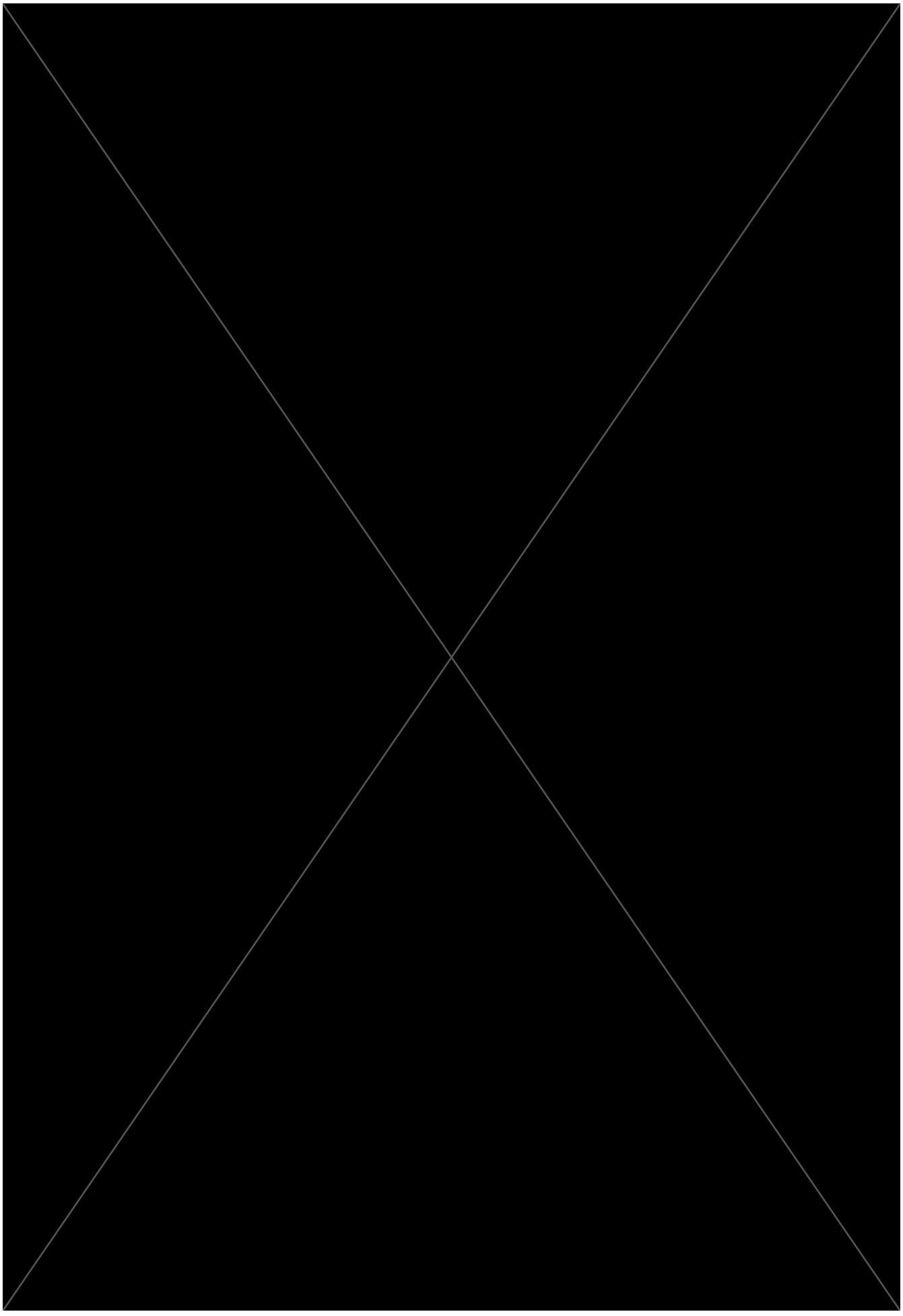

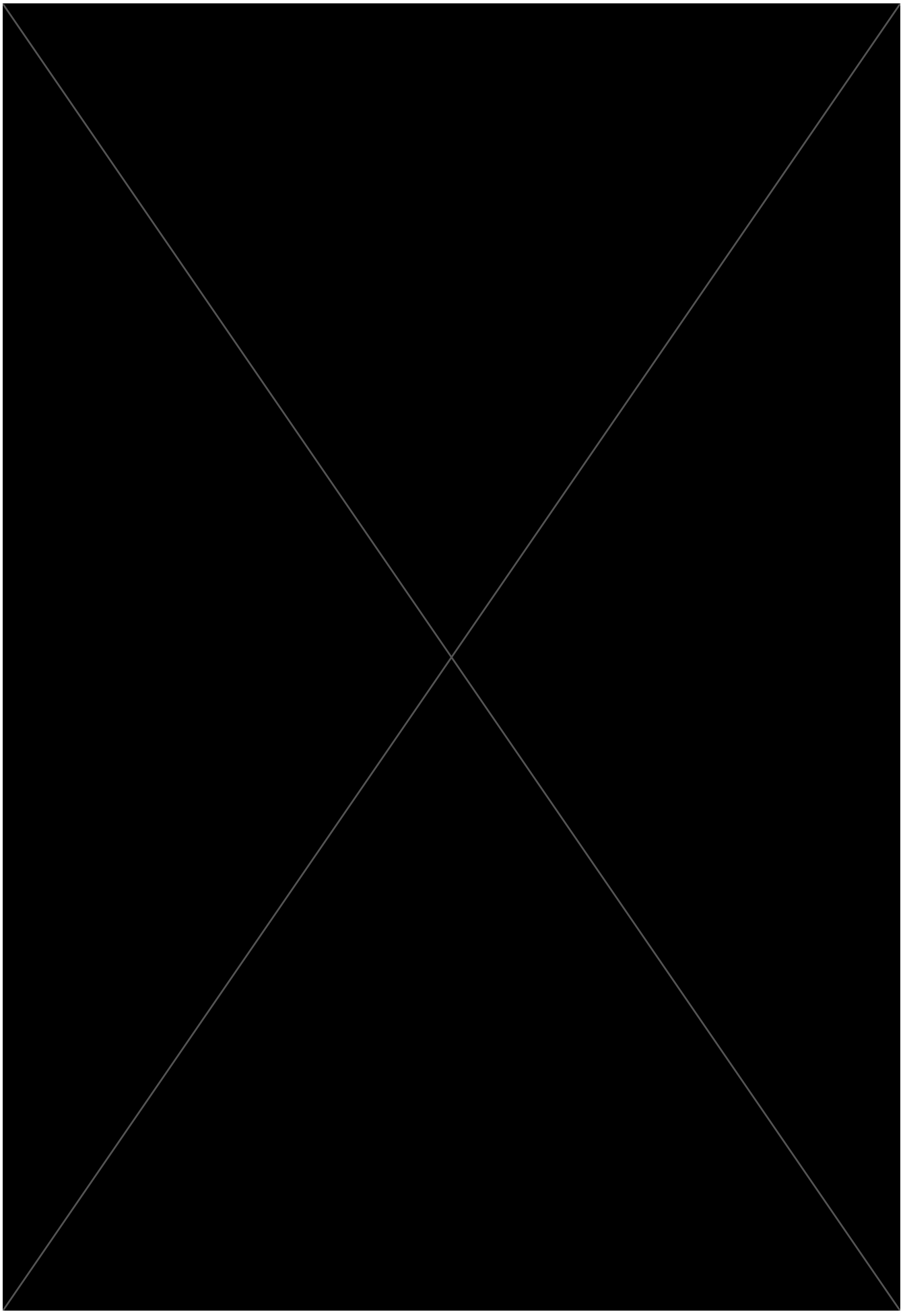

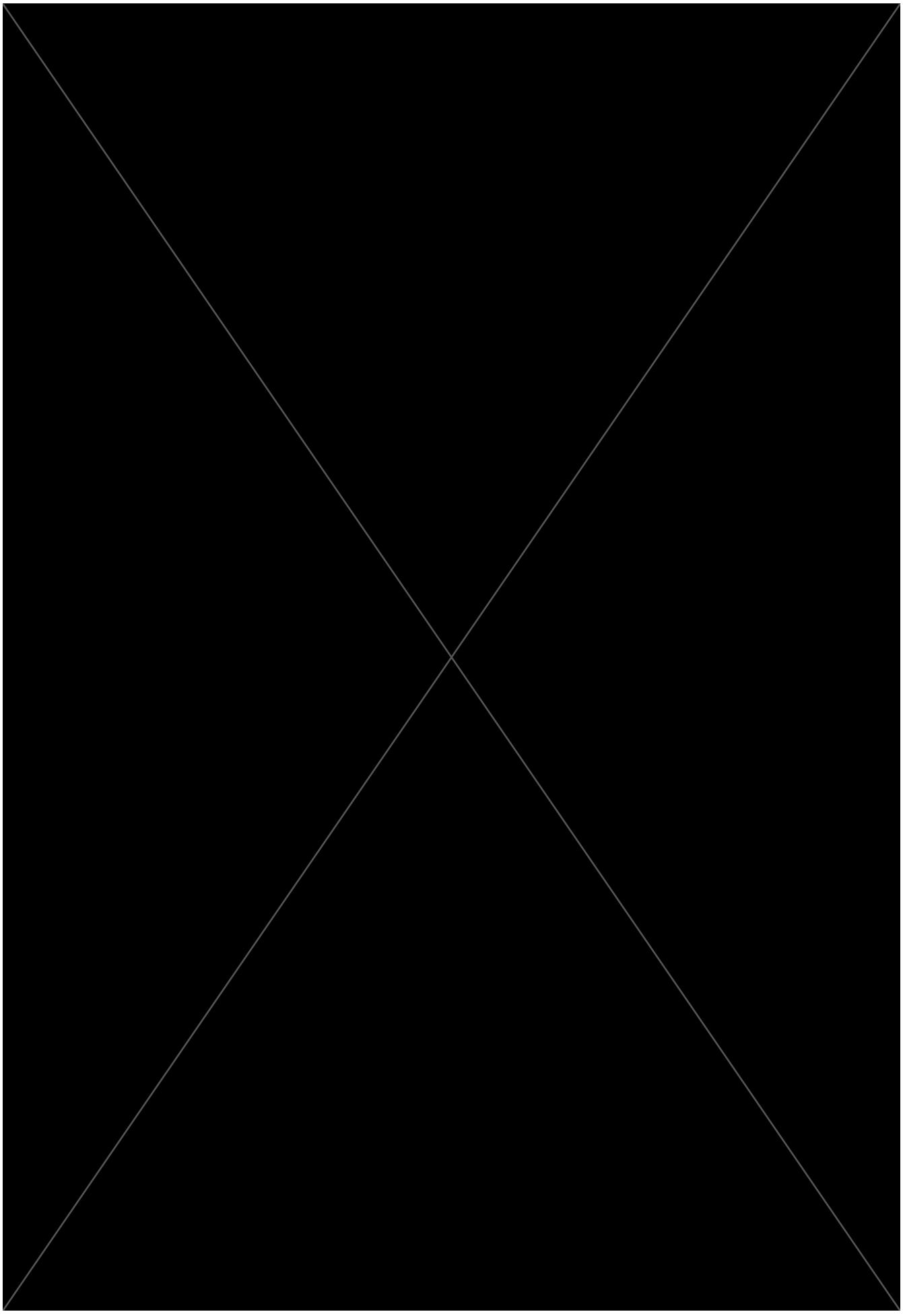

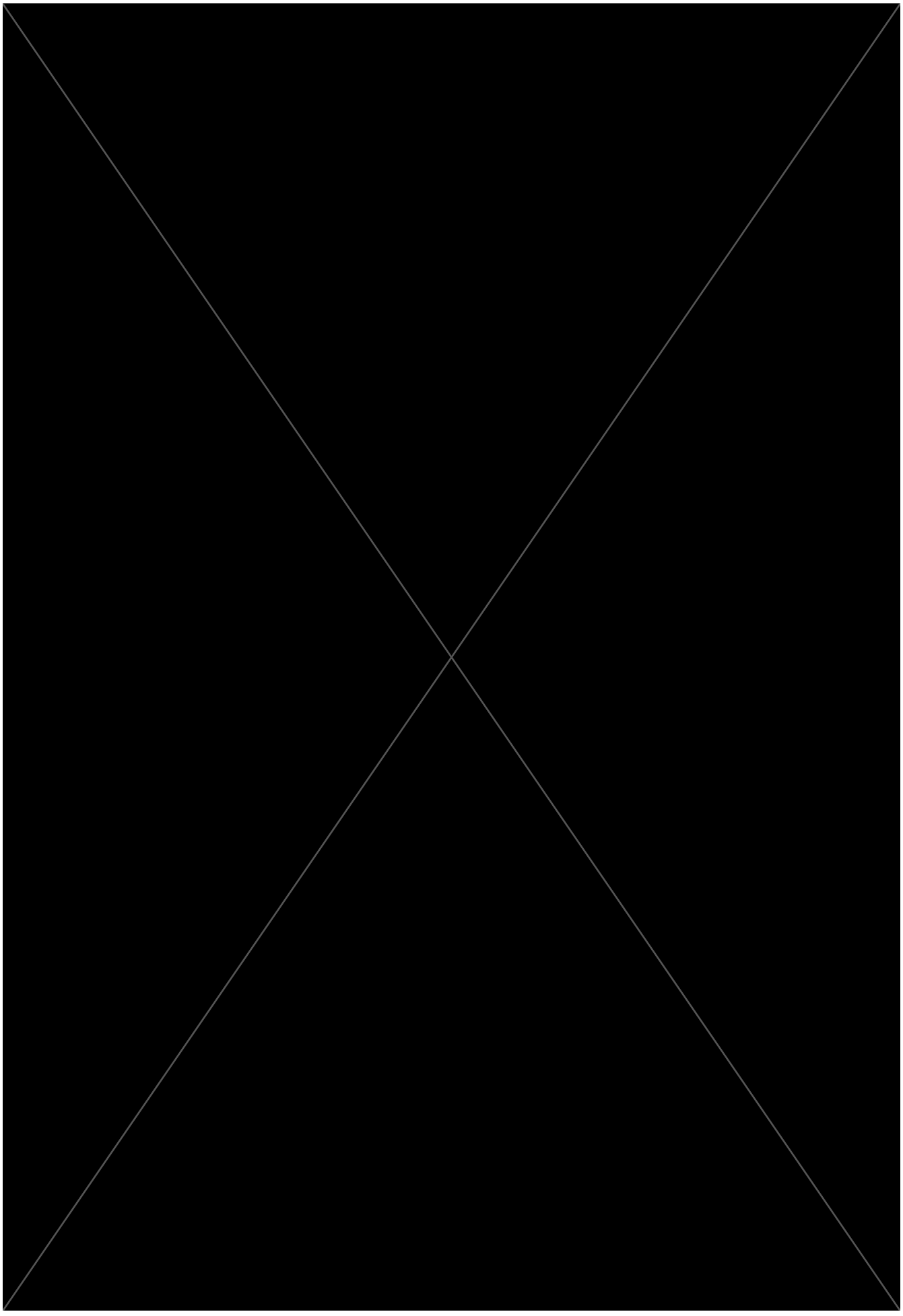

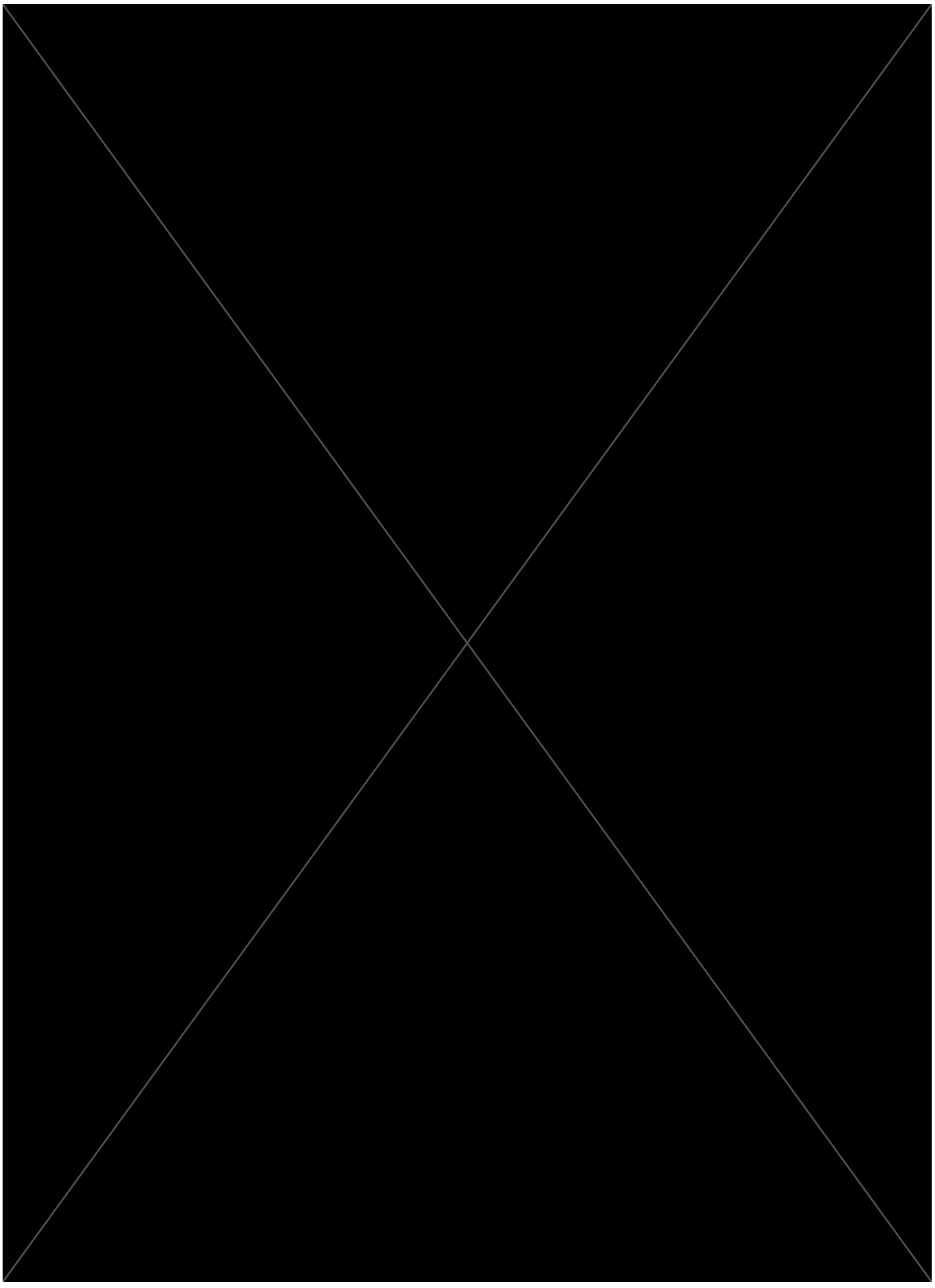

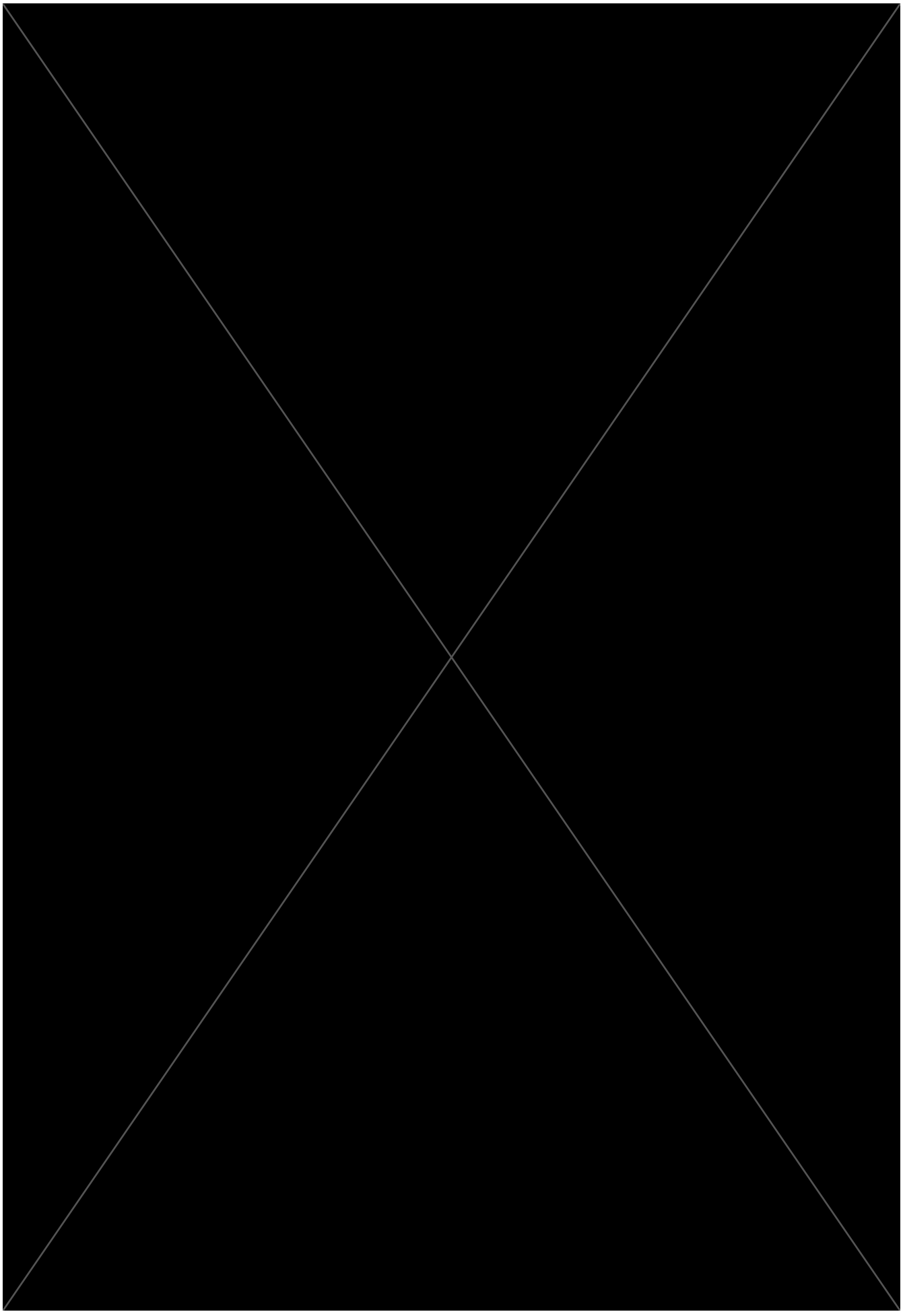

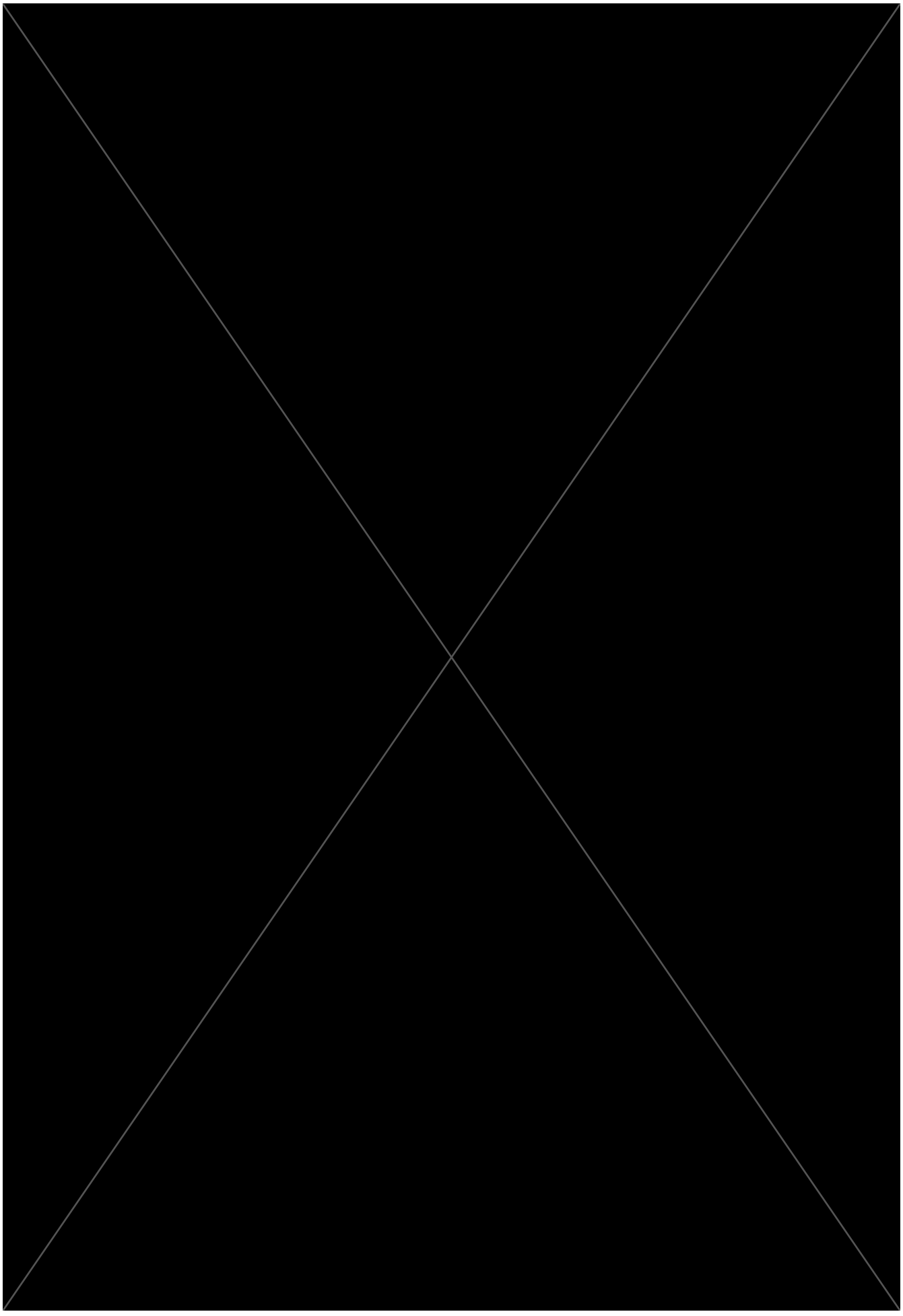

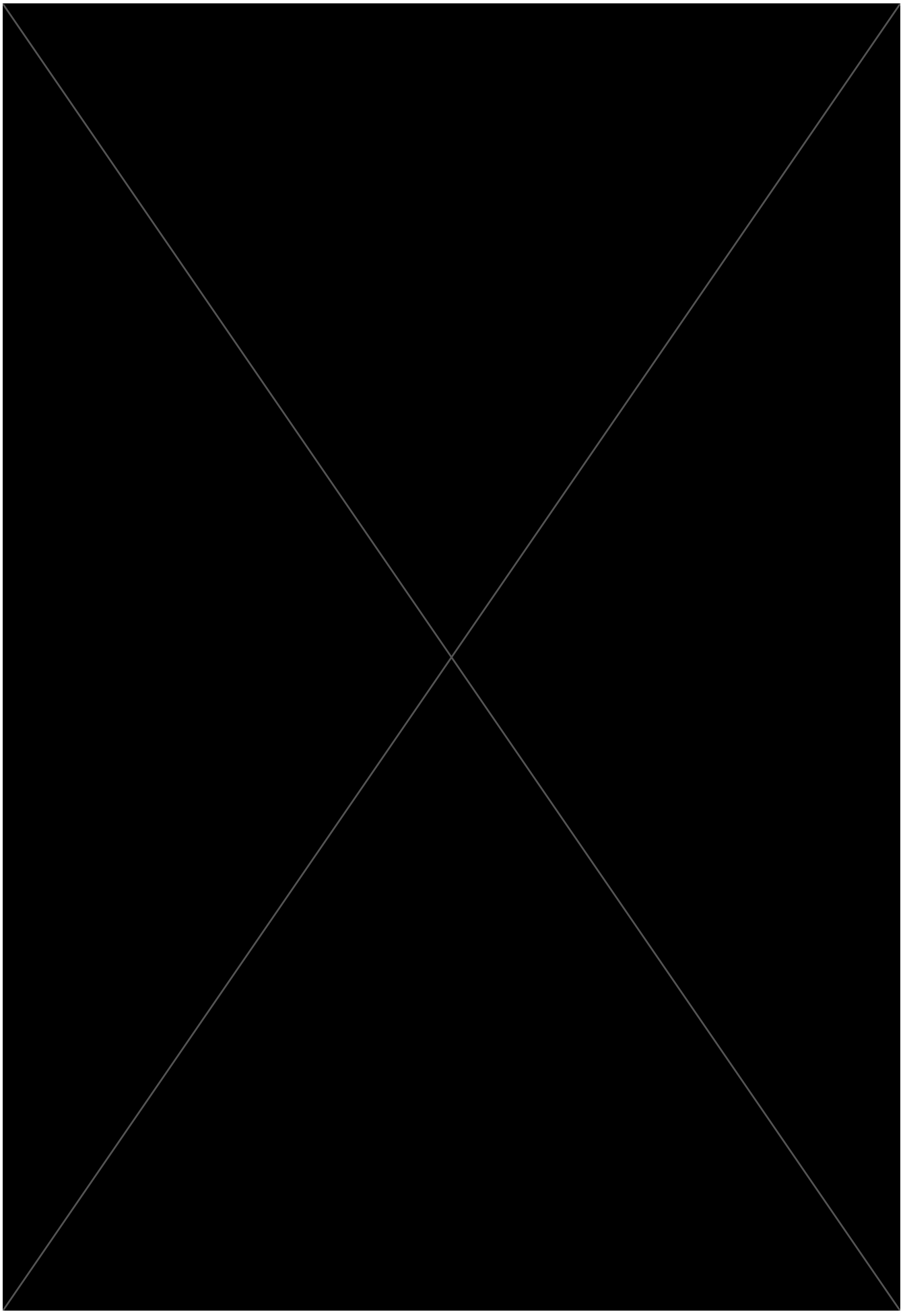

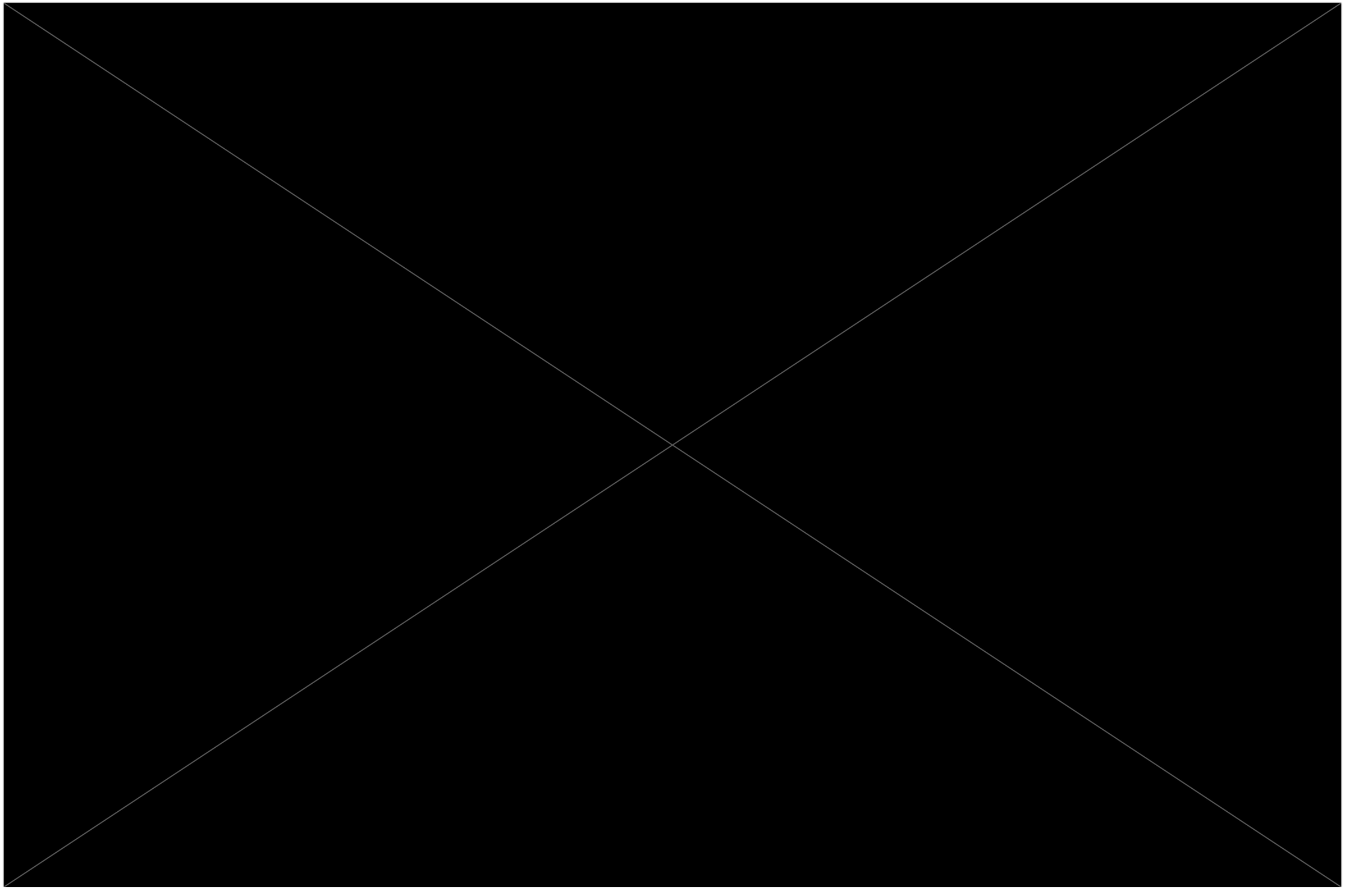

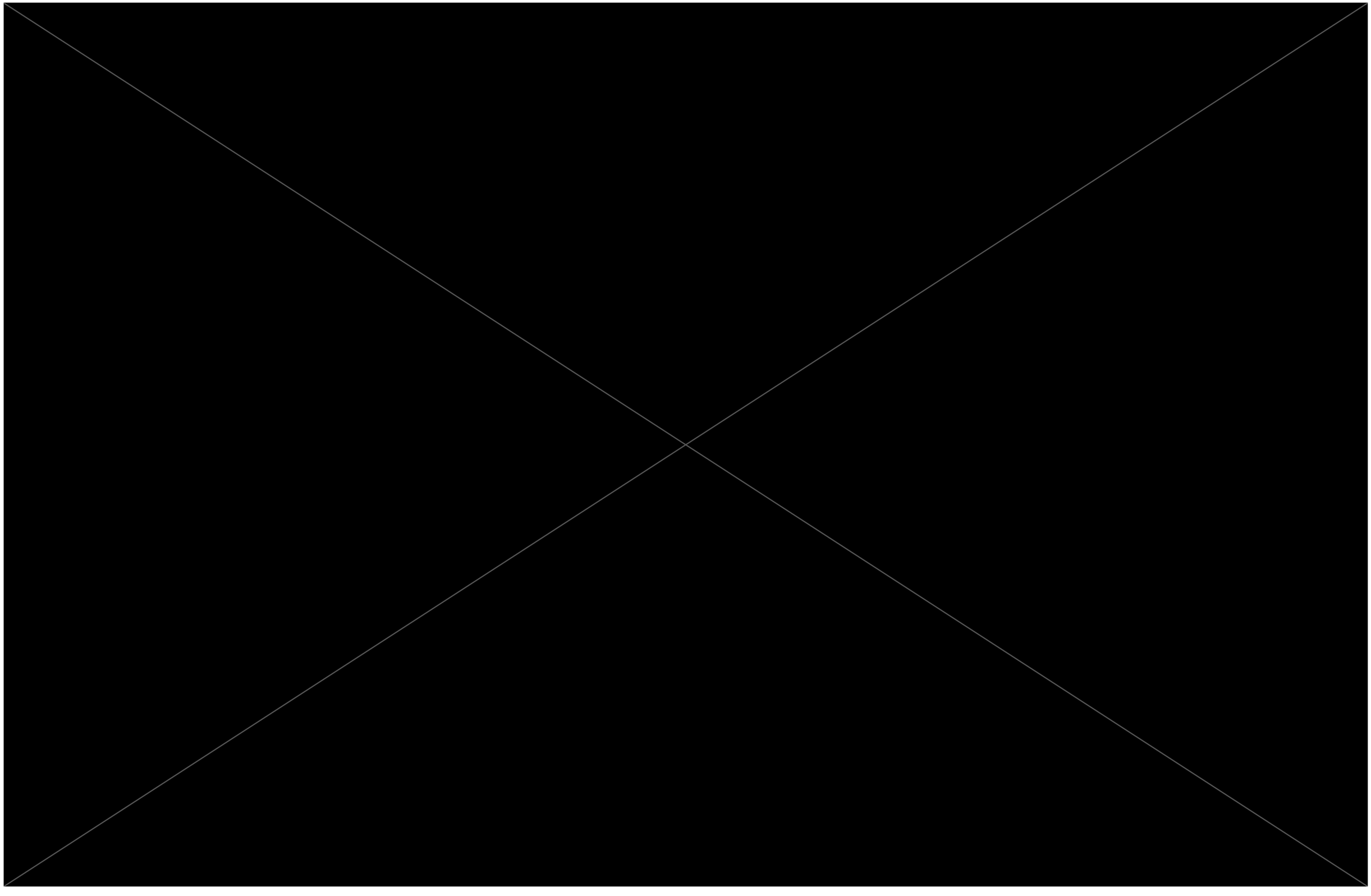

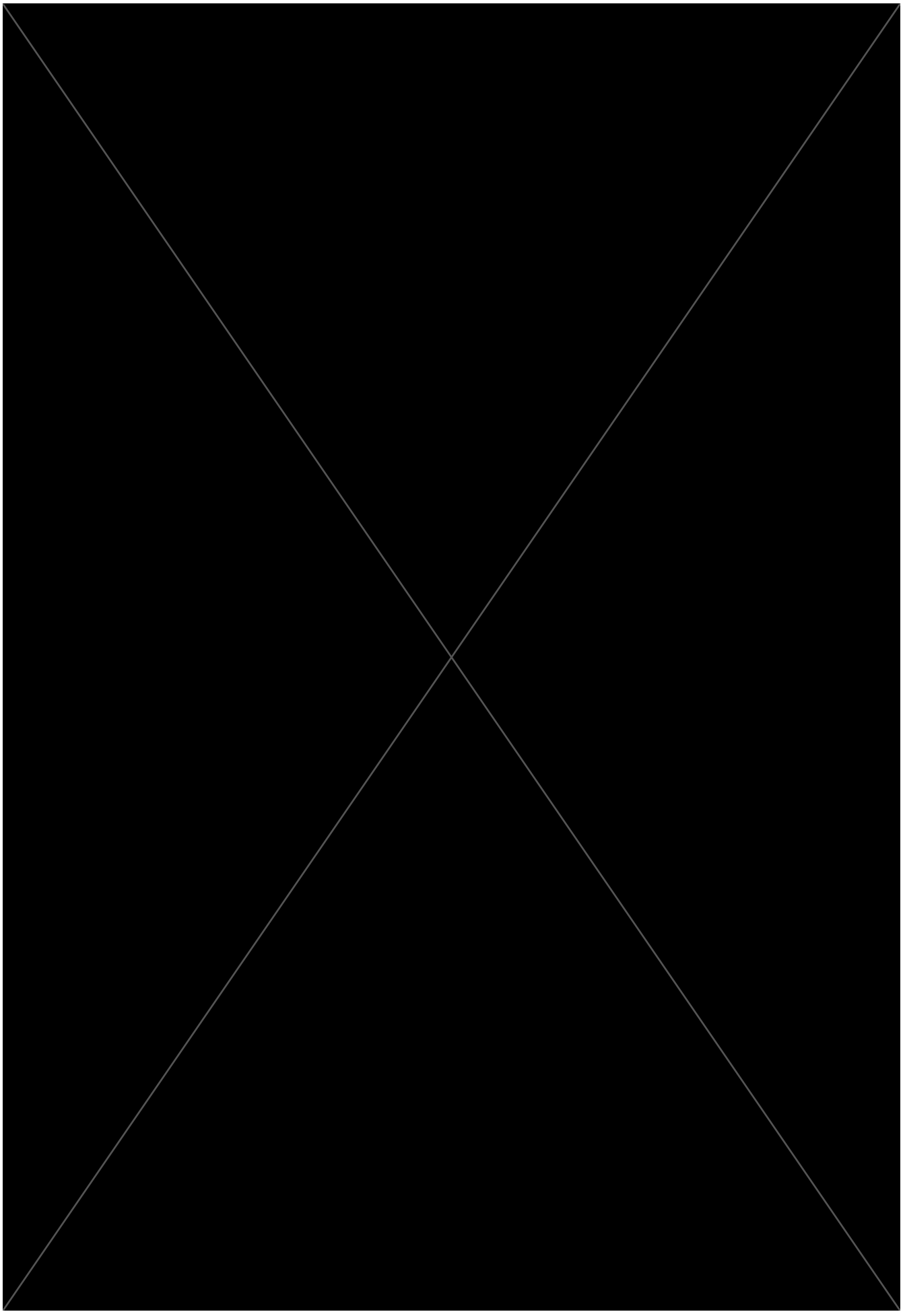

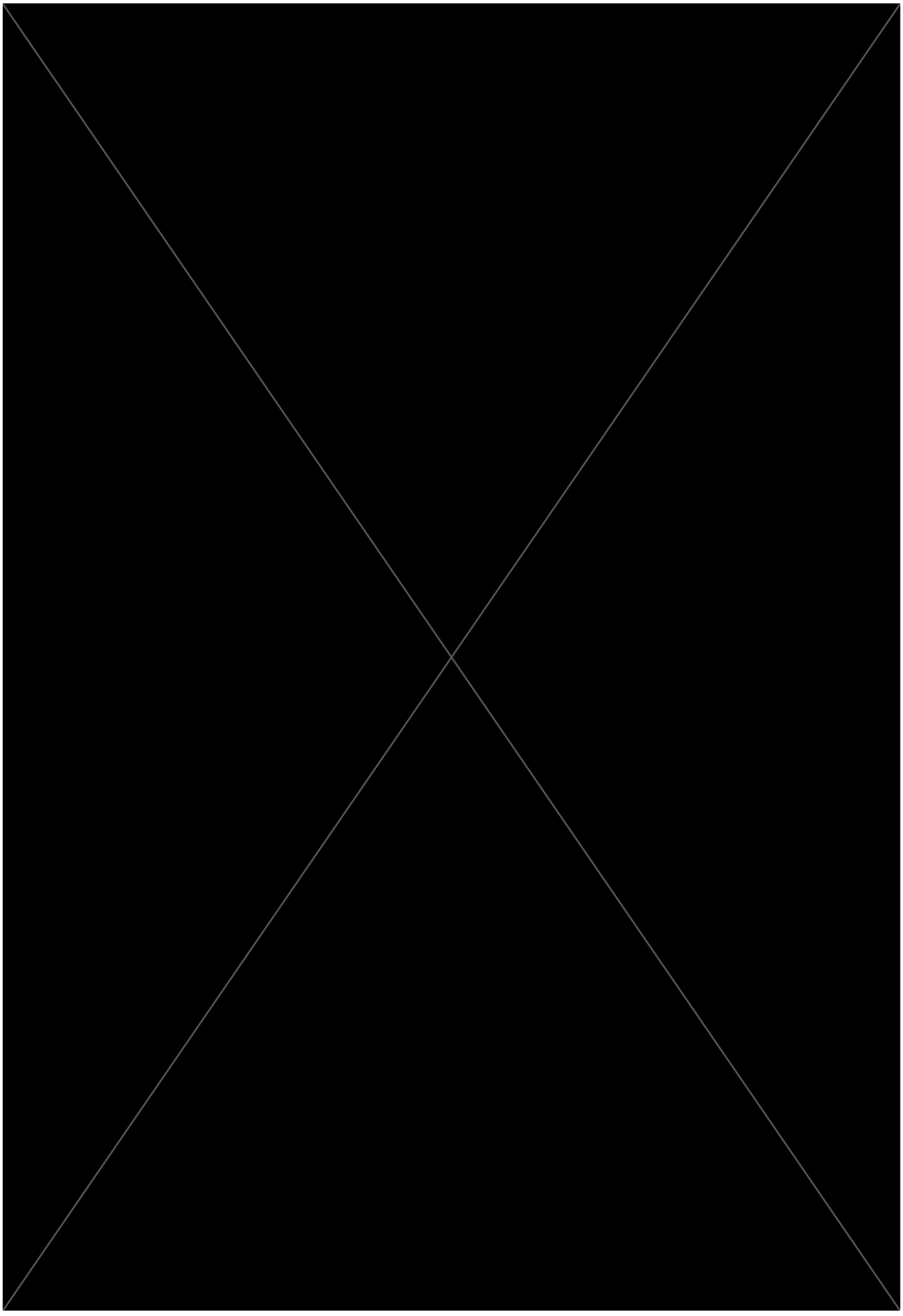

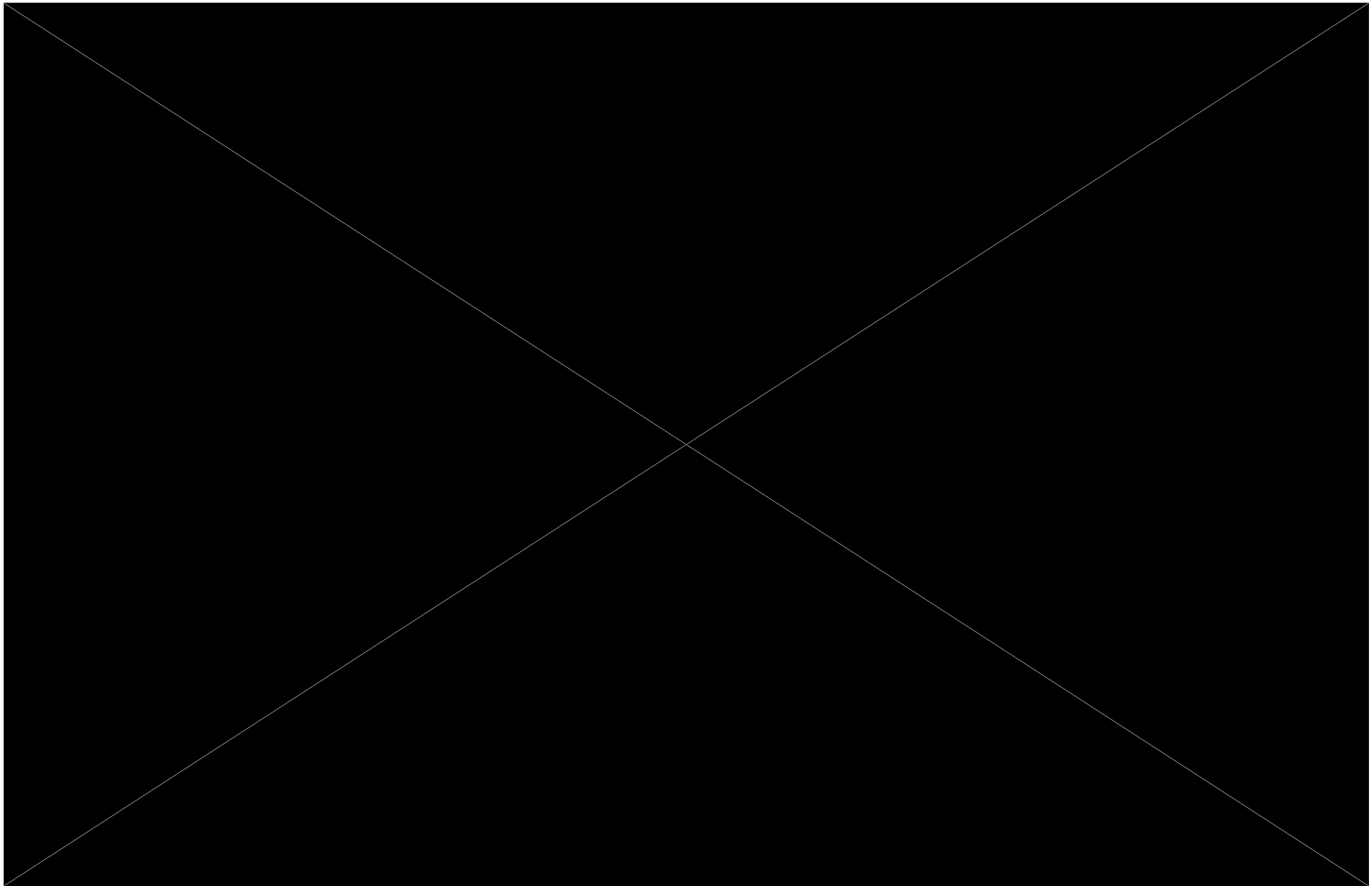

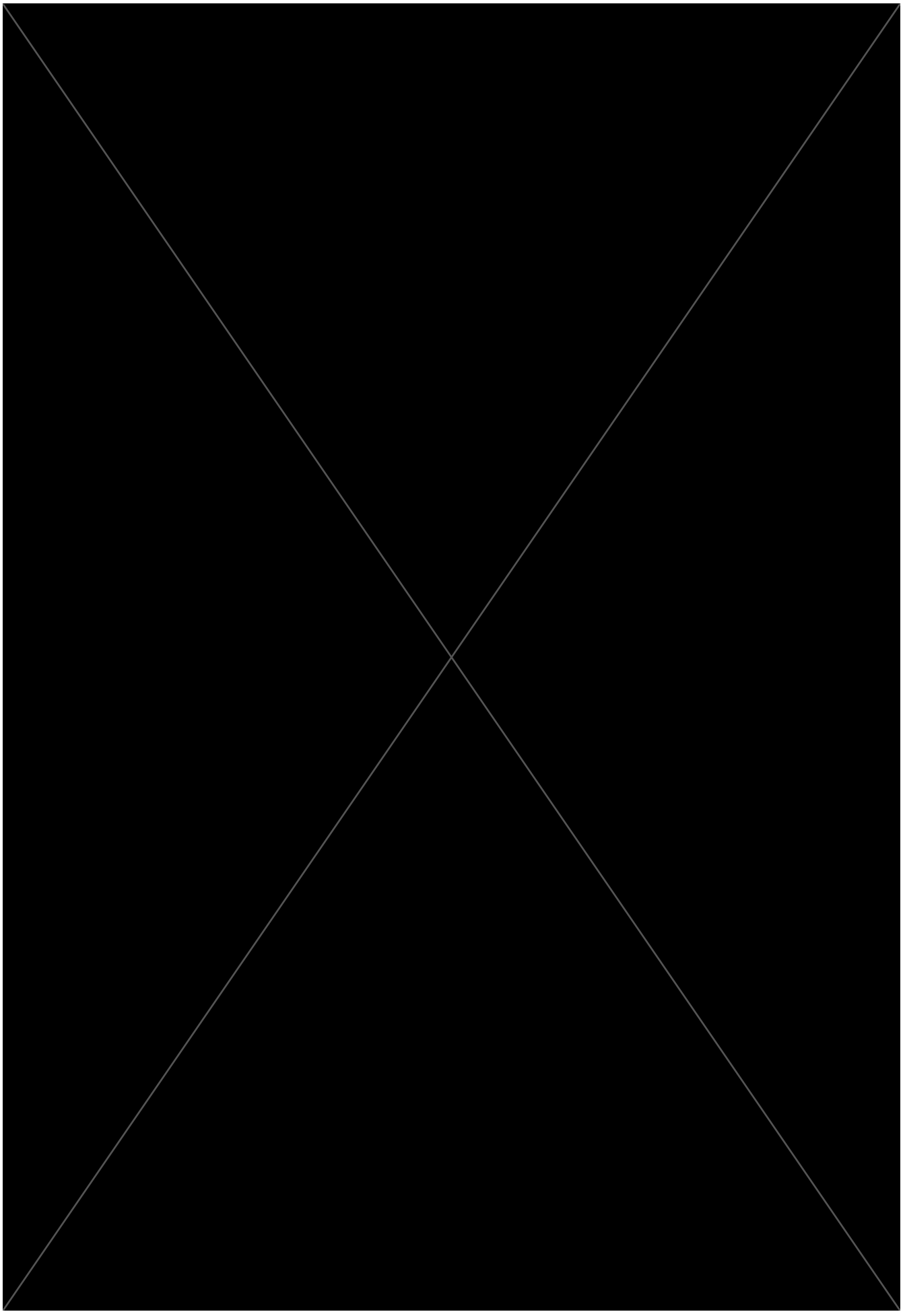

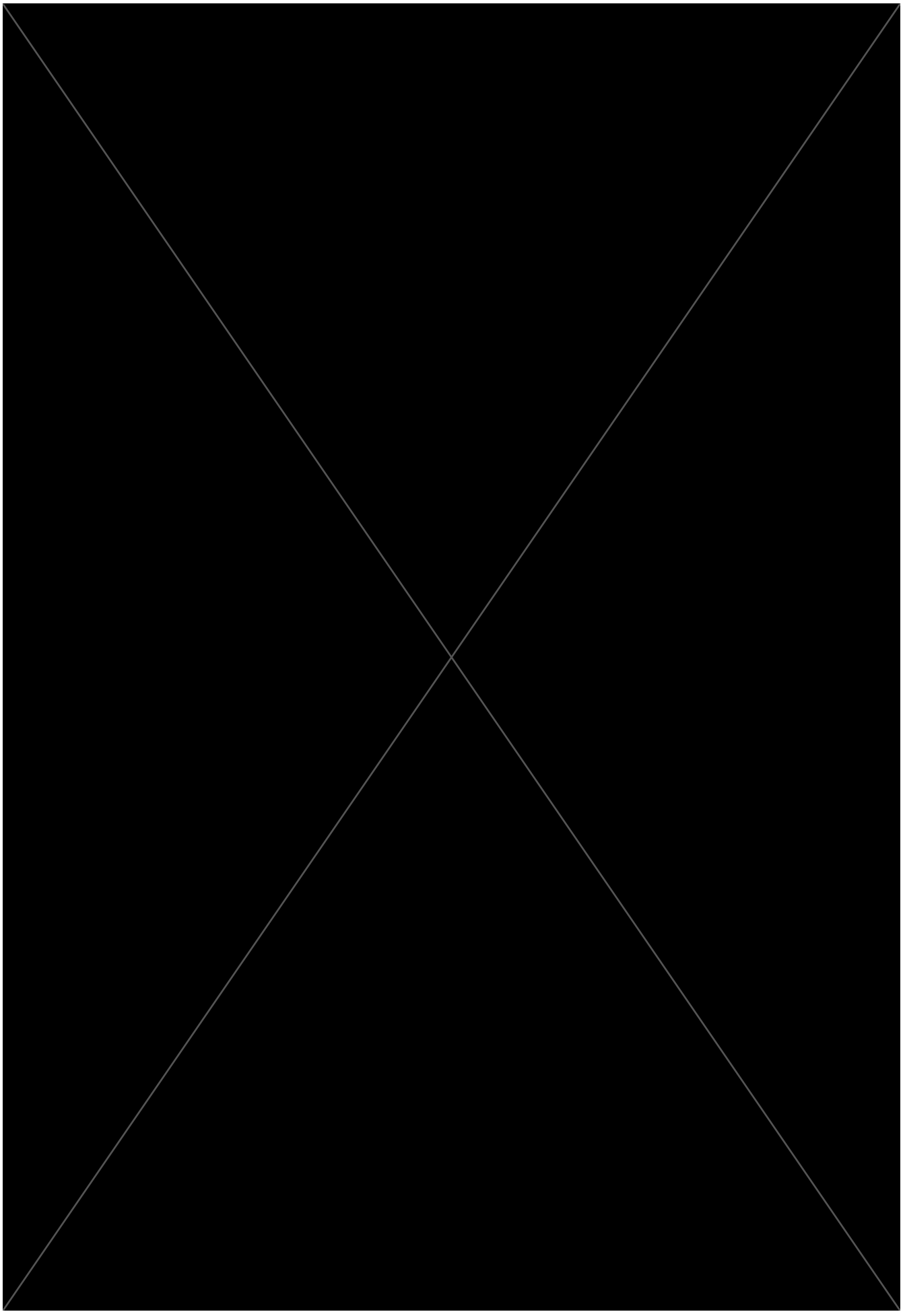

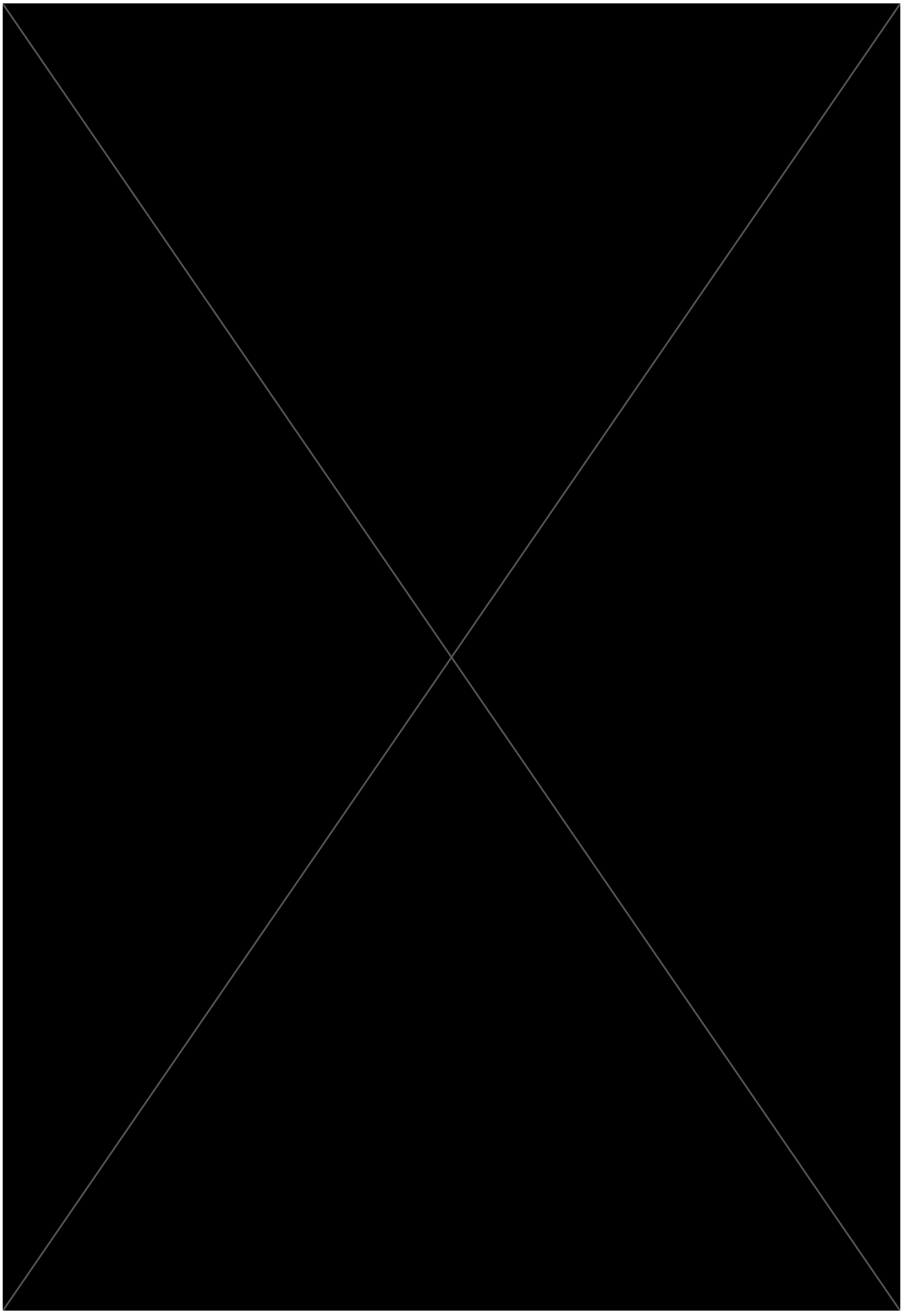

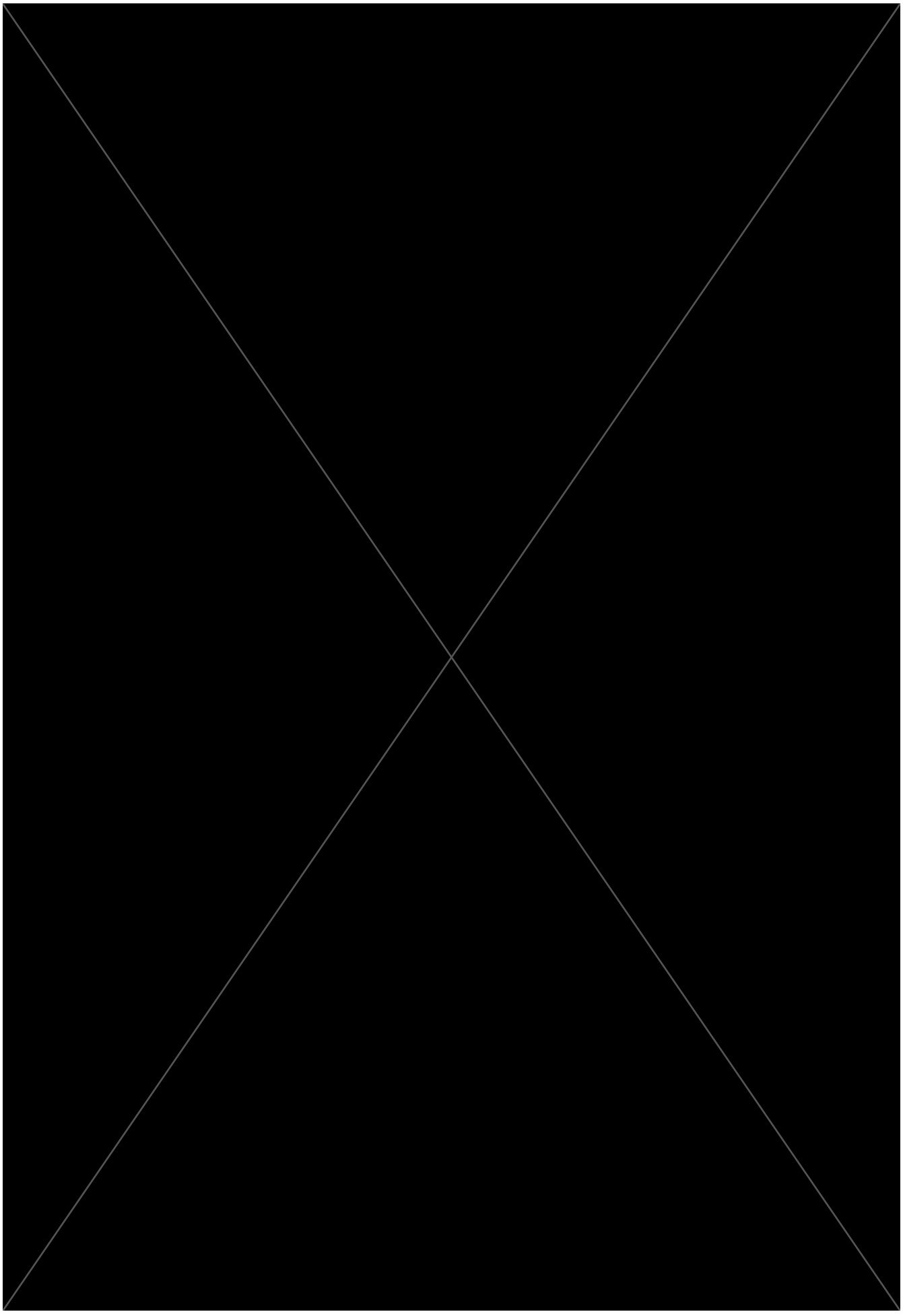

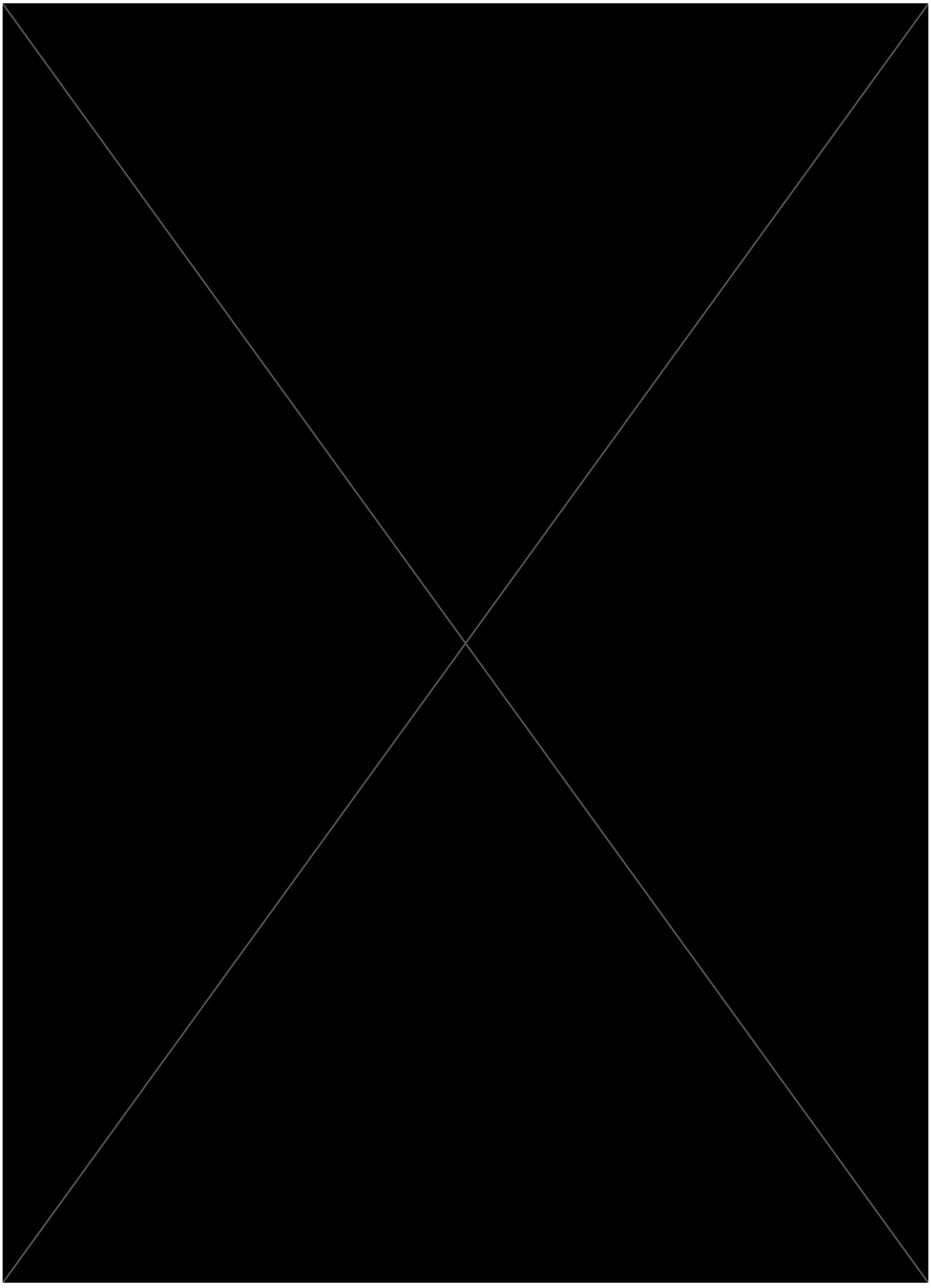

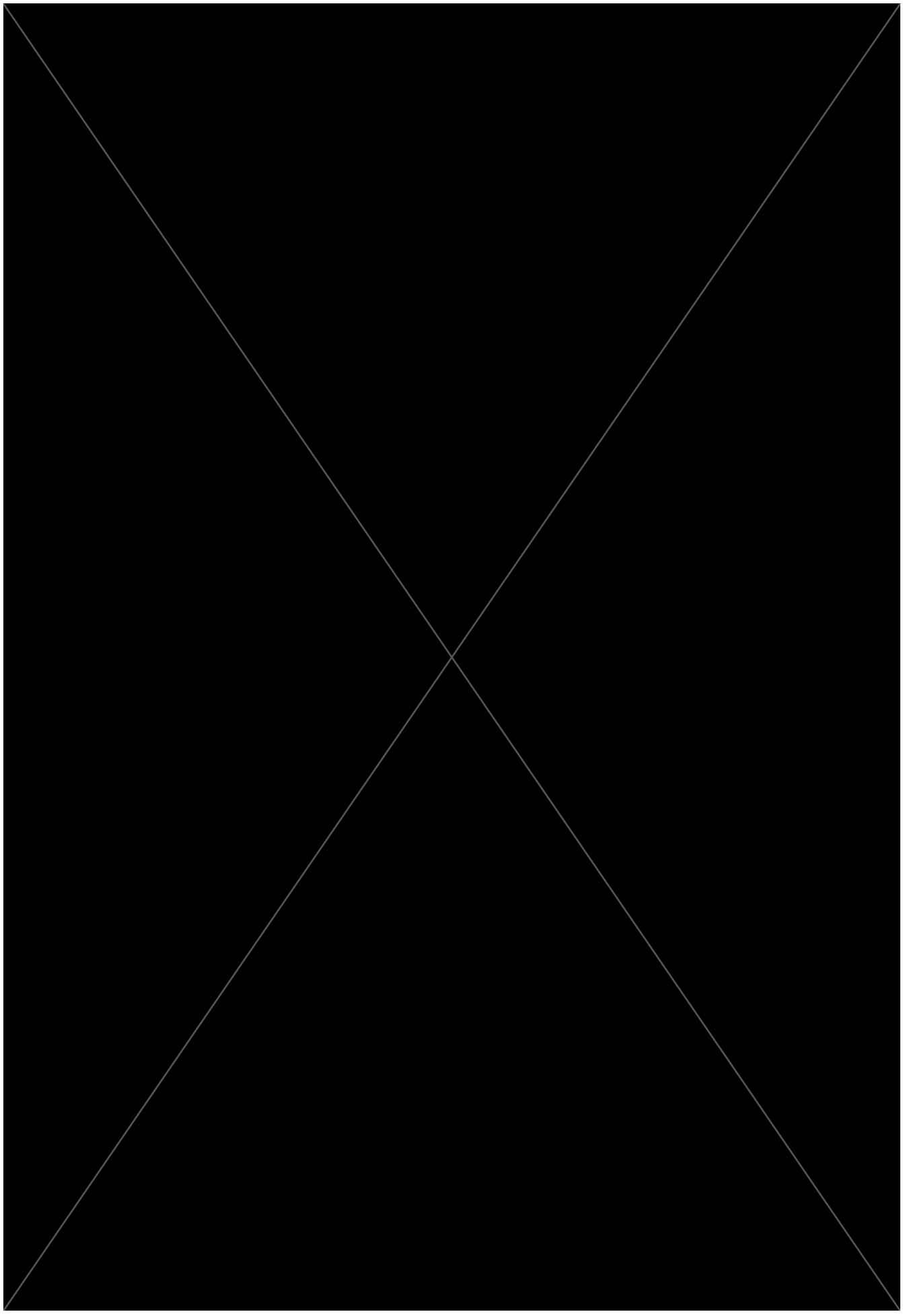

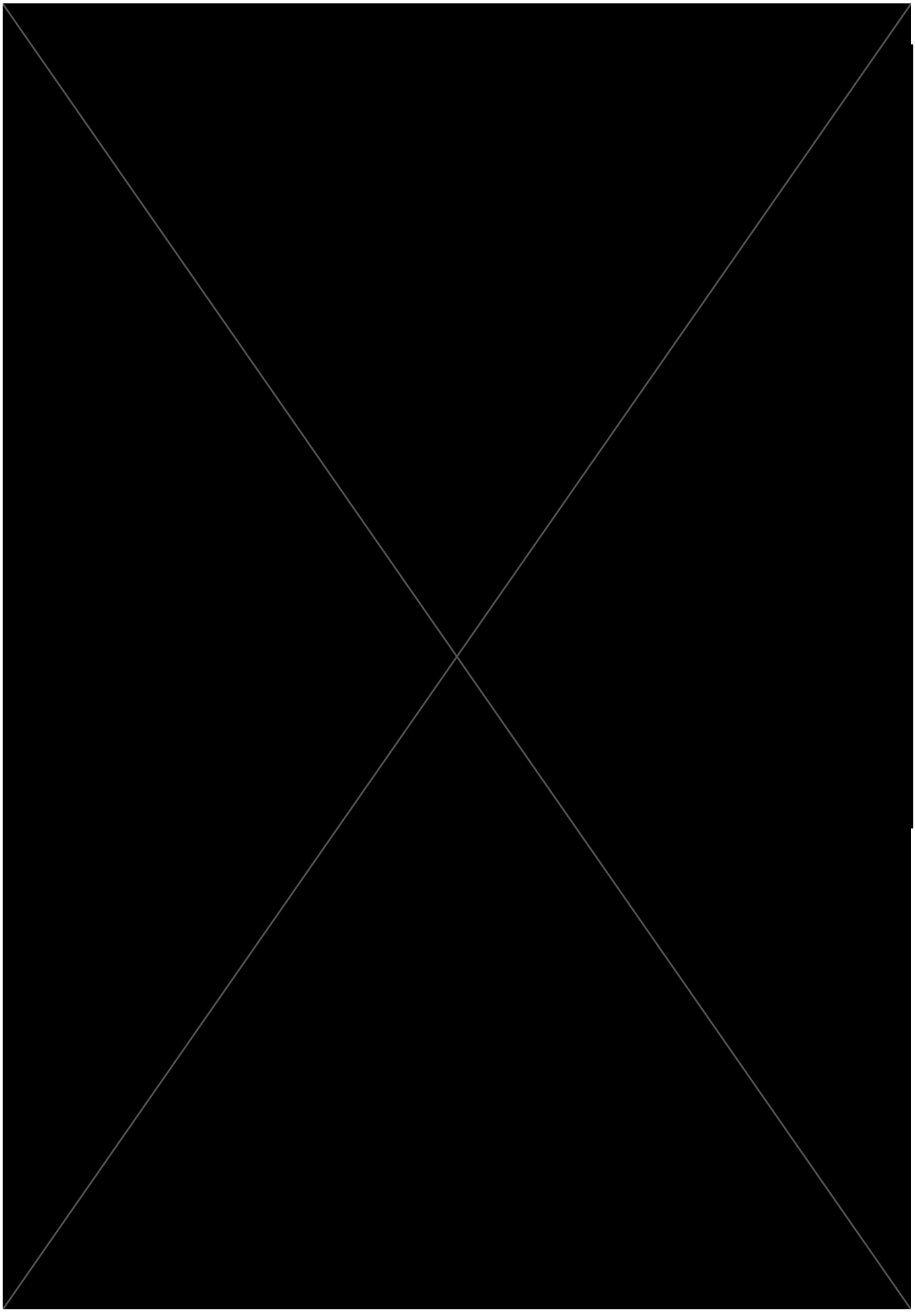

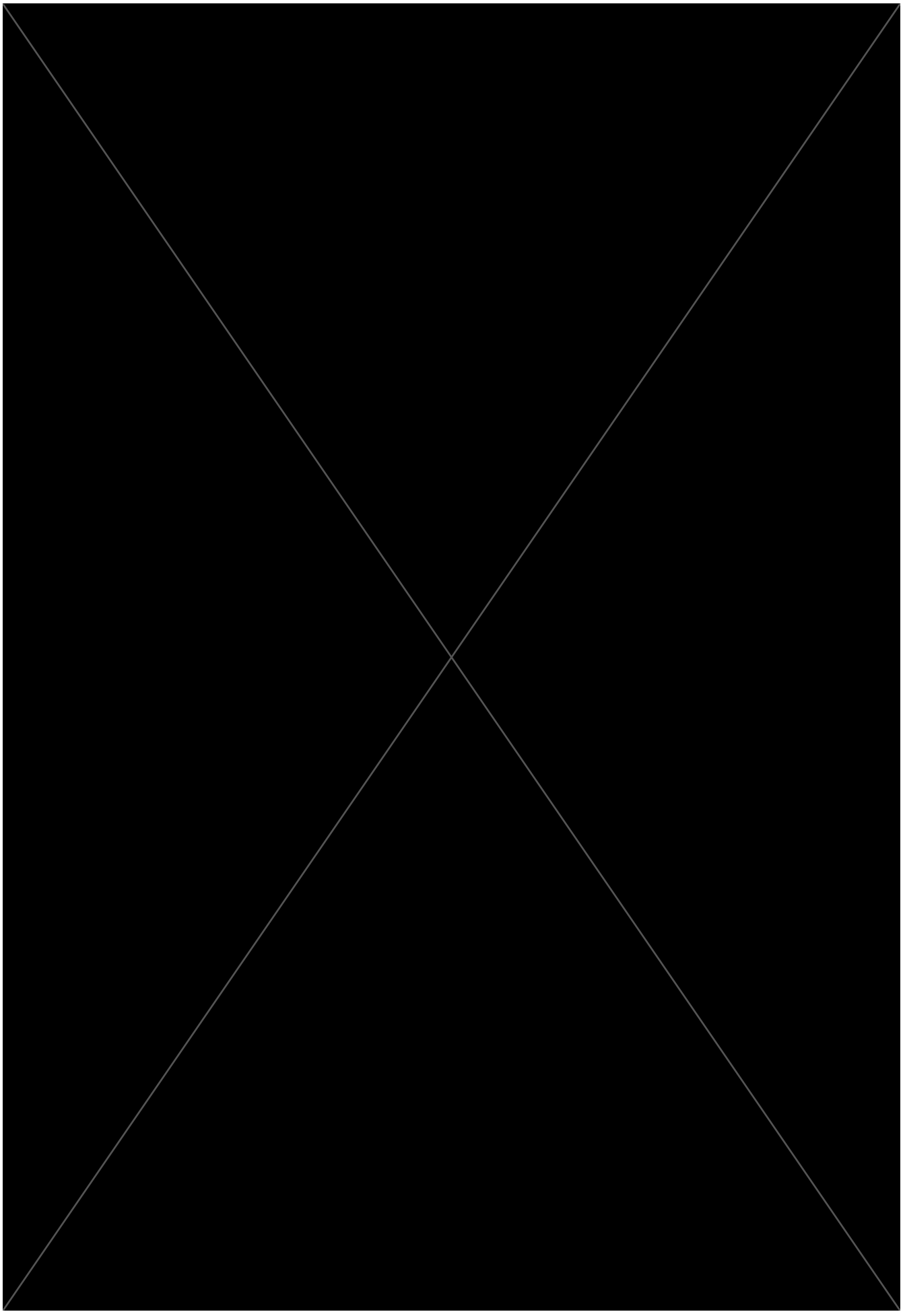

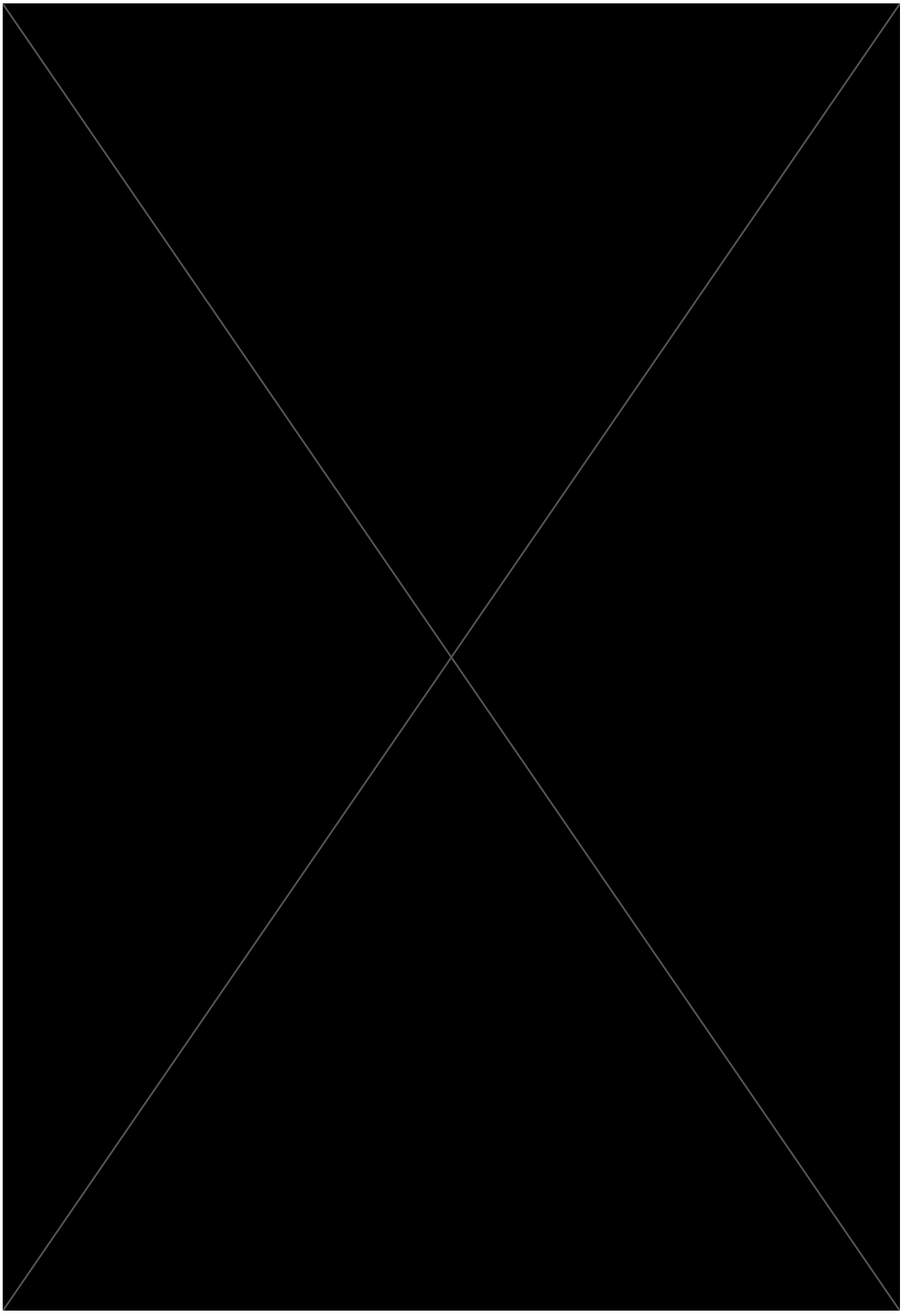

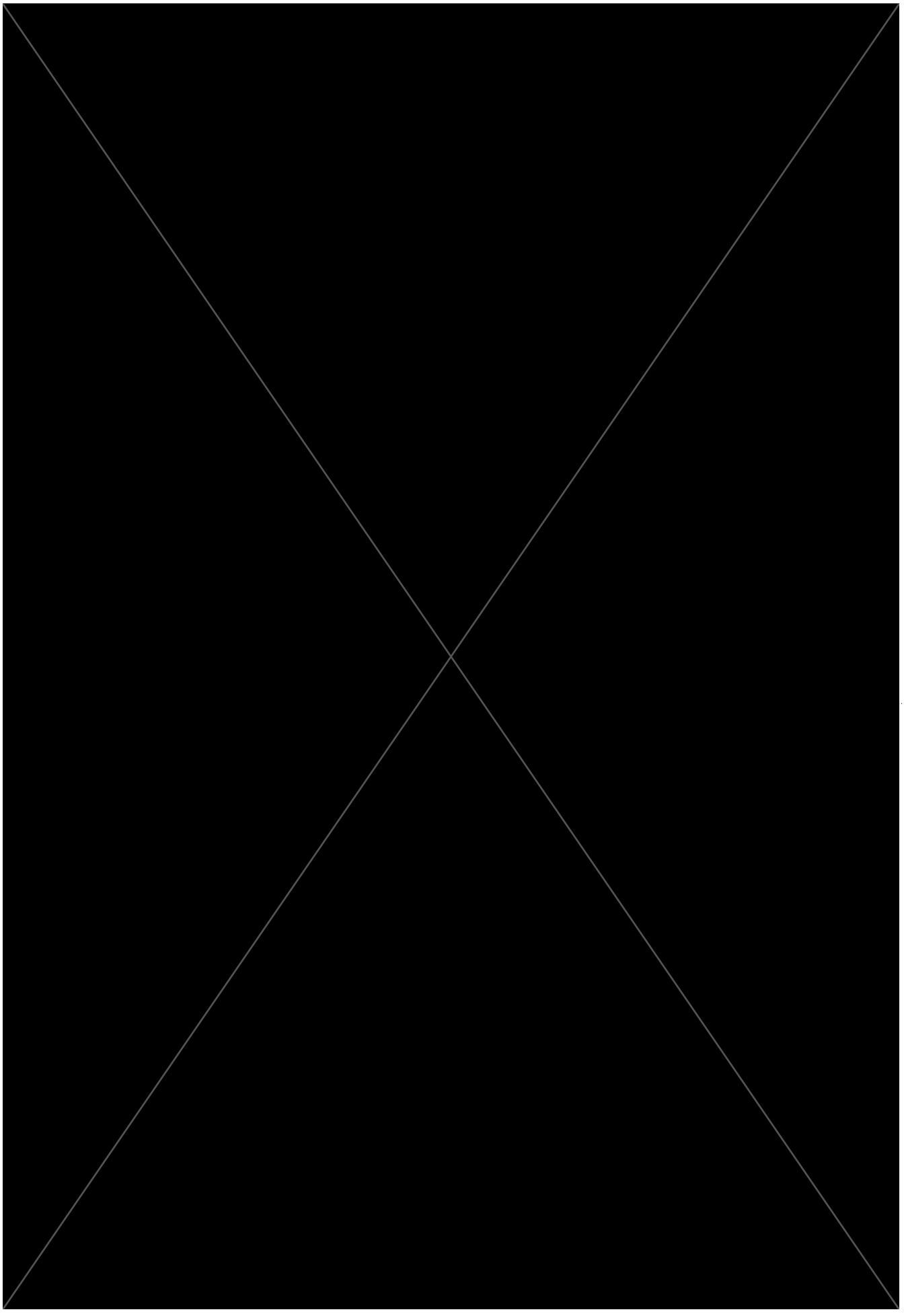

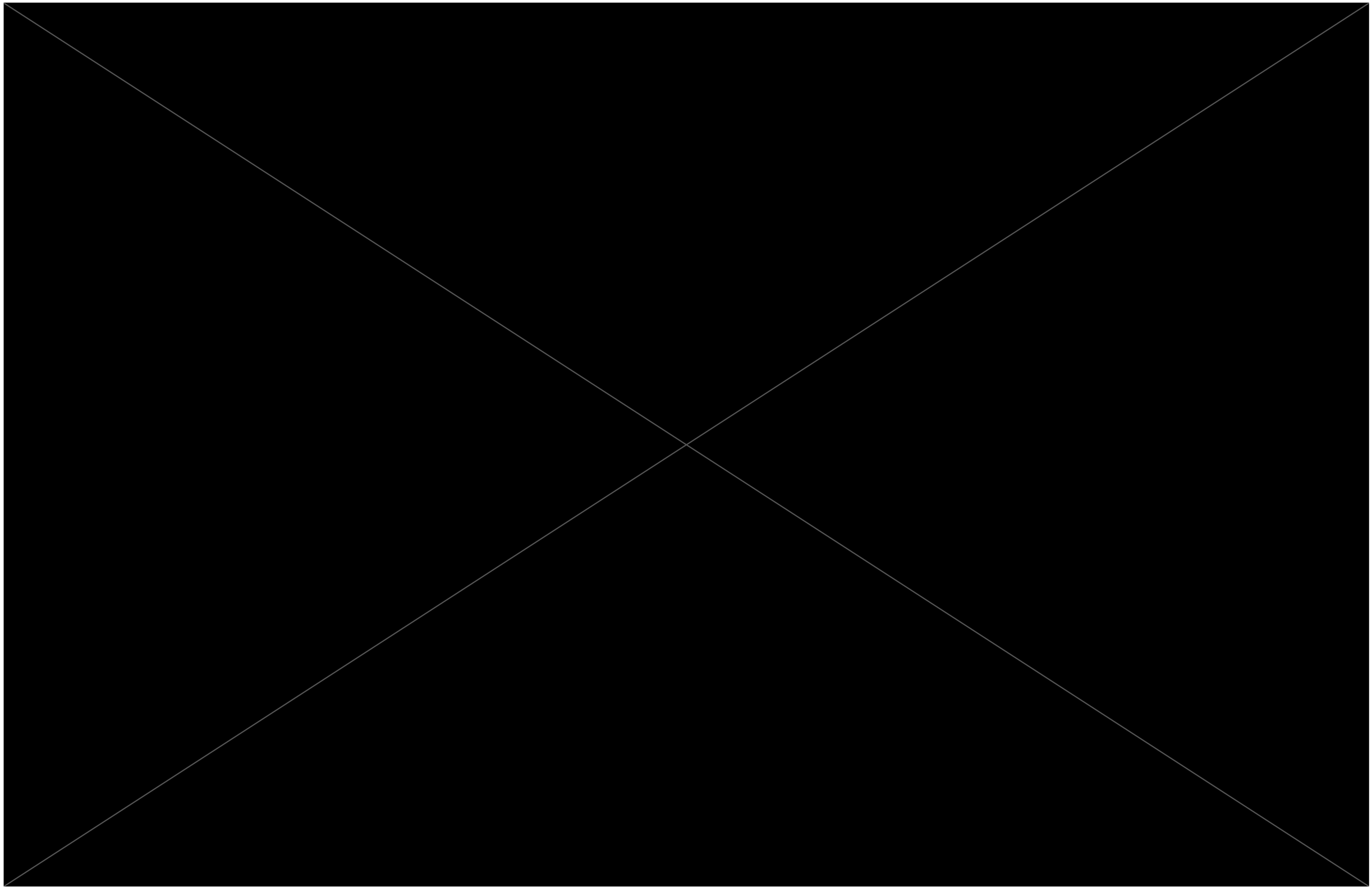

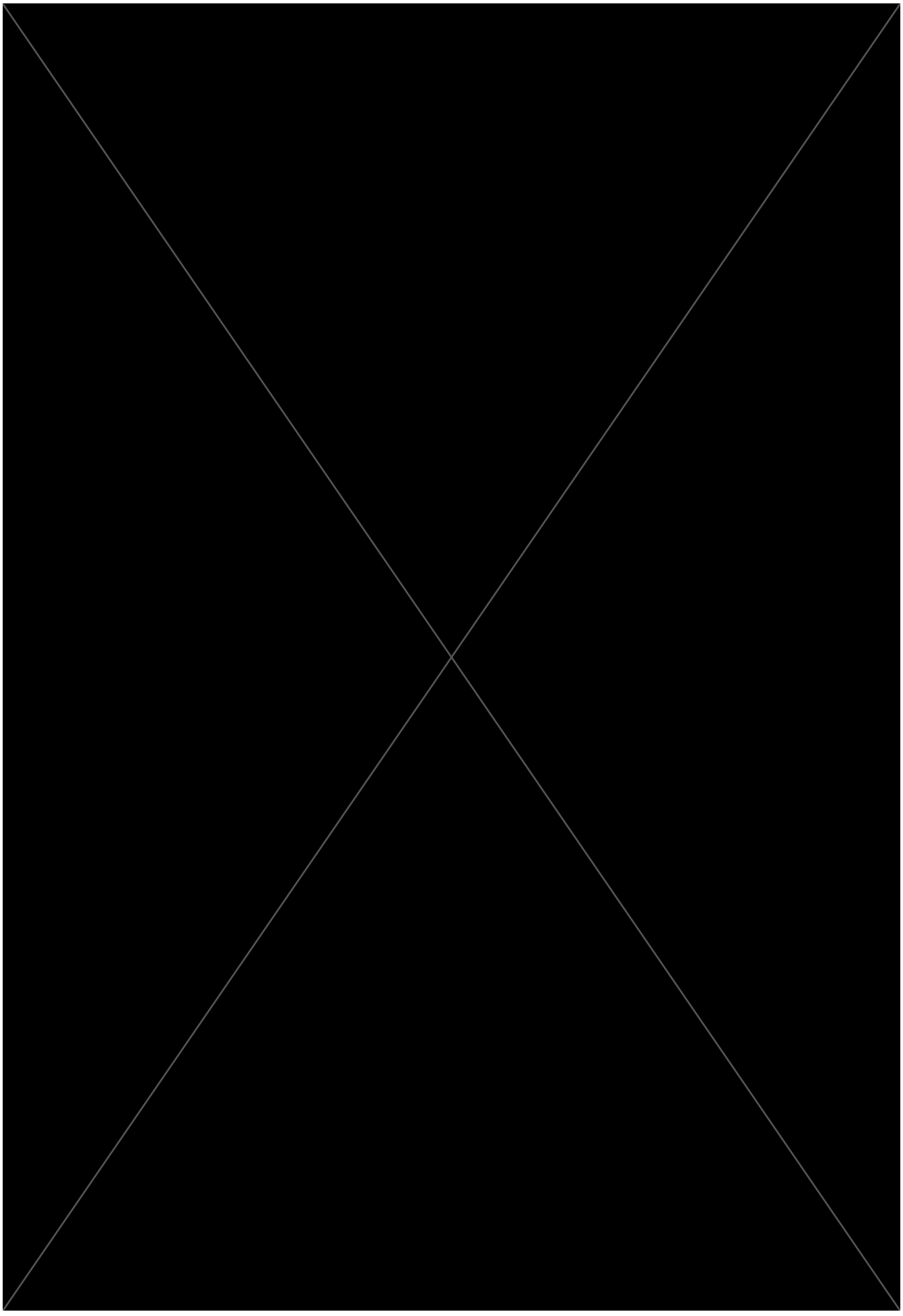

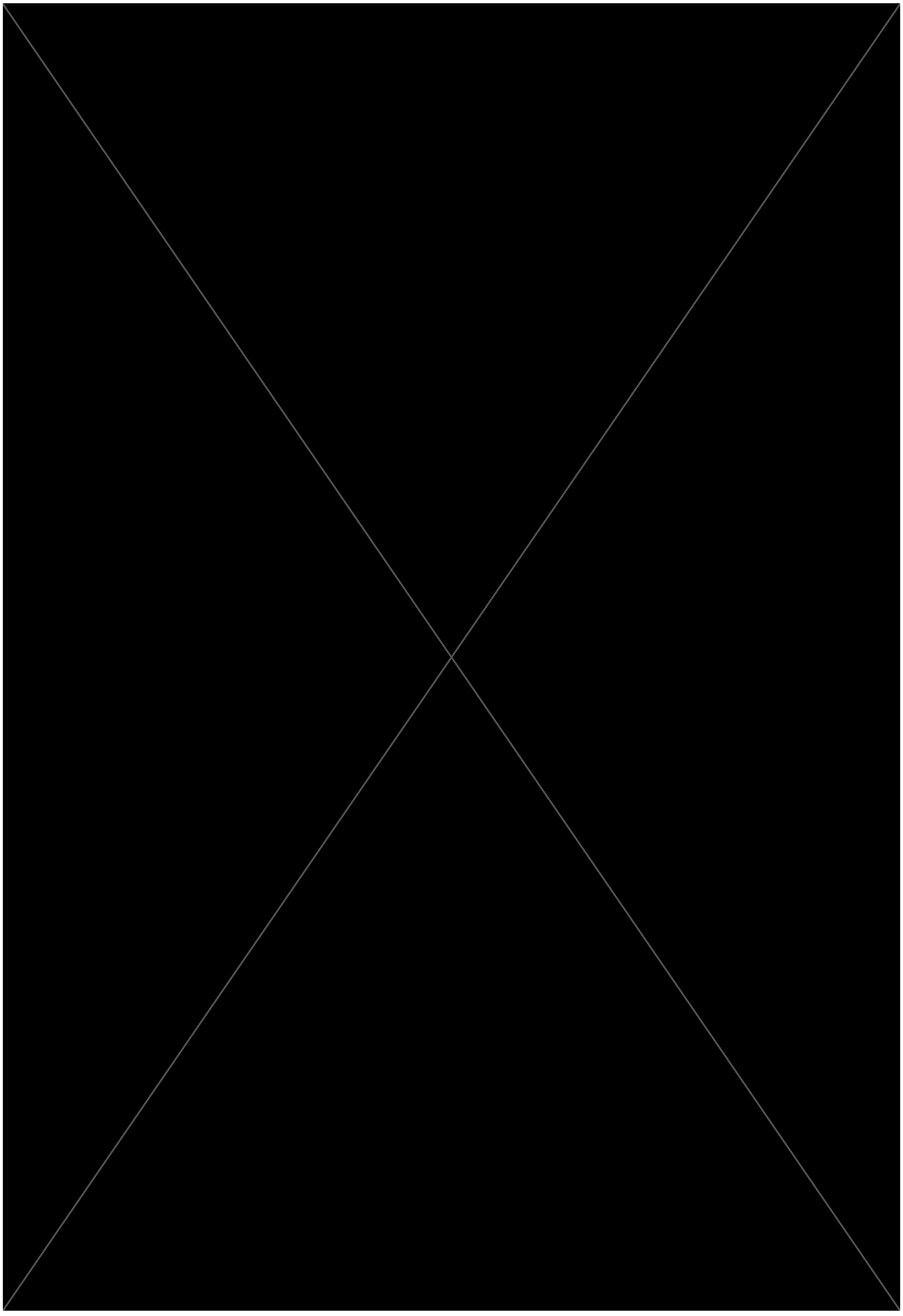

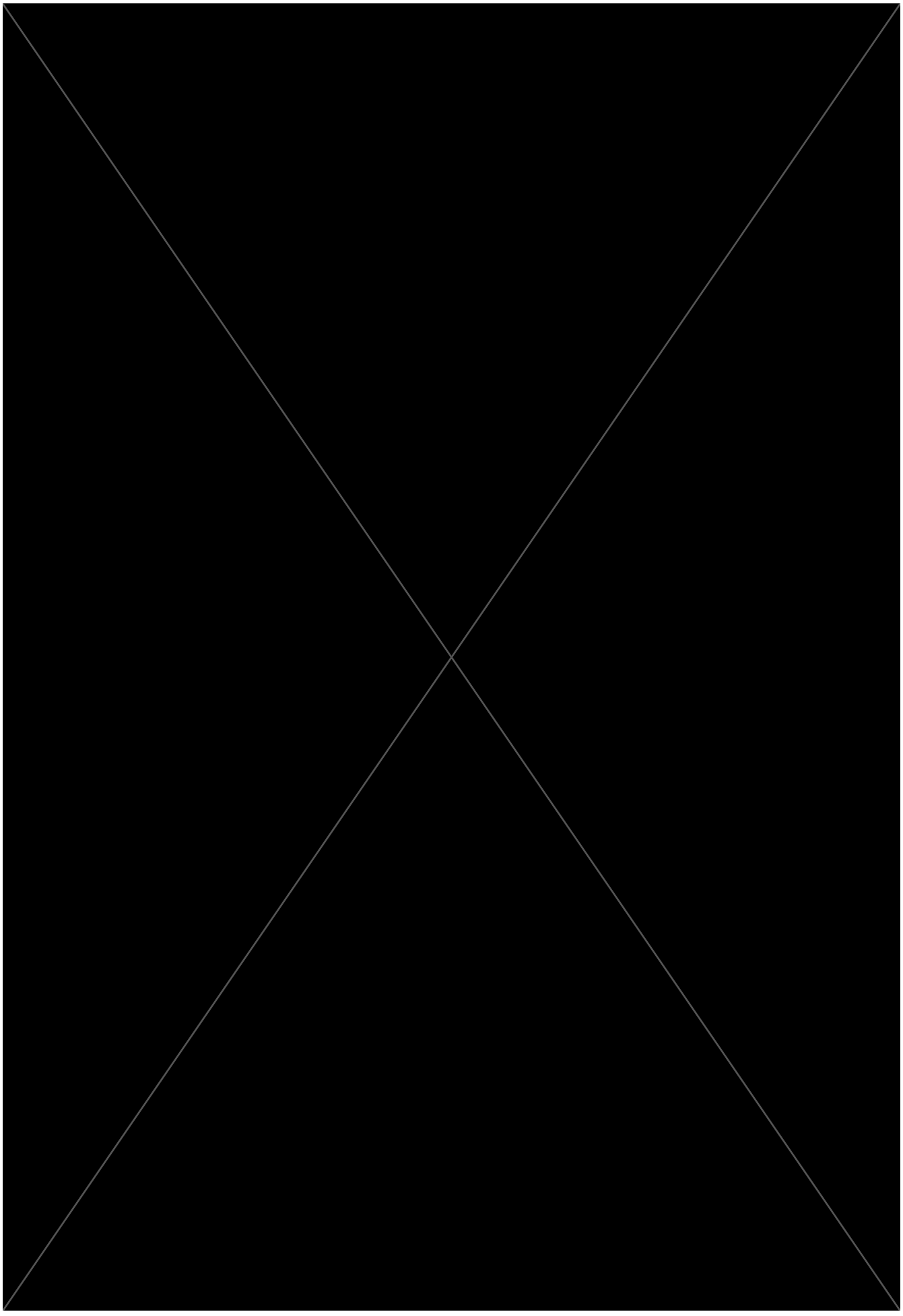

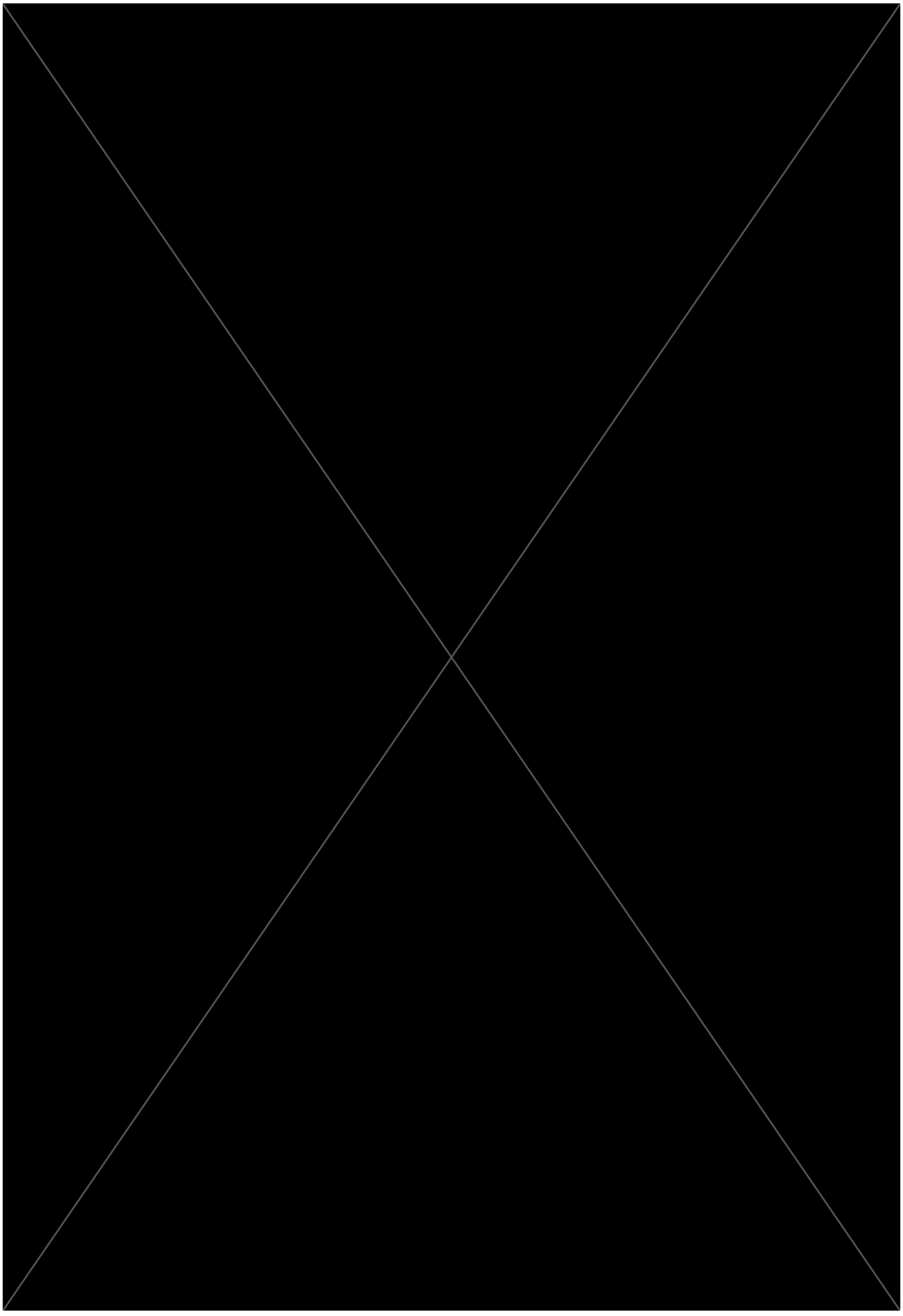

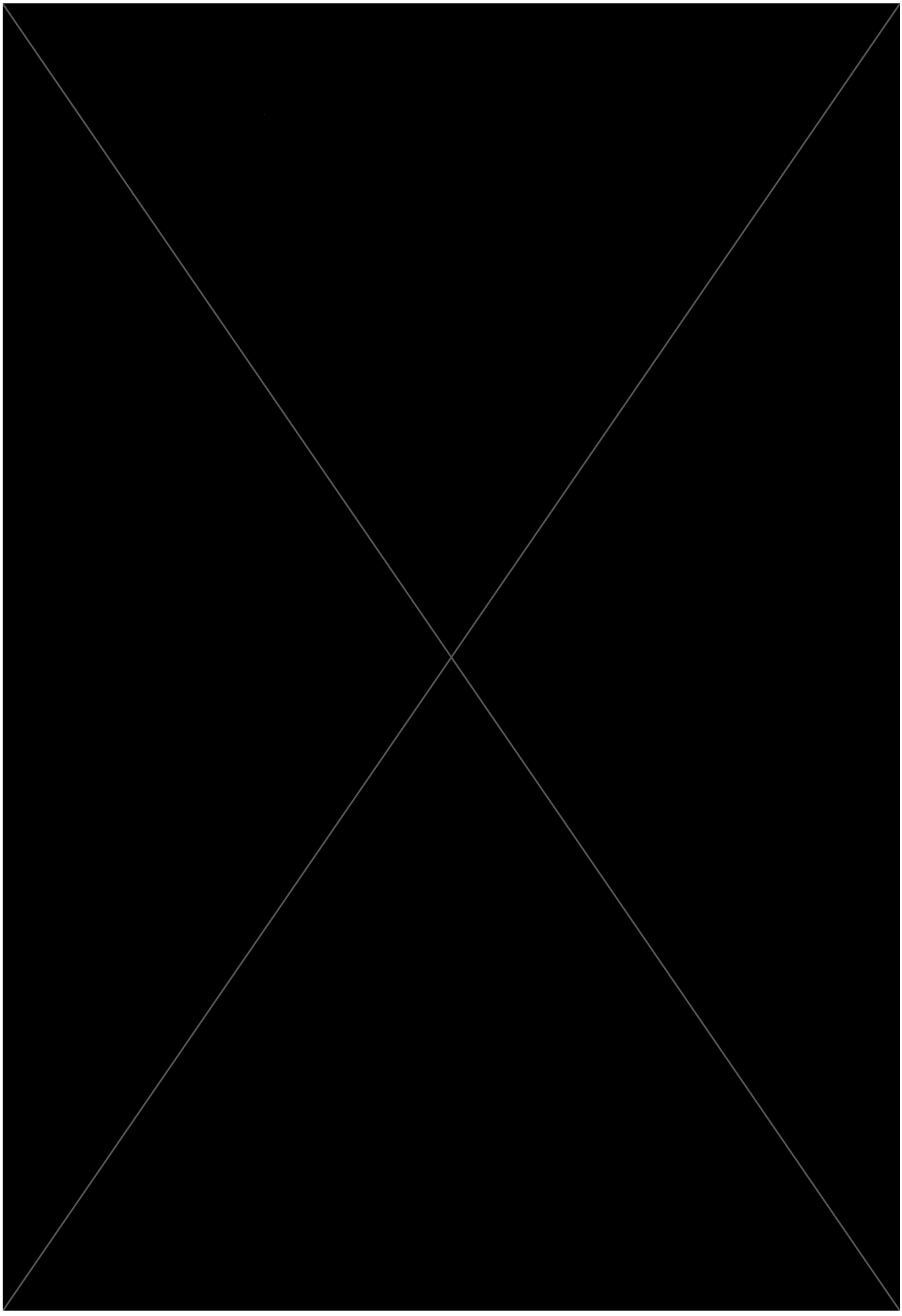

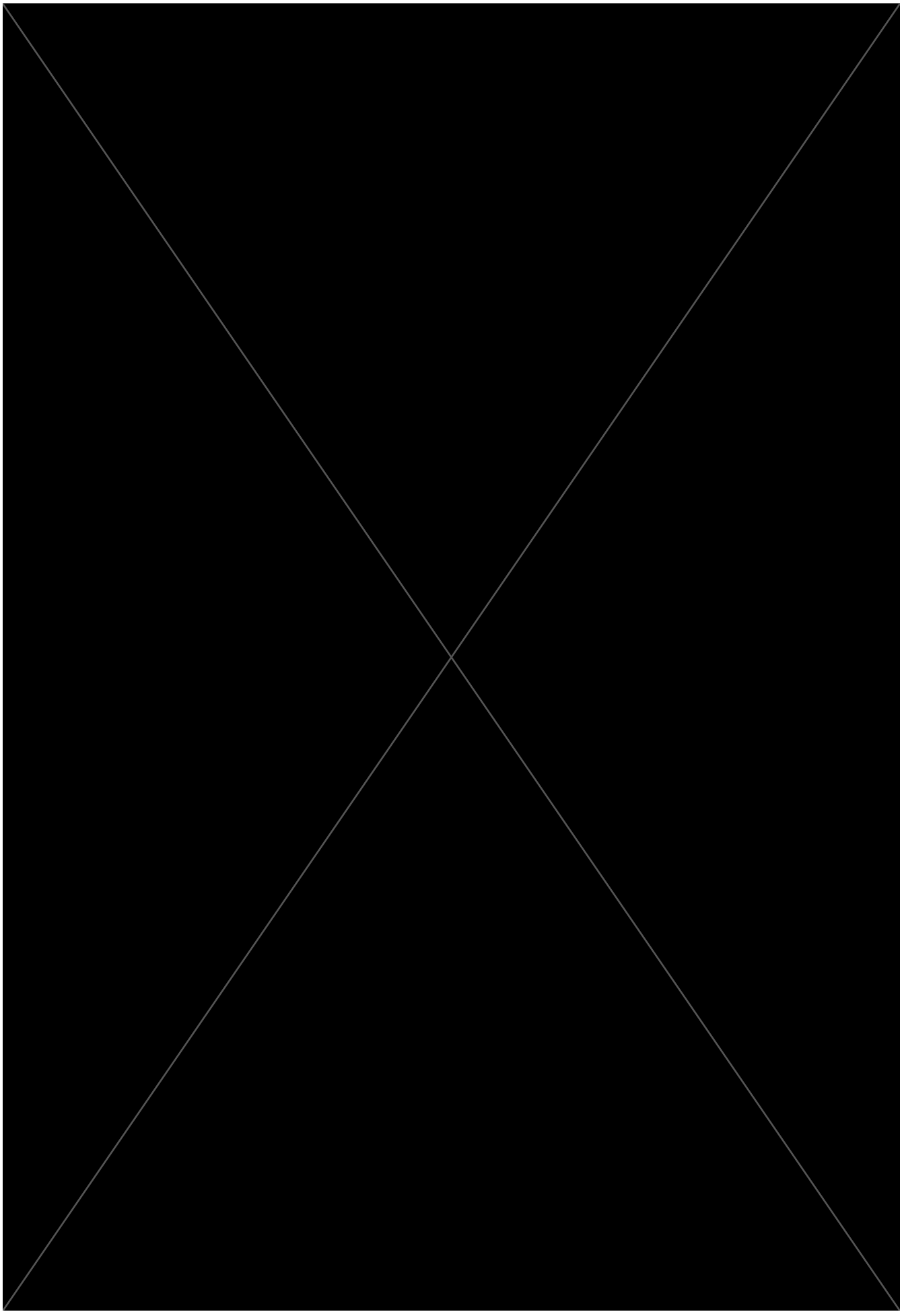

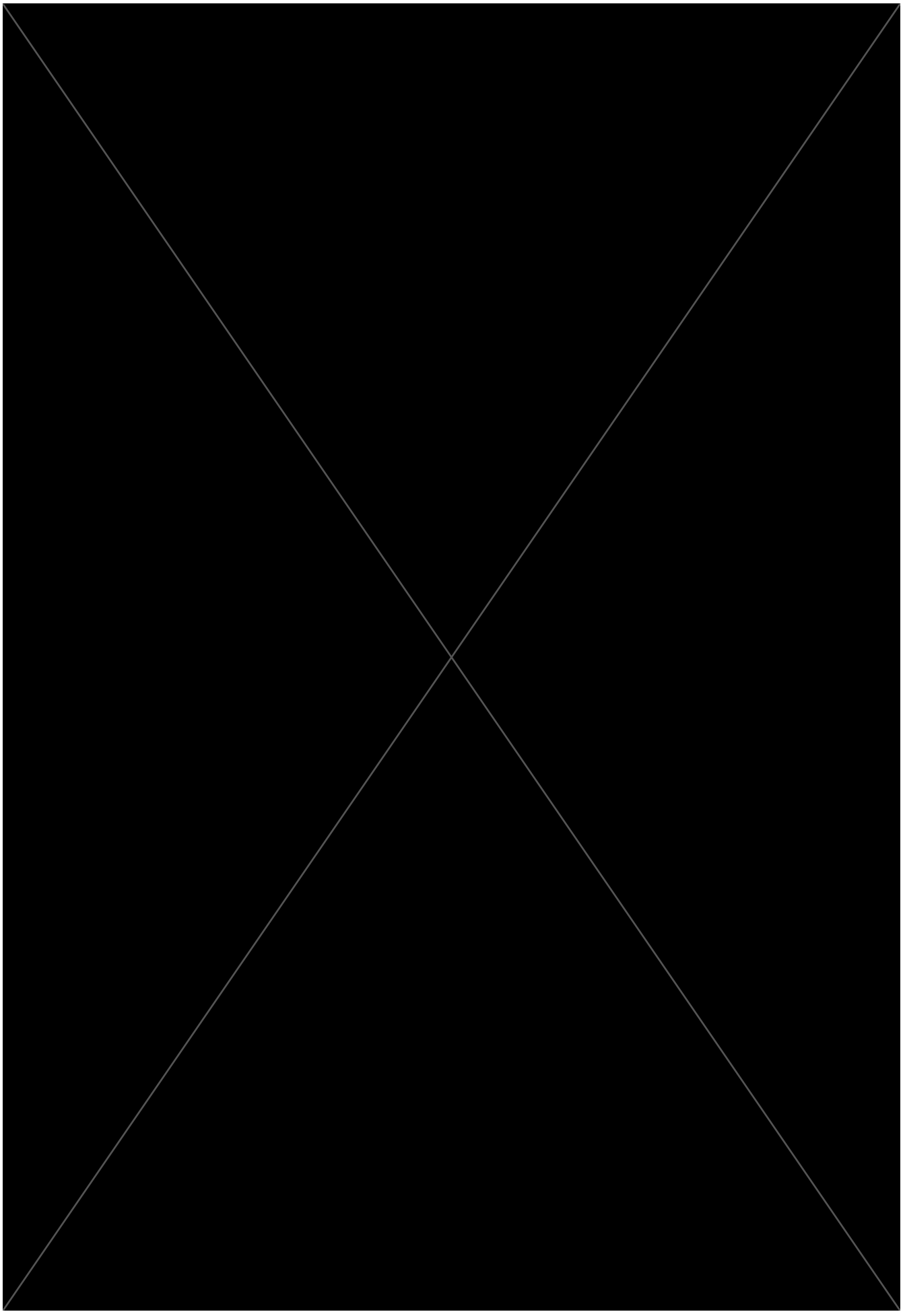

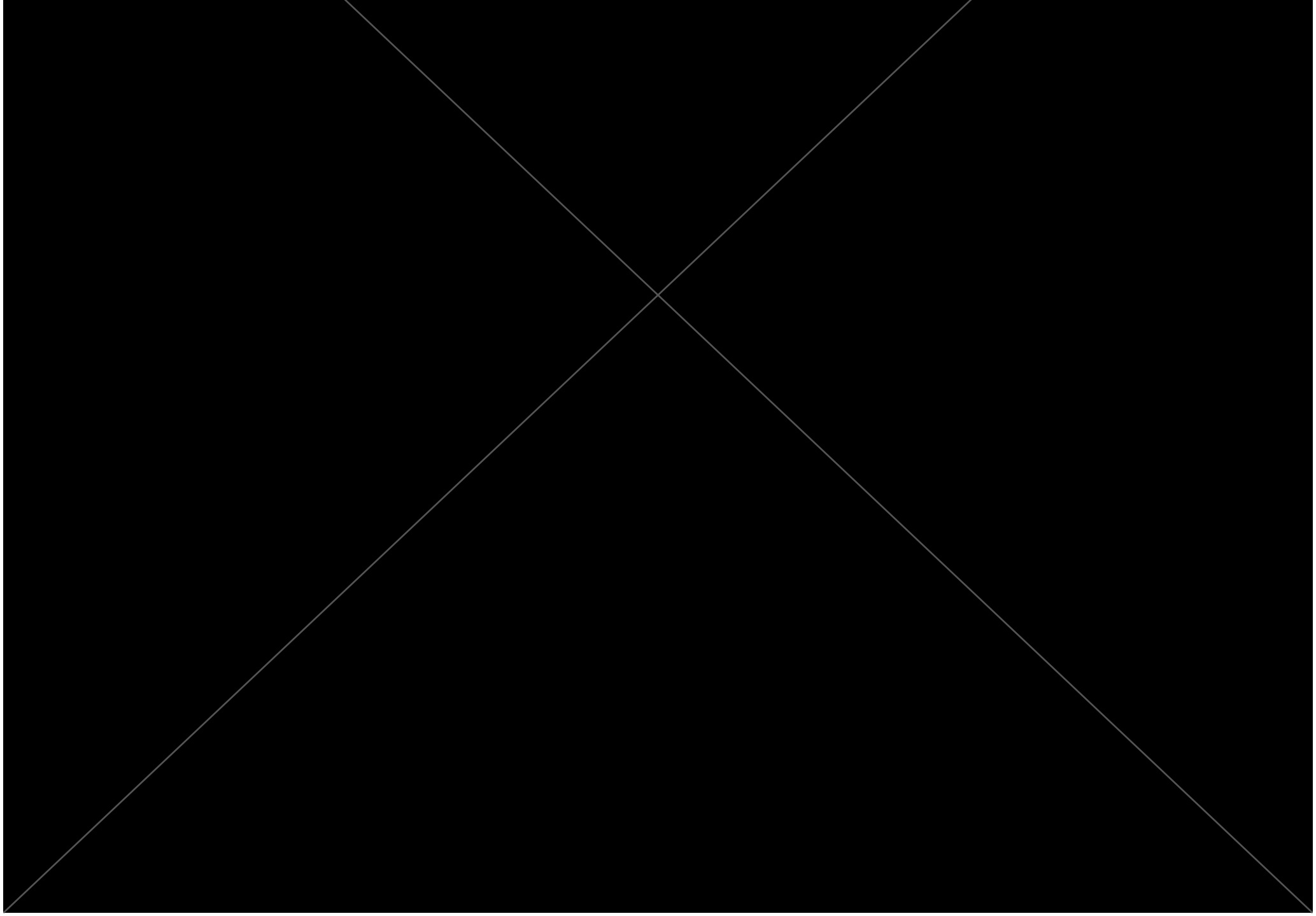

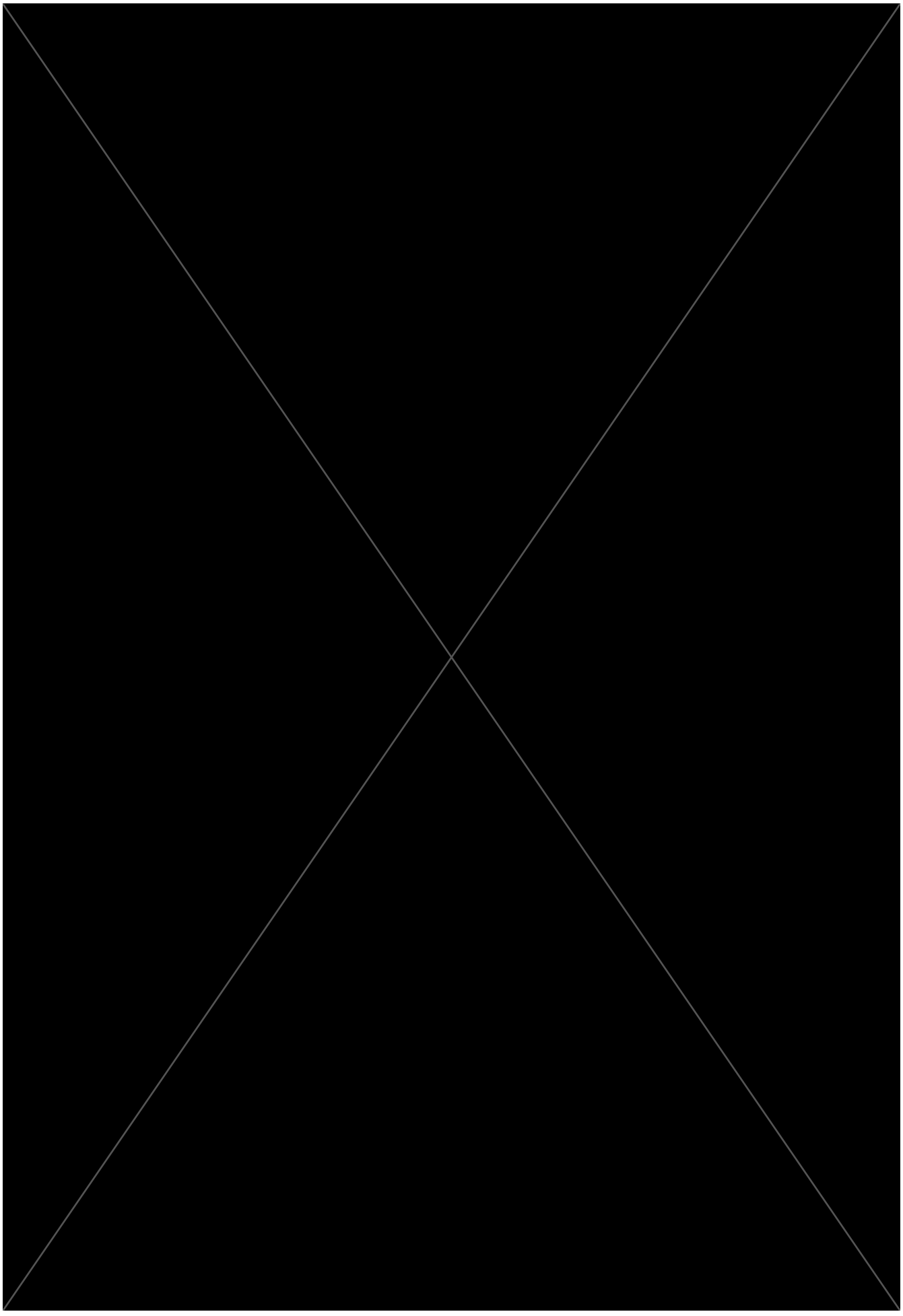

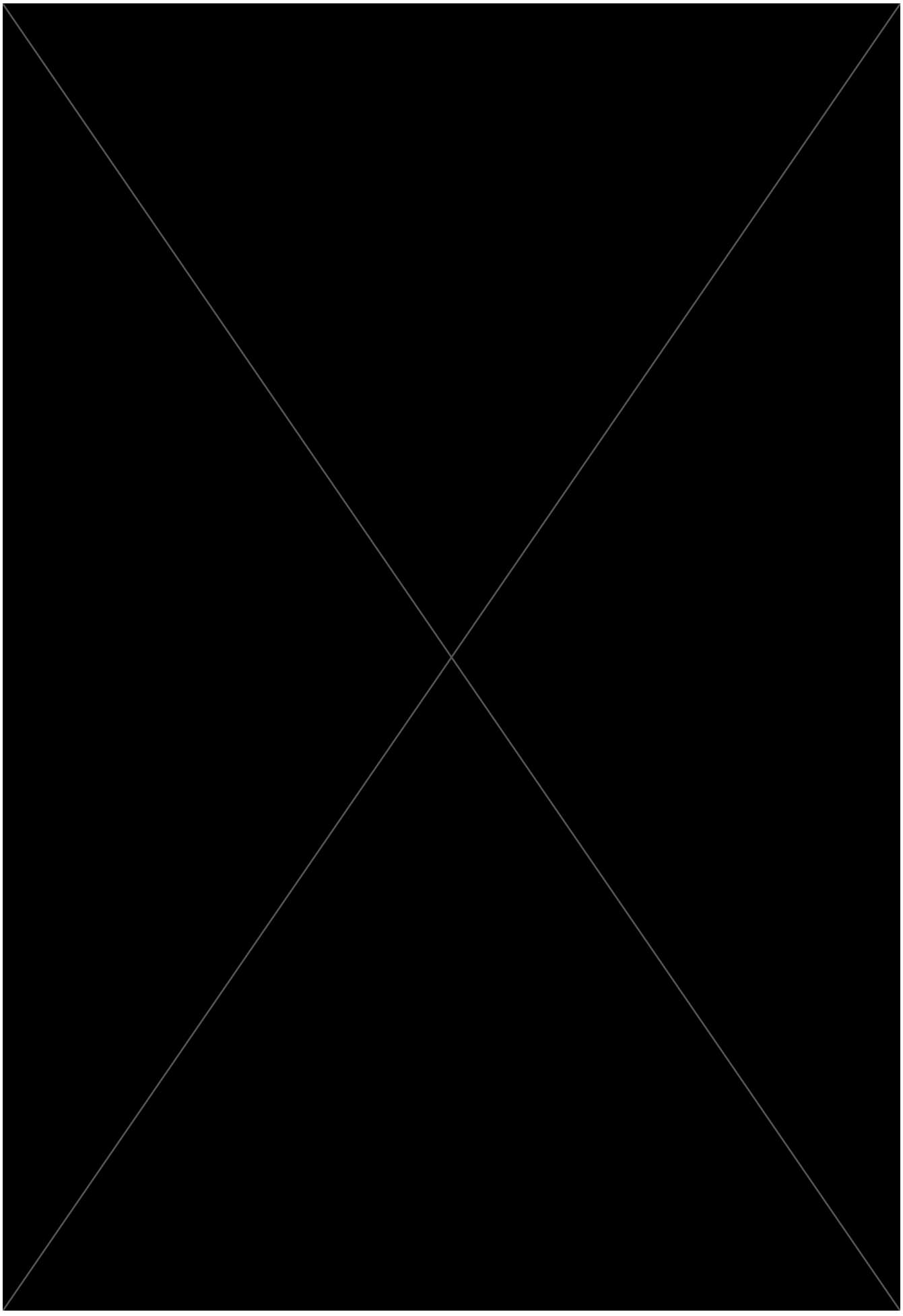

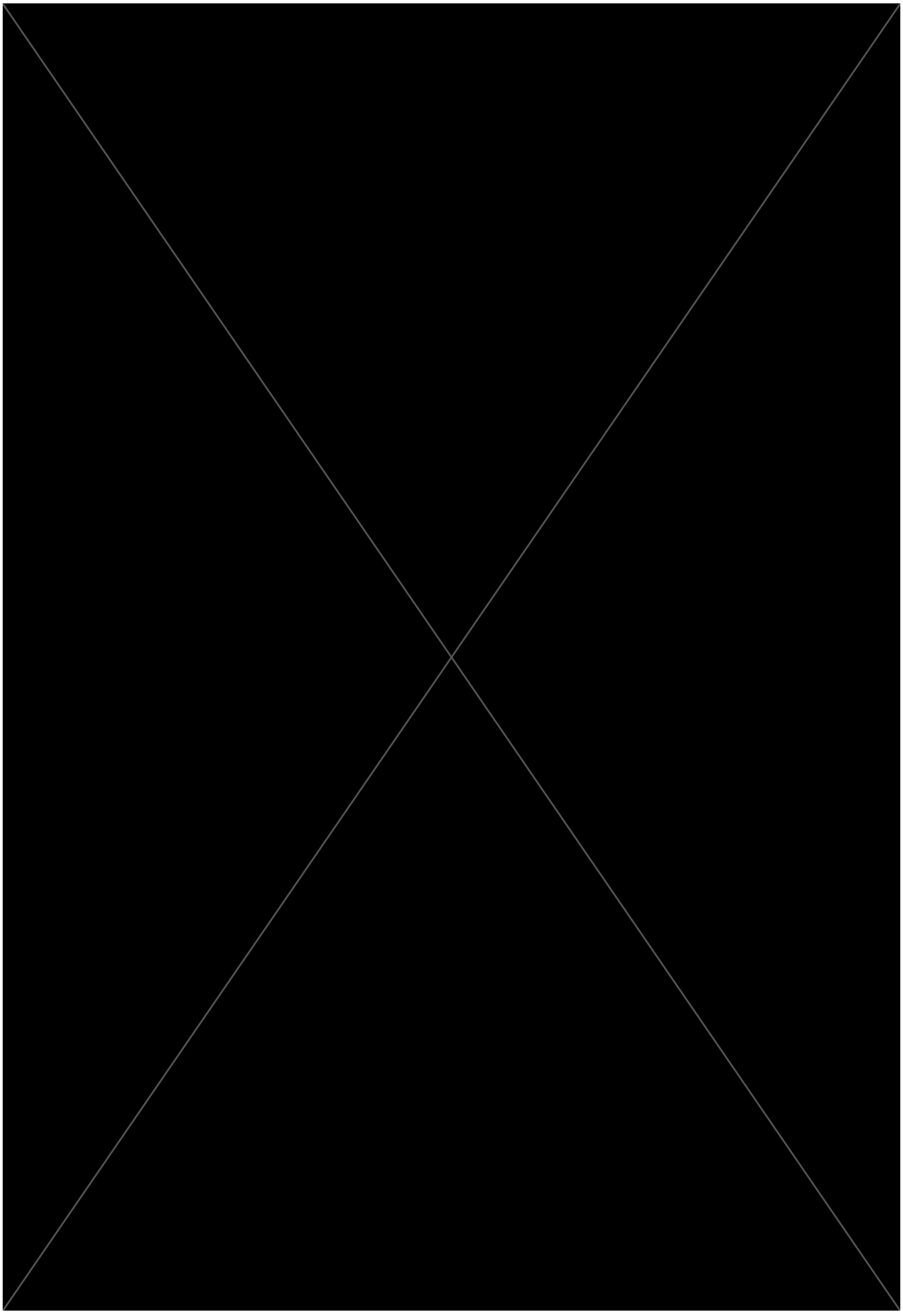

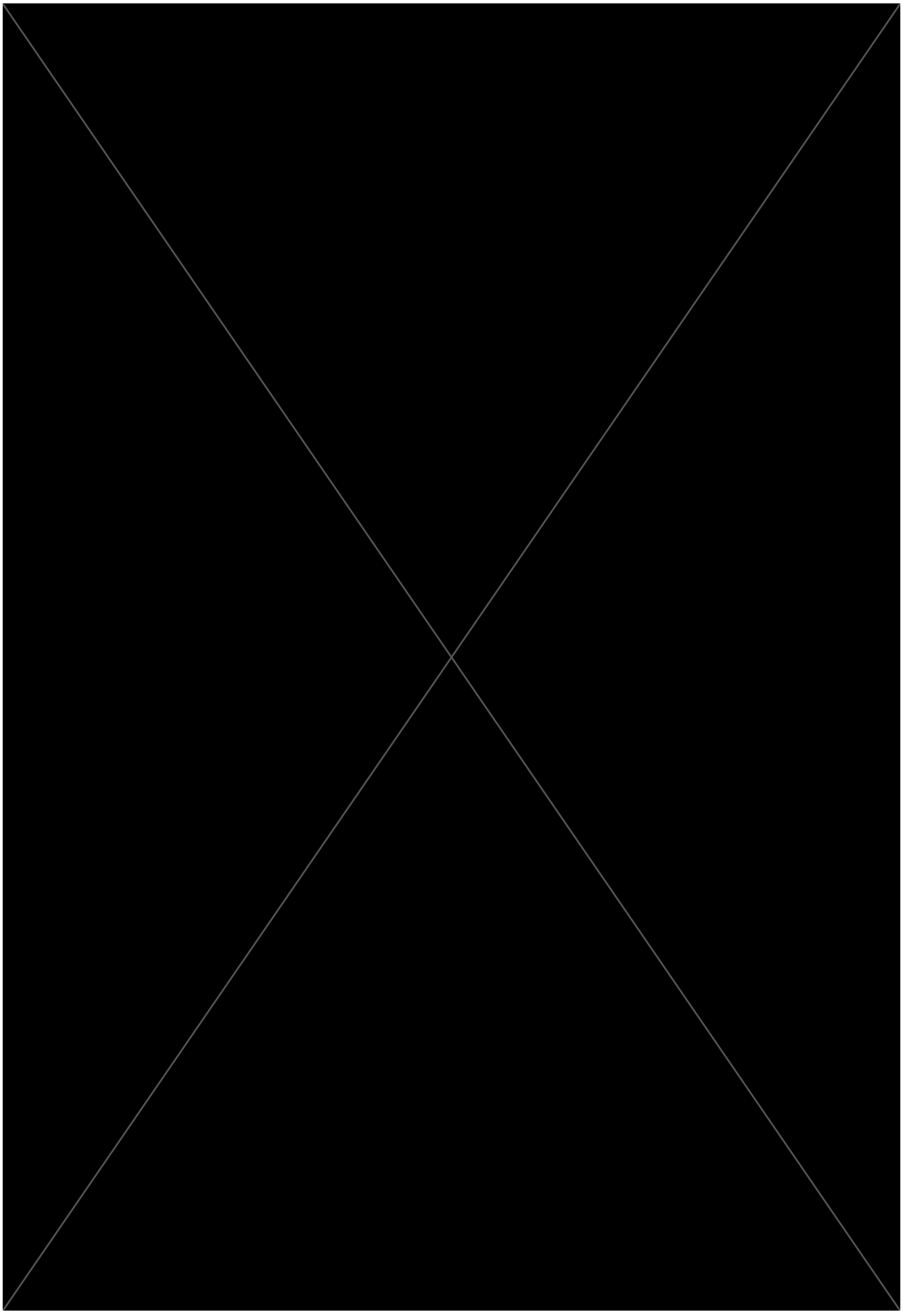

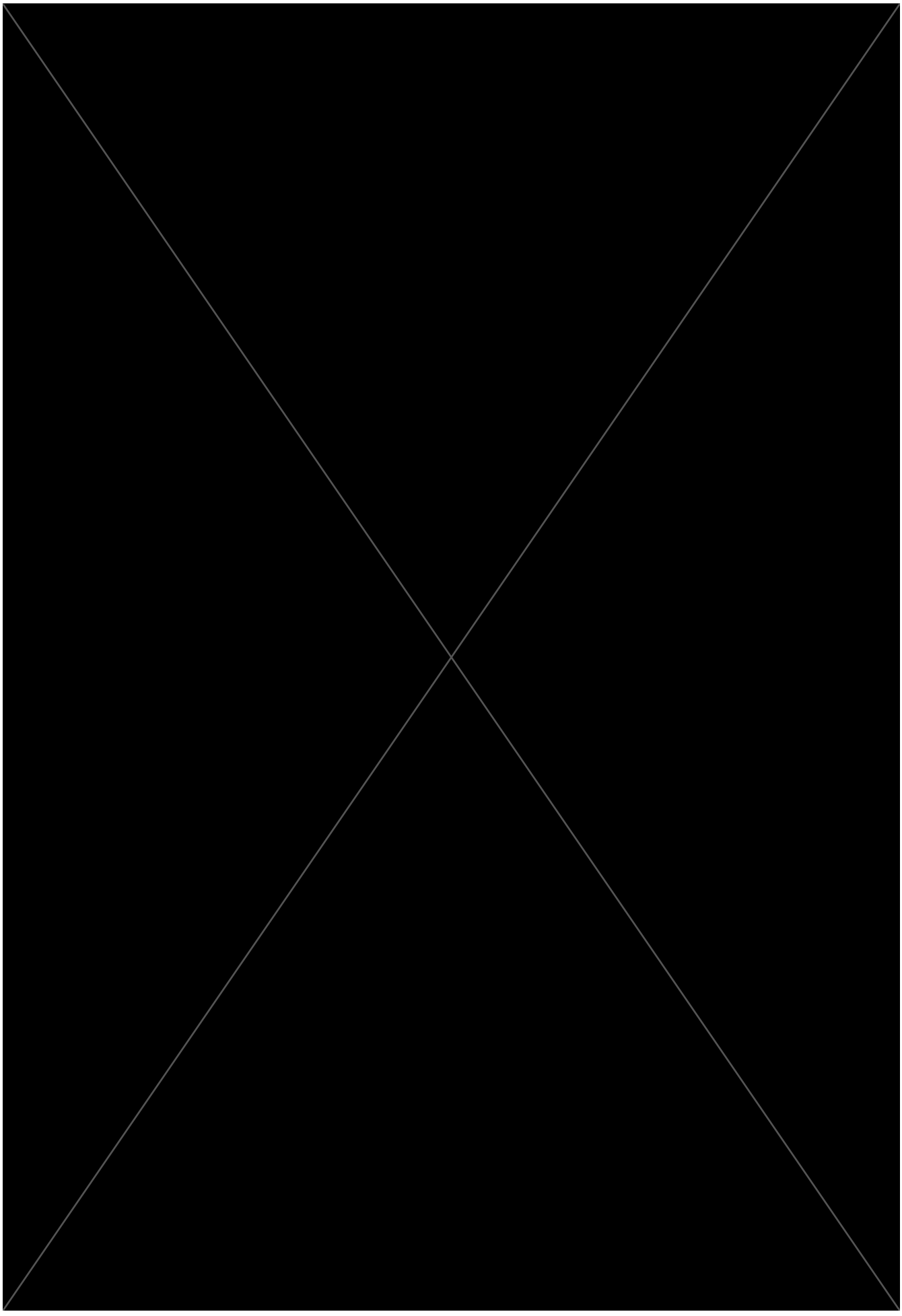

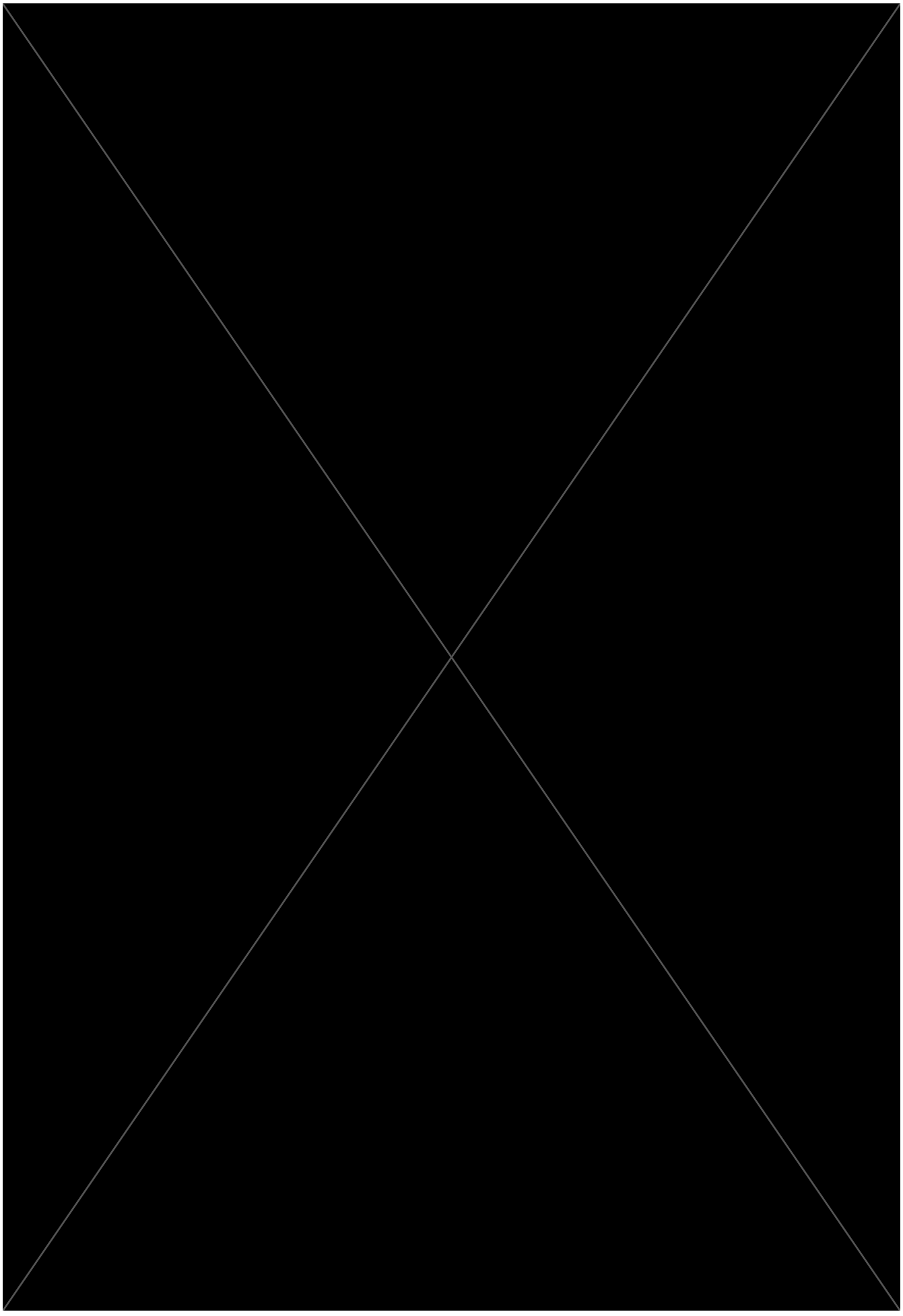

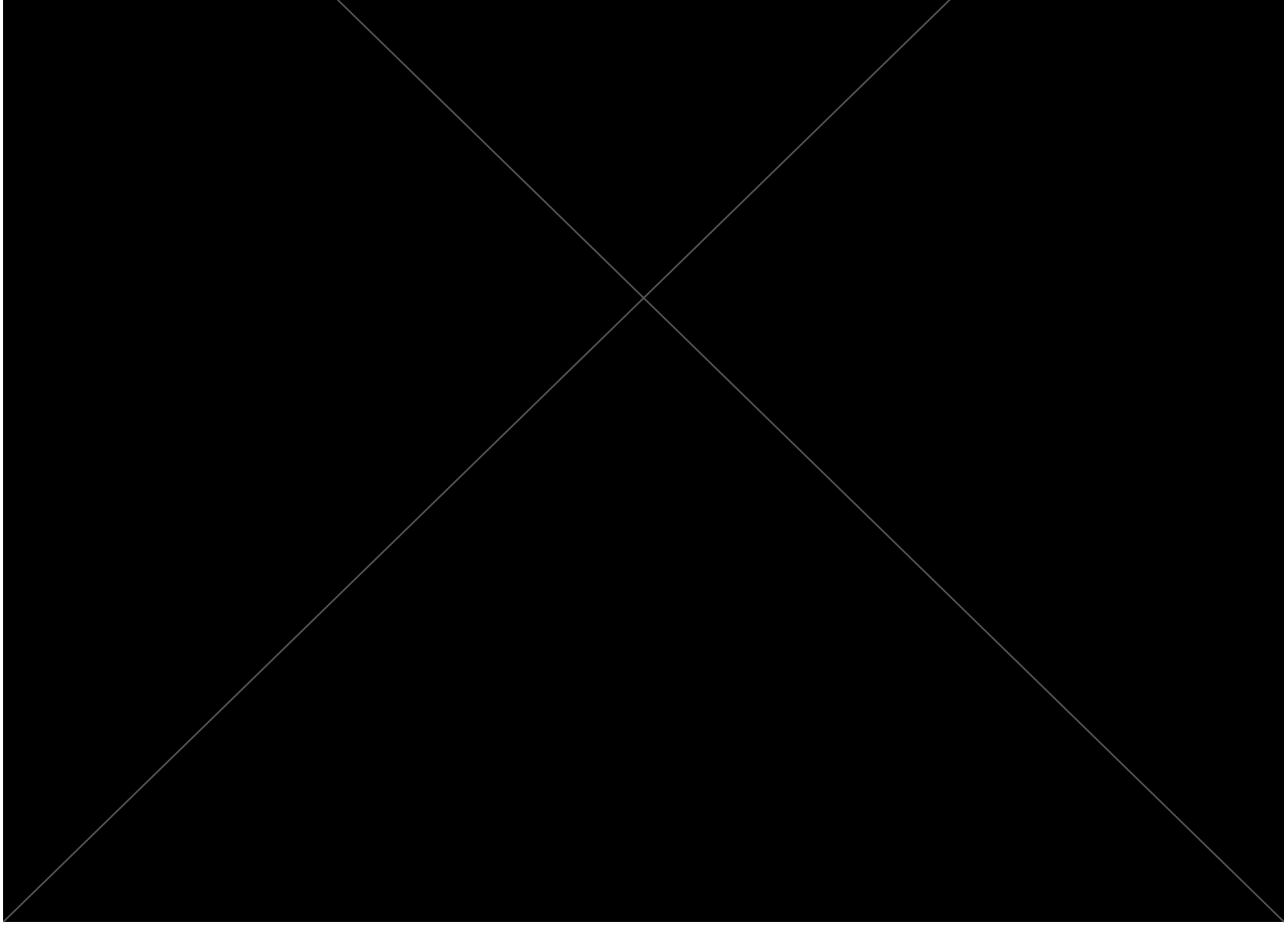

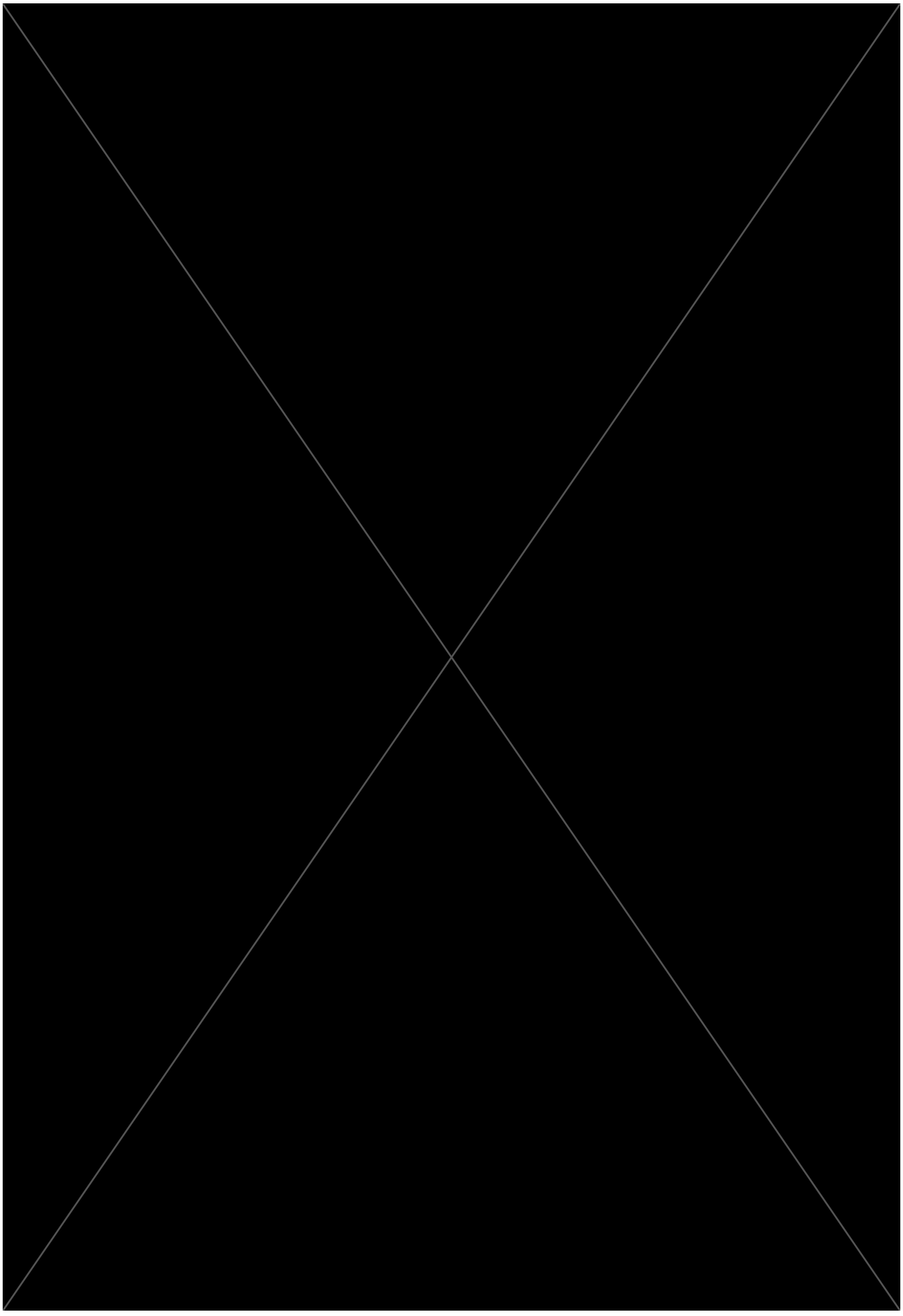

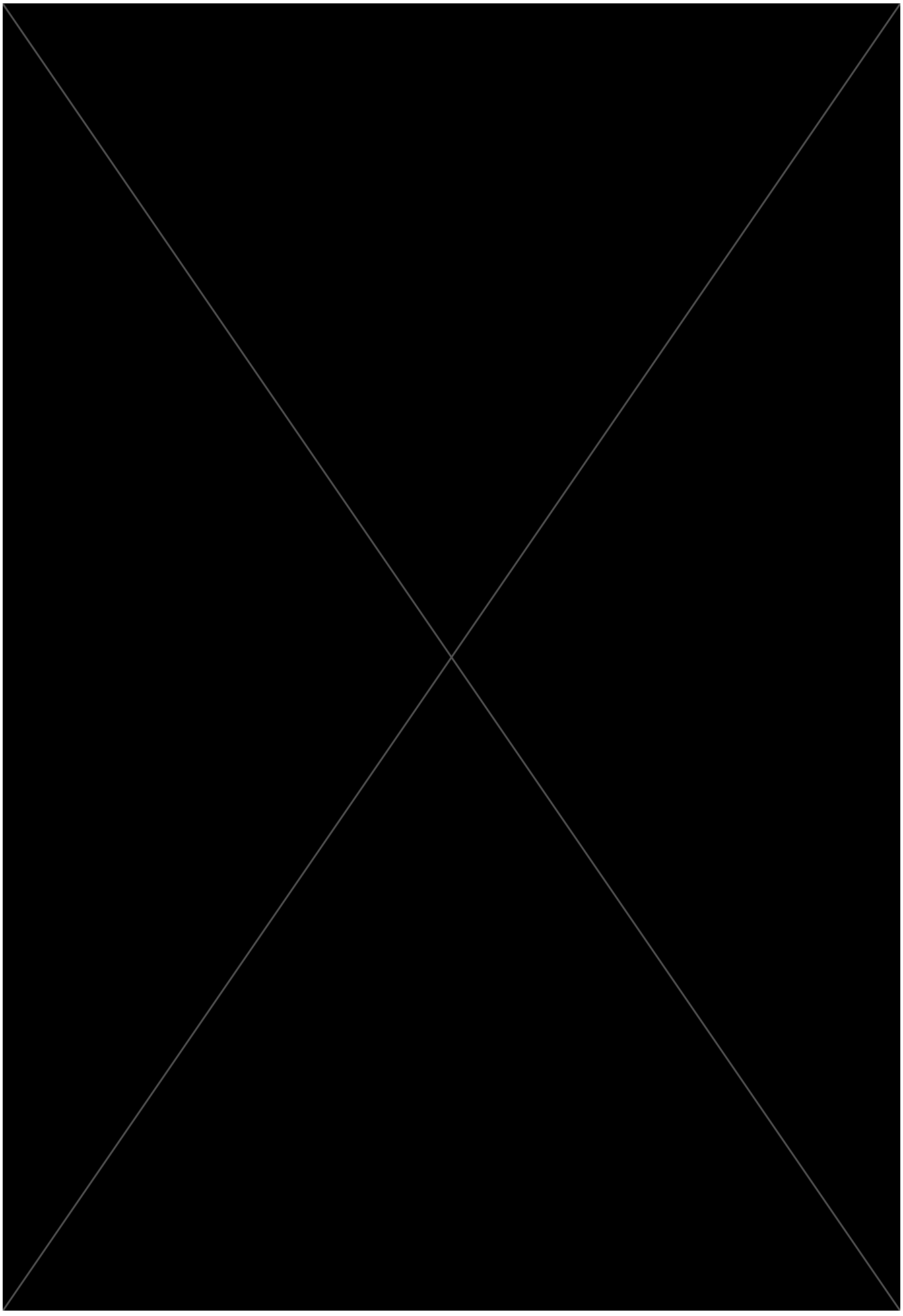

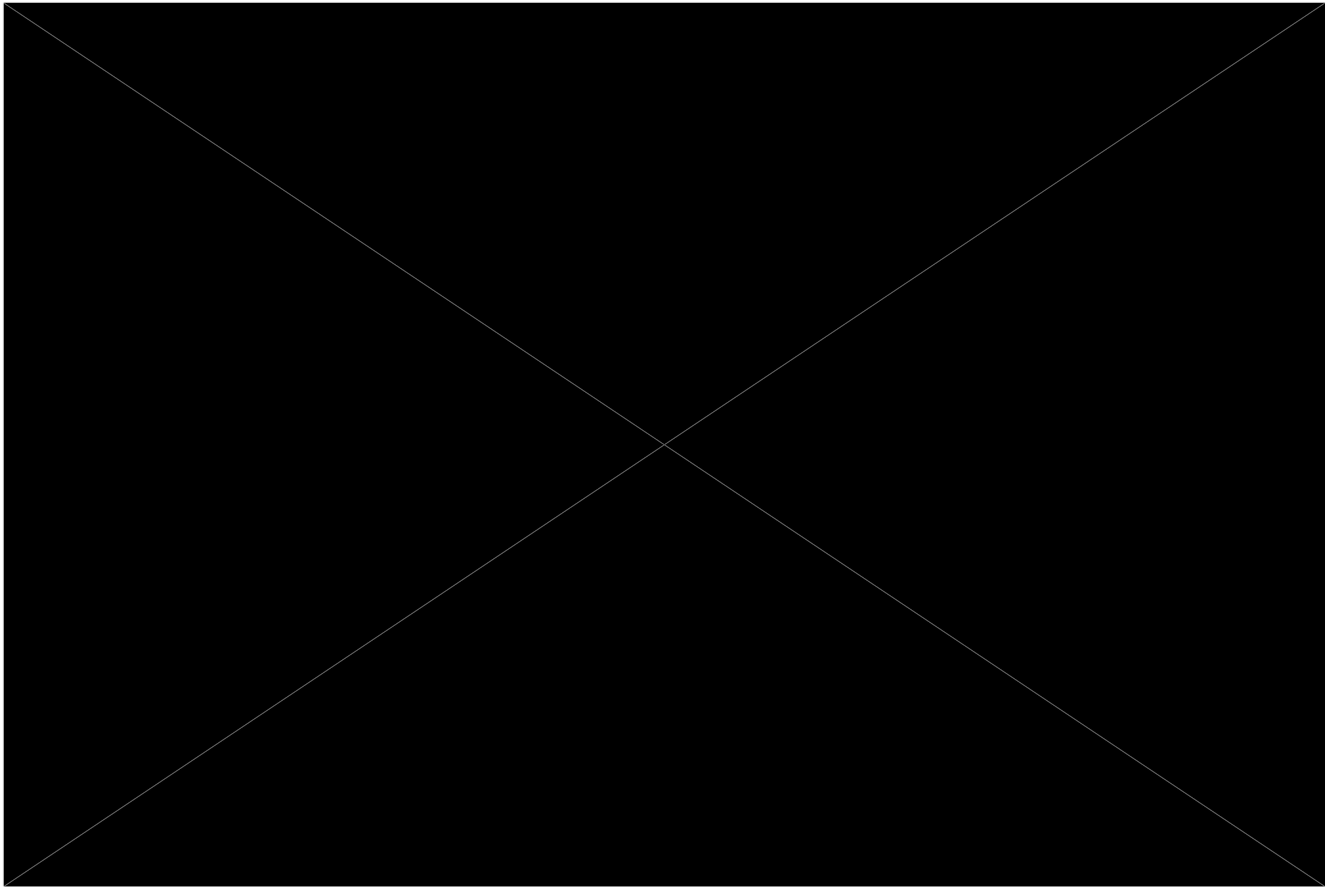

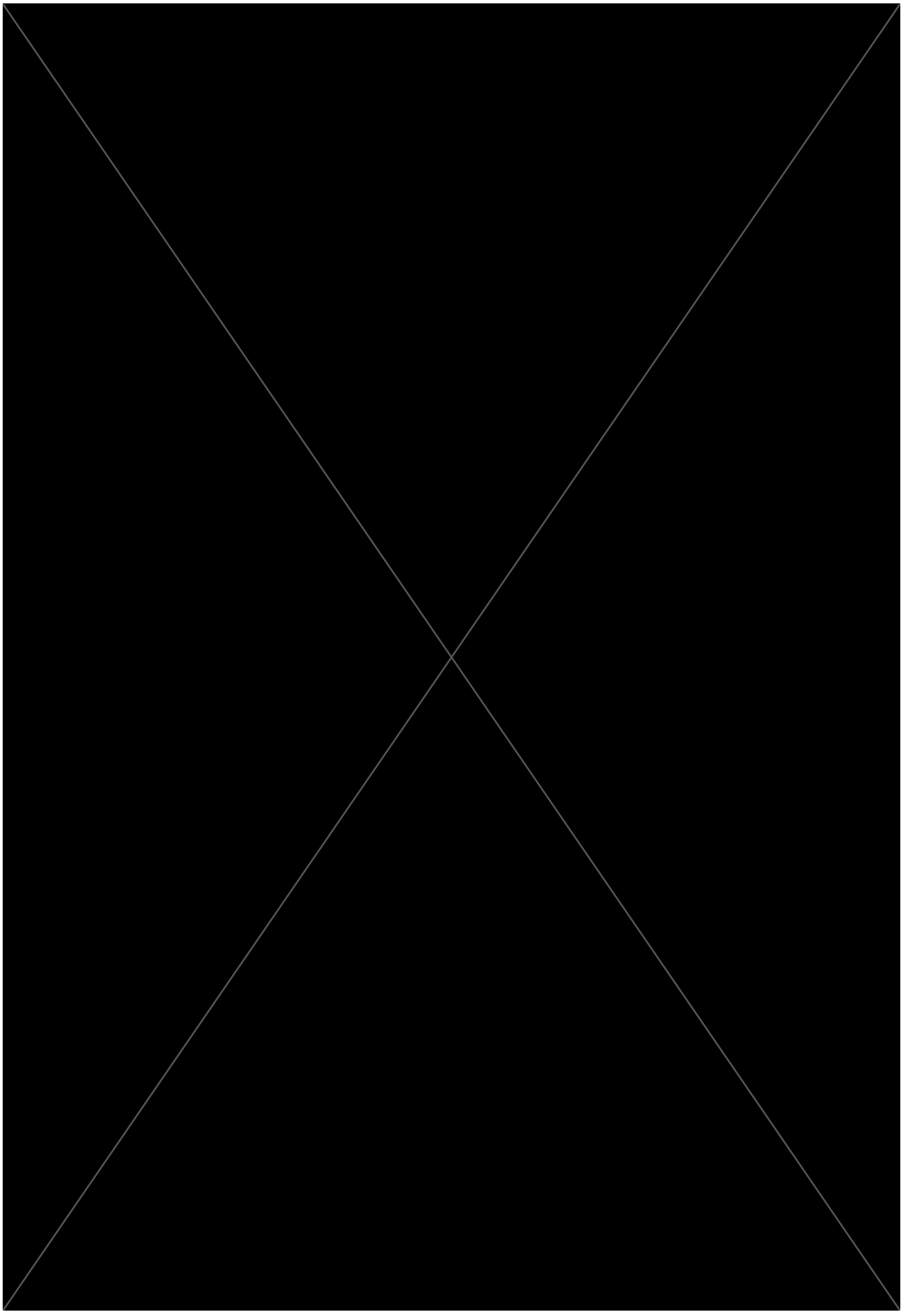

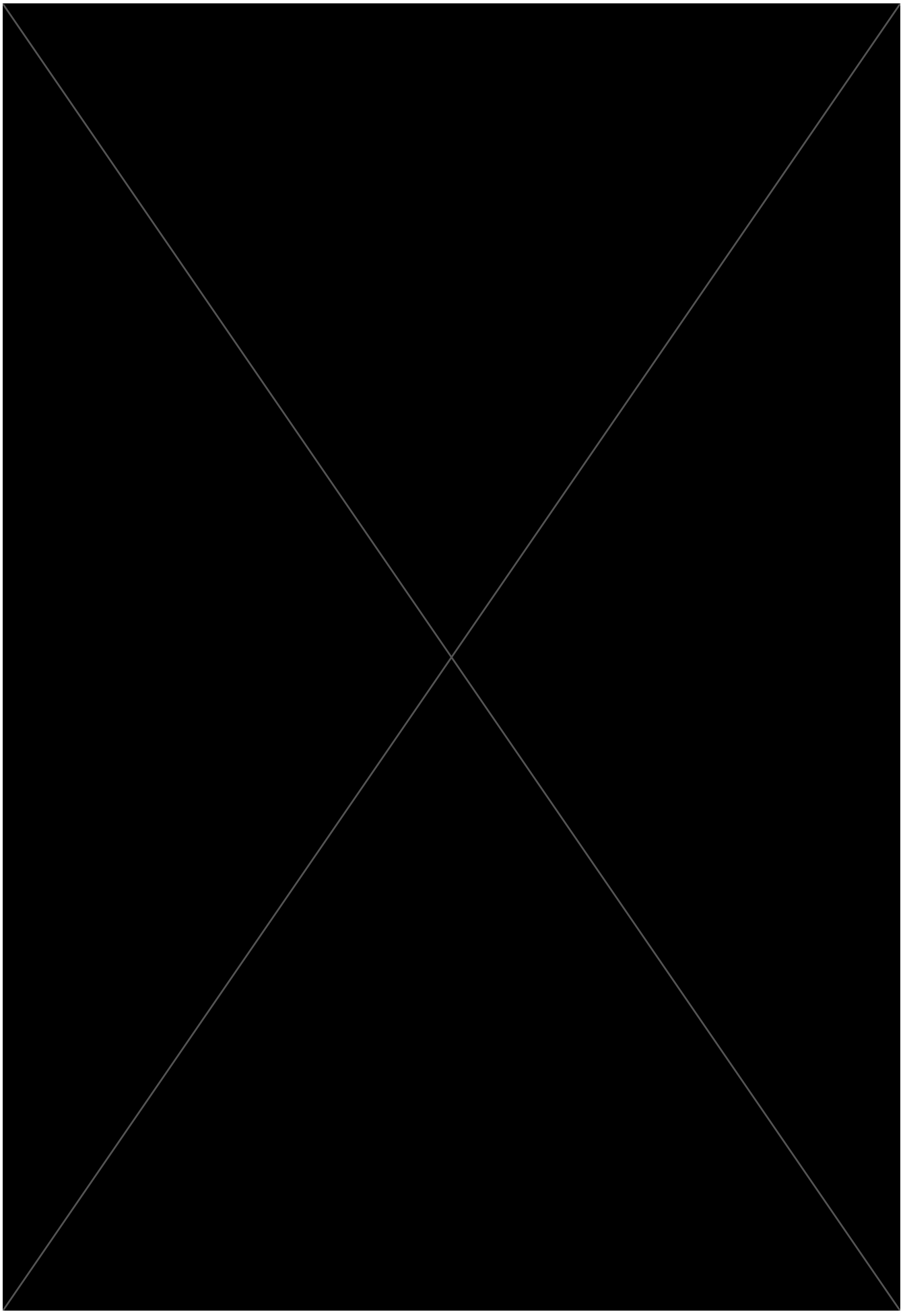

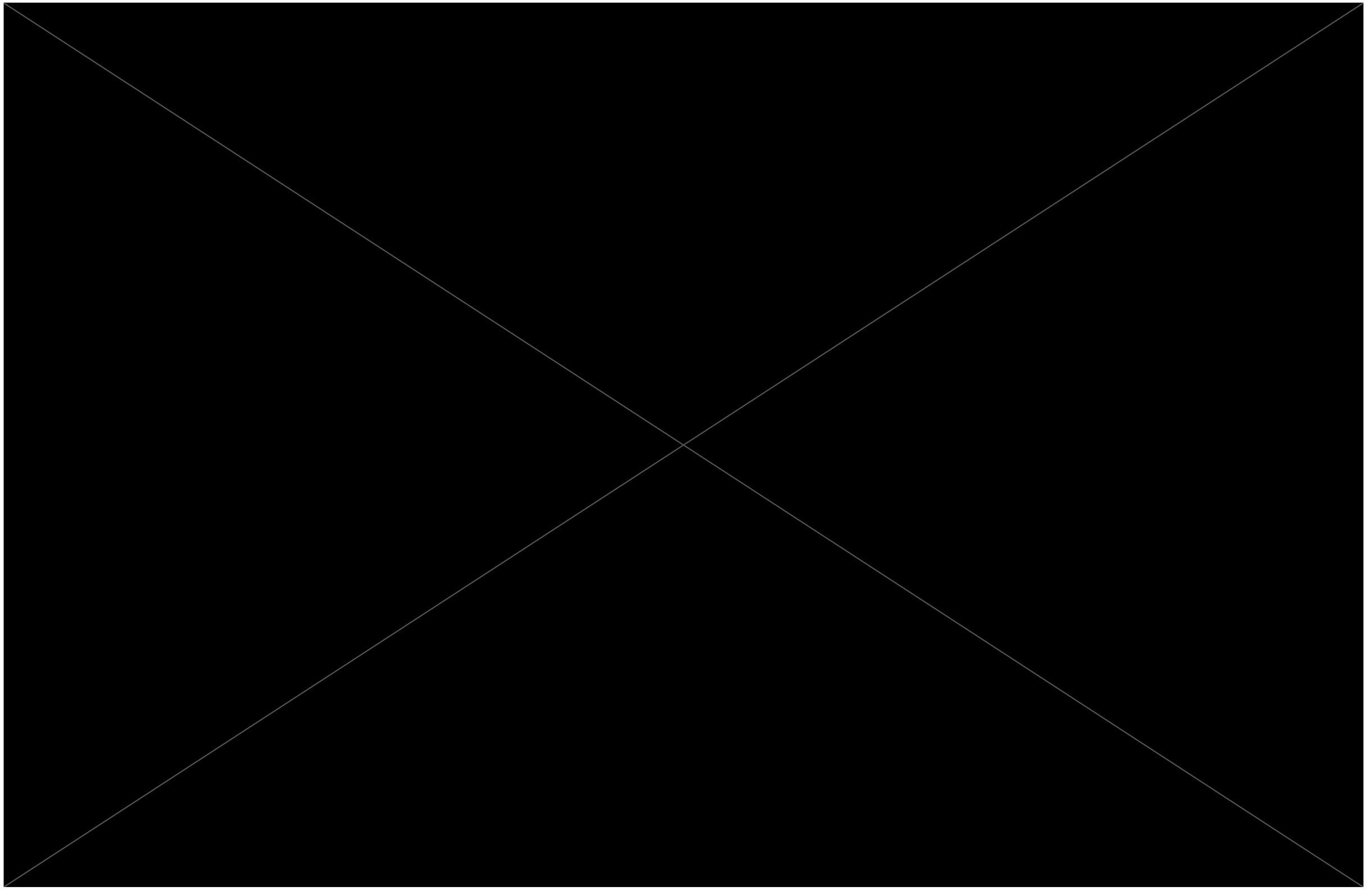

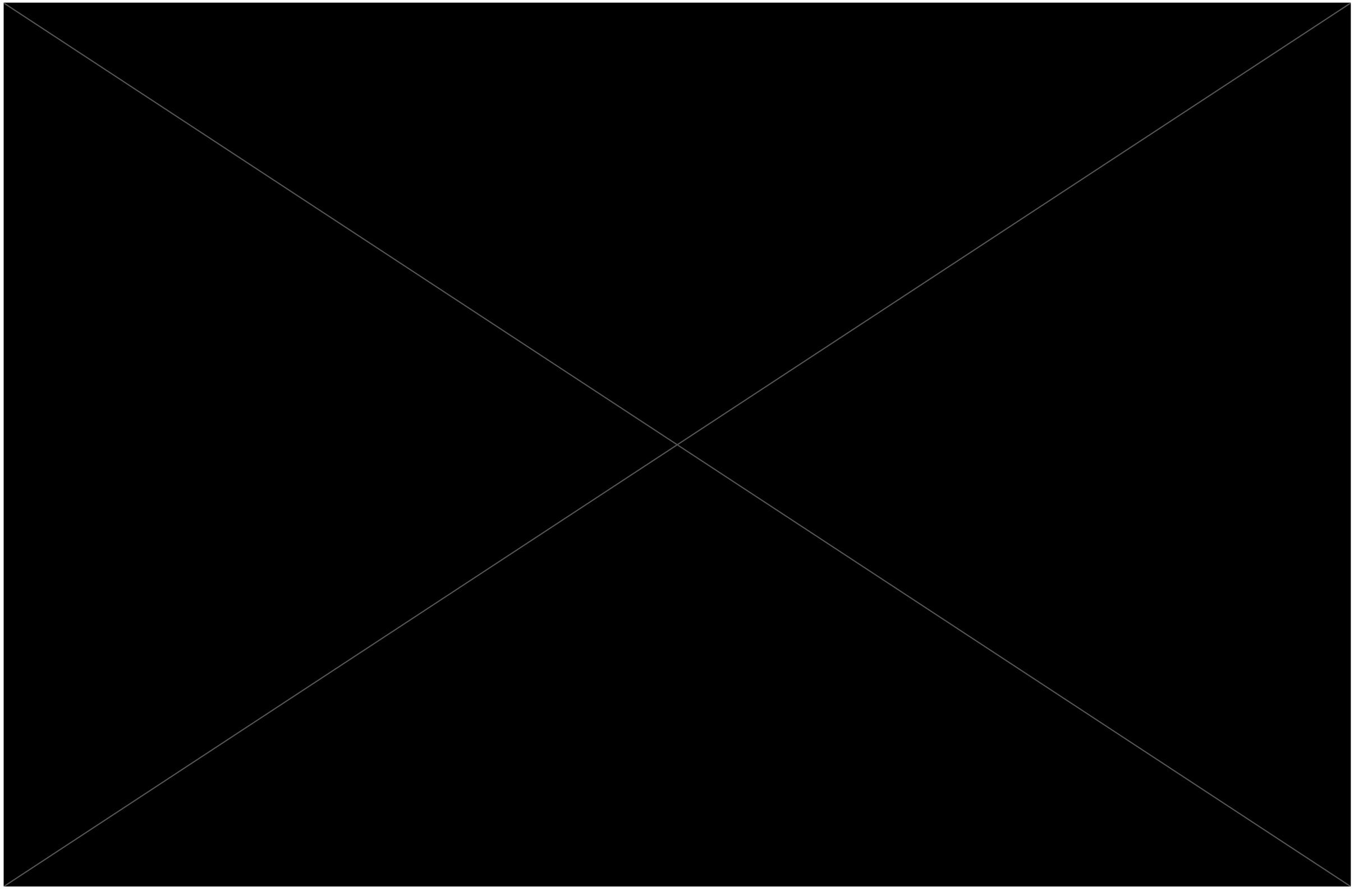

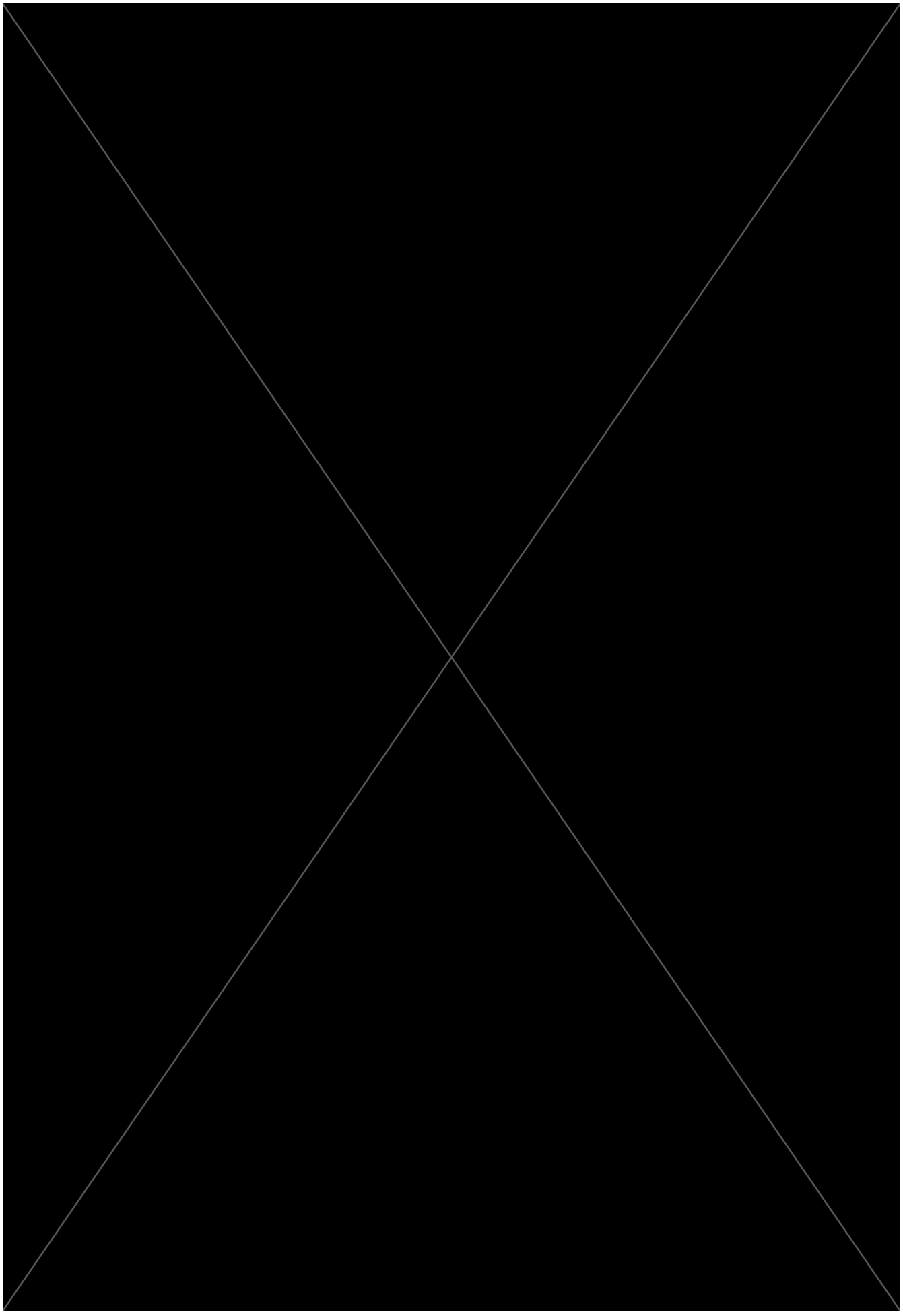

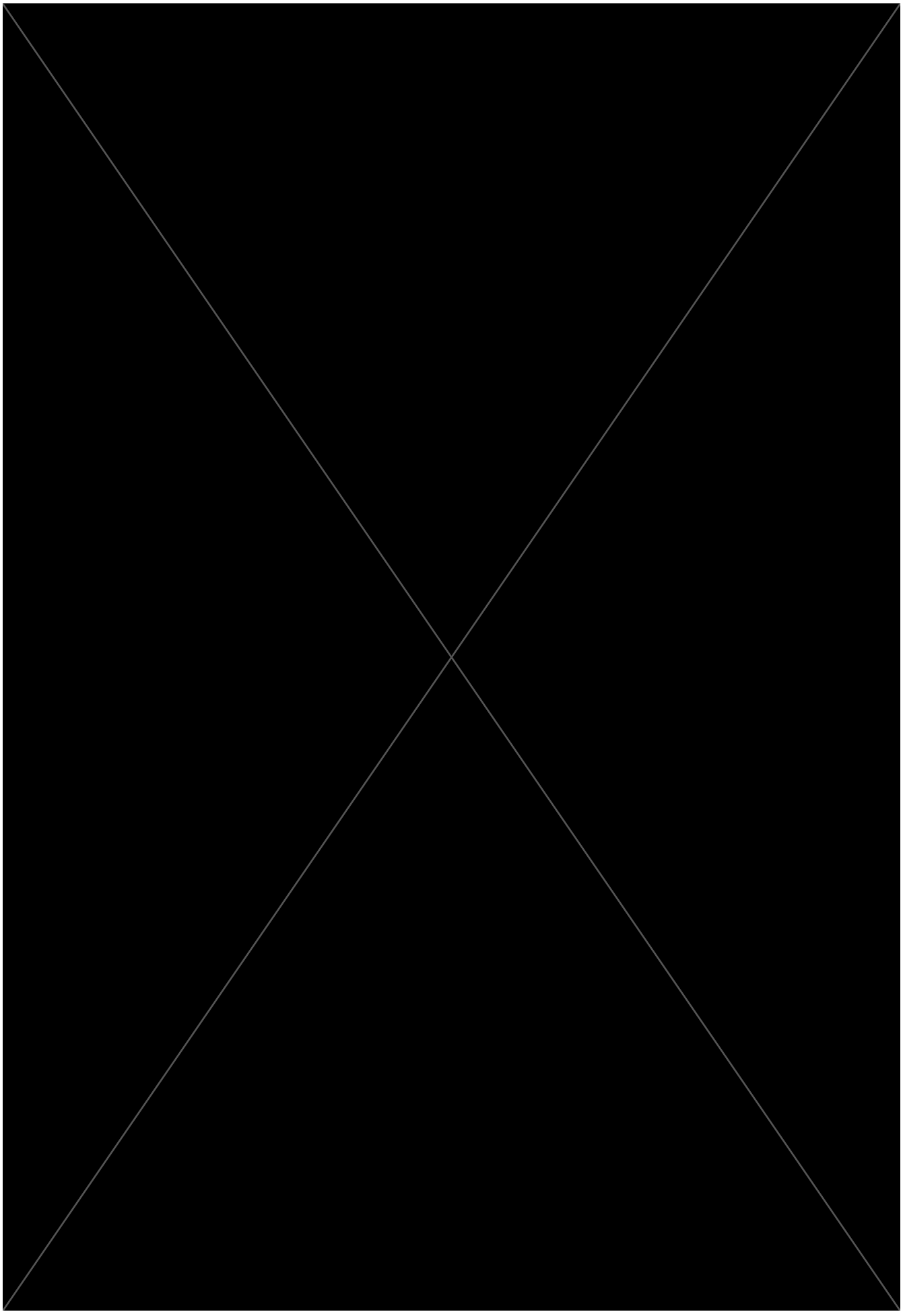

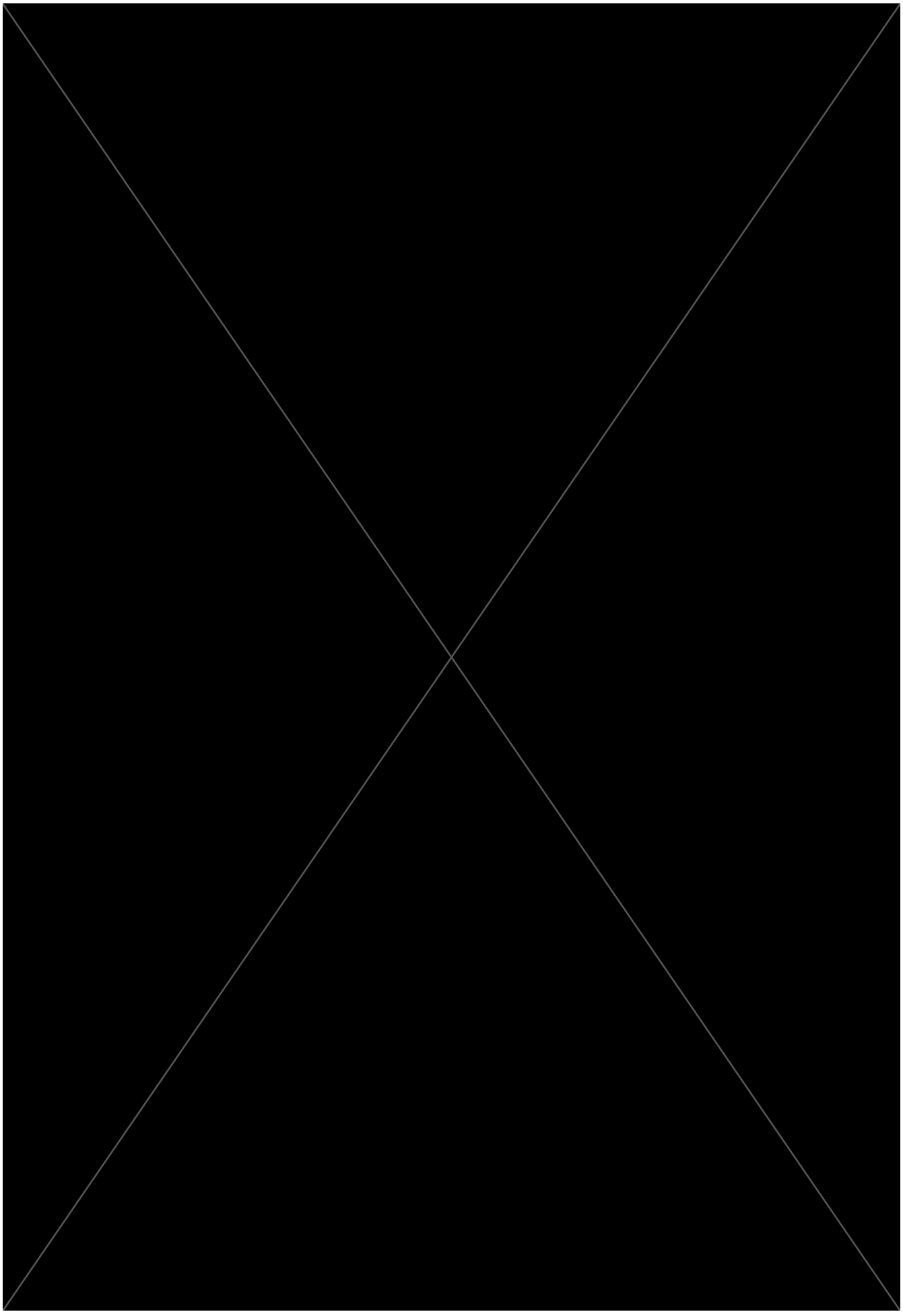

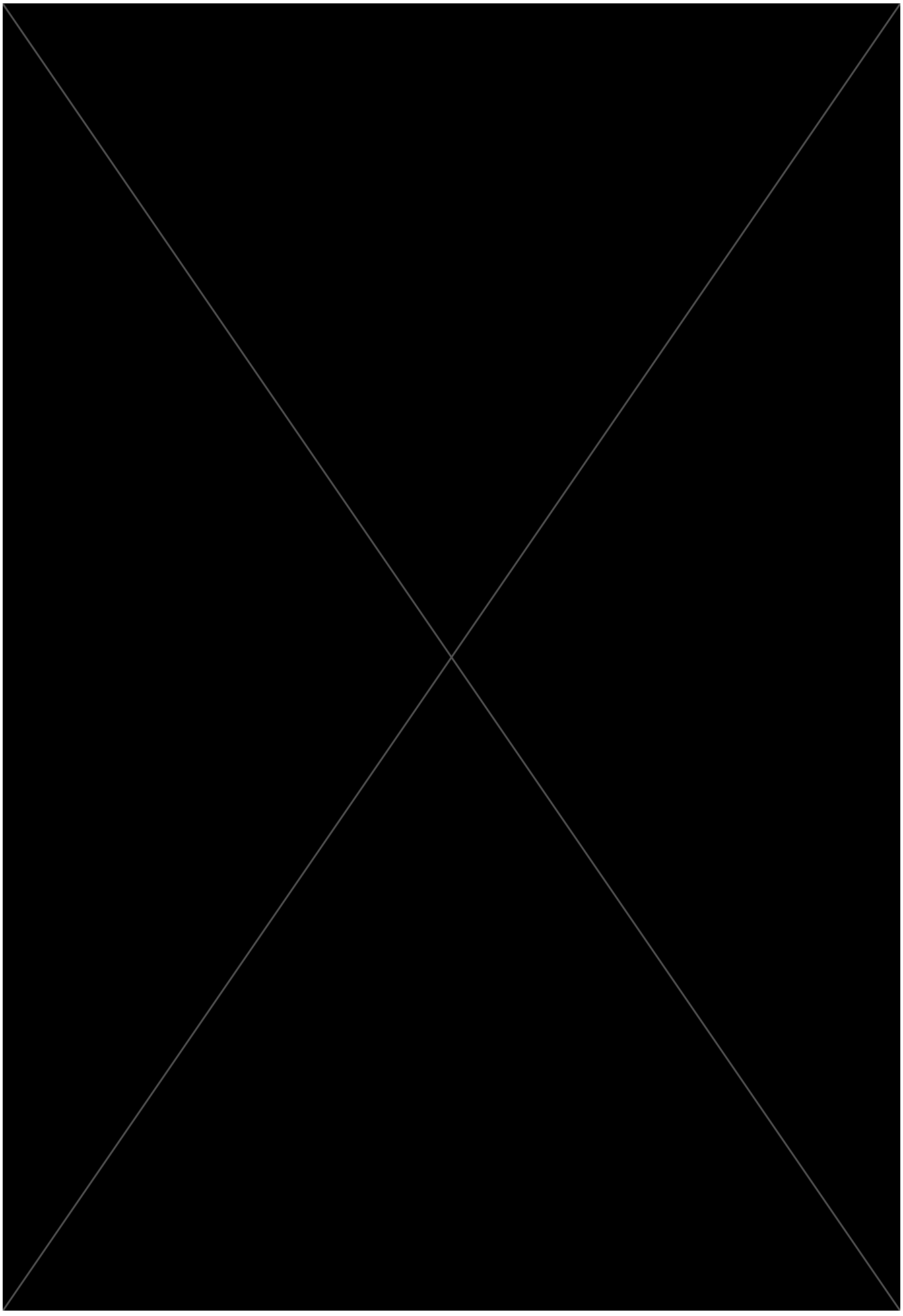

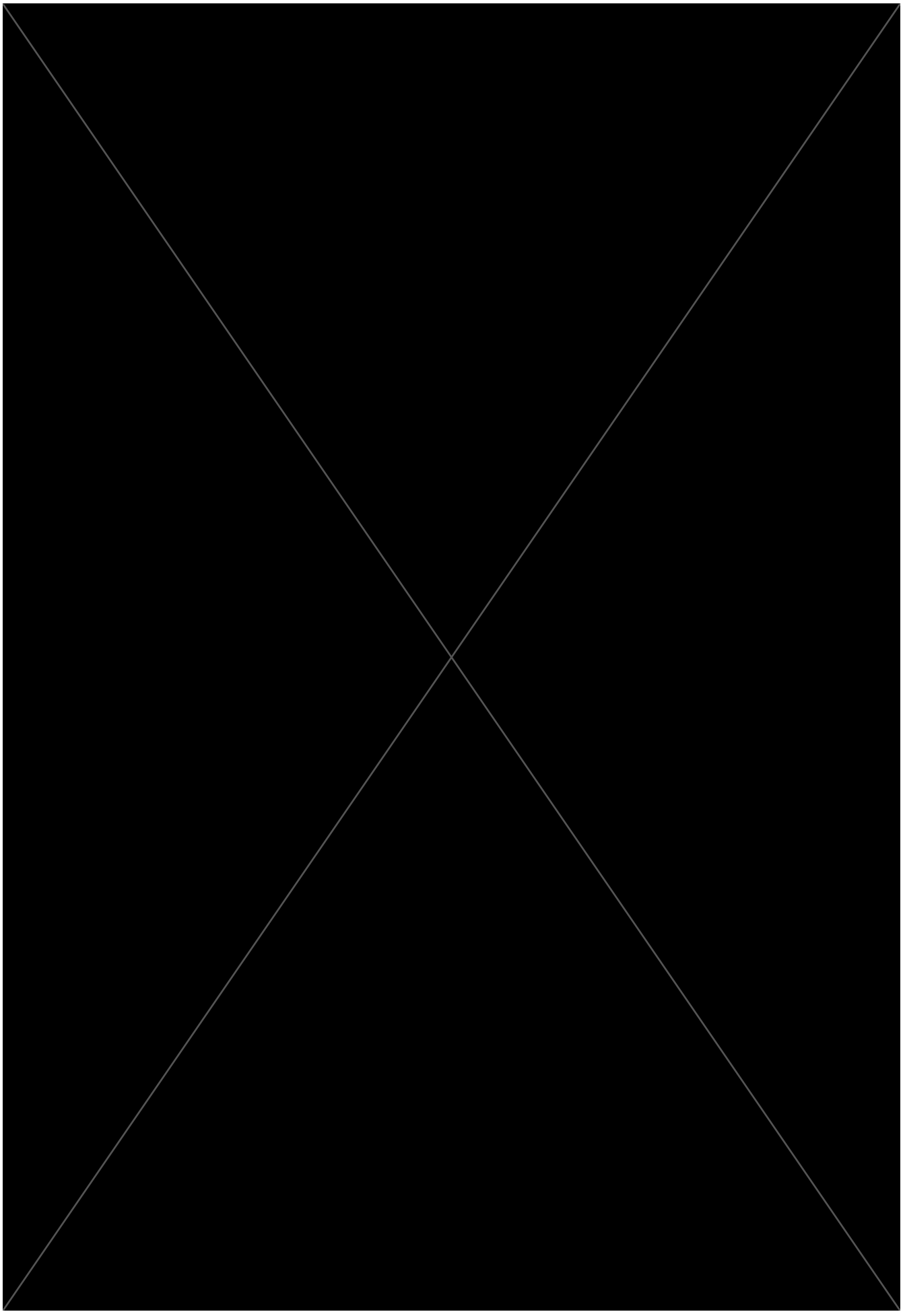

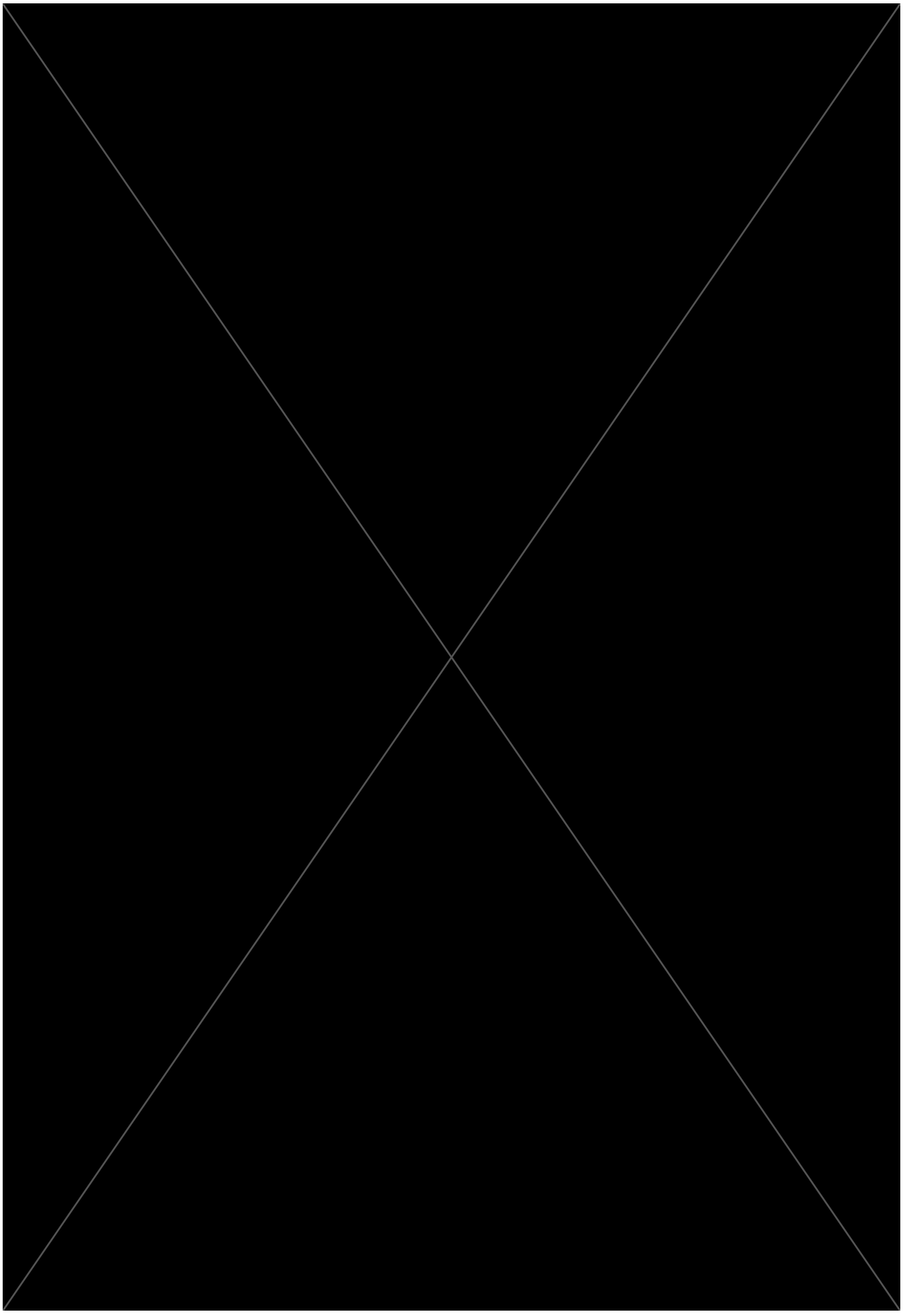

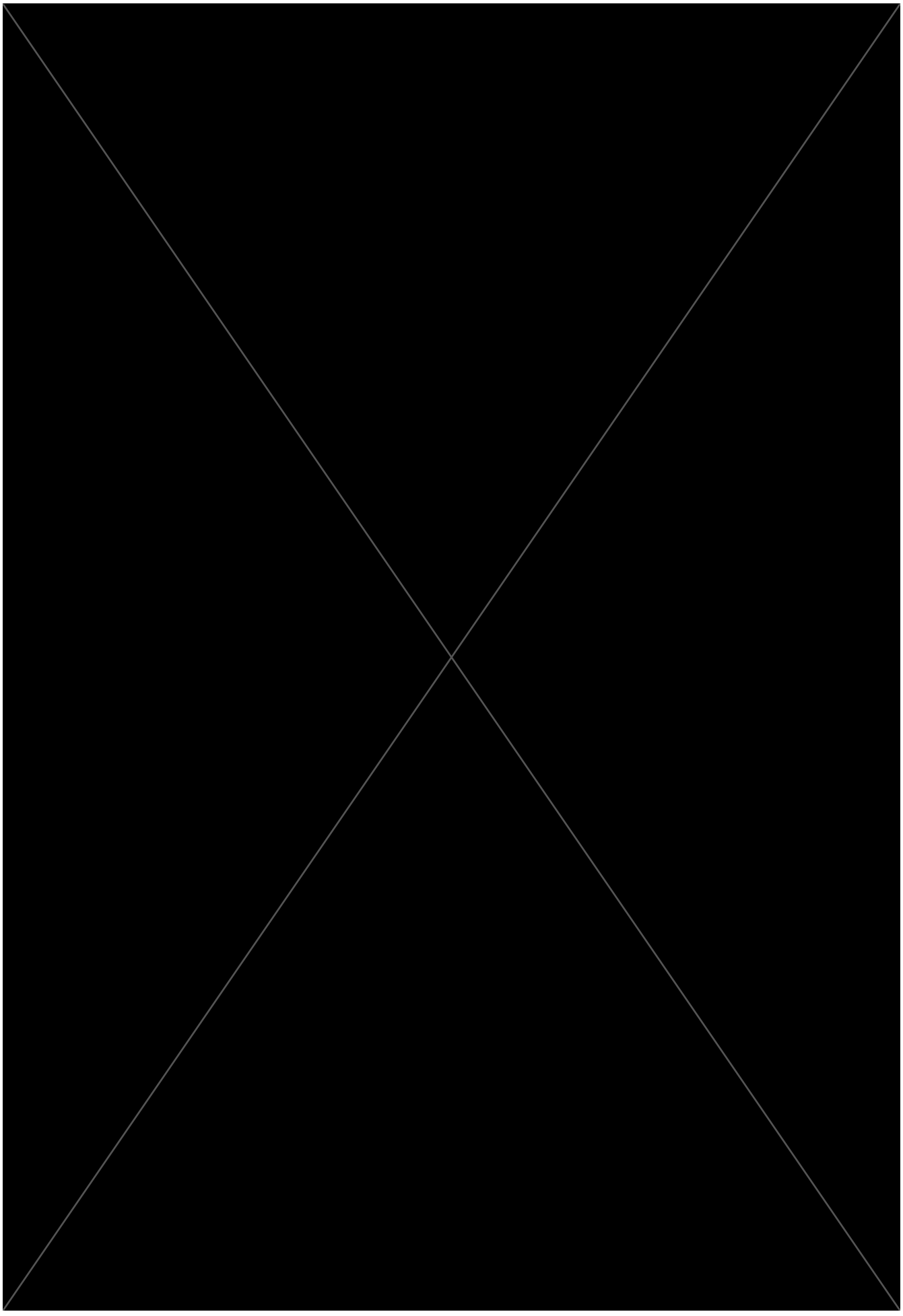

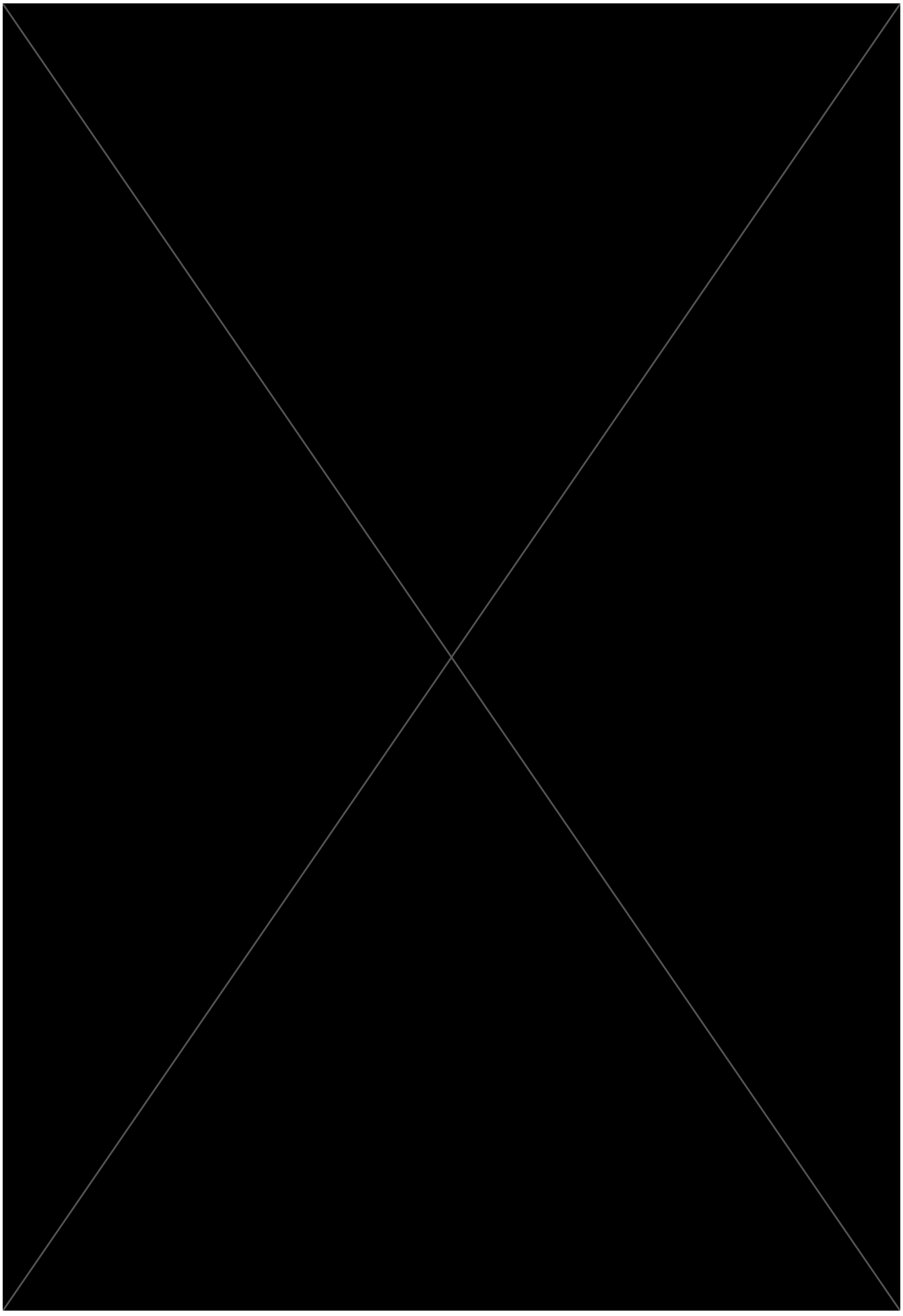

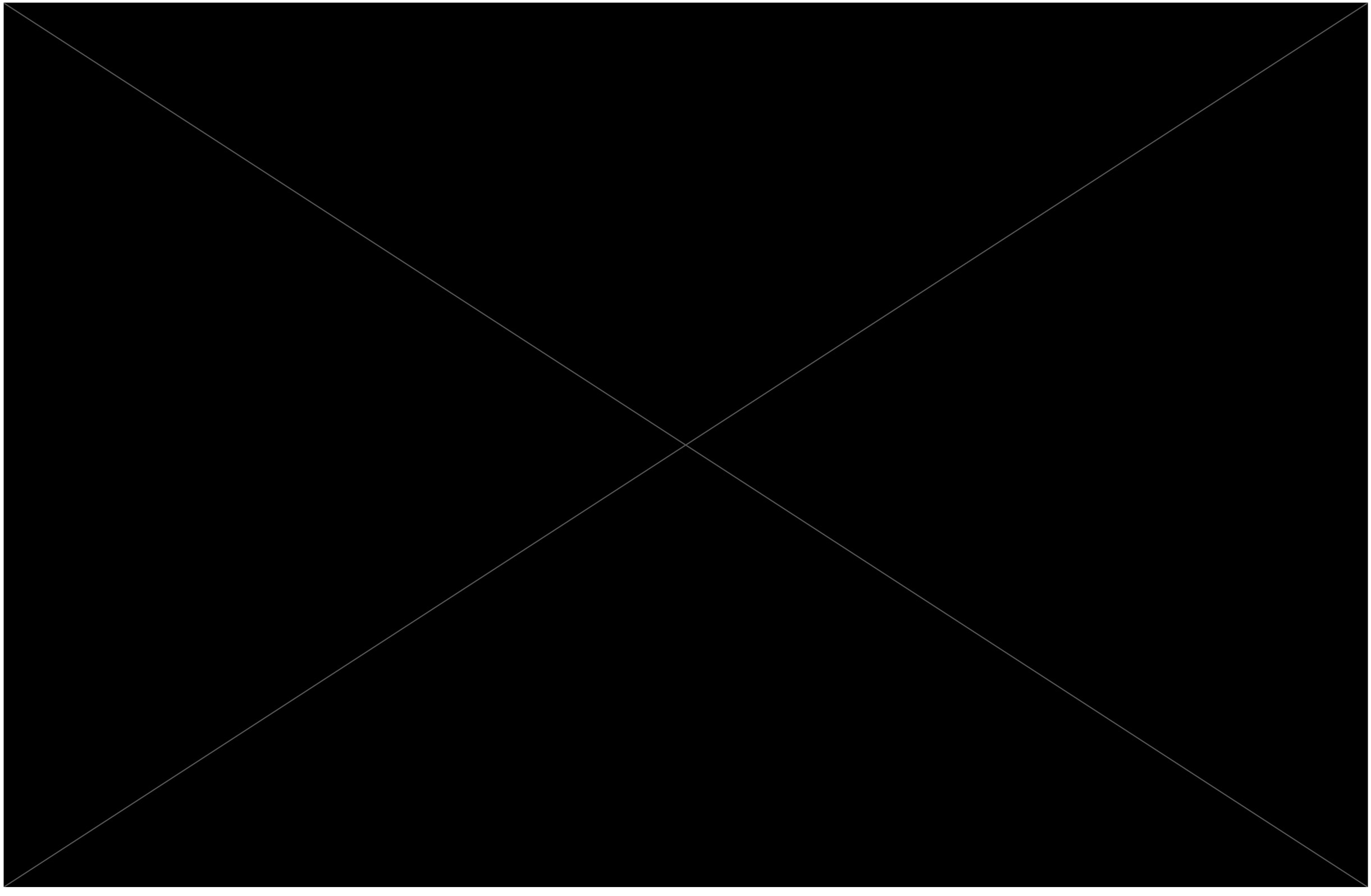

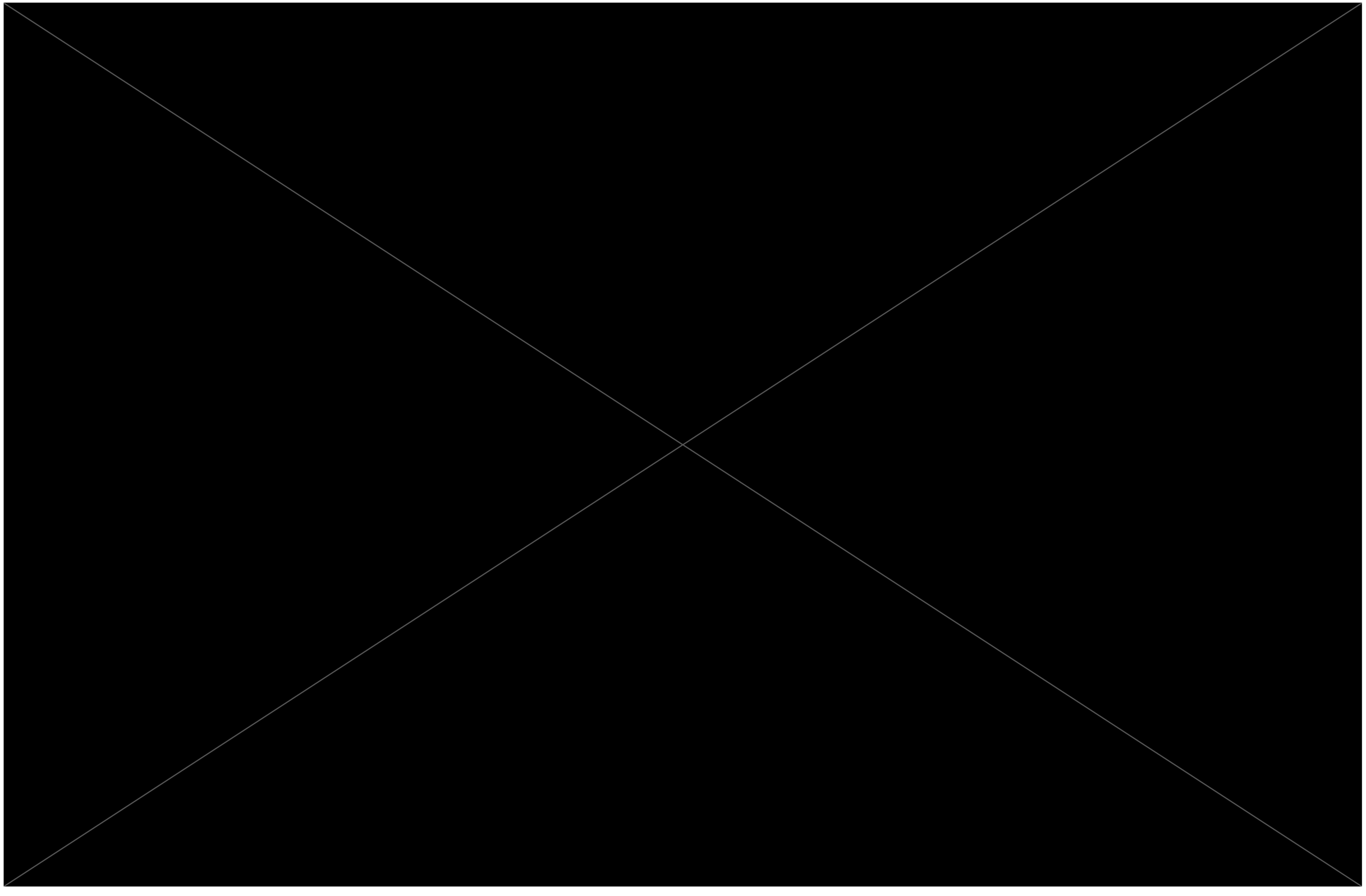

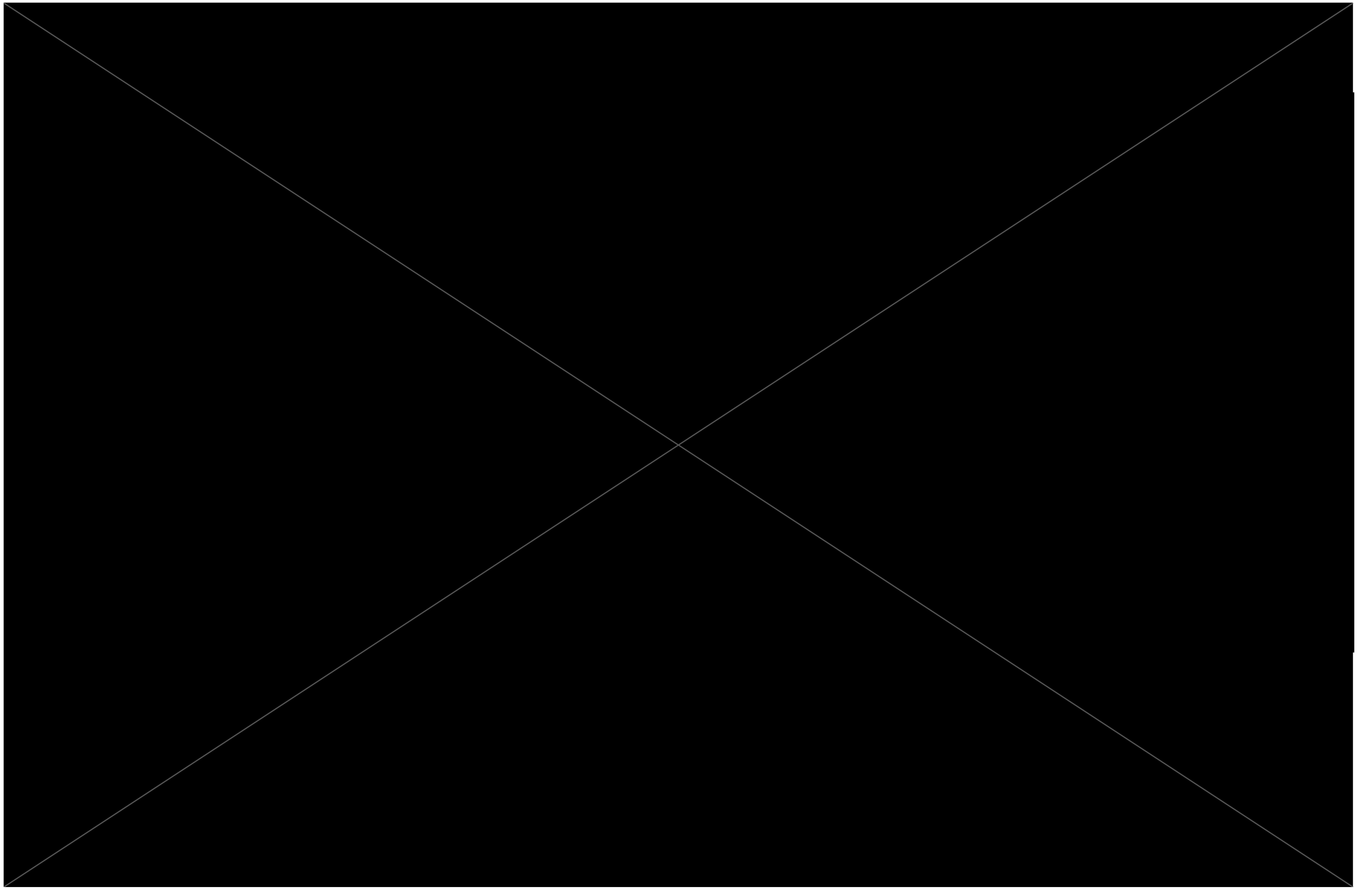

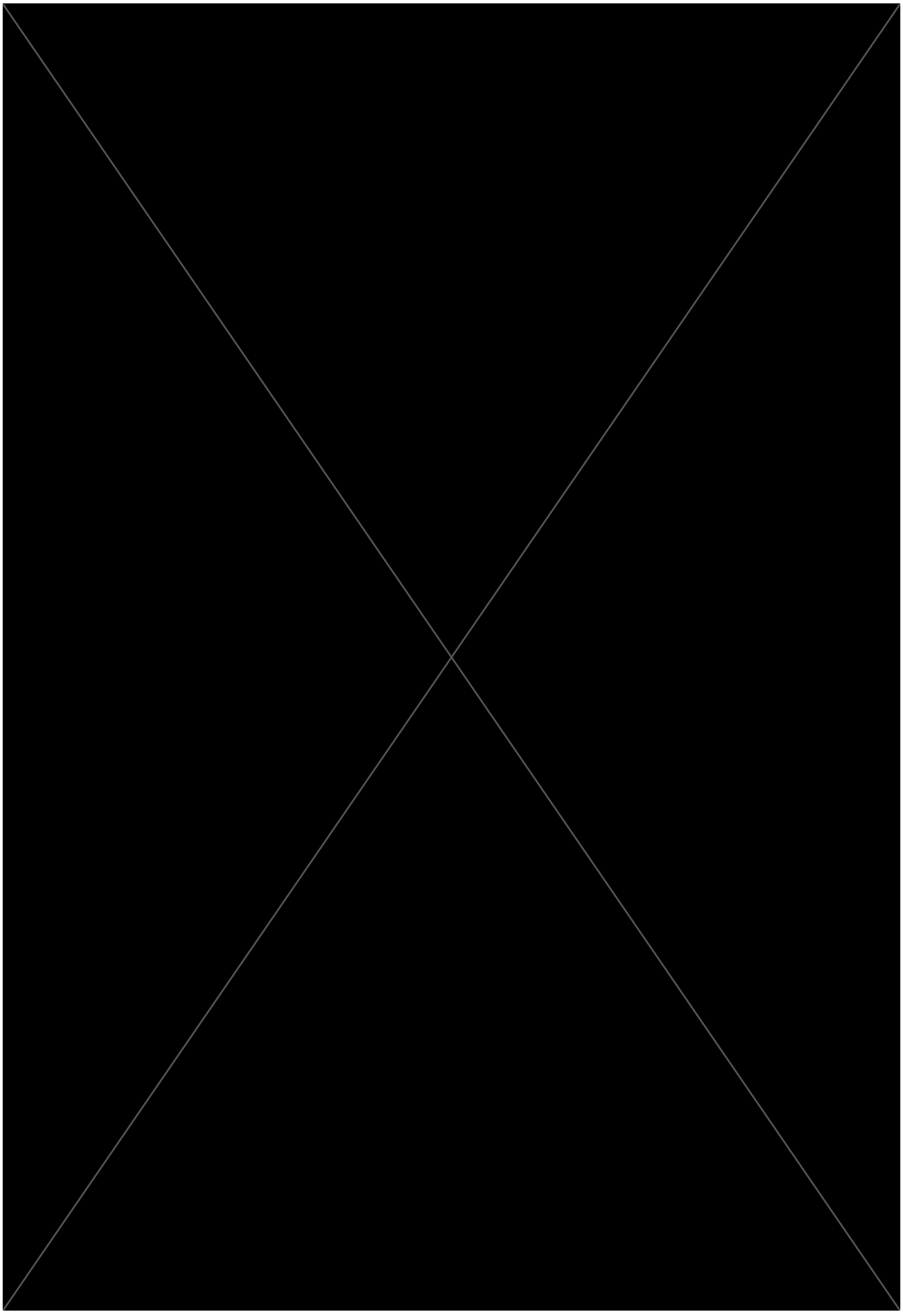

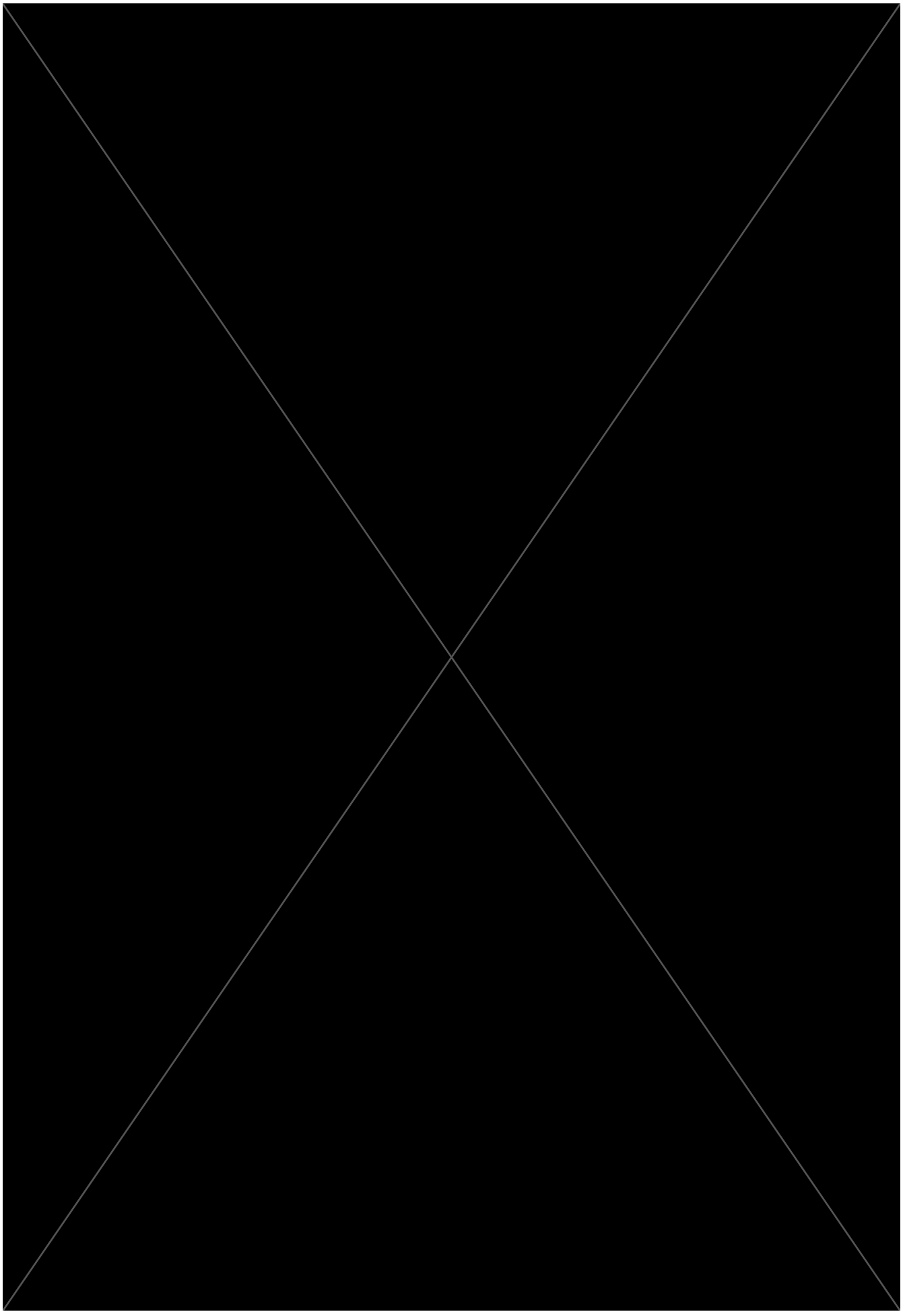

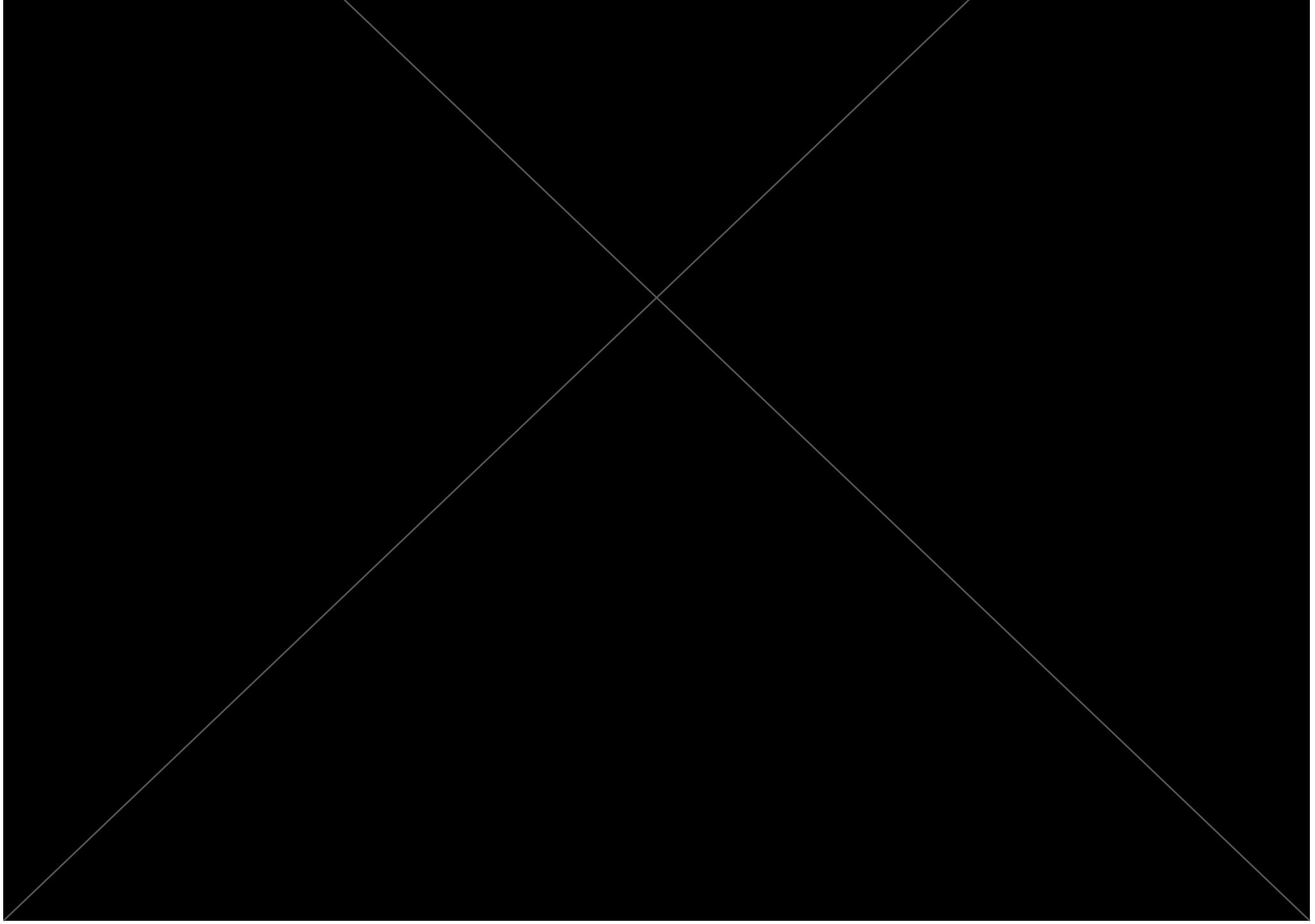

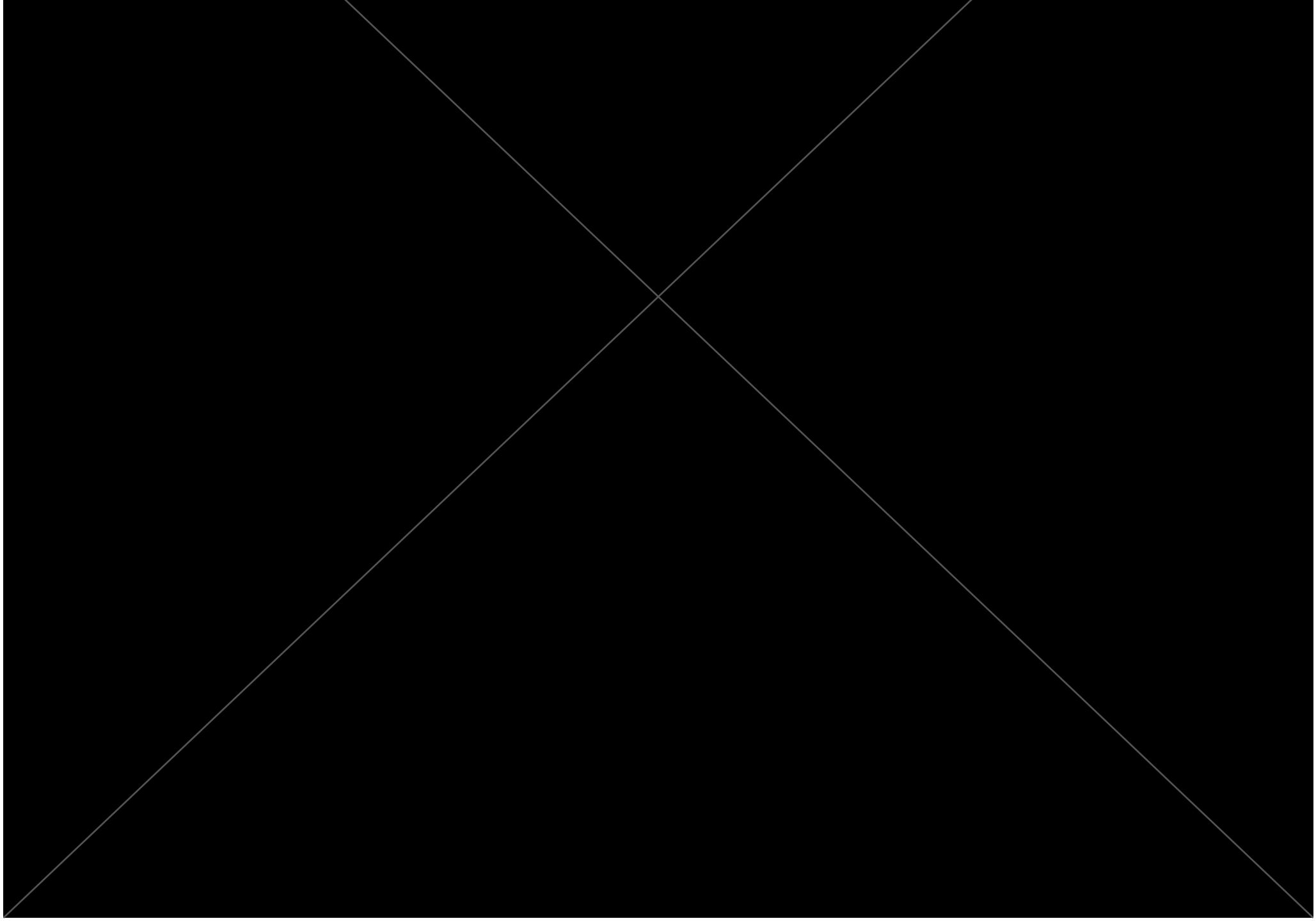

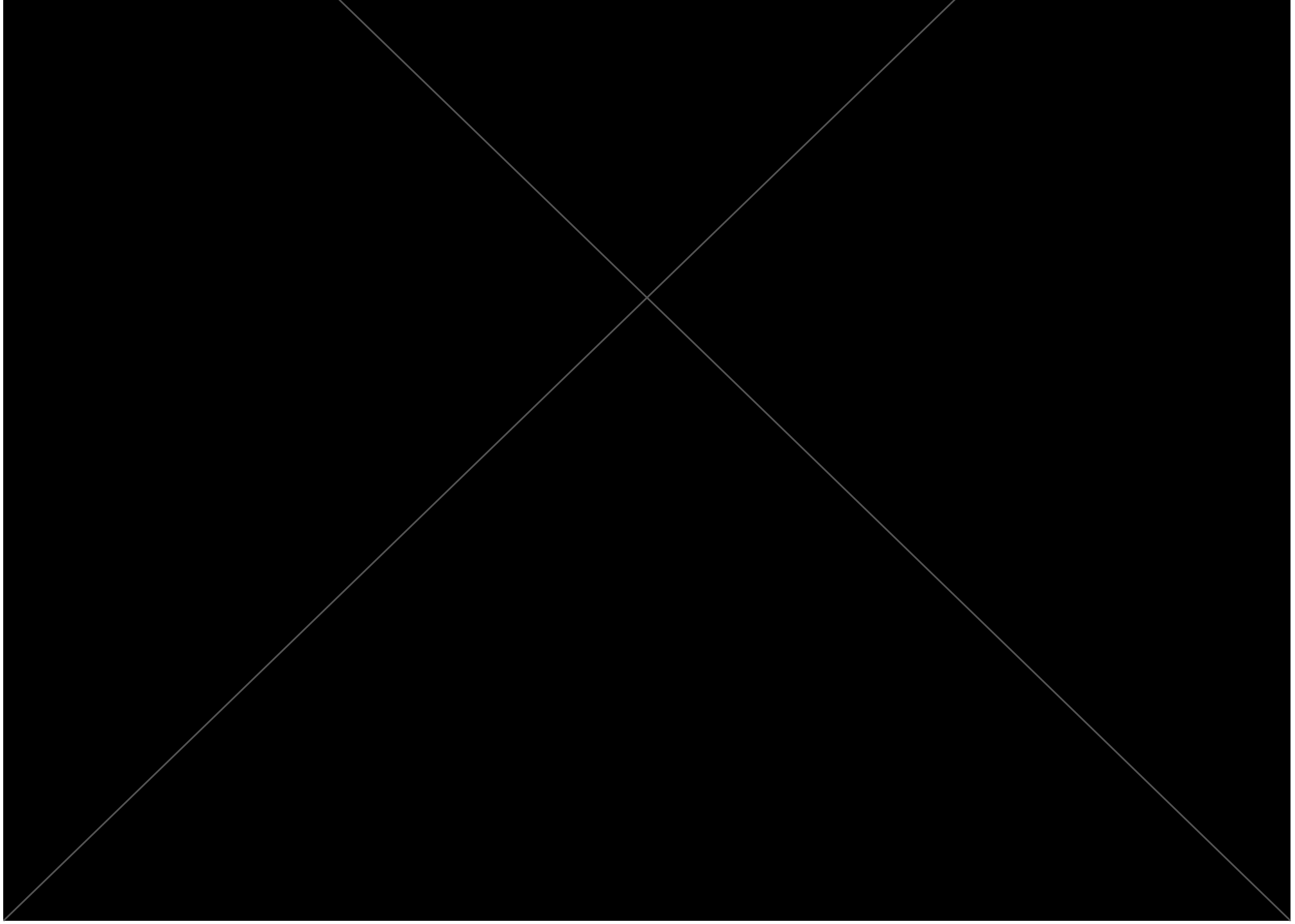

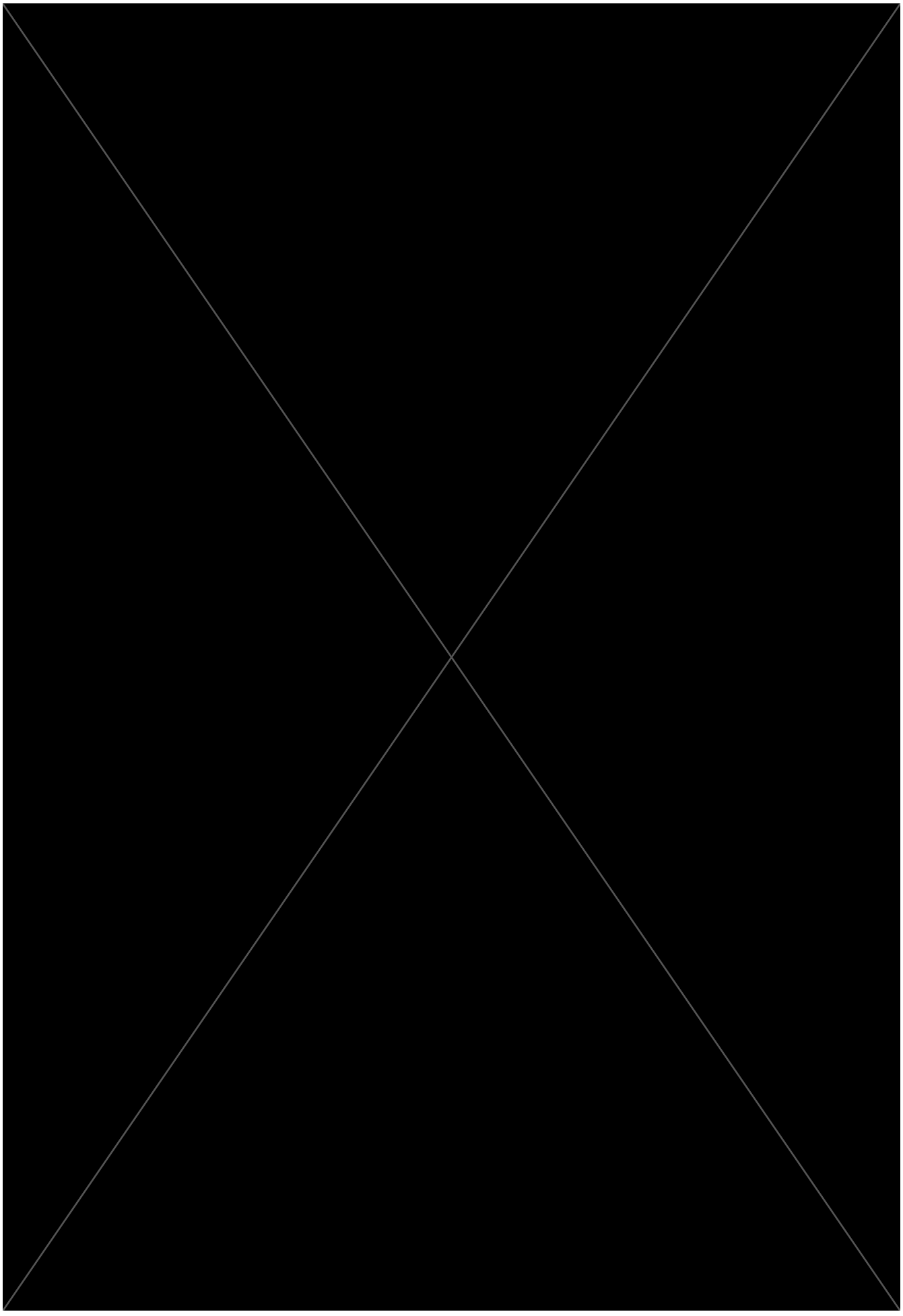

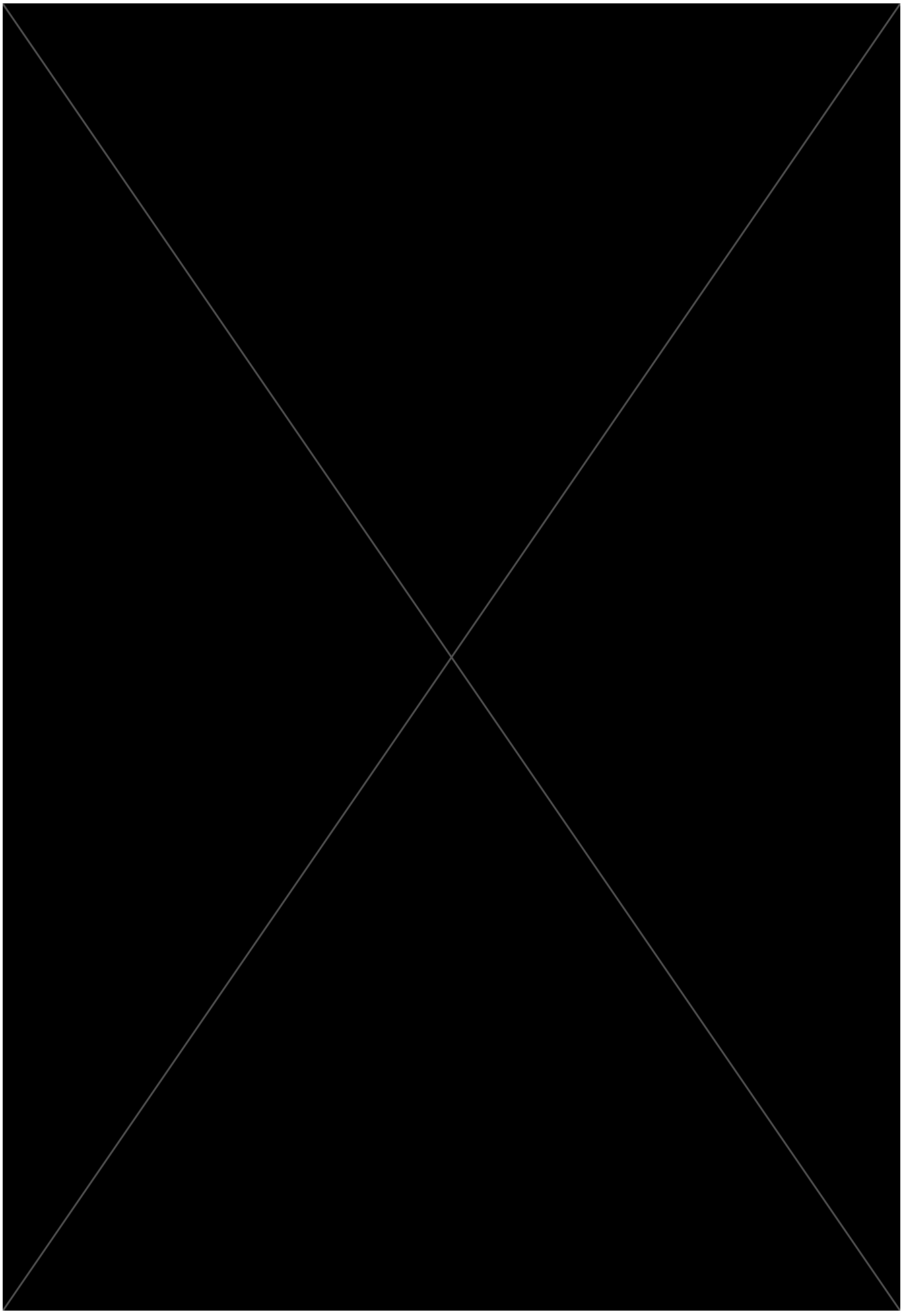

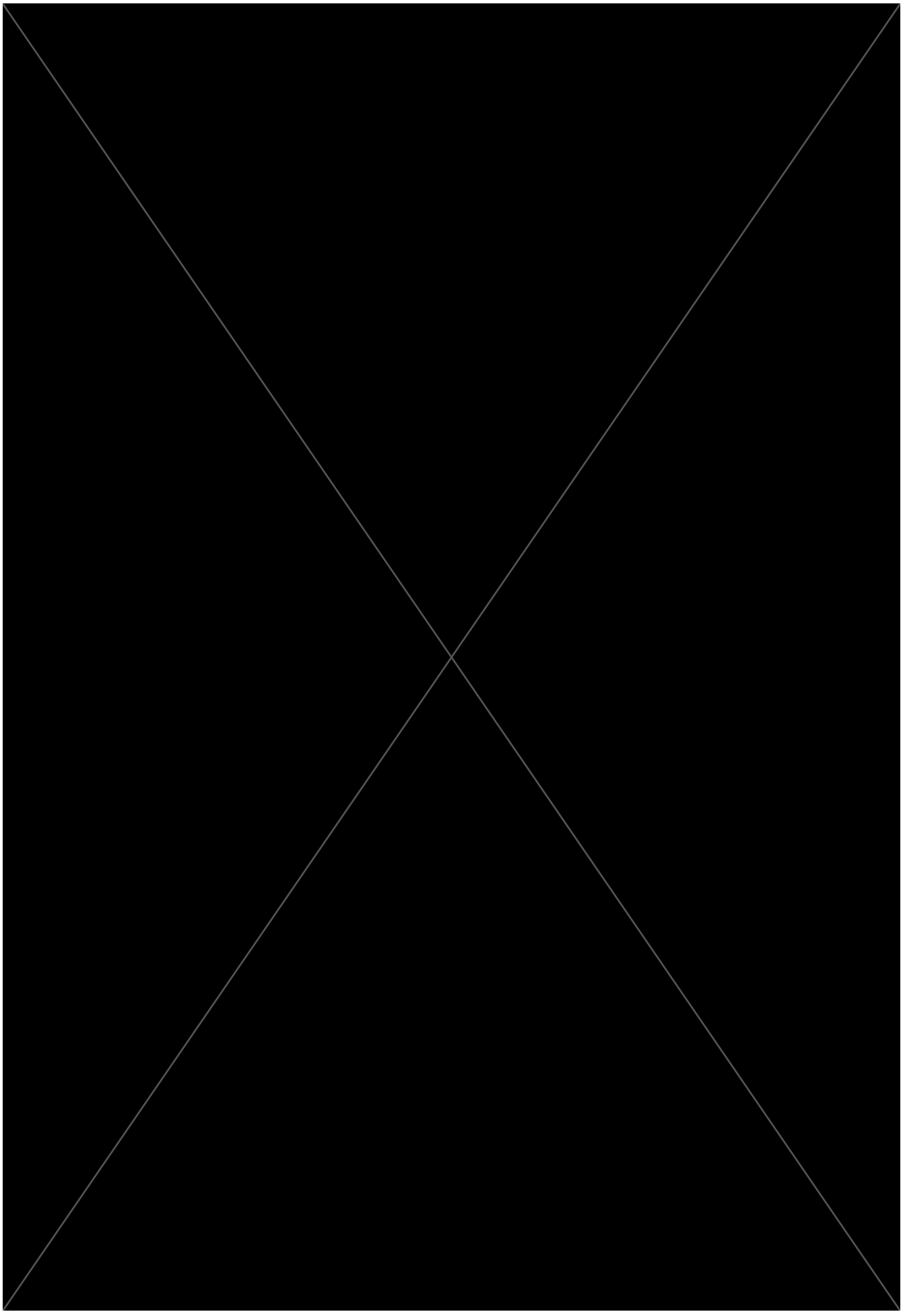

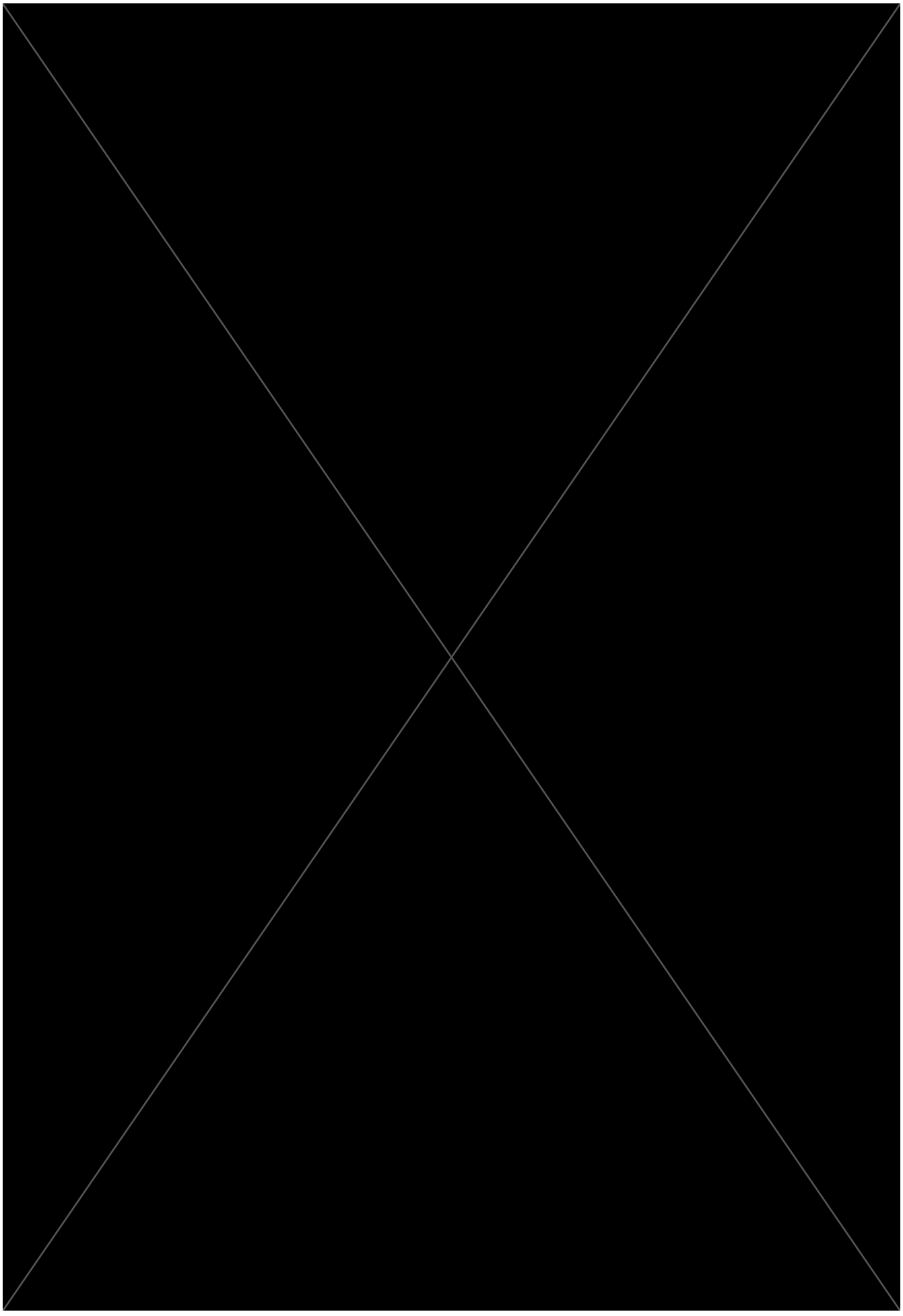

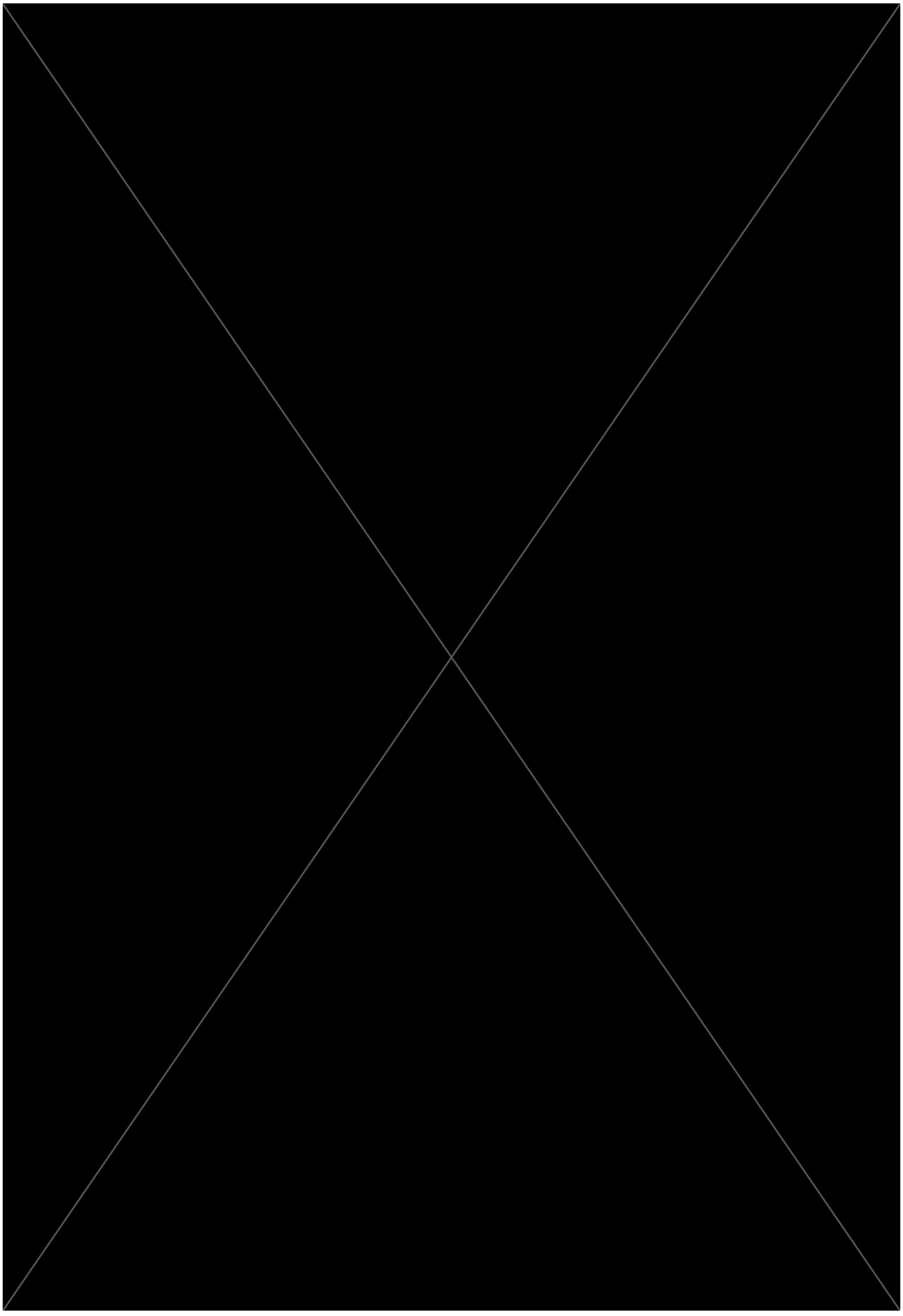

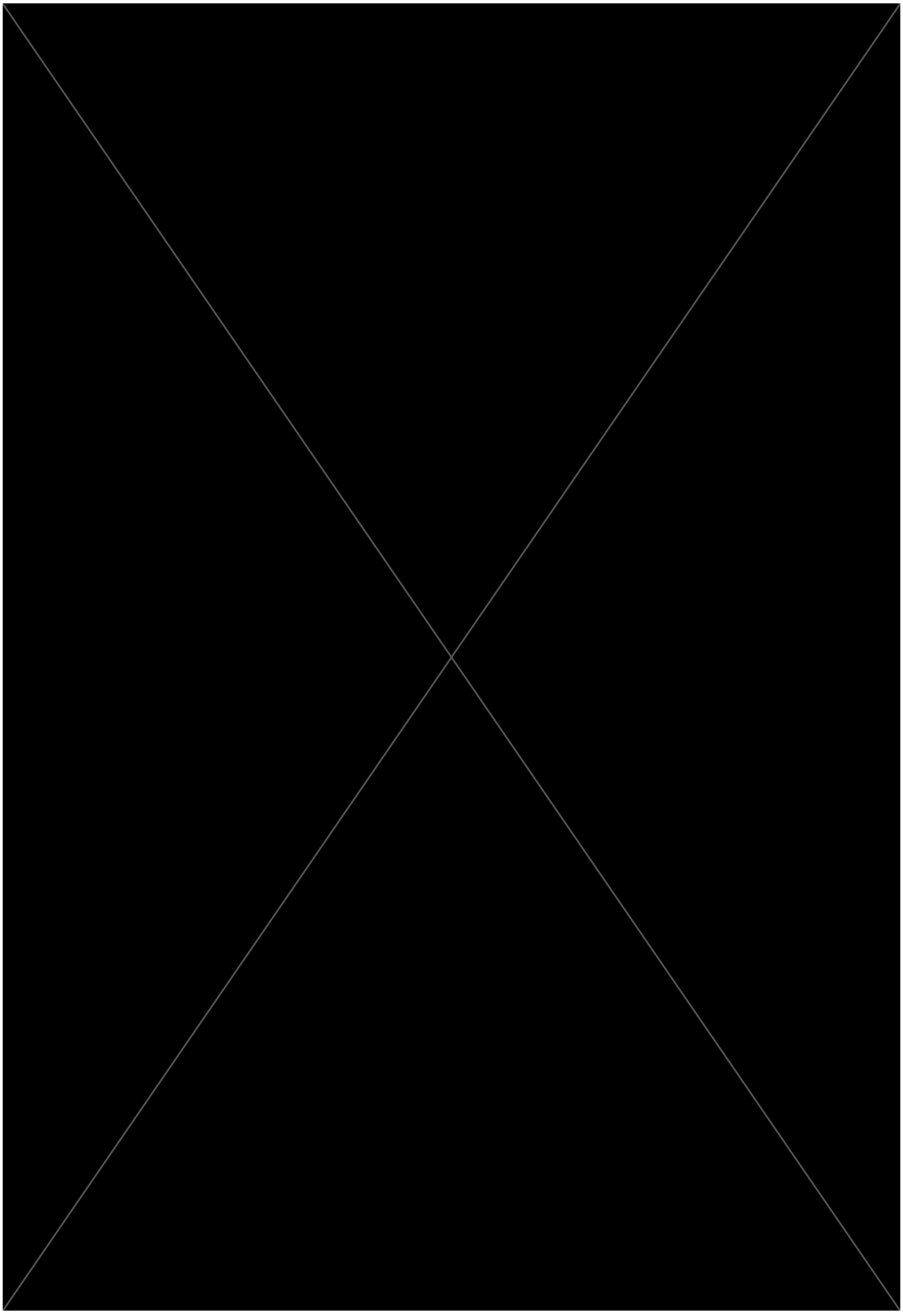

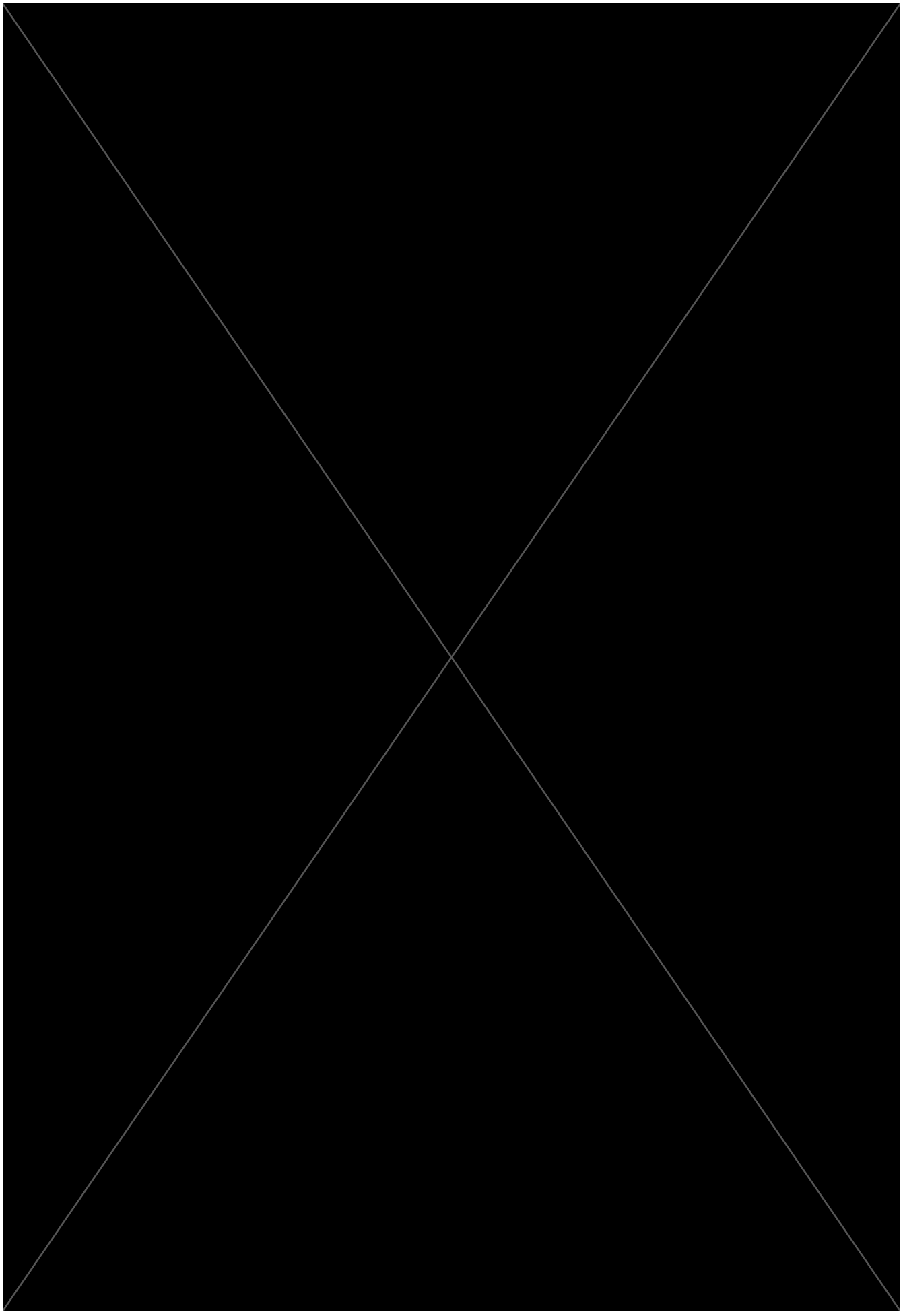

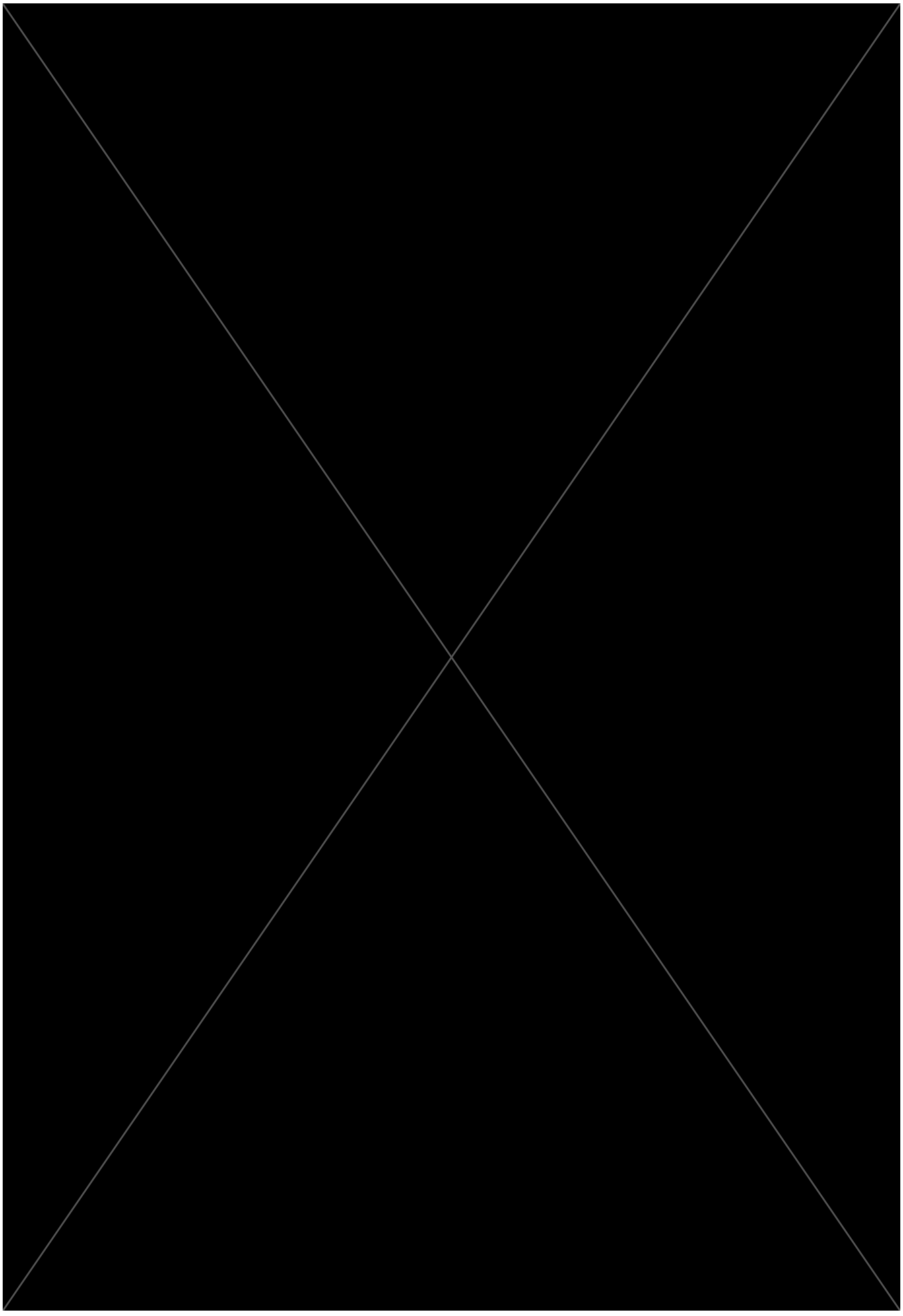

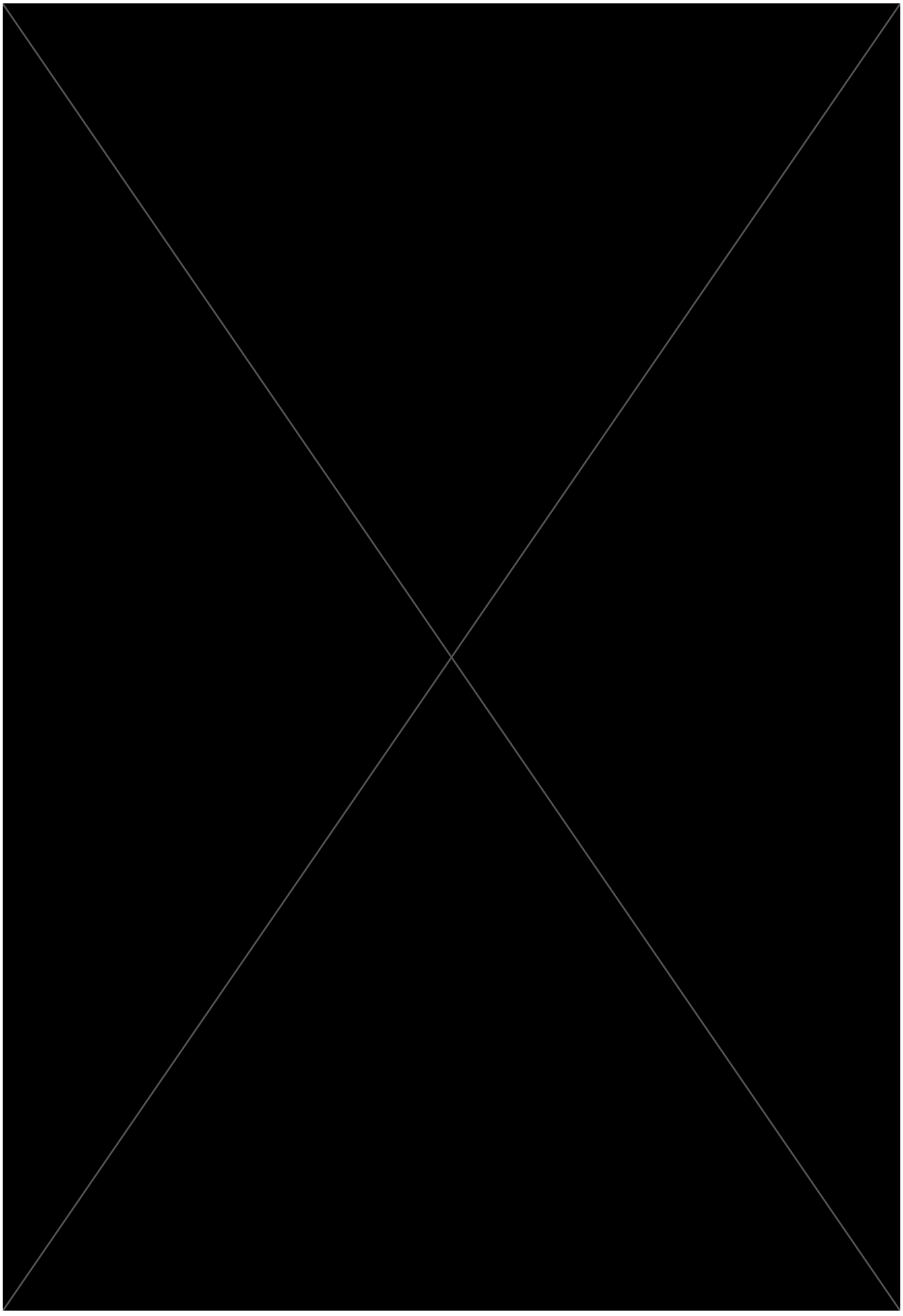

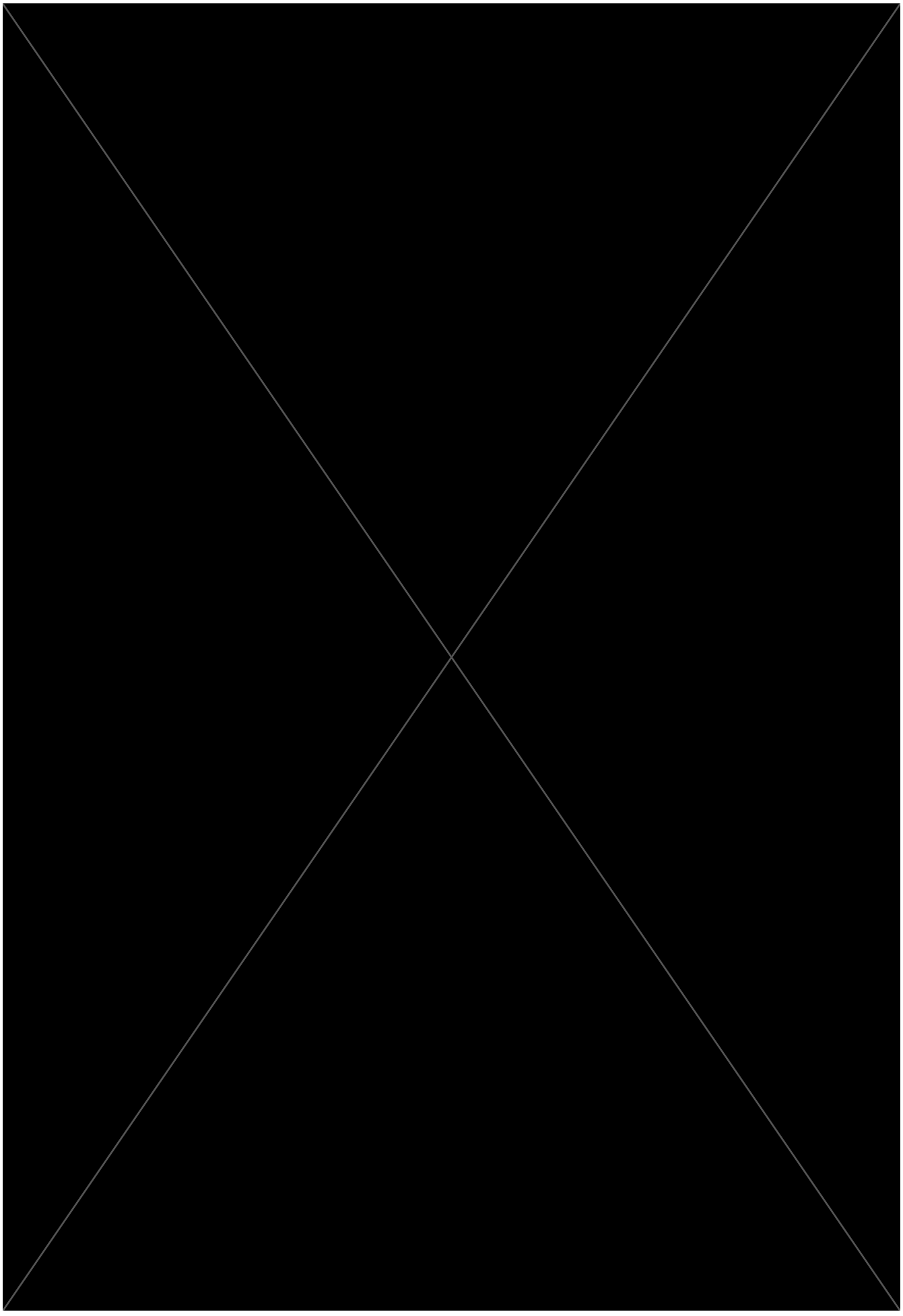

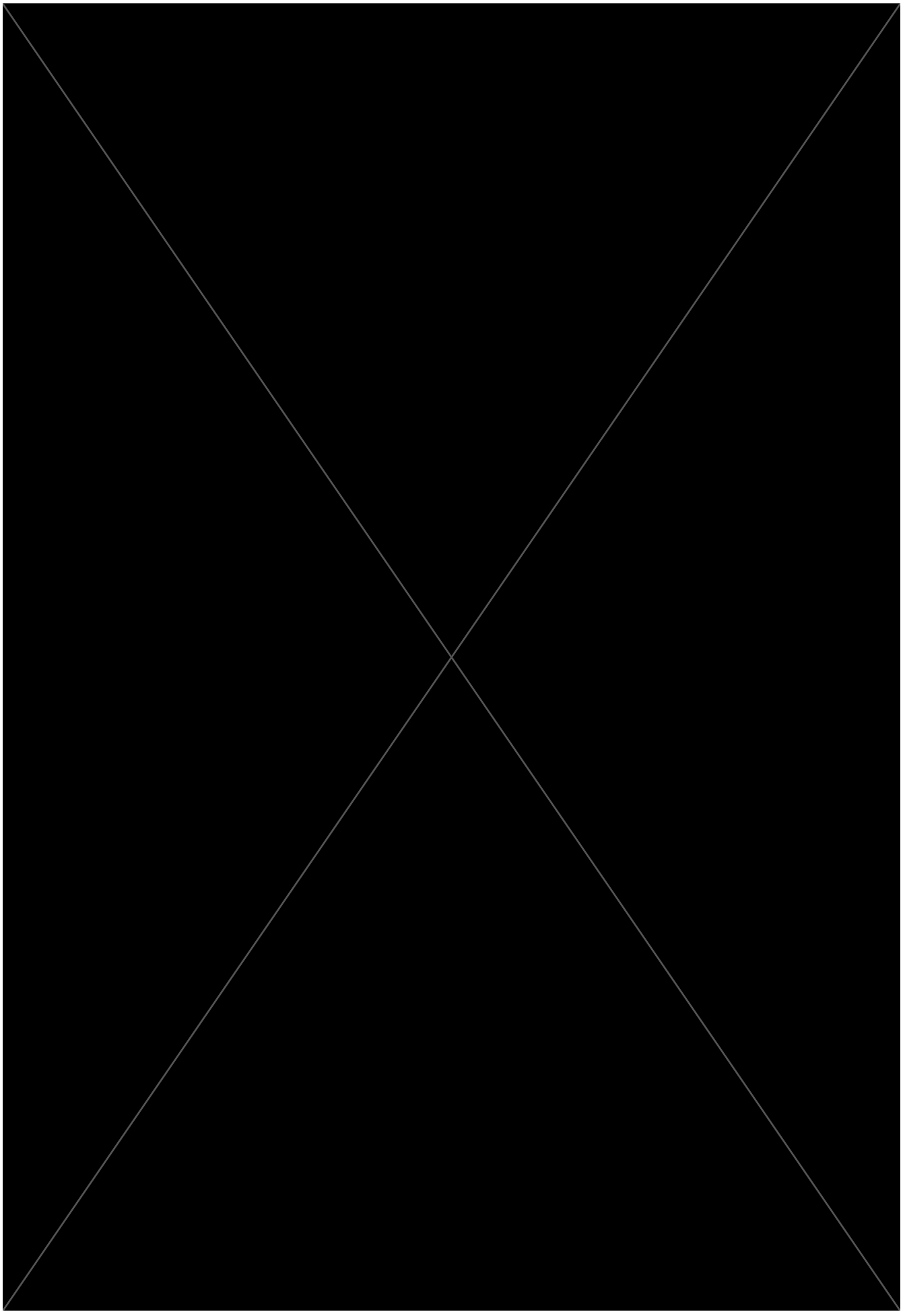

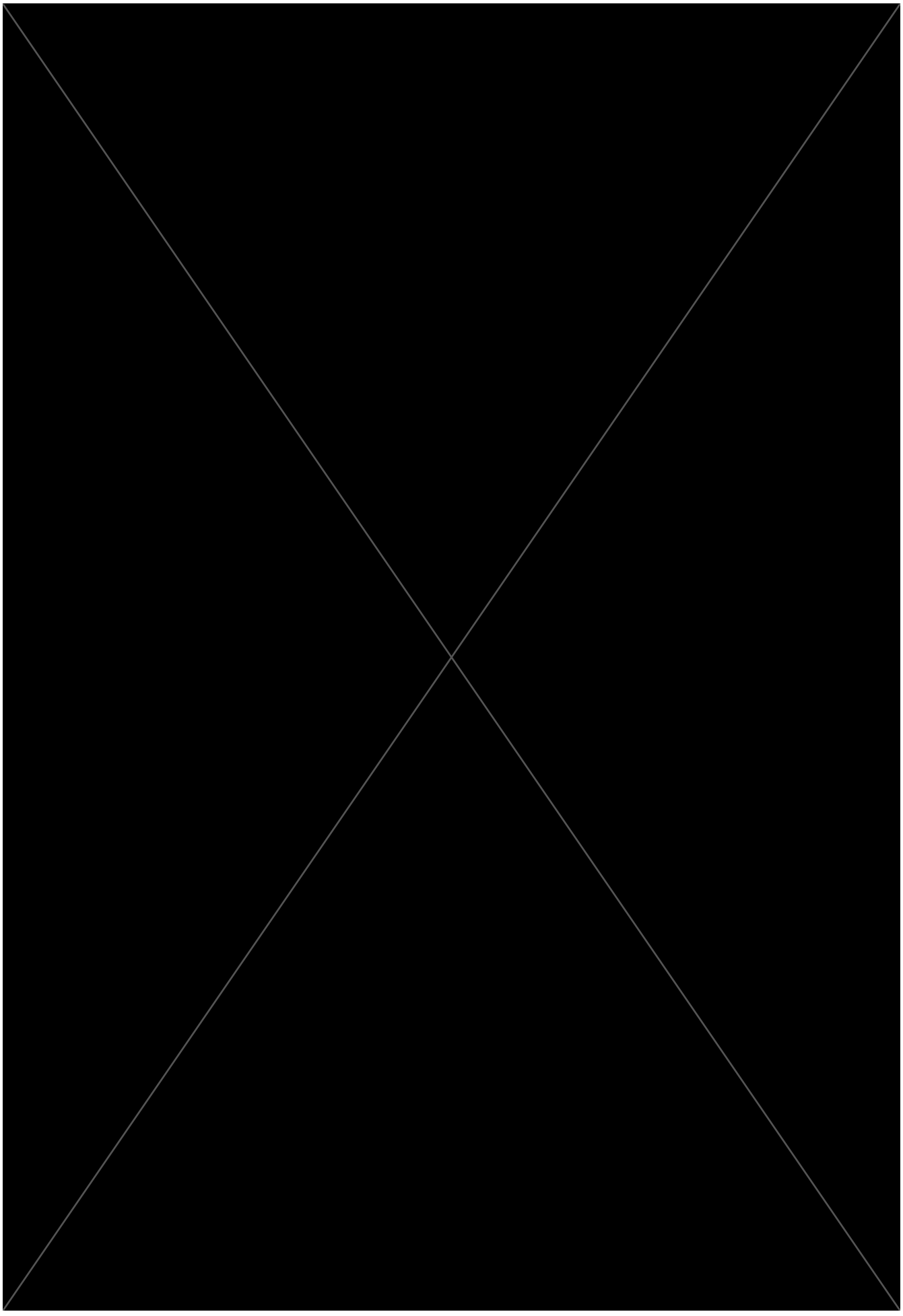

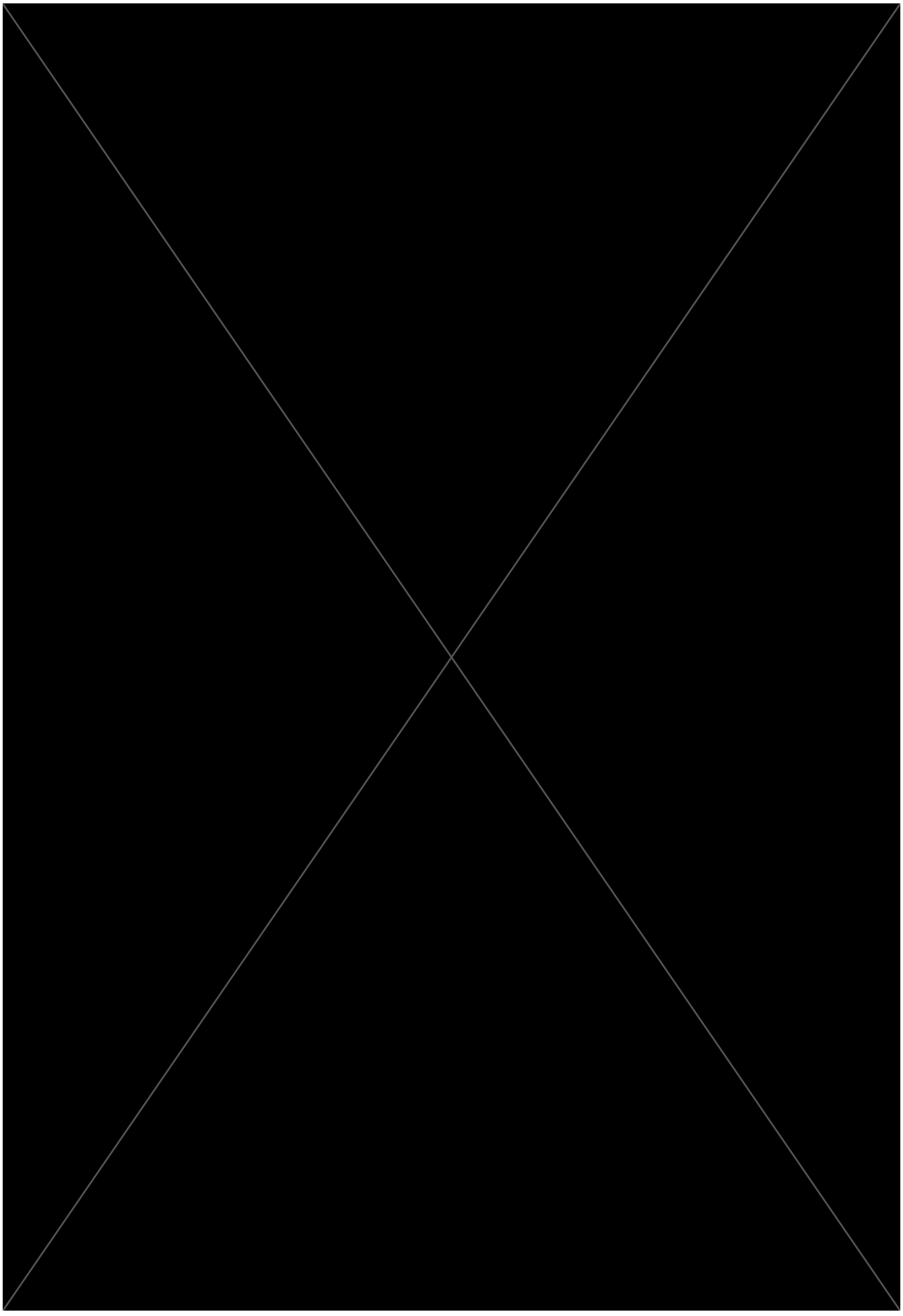

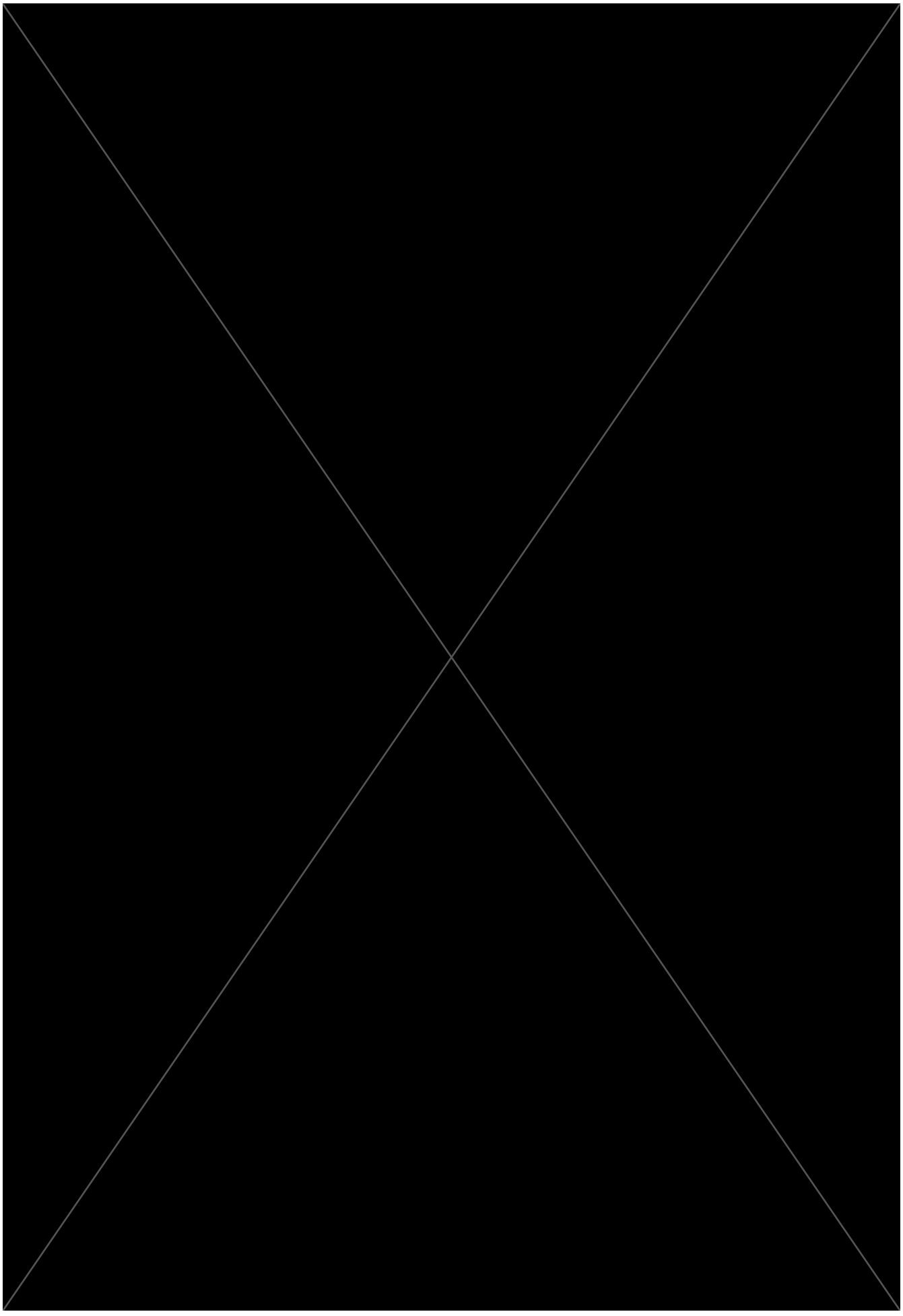

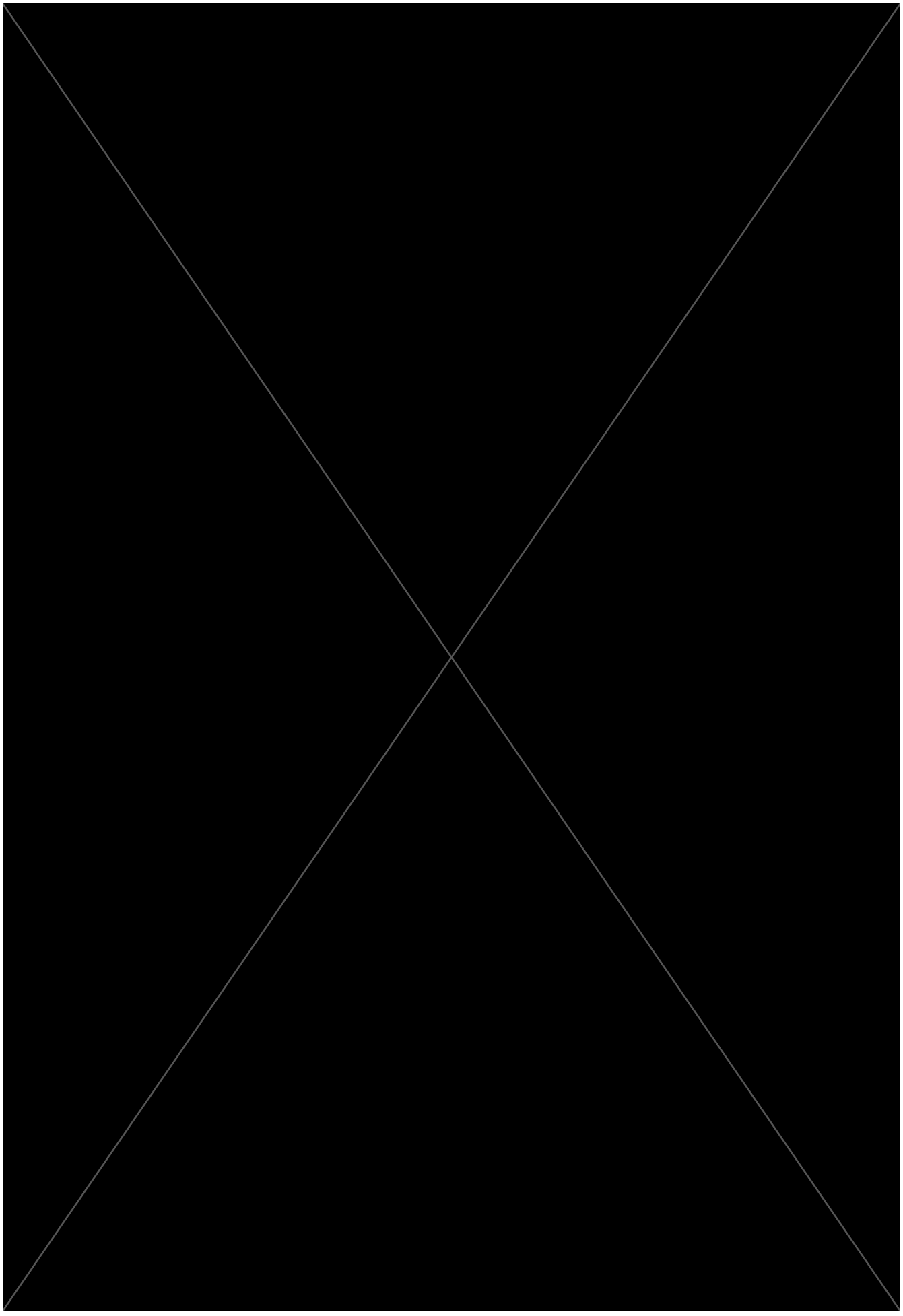

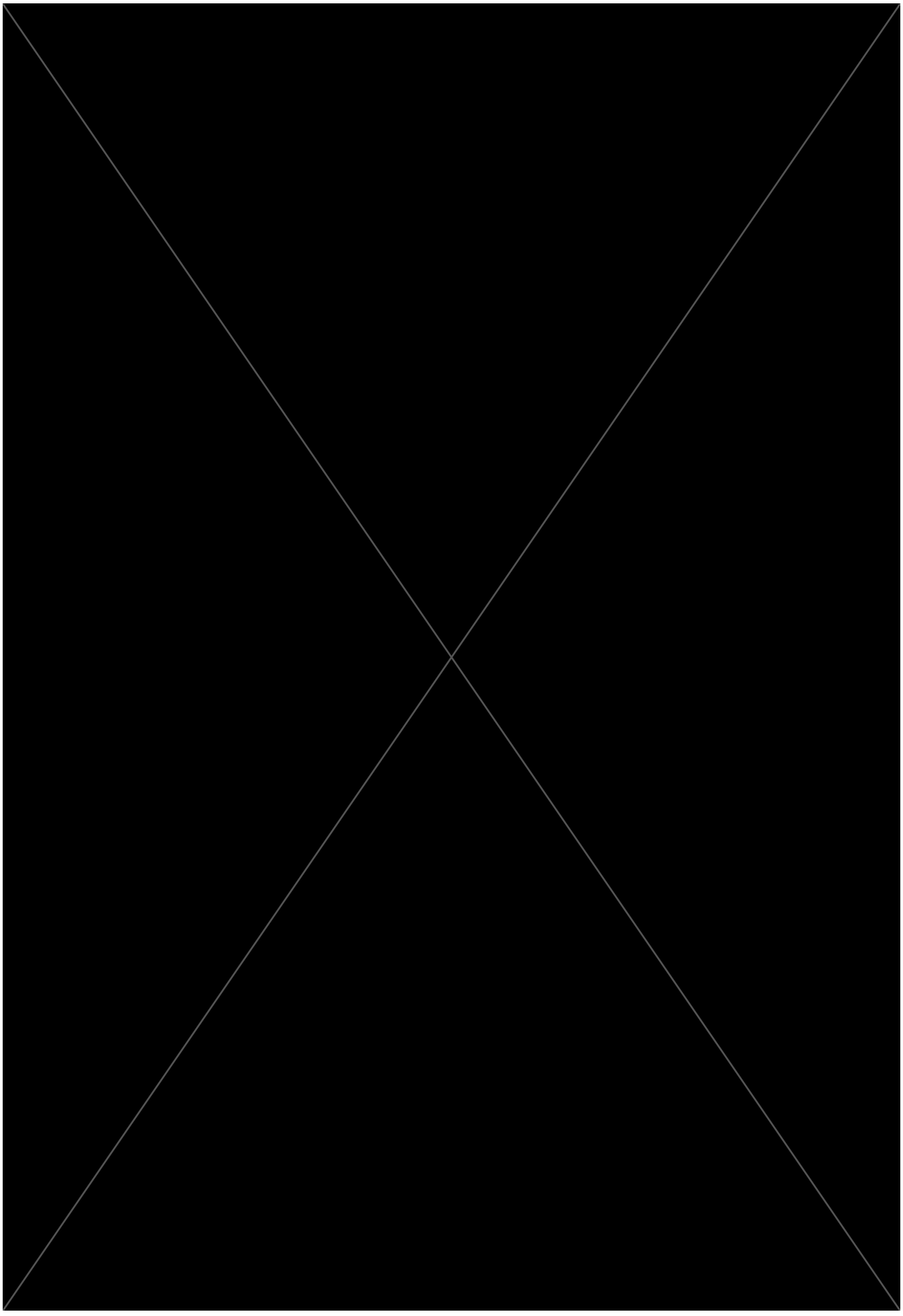

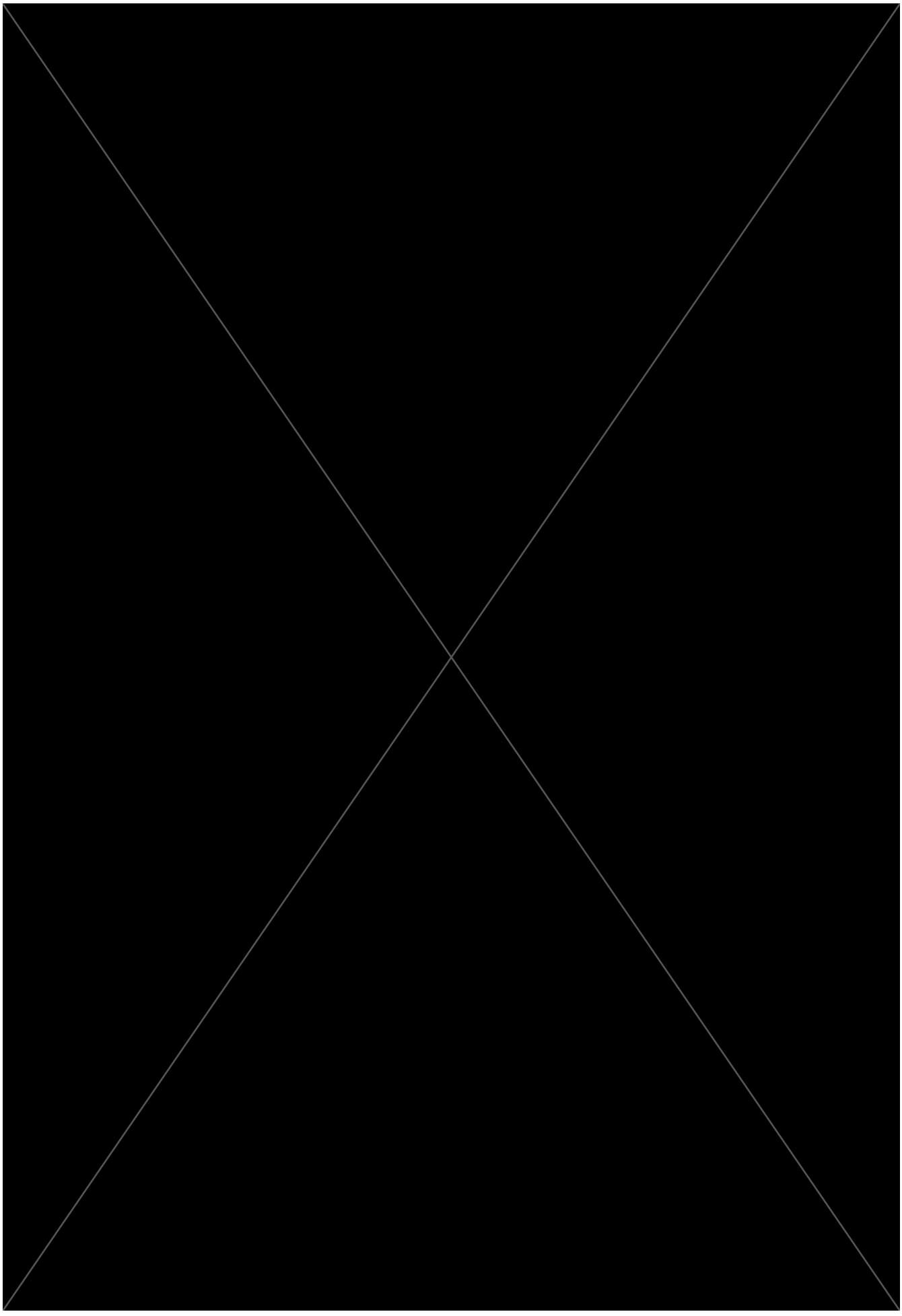

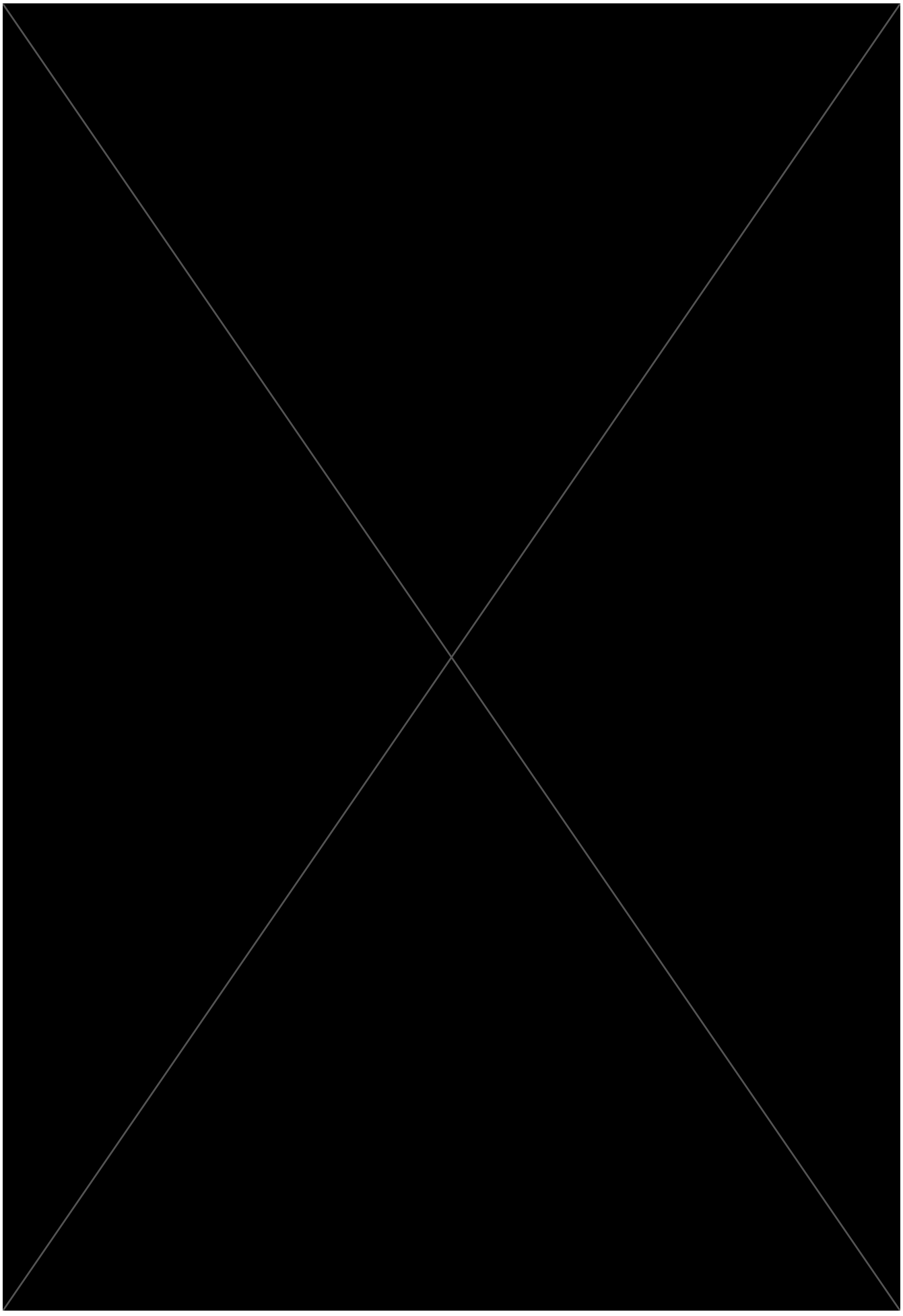

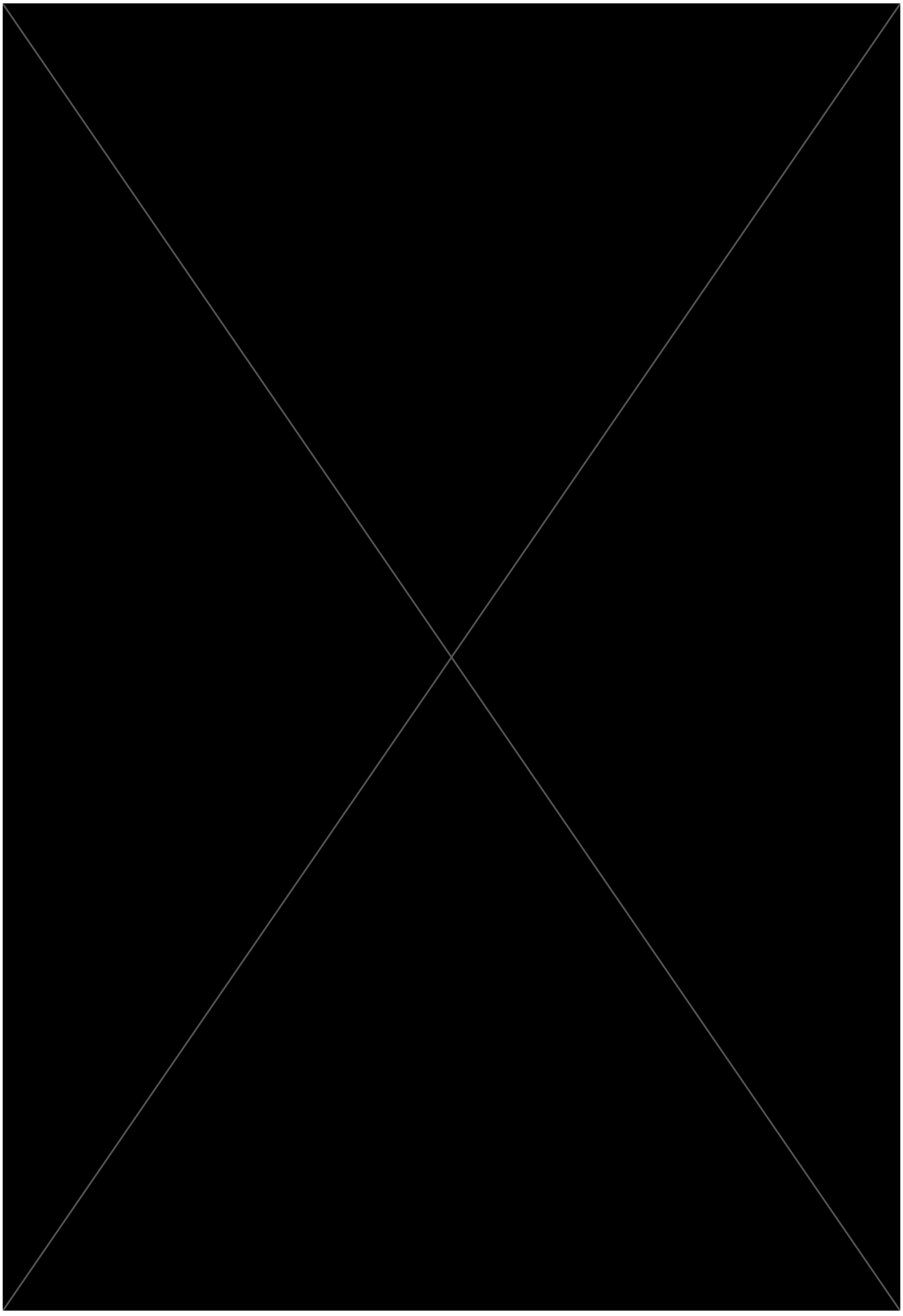

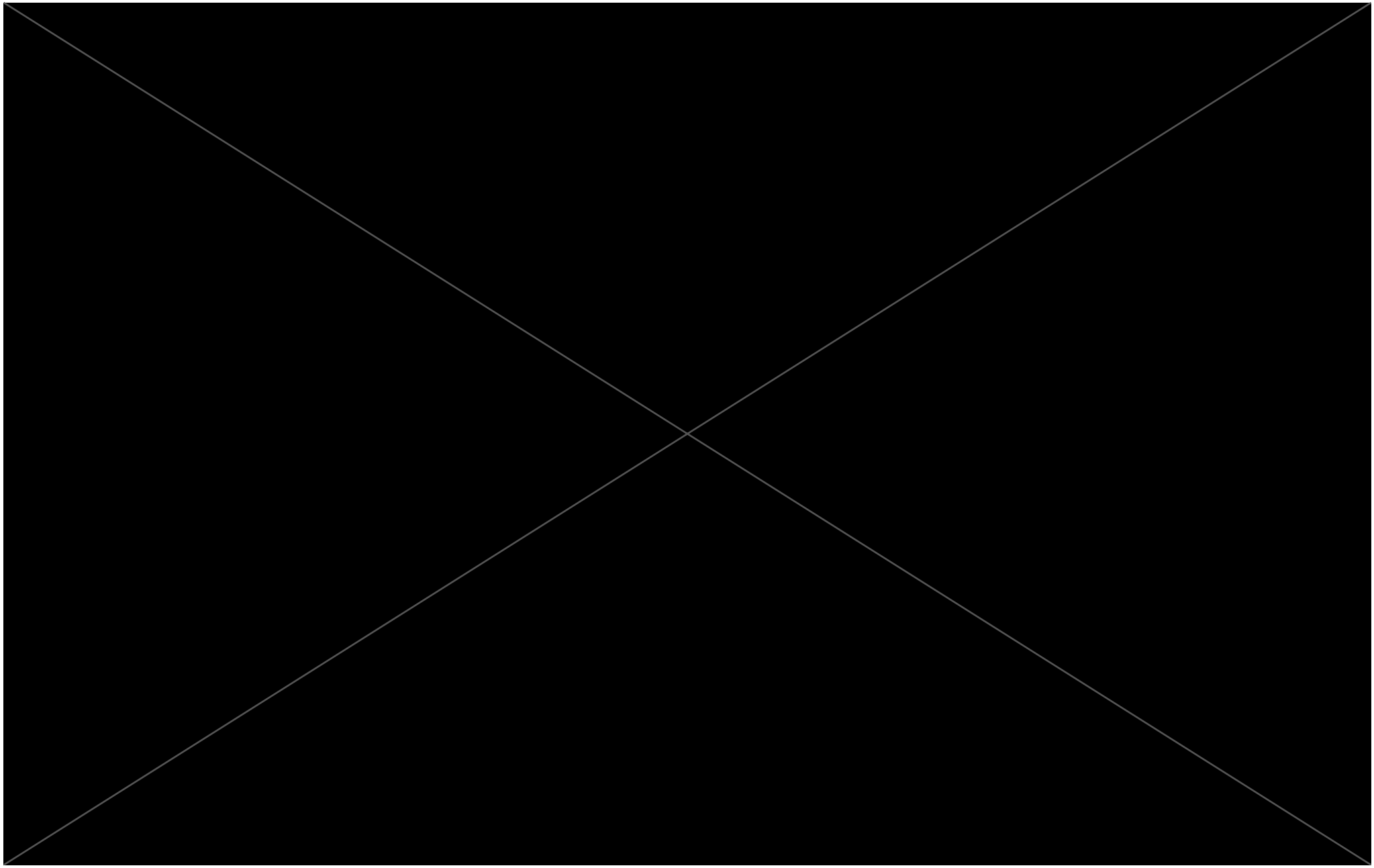

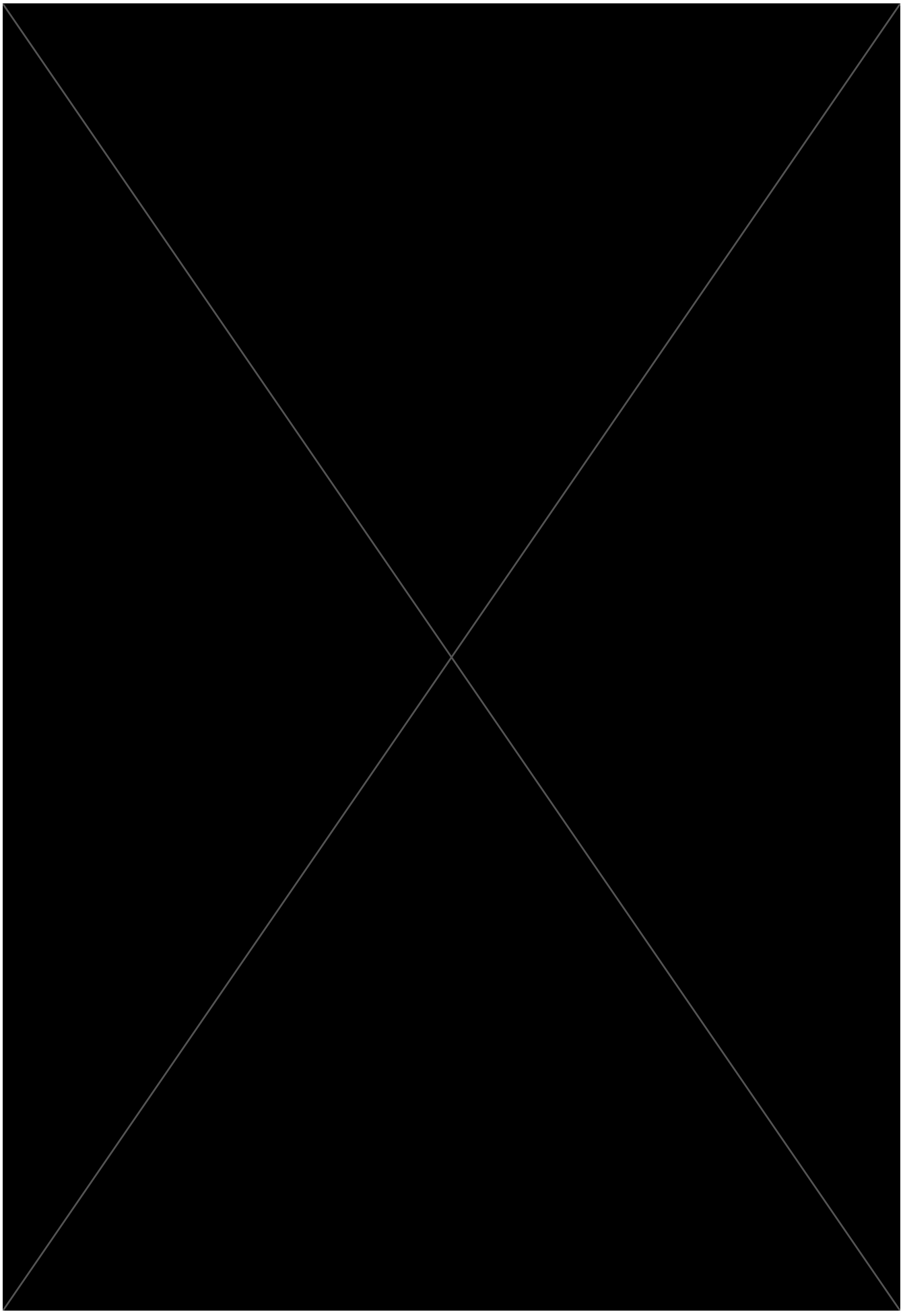

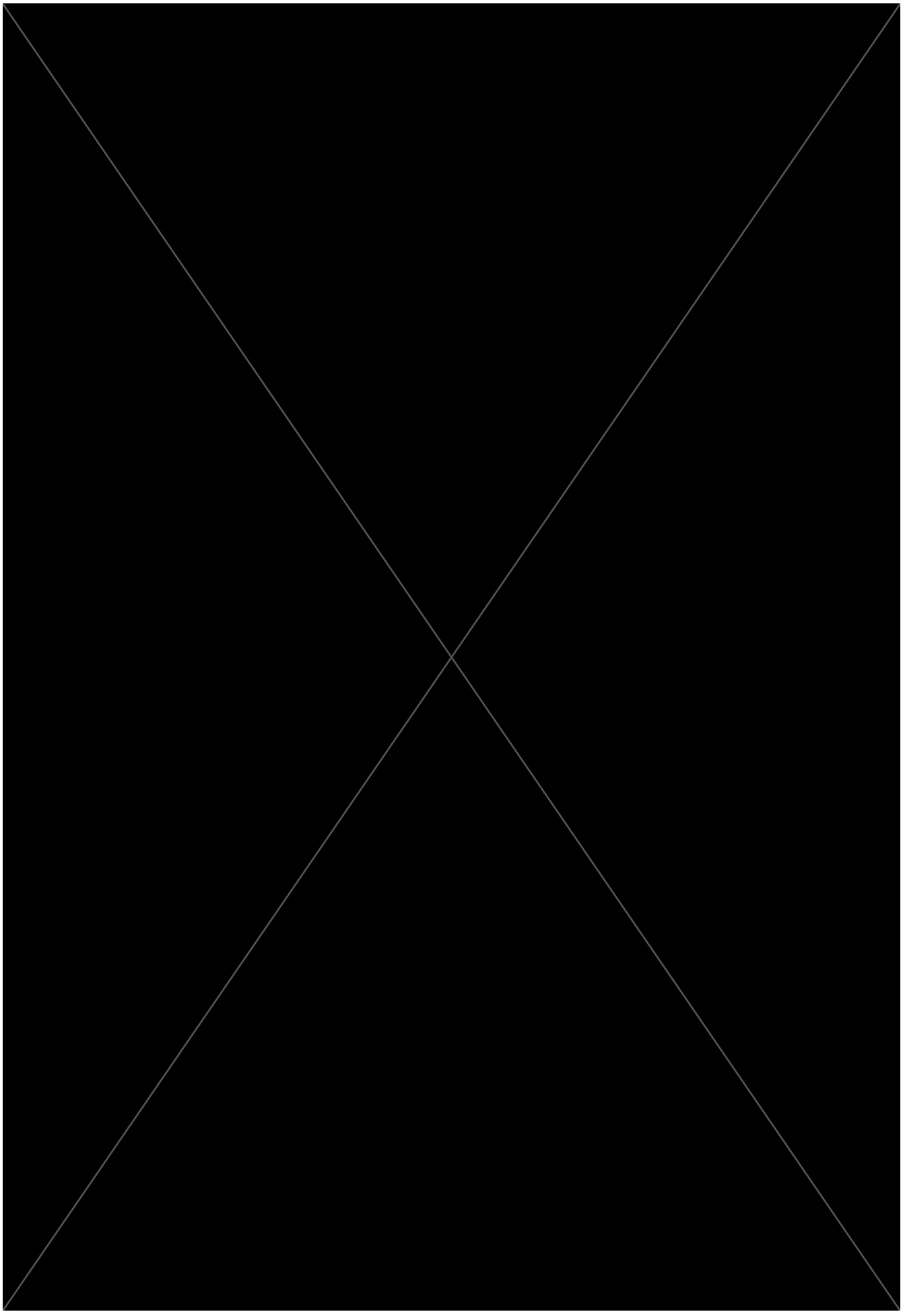

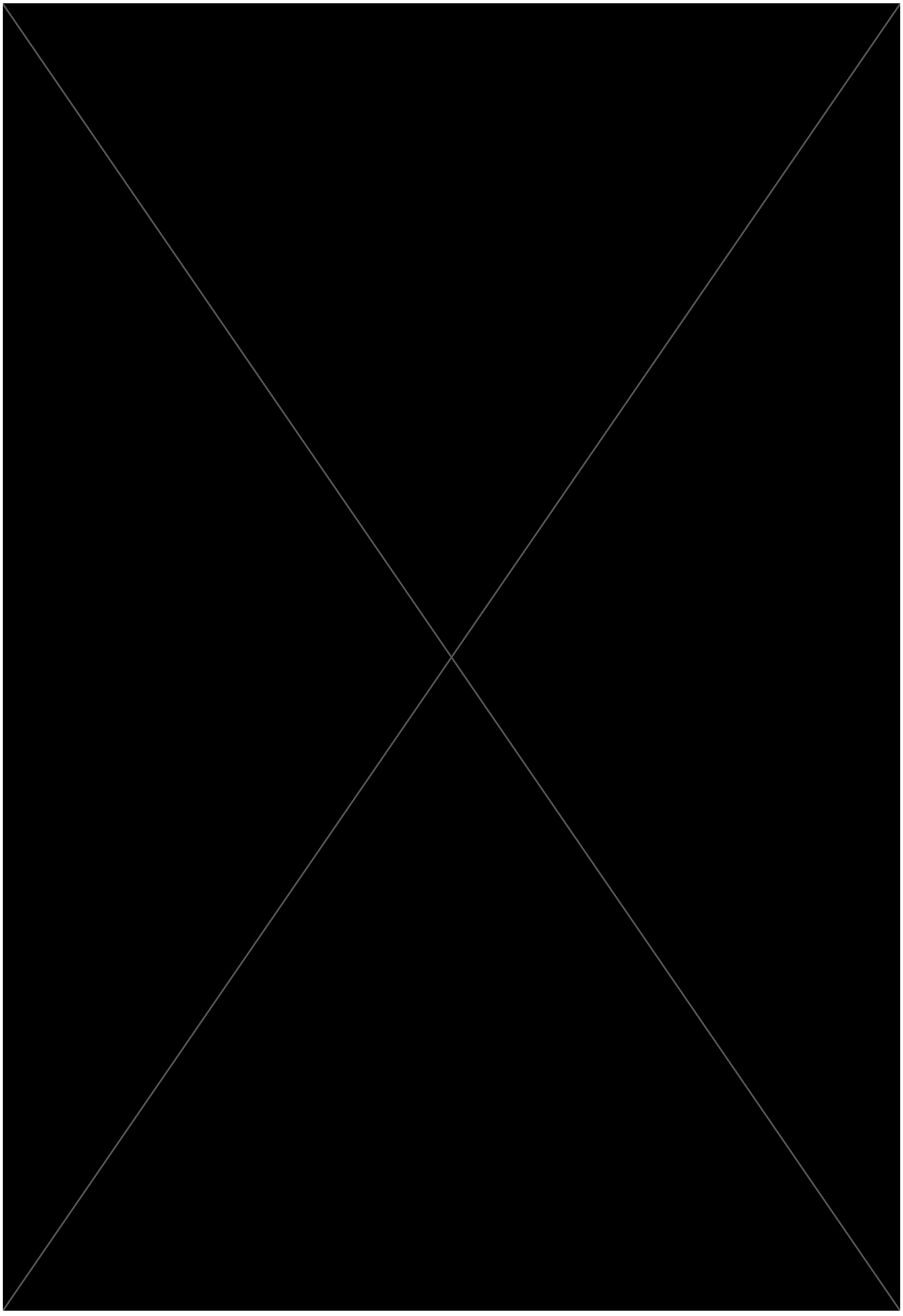

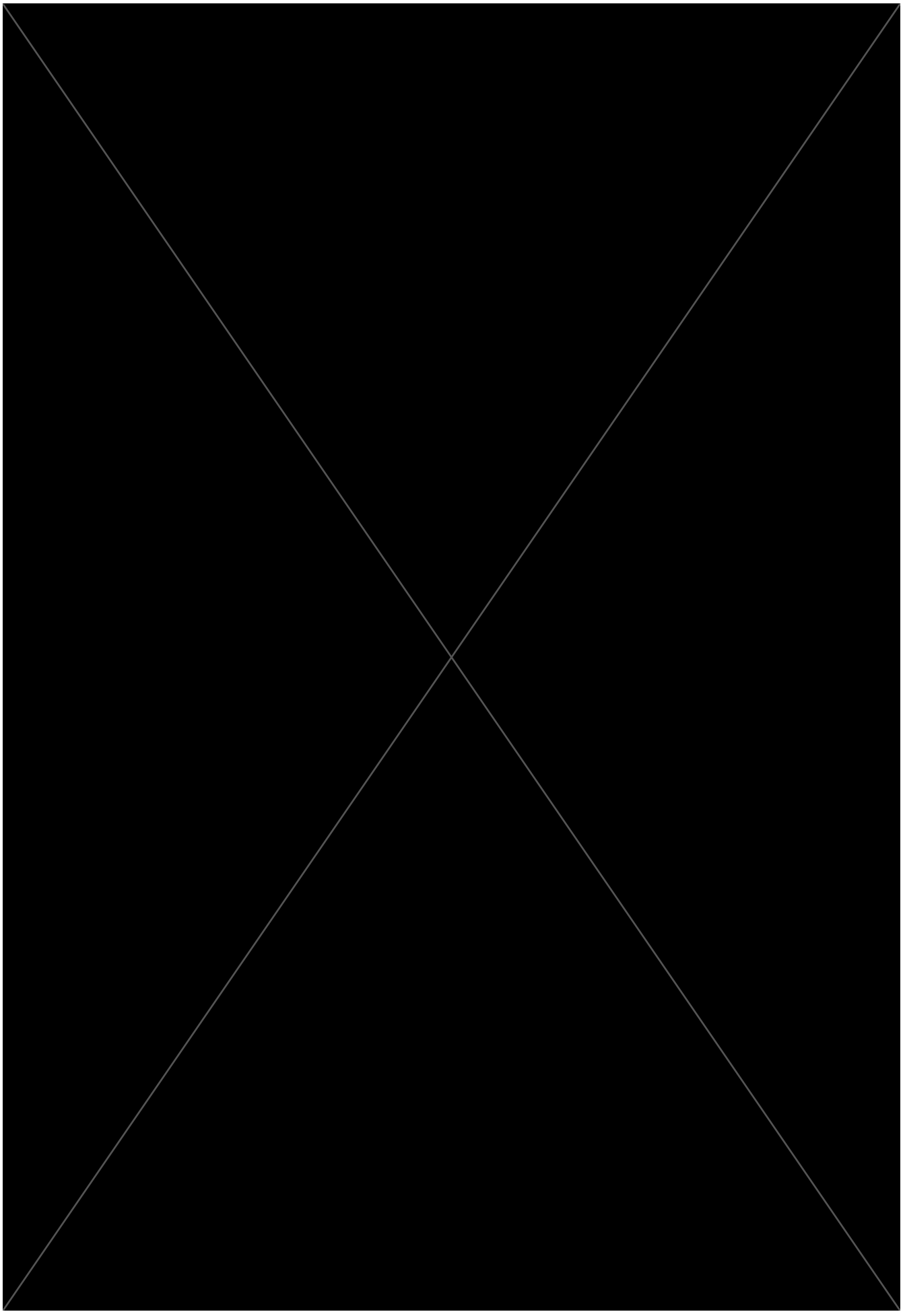

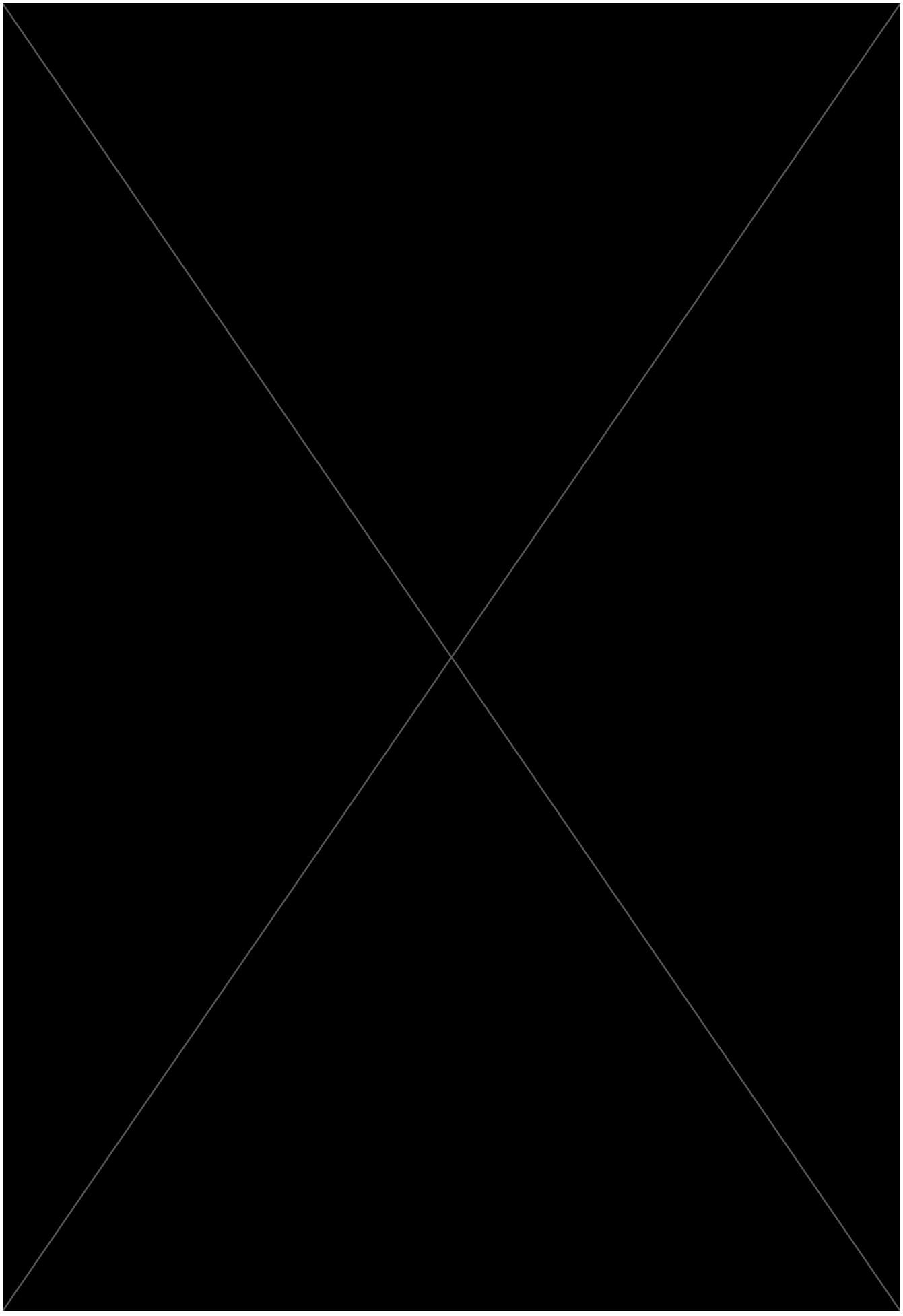

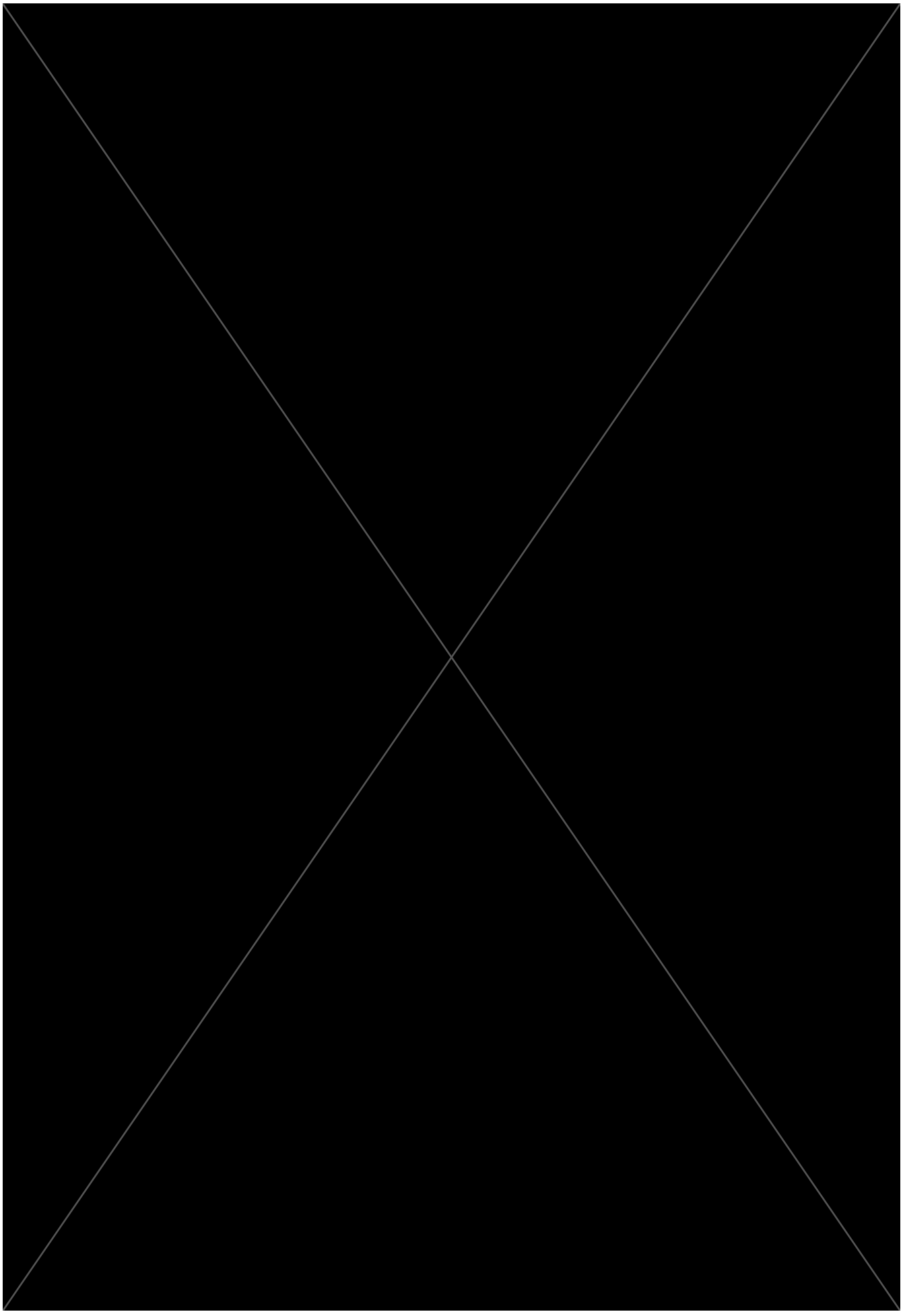

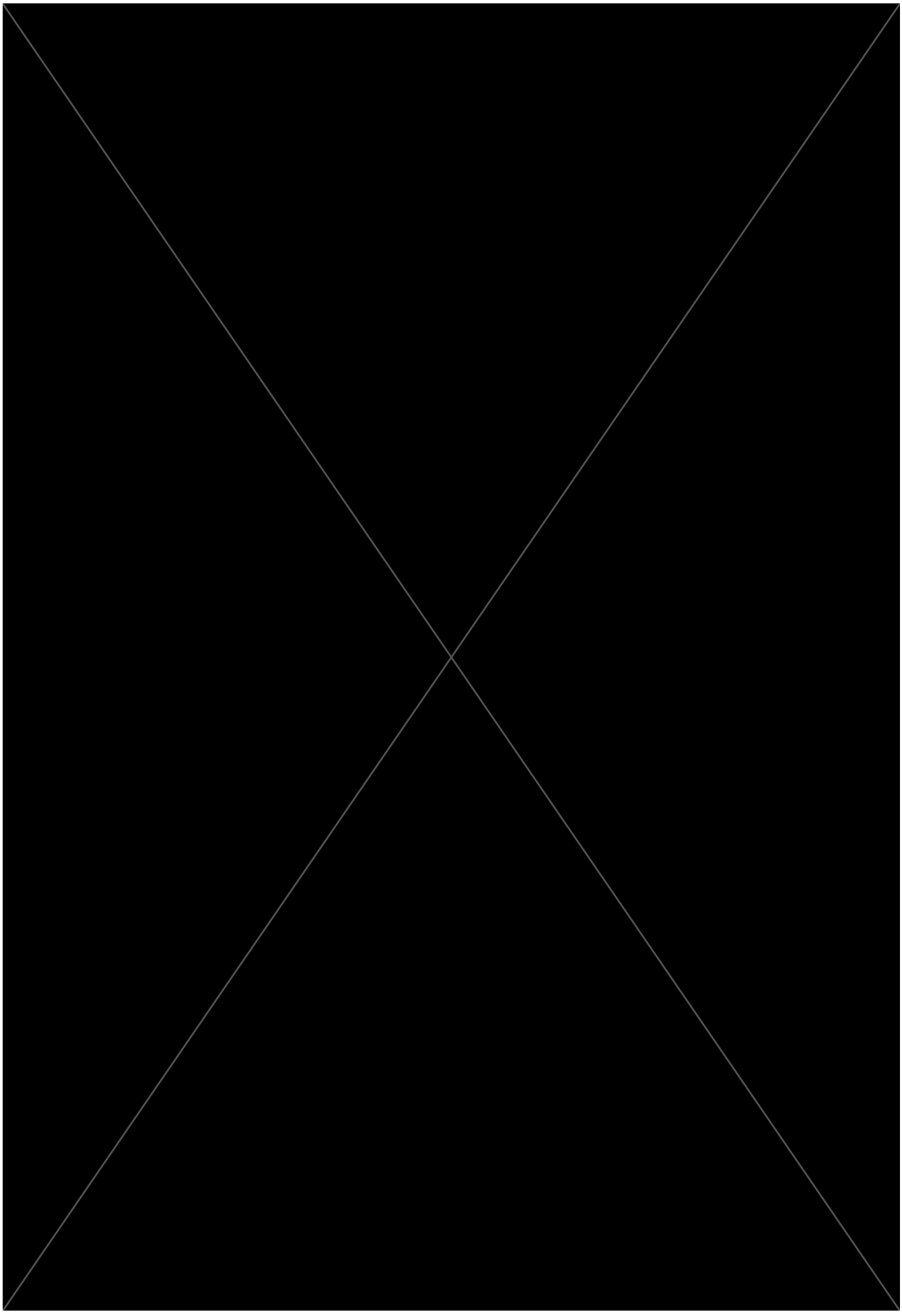

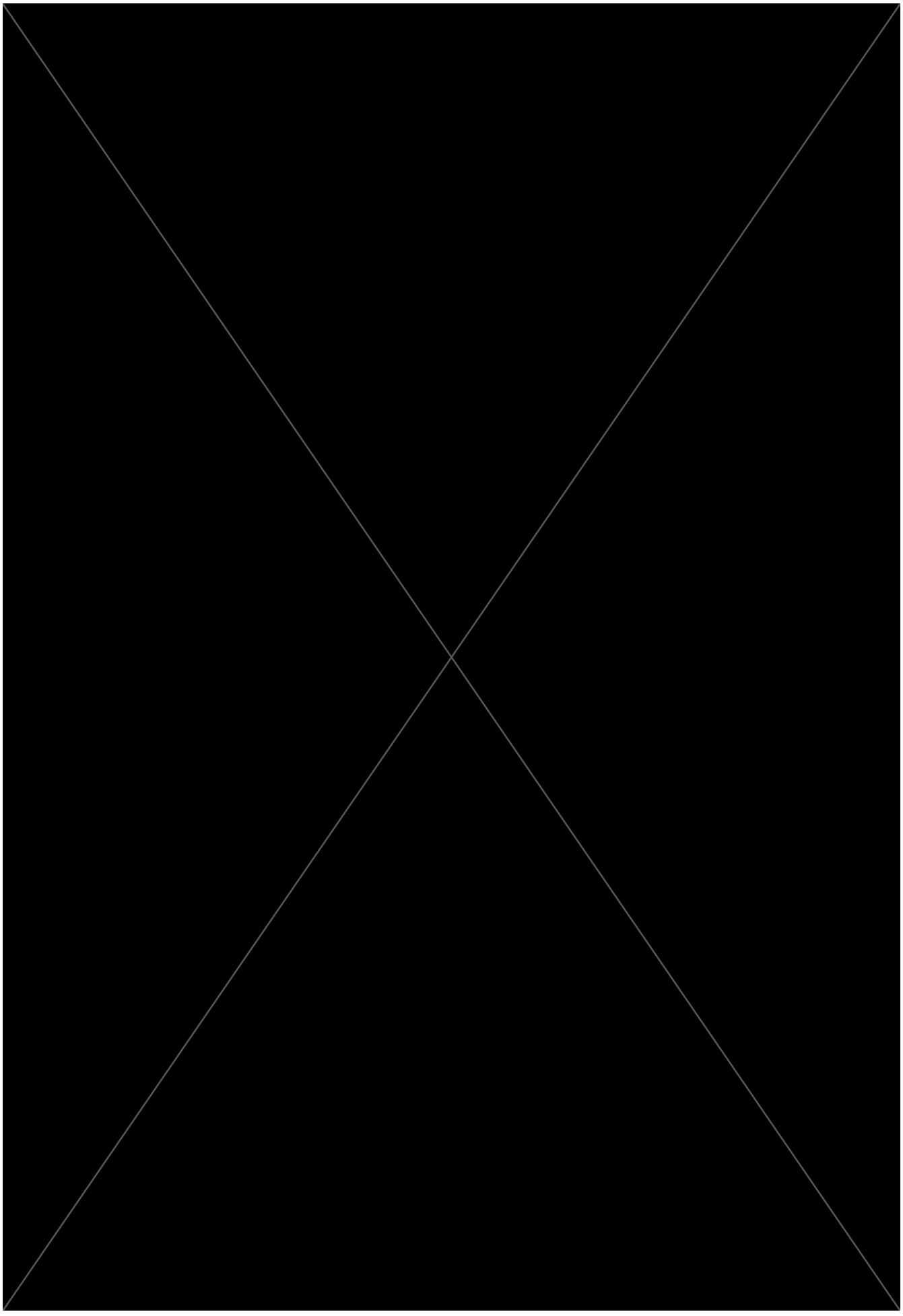

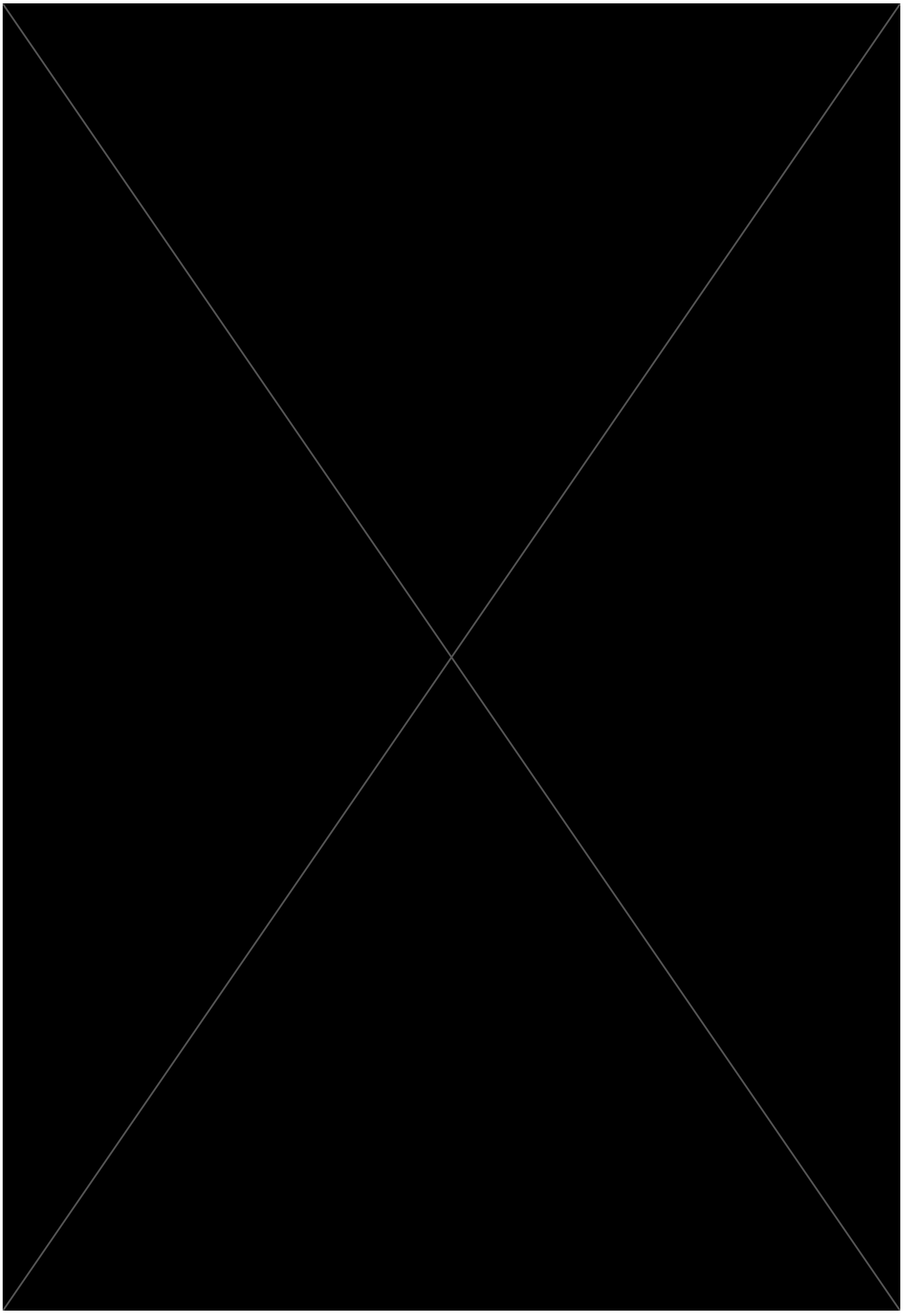

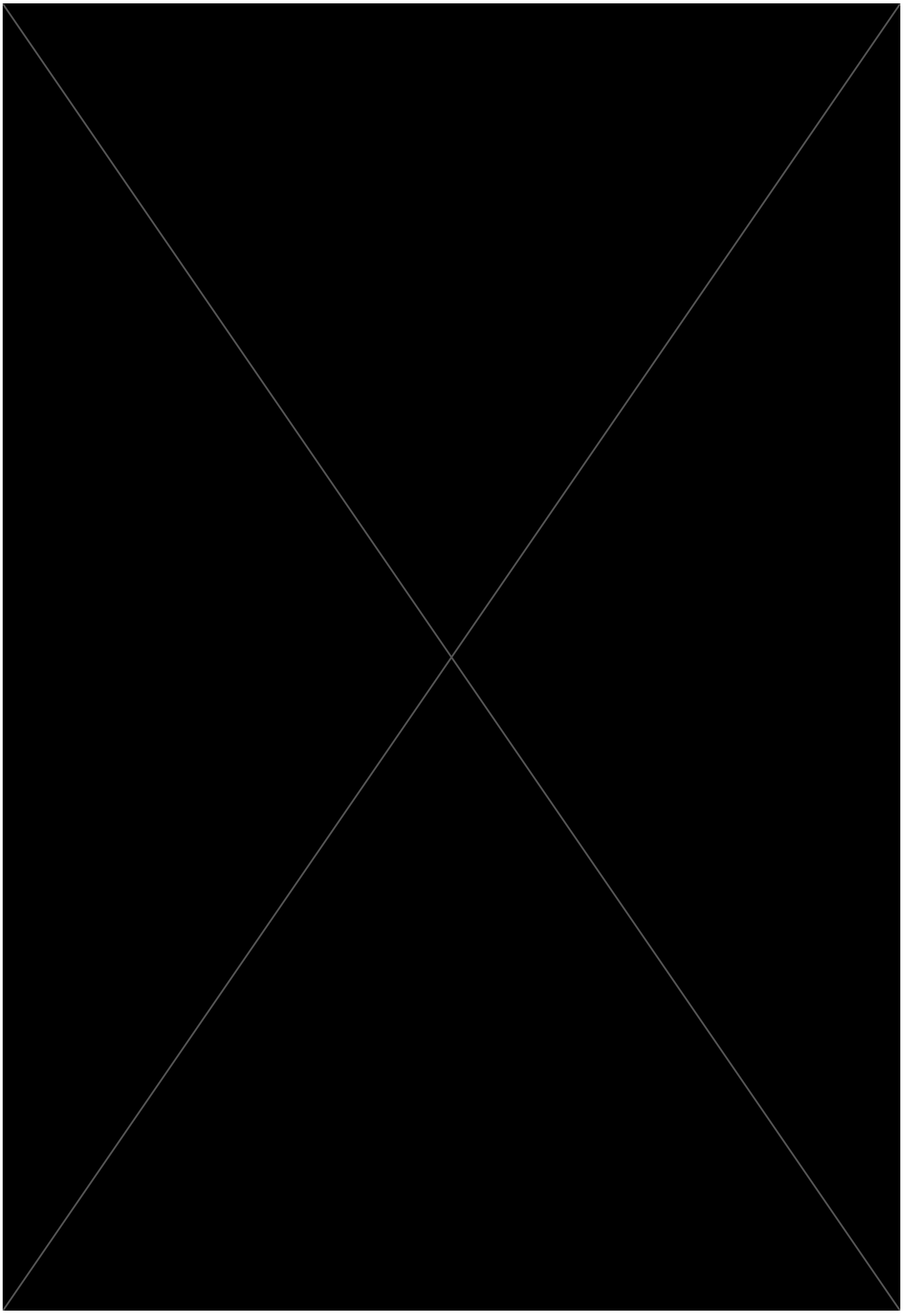

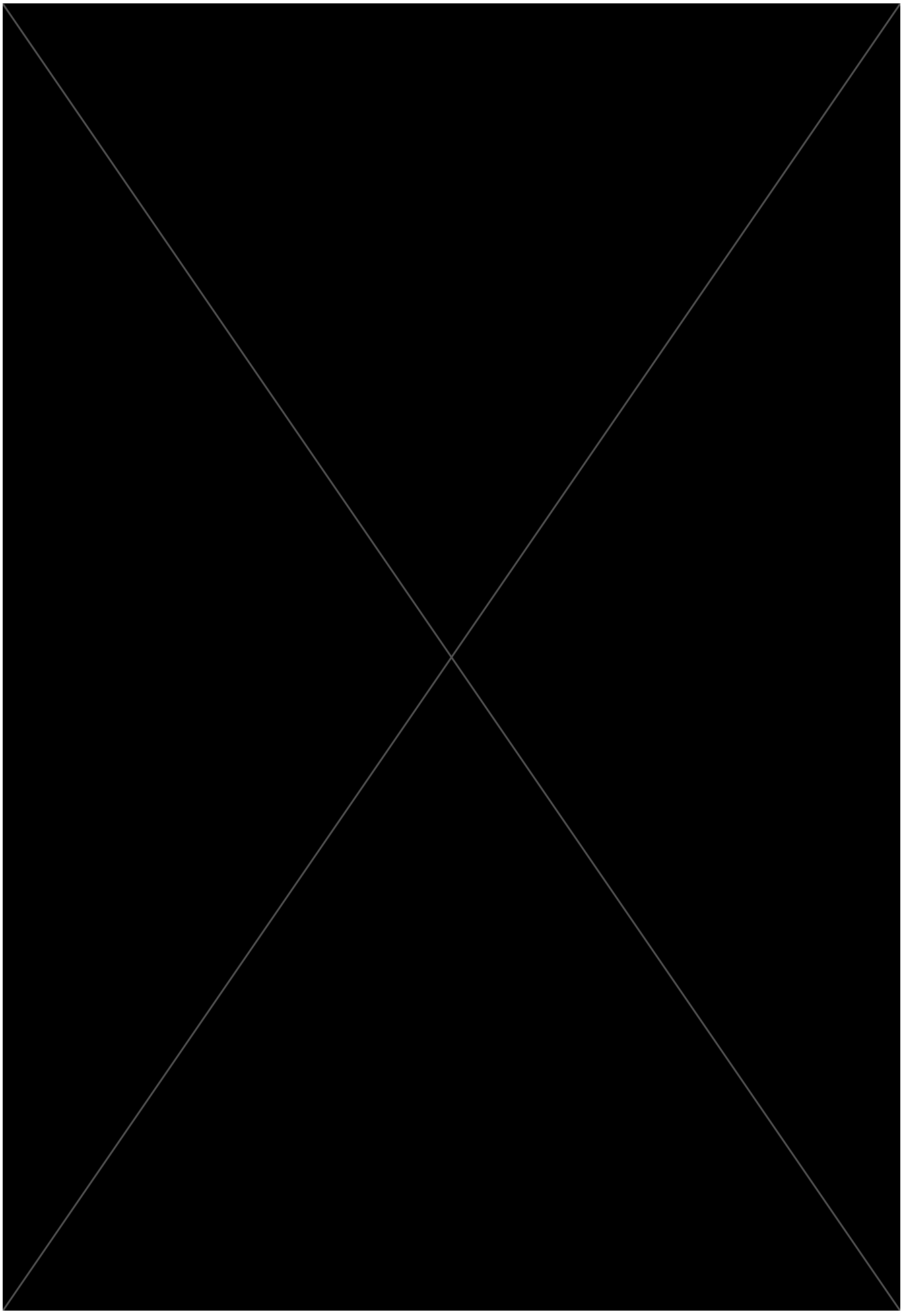

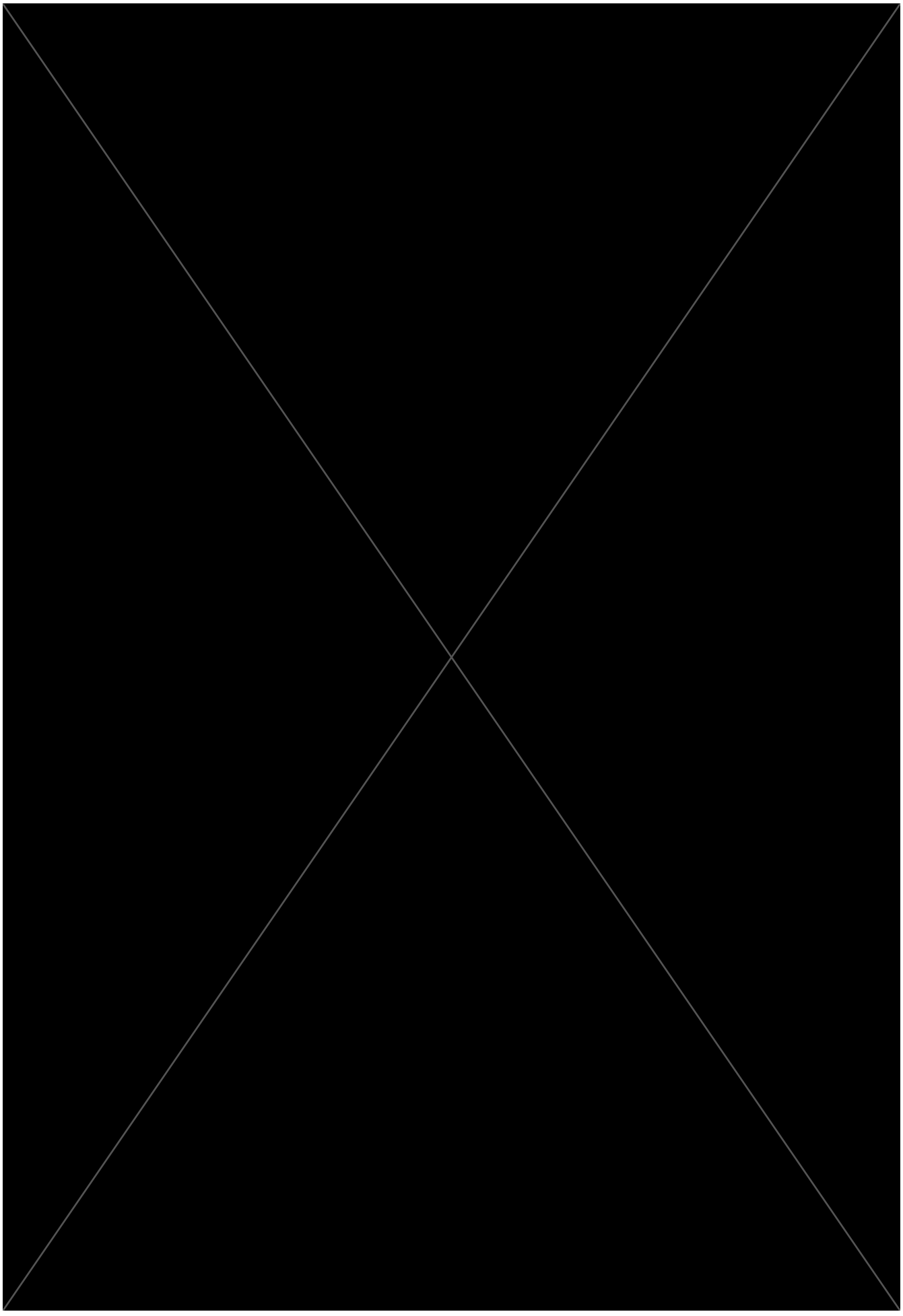

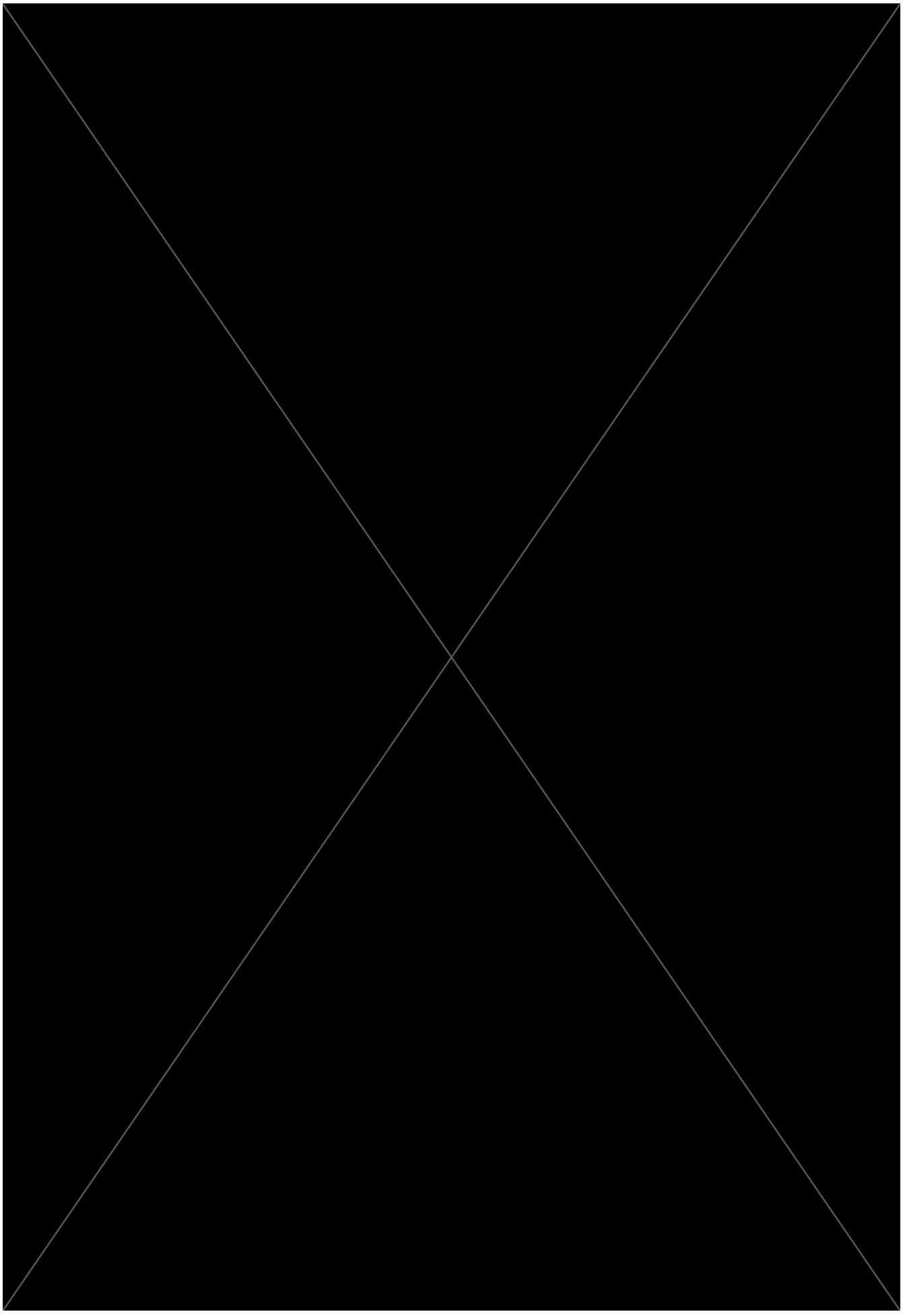

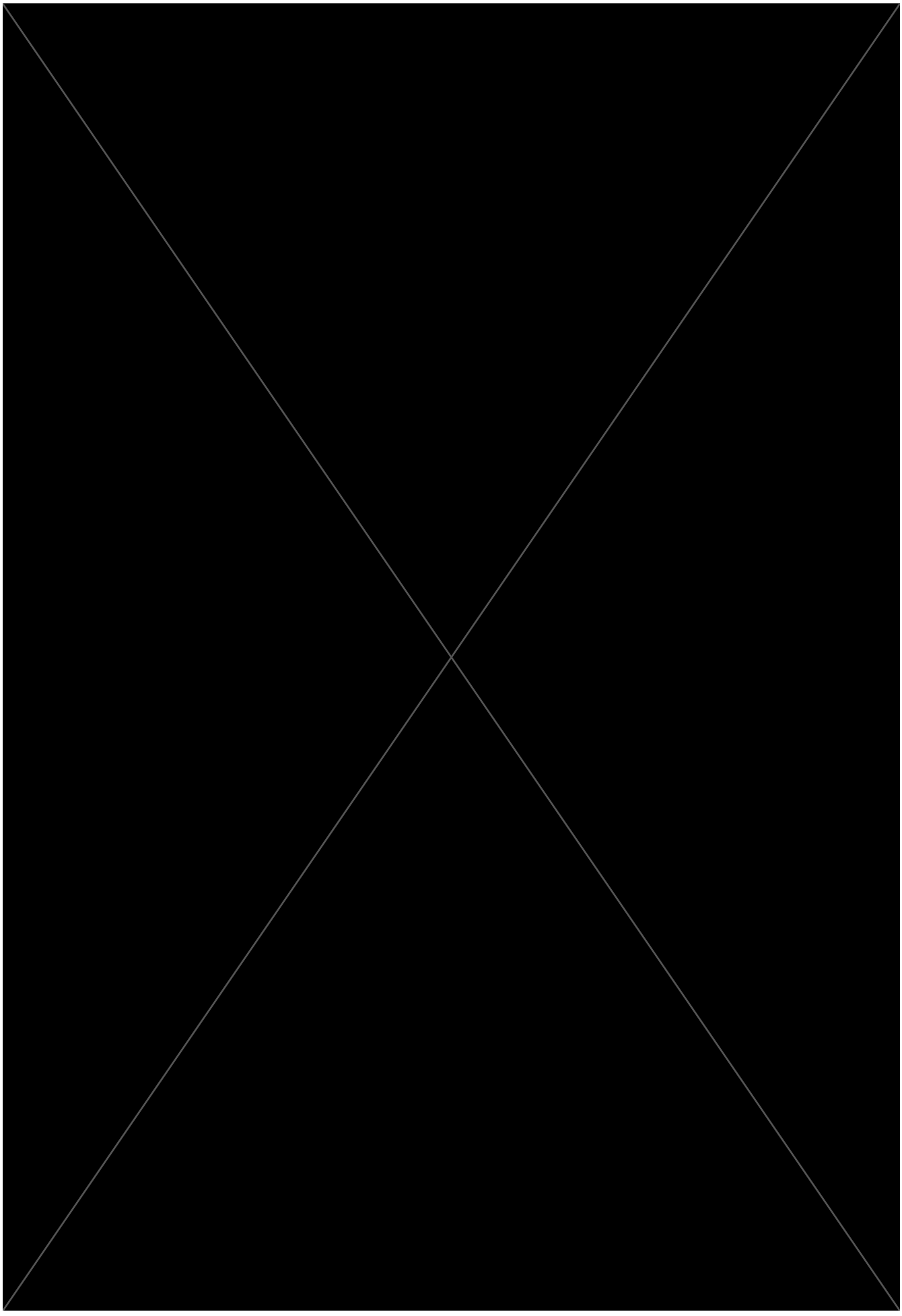

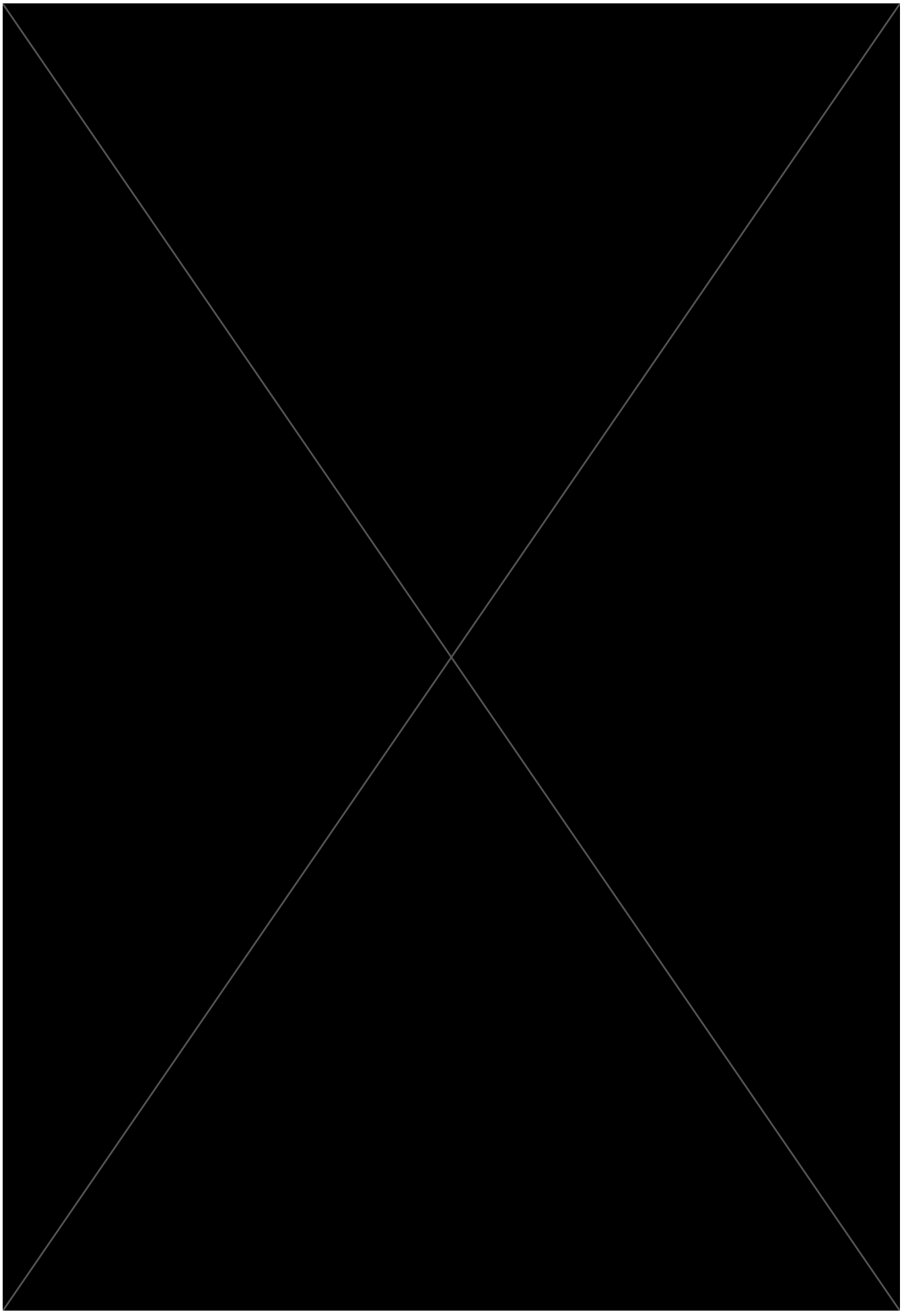

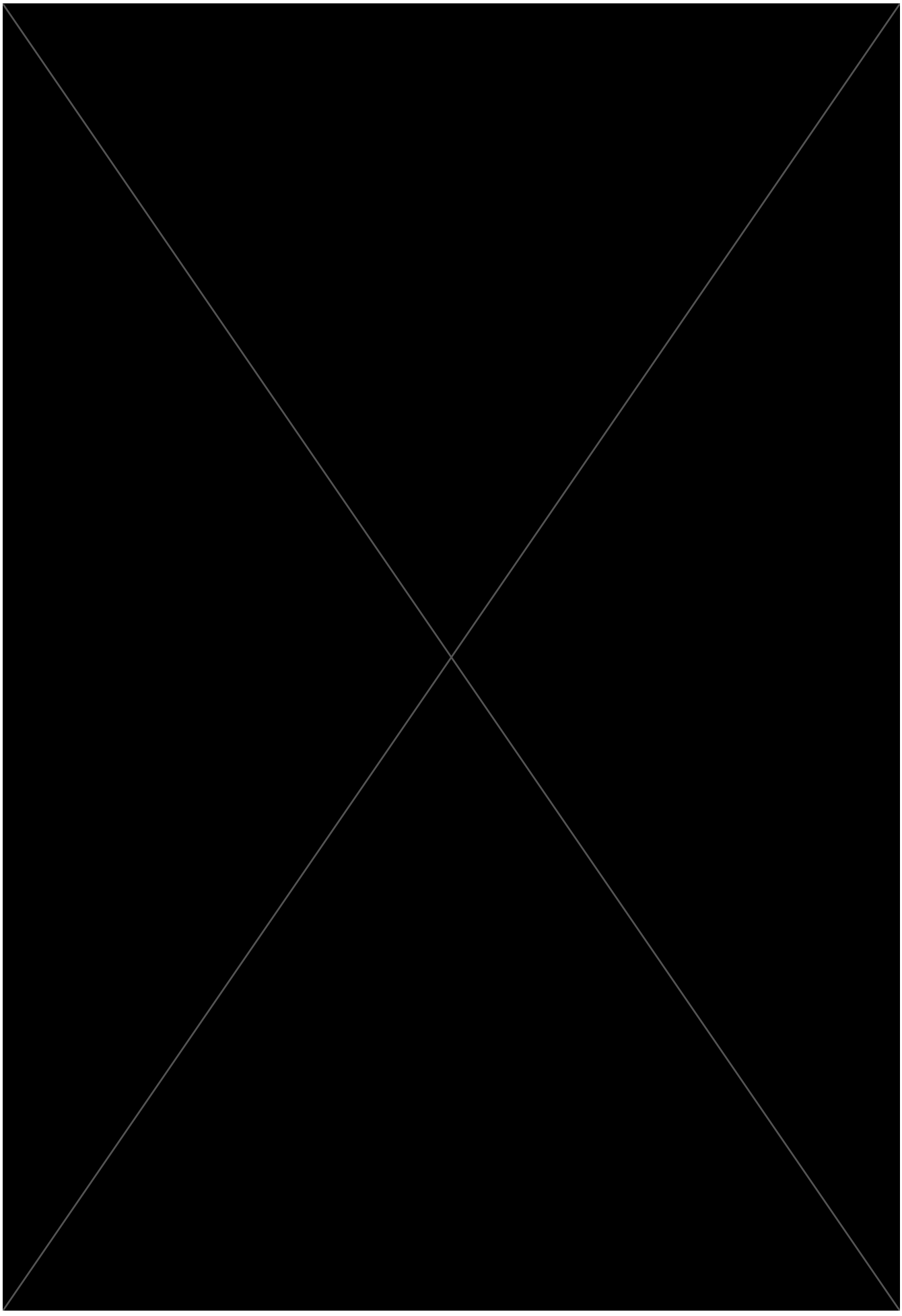

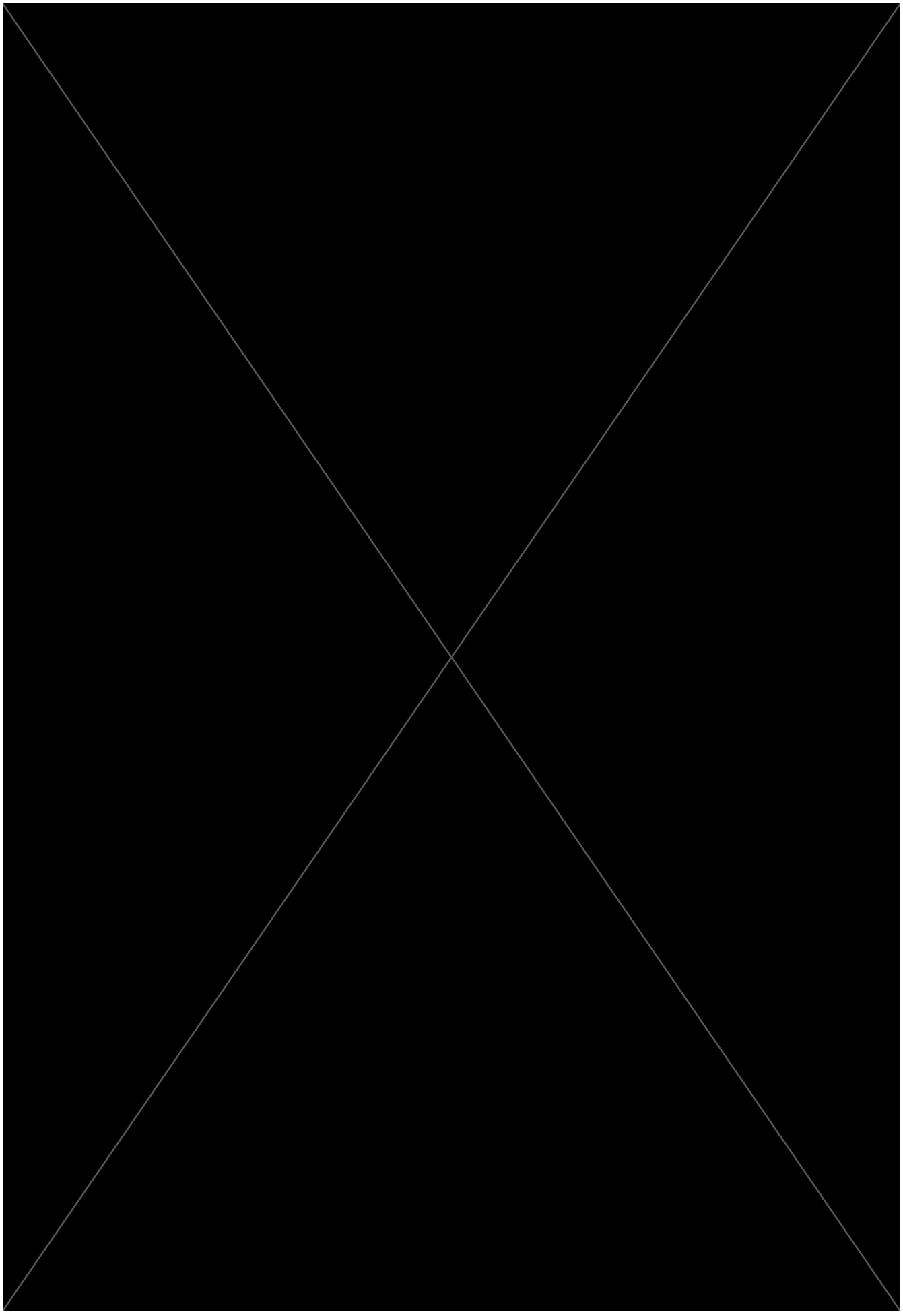

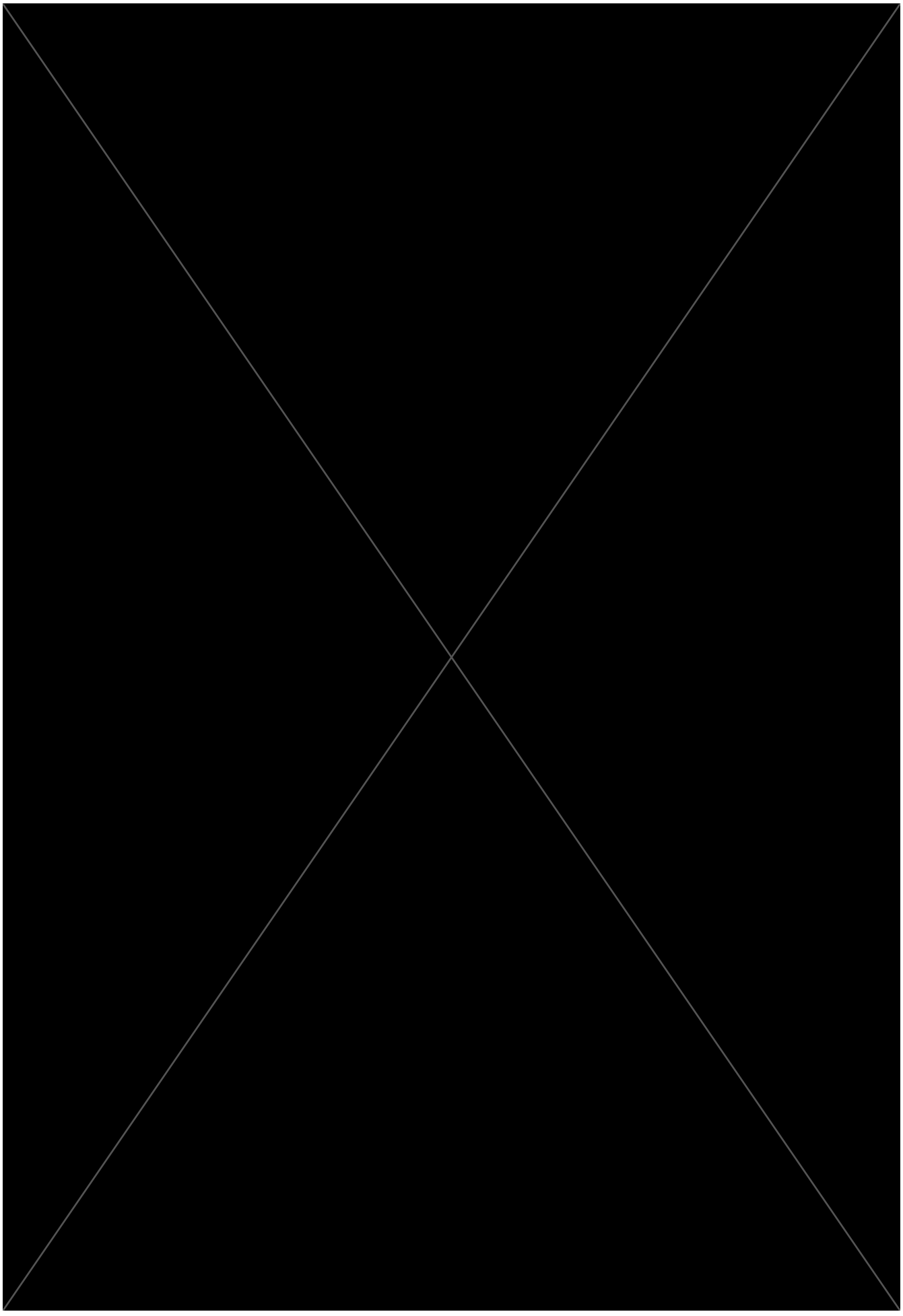

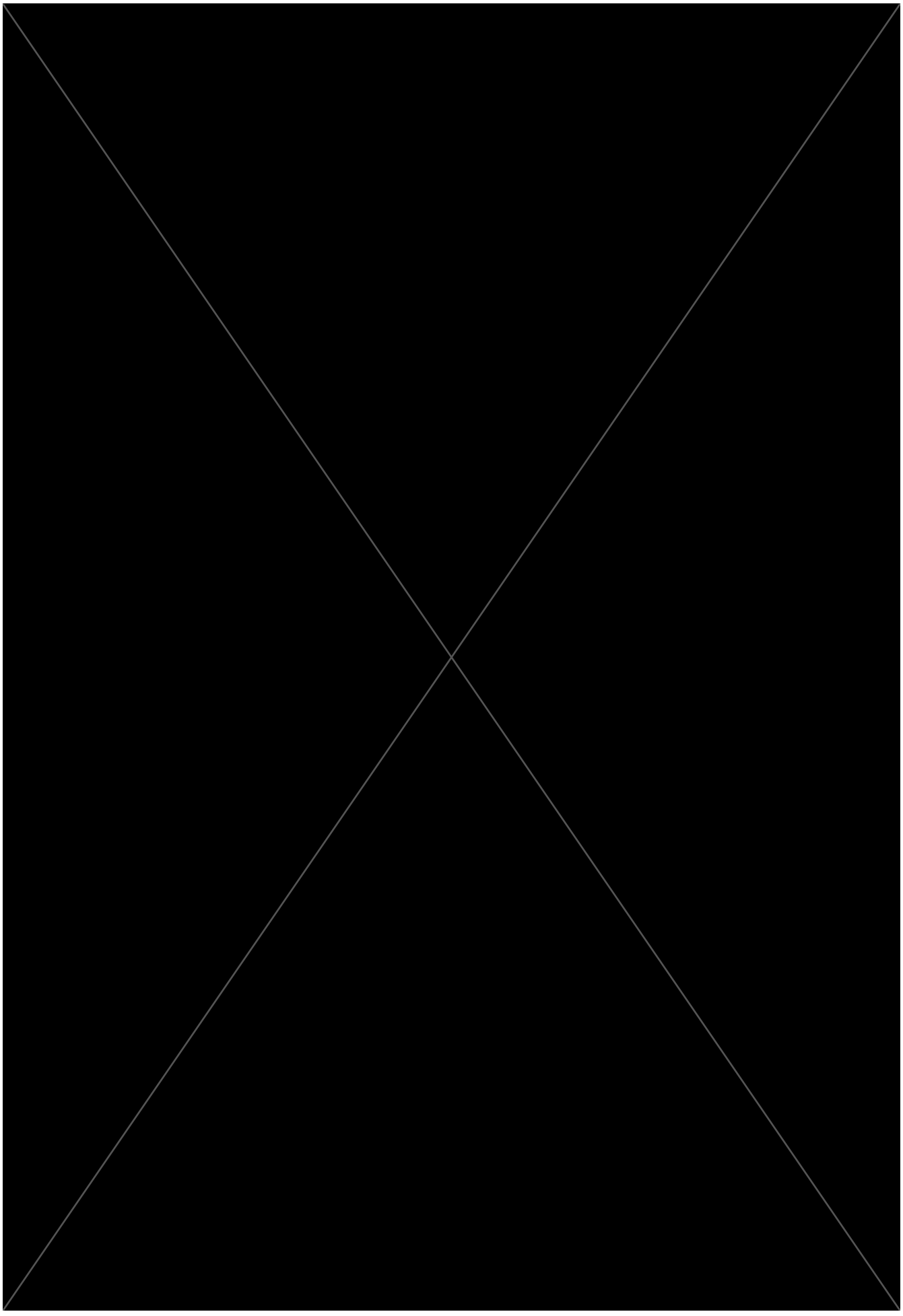

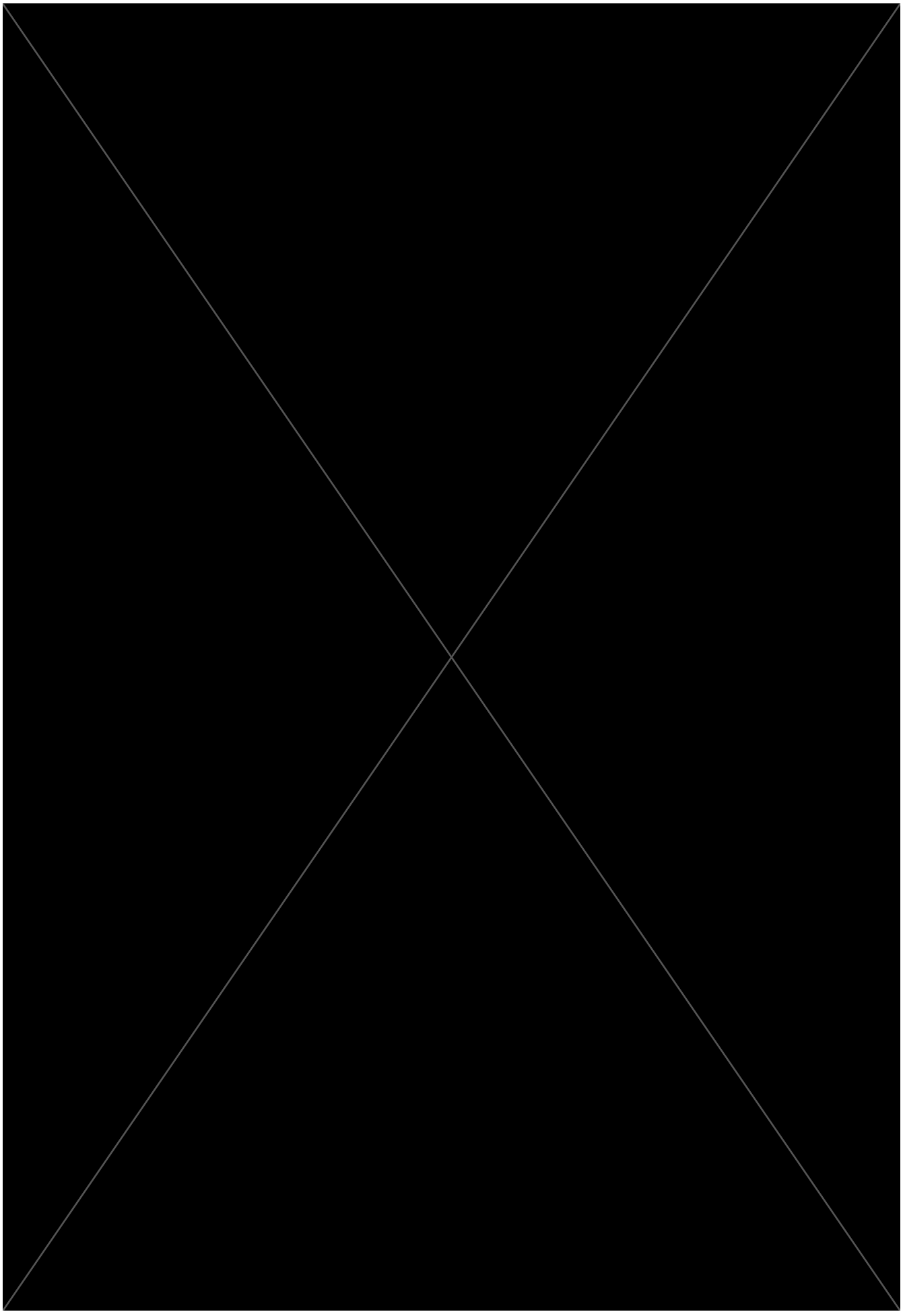

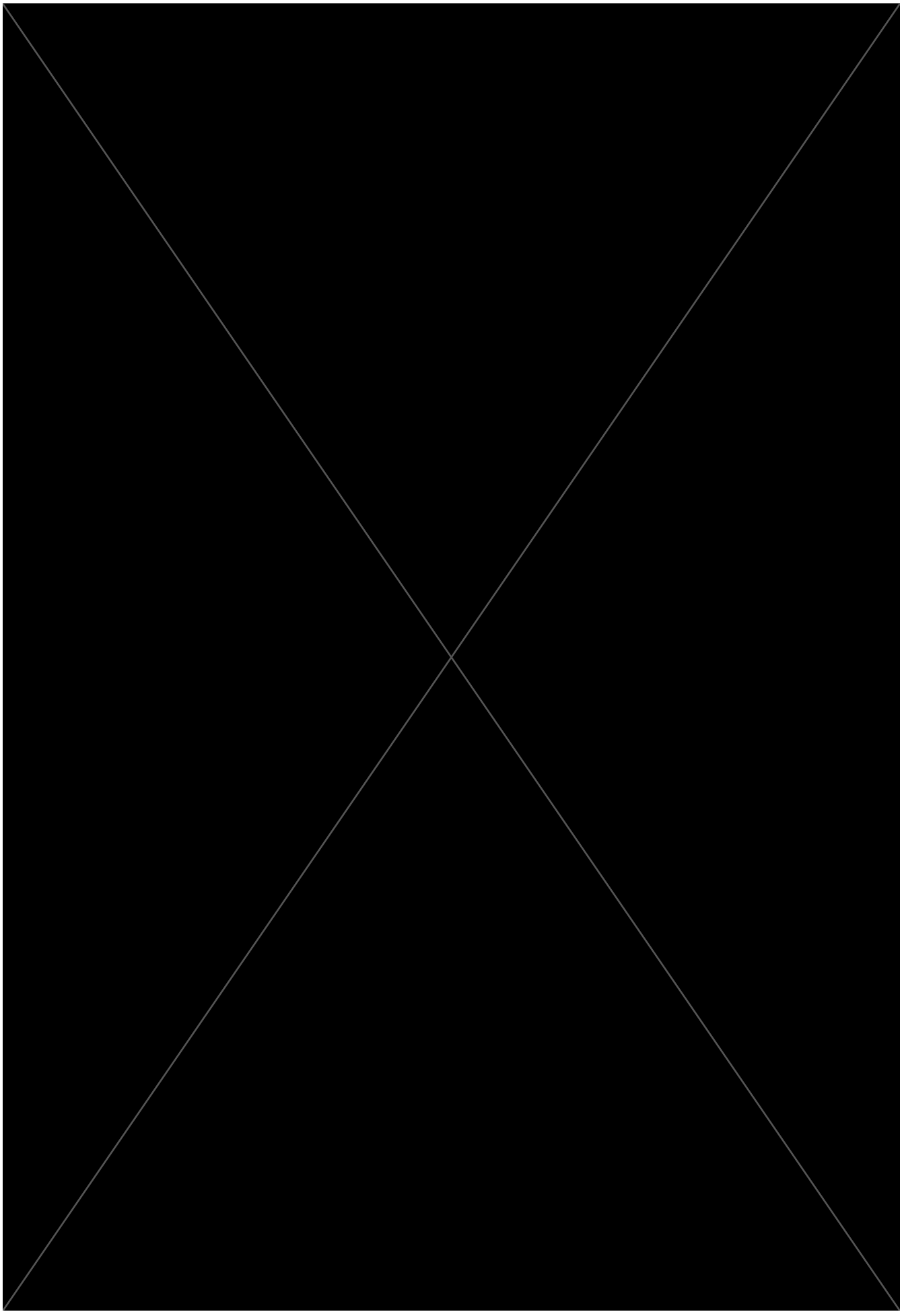

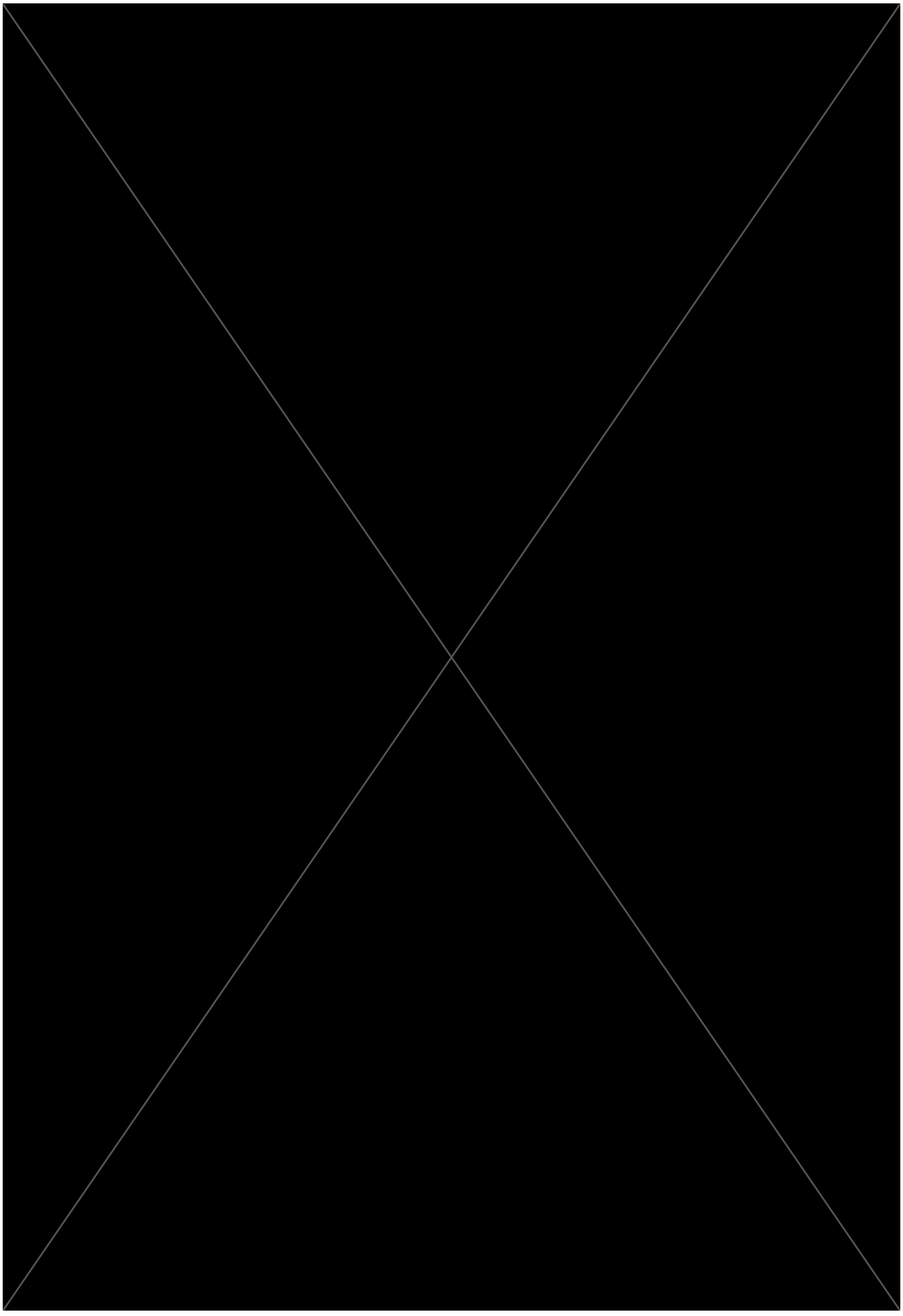

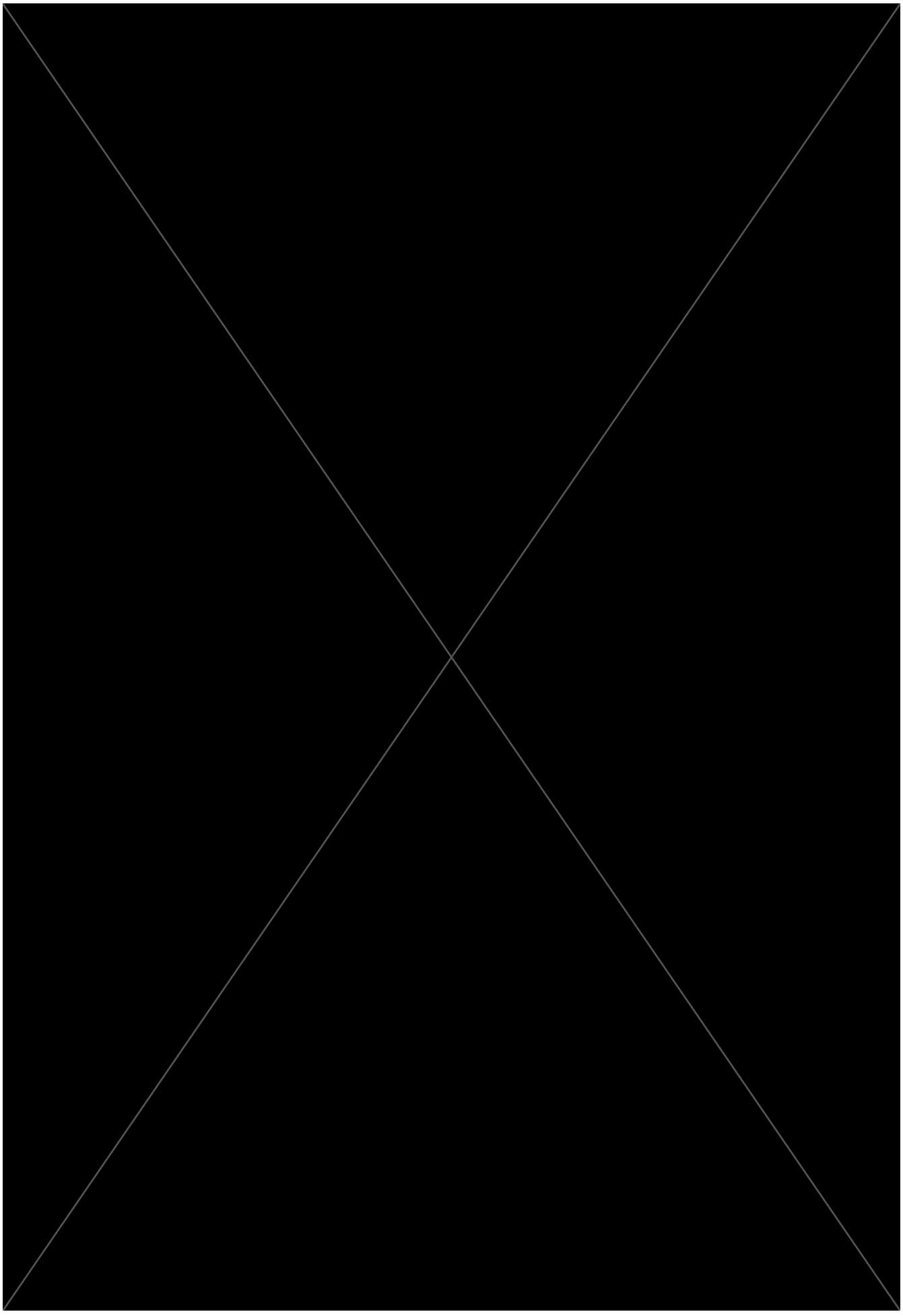

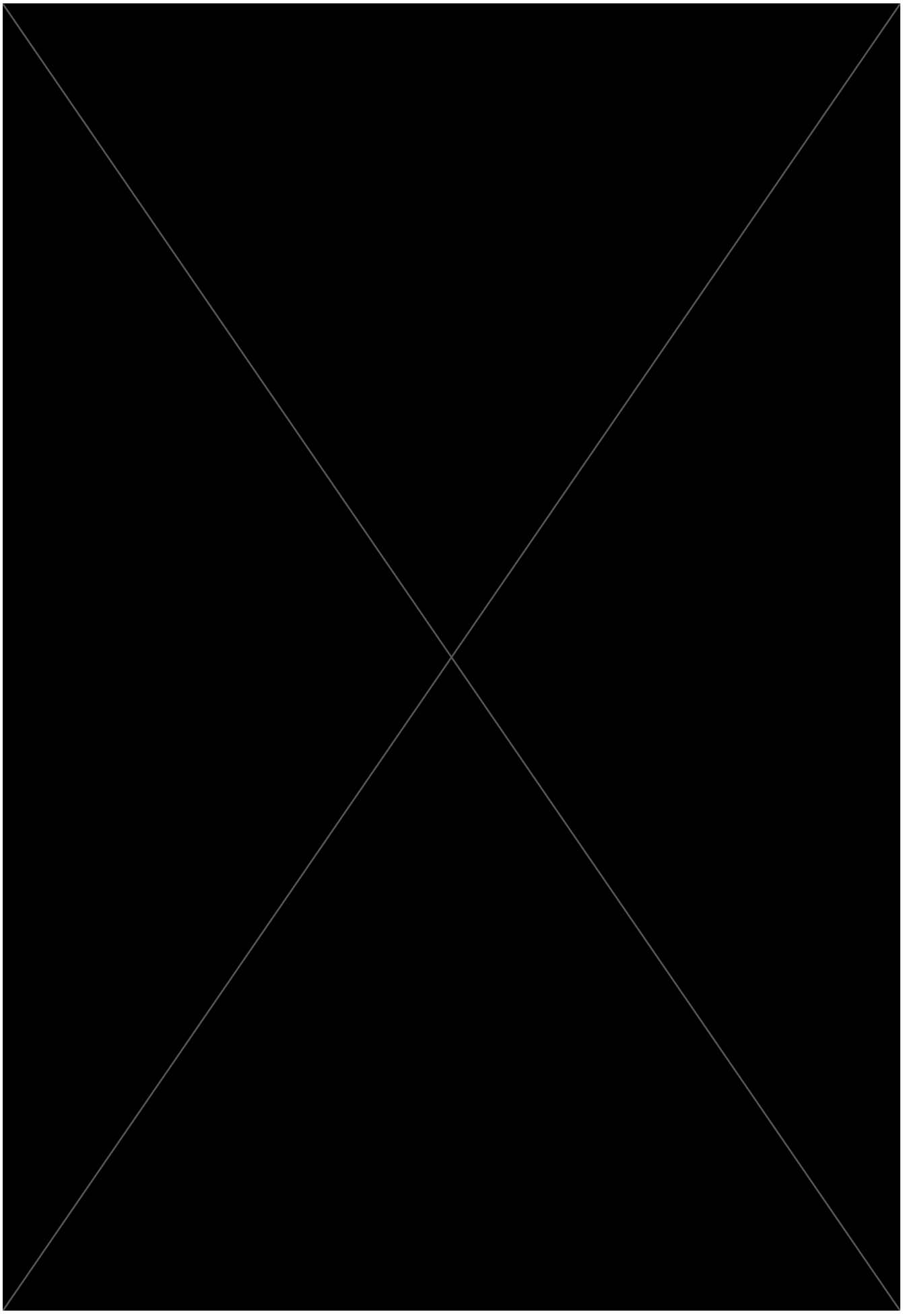

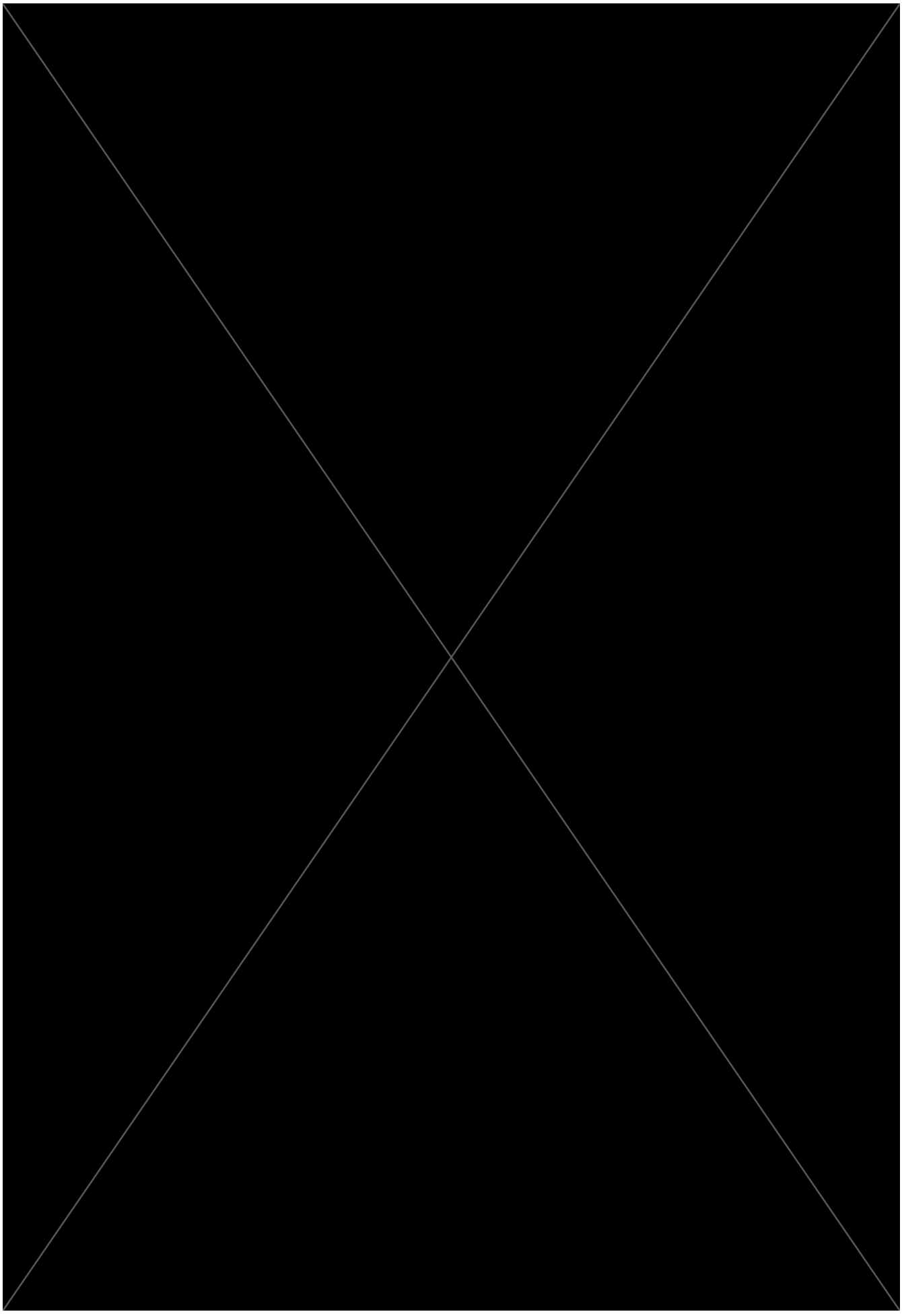

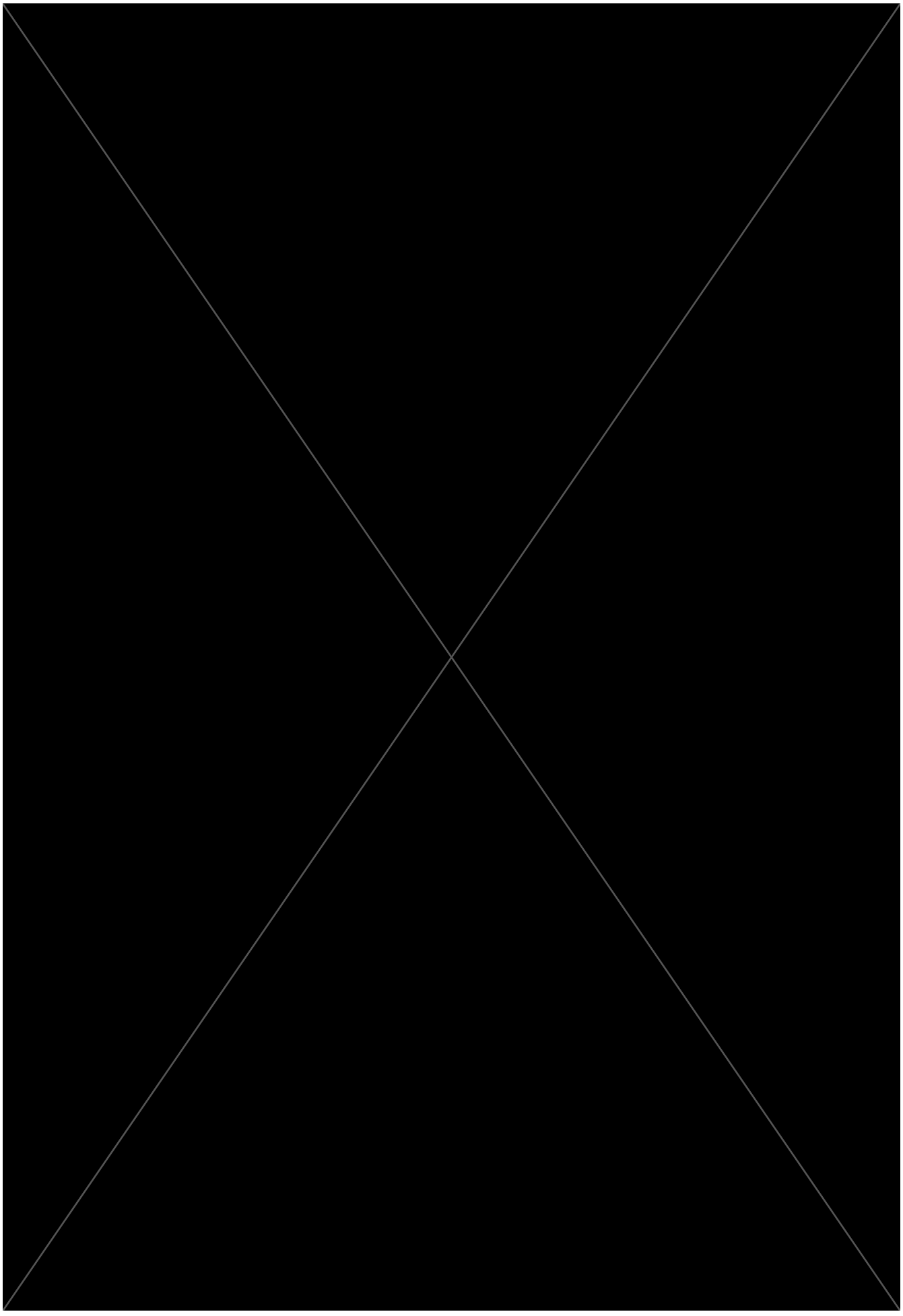

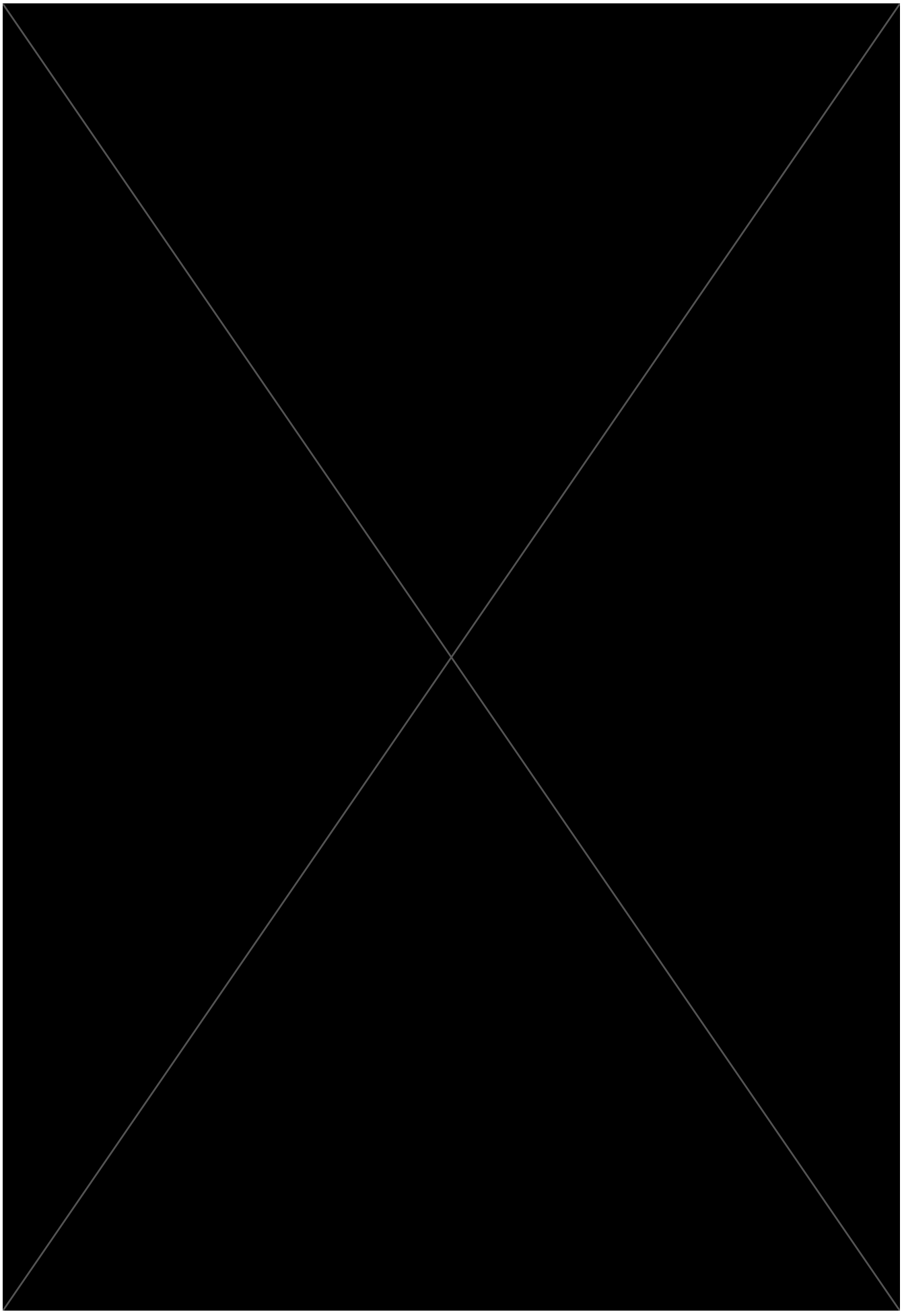

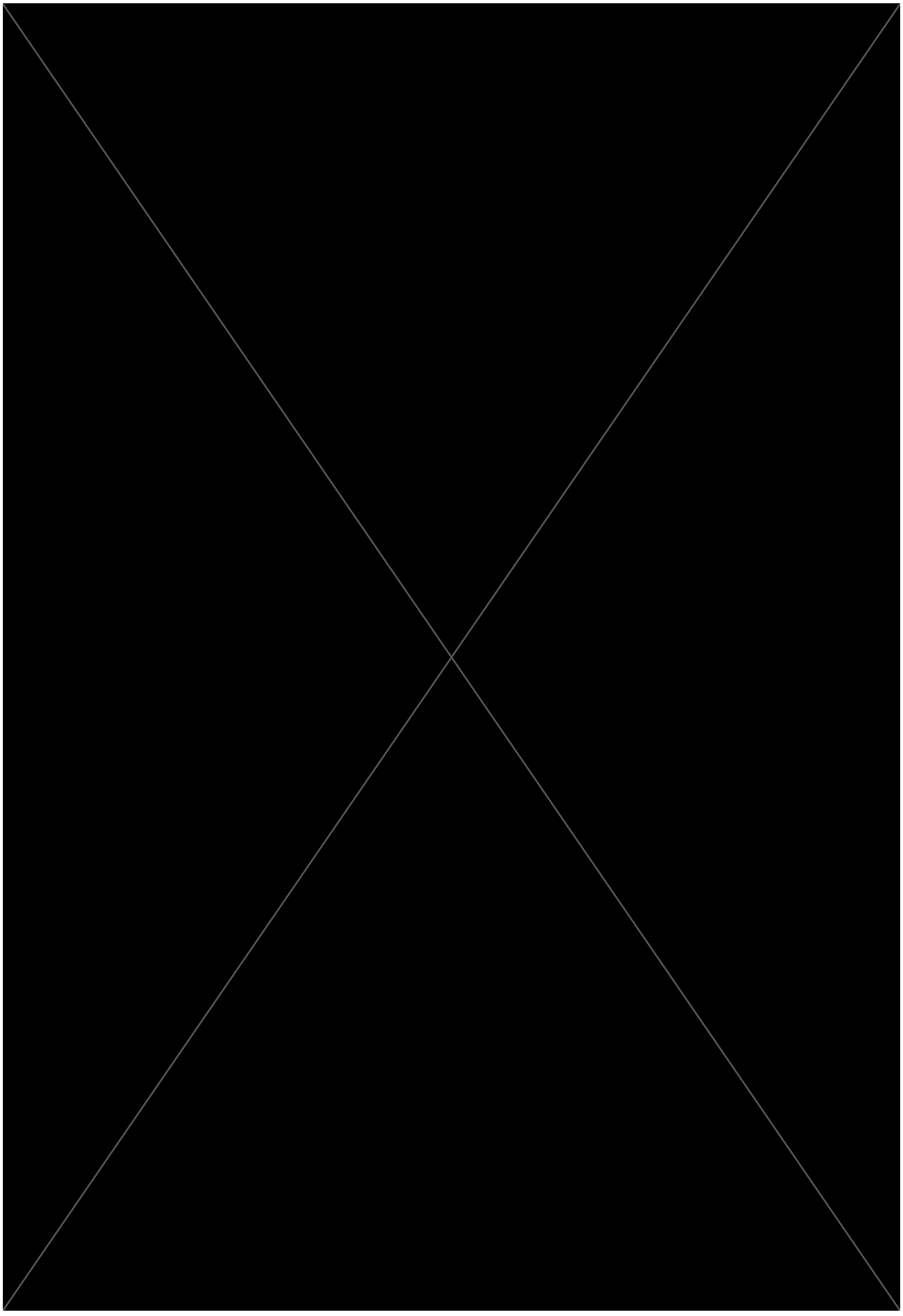

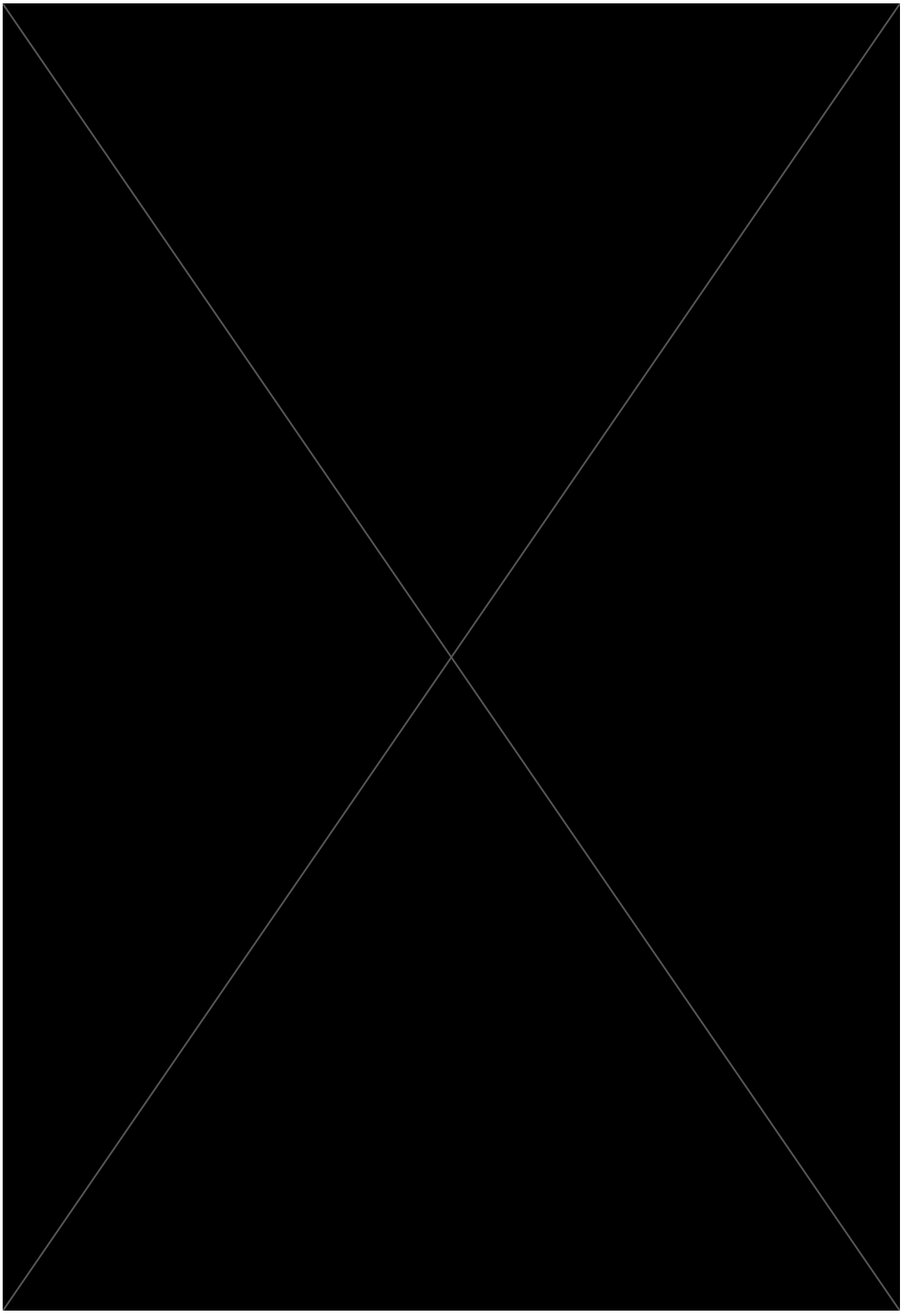

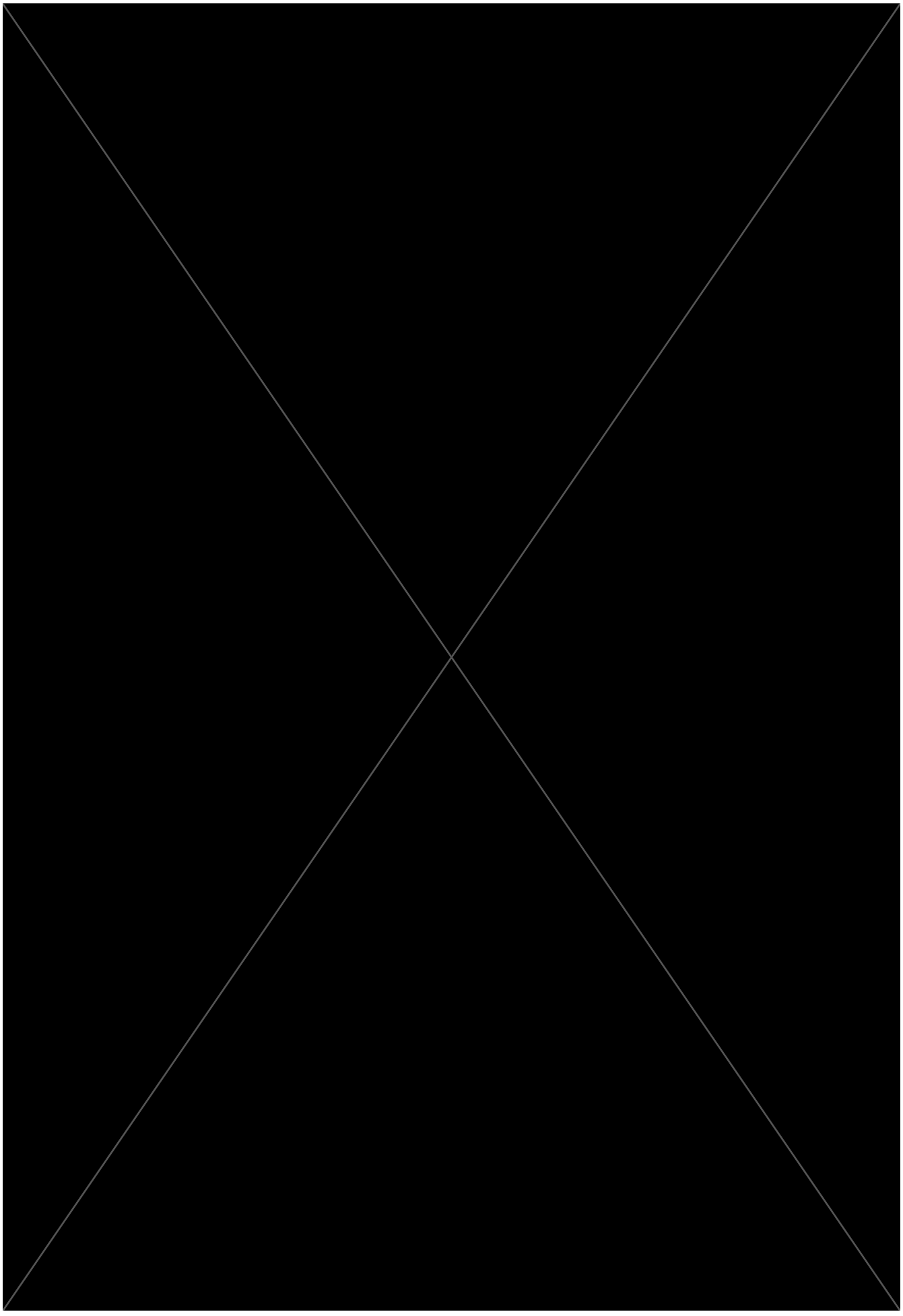

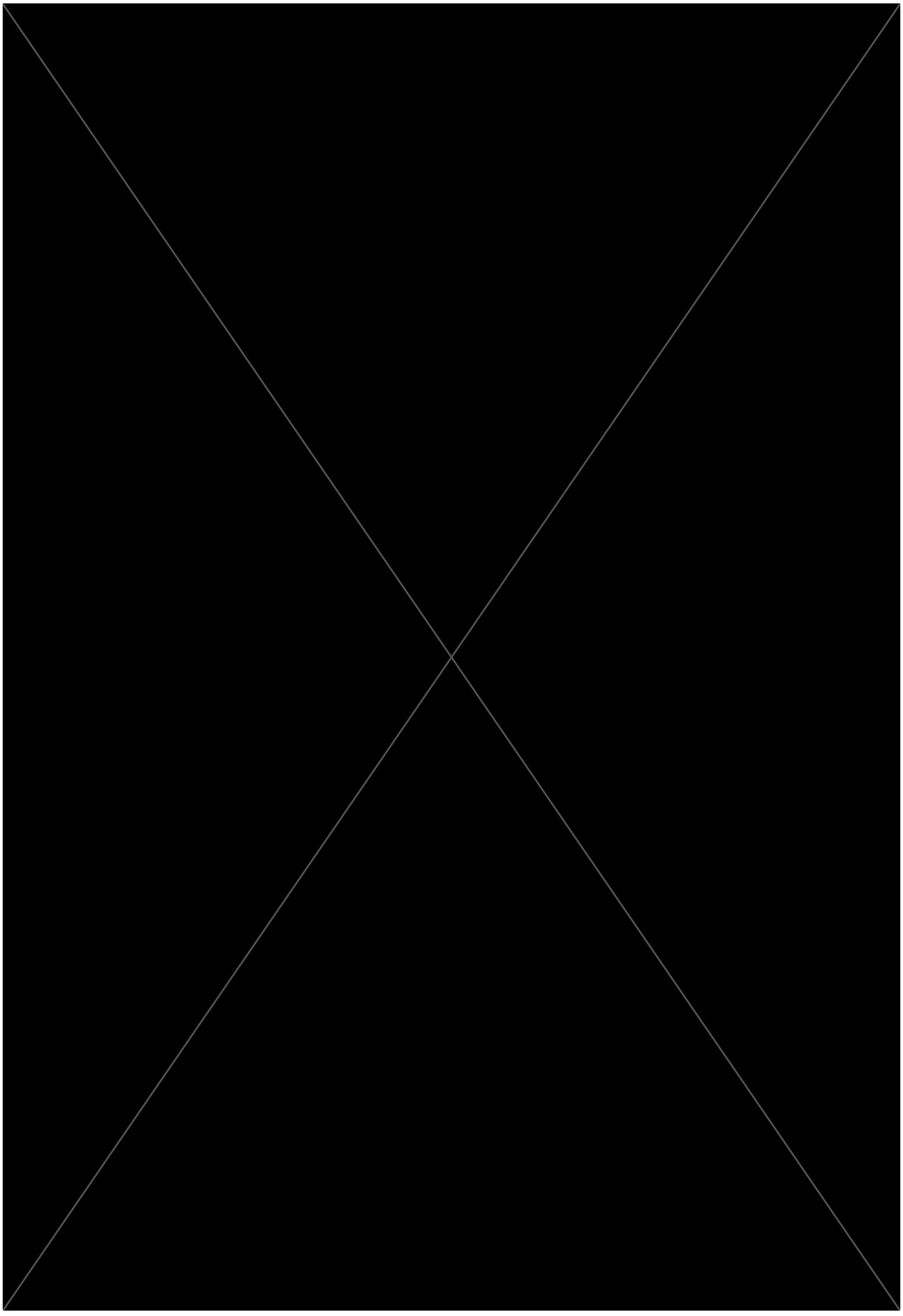

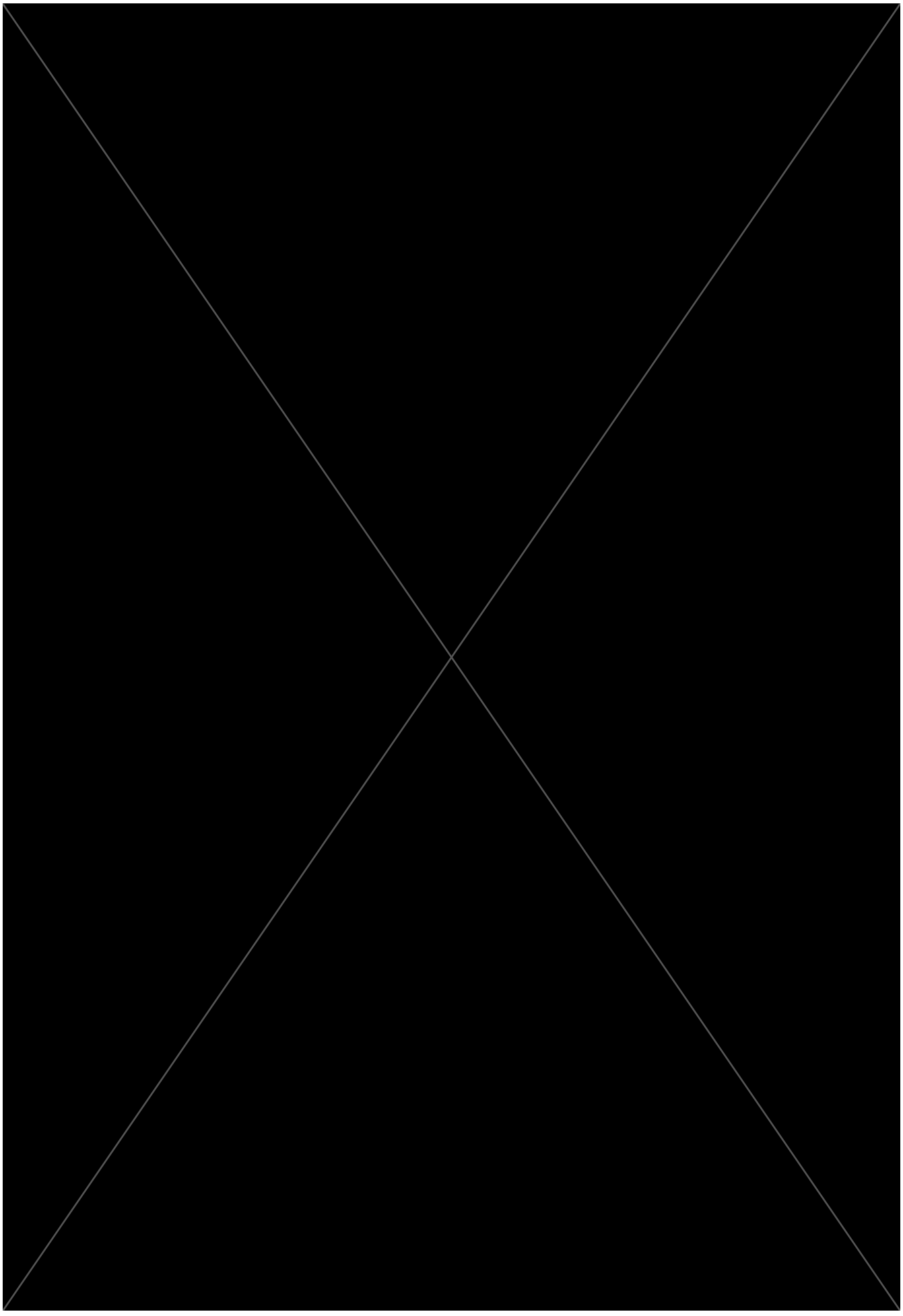

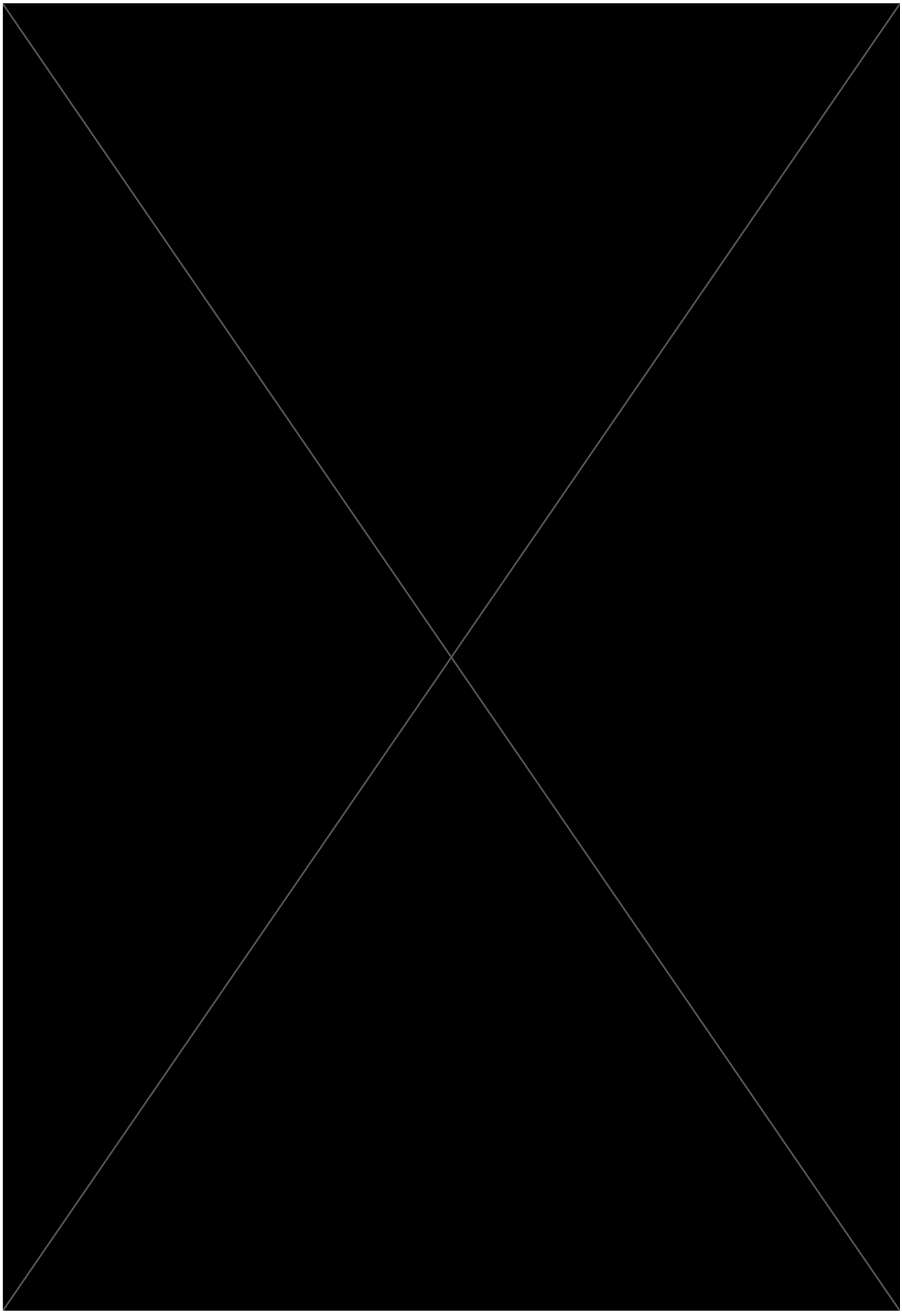

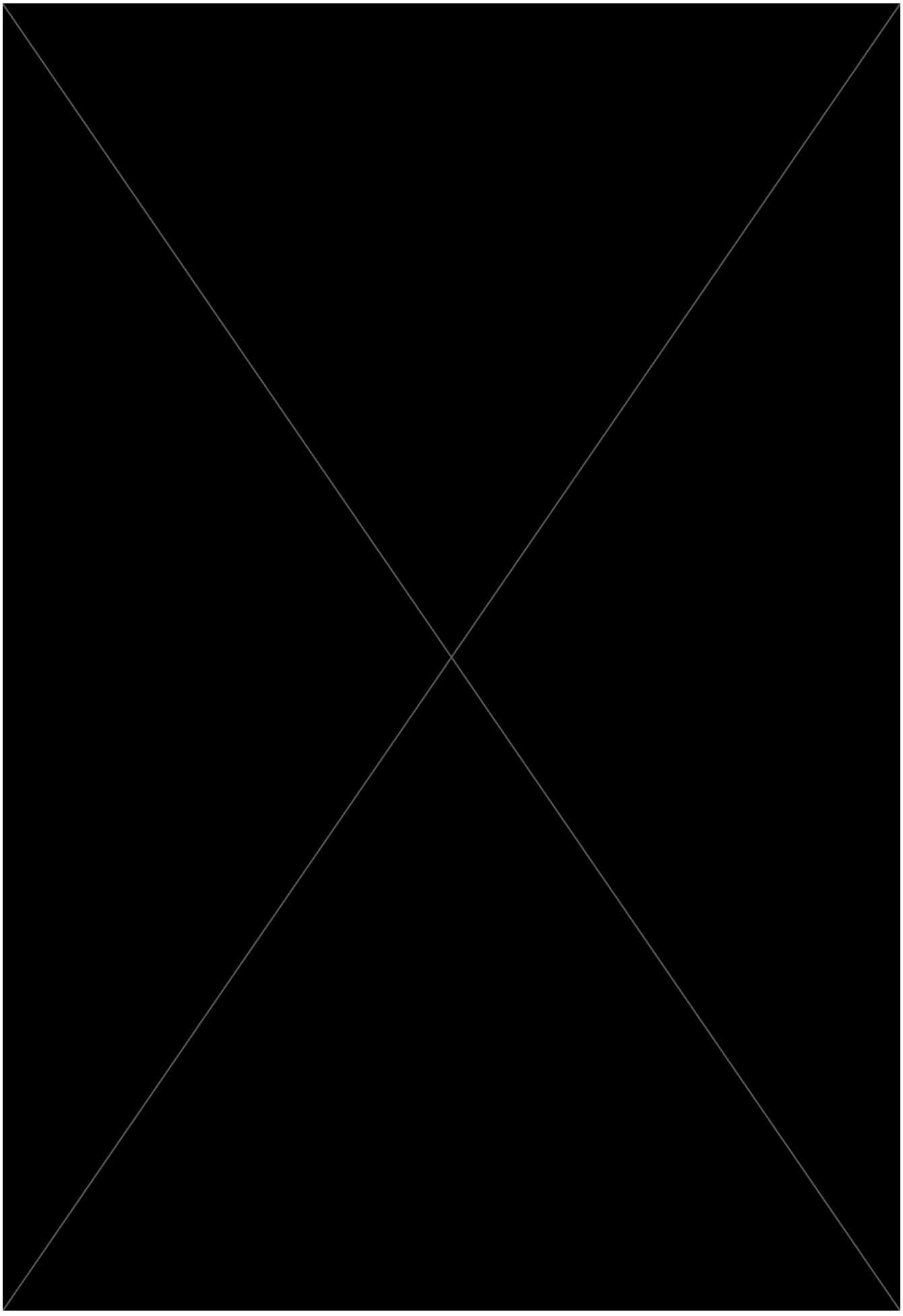

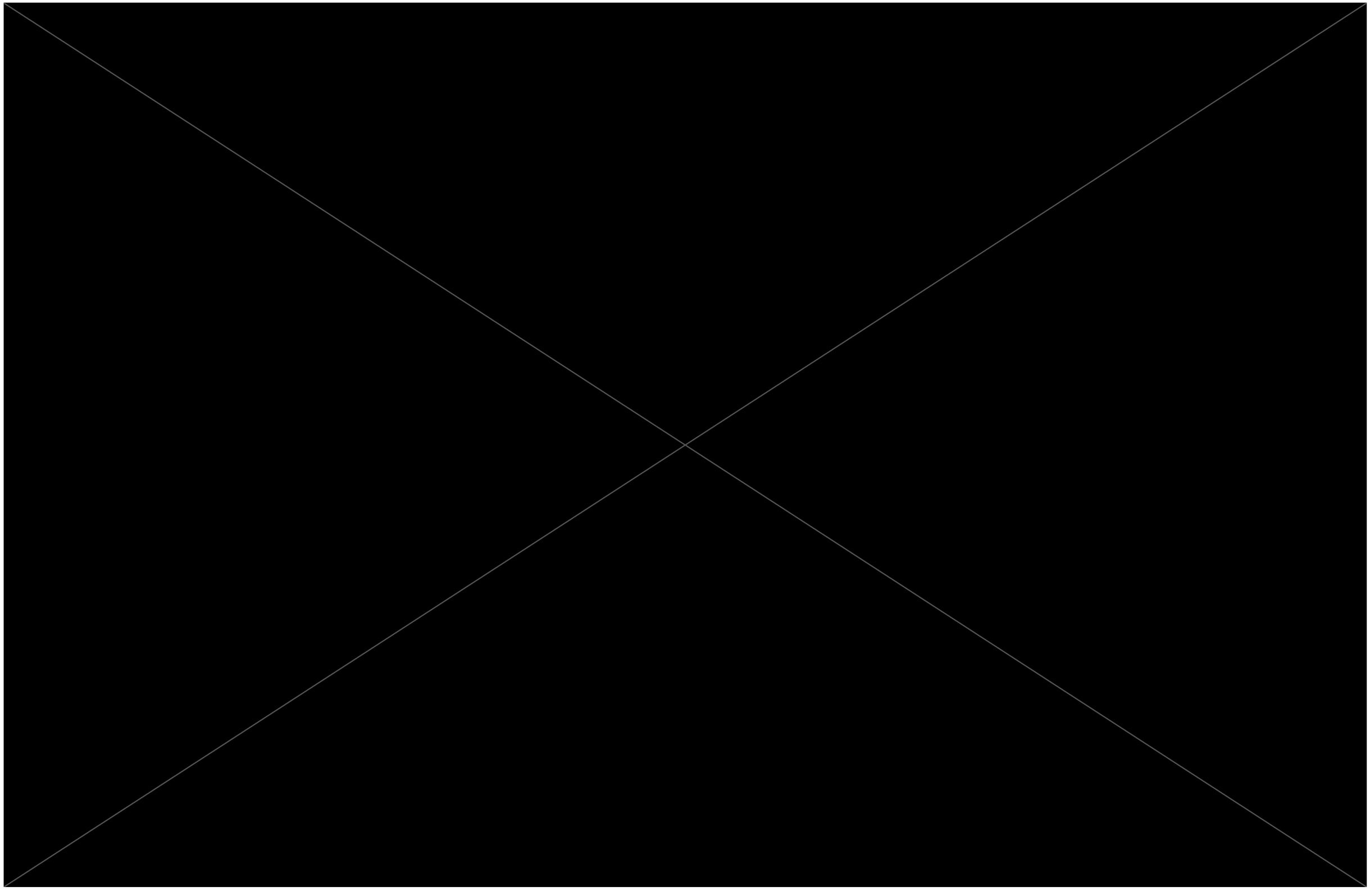

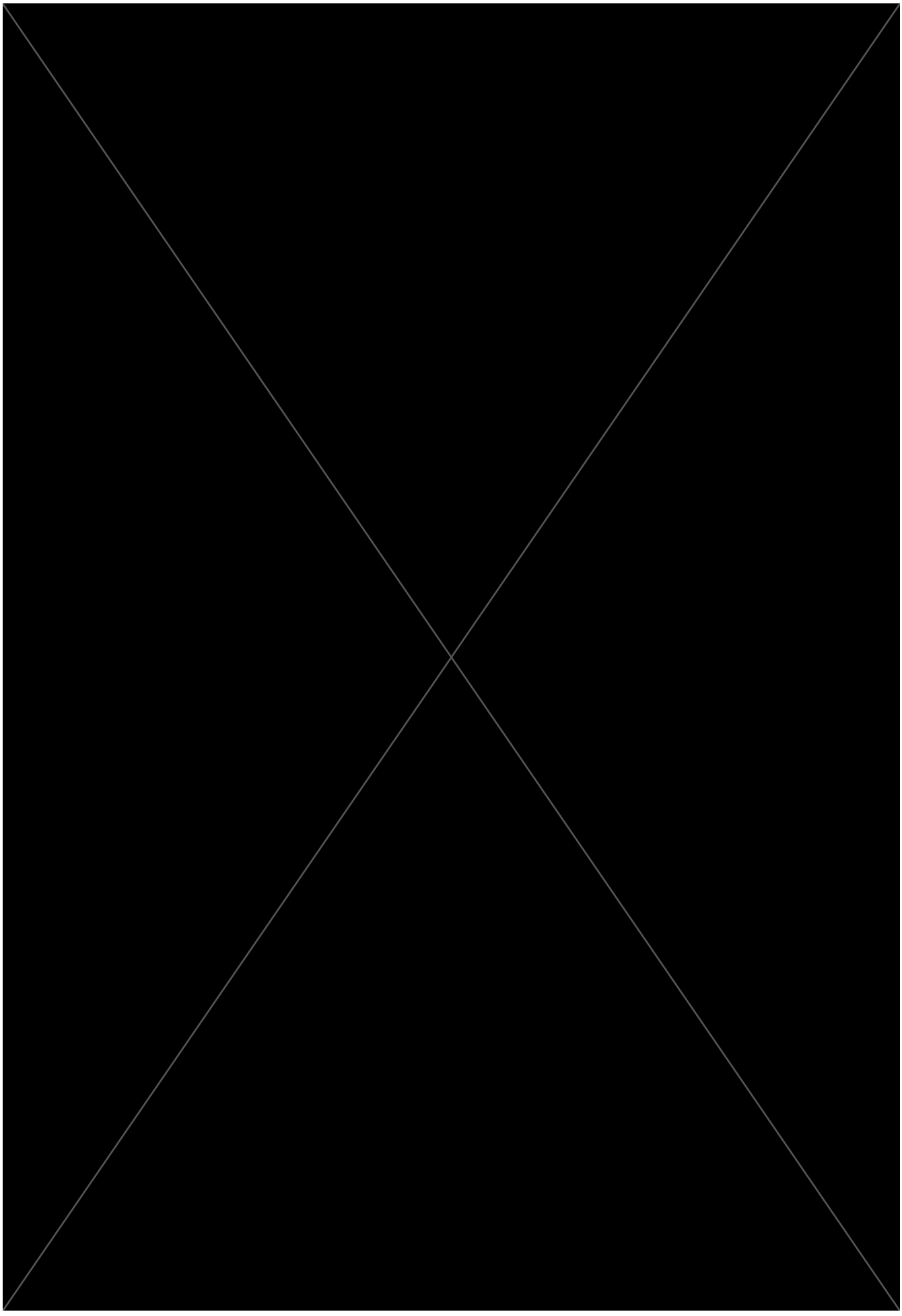

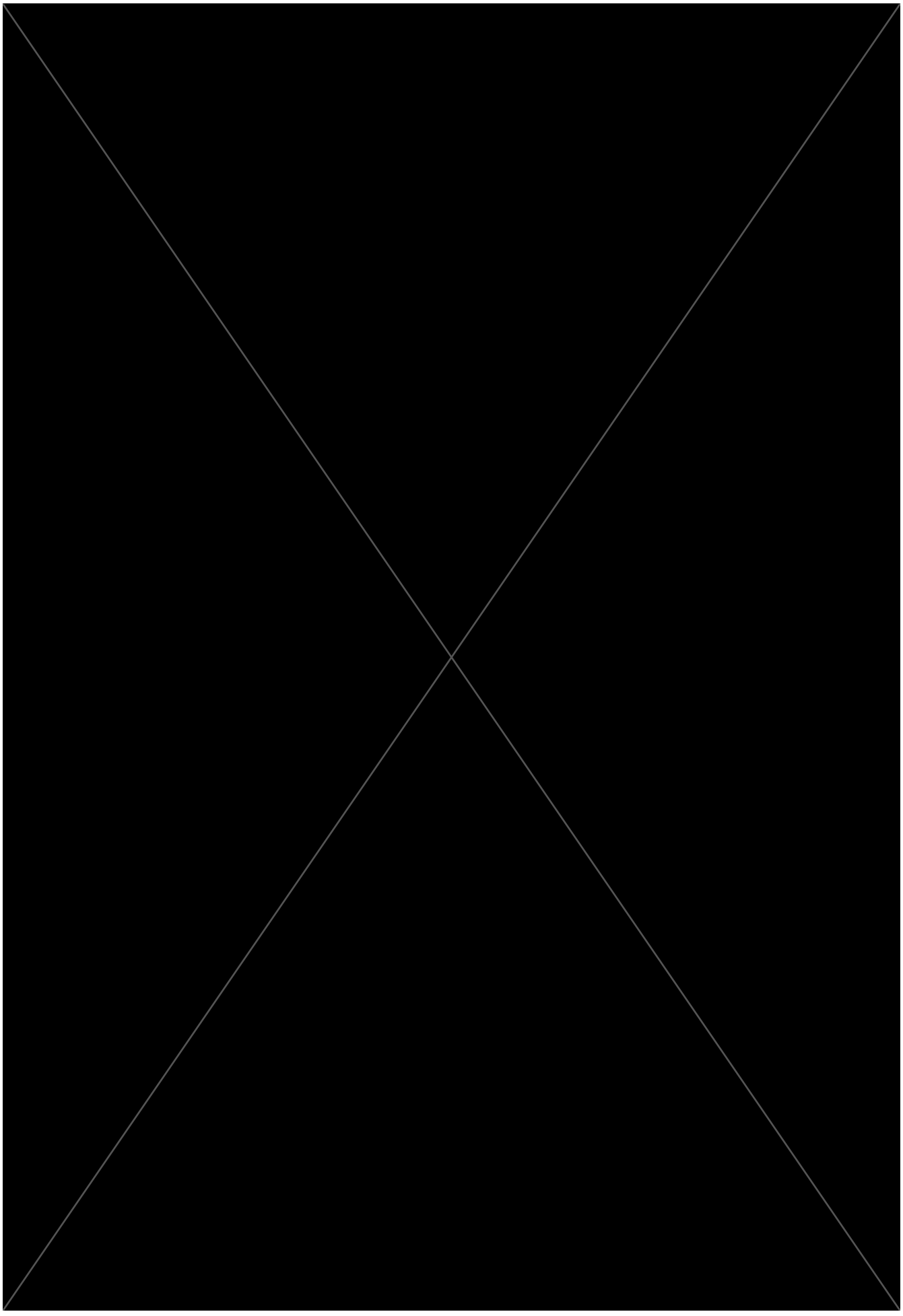

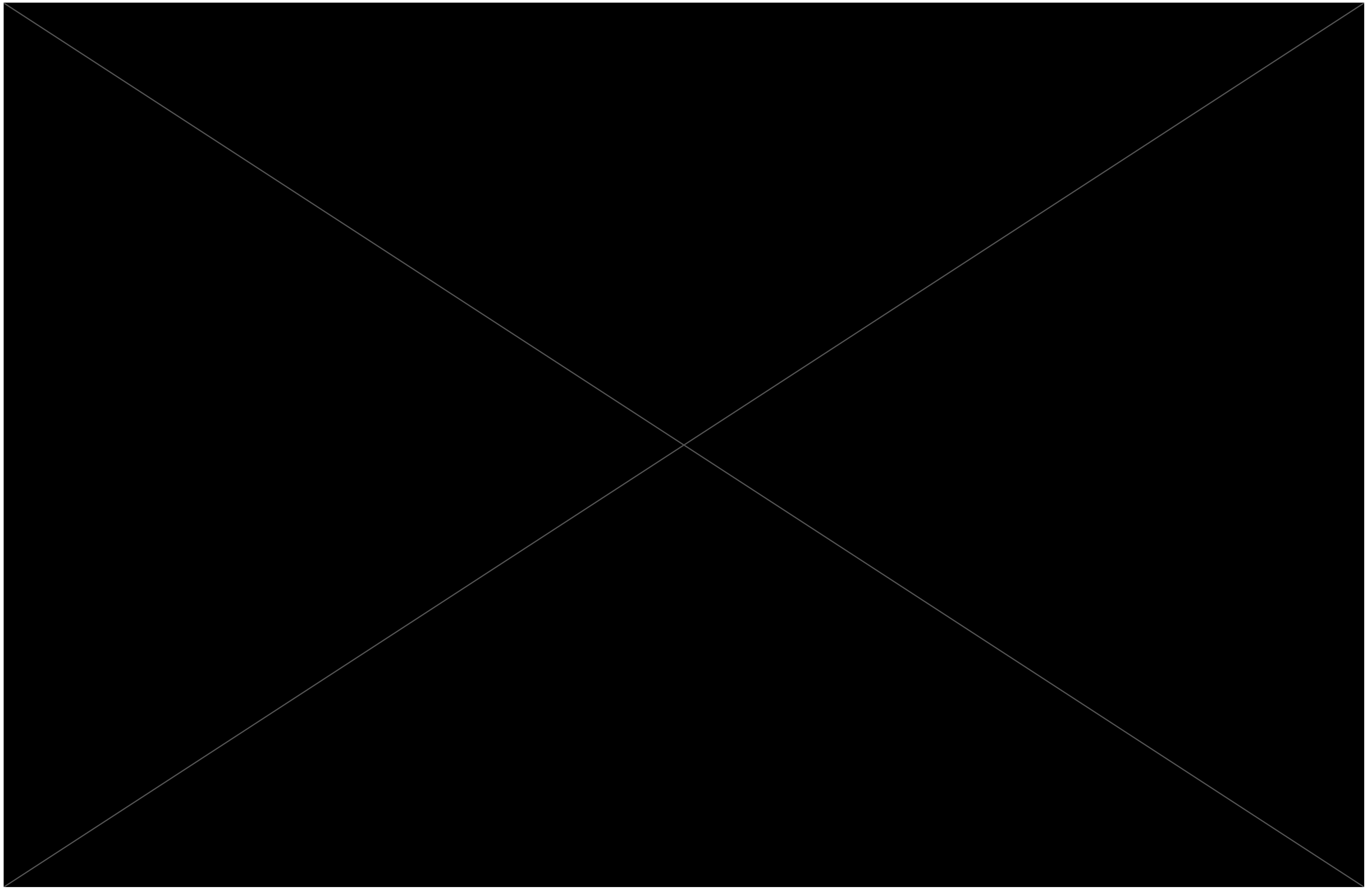

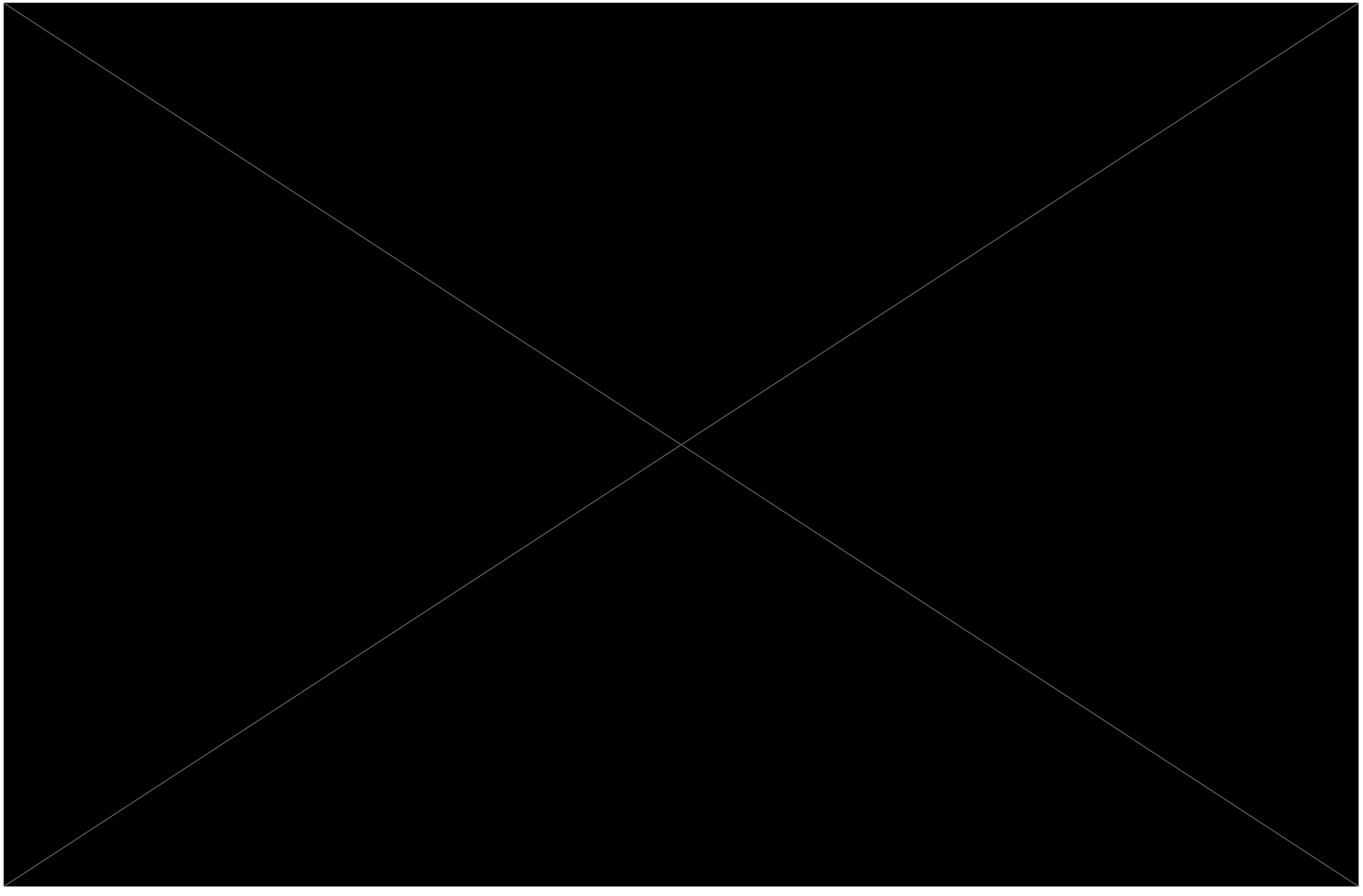

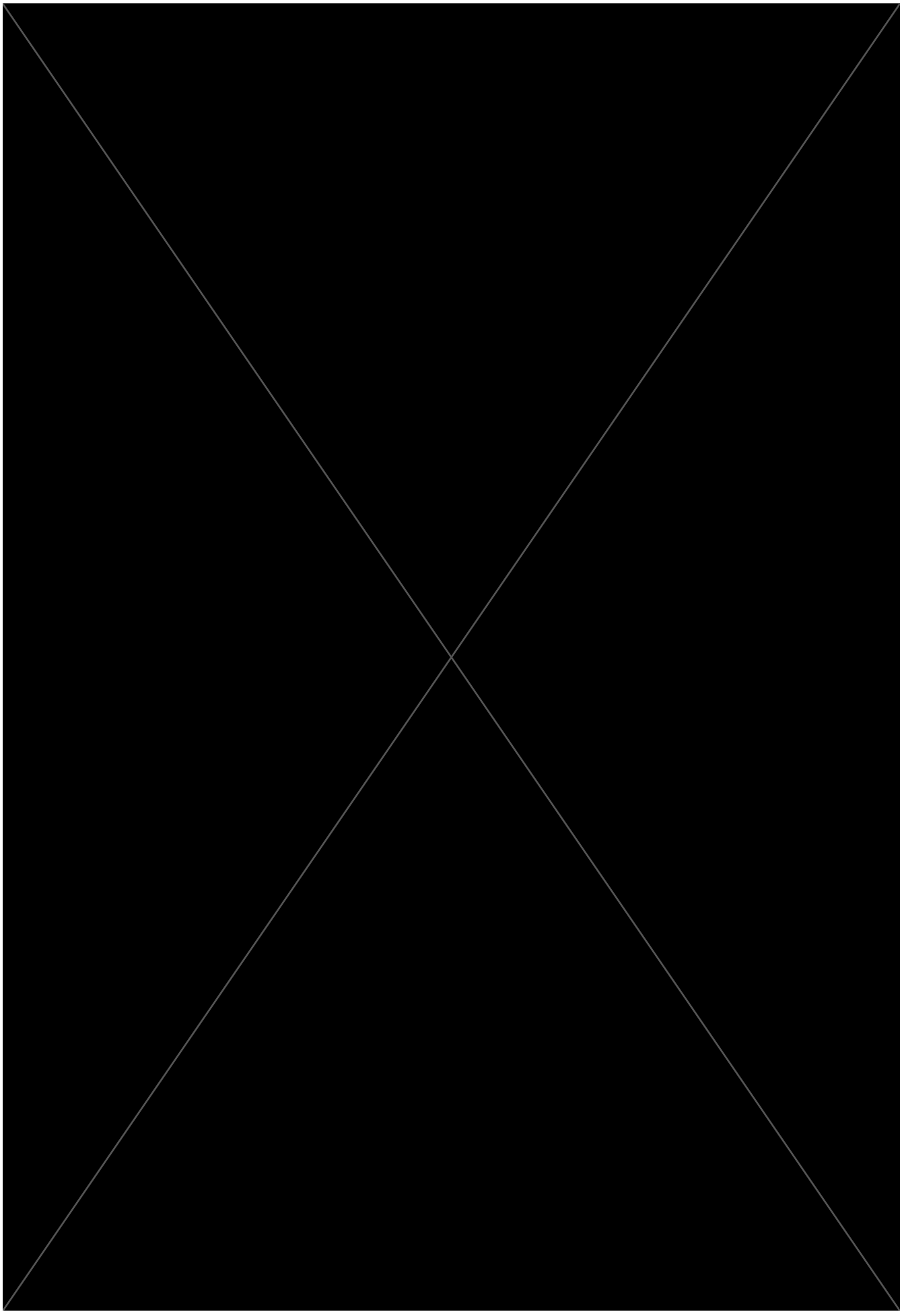

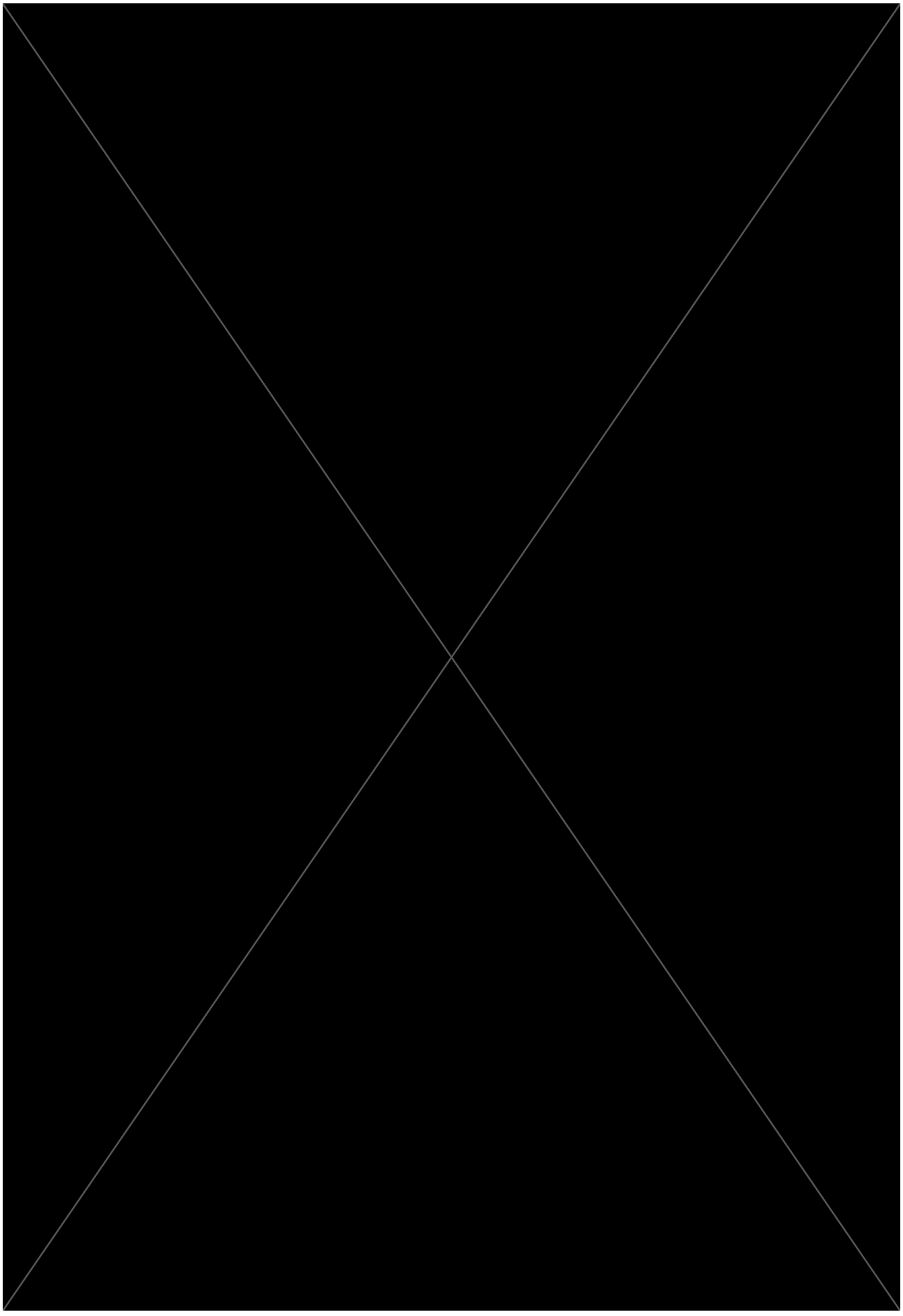

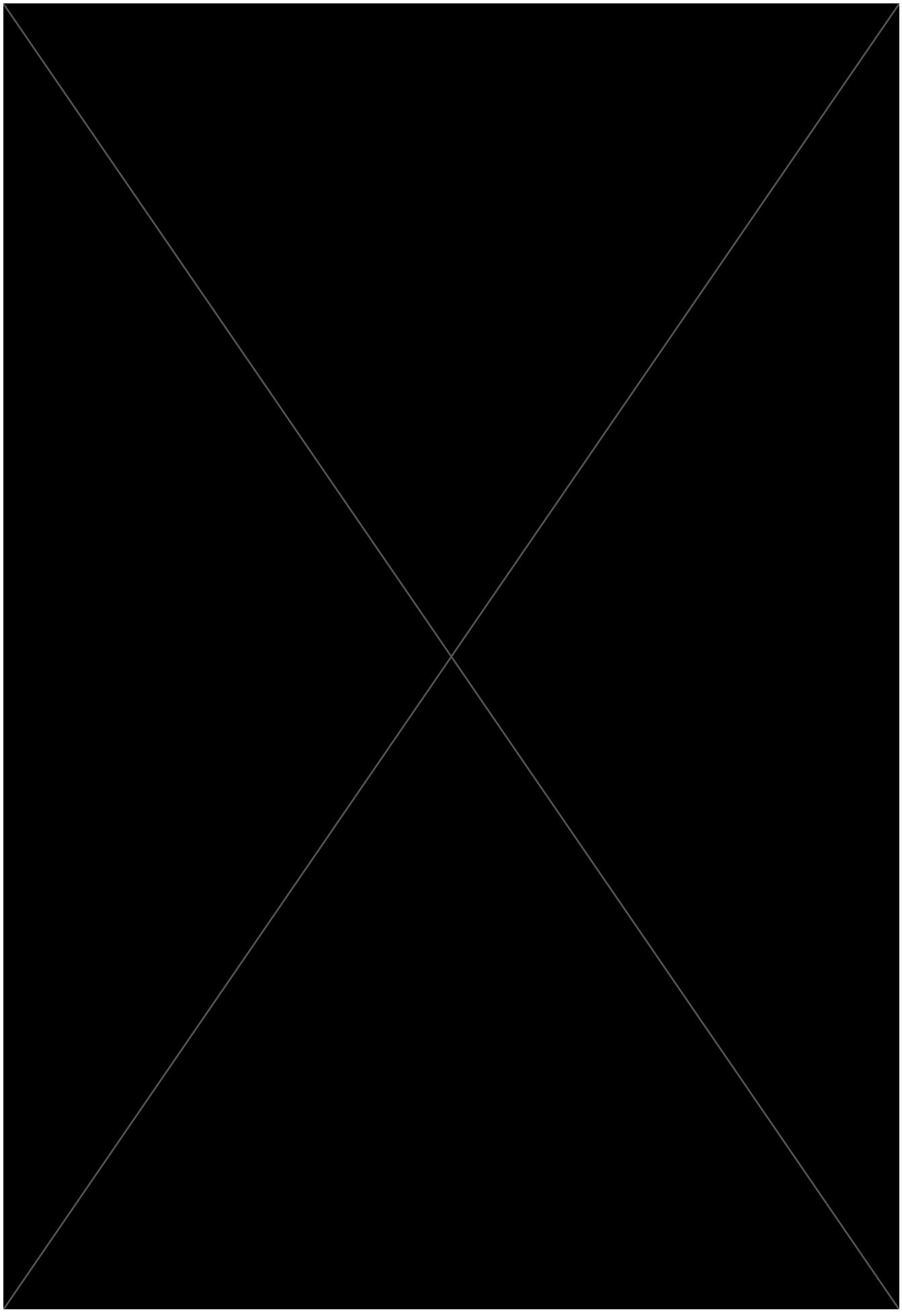

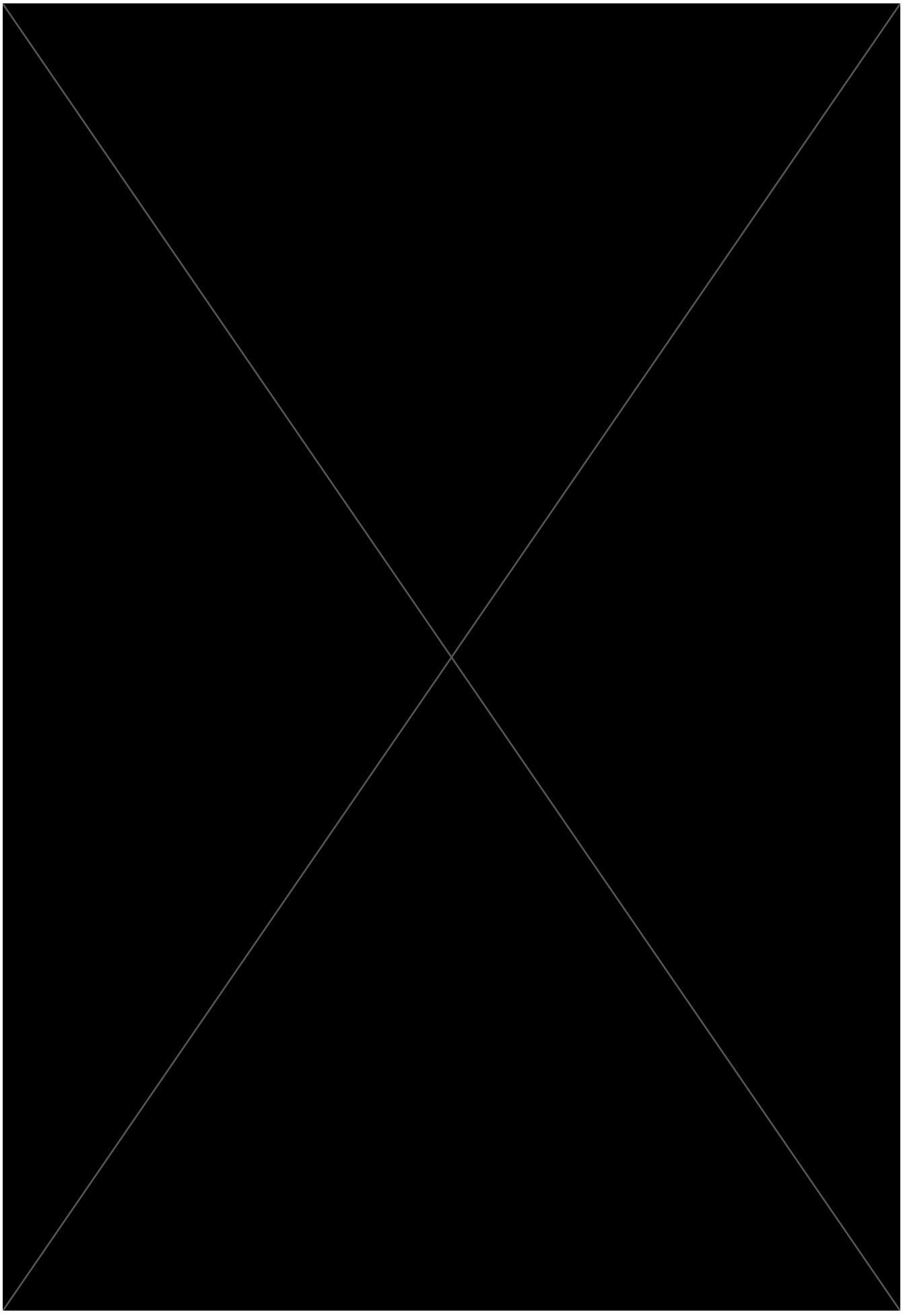

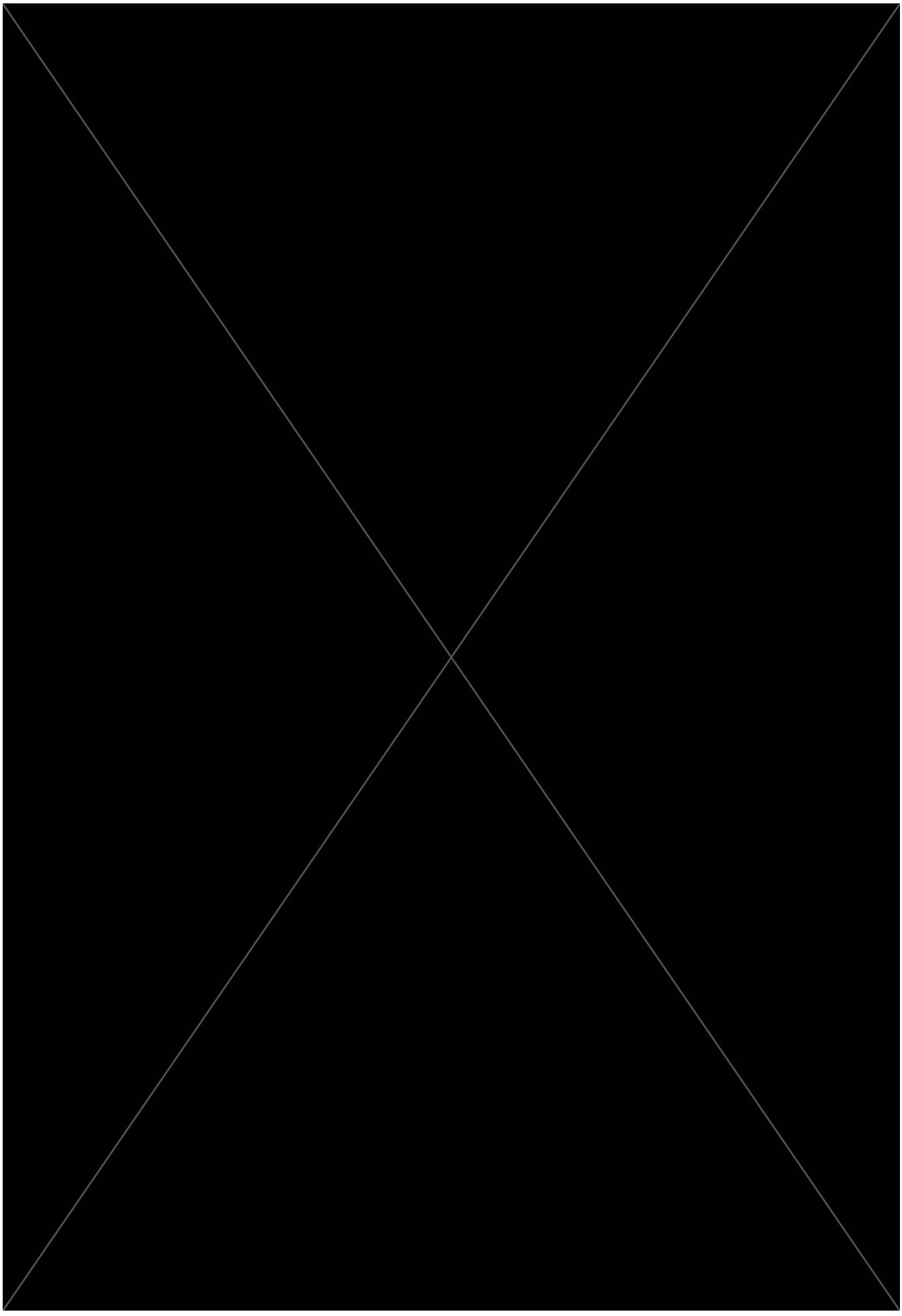

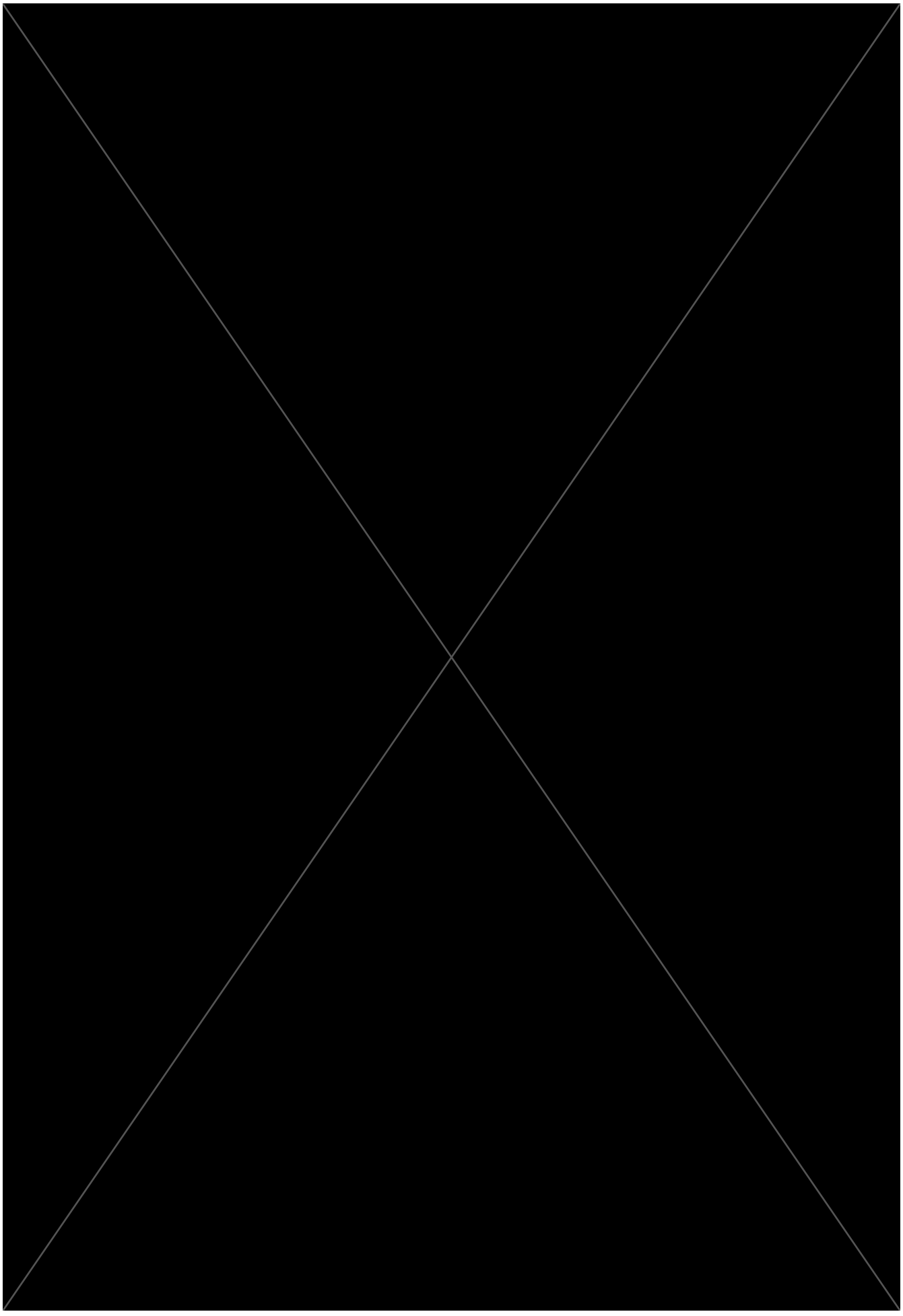

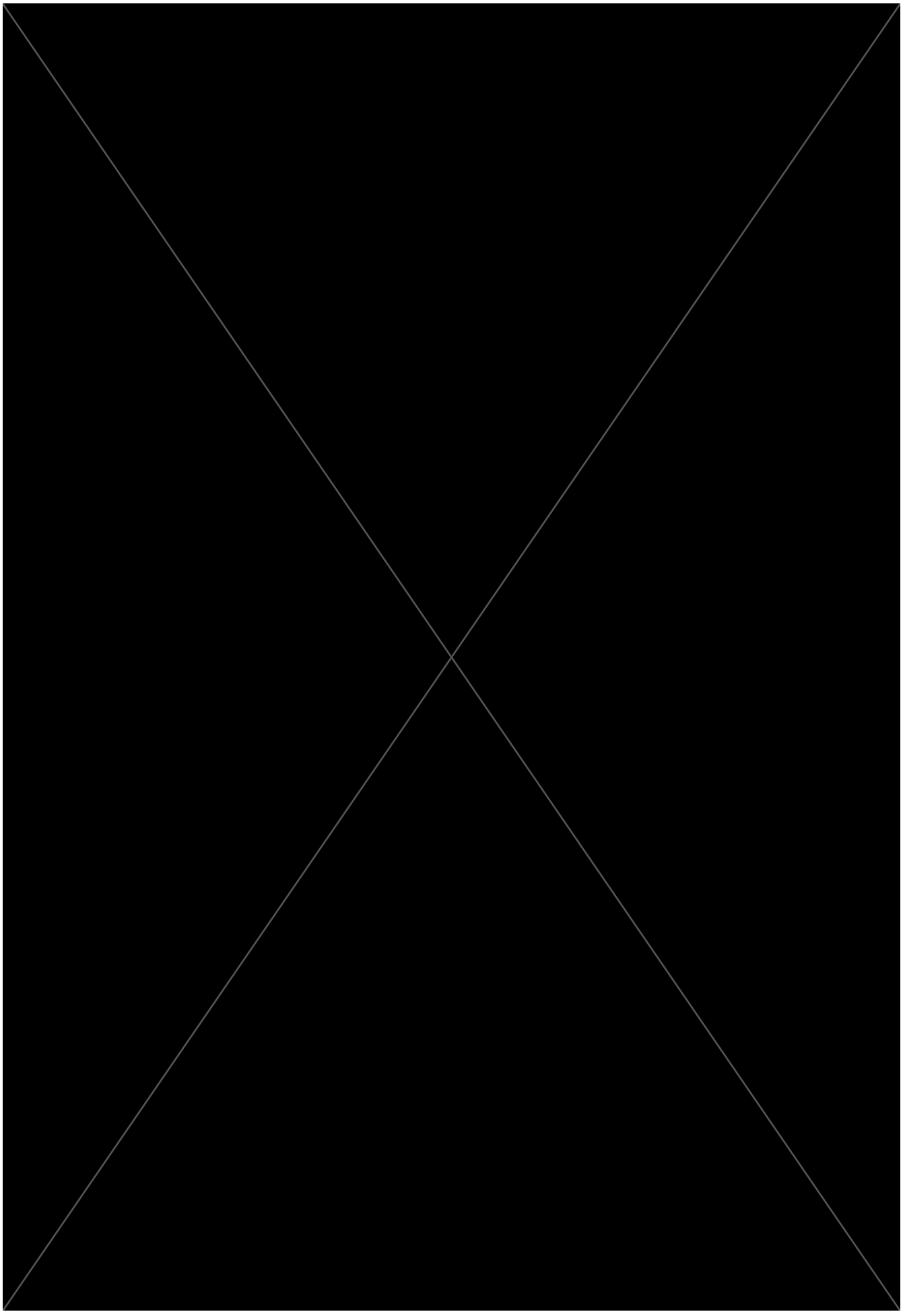

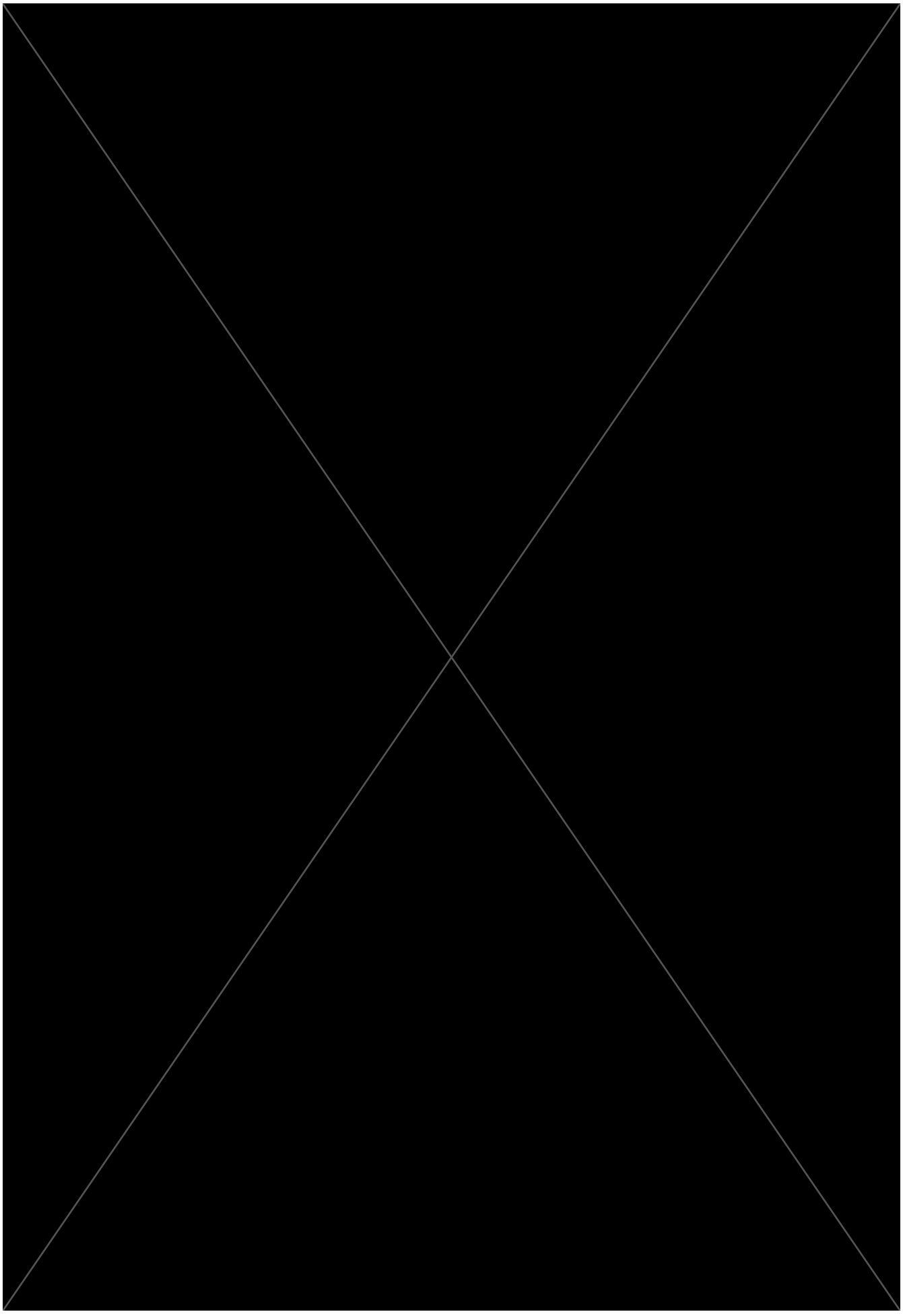

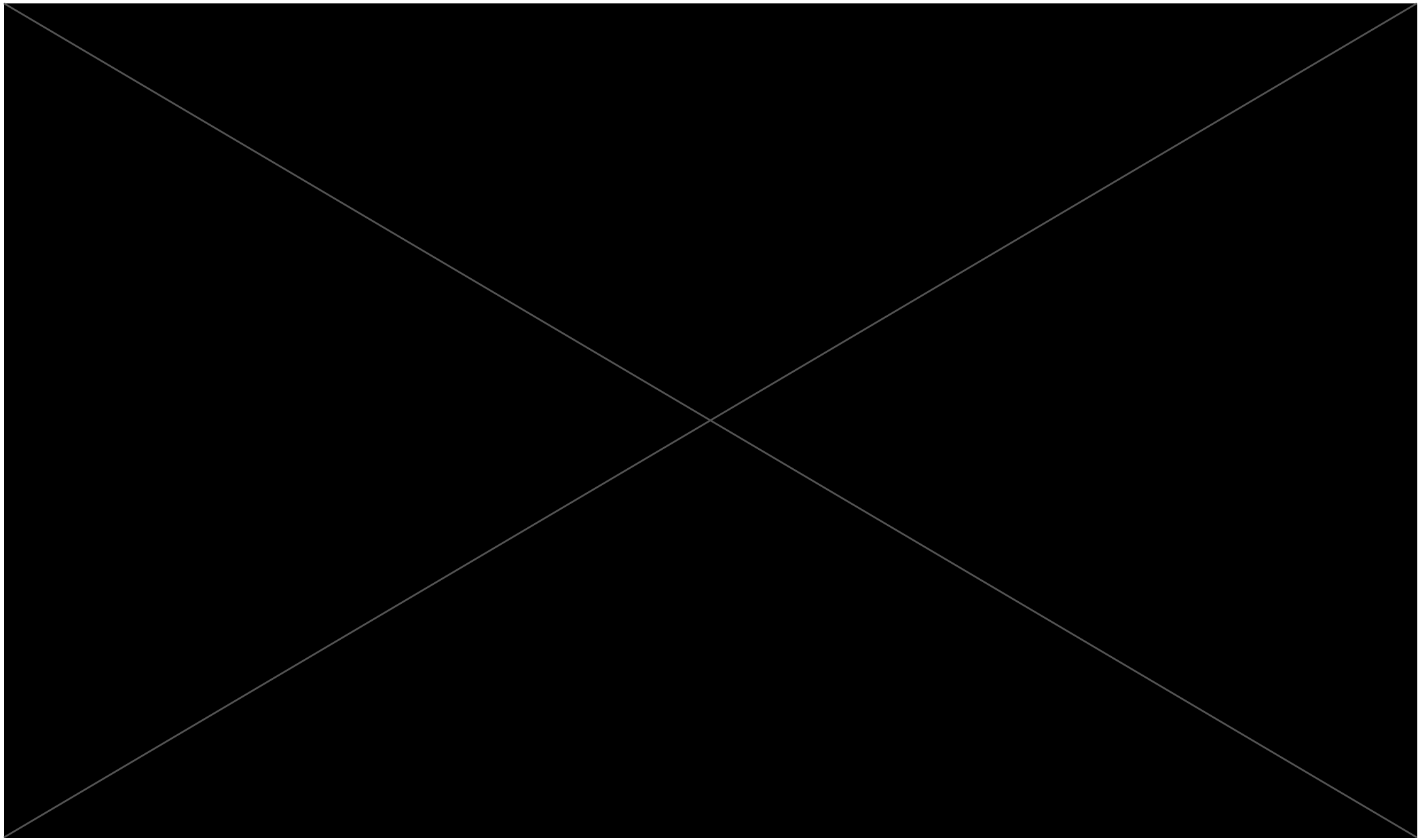

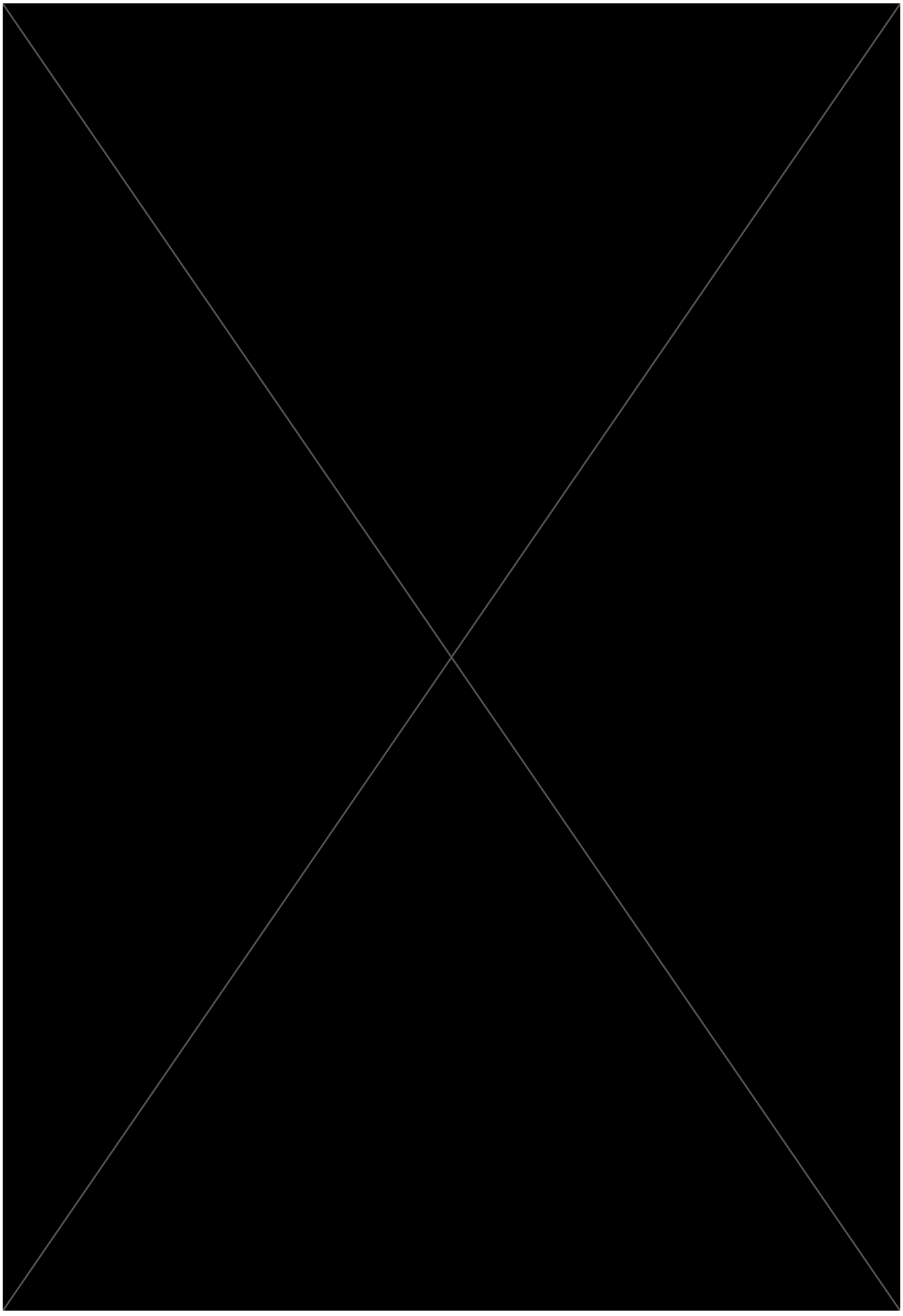

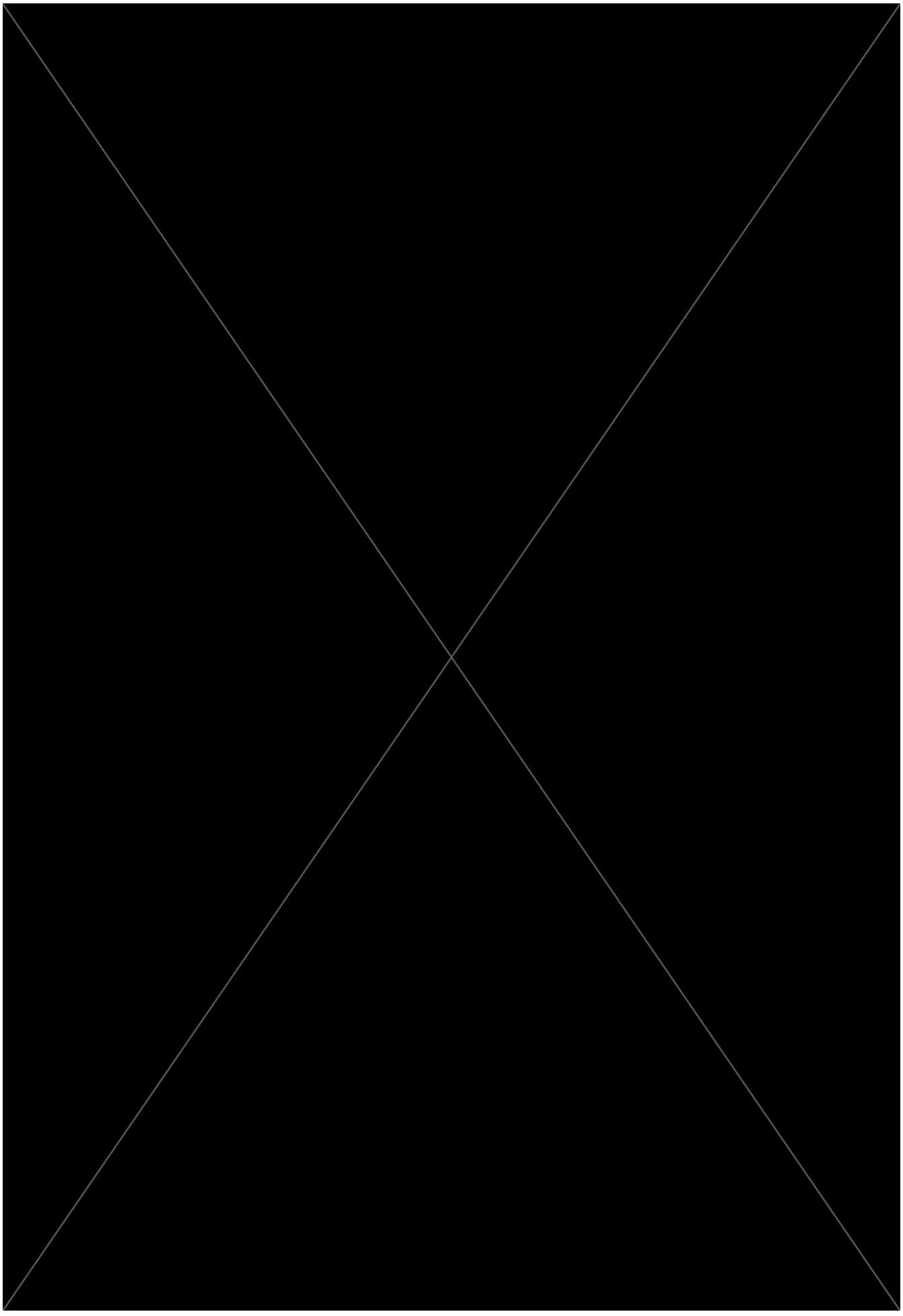

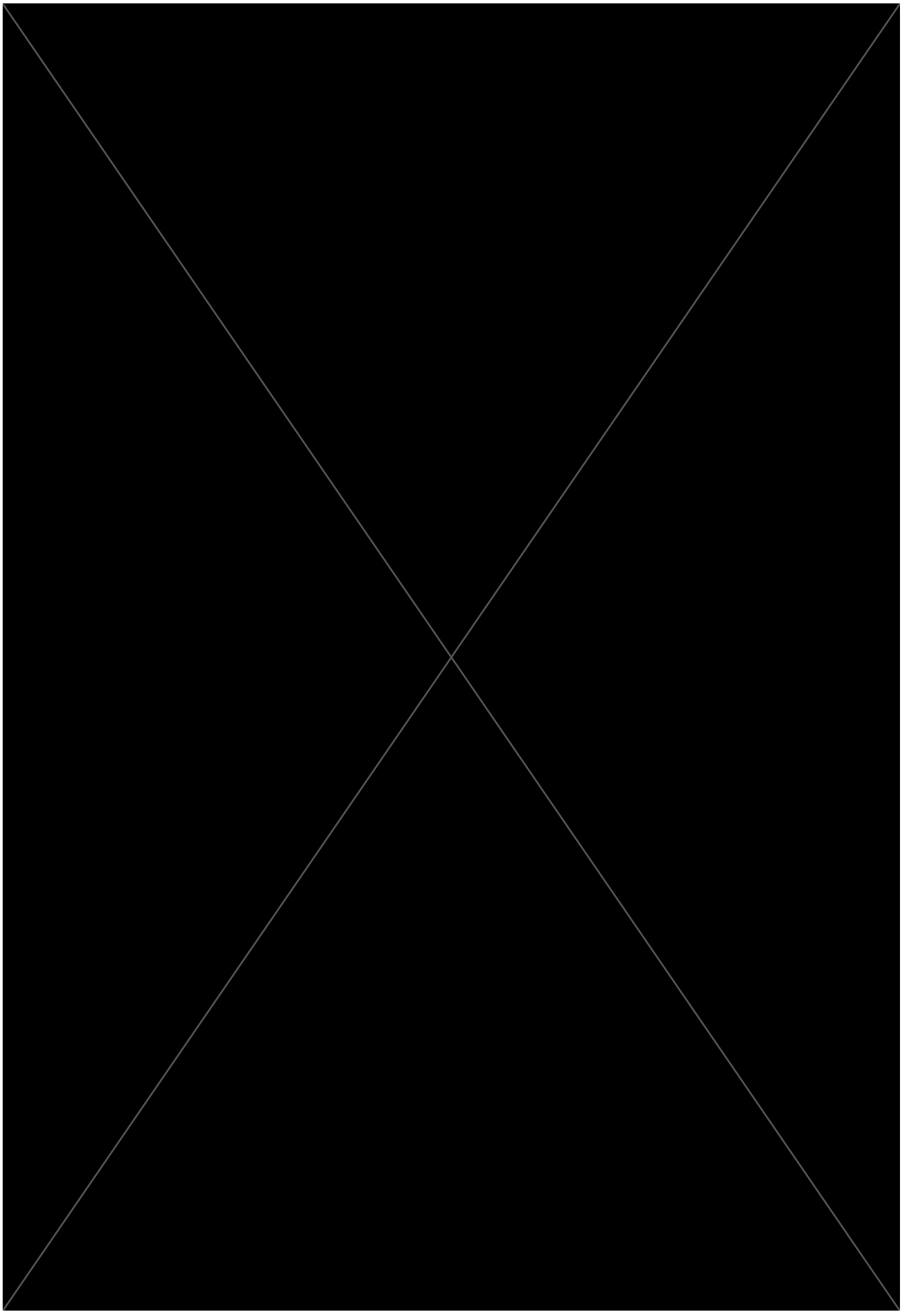

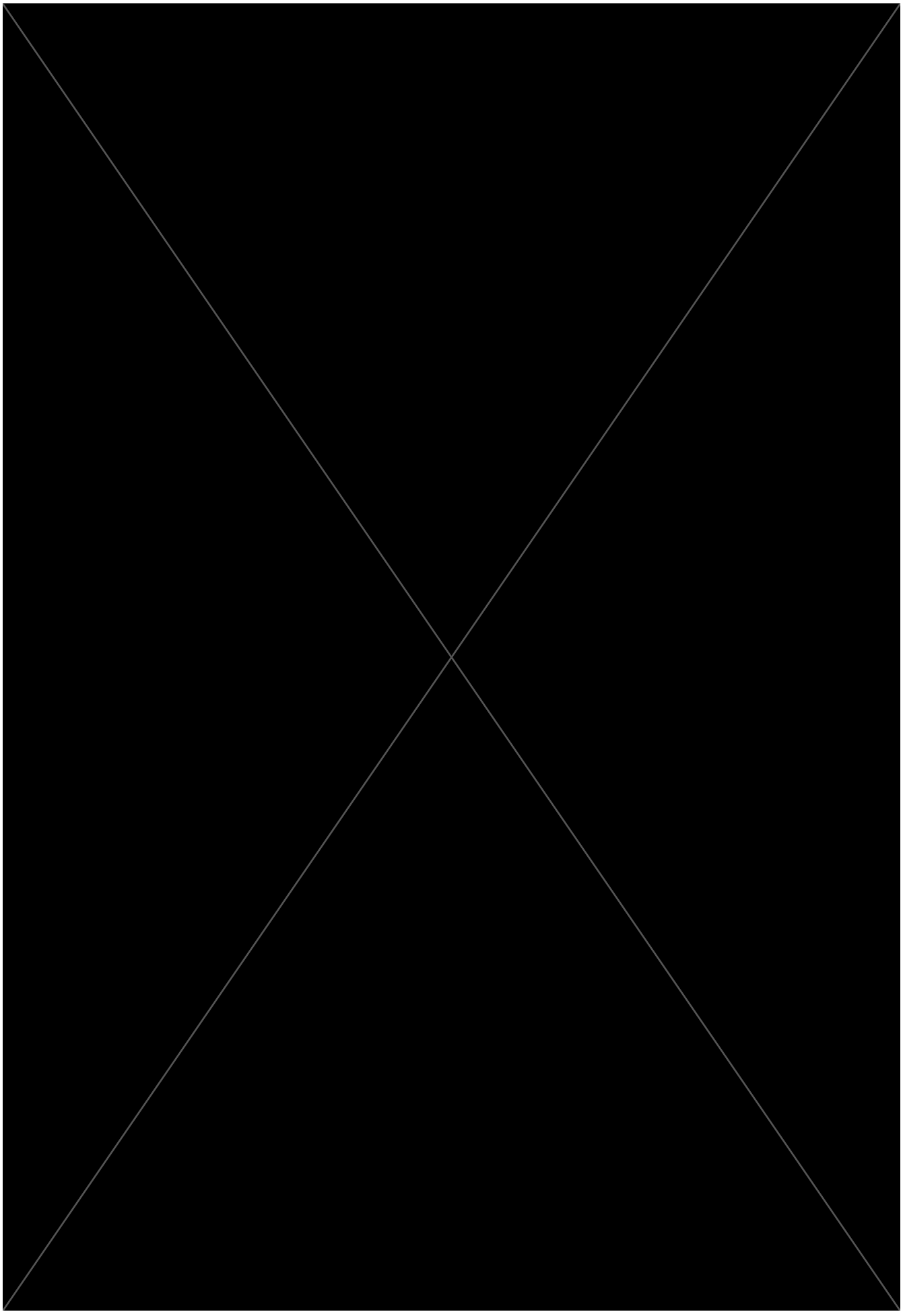

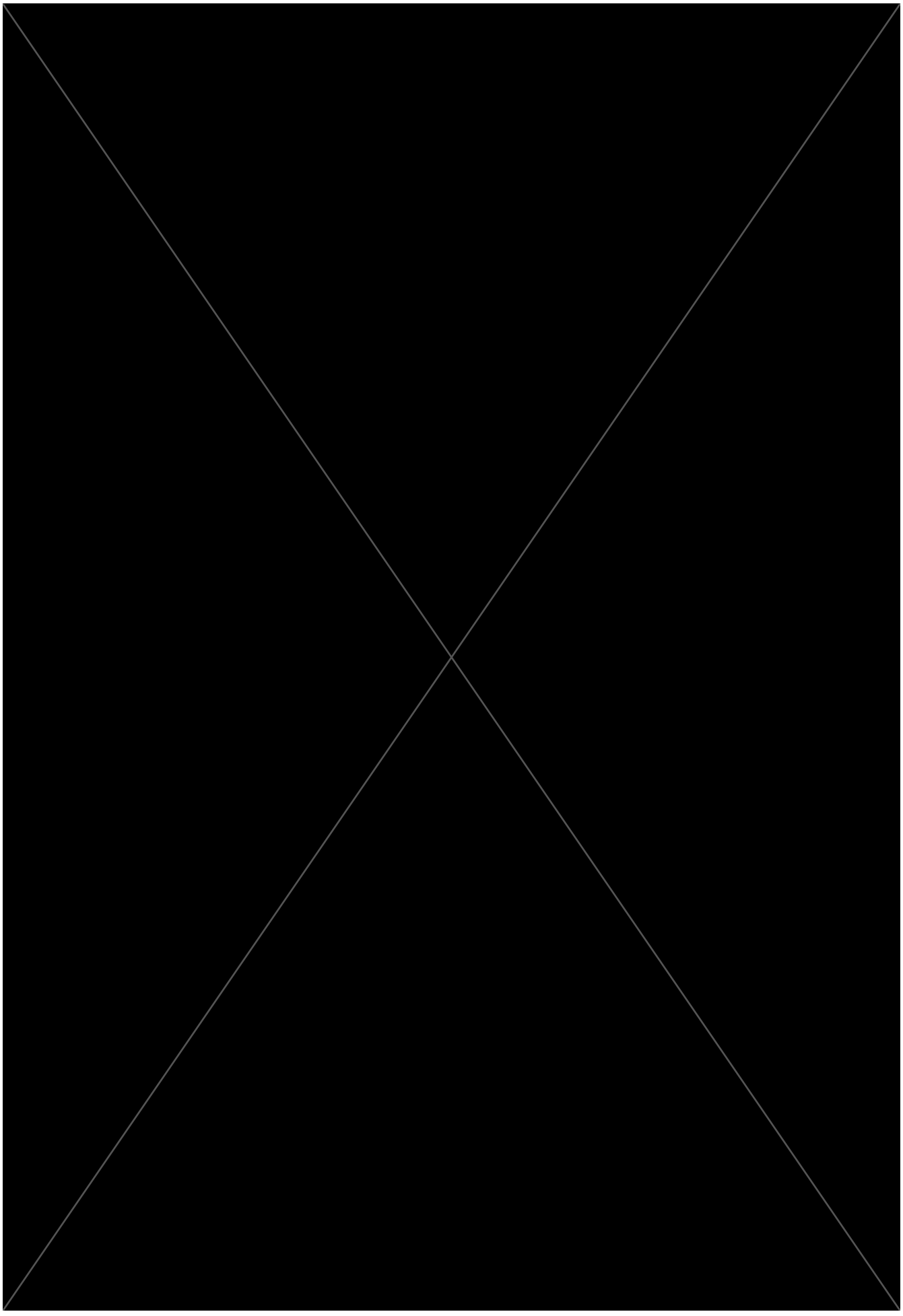

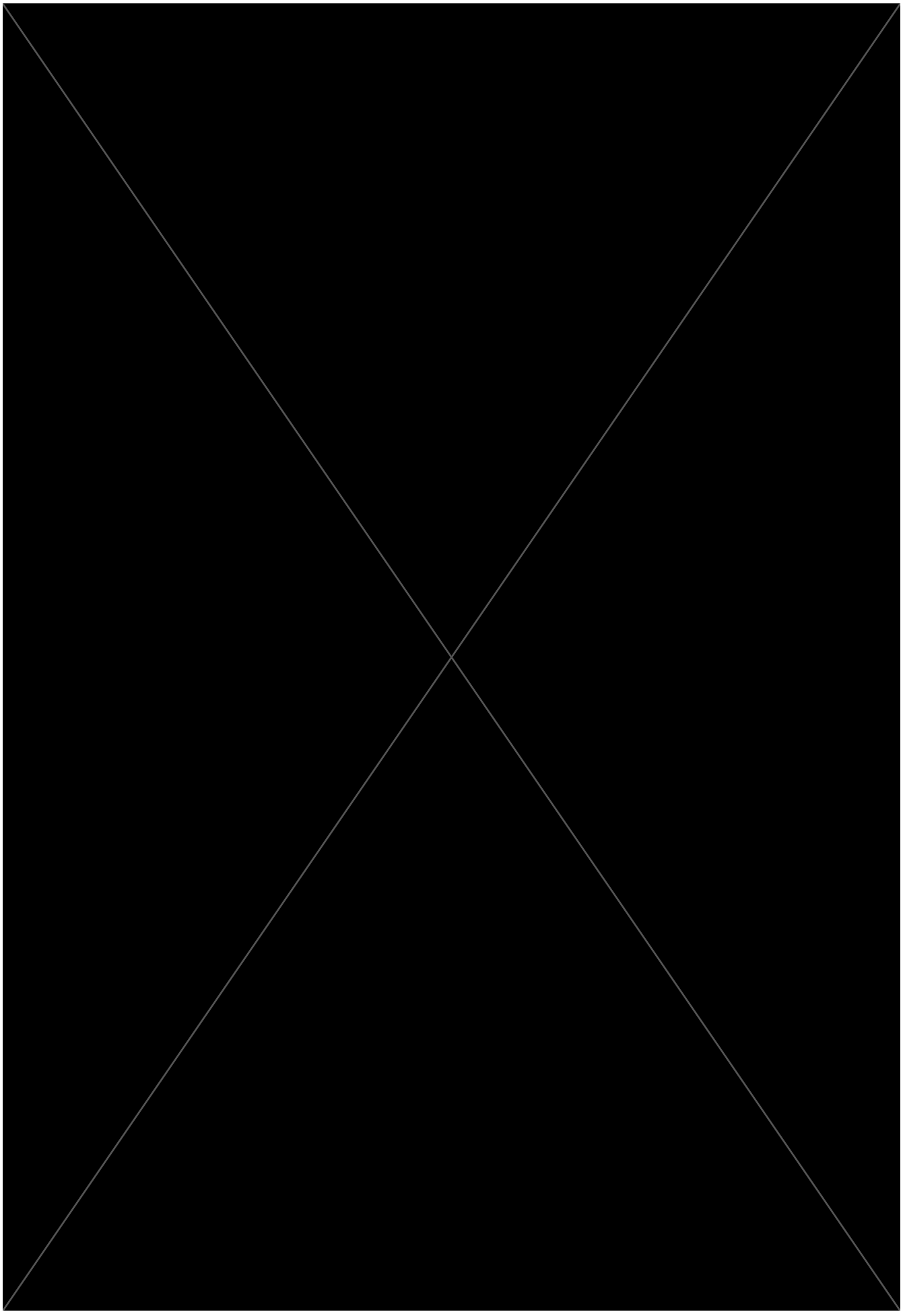

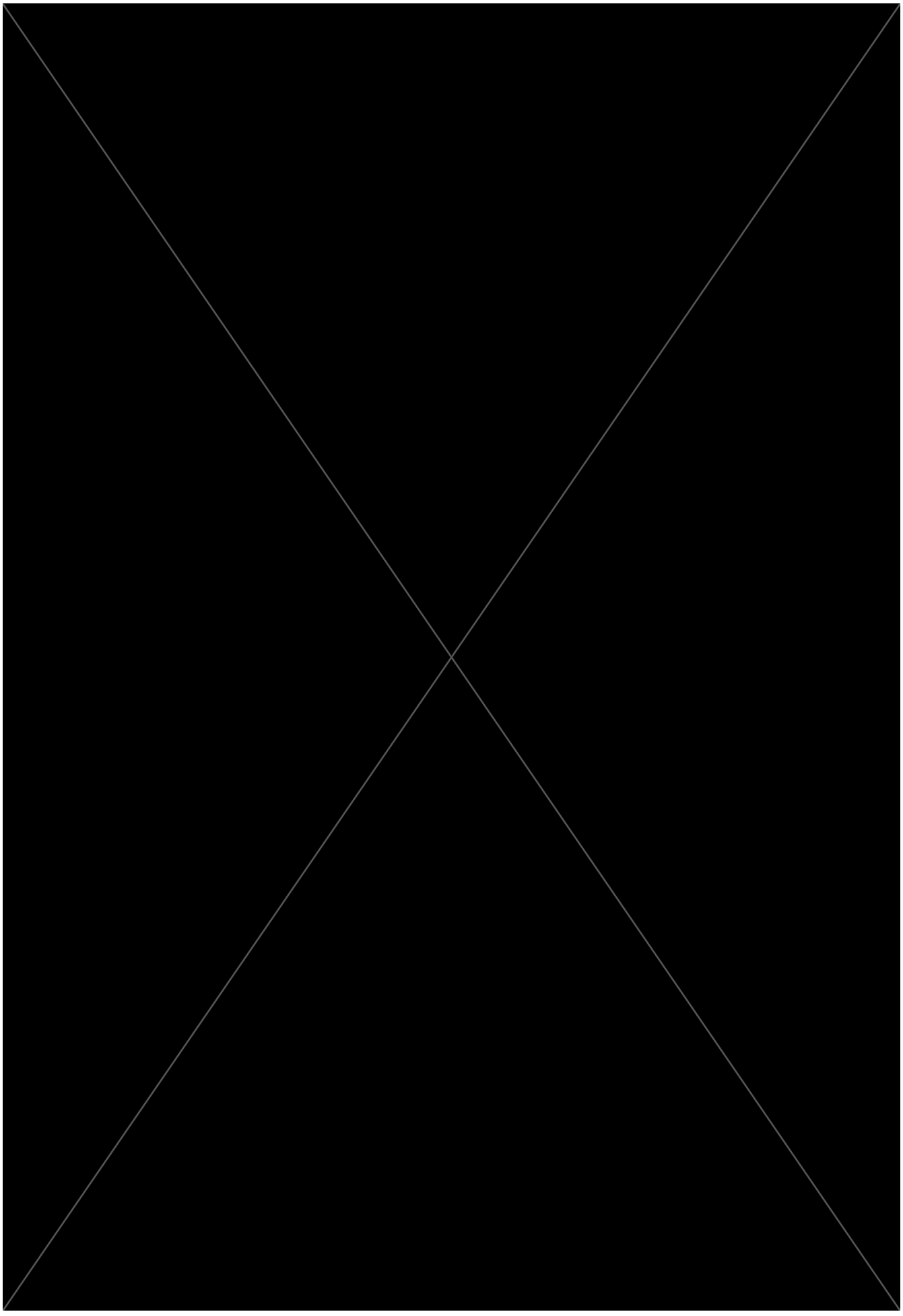

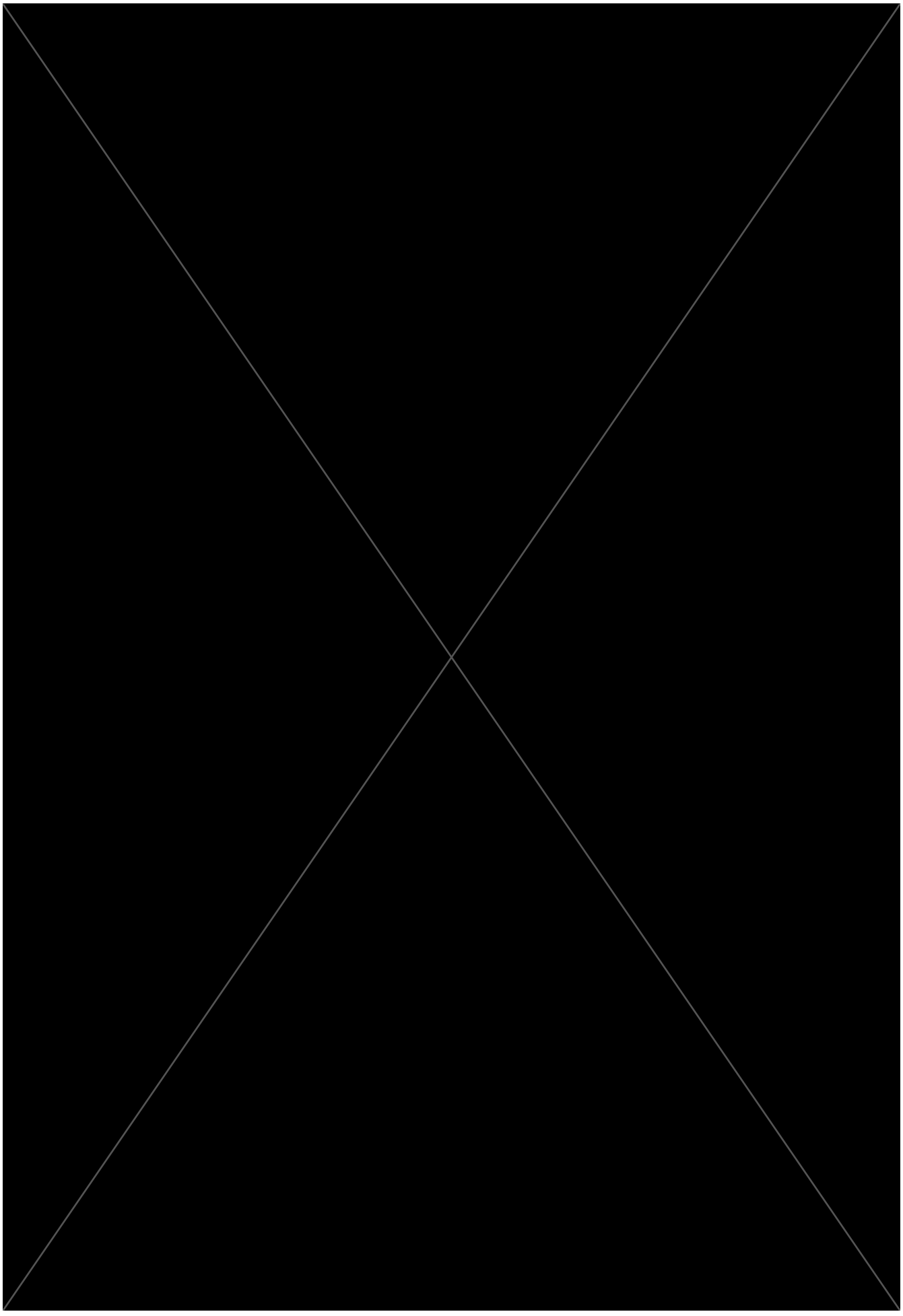

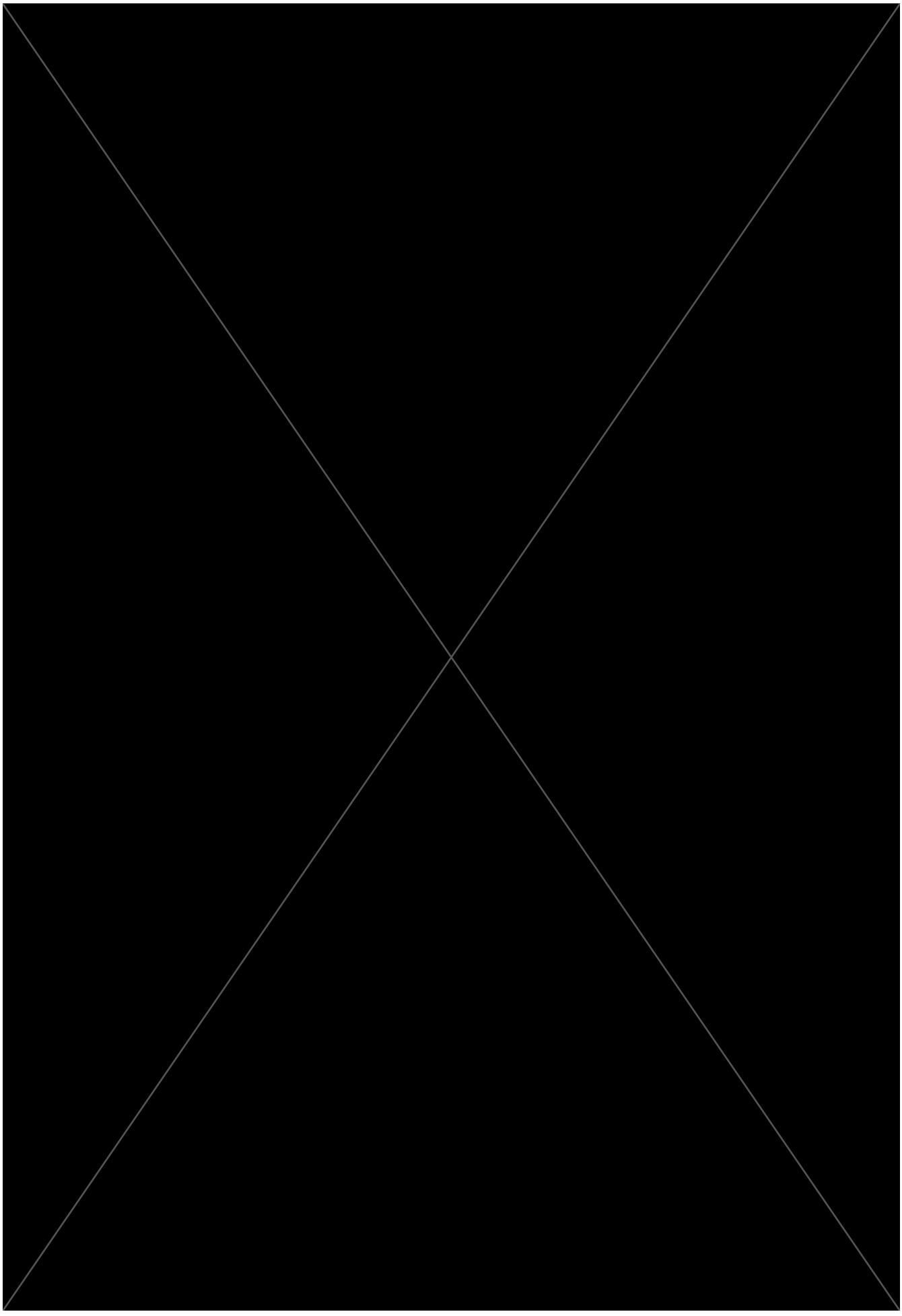

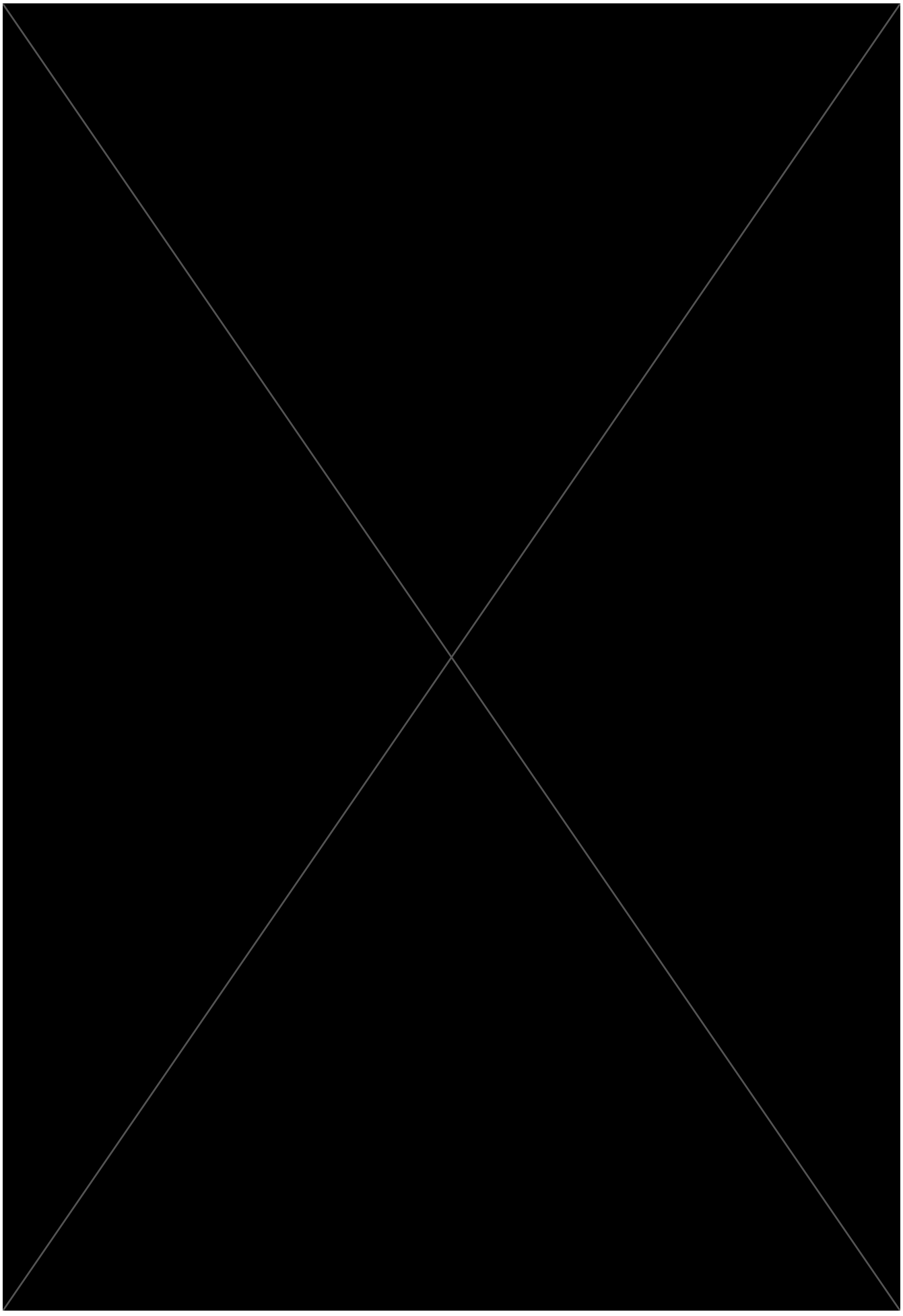

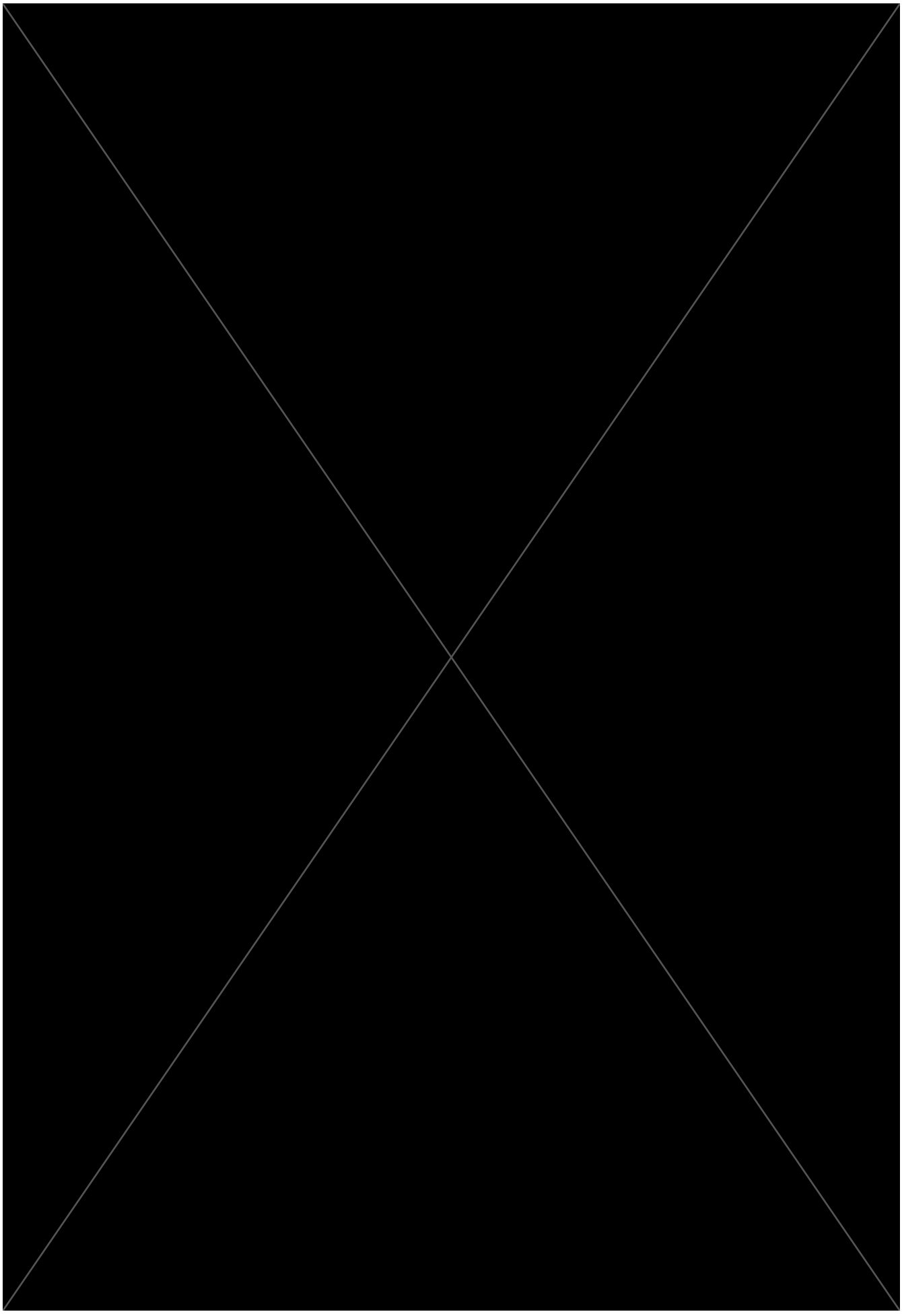

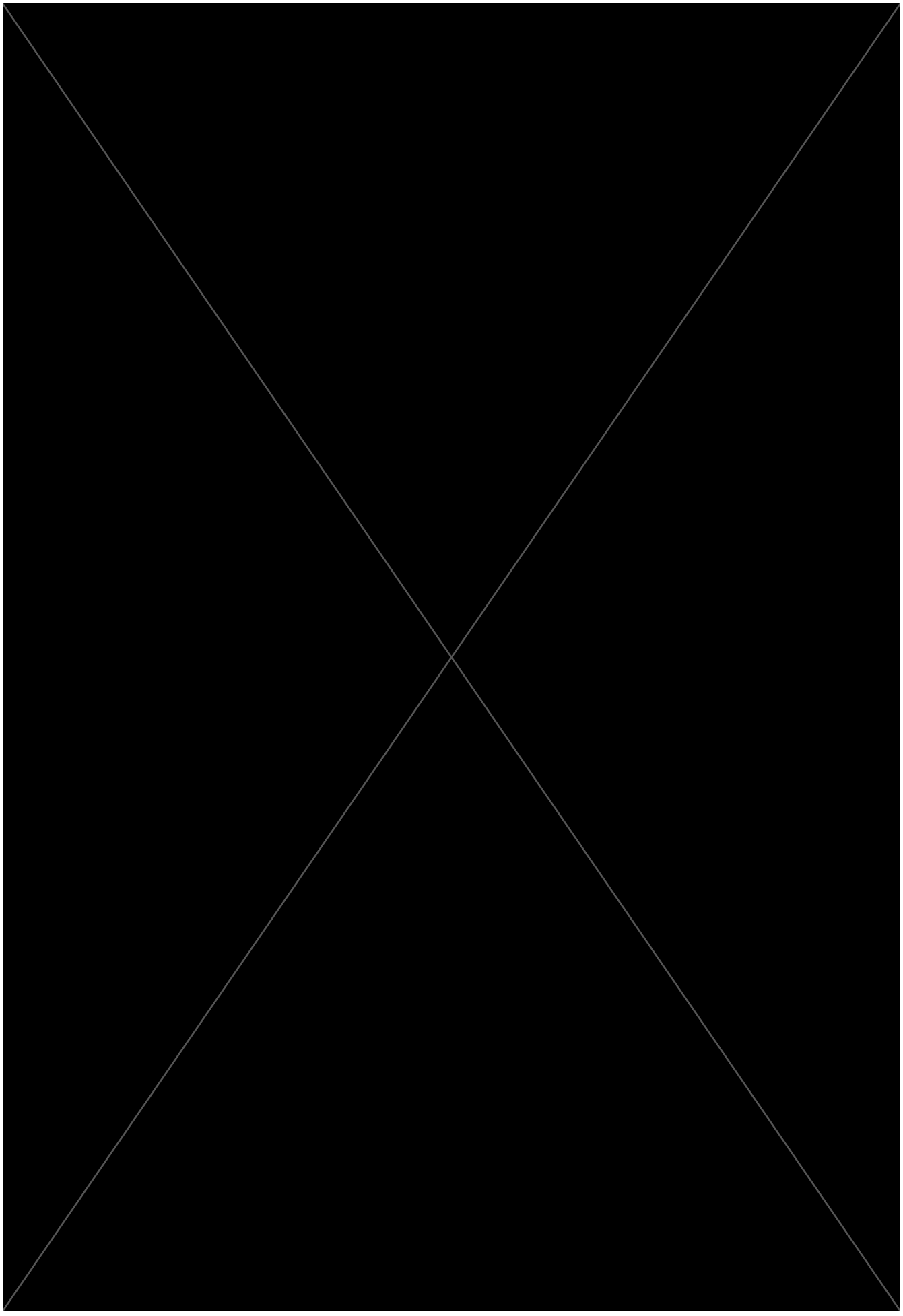

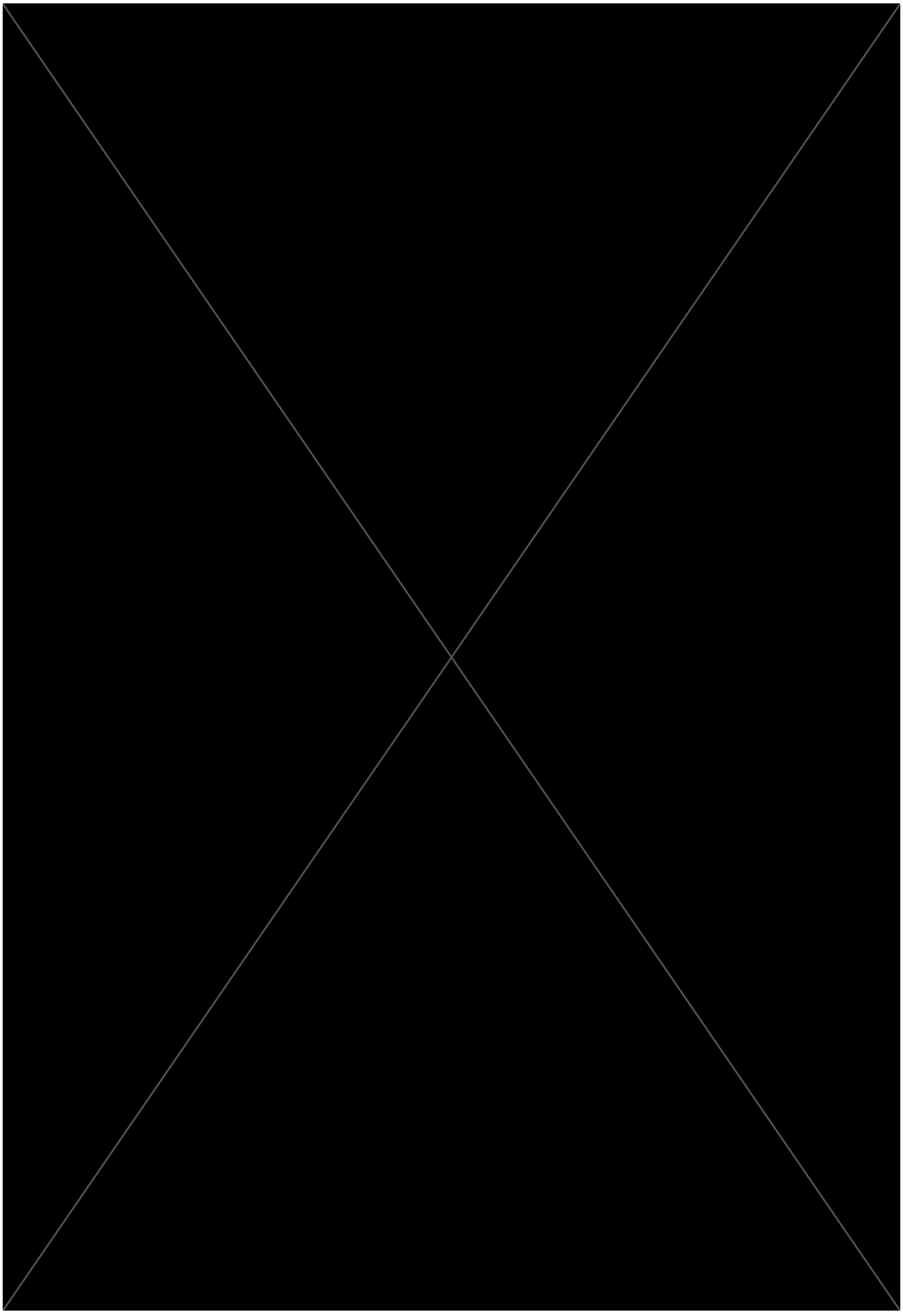

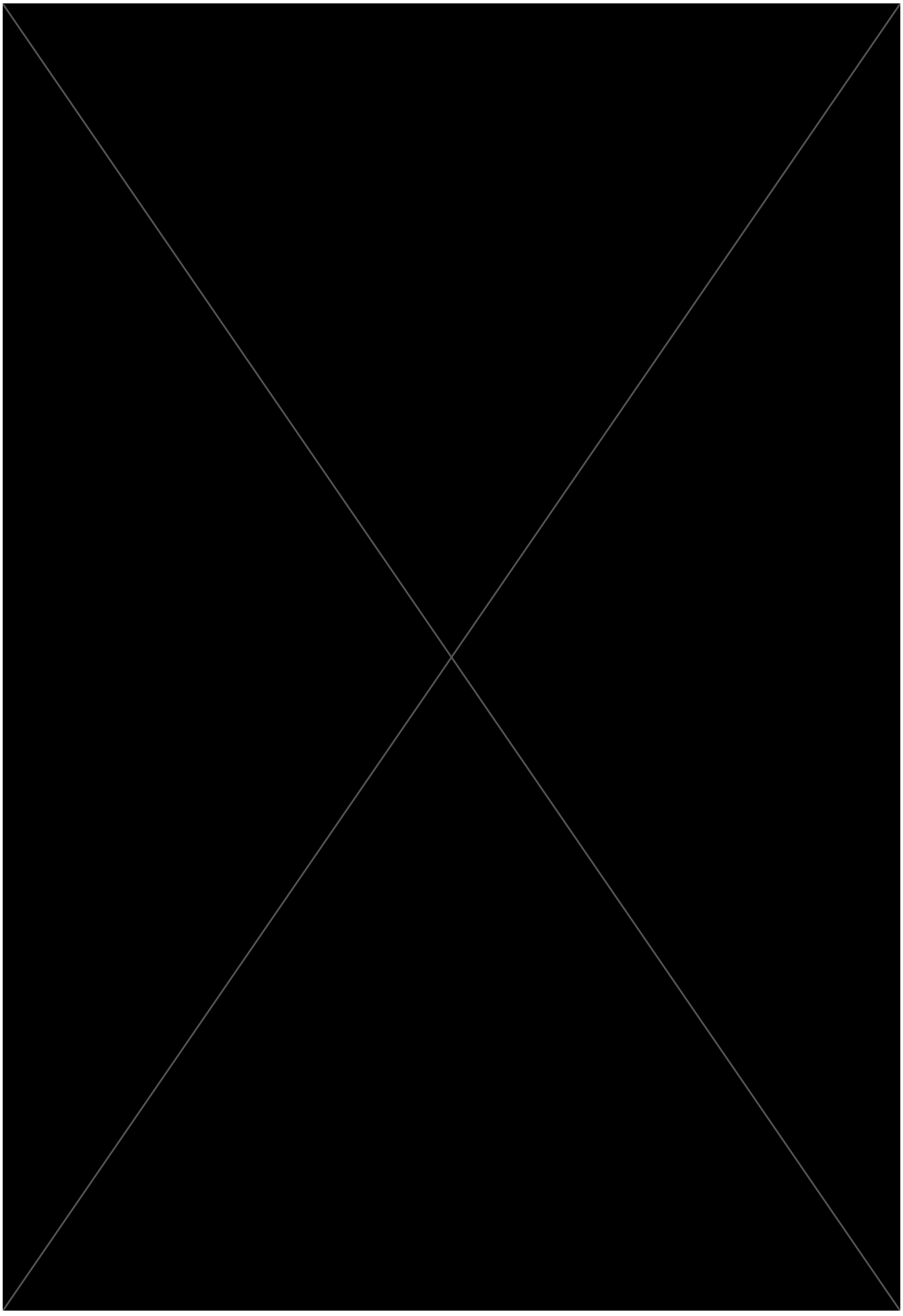

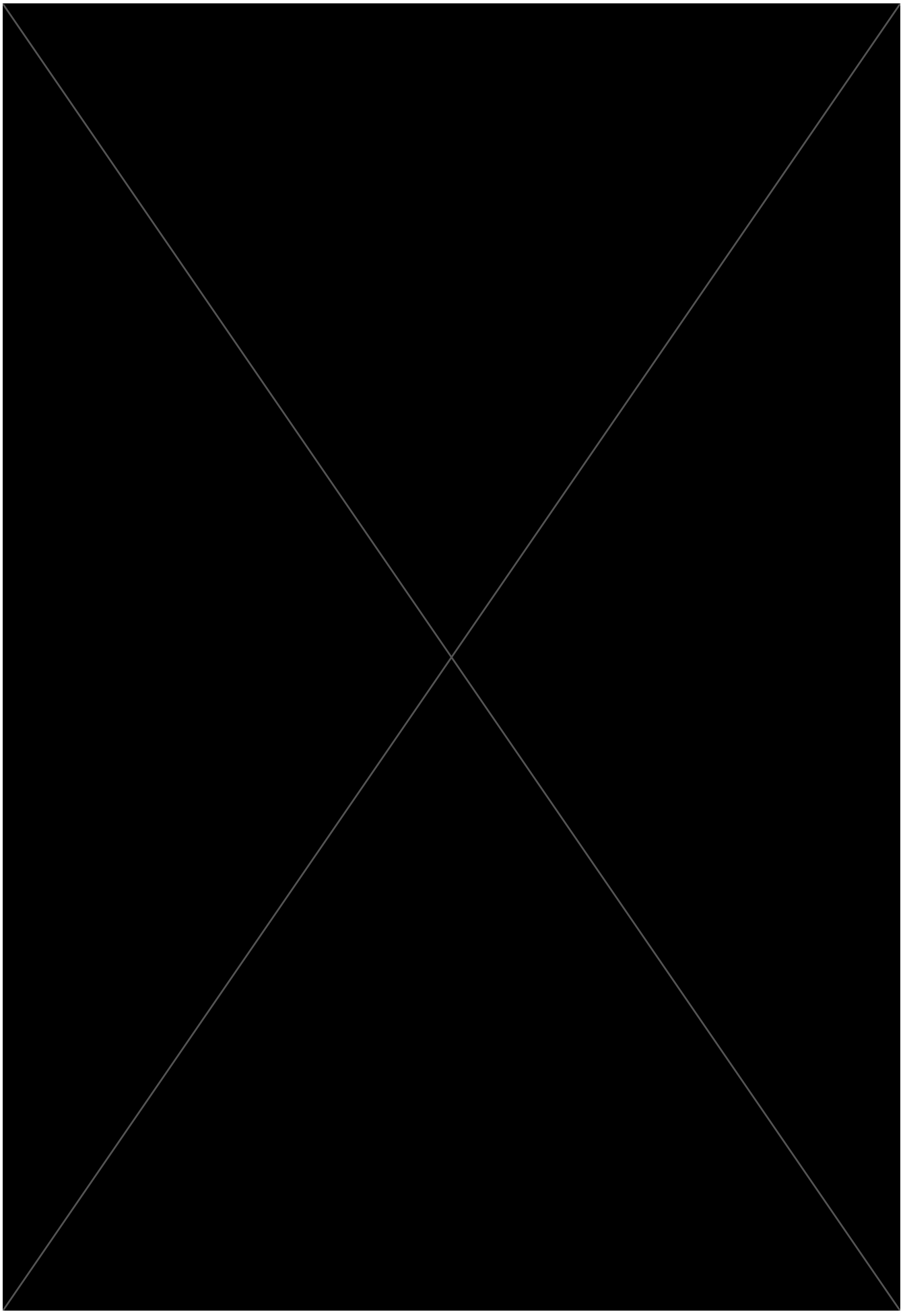

Chapter 9 Discussion and conclusions

9.1 Introduction

At the beginning of this thesis, four research questions were posed (Chapter 1, section 1.2). Here, the ways in which each of these questions have been answered are specified (section 9.2). The results presented throughout this thesis also point to several future areas of study, each of which is discussed below (section 9.3). Finally, the main conclusions drawn from this thesis are summarised (section 9.4).

9.2 Research questions

Research question 1: Do jumps of the rift-axis occur during SDR emplacement?

Recent models of SDR emplacement have included jumps of the *rift-axis* to explain the asymmetry observed between conjugate magma-rich margins (Buck, 2017; Morgan and Watts, 2018). However, these analytical models were not constrained by observations from high-quality seismic reflection data, thus limiting their applicability.

In this thesis it has been demonstrated that a series of Abandoned Sites of SDR Emplacement are embedded within the Orange Basin SDR sequence (Chapter 5, Chapter 6). When analysed in 2D dip-parallel seismic reflection profiles, many of these features record intra-SDR emplacement *rift-jumps*. That is, the abandonment of one rift-axis and the subsequent development of another. Hence these results support the inclusion of rift-jumps in numerical models of SDR emplacement (Buck, 2017).

The processes driving rift-axis jumps were investigated across a range of scales, from the local (Chapter 5) to the regional (Chapter 8). At the local scale, a 2D seismic grid in South African Orange Basin was used to map an Abandoned Site of SDR Emplacement in three dimensions. Through analysing thickness maps it was suggested that the abandonment of individual rift-axes was driven by along-strike interactions between separate magmatic segments. As such, the *rift-jumps* observed in 2D may in fact result from out-of-plane rift propagations. A similar phenomenon is observed at mid-ocean ridges, where

2D offsets of a spreading axis, as observed along a flow-line, may result from the lateral propagation of another ridge segment (Macdonald et al., 1988). The 3D maps presented in Chapter 5 indicate that the abandonment of individual rift-axes results in the development of a laterally continuous magmatic system. Accordingly, this process results in a loss of the along-strike segmentation present during earlier stages of SDR emplacement (Chapter 5; Norcliffe et al., 2018).

At the regional scale, it is possible that variations in spreading-rate control this process. Across the 800 km long Orange Basin there are significant along-strike variations in the width of the Outer SDRs, indicating lateral variations in spreading velocity during their emplacement (Chapter 8). Abandoned Sites of SDR Emplacement are often located in places where the Outer SDRs are relatively narrow, indicating slower spreading velocities. It is hence possible that, at the regional scale, relocations of the rift-axis are responding to variations in spreading velocity. For example, it is possible that the faster spreading segments propagated along-strike shortcutting areas of slower spreading velocity.

The results presented in this thesis are mainly from the SW African margin, however it is likely that they are representative of other magma-rich margins. It is notable that previous studies (Clemson et al., 1997; Gladczenko et al., 1998; Koopmann et al., 2013; Koopmann et al., 2014b; McDermott et al., 2015; Mohammed et al., 2016) in this region did not identify any of the five Abandoned Sites of SDR Emplacement mapped here. All of these studies were based on datasets that lacked the resolution and/or the coverage of those available for this study. Hence, as higher quality and more densely spaced seismic reflection data become available over magma-rich margins worldwide, it is possible that more of these features will be identified. Indeed, recent studies of the eastern margin of the U.S. have reported packages of landward dipping reflectors embedded in the SDR sequence (Davis et al., 2018b). Similar successions have also been identified in the Pelotas Basin, offshore Brazil (Stica et al., 2014; McDermott et al., 2018). Hence the processes described in this thesis may be common during magma-rich margin evolution.

Research question 2: What are the roles of faulting and loading in generating the dips displayed by SDRs?

The geometry of SDRs can be explained by either: lava-flow extrusion into the hanging-wall of landward-dipping normal faults (Geoffroy, 2005; Quirk et al., 2014; Clerc et al., 2015; Geoffroy et al., 2015; Nemčok and Rybár., 2017; Guan et al., 2019); or, magmatic loading of a thinned and weakened lithosphere (Mutter et al., 1982; Buck, 2017; Paton et al., 2017; Morgan and Watts, 2018; Tian and Buck, 2019). These different models assume fundamentally different crustal compositions and deformation mechanisms. In fault-controlled models, extension is accommodated via the generation of large normal faults and the crust is interpreted as stretched and intruded continental crust (Geoffroy, 2005; Clerc et al., 2015; Geoffroy et al., 2015; Nemčok and Rybár., 2017; Senkans et al., 2018; Guan et al., 2019). In loading-controlled models, extension is accommodated via axial magmatic accretion (Mutter et al., 1982; Buck, 2017; Paton et al., 2017; Morgan and Watts, 2018) and the crust is interpreted as coevally emplaced magmatic crust (Mutter et al., 1982; Eldhom and Grue, 1994; Gladczenko et al., 1998; Skogseid, 2000; Hopper et al., 2003; Paton et al., 2017; Collier et al., 2017; Tian and Buck, 2019).

These models are based on differing interpretations of the basal SDR-surface. In Chapter 6 it is demonstrated that seismic interpretations of this surface are inherently non-unique, giving rise to the competing models described above.

In Chapters 5 and 6 new insights into this debate have been gained through studying Abandoned Sites of SDR Emplacement, which record the syn-emplacement geometry of SDRs. These features contain thick (c. 2 km) unfaulted seismic facies units named Laterally Confined Volcanic Successions (LCVSs; Norcliffe et al., 2018). This seismic facies unit has a lens-shaped geometry where thickness is greatest above the abandoned rift-axis. Their unfaulted nature indicates that during SDR emplacement subsidence was driven by isostatic processes. Hence, interpretations from these systems supports magmatic-loading models of SDR emplacement (Mutter et al., 1982; Paton et al., 2017; Buck, 2017; Morgan and Watts, 2018; Tian and Buck, 2019). Their association with densely spaced upper-crustal reflectors, interpreted as dykes, further supports this conclusion.

Interpretations from Abandoned Sites of SDR Emplacement were then used to refine our understanding of loading-driven SDR emplacement. LCVS-geometry indicates that, during SDR emplacement, the rift-axis was characterised by a thick unfaulted volcanic mini-basin. To investigate the processes controlling the formation of this mini-basin, the observed geometries were compared to predictions from numerical and conceptual SDR emplacement models (Buck, 2017; Paton et al., 2017; Morgan and Watts, 2018). It was shown that the axial subsidence required could be generated through dyke emplacement (Morgan and Watts, 2018) and reductions in crustal thickness (Paton et al., 2017) due to waning magma-production. The geometry of SDRs is then produced through the splitting, via magma-intrusion, and stacking of these intra-LCVS reflectors. Throughout this process the mini-basin was continually filled at the surface via magma-extrusion.

The Orange Basin SDR sequence is often divided into Inner SDRs and Outer SDRs (Bauer et al., 2000; Blaich et al., 2010; McDermott et al., 2015). The Abandoned Sites of SDR Emplacement formed coevally with Outer SDRs. Hence they provide a snapshot of Outer SDR emplacement. The results presented above therefore support models whereby Outer SDRs form via magmatic-loading as the uppermost part of an entirely magmatic crust (Bauer et al., 2000; McDermott et al., 2015; Reuber, 2017).

The emplacement history of the Inner SDRs is less certain. On both the SW African margin and its conjugates offshore South America, these SDRs have been interpreted as fault-controlled features (McDermott et al., 2015; Paton et al., 2017; McDermott et al., 2018). Data presented in this thesis reveal that the in the Orange Basin, wedges of Inner SDRs terminate downdip against landward dipping surfaces. This supports interpretations of Inner SDRs as fault-controlled volcanics that were emplaced during continental stretching. However, as was noted above, interpretations of the basal-SDR surface is inherently non-unique. The identification of Abandoned Sites of SDR Emplacement within the Inner SDRs would help resolve this uncertainty.

Research question 3: What were the spatial and temporal relationships between subaerial and submarine magmatic spreading during South Atlantic opening?

The outermost SDRs along the South Atlantic magma-rich margins are often considered as the uppermost part of subaerially emplaced magmatic crust

(Gladczenko et al., 1998; McDermott et al., 2015; Collier et al., 2017; Paton et al., 2017; McDermott et al., 2018). This is a conclusion supported by the analyses presented in Chapters 5 and 6. Seaward of this SDR-bearing magmatic crust is normal oceanic crust (Gladczenko et al., 1998), which has thicknesses only slightly greater than global averages (Taposeea et al., 2016). In a 2D seismic section, the juxtaposition of these two crustal types record the subsidence of the margin below sea-level: during SDR emplacement, magmatic spreading was subaerial; during subsequent oceanic crust generation, the spreading centre was submarine (Mutter et al., 1982; Planke et al., 2000; McDermott et al., 2015; Paton et al., 2017; Collier et al., 2017).

The South Atlantic opened from south to north (Jackson et al., 2000; Moulin et al., 2010; Heine et al., 2013; Collier et al., 2017), indicating that the lateral transition from subaerial to submarine magmatic spreading was diachronous along the margin (Collier et al., 2017). In Chapter 7 new constraints were provided on the temporal and spatial relationship between subaerial and submarine magmatic spreading. Magnetic lineations, resulting from organised igneous accretion, were correlated from within the oceanic crust to within the SDR-bearing magmatic crust. These magnetic lineations are only present beneath the outermost SDRs, which is attributed to the reduced thickness of the SDRs in these areas. The continuity of magmatic spreading anomalies beneath both of these crustal types indicates that subaerial and submarine spreading were occurring coevally along the same organised axial system. The trend of this axial system is unaffected by a major transfer zone that segmented the basin during earlier stages of rifting and magmatism. Hence this presents an example of magmatic processes overprinting structural segmentation present earlier in the rifting process.

Regionally, it has been suggested that the northward younging of chrons within the oceanic crust can be used to date the northward propagation of continental breakup (Koopmann et al., 2013; Koopmann et al., 2014b). The results presented here instead indicate that these chrons record the northward transition from subaerial to submarine magmatic spreading.

Research question 4: What are the mechanisms and causes of asymmetric SDR emplacement?

As shown in Chapter 7, many of world's conjugate SDR sequences are asymmetric (Hopper et al., 2003; Blaich et al., 2009; Becker et al., 2014; Misra et al., 2015; Becker et al., 2016; Horni et al., 2017). This is problematic as the majority of SDR emplacement models assume a symmetrical system (Mutter et al., 1982; Geoffroy, 2005; Quirk et al., 2014; Paton et al., 2017; McDermott et al., 2018; Morgan and Watts, 2018; Tian and Buck, 2019). Here seismic reflection data from the Orange Basin and the conjugate portion of the South American margin were used to test models of asymmetric magma-rich margin evolution (Hopper et al., 2003; Becker et al., 2016; Buck, 2017).

The Abandoned Sites of SDR Emplacement embedded within the SW African SDR Sequence are absent on the conjugate South American margin (Franke et al., 2007; Franke et al., 2010; McDermott et al., 2018). In two dimensions, these abandoned magmatic systems can be considered to result from a jump of the rift-axis (see *research question 1*). Each of these jumps would have resulted in material from the South American side of the rift being transferred to the African side, thus contributing to asymmetry. The amount of asymmetry resulting from rift-jumps was calculated across three pairs of conjugate seismic reflection lines. In some places rift-jumps account for almost all of the asymmetry observed whereas elsewhere they fail to explain observations.

During Outer SDR emplacement it is suggested that two mechanisms accommodated asymmetry: symmetric magmatic spreading punctuated by rift-jumps (Buck, 2017); and, asymmetric magmatic spreading (Hopper et al., 2003). It is likely that both mechanisms were responding to the same geodynamic process. By analogy with the North Atlantic (Hopper et al., 2003), it is proposed that regional asymmetric magmatic accretion was driven by rift-axis migration towards South American side of the basin, which was characterised by thinner and warmer lithosphere (Autin et al., 2016).

The asymmetry of the Inner SDRs is not fully explained by either asymmetric magmatic spreading or by rift-jumps. These Inner SDRs at least partially overlie stretched continental crust and are often interpreted as fault-controlled features (McDermott et al., 2015; Paton et al., 2017; McDermott et al., 2018). Their

asymmetry therefore may result from the differential generation of accommodation space during continental stretching.

9.3 Future directions in magma-rich margin research

The results presented in this thesis point to several future areas of research, each of which is described below.

Analytical modelling of loading-driven SDR emplacement

In Chapter 6 a refined model of loading-driven SDR emplacement was presented. This model integrated new constraints on the syn-emplacement geometry of SDRs. It was proposed that during SDR emplacement, axial subsidence is driven by both dyke intrusion (Buck, 2017; Morgan and Watts, 2018; Tian and Buck, 2019) and reductions in crustal thickness (Paton et al., 2017). Two dimensional flexural models could be used to constrain the relative roles of each of these processes in producing the geometries observed. This would advance the results of previous numerical studies where crustal thickness was modelled as remaining constant through time (Buck, 2017; Morgan and Watts, 2018; Tian and Buck, 2019). These models could also address the subsidence of the evolving margin from a subaerial to a submarine environment.

Lithospheric necking in a magma-rich setting

As was demonstrated in Chapters 6 and 7, the innermost SDRs on the African margin overlie a zone of major crustal attenuation that is comparable to the *necking zone* identified across the Atlantic rifted margins (Péron-Pinvidic et al., 2013). It is possible that this necking zone formed coevally with the overlying Inner SDRs. This scenario suggests that the Inner SDRs are controlled by landward dipping normal faults (McDermott et al., 2015; Paton et al., 2017; McDermott et al., 2018). If this is the case, then the parameters controlling the generation of landward dipping normal faults need to be investigated. This is important as current simulations of continental extension predict the development of seaward dipping normal faults (e.g. Naliboff et al., 2017). Alternatively this necking zone could have formed prior to SDR emplacement via the same mechanisms as on a magma-poor margin (Mohn et al., 2012). Determining the mechanisms of lithospheric necking on magma-rich margins is unlikely to be solved by further interpretation of seismic reflection data. Rather,

field analogues (Geoffroy et al., 2001; Abdelmalak et al., 2015) and seismic refraction data could be used to better characterise this area of major crustal attenuation.

Segmentation from rift to drift

A number of studies suggest that the transfer zones segmenting early-stage rift basins (e.g. Morley et al., 1990) are present throughout the entire rifting process (Clemson et al., 1997; Franke et al., 2010; Koopmann et al., 2013; Koopmann et al., 2014b). Following breakup these transfer zones are then thought to control the nucleation of oceanic transform faults (Clemson et al., 1997; Stica et al., 2014). Evidence of these long-lived transfer zones have been found along rifted margins (Clemson et al., 1997; Koopmann et al., 2013; Stica et al., 2014; Koopmann et al., 2014b; Collier et al., 2017; McDermott et al., 2018) and in active rifts (Illsley-Kemp et al., 2018).

In Chapter 5 it was demonstrated that small-scale segmentation can be erased during the later stages of SDR emplacement. Then, in Chapter 7 it was shown that regional-scale segmentation associated with a large transfer zone can also become overprinted during this stage of basin evolution. These results contrast studies from elsewhere along this margin, which demonstrate the occurrence of segmentation from rift-initiation to seafloor spreading (Clemson et al., 1997; Koopmann et al., 2013; Collier et al., 2017).

Future work should address the question: *what factors control the preservation of structural segmentation from rift-drift?* In part this problem can be addressed via the regional characterisation of different transfer zones. However, 3D thermo-mechanical modelling would be useful in determining the parameters that control the longevity of structural segmentation.

The geodynamic processes driving asymmetric SDR emplacement

SDR sequences worldwide are asymmetric, however it is uncertain whether the processes controlling asymmetry are consistent along and between different rift-systems. In the North Atlantic, asymmetric SDR emplacement is thought to result from lithospheric heterogeneity (Hopper et al., 2003). By analogy with models of mid-ocean ridge accretion, it was suggested that asymmetry was driven by rift-axis migration towards the side of the rift characterised by thinner and warmer lithosphere (Hopper et al., 2003). A similar model can be used to

explain much of the asymmetry observed between the Orange Basin SDR sequence and its conjugates offshore Uruguay and Argentina (Chapter 8).

However, in parts of the South Atlantic (Reuber, 2017) and the NE Arabian Sea (Misra et al., 2015) plume motion may also have influenced asymmetric SDR emplacement. This process is also responsible for the rift-jumps observed in Iceland, an environment considered analogous to that recorded by SDRs (Mutter et al., 1982; Buck, 2017; McDermott et al., 2018).

Hence at least two factors influence asymmetric SDR emplacement: lithospheric heterogeneity and plume motion. To clarify the role of each of these factors, they need to be tested across a range of settings. Using published data, a database could be produced that constrains the distribution of SDRs, seafloor spreading anomalies, plumes, and failed rifts across the conjugate magma-rich margins of: the North Atlantic (Nielsen and Hopper, 2002; Hopper et al., 2003); the Central Atlantic (Oh et al., 1995; Klingelhoefer et al., 2016b; Davis et al., 2018a); the South Atlantic (Koopmann et al., 2014b; McDermott et al., 2015; Collier et al., 2017; McDermott et al., 2018); and the NE Arabian Sea (Corfield et al., 2010; Calvès et al., 2011; Misra et al., 2015). This would demonstrate what, if any, factors are consistent across all systems. For example, is the plume stem always located beneath the plate with the narrower SDR sequence, thus favouring the role of plume-motion in controlling asymmetry? Or, had the lithosphere always been asymmetrically thinned prior to SDR emplacement, thus favouring the role of lithospheric heterogeneity?

9.4 Conclusions

Within this thesis a series of Abandoned Sites of SDR Emplacement were identified within the Orange Basin SDR sequence. The occurrence of these features required the update of both regional (Bauer et al., 2000; McDermott et al., 2015) and generic (Planke et al., 1999; Planke et al., 2000) seismic-volcanostratigraphic frameworks.

In two dimensions, the majority of Abandoned Sites of SDR Emplacement can be considered a result of *rift-jumps*, such as have been included in recent numerical models (Buck, 2017). The processes driving these rift-jumps were investigated through the 3D characterisation of one such abandoned magmatic system. Results suggest that the abandonment of individual rift-axes are driven

by along-strike interactions between separate magmatic segments. A result of individual axis-abandonment is the establishment of a laterally continuous axial zone. Hence, the structural segmentation present in earlier stages of SDR emplacement becomes overprinted.

Abandoned Sites of SDR Emplacement also provide constraints on the syn-emplacement geometry of SDRs. They consistently demonstrate that during the later stages of SDR emplacement the rift-axis was characterised by a thick unfaulted package of volcanics named the Laterally Confined Volcanic Succession (LCVS). The architecture of LCVSs support magmatic-loading models of SDR emplacement (Mutter et al., 1982; Paton et al., 2017; Buck, 2017; Morgan and Watts, 2018; McDermott et al., 2018; Tian and Buck, 2019). Specifically, they indicate that during SDR emplacement, subsidence and rotation are driven by magma-intrusion (Buck, 2017; Morgan and Watts, 2018; Tian and Buck, 2019) and changes in crustal thickness (Paton et al., 2017). These results support regional models where the Outer SDRs are interpreted as the uppermost part of an entirely magmatic crust (McDermott et al., 2015; Collier et al., 2017).

The distribution of Abandoned Sites of SDR Emplacement and Outer SDRs were then used to map the extent of magmatic crust beneath the Orange Basin. This interpretation was then coupled with that of a regional total magnetic anomaly grid. It was demonstrated that linear magnetic anomalies, previously considered as seafloor spreading lineation (Koopmann et al., 2013; Collier et al., 2017), extend across both oceanic crust and SDR-bearing magmatic crust. This suggests that submarine and subaerial magmatic accretion were occurring coevally along the same organised spreading axis. Therefore, the northward younging of chrons in the South Atlantic is not indicative of the propagation of continental breakup (Koopmann et al., 2013), but of the northward younging of submarine seafloor spreading.

Finally, the scale of analysis was increases to encompass the conjugate magma-rich margins of South Africa-Argentina and Namibia-Uruguay. In both cases the African SDR Sequence is significantly wider than the South American. A forward model was used to test precisely how much asymmetry can be attributed to rift-jumps towards the South American plate. Whilst these jumps of the rift-axis explain the asymmetry observed in certain parts of the

SDR sequence, they fail to do so elsewhere. Instead the mechanisms controlling SDR emplacement are shown to vary spatially and temporally. In the early stages of magma-rich rifting, asymmetry is thought to result from the asymmetric stretching of the continental lithosphere, leading to the generation of differential accommodation space. In the later stages of SDR emplacement, asymmetry is a result of asymmetrical magmatic spreading and rift-jumps. It is suggested that both of these mechanisms were controlled by asymmetric lithosphere structure (Hopper et al., 2003) which lead to rift-axis migration towards the South American plate.

References

Abdelmalak, M.M., Andersen, T.B., Planke, S., Faleide, J.I., Corfu, F., Tegner, C., Shephard, G.E., Zastrozhnov, D. and Myklebust, R. 2015. The ocean-continent transition in the mid-Norwegian margin: Insight from seismic data and an onshore Caledonian field analogue. *Geology*. **43**(11), 1001-1014.

Abdelmalak, M.M., Faleide, J.I., Planke, S., Gernigon, L., Zastrozhnov, D., Shephard, G.E. and Myklebust, R. 2017. The T-Reflection and the Deep Crustal Structure of the Vøring Margin, Offshore mid-Norway. *Tectonics*. **36**(11), pp.2497–2523.

Allen, P.A. and Allen, J.R. 2013. Basin analysis: Principles and application to petroleum play assessment. Chichester: John Wiley and Sons

Armitage, J.J. and Collier, J.S. 2017. The thermal structure of volcanic passive margins. *Petroleum Geoscience*. **24**(4), pp.393–401.

Armitage, J.J., Collier, J.S. and Minshull, T. 2010. The importance of rift history for volcanic margin formation. *Nature*. **465**(7300), pp.913–917.

Austin, J.A.J. and Uchupi, E. 1982. Continental-Oceanic Crustal Transition Off Southwest Africa. *AAPG Bulletin*. **66**(9), pp.1328-1347.

Autin, J., Scheck-Wenderoth, M., Gottze, H.J., Reichert, C. and Marchal, D. 2016. Deep structure of the Argentine margin inferred from 3D gravity and temperature modelling, Colorado Basin. *Tectonophysics*. **676**, pp.198–210.

Bastow, I.D. and Keir, D. 2011. The protracted development of the continent–ocean transition in Afar. *Nature Geoscience*. **4**(4), pp.248–250.

Bauer, K., Neben, S., Schreckenberger, B., Emmermann, R., Hinz, K., Fechner, N., Gohl, K., Schulze, A., Trumbull, R.B. and Weber, K. 2000. Deep structure of the Namibia continental margin as derived from integrated geophysical studies. *Journal of Geophysical Research: Solid Earth*. **105**(B11), pp.25829–25853.

Bécel, A., Shillington, D.J., Nedimović, M.R., Webb, S.C. and Kuehn, H. 2015. Origin of dipping structures in fast-spreading oceanic lower crust offshore Alaska imaged by multichannel seismic data. *Earth and Planetary Science*

Letters. **424**, pp.26–37.

Becker, K., Franke, D., Trumbull, R.B., Schnabel, M., Heyde, I., Schreckenberger, B., Koopmann, H., Bauer, K., Jokat, W. and Krawczyk, C.M. 2014. Asymmetry of high-velocity lower crust on the South Atlantic rifted margins and implications for the interplay of magmatism and tectonics in continental breakup. *Solid Earth*. **5**(2), pp.1011–1026.

Becker, K., Tanner, D.C., Franke, D. and Krawczyk, C.M. 2016. Fault-controlled lithospheric detachment of the volcanic southern South Atlantic rift. *Geochemistry, Geophysics, Geosystems*., pp.1–21.

Behn, M.D. and Ito, G. 2008. Magmatic and tectonic extension at mid-ocean ridges: 1. Controls on fault characteristics. *Geochemistry, Geophysics, Geosystems*. **9**(8).

Bialas, R.W., Buck, W.R. and Qin, R. 2010. How much magma is required to rift a continent? *Earth and Planetary Science Letters*. **292**(1–2), pp.68–78.

Blaich, O. a., Faleide, J.I. and Tsikalas, F. 2011. Crustal breakup and continent-ocean transition at South Atlantic conjugate margins. *Journal of Geophysical Research*. **116**(B1).

Blaich, O. A., Faleide, J.I., Tsikalas, F., Franke, D. and León, E. 2009. Crustal-scale architecture and segmentation of the Argentine margin and its conjugate off South Africa. *Geophysical Journal International*. **178**(4064), pp.85–105.

Blaich, O. A., Faleide, J.I., Tsikalas, F., Gordon, a C. and Mohriak, W. 2013. Crustal-scale architecture and segmentation of the South Atlantic volcanic margin. *Geological Society, London, Special Publications*. **369**(0316), pp.167–183.

Blaich, O. A., Faleide, J.I., Tsikalas, F., Lilletveit, R., Chiossi, D., Brockbank, P. and Cobbold, P. 2010. Structural architecture and nature of the continent-ocean transitional domain at the Camamu and Almada Basins (NE Brazil) within a conjugate margin setting. *Petroleum Geology Conference Series*. **7**, pp.867–883.

Bodvarsson, G. and Walker, G.P.L. 1964. Crustal Drift in Iceland. *Geophysical Journal of the Royal Astronomical Society*. **8**(3), pp.285–300.

Boillot, G., Grimaud, S., Mauffret, A., Mougenot, D., Kornprobst, J., Mergoil-Daniel, J. and Torrent, G. 1980. Ocean-continent boundary off the Iberian margin: A serpentinite diapir west of the Galicia Bank. *Earth and Planetary Science Letters*. **48**(1), pp.23–34.

Boillot, G., Recq, M., Winterer, E.L., Meyer, A.W., Applegate, J., Baltuck, M., Bergen, J.A., Comas, M.C., Davies, T.A., Dunham, K., Evans, C.A., Girardeau, J., Goldberg, G., Haggerty, J., Jansa, L.F., Johnson, J.A., Kasahara, J., Loreau, J.P., Luna-Sierra, E., Moullade, M., Ogg, J., Sarti, M., Thurow, J. and Williamson, M. 1987. Tectonic denudation of the upper mantle along passive margins: a model based on drilling results (ODP leg 103, western Galicia margin, Spain). *Tectonophysics*. **132**(4), pp.335–342.

Brune, S., Williams, S.E. and Dietmar Müller, R. 2018. Oblique rifting: The rule, not the exception. *Solid Earth*. **9**(5), pp.1187–1206.

Buck, W.R. 2004. Consequences of asthenospheric variability on continental margins *In*: G. D. Karner, B. Taylor, N. W. Driscoll and K. D.L., eds. *Rheology and Deformation of the Lithosphere at Continetnal Margins*. Columbia University Press, pp.1–31.

Buck, W.R. 2017. The role of magmatic loads and rift jumps in generating seaward dipping reflectors on volcanic rifted margins. *Earth and Planetary Science Letters*. **466**, pp.62–69.

Buck, W.R., Lavier, L.L. and Poliakov, A.N.B. 2005. Modes of faulting at mid-ocean ridges. *Nature*. **434**(7034), pp.719–723.

Calvès, G., Schwab, A.M., Huuse, M., Clift, P.D., Gaina, C., Jolley, D., Tabrez, A.R. and Inam, A. 2011. Seismic volcanostratigraphy of the western Indian rifted margin: The pre-Deccan igneous province. *Journal of Geophysical Research*. **116**(B1).

Chappell, A.R. and Kusznir, N. 2008. Three-dimensional gravity inversion for Moho depth at rifted continental margins incorporating a lithosphere thermal gravity anomaly correction. *Geophysical Journal International*. **174**(1), pp.1–13.

Clemson, J., Cartwright, J. and Booth, J. 1997. Structural segmentation and the influence of basement structure on the Namibian passive margin. *Journal*

of the Geological Society. **154**(3), pp.477–482.

Clemson, J., Cartwright, J. and Swart, R. 1999. The Namib Rift: a rift system of possible Karoo age, offshore Namibia. *Geological Society, London, Special Publications*. **153**(1), pp.381–402.

Clerc, C., Jolivet, L. and Ringenbach, J.-C. 2015. Ductile extensional shear zones in the lower crust of a passive margin. *Earth and Planetary Science Letters*. **431**, pp.1–7.

Clerc, C., Ringenbach, J.-C., Jolivet, L. and Ballard, J.F. 2016. Rifted margins: Ductile deformation, boudinage, continentward-dipping normal faults and the role of the weak lower crust. *Gondwana Research*. **55**, 20-40

Collier, J.S., McDermott, C., Warner, G., Gyori, N., Schnabel, M., McDermott, K.G. and Horn, B.W. 2017. New constraints on the age and style of continental breakup in the South Atlantic from magnetic anomaly data. *Earth and Planetary Science Letters*. **477**, pp.27–40.

Collier, J.S., Minshull, T. a, Hammond, J.O.S., Whitmarsh, R.B., Kendall, J.-M., Sansom, V., Lane, C.I. and Rumpker, G. 2009. Factors influencing magmatism during continental breakup: New insights from a wide-angle seismic experiment across the conjugate Seychelles-Indian margins. *Journal of Geophysical Research*. **114**(B3), article no: B03101.

Collier, J.S., Sansom, V., Ishizuka, O., Taylor, R.N., Minshull, T.A. and Whitmarsh, R.B. 2008. Age of Seychelles – India break-up Age of Seychelles – India break-up. *Earth and Planetary Science Letters*. **272**(April 2018), pp.264–277.

Corfield, R.I., Carmichael, S., Bennett, J., Akhter, S., Fatimi, M. and Craig, T. 2010. Variability in the crustal structure of the West Indian Continental Margin in the Northern Arabian Sea. *Petroleum Geoscience*. **16**(3), pp.257–265.

Corner, B., Cartwright, J. and Swart, R. 2002. Volcanic passive margin of Namibia: A potential fields perspective. *Geological Society of America Special Papers*. **362**, pp.203–220.

Corti, G. 2009. Continental rift evolution: From rift initiation to incipient break-up in the Main Ethiopian Rift, East Africa. *Earth-Science Reviews*. **96**(1–2),

pp.1–53.

Corti, G., Agostini, A., Keir, D., van Wijk, J., Bastow, I.D. and Ranalli, G. 2015. Magma-induced axial subsidence during final-stage rifting: Implications for the development of seaward-dipping reflectors. *Geosphere*. **11**(3), pp.563–571.

Dalton, T.J.S., Paton, D. a. and Needham, D.T. 2016. Influence of mechanical stratigraphy on multi-layer gravity collapse structures: insights from the Orange Basin, South Africa. *Geological Society, London, Special Publications*. **438**, 211-228.

Davis, J.K., Bécel, A. and Buck, W.R. 2018a. Estimating emplacement rates for seaward-dipping reflectors associated with the U.S. East Coast Magnetic Anomaly. *Geophysical Journal International*. **215**(3), pp.1594–1603.

Davis, J.K., Bécel, A., Shillington, D.J. and Buck, W.R. 2018b. The Distribution and Characteristics of Seaward Dipping Reflectors Along the Eastern North American Margin. *In*: *American Geophysical Union, Fall Meeting 2018, Washington D.C., U.S.*.

Davison, I. 2007. Geology and tectonics of the South Atlantic Brazilian salt basins. *Geological Society, London, Special Publications*. **272**(1), pp.345–359.

Dix, C.H. 1955. Seismic Velocities From Surface Measurements. *Geophysics*. **20**(1), pp.68–86.

Doré, T. and Lundin, E. 2015. Hyperextended continental margins—Knowns and unknowns. *Geology*. **43**(1), pp. 95-96.

Ebinger, C.J. and Casey, M. 2001. Continental breakup in magmatic provinces: An Ethiopian example. *Geology*. **29**(6), pp.527–530.

Eldhom, O. 1991. Magmatic tectonic evolution of a volcanic rifted margin. *Marine Geology*. **102**(1–4), pp.43–61.

Eldhom, O. and Grue, K. 1994. North Atlantic volcanic margins : Dimensions and production rates a volume of flood basalts a mean eruption rate of the basalts were emplaced within volume in a mean crustal accretion rate. *Journal of Geophysical Research*. **99**, pp.2955–2968.

Elliott, G.M. and Parson, L.M. 2008. Influence of margin segmentation upon the

break-up of the Hatton Bank rifted margin, NE Atlantic. *Tectonophysics*. **457**(3–4), pp.161–176.

Franke, D. 2013. Rifting, lithosphere breakup and volcanism: Comparison of magma-poor and volcanic rifted margins. *Marine and Petroleum Geology*. **43**, pp.63–87.

Franke, D., Ladage, S., Schnabel, M., Schreckenberger, B., Reichert, C., Hinz, K., Paterlini, M., de Abelleyra, J. and Siciliano, M. 2010. Birth of a volcanic margin off Argentina, South Atlantic. *Geochemistry, Geophysics, Geosystems*. **11**(2).

Franke, D., Neben, S., Ladage, S., Schreckenberger, B. and Hinz, K. 2007. Margin segmentation and volcano-tectonic architecture along the volcanic margin off Argentina/Uruguay, South Atlantic. *Marine Geology*. **244**(1–4), pp.46–67.

Fromm, T., Planert, L., Jokat, W., Ryberg, T., Behrmann, J.H., Weber, M.H. and Haberland, C. 2015. South Atlantic opening: A plume-induced breakup? *Geology*. **43**(10), pp.931–935.

Geissler, W.H., Gaina, C., Hopper, J.R., Funck, T., Pe, G., Blischke, A., Arting, U.N.I., Jim, A. and Abdelmalak, M.M. 2017. Seismic volcanostratigraphy of the NE Greenland continental margin. *Geological Society, London, Special Publications.* **447**(1), pp. 149-170.

Geoffroy, L. 2001. The structure of volcanic margins: some problematics from the North-Atlantic/Labrador–Baffin system. *Marine and Petroleum Geology*. **20**(4), pp.566–584.

Geoffroy, L. 2005. Volcanic passive margins. *Comptes Rendus Geoscience*. **337**(16), pp.1395–1408.

Geoffroy, L., Burov, E.B. and Werner, P. 2015. Volcanic passive margins: another way to break up continents. *Scientific Reports*. **5(2015)**, article no.14828.

Geoffroy, L., Callot, J.-P., Scaillet, S., Skuce, A., Gélard, J.P., Ravilly, M., Angelier, J., Bonin, B., Cayet, C., Perrot, K. and Lepvrier, C. 2001. Southeast Baffin volcanic margin and the North American-Greenland plate separation. *Tectonics*. **20**(4), pp.566–584.

Gernigon, L., Blischke, A., Nasuti, A. and Sand, M. 2015. Conjugate volcanic rifted margins, seafloor spreading, and microcontinent: Insights from new high-resolution aeromagnetic surveys in the Norway Basin. *Tectonics*. **34**(5) pp.907–933.

Gernigon, L., Ringenbach, J.C., Planke, S. and Le Gall, B. 2004. Deep structures and breakup along volcanic rifted margins: Insights from integrated studies along the outer Vøring Basin (Norway). *Marine and Petroleum Geology*. **21**(3), pp.363–372.

Gerrard, I. and Smith, G. 1982. Post-Paleozoic succession and structure of the southwestern African continental margin. *M 34: Studies in continental margin geology. American Association of Petroleum Geologists Memoir, pp. 49-74*.

Gillard, M., Autin, J. and Manatschal, G. 2016. Fault systems at hyper-extended rifted margins and embryonic oceanic crust: Structural style, evolution and relation to magma. *Marine and Petroleum Geology*. **76**, pp.51–67.

Gillard, M., Autin, J., Manatschal, G., Sauter, D., Munschy, M. and Schaming, M. 2015. Tectonomagmatic evolution of the final stages of rifting along the deep conjugate Australian-Antarctic magma-poor rifted margins: Constraints from seismic observations. *Tectonics*. **34**, pp.753–783.

Gillard, M., Sauter, D., Tugend, J., Tomasi, S., Epin, M. and Manatschal, G. 2017. Birth of an oceanic spreading center at a magma-poor rift system. *Scientific Reports*. **7**(1), article no. 15072.

Gladczenko, T.P., Hinz, K., Eldhom, O., Meyer, H., Neben, S. and Skogseid, J. 1997. South Atlantic volcanic margins. *Journal of the Geological Society*. **154**(3), pp.465–470.

Gladczenko, T.P., Skogseid, J. and Eldhom, O. 1998. Namibia volcanic margin. *Marine Geophysical Researches*. **20**(4), pp.313–341.

Gouiza, M. and Paton, D.A. 2019. The role of inherited lithospheric heterogeneities in defining the crustal architecture of rifted margins and the magmatic budget during continental breakup. *Geochemistry, Geophysics, Geosystems*. **20**(4), pp.1836-1853.

Granado, P., Vera, J. De and McClay, K. 2009. Tectonostratigraphic evolution

of the Orange Basin, SW Africa. *Trabajos de geología*. **328**, pp.321–328.

Guan, H., Geoffroy, L., Gernigon, L., Chauvet, F., Grigné, C. and Werner, P. 2019. Magmatic ocean-continent transitions. *Marine and Petroleum Geology*. **104**, pp.438–450.

Hayward, N.J. and Ebinger, C.J. 1996. Variations in the along-axis segmentation of the Afar Rift system. *Tectonics*. **15**(2), p.244-257.

Heine, C., Zoethout, J. and Müller, R.D. 2013. Kinematics of the South Atlantic rift. *Solid Earth*. **4**(2), pp.215–253.

Hey, R. 1977. A new class of 'pseudofaults' and their bearing on plate tectonics: A propagating rift model. *Earth and Planetary Science Letters*. **37**(2), pp.321–325.

Hinz, K. 1981. A hypothesis on the terrestrial catastrophes wedges of very thick oceanward dipping layers beneath passive continental margind — their origin and paleonevironmental significance. *Geologisches Jahrbuch Reihe E*. **22**, pp.3–27.

Hirsch, K.K., Bauer, K. and Scheck-Wenderoth, M. 2009. Deep structure of the western South African passive margin - Results of a combined approach of seismic, gravity and isostatic investigations. *Tectonophysics*. **470**, pp.57–70.

Hjartardóttir, Á.R., Einarsson, P., Gudmundsson, M.T. and Högnadóttir, T. 2016. Fracture movements and graben subsidence during the 2014 Bárdarbunga dike intrusion in Iceland. *Journal of Volcanology and Geothermal Research*. **310**, pp.242–252.

Hoggard, M.J., Winterbourne, J., Czarnota, K. and White, N. 2017. Oceanic residual depth measurements, the plate cooling model, and global dynamic topography. *Journal of Geophysical Research: Solid Earth*. **122**(3), pp.2328–2372.

Hopper, J.R., Dahl-Jensen, T., Holbrook, W.S., Larsen, H.C., Lizarralde, D., Korenaga, J., Kent, G.M. and Kelemen, P.B. 2003. Structure of the SE Greenland margin from seismic reflection and refraction data: Implications for nascent spreading center subsidence and asymmetric crustal accretion during North Atlantic opening. *Journal of Geophysical Research: Solid*

Earth. **108**(B5).

Horni, J.Á., Hopper, J.R., Blischke, A., Geisler, W.H., Stewart, M., McDermott, K., Judge, M., Erlendsson, Ö. and Árting, U. 2017. Regional distribution of volcanism within the North Atlantic Igneous Province. *Geological Society, London, Special Publications*. **447**(1), pp.105–125.

Hubbard, R.J., Pape, J. and Roberts, D.G. 1985. Depositional sequence mapping as a technique to establish tectonic and stratigraphic framework and evaluate hydrocarbon potential on a passove continental margin *In*: O. R. Berg and D. Woolverton, eds. *Seismic Stratigraphy II: An Integrated Approach*. American Association of Petroleum Geologists Memoir, pp.79–91.

Illsley-Kemp, F., Bull, J.M., Keir, D., Gerya, T. V., Pagli, C., Gernon, T., Ayele, A., Goitom, B., Hammond, J. and Kendall, J.M. 2018. Initiation of a Proto-Transform Fault Prior to Seafloor Spreading. *Geochemistry, Geophysics, Geosystems*.

Jackson, M.P., Cramez, C. and Fonck, J.-M. 2000. Role of subaerial volcanic rocks and mantle plumes in creation of South Atlantic margins: implications for salt tectonics and source rocks. *Marine and Petroleum Geology*. **17**(4), pp.477–498.

Jagoutz, O., Müntener, O., Manatschal, G., Rubatto, D., Péron-Pinvidic, G., Turrin, B.D. and Villa, I.M. 2007. The rift-to-drift transition in the North Atlantic: A stuttering start of the MORB machine? *Geology*. **35**(12), p.1087-1090.

Jungslager, E.H.A. 1999. Petroleum habitats of the Atlantic margin of South Africa. *Geological Society, London, Special Publications*. **153**(1), pp.153–168.

Karner, G.D. and Gambôa, L. 2007. Timing and origin of the South Atlantic pre-salt sag basins and their capping evaporites. *Geological Society, London, Special Publications.* **285**(1), pp.15–35.

Karson, J. a and Brooks, C. 1999. Structural and magmatic segmentation of the Tertiary East Greenland volcanic rifted margin. *Geological Society, London, Special Publications*. **164**, pp.313–338.

Kearey, P., Brooks, M. and Hill, I. 2002. *An Introduction to Geophysical Exploration* 3rd ed. Blackwell Science Ltd.

Keen, C.E. and Boutilier, R.. 2000. Interaction of rifting and hot horizontal plume sheets at volcanic margins. *Journal of Geophysical Research*. **105**(B6), pp.13375–13387.

Keir, D., Bastow, I.D., Pagli, C. and Chambers, E.L. 2013. The development of extension and magmatism in the Red Sea rift of Afar. *Tectonophysics*. **607**, pp.98–114.

King, S.D. and Anderson, D.L. 1998. Edge-driven convection. *Earth and Planetary Science Letters*. **160**(3–4), pp.289–296.

Klimke, J., Franke, D., Gaedicke, C., Schreckenberger, B., Schnabel, M., Stollhofen, H., Rose, J. and Chaheire, M. 2015. How to identify oceanic crust—Evidence for a complex break-up in the Mozambique Channel, off East Africa. *Tectonophysics*. **693**, pp. 436-452.

Klingelhoefer, F., Biari, Y., Sahabi, M., Aslanian, D., Schnabel, M., Matias, L., Benabdellouahed, M., Funck, T., Gutscher, M.A., Reichert, C. and Austin, J.A. 2016a. Crustal structure variations along the NW-African continental margin: A comparison of new and existing models from wide-angle and reflection seismic data. *Tectonophysics*. **674**, pp.227–252.

Koopmann, H., Brune, S., Franke, D. and Breuer, S. 2014a. Linking rift propagation barriers to excess magmatism at volcanic rifted margins. *Geology*. **42**(12), pp.1071–1074.

Koopmann, H., Franke, D., Schreckenberger, B., Schulz, H., Hartwig, A., Stollhofen, H. and di Primio, R. 2013. Segmentation and volcano-tectonic characteristics along the SW African continental margin, South Atlantic, as derived from multichannel seismic and potential field data. *Marine and Petroleum Geology*. **50**, pp.22–39.

Koopmann, H., Schreckenberger, B., Franke, D., Becker, K. and Schnabel, M. 2014b. The late rifting phase and continental break-up of the southern South Atlantic: the mode and timing of volcanic rifting and formation of earliest oceanic crust. *Geological Society, London, Special Publications*. **420**(1), pp. 315-450.

Larsen, H.C., Mohn, G., Nirrengarten, M., Sun, Z., Stock, J., Jian, Z., Klaus, A., Alvarez-Zarikian, C.A., Boaga, J., Bowden, S.A., Briais, A., Chen, Y., Cukur, D., Dadd, K., Ding, W., Dorais, M., Ferré, E.C., Ferreira, F., Furusawa, A., Gewecke, A., Hinojosa, J., Höfig, T.W., Hsiung, K.H., Huang, B., Huang, E., Huang, X.L., Jiang, S., Jin, H., Johnson, B.G., Kurzawski, R.M., Lei, C., Li, B., Li, L., Li, Y., Lin, J., Liu, C., Liu, C., Liu, Z., Luna, A.J., Lupi, C., McCarthy, A., Ningthoujam, L., Osono, N., Peate, D.W., Persaud, P., Qiu, N., Robinson, C., Satolli, S., Sauermilch, I., Schindlbeck, J.C., Skinner, S., Straub, S., Su, X., Su, C., Tian, L., van der Zwan, F.M., Wan, S., Wu, H., Xiang, R., Yadav, R., Yi, L., Yu, P.S., Zhang, C., Zhang, J., Zhang, Y., Zhao, N., Zhong, G. and Zhong, L. 2018. Rapid transition from continental breakup to igneous oceanic crust in the South China Sea. *Nature Geoscience*. **11**(10), article no. 782.

Larsen, H.C. and Saunders, A.D. 1998. 41. Tectonism and volcanism at the southeast Greenland rifted margin: a record of plume impact and later continental rupture. *Proceedings of the Ocean Drilling Program, Scientific Results*. **152**.

Lentini, M.R., Fraser, S.I., Sumner, H.S. and Davies, R.J. 2010. Geodynamics of the central South Atlantic conjugate margins: implications for hydrocarbon potential. *Petroleum Geoscience*. **16**(3), pp.217–229.

Light, M.P.R., Maslanyj, M.P., Greenwood, R.J. and Banks, N.L. 1993. Seismic sequence stratigraphy and tectonics offshore Namibia. *Geological Society of London Special Publications*. **71**, pp.163–191.

Lymer, G., Cresswell, D.J.F., Reston, T.J., Bull, J.M., Sawyer, D.S., Morgan, J.K., Stevenson, C., Causer, A., Minshull, T.A. and Shillington, D.J. 2019. 3D development of detachment faulting during continental breakup. *Earth and Planetary Science Letters*. **515**, pp.90–99.

Macdonald, K.C., Fox, P.J., Perram, L.J., Eisen, M.F., Haymon, R.M., Miller, S.P., Carbotte, S.M., Cormier, M.-H. and Shor, A.N. 1988. A new view of the mid-ocean ridge from the behaviour of ridge-axis discontinuities. *Nature*. **335**(6187), pp.217–225.

Magee, C. and Jackson, C.A.-L. 2018. How do normal faults grow above dykes? *EarthArXiv*, 14 Dec. 2018, available at:

https://doi.org/10.31223/osf.io/ahxn5.

Manatschal, G. 2004. New models for evolution of magma-poor rifted margins based on a review of data and concepts from West Iberia and the Alps. *International Journal of Earth Sciences*. **93**(3), pp.432–466.

Manatschal, G., Lavier, L.L. and Chenin, P. 2015. The role of inheritance in structuring hyperextended rift systems: Some considerations based on observations and numerical modeling. *Gondwana Research*. **27**(1), pp.140–164.

Maslanyj, M.P., Light, M.P.R., Greenwood, R.J. and Banks, N.L. 1992. Extension tectonics offshore Namibia and evidence for passive rifting in the South Atlantic. *Marine and Petroleum Geology*. **9**, pp.590–601.

Matthews, K.J., Maloney, K.T., Zahirovic, S., Williams, S.E., Seton, M. and Müller, R.D. 2016. Global plate boundary evolution and kinematics since the late Paleozoic. *Global and Planetary Change*. **146**, pp.226–250.

Maus, S., Barckhausen, U., Berkenbosch, H., Bournas, N., Brozena, J., Childers, V., Dostaler, F., Fairhead, J.D., Finn, C., Von Frese, R.R.B., Gaina, C., Golynsky, S., Kucks, R., Lühr, H., Milligan, P., Mogren, S., Müller, R.D., Olesen, O., Pilkington, M., Saltus, R., Schreckenberger, B., Thébault, E. and Tontini, F.C. 2009. EMAG2: A 2-arc min resolution Earth Magnetic Anomaly Grid compiled from satellite, airborne, and marine magnetic measurements. *Geochemistry, Geophysics, Geosystems*. **10**(8).

Maystrenko, Y.P., Scheck-Wenderoth, M., Hartwig, A., Anka, Z., Watts, A.B., Hirsch, K.K. and Fishwick, S. 2013. Structural features of the Southwest African continental margin according to results of lithosphere-scale 3D gravity and thermal modelling. *Tectonophysics*. **604**, pp.104–121.

McDermott, C., Lonergan, L., Collier, J.S., McDermott, K.G. and Bellingham, P. 2018. Characterization of seaward-dipping reflectors along the S. American Atlantic margin and implications for continental breakup. *Tectonics*. (9), pp.3303-3327.

McDermott, K.G., Gillbard, E. and Clarke, N. 2015. From Basalt to Skeletons – the 200 million-year history of the Namibian margin uncovered by new seismic data. *First Break*. **33**(12), pp.77–85.

McKenzie, D. 1978. Some remarks on the development of sedimentary basins. *Earth and Planetary Science Letters*. **40**(1), pp.25–32.

McKenzie, D. 1984. The generation and compaction of partial melts. *J. Petrol.* **25**(September), pp.713–765.

McKenzie, D. and Bickle, M.J. 1988. The volume and composition of melt generated by extension of the lithosphere. *Journal of petrology.* **29**(3), pp.625–679.

Menzies, M. and Klemperer, S. 2002. Characteristics of volcanic rifted margins. *Geological Society of America Special Papers*. **362**, pp.1–14.

Mercier de Lépinay, M., Loncke, L., Basile, C., Roest, W.R., Patriat, M., Maillard, A. and De Clarens, P. 2016. Transform continental margins – Part 2: A worldwide review. *Tectonophysics*. **693**, pp.96–115.

Minshull, T.A., Dean, S.M., White, R.S. and Whitmarsh, R.B. 2008. Anomalous melt production after continental break-up in the southern Iberia Abyssal Plain. *Geological Society, London, Special Publications*. **187**(1), pp.537–550.

Minshull, Timothy A, Lane, C.I., Collier, J.S. and Whitmarsh, R.B. 2008. The relationship between rifting and magmatism in the northeastern Arabian Sea. *Nature Geoscience*. **1**(7), pp. 463–467.

Misra, A.A., Sinha, N. and Mukherjee, S. 2015. Repeat ridge jumps and microcontinent separation : Insights from NE Arabian Sea. *Marine and Petroleum Geology*. **59**, pp.406–428.

Mitchum, R.M.J., Vail, P.R. and Sangree, J.B. 1977. Seismic stratigraphy and global changes of sea level, Part six: stratigraphic interpretation of seismic reflection patterns in depositional sequences. *Seismic Stratigraphy — applications to hydrocarbon exploration*. **165**, pp.117–134.

Mittelstaedt, E., Ito, G. and Van Hunen, J. 2011. Repeat ridge jumps associated with plume-ridge interaction, melt transport, and ridge migration. *Journal of Geophysical Research: Solid Earth*. **116**(B1).

Mohammed, M., Paton, D. a., Collier, R.E.L. and Hodgson, N. 2016. Interaction of crustal heterogeneity and lithospheric processes in determining passive margin architecture on the southern Namibian margin. *Geological Society,*

London, Special Publications. **438**(1), pp. 177-193.

Mohn, G., Manatschal, G., Beltrando, M., Masini, E. and Kusznir, N. 2012. Necking of continental crust in magma-poor rifted margins: Evidence from the fossil Alpine Tethys margins. *Tectonics*. **31**(1).

Morgan, J.P. and Chen, Y.J. 1993. The genesis of oceanic crust: Magma injection, hydrothermal circulation, and crustal flow. *Journal of Geophysical Research: Solid Earth*. **98**(B4), pp.6283–6297.

Morgan, R. and Watts, A.B. 2018. Seismic and gravity constraints on flexural models for the origin of seaward dipping reflectors. *Geophysical Journal International*. **214**(3), pp.2073–2083.

Morley, C.K., Nelson, R.A., Patton, T.L. and Munn, S.G. 1990. Transfer zones in the East African rift system and their relevance to hydrocarbon exploration in rifts. *American Association of Petroleum Geologists Bulletin*. **74**(8), pp.1234–1253.

Moulin, M., Aslanian, D. and Unternehr, P. 2010. A new starting point for the South and Equatorial Atlantic Ocean. *Earth-Science Reviews*. **98**(1–2), pp.1–37.

Müller, R.D., Roest, W.R. and Royer, J.Y. 1998. Asymmetric sea-floor spreading caused by ridge-plume interactions. *Nature*. **396**(6710), pp.455–459.

Müller, R.D., Sdrolias, M., Gaina, C. and Roest, W.R. 2008. Age, spreading rates, and spreading asymmetry of the world's ocean crust. *Geochemistry, Geophysics, Geosystems*. **9**(4) article no: Q04006 [no pagination].

Muntingh, A. and Brown, L.F. 1993. Sequence stratigraphy of Petroleum Plays, Post-Rift Cretaceous Rocks (Lower Aptian to Upper Maastrchtian), Orange Basin, Western Offshore, South Africa *In*: *Siliciclastic Sequence Stratigraphy. Recent Develepments and Apllications*.

Mutter, J., Talwani, M. and Stoffa, P. 1982. Origin of seaward-dipping reflectors in oceanic crust off the Norwegian margin by "subaerial sea-floor spreading". *Geology*. **10**(7), pp.353–357.

Mutter, J.C. 1985. Multichannel seismic images of the oceanic crust's internal structure: Evidence for a magma chamber beneath the Mesozoic Mid-

Atlantic Ridge. *Geology*. **13**(9), pp. 629-632.

Mutter, J.C., Buck, W.R. and Zehnder, C.M. 1988. Convective partial melting 1. A model for the formation of thick basaltic sequences during the initiation of spreading. *Journal of Geophysical Research*. **93**(B2), pp.1031–1048.

Mutter, J.C. and Carton, H.D. 2013. The mohorovicic discontinuity in ocean basins: Some observations from seismic data. *Tectonophysics*. **609**, pp.314–330.

Naliboff, J.B., Buiter, S.J.H., Péron-Pinvidic, G., Osmundsen, P.T. and Tetreault, J. 2017. Complex fault interaction controls continental rifting. *Nature Communications*. **8**(1), article no. 1179

Nelson, C.E., Jerram, D. a. and Hobbs, R.W. 2009. Flood basalt facies from borehole data: implications for prospectivity and volcanology in volcanic rifted margins. *Petroleum Geoscience*. **15**(4), pp.313–324.

Nemčok, M. and Rybár., S. 2017. Rift–drift transition in a magma-rich system: the Gop Rift–Laxmi Basin case study, West India. *Geological Society, London, Special Publications*. **445**(1), pp.95–117.

Nielsen, T.K. and Hopper, J.R. 2002. Formation of volcanic rifted margins: Are temperature anomalies required? *Geophysical Research Letters*. **29**(21).

Nielsen, T.K., Larsen, H.C. and Hopper, J.R. 2002. Contrasting rifted margin styles south of Greenland: Implications for mantle plume dynamics. *Earth and Planetary Science Letters*. **200**(3–4), pp.271–286.

Norcliffe, J.R., Paton, D.A., Mortimer, E.J., McCaig, A.M., Nicholls, H., Rodriguez, K., Hodgson, N. and Van Der Spuy, D. 2018. Laterally Confined Volcanic Successions (LCVS); recording rift-jumps during the formation of magma-rich margins. *Earth and Planetary Science Letters*. **504**, pp.53–63.

Norton, I.O., Carruthers, D.T. and Hudec, M.R. 2015. Rift to drift transition in the South Atlantic salt basins: A new flavor of oceanic crust. *Geology*. **44**(1), pp. 55-58.

O'Connor, J.M. and Duncan, R. a. 1990. Evolution of the Walvis Ridge-Rio Grande Rise Hot Spot System: Implications for African and South American Plate motions over plumes. *Journal of Geophysical Research*. **95**, p.17475-17502.

Ogilvie, J.S., Crompton, R. and Hardy, N.M. 2001. Characterization of volcanic units using detailed velocity analysis in the Atlantic Margin, West of Shetlands, United Kingdom. *The Leading Edge*. **20**(01), pp.34–50.

Oh, J., Austin, J.A., Phillips, J.D., Coffin, M.F. and Stoffa, P.L. 1995. Seaward-dipping reflectors offshore the southeastern United States : Seismic evidence for extensive volcanism accompanying sequential formation of the Carolina trough and Blake Plateau basin Along the Hinge Zone. *Geology*. **23**(1), pp.9–12.

Osmundsen, P.T. and Ebbing, J. 2008. Styles of extension offshore mid-Norway and implications for mechanisms of crustal thinning at passive margins. *Tectonics*. **27**(6), pp.1–25.

Osmundsen, P.T. and Péron-Pinvidic, G. 2018. Crustal-Scale Fault Interaction at Rifted Margins and the Formation of Domain-Bounding Breakaway Complexes: Insights From Offshore Norway. *Tectonics*. **37**(3), pp.935–964.

Osmundsen, P.T., Sommaruga, A., Skilbrei, J.R. and Olesen, O. 2002. Deep structure of the Mid Norway rifted margin. *Norsk Geologisk Tidsskrift*. **82**(4), pp.205–224.

Pálmason, G. 1973. Kinematics and heat flow in a volcanic rift zone with application to Iceland. *Geophysical Journal of the Royal Astronomical Society*. **26**, pp.515–535.

Palmason, G. and Saemundsson, K. 1974. Iceland in Relation to the Mid-Atlantic Ridge. *Annual Review of Earth and Planetary Sciences*. **2**(1), pp.25–50.

Pángaro, F. and Ramos, V. a. 2012. Paleozoic crustal blocks of onshore and offshore central Argentina: New pieces of the southwestern Gondwana collage and their role in the accretion of Patagonia and the evolution of Mesozoic south Atlantic sedimentary basins. *Marine and Petroleum Geology*. **37**(1), pp.162–183.

Paton, D. A., Mortimer, E.J., Hodgson, N. and Van Der Spuy, D. 2016. The missing piece of the South Atlantic jigsaw - when continental break-up ignores crustal heterogeneity. *Petroleum Geoscience of the West Africa Margin, Geological Society, London, Special Publications*. **438**.

Paton, D. A., Pindell, J., McDermott, K.G., Bellingham, P., Horn, B.W. and Repository, G.S.A.D. 2017. Evolution of seaward-dipping reflectors at the onset of oceanic crust formation at volcanic passive margins: Insights from the South Atlantic. *Geology*. **45**(5), pp. 439-442.

Paton, D. A., di Primio, R., Kuhlmann, G., van der Spuy, D. and Horsfield, B. 2007. Insights into the Petroleum System Evolution of the southern Orange Basin, South Africa. *South African Journal of Geology*. **110**, pp.261–274.

Paton, D. A., van der Spuy, D., di Primio, R. and Horsfield, B. 2008. Tectonically induced adjustment of passive-margin accommodation space; influence on the hydrocarbon potential of the Orange Basin, South Africa. *AAPG Bulletin*. **92**(5), pp.589–609.

Pérez-Diaz, L. and Eagles, G. 2014. Constraining South Atlantic growth with seafloor spreading data. *Tectonics*. **33**(9), pp.1848–1873.

Pérez-Gussinyé, M., Morgan, J.P., Reston, T.J. and Ranero, C.R. 2006. The rift to drift transition at non-volcanic margins: Insights from numerical modelling. *Earth and Planetary Science Letters*. **244**(1–2), pp.458–473.

Pérez-Gussinyé, M., Reston, T.J. and Phipps Morgan, J. 2008. Serpentinization and magmatism during extension at non-volcanic margins: the effect of initial lithospheric structure. *Geological Society, London, Special Publications*. **187**(1), pp.551–576.

Péron-Pinvidic, G. and Manatschal, G. 2008. The final rifting evolution at deep magma-poor passive margins from Iberia-Newfoundland: a new point of view. *International Journal of Earth Sciences*. **98**(7), pp.1581–1597.

Péron-Pinvidic, G., Manatschal, G., Masini, E., Sutra, E., Flament, J.M., Haupert, I. and Unternehr, P. 2015. Unravelling the along-strike variability of the Angola–Gabon rifted margin: a mapping approach. *Geological Society, London, Special Publications*. **438**(1), pp.49–76.

Péron-Pinvidic, G., Manatschal, G. and Osmundsen, P.T. 2013. Structural comparison of archetypal Atlantic rifted margins: A review of observations and concepts. *Marine and Petroleum Geology*. **43**, pp.21–47.

Péron-Pinvidic, G., Osmundsen, P.T. and Ebbing, J. 2016. Mismatch of geophysical datasets in distal rifted margin studies. *Terra Nova*. **28**(5), pp.

340-347.

Phillips, T.B., Magee, C., Jackson, C.A.L. and Bell, R.E. 2018. Determining the three-dimensional geometry of a dike swarm and its impact on later rift geometry using seismic reflection data. *Geology*. **46**(2), pp.119–122.

Pindell, J., Graham, R. and Horn, B.W. 2014. Rapid outer marginal collapse at the rift to drift transition of passive margin evolution, with a Gulf of Mexico case study. *Basin Research*. **26**(6), pp.701–725.

Planke, S., Alvestad, E. and Eldhom, O. 1999. Seismic characteristics of basaltic extrusive and intrusive rocks. *The Leading Edge*. **18**(3), pp.342–348.

Planke, S. and Eldhom, O. 1994. Seismic response and construction of seaward dipping wedges of flood basalts : Voring volcanic margin. *Journal of Geophysical Research: Solid Earth*. **99**(B5), pp.9263–9278.

Planke, S., Rasmussen, T., Rey, S.S. and Myklebust, R. 2005. Seismic characteristics and distribution of volcanic intrusions and hydrothermal vent complexes in the Vøring and Møre basins. *Geological Society, London, Petroleum Geology Conference series*. **6**, pp.833–844.

Planke, S., Symonds, P.A., Alvestad, E. and Skogseid, J. 2000. Seismic volcanostratigraphy of large-volume basaltic extrusive complexes on rifted margins. *Journal of Geophysical Research: Solid Earth*. **105**(B8), pp.19335–19351.

Quirk, D.G. and Hertle, M. 2013. Rifting, subsidence and continental break-up above a mantle plume in the central South Atlantic. *Geological Society, London, Special Publication.* **269**(1), pp.185–214.

Quirk, D.G., Shakerley, A. and Howe, M.J. 2014. A mechanism for construction of volcanic rifted margins during continental breakup. *Geology*. **42**(12), pp.1079–1082.

Ranero, C.R., Reston, T., Belykh, I. and Gnibidenko, H. 1997. Reflective oceanic crust formed at a fast-spreading center in the Pacific. *Geology*. **25**(6), pp.499–502.

Reston, T. 2005. Polyphase faulting during the development of the west Galicia rifted margin. *Earth and Planetary Science Letters*. **237**(3–4), pp.561–576.

Reston, T. 2009. The structure, evolution and symmetry of the magma-poor rifted margins of the North and Central Atlantic: A synthesis. *Tectonophysics*. **468**(1–4), pp.6–27.

Reston, T., Ranero, C.R. and Belykh, I. 1999. The structure of Cretaceous oceanic crust of the NW Pacific: Constraints on processes at fast spreading centers. *Journal of Geophysical Research*. **104**, p.629.

Reston, T.J. and Morgan, J.P. 2004. Continental geotherm and the evolution of rifted margins. *Geology*. **32**(2), pp.133–136.

Reuber, K.R. 2017. *Crustal Structure and Mesozoic Tectonic Evolution of Conjugate Volcanic Passive Margins of the South-Central and South Atlantic Oceans*. PhD Thesis, University of Houston.

Reuber, K.R., Pindell, J. and Horn, B.W. 2016. Demerara Rise , offshore Suriname : Magma-rich segment of the Central Atlantic Ocean , and conjugate to the Bahamas hot spot. *Interpretation*. **4**(2), pp.131-155

Rey, S.S., Planke, S., Symonds, P.A. and Faleide, J.I. 2008. Seismic volcanostratigraphy of the Gascoyne margin, Western Australia. *Journal of Volcanology and Geothermal Research*. **172**(1–2), pp.112–131.

Rivalta, E., Taisne, B., Bunger, A.P. and Katz, R.F. 2015. A review of mechanical models of dike propagation: Schools of thought, results and future directions. *Tectonophysics*. **638**, pp.1–42.

Roberts, A.M., Alvey, A.D. and Kusznir, N.J. 2018. Crustal structure and heat-flow history in the UK Rockall Basin, derived from backstripping and gravity-inversion analysis. *Petroleum Geoscience*. **25**(2), pp. 131-150.

Roberts, D.G., Backman, J., Morton, A.C., Murray, J.W. and Keene, J.B. 1984. 39. Evolution of Volcanic Rifted Margins: Synthesis of Leg 81 Results on the Western Margin of the Rockall Plateau. *Initial Reports of the Deep Sea Drilling Project 81*., pp.883–991.

Sawyer, D.S., Coffin, M.F., Reston, T.J., Stock, J.M. and Hopper, J.R. 2007. COBBOOM: The Continental Breakup and Birth of Oceans Mission. *Scientific Drilling*. **5**, pp.13–25.

Senkans, A., Leroy, S., D'Acremont, E., Castilla, R. and Despinois, F. 2018. Polyphase rifting and break-up of the central Mozambique margin. *Marine*

and Petroleum Geology. **100**, pp.412–433.

Séranne, M. and Anka, Z. 2005. South Atlantic continental margins of Africa: A comparison of the tectonic vs climate interplay on the evolution of equatorial west Africa and SW Africa margins. *Journal of African Earth Sciences*. **43**(1–3), pp.283–300.

Sheriff, R.E. 1980. *Seismic Stratigraphy*. Boston: IHRDC.

Shillington, D.J., Scott, C.L., Minshull, T.A., Edwards, R.A., Brown, P.J. and White, N. 2009. Abrupt transition from magma-starved to magma-rich rifting in the eastern Black Sea. *Geology*. **37**(1), pp.7–10.

Sigmundsson, F., Hooper, A., Hreinsdóttir, S., Vogfjörd, K.S., Ófeigsson, B.G., Heimisson, E.R., Dumont, S., Parks, M., Spaans, K., Gudmundsson, G.B., Drouin, V., Árnadóttir, T., Jónsdóttir, K., Gudmundsson, M.T., Högnadóttir, T., Fridriksdóttir, H.M., Hensch, M., Einarsson, P., Magnússon, E., Samsonov, S., Brandsdóttir, B., White, R.S., Ágústsdóttir, T., Greenfield, T., Green, R.G., Hjartardóttir, Á.R., Pedersen, R., Bennett, R.A., Geirsson, H., la Femina, P.C., Björnsson, H., Pálsson, F., Sturkell, E., Bean, C.J., Möllhoff, M., Braiden, A.K. and Eibl, E.P.S. 2014. Segmented lateral dyke growth in a rifting event at Bárðarbunga volcanic system, Iceland. *Nature*. **517**(7533), pp. 191-195.

Skogseid, J. 1994. Dimensions of the Late Cretaceous-Paleocene Northeast Atlantic rift derived from Cenozoic subsidence. *Tectonophysics*. **240**(1–4), pp.225–247.

Skogseid, J. 2000. NE Atlantic continental rifting and volcanic margin formation. *Geological Society, London, Special Publications.* **167**(1), pp.295-326.

Skogseid, J. 2001. Volcanic margins: Geodynamic and exploration aspects. *Marine and Petroleum Geology*. **18**(4), pp.457–461.

Smallwood, J.R. and White, R.S. 2012. Ridge-plume interaction in the North Atlantic and its influence on continental breakup and seafloor spreading Ridge-plume interaction in the North Atlantic and its influence on continental breakup and seafloor spreading. *Geological Society, London, Special Publications.* **197**(1), pp.15–37.

Soto, M., Morales, E., Veroslavsky, G., de Santa Ana, H., Ucha, N. and

Rodríguez, P. 2011. The continental margin of uruguay: Crustal architecture and segmentation. *Marine and Petroleum Geology*. **28**(9), pp.1676–1689.

Stewart, J., Watts, A.B. and Bagguley, J.G. 2000. Three-dimensional subsidence analysis and gravity modelling of the continental margin offshore Namibia. *Geophysical Journal International*. **141**, pp.724–746.

Stica, J.M., Zalán, P.V. and Ferrari, A.L. 2014. The evolution of rifting on the volcanic margin of the Pelotas Basin and the contextualization of the Paraná–Etendeka LIP in the separation of Gondwana in the South Atlantic. *Marine and Petroleum Geology*. **50**, pp.1–21.

Taposeea, C.A., Armitage, J.J. and Collier, J.S. 2016. Asthenosphere and lithosphere structure controls on early onset oceanic crust production in the southern South Atlantic. *Tectonophysics*. **716**, pp.4–20.

Tian, X. and Buck, W.R. 2019. Lithospheric Thickness of Volcanic Rifting Margins: Constraints From Seaward Dipping Reflectors. *Journal of Geophysical Research: Solid Earth*. **124**(4), pp.3254-3270.

Torsvik, T.H., Rousse, S., Labails, C. and Smethurst, M. a. 2009. A new scheme for the opening of the South Atlantic Ocean and the dissection of an Aptian salt basin. *Geophysical Journal International*. **177**(3), pp.1315–1333.

Tugend, J., Gillard, M., Manatschal, G., Nirrengarten, M., Harkin, C., Epin, M., Sauter, D., Autin, J., Kusznir, N. and McDermott, K.G. 2018. Reappraisal of the magma-rich versus magma-poor rifted margin archetypes. *Geological Society, London, Special Publications*., **476**, article no. SP476-9.

Tugend, J., Manatschal, G., Kusznir, N. and Masini, E. 2015. Characterizing and identifying structural domains at rifted continental margins: application to the Bay of Biscay margins and its Western Pyrenean fossil remnants. *Geological Society, London, Special Publications*. **413**(1), pp.171–203.

Unternehr, P., Curie, D., Olivet, J.L., Goslin, J. and Beuzart, P. 1988. South Atlantic fits and intraplate boundaries in Africa and South America. *Tectonophysics*. **155**, pp.169–179.

Unternehr, P., Péron-Pinvidic, G., Manatschal, G. and Sutra, E. 2010. Hyper-

extended crust in the South Atlantic: in search of a model. *Petroleum Geoscience*. **16**(3), pp.207–215.

Walker, G.P.L. 1965. Evidence of crustal drift from Icelandic geology. *Philosophical Transactions of the Royal Society of London.* **258**(1088), pp.199–204.

White, R.S., Bown, J.W. and Smallwood, J.R. 1995. The temperature of the Iceland plume and origin of outward-propagating V-shaped ridges. *Journal of the Geological Society*. **152**, pp.1039–1045.

White, R.S. and McKenzie, D. 1989. Magmatism at rift zones: The generation of volcanic continental margins and flood basalts. *Journal of Geophysical Research*. **94**(B6), pp.7685-7729.

White, R.S., McKenzie, D. and O'Nions, R.K. 1992. Oceanic crustal thickness from seismic measurements and rare earth element inversions. *Journal of Geophysical Research*. **97**(B13), p.19683-19715.

White, R.S., Smith, L.K., Roberts, A.W., Christie, P.A.F., Kusznir, N.J., Roberts, A.M., Healy, D., Spitzer, R., Chappell, A., Eccles, J.D., Fletcher, R., Hurst, N., Lunnon, Z., Parkin, C.J. and Tymms, V.J. 2008. Lower-crustal intrusion on the North Atlantic continental margin. *Nature*. **452**(7186), pp.460–464.

White, R.S., Spence, G.D., Fowler, S.R., McKenzie, D.P., Westbrook, G.K. and Bowen, A.N. 1987. Magmatism at rifted continental margins. *Nature*. **330**(6147), pp.439–444.

Whitmarsh, R.B., Manatschal, G. and Minshull, T. A. 2001. Evolution of magma-poor continental margins from rifting to seafloor spreading. *Nature*. **413**(6852), pp.150–154.

Wickens, H.D. V and McLachlan, I.R. 1990. The stratigraphy and seidmentology of the reservoir interval of the Kudu 9A-2 and 9A-3 boreholes. *Communications of the Geological Survey of Namibia*. **6**, pp.9–22.

van Wijk, J.W., Huismans, R.S., ter Voorde, M. and Cloetingh, S.A.P.. 2001. Melt generation at volcanic continental margins: No need for a mantle plume? *Geophysical Research Letters*. **28**(20), pp.3995–3998.

Wolfenden, E., Ebinger, C.J., Yirgu, G., Renne, P.R. and Kelley, S.P. 2005. Evolution of a volcanic rifted margin: Southern Red Sea, Ethiopia.

Geological Society of America Bulletin. **117**(7–8), pp.846–864.

Wright, T.J., Ebinger, C.J., Biggs, J., Ayele, A., Yirgu, G., Keir, D. and Stork, A. 2006. Magma-maintained rift segmentation at continental rupture in the 2005 Afar dyking episode. *Nature*. **442**(7100), pp.291–294.

Wright, T.J., Sigmundsson, F., Pagli, C., Belachew, M., Hamling, I.J., Brandsdóttir, B., Keir, D., Pedersen, R., Ayele, A., Ebinger, C.J., Einarsson, P., Lewi, E. and Calais, E. 2012. Geophysical constraints on the dynamics of spreading centres from rifting episodes on land. *Nature Geoscience*. **5**(4), pp.242–250.

Appendix A

A.1. Seismic velocity analysis

Interval velocity can be a distinguishing feature of a seismic facies unit (Mitchum et al., 1977). Here, semblance analysis was used to estimate the velocity-depth profiles of several seismic facies units. Below an overview of the technique is provided, alongside a description of how the raw seismic data were prepared for analysis.

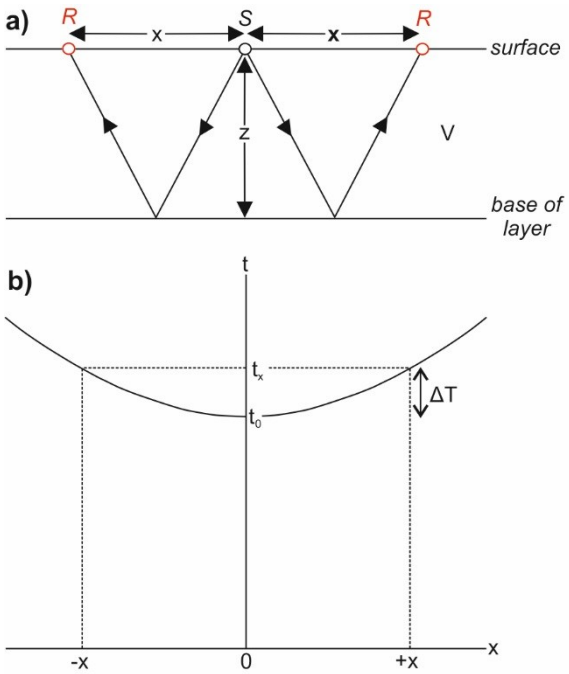

Figure A.1. a) Reflected raypaths from source (S) to receivers (R). Rays are reflected off the base of a horizontal layer with velocity (V). The depth of the basal surface is located at depth z. Both receivers are offset from the source by distance x. b) graph showing travel time (t) vs offset (x) for reflections off the base of a single layer with uniform velocity and thickness. 'Travel time' is the time taken for the reflected ray to travel from the source to the receiver. Figure is modified from Kearey et al. (2002).

A.1. The velocity of a single horizontal layer

The time taken for a wave to travel from source to receiver is known as travel time (t). If we consider a horizontal layer (Figure A.1a) with constant velocity (V), then the travel time of a ray reflected off its base can be calculated by:

Equation A.1

$$t = \frac{(x^2 + 4z^2)^{1/2}}{V}$$

Where x is the offset between the source and the receiver and z is the depth to the base of the layer (Figure A.1a).

In a typical seismic reflection survey, both V and z are unknown, meaning data from a single source-receiver pair are insufficient to solve this equation. However, seismic data are commonly acquired across a range of offsets. A consequence of this is that we can analyse variations in travel time with offset to statistically estimate V and z. As source-receiver offset increases, travel time also increases (Figure A.1b), resulting in a relationship known as *moveout*. The amount of *moveout* recorded can be used to estimate the velocity of a layer.

At zero-offset, the ray travels vertically from source to receiver and hence travel time (t_0) can be calculated via:

Equation A.2

$$t_0 = \frac{2z}{V}$$

It follows that where x is greater than 0, the travel time will be greater than t_0. At the offsets typical in seismic reflection surveying, moveout is approximately hyperbolic (Figure A.1b). Therefore, travel time at offset x (t_x) can be calculated by the following truncated binomial equation:

Equation A.3

$$t_x \approx t_0 + \frac{x^2}{2V^2 t_0}$$

Normal moveout (ΔT), or NMO, is defined as the difference between the travel time at offset x (t_x) and zero-offset (t_0):

Equation A.4

$$\Delta T = t_x - t_o \approx \frac{x^2}{2V^2 t_0}$$

Given that x, t_0, and ΔT are known, this equation can be re-arranged to calculate velocity:

Equation A.5

$$V \approx \frac{x}{(2t_0 \Delta T)^{1/2}}$$

A.2. velocities in a multi-layered subsurface

The equations shown above are valid for a single layer with a homogeneous velocity. In practise, the rays recorded at a receiver will have travelled through many layers with varying velocities. Hence these relationships have to be adapted for reflections from the *n*th layer in a multi-layered subsurface (Figure A.2).

Inter-layer variations in velocity will cause the ray path to diffract at interfaces. These diffractions lead to markedly different raypaths (Figure A.2) than those characterising a single homogeneous layer (Figure A.1a), resulting in a breakdown of the simple NMO relationship presented above.

In order to estimate NMO in a multi-layered subsurface, the homogeneous velocity V should be replaced with an average velocity (V_{av}) of all of the layers that the ray has travelled through. In general, velocity increases with depth and hence V_{av} should be weighted towards these higher velocities. The Root-Mean-Square Velocity (V_{rms}) offers one such weighted average:

Equation A.6

$$V_{rms} = \sqrt{\frac{\sum_{i=1}^{n} v_i^2 \, t_i}{\sum_{i=1}^{n} t_i}}$$

V_{rms} can then be used to calculate travel time at offset x for reflections from the *n*th layer:

Equation A.7

$$t_n \approx t_0 + \frac{x^2}{2V_{rms}^2 t_0}$$

Through adapting the equations shown in section A.1, it follows that NMO at the nth reflector ($\Delta T_{n)}$ can also be calculated:

Equation A.8

$$\Delta T_n = \frac{x^2}{2V_{rms}^2 t_0}$$

If V_{rms} is calculated for the top (n-1) and base (n) of a layer then the interval velocity of the layer (V_n) can be calculated using the Dix equation (Dix, 1955):

Equation A.9

$$V_n = \sqrt{\frac{V_{rms,n}^2 t_n - V_{rms,n-1}^2 t_{n-1}}{2V^2 t_0}}$$

Where t_n is the travel time for the ray reflected off the base of layer n, and t_{n-1} is the travel time for that reflected off the base of layer n-1 (which is also the top of layer n).

The interval velocity resulting from this calculation is itself an average of the velocity field across a specified interval. Depending on the resolution of the study, this interval can consist of one or many seismically resolved layers.

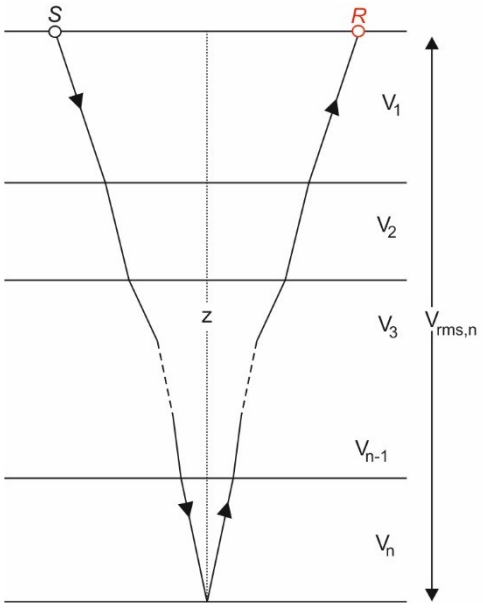

Figure A.2. Ray path from source (S) to receiver (R) through a multi-layered subsurface. Each layer has a uniform velocity, V. The raypath refracts at layer interfaces due to velocity variations between layers. Here, the reflected raypath to the base of the *n*th layer is shown. Modified from Kearey et al. (2002).

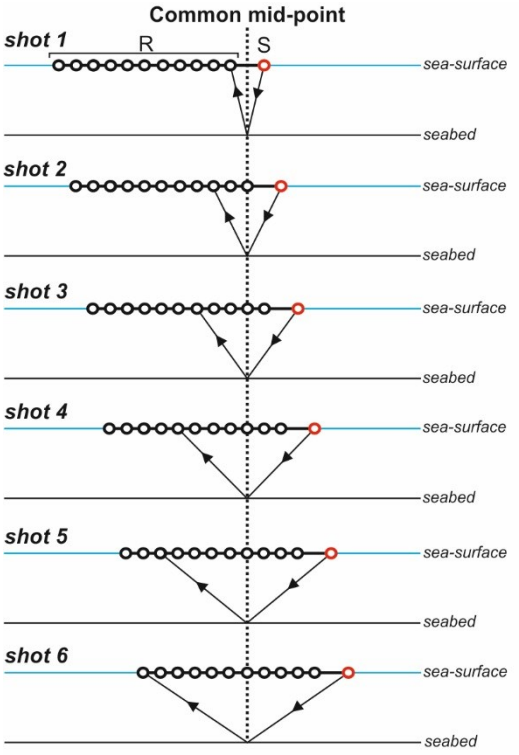

Figure A.3. Schematic representation of a 2D marine seismic reflection survey. After each shot the entire array is moved a specified distance. A consequence is that several source-receiver pairs share a common mid-point. Modified from Kearey et al. (2002).

A.3. Velocity analysis

Multichannel seismic reflection surveying is characterised by one source and many receivers (Figure A.3). After each shot the entire array is moved a specified distance, meaning that reflections from the same subsurface location are recorded across a range of source-receiver offsets (Figure A.3). Raw seismic reflection data are commonly stored in *common shot gathers*, meaning all of the traces recording one shot are stored together. For processing purposes, these common shot gathers are often re-sorted into *common mid-point* (CMP) *gathers*, each of which contains all of the traces recorded from a common source-receiver midpoint. This midpoint is calculated geographically as a point either on the seabed, at sea-level, or on the land-surface (Figure A.3). Assuming near-horizontal layering, each trace within a CMP gather will contain reflections from all of the interfaces located vertically beneath the midpoint. As offset increases, reflections from the same subsurface interface will show moveout. If a CMP gather is ordered such that TWTT is shown on the Y-axis, and source-receiver offset on the x-axis, then this moveout should be visually evident (Figure A.4).

The technique of semblance analysis was developed to enable the *stacking* of reflections within a CMP gather. *Stacking* refers to the addition of reflections from the same subsurface location that are recorded across a range of offsets.

This process is undertaken in order to boost the amplitude of primary reflections and decrease the prevalence of coherent and incoherent noise. In order to stack reflections from the same subsurface location, the amount of moveout must be calculated, which is reliant on velocity estimation.

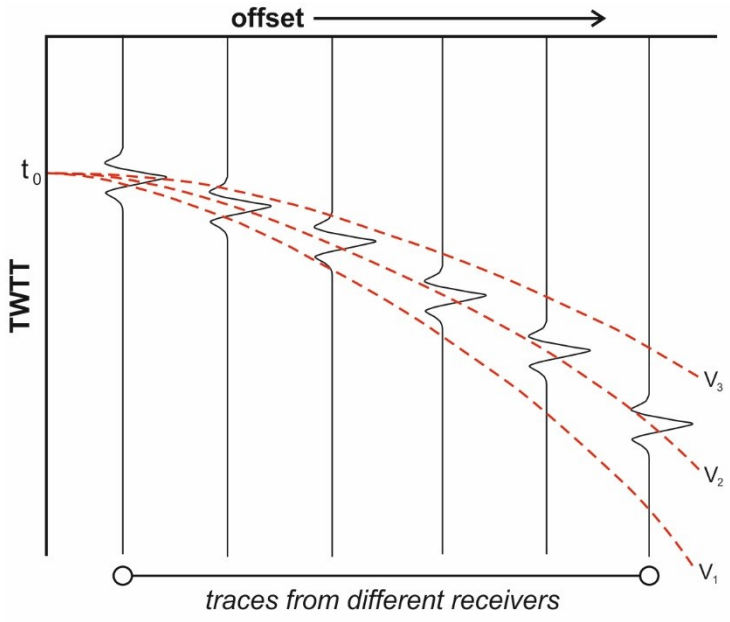

Figure A.4. Schematic representation of a CMP gather containing one reflection recorded across numerous offsets. For the t_0 of this reflection, the NMO equation has been solved with three different velocities (V_1, V_2, V_3). The hyperbolas resulting from these calculations are plotted onto the gather (red dashed lines). The hyperbola produced by V_2 provides the best match to the observed moveout, this is a case where *semblance* is high.

Semblance analysis is one such method of estimating subsurface velocities. During this procedure the NMO equation for a multi-layered subsurface is solved using a range of velocities and at a set t_0-interval within a CMP gather (Figure A.4). The hyperbolas resulting from these calculations are plotted onto the gather, where they intersect the reflections recorded across a range of offsets (Figure A.4). A measurement of similarity, known as *semblance*, is made between the reflections a hyperbola intersects. Where semblance is high, all of the reflections intersected by the hyperbola are similar (e.g. V_2 in Figure A.4). An inference of this situation is that all of these reflections are from the same subsurface interface. Conversely, where semblance is low, the hyperbola is considered to intersect reflections from different interfaces (e.g. V_a and V_2 in Figure A.4).

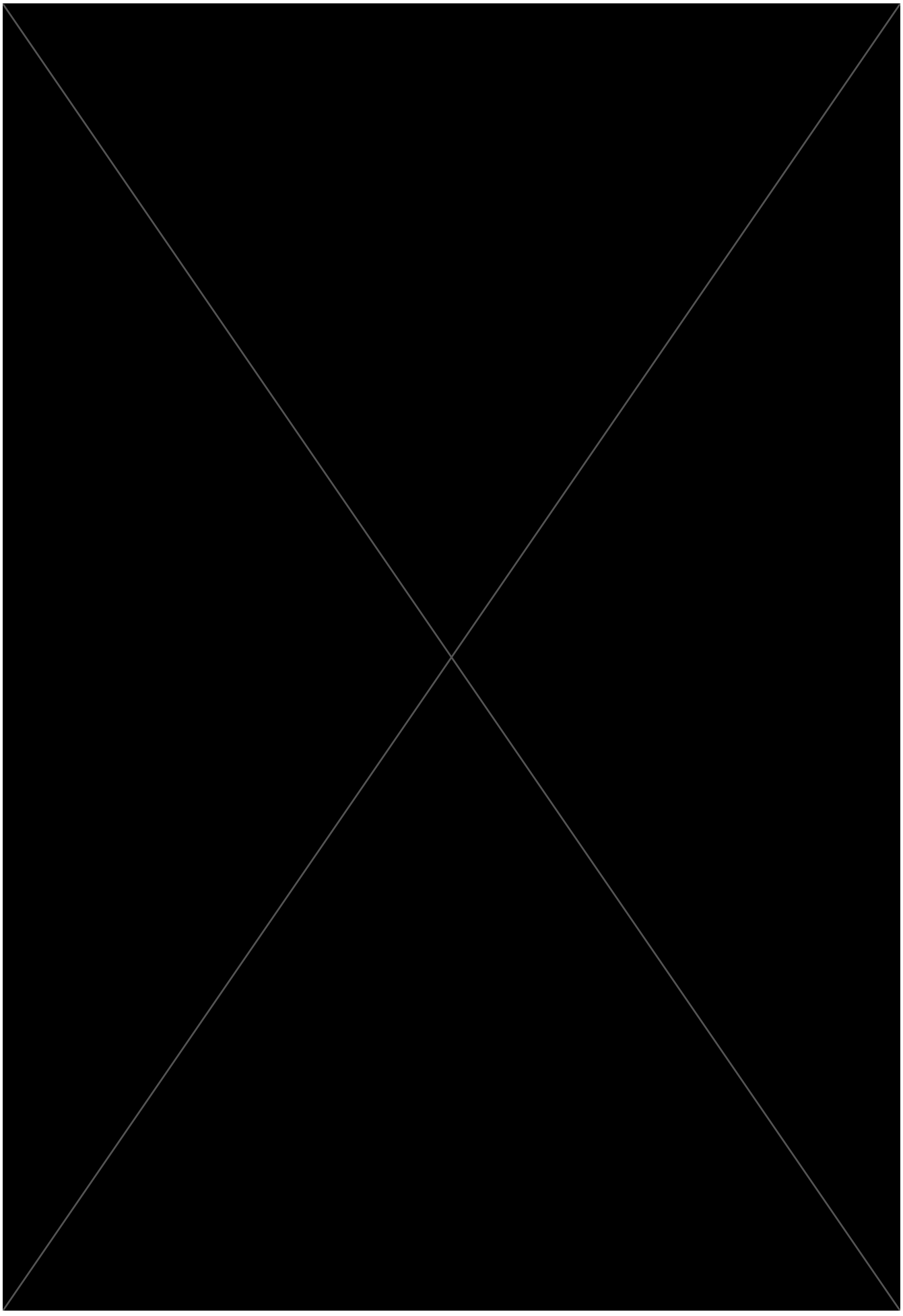

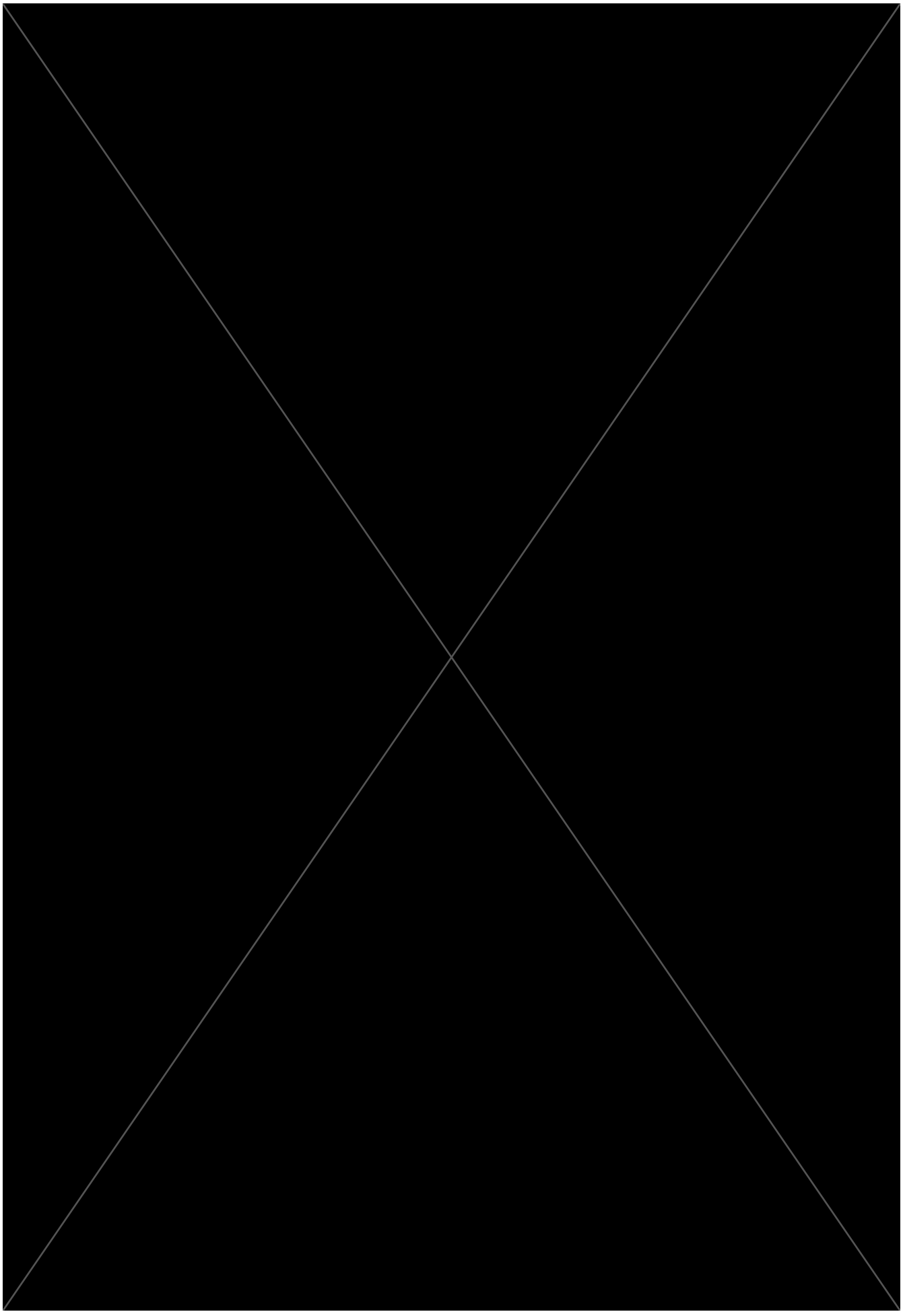

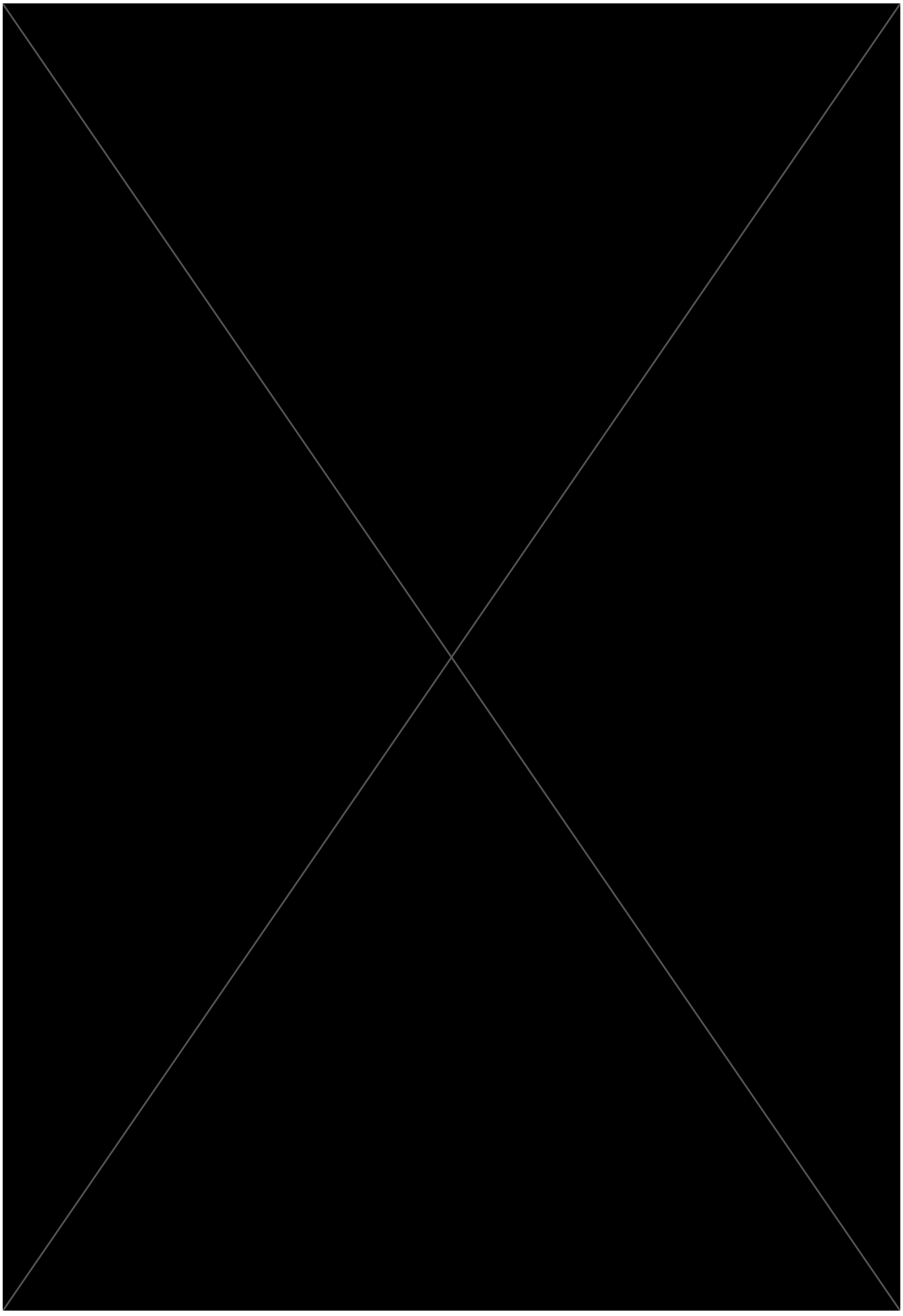

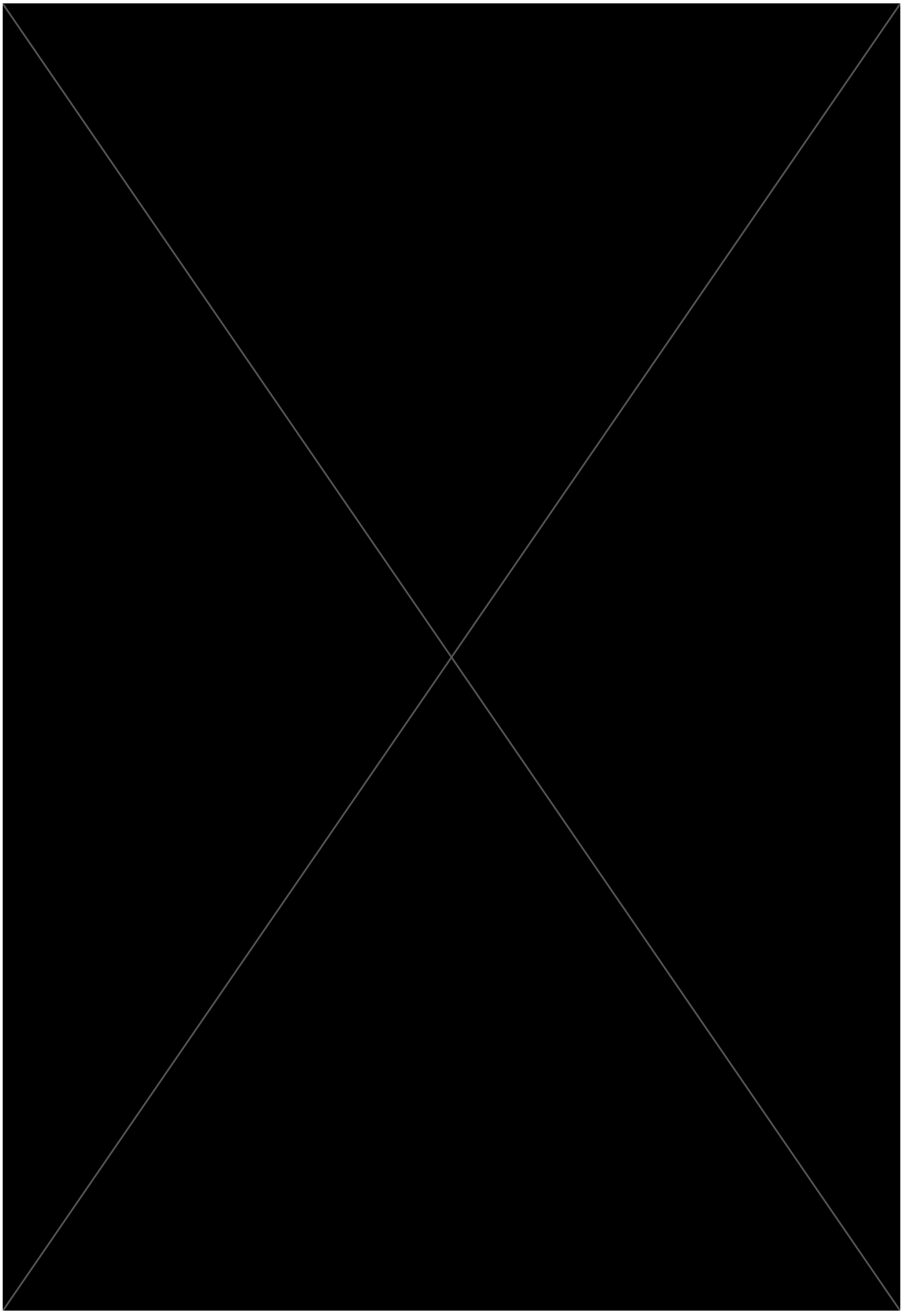

Appendix C

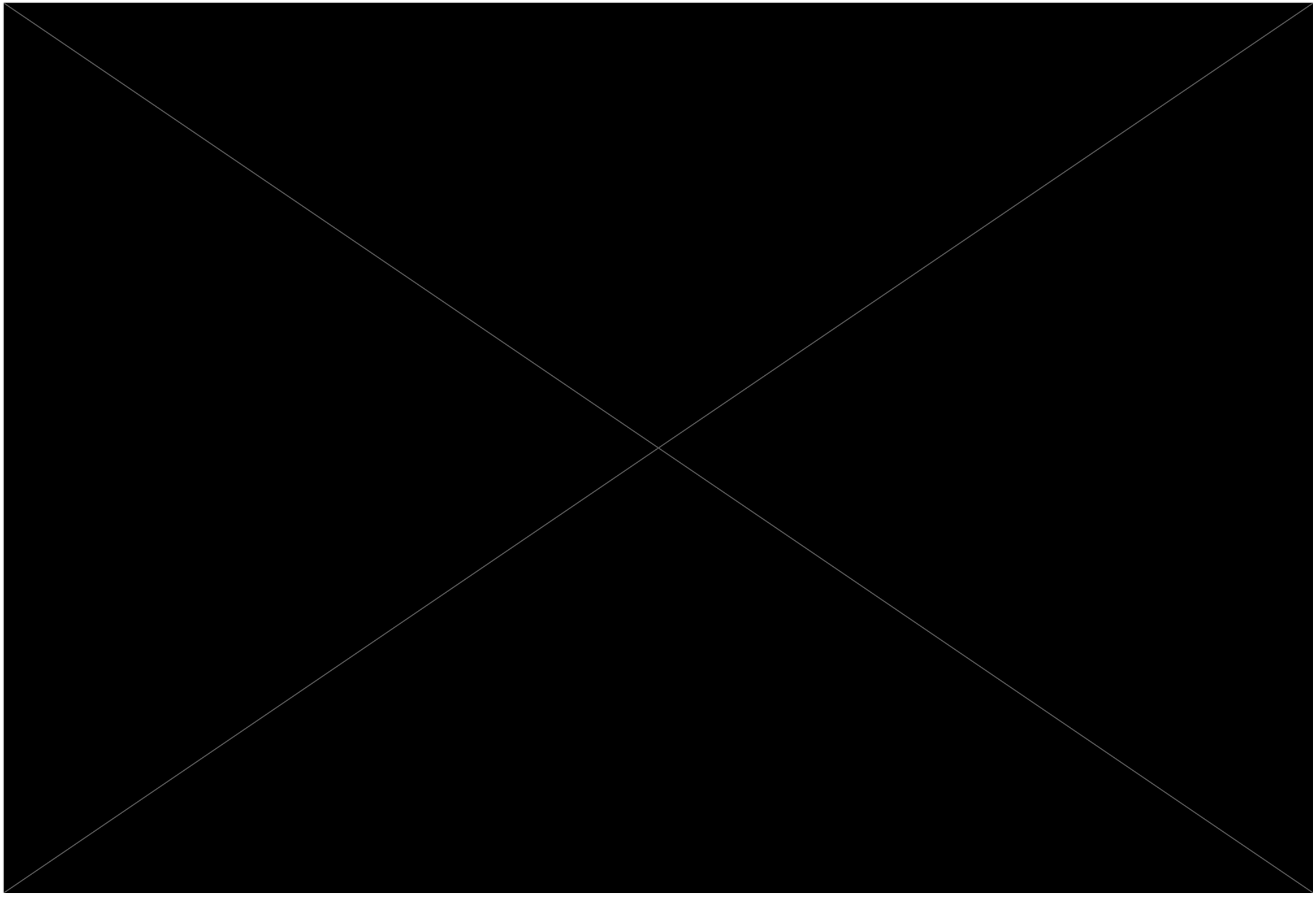

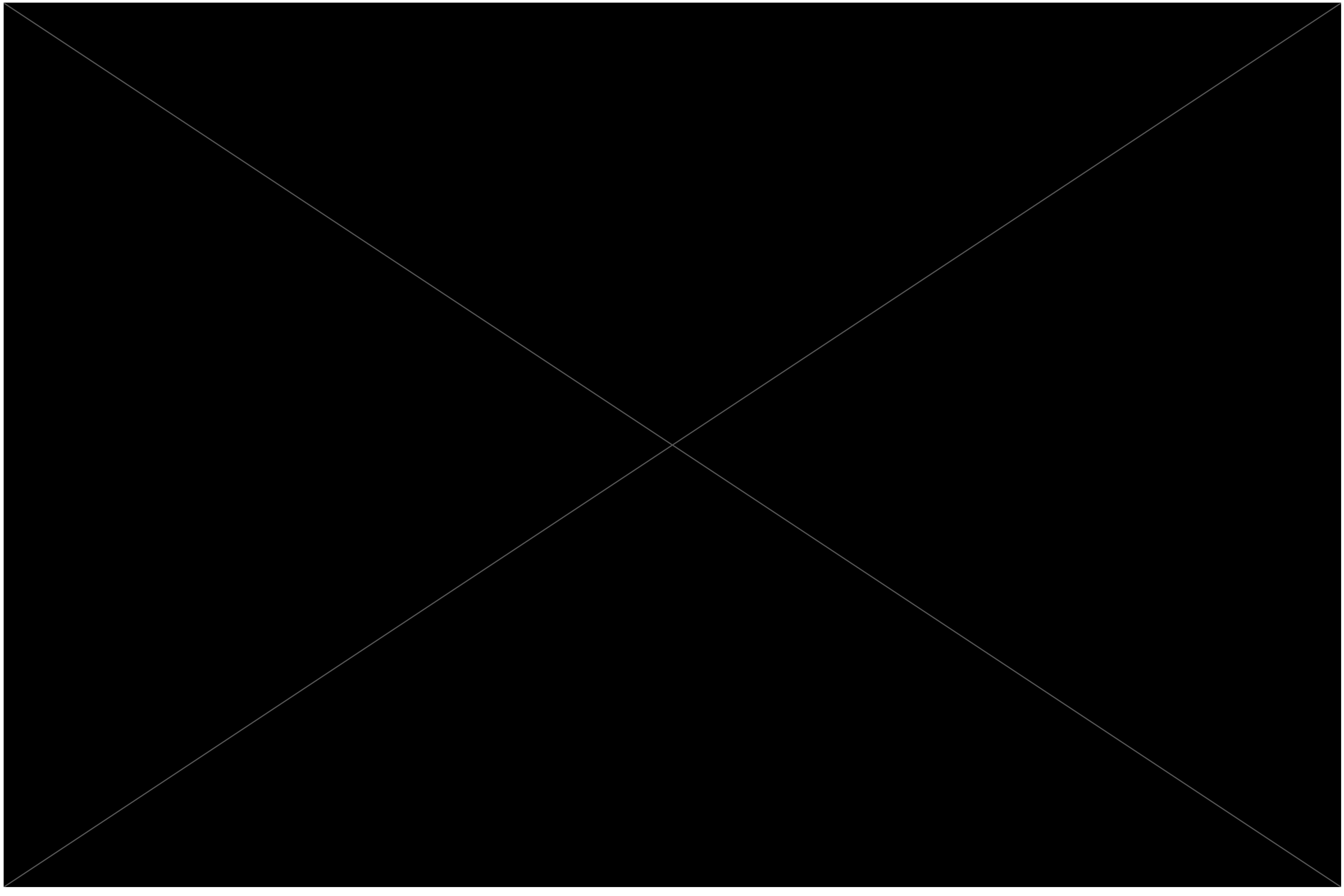

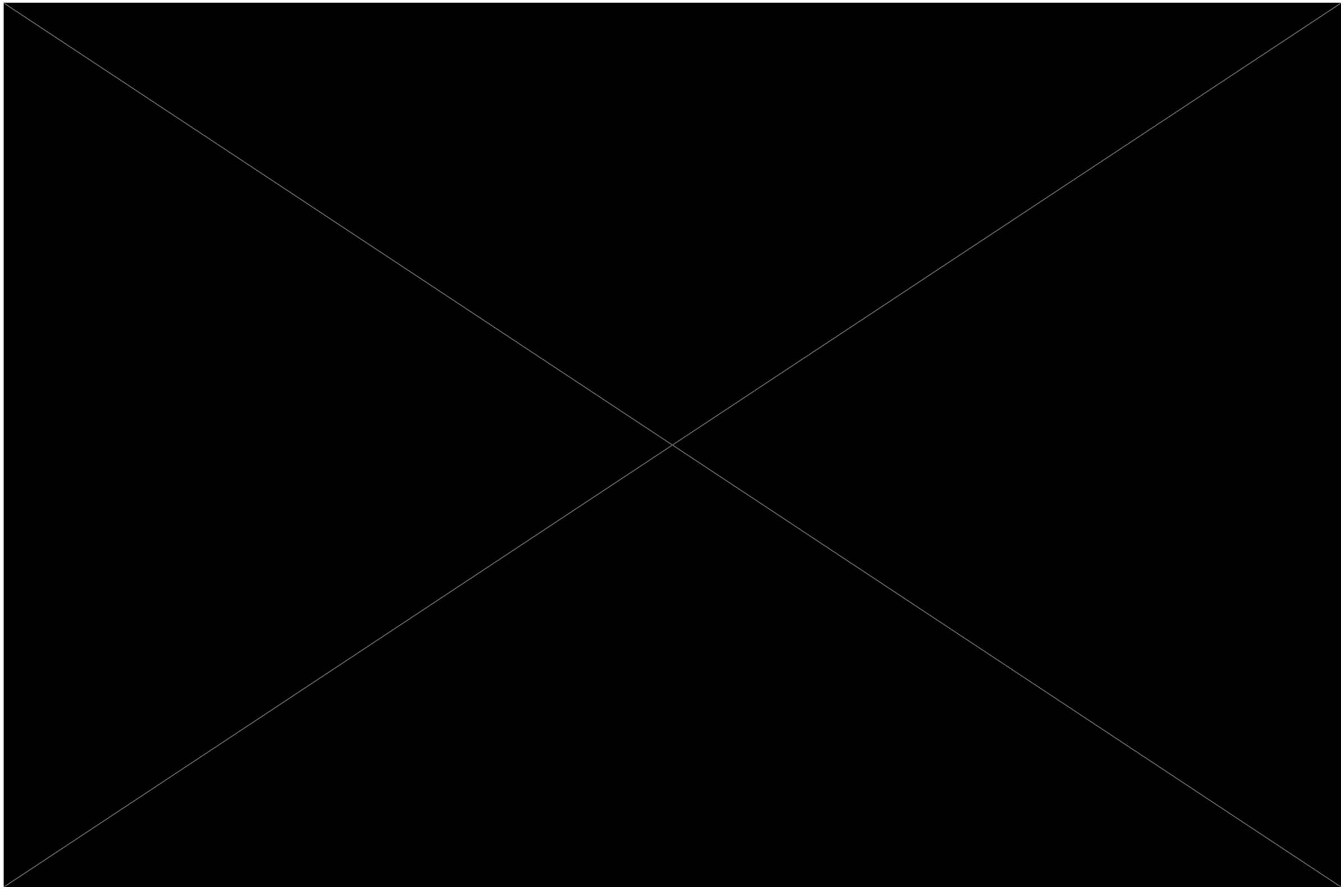

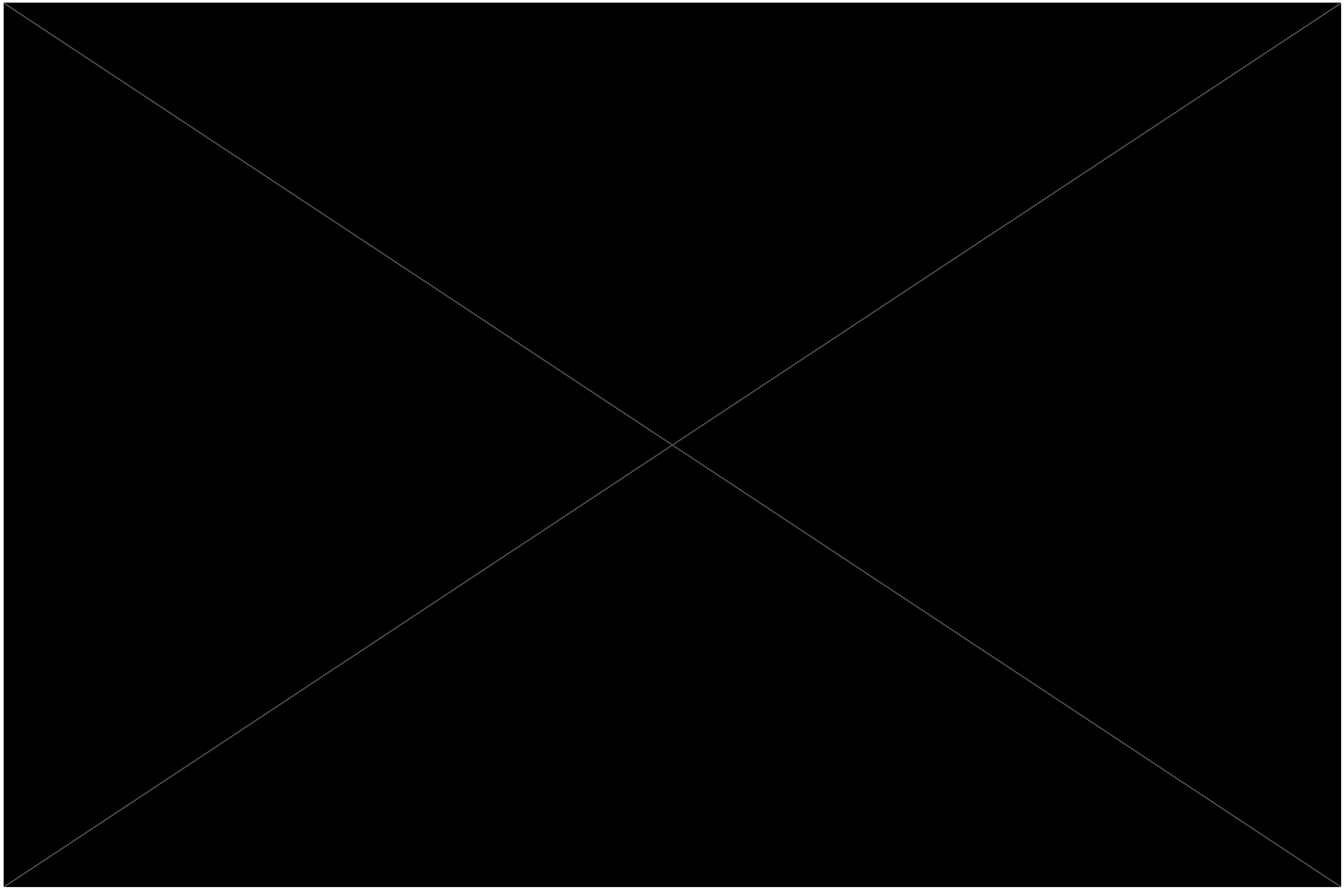

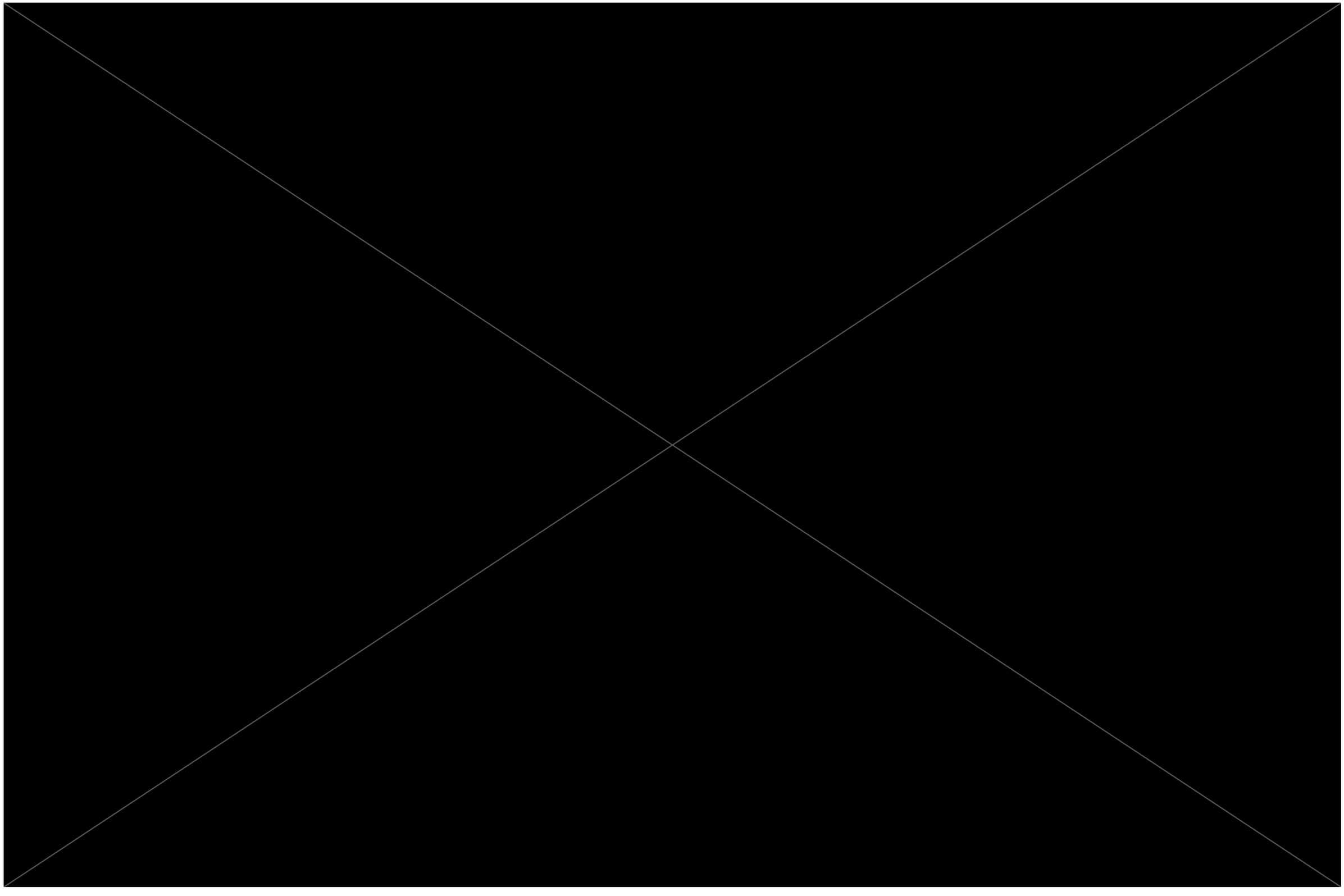

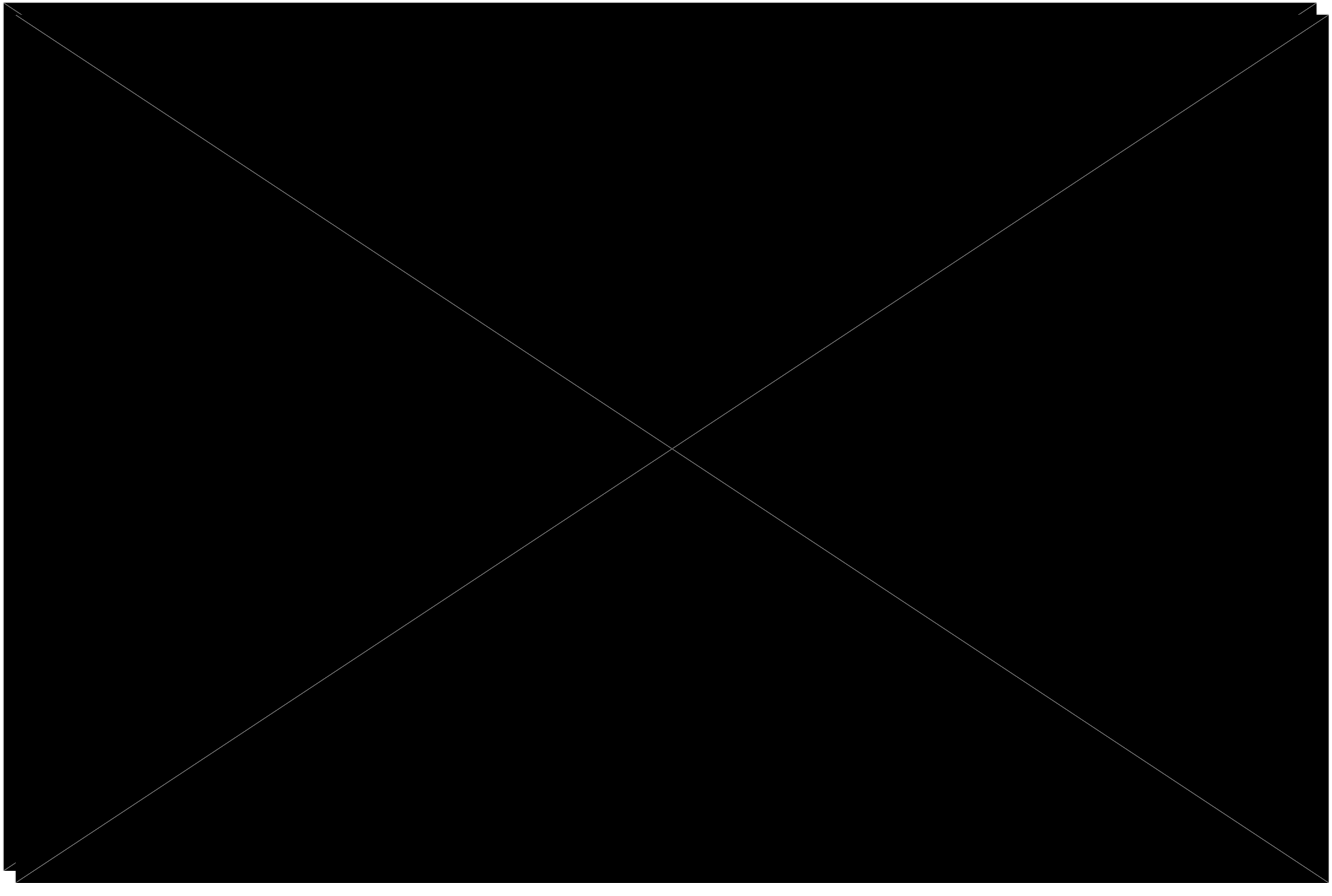

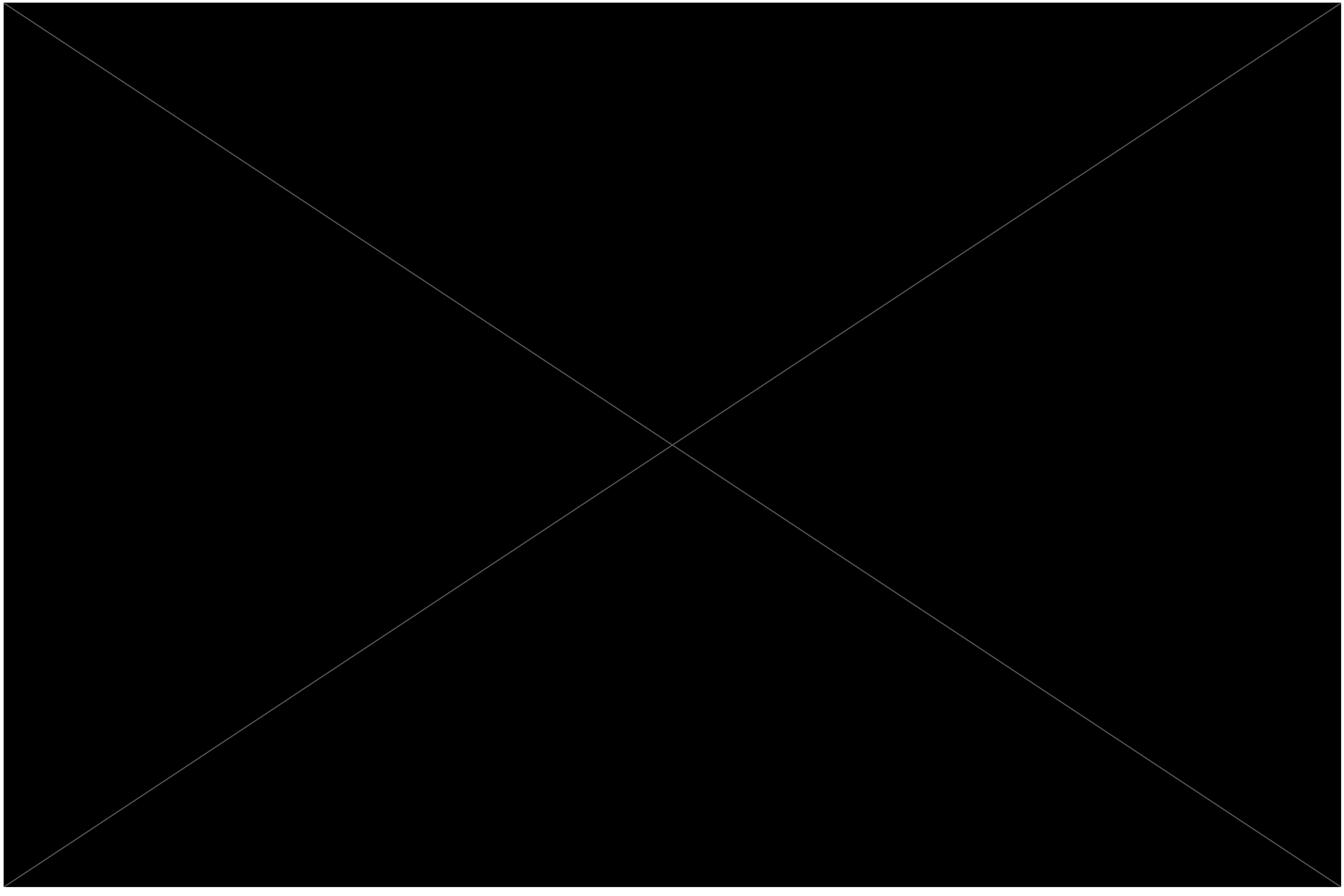

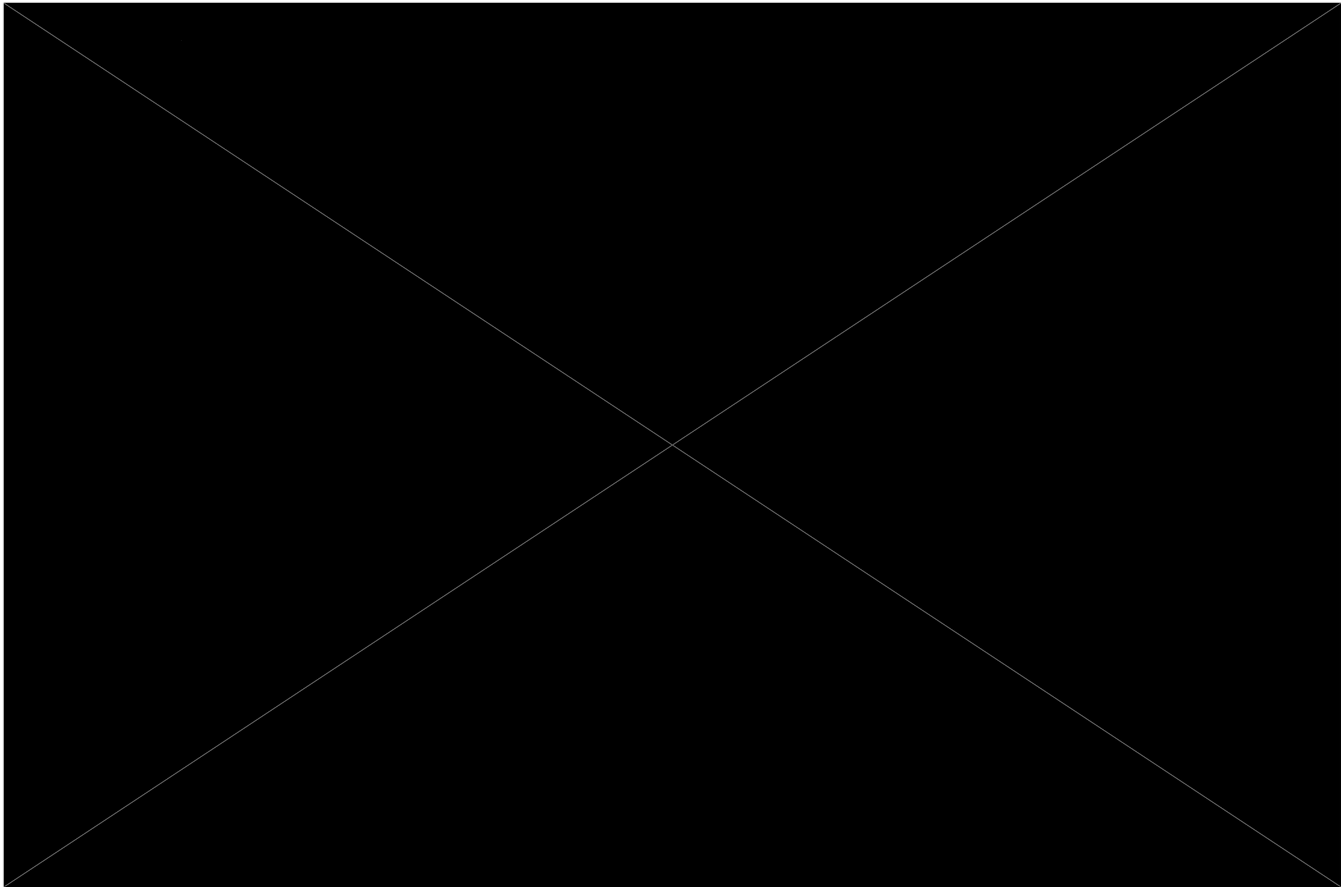

Appendix D

Details of publication which chapter 5 is based on:

Norcliffe, J.R., Paton, D.A., Mortimer, E.J., McCaig, A.M., Nicholls, H., Rodriguez, K., Hodgson, N. and Van Der Spuy, D. 2018. Laterally Confined Volcanic Successions (LCVS); recording rift-jumps during the formation of magma-rich margins. Earth and Planetary Science Letters. 504,pp.53–63. 10.1016/j.epsl.2018.09.033